Impacts of global climate changes on continental environments : case study of the eocene-oligocene transition in the upper Rhine graben

Emile Simon

To cite this version:

Emile Simon. Impacts of global climate changes on continental environments : case study of the eocene-oligocene transition in the upper Rhine graben. Sciences de la Terre. Université de Strasbourg, 2023. Français. NNT : 2023STRAH009 . tel-04613933

HAL Id: tel-04613933
https://theses.hal.science/tel-04613933v1

Submitted on 17 Jun 2024

UNIVERSITÉ DE STRASBOURG

École Doctorale des Sciences de la Terre et de l'Environnement (ED 413)

Institut Terre et Environnement de Strasbourg (UMR 7063)

THÈSE

présentée par :

Emile SIMON

Soutenue le **14 novembre 2023**

pour obtenir le grade de : **Docteur de l'Université de Strasbourg**

Discipline/Spécialité : Sédimentologie, Paléoclimatologie

Impacts of global climate changes on continental environments: case study of the Eocene-Oligocene transition in the Upper Rhine Graben

Impacts des changements climatiques globaux sur les environnements continentaux : étude de cas de la transition Éocène-Oligocène dans le Fossé Rhénan

THÈSE dirigée par :

M. SCHUSTER Mathieu	Directeur de recherche, CNRS, Institut Terre & Environnement de Strasbourg, UMR7063
M. VOGEL Hendrik	Professeur, Université de Berne, Suisse

RAPPORTEURS :

Mme. FOUBERT Anneleen	Professeure, Université de Fribourg, Suisse
M. HINDERER Matthias	Professeur, Université technique de Darmstadt, Allemagne

AUTRES MEMBRES DU JURY :

Mme. SCHMITT Anne-Désirée	Professeure, Université de Strasbourg
M. GINDRE-CHANU Laurent	Consultant, Terra Geosciences, Dijon, France

Table of Contents

List of acronyms

EOT: Eocene-Oligocene Transition

EOB: Eocene-Oligocene Boundary

EOIS: Earliest Oligocene Isotope Step

EOGM: Early Oligocene Glacial Maximum

AIS: Antarctic Ice Sheet

ACC: Antarctic Circumpolar Current

NAO: North Atlantic Oscillation

AMOC: Atlantic Meridional Overturning Circulation

GSR: Greenland-Scotland Ridge

ITCZ: InterTropical Convergence Zone

CCD: Carbonate Compensation Depth

PETM: Paleocene-Eocene Thermal Maximum

EECO: Early Eocene Climatic Optimum

MECO: Middle Eocene Climatic Optimum

MMCO: Middle Miocene Climatic Optimum

URG: Upper Rhine Graben

MAR: Maximum Accumulation Rate

Acknowledgements

I would like to sincerely thank:

- my PhD directors Mathieu SCHUSTER and Hendrik VOGEL for creating this research opportunity, giving me the freedom to pursue it how I saw fit, and for providing precious advice and feedback.
- the members of the jury, Anneleen FOUBERT, Matthias HINDERER, Anne-Désirée SCHMITT, and Laurent GINDRE-CHANU for reviewing this manuscript and providing rich feedback during the defense.
- the “Région Grand-Est” and “MESRI” for funding this PhD.
- the “CNRS” and “INSU” (TelluS/SysTer program) for funding the field and analytical work of this PhD.
- the “Musée d’Histoire Naturelle et d’Ethnographie de Colmar” (Martial BOUTANTIN, Claire PRÊTRE, Manuelle VIGNES) for providing access to the core samples of the DP-XXVIII borehole.
- the “Musée de la Mine et de la Potasse” (“KALIVIE”) (Chantal VIS, Laurent GINDRE-CHANU, Loïc DEMESY, and all the volunteers) for providing access to their geological collection and to historical documents.
- “ES Géothermie” and Albert GENTER for providing the cuttings and numerical data from the GRT-1 and GPK-2 boreholes.
- the “Mines De Potasse d’Alsace” (previously “Mines Domaniales de Potasse d’Alsace”) and Régis FISCHER for providing access to a mining gallery 500 m underground to log and sample its sedimentary record.
- Kirsten and Matthias GRIMM for insightful discussions on the biostratigraphy of the Upper Rhine Graben.
- Andreas KOUTSODENDRIS and Joerg PROSS from the University of Heidelberg for guiding me through the basics of palynology.
- the “Geological Systems” research team at ITES, as well as all the colleagues I’ve spent time with.
- Magalie LINDENMAYER and the workers of the Holcim quarry in Altkirch for granting us access to the quarry.
- the Collectivité européenne d’Alsace and Samuel AUDINOT for providing access to quarries and for insightful discussions.
- the members of my PhD Committee (Guillaume DUPONT-NIVET, Fritz SCHLUNEGGER, Alexis NUTZ, Jean-François GHIENNE, Mathieu MARTINEZ, Guilherme BOZETTI, Laurent GINDRE-CHANU, François GUILLOCHEAU) for insightful discussions and for their advice on the various disciplines in which they excel.
- my family and friends.

> “Look back over the past, with its changing empires that rose and fell, and you can foresee the future, too.”
>
> **Marcus Aurelius**

Abstract

Understanding past climate changes is an important step to better assess the future of our warming Earth. This thesis is a contribution to the collective effort of paleoclimate studies, focused on the impacts of the Eocene-Oligocene Transition (EOT) on the continental environments of the Upper Rhine Graben (URG). The EOT is a ~790 kyr period that marked the transition from the late Eocene “greenhouse” world to the early Oligocene “icehouse” world, notably associated with an average global cooling of 4 to 6 °C and the onset of the Antarctic icesheet. Sedimentary records of the URG were investigated through the lenses of sedimentology, cyclostratigraphy, geochemistry, palynology, and paleomagnetism.

Chapter I, II, and III. Chapter I introduces the rationale and objective of this thesis, dwelling on the importance of documenting paleoclimates. In the second chapter, state of the art syntheses are presented on our modern climate, on the EOT, on the geological setting of the URG, and on orbital cycles theory and their impacts on climate and sedimentation. In the third chapter, the material and methods used throughout the thesis are detailed.

Chapter IV. In this chapter, the sedimentology of the Mulhouse basin is detailed through the study of core samples and documents from the DP-XXVIII well, from the Jurassic to the “Série Grise”, through the sedimentological analysis of a mine gallery, and through the investigation of potash seams. The evolution of paleoenvironments is detailed based on the interpretation of sedimentary structures and lithofacies. In addition to these distal records, proximal records of the URG are detailed through the description and interpretation of sedimentary structures and lithofacies from several outcrops.

Chapter V. In this chapter, the observations made from the study of the DP-XXVIII well are interpreted in the scope of the EOT. At the base of the “Sel III”, a transition from structureless mudstones to laminites and varves is detailed, along the onset of metric to decametric mudstone-evaporite cycles induced by orbital cycles. These changes are interpreted as being the result of an increased seasonal climatic contrast and sensitivity of the climate to orbital variations across the EOT. Previous palynological investigations also suggested increased seasonality in the “Sel III”, along with cooling and aridification.

Chapter VI. In this chapter, cyclostratigraphic investigations are performed on the sedimentary records of the Mulhouse and Pechelbronn basins using gamma-ray well-logs, showing the imprint of orbital forcing in both basins. In the Mulhouse basin, the metric to decametric mudstone-evaporite alternations mostly correspond to precession cycles with cases of obliquity, modulated by short eccentricity. Minimum durations of each investigated interval are proposed, and an orbital tuning solution is proposed for the “Zone Salifère Supérieure”. A new chronostratigraphic framework is proposed based on these new results.

Chapter VII. This chapter deals with the geochemistry (TOC, TIC, C/N, C/S) and palynology (dinocysts, pollen) of the GRT-1 and GPK-2 boreholes of the Pechelbronn basin. The geochemistry results suggest that from the “basal Eocene” to the “Série Grise”, the environment was brackish to marine, and that the organic matter was derived from both algae and land plants, expect for samples with high TOC values (>1%) for which they mainly derived from land plants. The palynology results suggest that part of the “Couches de Pechelbronn Moyennes” and “Inférieures” were influenced by a marine transgression due to the presence of marine dinocysts. Pollen counting results show an aridification event at the base of the “Couches de Pechelbronn Supérieures”.

Chapter VIII. Paleomagnetic measurements show that most outcrops did not hold any magnetic signal, except for the “Strangenberg” outcrop for which most samples recorded inverse signals, and in the mine gallery.

Résumé étendu en langue française

Chapitre I : Introduction

La Terre est impactée par un changement climatique dont la vitesse et l'amplitude excèdent tout processus géologiques naturels, largement à cause des émissions de gaz à effet de serre d'origines humaine (Foster et al., 2018). Des effets néfastes de ce réchauffement climatique anthropique peuvent déjà être observés sur les écosystèmes naturels (e.g. modifications de l'aire de répartition des espèces, modifications du calendrier phénologique et de la structure globale des écosystèmes) et sur les systèmes humains (e.g. pénuries d'eau, réduction de la productivité alimentaire, dégradation de la santé et du bien-être, dégâts sur les infrastructures) (Shukla et al., 2019). Bien que les principaux impacts et mécanismes des changements climatiques sont relativement bien compris, ils restent associés à des incertitudes, dont les facteurs incluent la variabilité naturelle et la sensibilité climatique. Afin de mieux les comprendre, une partie de la communauté scientifique s'est tournée vers l'étude des changements climatiques du passé (Zachos et al., 2001). Comprendre l'histoire climatique de la Terre est crucial pour mieux appréhender son présent et concevoir son futur. Les changements climatiques du Cénozoïque sont particulièrement prometteurs à cet égard, car la configuration des continents au cours de cette période est relativement proche, à quelques différences près, de leur configuration actuelle. L'étude des archives sédimentaires de ces changements climatiques nous permet de mieux comprendre les impacts qu'ils ont eu sur les environnements passés.

La transition Éocène-Oligocène (TEO) signe le passage de la période « greenhouse » de l'Éocène à la période « icehouse » de l'Oligocène, marqué par un refroidissement de la température moyenne globale de 4 à 6°C et par la glaciation de l'Antarctique (Hutchinson et al., 2020 ; Lear et al., 2008). Les enregistrements pré-TEO (i.e. Paléocène, Éocène) contiennent des informations sur le climat terrestre sous des conditions caractérisées par de hautes températures et taux de CO_2. Les enregistrements post-TEO (i.e. Oligocène à Holocène) renferment des informations sur des conditions plus proches de l'actuel. Ces périodes peuvent servir comme homologues à ce que le futur nous réserve en fonction des scénarios climatiques (Tierney et al., 2020). L'étude de la TEO se révèle être une clé vers la compréhension des mécanismes pouvant pousser le climat à rapidement basculer d'un état « greenhouse » à un état « icehouse ». La communauté scientifique s'efforce de documenter cette période à divers points du globe (Hutchinson et al., 2020 ; Coxall & Pearson, 2007), et cette documentation permet aux modélisateurs d'affiner leurs modèles climatiques.

Le Fossé Rhénan, zone d'étude de cette thèse, contient des enregistrements sédimentaires du Cénozoïque, et notamment des dépôts datant de l'Éocène et de l'Oligocène. C'est une zone propice à l'étude de la transition Éocène-Oligocène. Grâce à ses riches ressources souterraines exploitées par le passé (e.g. pétrole, potasse) et actuellement (e.g. géothermie, carrières), de nombreuses données géologiques ont été mises à disposition et permettent de documenter l'évolution passée du Fossé Rhénan.

Comprendre le passé est une étape cruciale pour évaluer l'avenir de notre monde soumis à une perturbation climatique d'origine anthropique (**Figure 1**). C'est un effort collectif mené par des scientifiques de différentes disciplines et horizons, dont l'objectif est de documenter comment les environnements et climats étaient à des périodes données, et comment ils ont évolué depuis. L'objectif de cette thèse est de contribuer à cet effort en documentant les impacts de la transition Éocène-Oligocène sur les environnements continentaux du Fossé Rhénan. Une attention particulière est également portée sur « l'avant » et « l'après » de cette transition, car tout aussi importants que le « pendant ». Pour ce faire, les enregistrements sédimentaires du Fossé Rhénan ont été étudié à travers l'angle de vue de la sédimentologie, de la cyclostratigraphie, de la géochimie, de la palynologie, et du paléomagnétisme.

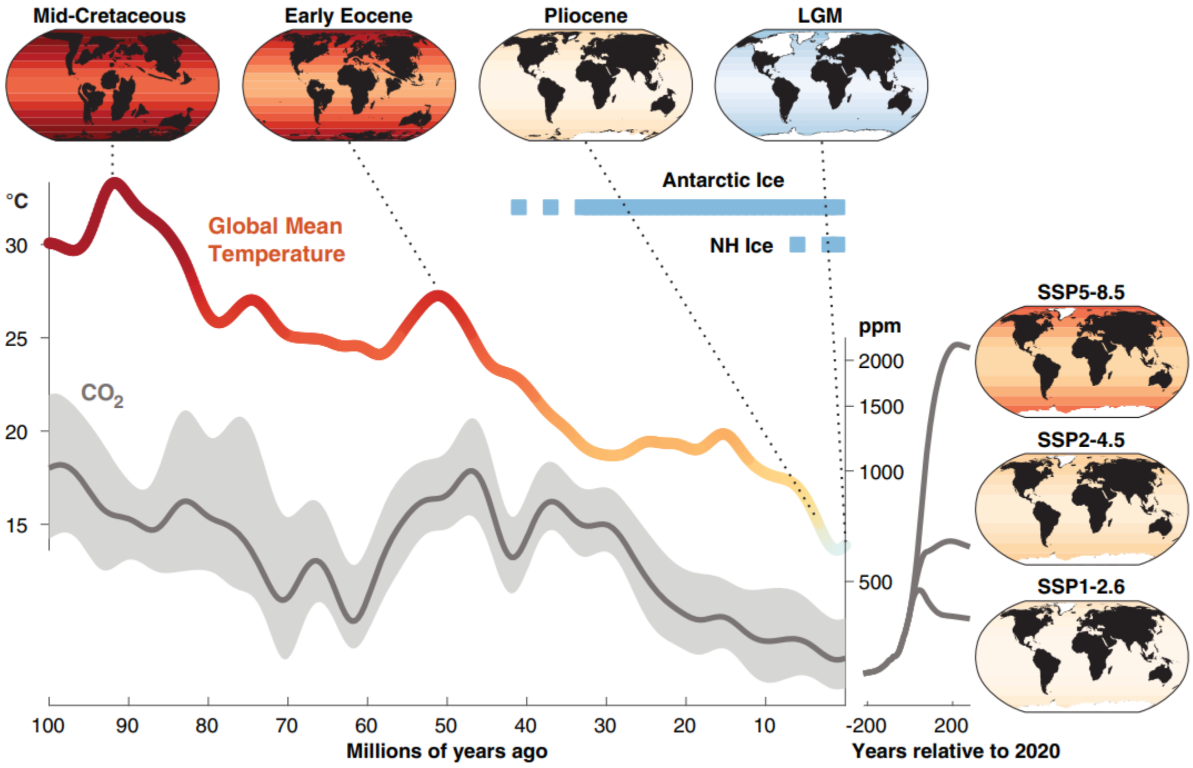

Figure 1: Températures moyennes à la surface du globe et taux de CO_2 pour les 100 derniers millions d'années comparés aux scénarios climatiques futurs, tels que synthétisés par Tierney et al. (2020). Les courbes ont été lissées pour mettre en évidence les tendances à long terme. LGM = Dernier Maximum Glaciaire, NH = Hémisphère Nord. SSP = Shared Socioeconomic Pathways (voies socio-économiques partagées). D'après Tierney et al. (2020).

Chapitre II : Contextes scientifique et géologique

II.1 : Climat moderne, réchauffement climatique, et cycles glaciaire-interglaciaire

Climat moderne. La météo (= le temps) caractérise les conditions de l'atmosphère sur de courtes périodes, principalement en fonction de la température, des précipitations, et de la disposition des nuages. Le climat est défini comme le modèle météo à plus long terme d'une région donnée (Peixoto & Oort, 1992 ; Schneider & Dickinson, 1974). Les climats terrestres sont partiellement dictés par l'agencement de plusieurs caractéristiques physiques de la Terre, comprenant la disposition des continents et des passages océaniques qui influent sur les mouvements des courants océaniques. Ces derniers jouent un rôle majeur dans la mise en place des climats, car ils influencent les températures et précipitations de diverses zones en transportant la chaleur et l'humidité (Clark et al., 2002 ; Wunsch, 2002 ; Rahmstorf, 2003). La circulation thermohaline (= circulation océanique profonde) est un courant océanique de grande envergure entraînée par des gradients de densités issues des flux d'eau douce et de la chaleur de surface (Wunsch, 2002). D'autres courants océaniques comme le Gulf Stream sont alimentés par des vents de surfaces tels que les vents d'ouest (= westerlies), l'un des vents dominants sur Terre (Seager et al., 2002 ; Taylor & Stephens, 1998). Les vents dominants sont les principaux vents de surfaces qui soufflent dans des directions données, liés aux cellules atmosphériques existantes à des latitudes précises dans les deux hémisphères (Oort, 1983 ; Budikova, 2009 ; Kushner et al., 2001). Ces cellules sont connues sous les noms « cellules de Hadley » (entre 0 et 30°), « cellule des Ferrel » (entre 30 et 60°), et « cellules polaires » (entre 60 et 90°). Ces vents existent en raison de processus induits par l'insolation solaire, qui chauffent préférentiellement l'équateur plutôt que les pôles à cause de la courbure de la Terre, ainsi qu'à cause de la rotation terrestre. Ces différences de températures se traduisent en différences de densités qui provoquent les mouvements des masses d'air. À plus petite échelles, ces vents sont également entre autres influencés par la présence de montagnes et par les processus de rétroaction en lien avec les courants océaniques. Le Gulf Stream transporte les eaux chaudes du golfe du Mexique vers l'océan Atlantique, qui influence grandement le climat en Europe occidentale, et plus largement de l'hémisphère Nord (Stommel, 2022 ; Taylor et al., 1998). En Europe occidentale, les températures de l'air sont jusqu'à 10°C plus élevées que la moyenne à des latitudes équivalentes, et ce en partie grâce au Gulf Stream (Palter, 2015). En raison du réchauffement climatique actuel, l'équilibre des courants océaniques, et donc des climats régionaux et mondiaux, est menacé.

Réchauffement climatique

Depuis la révolution industrielle des XVIIIe et XIXe siècles, de grandes quantités de gaz à effet de serre ont été injectées dans l'atmosphère, notamment induits par la combustion d'énergies fossiles et de la déforestation à grande échelle (Salam & Noguchi, 2005). En raison de l'effet de serre, processus par lequel la chaleur est partiellement absorbée, redirigée et piégée dans l'atmosphère, la température moyenne de la Terre a augmenté de plus de 1°C depuis le début des années 1900. Les effets de ces changements rapides sont déjà perceptibles et devraient s'aggraver si rien n'est fait (GIEC, 2022). L'augmentation des concentrations de CO_2 dans l'atmosphère entraîne une acidification croissante des océans, ce qui provoque d'énormes changements dans la chimie des carbonates de l'eau de mer (Doney et al., 2009). L'équilibre des calottes glaciaires est menacé, et leur fonte est observée à des vitesses alarmantes aux deux pôles. En raison de la fonte des calottes glaciaires et de la dilatation de l'eau de mer induite par le réchauffement global, le niveau moyen des océans s'élève (Alley et al., 2005 ; Lombard et al., 2005). Les risques naturels extrêmes tels que les tempêtes, les incendies de forêt et les inondations sont de plus en plus graves et fréquents (Van Aalst, 2006). Ces changements rapides menacent l'existence d'espèces adaptées à des environnements et des conditions climatiques spécifiques.

Cycles glaciaires-interglaciaires

Au cours des temps géologiques, les variations climatiques ont été induites par des processus naturels, tel que la répartition changeante de l'insolation sur Terre due aux cycles orbitaux (= cycles de Milankovitch) qui ont engendré les cycles glaciaires-interglaciaires (Berger, 1988 ; Berger, 2001 ; Archer et al., 2020). Les cycles glaciaires-interglaciaires font référence aux changements observés dans la pression partielle de CO_2, la température, l'aridité et l'étendue des glaces aux pôles au cours des derniers millions d'années (Lüthi et al., 2008). Les périodes glaciaires sont plus froides et plus sèches que les périodes interglaciaires. L'étude des carottes de glace de l'Antarctique a permis d'étudier les proxys climatiques dans le passé et a montré que les changements des gaz à effet de serre sont en corrélation avec les variations de la température (Lüthi et al., 2008). Pour les 1,2 derniers millions d'années, les observations montrent que les cycles glaciaires-interglaciaires se sont produits tous les 100 000 ans, alors qu'ils semblent s'être produits tous les ~41 000 ans entre 1,2 millions d'années et 5,4 millions d'années (Lisiecki & Raymo, 2005). Ces observations sont très intéressantes car le cycle qui a le plus d'impact sur l'insolation est la précession, or le cycle de précession (23 000 ans) n'apparaît pas vraiment dans les enregistrements de ces périodes. Cette observation fait toujours l'objet de recherches actives qui se concentrent notamment sur les processus non linéaires et les mécanismes de rétroaction qui auraient pu provoquer ces cycles glaciaires-interglaciaires.

II.2 : La transition Éocène-Oligocène (TEO)

Définition de la TEO

La TEO fait référence à l'intervalle transitoire en l'Éocène et l'Oligocène au cours duquel la Terre a connu une phase de réorganisation climatique et biotique rapide et importante. La durée complète de la TEO est estimée à 790 000 ans, commençant avant et se terminant après la limite Éocène-Oligocène (33.9 Ma) (Hutchinson et al., 2020) (**Figure 2**). D'un point de vue stratigraphique, la limite Éocène-Oligocène a été définie à l'affleurement de Massignano en Italie, au niveau où la famille de foraminifère planctonique *Hantkeninidae* s'est éteinte (Nocchi et al. 1986 ; Premoli Silva & Jenkins, 1993). La transition climatique Éocène-Oligocène a été définie par les enregistrements $\delta^{18}O$ des foraminifères benthiques provenant de sites en eaux profondes (Coxall et al., 2005 ; Zachos et al., 2001), qui montrent une augmentation de 1,5 ‰ en moyenne due à la combinaison de la croissance des glaces terrestres et du refroidissement des eaux profondes. La TEO est définie comme un évènement composite comprenant trois étapes principales connue sous le nom de « événement de l'Éocène tardif » (= late Eocene event), « étape 1 » (= step 1), et « étape isotopique de l'oxygène de l'Oligocène précoce » (= Earliest Oligocene oxygen Isotope Step, EOIS) (Hutchinson et al., 2020). Le début de la TEO correspond à la disparition du foraminifère *Discoaster saipanensis* et sa fin correspond à la fin de l'EOIS, de 34.44 à 33.65 Ma.

- **Événement de l'Éocène tardif**. C'est un court événement froid intervenant dans la Priabonien supérieur, correspondant à un pic de $\delta^{18}O$ observés dans certains enregistrements et corrélé à l'extinction du foraminifère *Discoaster saipanensis*. Cet événement est parfois interprété comme une première glaciation antarctique avortée et pourrait être associé à un changement important des courants de l'Atlantique Nord (Coxall et al., 2018).
- **Étape 1**. Elle correspond à la première excursion de $\delta^{18}O$ observée peu avant la limite Éocène-Oligocène. Elle début à 34.15 Ma, dure environ 40 000 ans, et correspond principalement à un refroidissement des eaux profondes et des basses latitudes d'environ 2°C (Bohaty et al., 2012 ; Peck et al., 2010 ; Pusz et al., 2011 ; Lear et al., 2010, 2008, 2004). Cet événement est également connu sous le nom de « EOT-1 » (Katz et al., 2008).
- **Étape Isotopique de l'oxygène de l'Éocène précoce**. C'est une courte seconde période d'augmentation rapide du $\delta^{18}O$ postérieure à la limite Éocène-Oligocène située dans la partie inférieure de l'épisode magnétique C13n. Elle dure environ 40 000 ans et le maximum de $\delta^{18}O$ est atteint à environ 33.65 Ma, marquant l'apparition et/ou le développement majeur de la calotte glaciaire Antarctique, possiblement également associé à un refroidissement (Kennedy et al., 2015). Cet événement est également connu sous le nom de « Oi1 » (Miller et al., 1991) et « Oi-1a » (Zachos et al., 1996).

La fin de cette période marque la fin de la TEO, suivi par le « maximum glaciaire de l'Oligocène précoce » (= Early Oligocene Glacial Maximum, EOGM), qui est une période d'environ 490 000 ans durant laquelle l'étendue de la nouvelle calotte glaciaire Antarctique atteint son maximum, probablement équivalente à son étendue actuelle (Lear et al., 2008). À la fin de l'EOGM, le $\delta^{18}O$ diminue et marque la fonte partielle de la calotte glaciaire nouvellement formée et/ou un réchauffement relatif des eaux profondes.

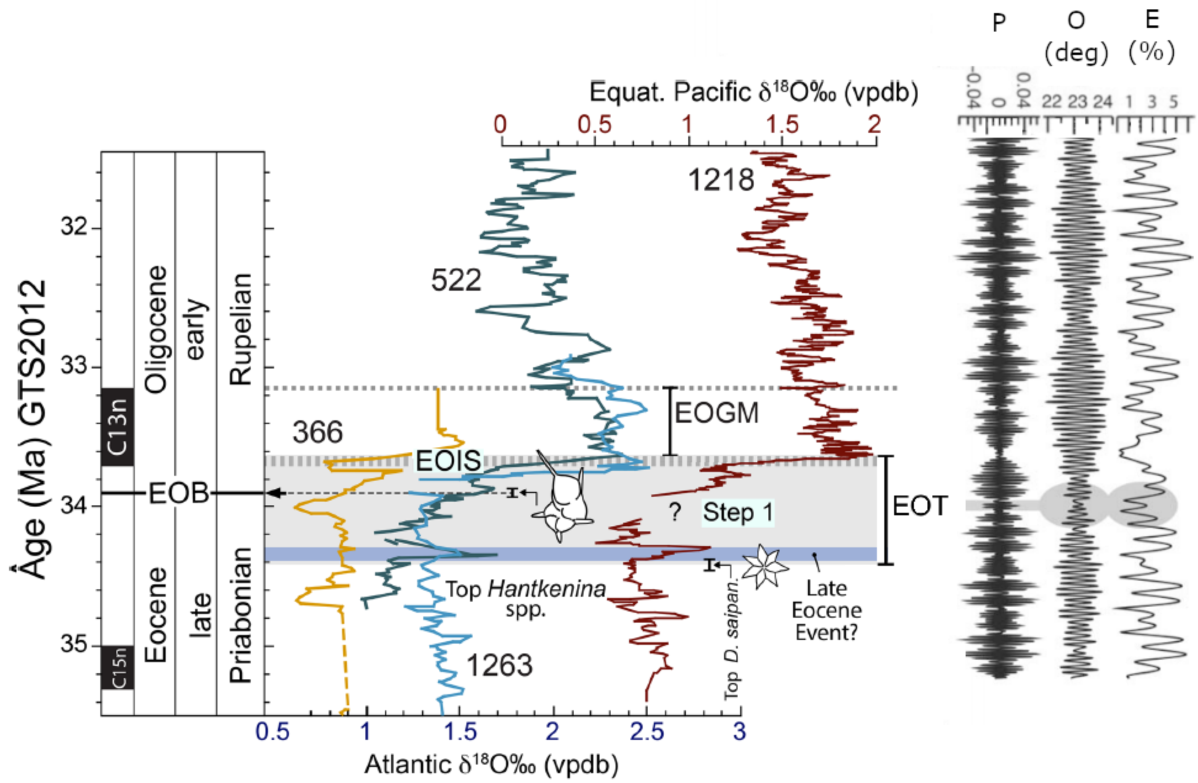

***Figure 2**: Expression de la TEO à travers les variations du $\delta^{18}O$ des foraminifères dans les carottes océaniques, montrant ses principales étapes ainsi que les paramètres orbitaux (P : précession, O : obliquité, E : excentricité). L'étape 1 (« Step 1 ») est précédée d'une courte période pendant laquelle la configuration des cycles orbitaux a induit de faibles valeurs d'insolation dans l'hémisphère sud, provoquant des étés plus froids, permettant à la glace de se développer plus facilement en Antarctique. Modifié d'après Hutchinson et al. (2020) et Coxall & Pearson (2007).*

Causes de la TEO

Les deux principales causes évoquées pour expliquer la TEO sont une baisse drastique des taux de CO_2 d'une part, et une modification des passages et courants océaniques de l'autre (Kennedy et al., 2015 ; Pearson et al., 2009 ; Livermore et al, 2007). De plus, les variations d'insolation perçues par la Terre, expliquées par une configuration particulière des paramètres orbitaux, ont pu permettre à la glace de persister pendant l'été dans certains points de nucléation et de se propager rapidement à l'ensemble du continent antarctique (DeConto & Pollard, 2003 ; Ladant et al., 2014). Pendant longtemps, l'explication pour la glaciation de l'Antarctique avait été l'établissement du Courant Circumpolaire Antarctique (courant qui isole thermiquement l'Antarctique en bloquant l'arrivée d'eau chaude en provenance de l'équateur) induit par l'approfondissement du passage de Drake et l'ouverture de la voie maritime de Tasmanie (Livermore et al., 2007 ; Kennedy et al., 2015, Abelson & Erez, 2017), mais cette hypothèse est aujourd'hui débattue car le passage de Drake n'aurait pas été assez profond à cette période pour permettre une circulation importante des eaux profondes (Eagles et al., 2005). Récemment, une étude a suggéré que des changements tectoniques au niveau des passages atlantiques-arctiques auraient influencé la circulation océanique et provoqué la croissance des calottes glaciaires continentales parallèlement à l'abaissement du CO_2. Les modélisations numériques suggèrent que la chute de CO_2 a eu un impact majeur sur l'existence de la TEO (DeConto & Pollard., 2003 ; Ladant et al., 2014). Les taux de CO_2 seraient passés d'environ 1100 ppm au Priabonien supérieur à environ 600 ppm au Rupélien inférieur (Pearson et al., 2009). La glaciation antarctique aurait débuté après le dépassement d'une valeur critique de CO_2 estimée à ~750 ppm, qui reste cependant débattue (Pearson et al., 2009). Selon Ladant et al. (2014), ce seuil se situerait plutôt autour de 900 ppm. Les causes proposées pour la réduction du CO_2 atmosphérique autour de la TEO restent très discutées. Elles comprennent des causes à long terme telles que l'augmentation de l'altération chimique des silicates potentiellement liée à l'orogenèse himalayenne (Raymo & Ruddiman, 1992 ; Ruddiman et al., 1997), une augmentation du taux d'enfouissement du carbone organique (Diester Haass & Zachos, 2003), et une forte réduction du dégazage volcanique et hydrothermal en relation avec une diminution du taux d'expansion des océans (Berner, 1990). Cependant, les modèles numériques (e.g. DeConto & Pollard, 2003 ; Ladant et al., 2014) indiquent que la diminution rapide du CO_2 atmosphérique se serait produite dans un intervalle de temps limité à la TEO. Bien que l'influence des changements bathymétriques des passages océaniques Atlantique-Arctique suggérée par Straume et al. (2022) puisse être un argument de poids, elle n'a pas déclenché la baisse du CO_2, dont la véritable cause reste encore à découvrir. La modification des courants océaniques pourrait avoir modifié les taux de précipitations sur les continents, renforçant l'absorption du CO_2 par l'altération des silicates, et pourrait avoir transporté des eaux riches en nutriments vers la surface, renforçant également l'absorption du CO_2 par une productivité biologique accrue (Straume et al., 2022).

Conséquences de la TEO

Les principales conséquences associées au changement climatique de la TEO sont notamment (i) une forte baisse de la température moyenne globale, (ii) l'apparition de la calotte glaciaire Antarctique et une baisse du niveau eustatique absolu d'environ 70 m, (iii) des changements faunistiques et floristiques majeurs, ainsi que (iv) un approfondissement de la profondeur de compensation des carbonates dans les océans lié à un changement de la chimie de l'eau. Dans le domaine marin, des chutes de températures ont été observées tant à la surface des océans que dans les eaux profondes. Des études suggèrent que les températures de surfaces auraient chutées de 2.5 °C en Tanzanie (Lear et al., 2008), de 3 à 4 °C dans le Golfe du Mexique (Wade et al., 2012), et entre 0 et 8 °C à diverses autres latitudes (Hutchinson et al., 2020). Les eaux profondes se seraient refroidies de 2 à 3°C dans l'océan Austral (Bohaty et al., 2012). En comparaison au domaine marin, les enregistrements sédimentaires continentaux montrent des réponses plus hétérogènes au cours de la TEO, démontrant une plus grande variabilité climatique sur les continents (Hutchinson et al., 2020 ; Pound & Salzmann, 2017 ; Toumoulin et al., 2021). En général, les climats sont devenus plus froids et arides, mais il y a des exceptions. En **Europe**, dans les bassins de Paris (France) et du Hampshire (Royaume-Uni), les observations de Stehlin (1910) suggèrent un remplacement des mammifères endémiques européens par des espèces asiatiques mieux adaptées à des climats plus froids, suggérant un refroidissement marqué, événement qu'il appela « Grande Coupure ». Plus récemment, dans le bassin du Hampshire, Hooker et al. (2004) ont confirmé les observations de Stehlin (1910) et ont corrélé la « Grande Coupure » avec l'étape Isotopique de l'oxygène de l'Éocène inférieur. D'autres analyses dans le même bassin ont révélé un refroidissement de la température moyenne de l'air de 4 à 6 °C au cours de la TEO (Hren et al., 2013). Dans le bassin de Rennes, le climat chaud et humide de l'Éocène supérieur s'est détérioré jusqu'à l'Oligocène inférieur, où les conditions sont devenues plus froides et plus arides (Tramoy et al., 2016). Dans le Fossé Rhénan (France), des études palynologiques ont révélé un refroidissement à long terme du Lutétien au Rupélien inférieur supérieur, avec une phase de refroidissement d'aridification et de saisonnalité accrue dans l'unité "Sel III" (Schuler, 1988), corrélé à la TEO dans cette thèse. En **Antarctique**, la végétation est passée de l'Éocène moyen au début de l'Oligocène de forêts sempervirentes à une végétation de basse altitude (Pound & Salzmann, 2017). Dans la partie orientale du continent, la végétation est passée de forêts subtropicales très diversifiées à des forêts de type tempérée froide à travers la TEO (Strother et al., 2017 ; Pross et al., 2012). En **Asie**, la TEO a été rattachée à une aridification et augmentation de la mousson en Chine (Dupont-Nivet et al., 2007), ainsi qu'à un grand changement faunistique observé en Mongolie et au nord de la Chine (Sun et al., 2014). Au sud-est de l'**Australie**, des études indiquent une transition de forêts tropicales chaudes à des forêts tropicales tempérées indiquant un refroidissement à travers la TEO (Korasidis et al., 2019 ; Sluiter et al., 2022), tandis que d'autres études indiquent une perte de diversité plutôt qu'un changement majeur (Macphail, 2007 ; Martin, 2006). En **Amérique du Nord**, des changements floristiques indiquent également une tendance au refroidissement et à l'aridification à travers la TEO (Wing, 1987 ; Ridgway & Sweet, 1995 ; Breedlovestrout et al., 2013 ; Yancey et al., 2003). Des analyses isotopiques suggèrent un refroidissement de 7 à 8 °C (Fan et al., 2018 ; Zanazzi et al., 2007). C'est en **Amérique du Sud** où les conséquences de la TEO sont plus hétérogènes. Tandis que des études montrent que la végétation est restée relativement inchangée à travers la TEO en Patagonie (Kohn et al., 2004, 2015 ; Strömberg et al, 2013 ; Quattrocchio et al., 2013), une autre étude plus récente suggère un refroidissement de près de 5 °C à travers la TEO (Colwyn & Hren, 2019), et d'autres encore suggèrent le passage de forêts tempérées chaudes à des forêts tempérées froides (Barreda & Palazzesi, 2010). Il y a très peu de données relatives à la TEO en **Afrique** à cause de manque de données paléobotaniques sur l'intervalle de temps Éocène-Oligocène. Cependant, la disparition des palmiers africains a été corrélée à la TEO par Pan et al. (2006).

La saisonnalité sur les continents à travers la TEO

La saisonnalité, définie comme les variations saisonnières de la température et des précipitations (Kwiecien et al., 2022), est une notion importante à documenter lors de l'étude de changements climatiques. Des études récentes suggèrent que les changements biotiques attribués à la TEO se seraient produits principalement à cause d'une augmentation du contraste climatique saisonnier exprimé par des hivers plus froids (Page et al., 2019 ; Eldrett et al., 2009). Ces changements de contraste climatique saisonnier se seraient principalement produits à des latitudes moyennes et hautes (Hren et al., 2013 ; Ivany et al., 2000 ; Eldrett et al., 2009 ; Boulila et al., 2021 ; Bauer et al., 2016), comme dans le Fossé Rhénan (cette thèse ; Schuler, 1988).

Simulations numériques des changements paléoclimatiques à travers la TEO

De nombreuses études de simulations numériques ont été produites afin de proposer des explications aux causes et conséquences de la TEO. D'après les simulations numériques de DeConto & Pollard (2003), le moteur de la TEO est une diminution des taux de CO_2 atmosphérique. Cette diminution a conduit à la formation de petites calottes glaciaires sur les hautes terres de l'Antarctique, suivie par des mécanismes de rétroaction une fois qu'un seuil de CO_2 a été dépassé, provoquant la croissance rapide de la calotte glaciaire Antarctique. Plus récemment, les simulations numériques de Tardif et al. (2021) suggèrent que les variations orbitales ont joué un rôle crucial, avec la diminution des taux de CO_2, dans l'événement biotique majeur autour de l'EOT, tel que la "Grande Coupure". Les simulations numériques de Toumoulin et al. (2022) suggèrent que la diminution des taux de CO_2 n'était pas suffisante à elle seule pour expliquer les changements de saisonnalité observés à travers la TEO, mais qu'il s'agissait d'un effet combiné de cette diminution, de la formation de calotte glaciaire Antarctique et de l'augmentation de la continentalité. Ils suggèrent également que les zones de continentalité accrue due à l'abaissement du niveau de la mer sont les zones où la saisonnalité a le plus augmenté, ce qui explique en grande partie l'hétérogénéité des changements de température sur les continents. D'autres chercheurs se sont intéressés aux simulations numériques des changements des courants océaniques. Bien que l'ouverture des passages de l'océan Austral ait longtemps été considérée comme le principal facteur à l'origine de l'apparition de la circulation méridienne de retournement de l'Atlantique (AMOC) et de la glaciation de l'Antarctique (Livermore et al., 2007), des études de simulation numérique utilisant les conditions limites de l'Éocène invalident cette hypothèse. Elles montrent que l'ouverture de ces passages n'a eu qu'un impact modeste sur le transport de chaleur vers le pôle de l'océan, ce qui signifie qu'elle n'est pas directement responsable de l'apparition de la calotte glaciaire Antarctique (Goldner et al., 2014). En outre, une autre étude a montré que même si les passages de l'océan Austral permettaient des connexions en eau profonde, un courant circumpolaire antarctique (ACC) suffisamment fort n'aurait pas pu se développer avant que l'Australie ne se soit suffisamment déplacée vers le nord pour ne plus arrêter le fort flux zonal dans l'océan Austral (Hill et al., 2013). Cependant, l'évolution à long terme de ces passages pourrait expliquer les observations locales de la température benthique, car elle pourrait avoir provoqué un refroidissement de ~3°C des eaux profondes (Sijp et al., 2014). Les changements de circulation océanique sont plus probablement une conséquence de la glaciation qu'une cause, car la présence des EAE semble avoir renforcé les circulations d'eaux profondes de l'océan Austral et leur refroidissement (Goldner et al., 2014). Cependant, une étude récente suggère que les changements bathymétriques au niveau des passages océaniques Atlantique-Arctique pourraient avoir été un des principaux moteurs de la TEO à travers le renforcement de l'AMOC (Straume et al., 2022).

II.3 : Contexte géologique

Rift ouest-européen.

Le système de rift ouest-européen s'étend sur ~1100 km de la mer Méditerranée à la mer du Nord et contient plusieurs rifts intracontinentaux (Ziegler, 1992 ; Bergerat, 1985 ; Illies et al., 1967) (**Figure 3**). La localisation de ces rifts est corrélée à la position des systèmes de fractures hérités de l'orogenèse hercynienne (Edel et al., 2007). La formation du rift ouest-européen s'explique par la réactivation de ces systèmes de fractures sous l'effet des contraintes transpressives nord induites par les collisions continentales des orogènes pyrénéennes et alpines (Dèzes et al., 2004 ; Schumacher, 2002 ; Bergerat, 1987). Les vallées de rift du rift ouest-européen sont le Fossé Rhénan (URG), la vallée de la Roer (= Lower Rhine Graben, LRG), le fossé hessois (HG), le fossé d'Eger (EG) (également connu sous le nom de fossé de l'Ohre), le fossé bressan (BG) et le fossé de la Limagne (LG). Il existe également plusieurs autres grabens et bassins cénozoïques près de la mer Méditerranée liés à l'ECRS.

Fossé Rhénan.

Le Fossé Rhénan est un système de horsts et grabens en relais complexe. Son histoire structurelle a débuté au Paléozoïque, au cours de l'orogénèse Hercynienne (ou Varisque) de laquelle il tire ses principales tendances structurelles. La chaîne Hercynienne fut le résultat de la collision et de l'accrétion entre deux continents ; Laurussia au Nord et Gondwana au Sud (Ziegler, 1990). Les principales structures héritées par le Fossé Rhénan le l'orogénèse Hercynienne sont les zones de dislocations NE-ENE appelées (1) Hunsrück-Taurus (Anderle, 1987), (2) Lalaye-Lubine-Baden-Baden (Wickert & Eisbacher, 1988), et (3) Badenweiler-Lenzkirch (Krohe & Eisbacher, 1988). Ces structures Hercyniennes ont fortement influencé la formation du Fossé Rhénan au cours du Cénozoïque (Schumacher, 2002).

Au cours du Mésozoïque, du Permien supérieur jusqu'au Trias, la formation de larges bassins sédimentaires tel que le Bassin Germanique a été induite par l'initiation du démantèlement de la Pangée. En France, dans la zone où se formera le Fossé Rhénan, les sédiments du Bassin Germanique datent du Permien terminal au Jurassique supérieur et sont, de bas en haut les formations appelées « Buntsandstein », « Muschelkalk », « Keuper », « Lias » et « Dogger ». Des descriptions détaillées de ces formations à travers des données de forages sont proposées par Aichholzer et al. (2016), Duringer et al. (2019), and Aichholzer

(2019). Le « Buntsandstein » (Permien supérieur à Trias inférieur) contient des grès et conglomérats fluviatiles et éoliens issus de l'altération du socle Paléozoïque. Le « Muschelkalk » (Trias moyen) est un épisode marin composé de calcaire, d'alternances marno-calcaire, de dolomie, et de quelques passées anhydritiques. Le « Keuper » (Trias supérieur) est principalement composé d'argile, de marne, de dolomie, et d'anhydrite, avec quelques passées gréseuses. Le « Lias » (Jurassique inférieur) est principalement composé d'argile monotones avec quelques passées calcaires. Le « Dogger » (Jurassique supérieur) contient des argiles, grès, et calcaires. C'est dans cette formation qu'est trouvée la « Grande Oolithe », qui est un dépôt calcaire caractéristique du Bassin Germanique complètement formé d'oolithes. Ces diverses formations, ainsi que le socle Paléozoïque, vont être les principales sources de sédiments lors de la formation et du remplissage du Fossé Rhénan. Le Crétacé est absent de l'archive sédimentaire du Fossé Rhénan, ce qui est expliqué par soulèvement de la zone.

C'est au cours du Cénozoïque, et plus particulièrement au cours du Lutétien, que démarre la formation du Fossé Rhénan. L'évolution tectonique du Fossé Rhénan est principalement liée aux contraintes exercées sur l'avant-pays alpin à la suite des collisions liées aux orogènes alpin et pyrénéen. Avant le rifting à proprement parlé, la subsidence tectonique est initiée au Lutétien entraînant l'altération karstique des calcaires du Jurassique, suivie par l'apparition de petits lacs épars disposés sur les dépressions structurales héritées du socle Paléozoïque. La première phase de subsidence principale ayant probablement débuté au Lutétien supérieur ou Bartonien inférieur est associée à une extension ONO-ESE. La subsidence s'est amplifiée au cours du Priabonien jusqu'au Rupélien inférieur, induisant d'intenses fracturations et le développement de blocs basculés. À ce stade, alors que le bassin du rift s'est affaissé, les épaules du rift se sont soulevées, entraînant le dépôt de cônes alluviaux le long des marges sud, ouest et est de l'URG méridionale (Duringer, 1988), régis par un régime de contraintes d'extension orienté ONO-ESE (Illies, 1977). Les failles maîtresses séparant le bassin des épaules du rift sont devenues évidentes à cette époque (Schumacher, 2002). Une transgression induite par la tectonique et/ou le climat et influencée par le milieu marin (Lavoyer, 2013) a entraîné le dépôt d'une formation marneuse uniforme dans l'ensemble de l'URG, connue sous le nom de "Zone Fossilifère". Cette formation est probablement liée à l'élévation eustatique du niveau de la mer entre les séquences PaRu1 et PaRu2 (Berger, 2005 ; Haq et al., 1998) correspondant à la fin de l'EOGM. La connexion avec le domaine marin a été interrompue jusqu'au Rupélien supérieur. Au cours du Rupélien supérieur, la dépression hessoise au nord et la dépression raurachienne au sud ont relié le Fossé Rhénan au bassin de la mer du Nord et à la partie orientale du bassin de l'avant-pays alpin (Berger, 1996 ; Martini, 1990) en raison de l'augmentation eustatique du niveau de la mer entre les séquences PaRu2 et PaRu3. Le Fossé Rhénan est ainsi devenu un chenal marin dont les dépôts de schiste ("**Série Grise**") présentent une épaisseur et une évolution de faciès uniformes au premier ordre dans l'ensemble du bassin du rift (Roussé, 2006). Vers la limite Rupélien-Chattien, la baisse du niveau de la mer a isolé le Fossé Rhénan des domaines marins, marquant le passage des schistes marins du Rupélien supérieur aux dépôts fluvio-lacustres d'eau saumâtre à douce du Chattien. Pendant le Chattien, le segment médian du Fossé Rhénan a continué à s'affaisser tandis que les segments nord et sud ont été temporairement soulevés, ce qui a entraîné une discordance intra-Chattien (Rothausen et Sonne, 1984). Au cours du Miocène, la subsidence s'est poursuivie dans le nord de l'URG, tandis que le sud du Fossé Rhénan a subi un soulèvement et une érosion qui ont effacé les traces de la subsidence de la fin du Chattien (Villemin et al., 1986) et qui ont probablement été accompagnés par le volcanisme du Kaiserstuhl. À la fin du Miocène, un régime compressif entre en jeu et marque la fin de l'extension du fossé rhénan supérieur. Depuis le Pliocène supérieur, le Fossé Rhénan est affecté par des déformations de trans-tension et des failles de glissement. Le soulèvement quaternaire différentiel des épaules du rift a signé la morphologie moderne du Fossé Rhénan (Lutz & Cleintuar, 1999).

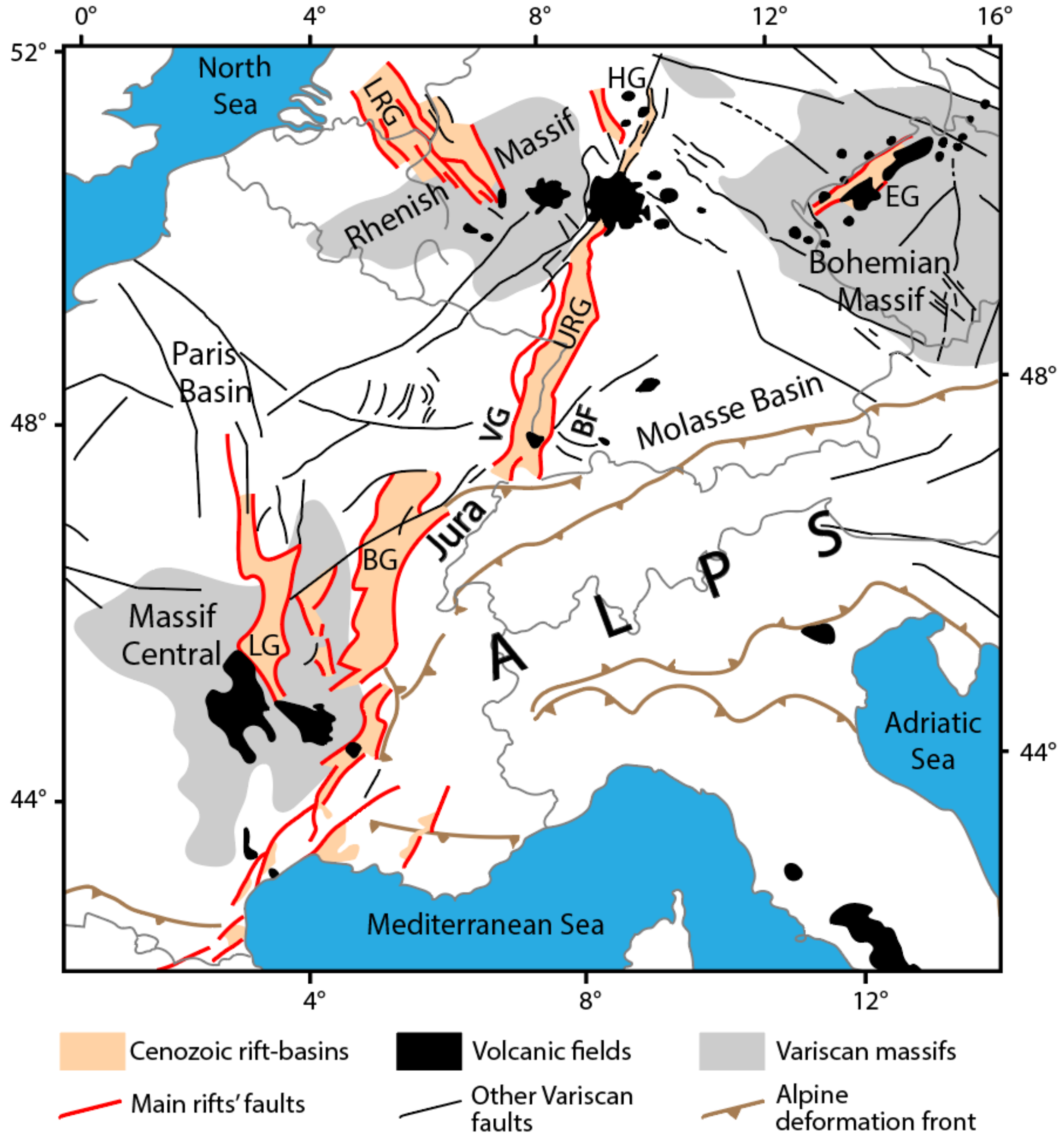

Figure 3: Carte de localisation et structures principales du système de rift ouest-européen. URG = Fossé Rhénan, LRG = Vallée de la Roer, HG = Fossé hessois, EG = Fossé d'Eger (Ohre), BG = Fossé bressan, LG = Fossé de la Limagne, VG = Vosges, BF = Forêt Noire. Modifié d'après Dèzes et al. (2004).

Contexte paléclimatique

L'évolution du paléoclimat régional au cours de l'Eocène et de l'Oligocène dans le Fossé Rhénan est relativement bien connue grâce aux recherches palynologiques de Schuler (1988). Ces études ont été menées dans diverses localités et forages du Fossé Rhénan, ce qui a permis d'obtenir une vue d'ensemble des principales tendances climatiques.

Le Lutétien (« Éocène basal ») est caractérisé par un climat tropical chaud et humide, avec des températures annuelles moyennes estimées de 17 à 20°C et une pluviométrie de 1500 à 2000 mm/an. Le Lutétien supérieur, le Bartonien, et le Priabonien inférieur (« Marnes à Limnées I », « Sel I », « Marnes à Limnées II », « Sel II ») sont caractérisés par un climat chaud et humide subtropical, avec des températures moyennes annuelles estimées de 15 à 20°C et une pluviométrie de 1000 à 1500 mm/an.

Le Priabonien supérieur jusqu'au Rupélien inférieur (base du « Sel III ») est une période marquée par du refroidissement, de l'aridification, et une augmentation du contraste saisonnier indiquée par l'apparition d'une saison sèche très marquée. Dans cette thèse, je corrèle ces changements climatiques à la TEO. À la base du « Sel III », le climat apparaît comme intermédiaire entre subtropical (Température moyenne annuelle : 15-20°C ; Précipitations : 1500-2000 mm/an) et Méditerranéen avec une longue saison sèche marquée (Température moyenne annuelle : 12-15°C ; Précipitations : 1100-1500 mm/an). Le climat de la « Zone Fossilifère » (Rupélien inférieur) est considéré comme étant similaire à celui du « Sel III ».

Le Rupélien inférieur (« Sel IV », « Sel V », « Marnes sans Sel ») est marqué par une majorité de taxons mésothermaux et une augmentation de taxons microthermaux. Le « Sel IV » est caractérisé par un climat Méditerranéen avec une long saison sèche, avec des températures moyennes annuelles de 12 à 15°C et une pluviométrie de 1000 à 1200 mm/an, révélant une période d'aridification marquée. Le climat devient plus froid et humide au cours du « Sel V » et « Marnes sans Sel ». Le Rupélien supérieur (« Série Grise ») est caractérisé par la domination des Pinacées. En comparaison avec le Rupélien inférieur, les températures étaient potentiellement plus basses et les précipitations plus importantes.

Sous-bassins

Bassin de Mulhouse

Le bassin de Mulhouse (aussi appelé bassin Potassique) a été extensivement étudié par Blanc-Valleron (1990) et Maïkovsky (1941). Il se situe au sud du Fossé Rhénan (**Figure 4**). Ce bassin est caractérisé par un important volume d'évaporites éocènes et oligocènes (anhydrite, gypse, halite, sylvite, carnallite) et est le seul dans le Fossé Rhénan où de la potasse a été accumulée. Il se trouve au sud du Fossé Rhénan, Les lithologies des différentes formations du bassin de Mulhouse sont détaillées ci-dessous.

L' « **Éocène basal** » (terme qui inclue les appellations « Sidérolithique », « Zone de Transition », « Formation de Bouxwiller ») est caractérisé par des dépôts carbonatés, détritiques, et karstiques déposés en discordance sur les dépôts jurassiques sous-jacent. Cette formation appartient au Lutétien.

La « **Zone Salifère Inférieure** » est une formation subdivisée en quatre unités appelées « Marnes à Limnées I », « Sel I », « Marnes à Limnées II », et « Sel II ». Elle s'étend du Lutétien supérieur jusqu'à la fin de Bartonien, et potentiellement au début du Priabonien. Les « Marnes à Limnées I » et « Marnes à Limnées » sont des unités caractérisées par des marnes lacustres massives, parsemées d'occasionnels bancs et nodules d'anhydrite. Le « Sel I » et le « Sel II » sont caractérisés par d'épais dépôts de halite dans lesquels des passages anhydritiques et marneux sont présents.

La « **Zone Salifère Moyenne** » est une formation subdivisée en deux unités appelées « Sel III » et « Zone Fossilifère » et s'étend du Priabonien supérieur au Rupélien inférieur. Le « Sel III » est caractérisé par l'apparition de sédiments finement laminés et d'alternances de marne et de halite décamétriques. La « Zone Fossilifère » est une unité trouvée partout dans le Fossé Rhénan avec une très bonne continuité latérale. Elle est caractérisée par des marnes et anhydrites laminées, et les fossiles trouvés à la base de la formation suppose une connexion momentanée avec le domaine marin.

La « **Zone Salifère Supérieure** » est une formation subdivisée en trois unités appelées « Sel IV », « Sel V », et « Marnes sans Sel » appartenant au Rupélien inférieur. Le « Sel IV » est caractérisé par des alternances marne-halite cycliques de plusieurs mètres d'épaisseurs, ainsi que par la présence de deux bancs de potasse dans le centre du bassin. Le « Sel V » est également caractérisé par des alternances marne-halite cycliques. Les « Marnes sans Sel » par des alternances de bancs de marne et d'anhydrite, et par l'absence complète de halite.

La « **Série Grise** » est une formation subdivisée en quatre unités appelées « Marnes à Foraminifères », « Schistes à Poissons », « Couches à Mélettes », et « Marnes à Cyrènes ». Cette formation est marquée à sa base par une riche diversité de foraminifères marquant une transgression marine qui combla la totalité du Fossé Rhénan au cours du Rupélien moyen. Elle consiste principalement de marnes et grès riches en microfossiles et en poissons.

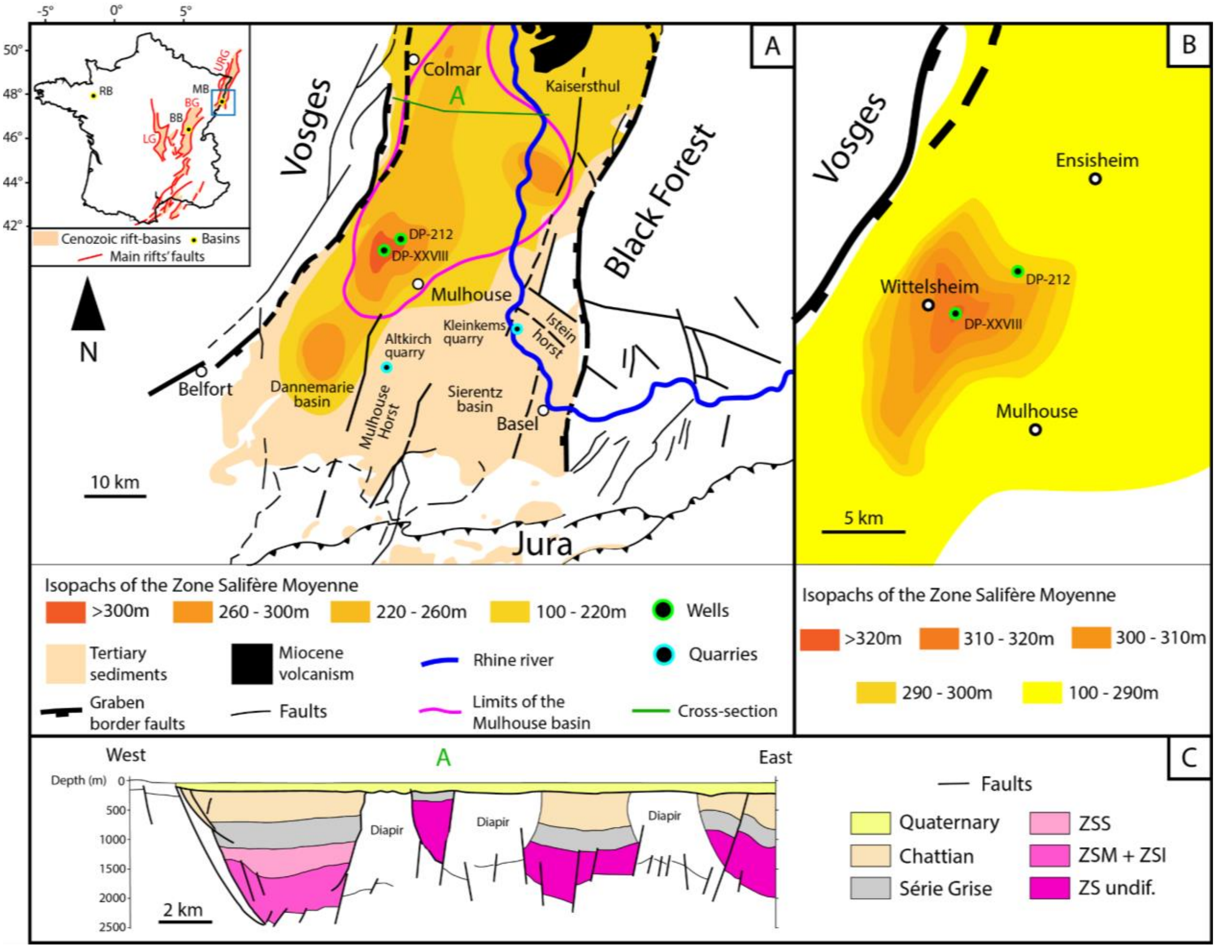

Figure 4*: Carte de localisation et structure géologique du Fossé Rhénan méridional. (**A**) Localisation et détails du Fossé Rhénan méridional, avec les isopaques de la "Zone Salifère Moyenne", d'après Blanc-Valleron (1990), Roussé (2006) et la carte géologique française. (**B**) Isopaques détaillées de la "Zone Salifère Moyenne" dans le bassin de Mulhouse près du puits DP-XXVIII, d'après Blanc-Valleron (1990). (C) Coupe géologique de la partie supérieure du bassin de Mulhouse, d'après Roussé (2006), montrant la structure classique du graben et la présence d'énormes diapirs de sel. URG = Fossé Rhénan, MB = Bassin de Mulhouse, BG = Fossé bressan, BB = Bassin Bourg-en-Bresse, LG = Fossé de la Limagne, RB = Bassin de Rennes, ZSS = Zone Salifère Supérieure, ZSM = Zone Salifère Moyenne, ZSI = Zone Salifère Inférieure, undif. = indifférencié.*

Bassin de Pechelbronn

Le bassin de Pechelbronn est situé au nord de la partie française du Fossé Rhénan. Ce bassin a été fortement exploré à travers des campagnes de forages à des fins d'exploitation de pétrole, notamment dans la localité de Merkwiller-Pechelbronn. Schnaebele (1948) a produit une large monographie sur la géologie du champ pétrolifère, à travers laquelle les lithologies ont été détaillées. Le bassin de Pechelbronn est principalement caractérisé par des dépôts silico-clastiques et par ses gisements d'huile. Un volume non négligeable d'évaporite sont également présentes dans cette région, avec notamment du gypse, de l'anhydrite et de l'halite.

Dans le bassin de Pechelbronn, l' « **Éocène basal** » (Lutétien) est subdivisé en deux unités appelées « Zone de Transition » et « Calcaire à Planorbes ». La « Zone de Transition » est principalement constituées de dépôts continentaux fluvio-lacustres déposés en discordances sur le substratum jurassique, similairement au bassin de Mulhouse. Le « Calcaire à Planorbes », comme son nom l'indique, est une unité calcaire comprenant des fossiles de planorbes.

La « **Zone Dolomitique** » est subdivisée en deux unités appelées « Zone des Marnes à Anhydrite » et « Zone des Marnes Dolomitiques ». La première est principalement composée de marnes dans lesquelles l'anhydrite est abondante et déposée soit en couches, soit en nodules. La seconde est composée de marnes sans (ou avec très peu) d'anhydrite, marquant une transition de tendance d'eau saumâtre à douce. Des variations de facies et lithologies latérales peuvent être observées en s'éloignant du centre du bassin.

La « **Couche Rouge** » est une formation monotone formée de marnes dolomitiques et de marnes argileuses, de couleur rougeâtre, contenant des nodules d'anhydrite de manière occasionnelle. Elle est seulement observée dans la région du bassin de Pechelbronn et a servi de repère lors des campagnes d'exploration pétrolière.

Les « **Couches de Pechelbronn Inférieures** », aussi connues sous le nom de « Zone Bitumineuse Inférieure », sont constituées d'alternances de marnes, de marnes dolomitiques, de grès, et de plus rares dolomies et calcaires. Les marnes y sont décrites comme étant laminées, et c'est dans cette formation que les gisements d'huile furent exploités au cours du 20ème siècle.

Les « **Couches de Pechelbronn Moyennes** » sont l'équivalent de la « Zone Fossilifère ». Cette dernière est subdivisée en trois zones appelées « Zone à Mytilus », « Zone à Bryozoaires », et « Zone à Hydrobies », due à la riche présence de certains fossiles. D'un point de vue lithologique, ces trois zones sont caractérisées par des marnes laminées à tendances parfois gréseuses. D'un point de vue paléo-environnemental, la première contient à sa base de nombreux fossiles marquant un milieu marin momentané (Lavoyer, 2013 ; Schuler, 1988), liée à une transgression (Berger et al., 2005 ; Pirkenseer et al., 2010). En remontant jusqu'à la dernière zone, la tendance devient saumâtre puis d'eau douce.

Les « **Couches de Pechelbronn Supérieures** », contrairement aux deux formations précédentes, affiche de fortes variations de faciès nu nord au sud du bassin, dont la principale différence est la présence ou l'absence de gypse et d'anhydrite. Le faciès nord fût décrit par Schaebele (1948) comme d'eau douce, et le faciès sud comme saumâtre, indiquant des conditions marines et potentiellement marines. D'une manière générale, ce sont des dépôts marneux intercalés de grès et conglomérats.

II.4 : Cycles orbitaux, insolation, et sédimentation

L'orbite de la Terre autour du soleil est affectée par des mouvements cycliques qui modifient la répartition de l'insolation autour du globe au fil du temps. L'insolation désigne la quantité de rayonnement solaire perçue à un endroit donné sur Terre. Cette modification module les contrastes saisonniers qui induisent des changements climatiques et environnementaux à des échelles de temps de 10^1 ka à 10^3 ka (Berger, 1978 ; Milankovitch, 1920, 1941). Certains environnements sédimentaires sont particulièrement sensibles à ces changements et forment des alternances sédimentaires régulières qui sont les archives de ces changements climatiques passés. C'est pourquoi les alternances sédimentaires régulières sont souvent étudiées pour étudier les changements climatiques passés par le biais de la discipline de la cyclostratigraphie. Les trois principaux cycles orbitaux qui induisent ces changements climatiques sont l'excentricité, l'obliquité et la précession (**Figure 5**).

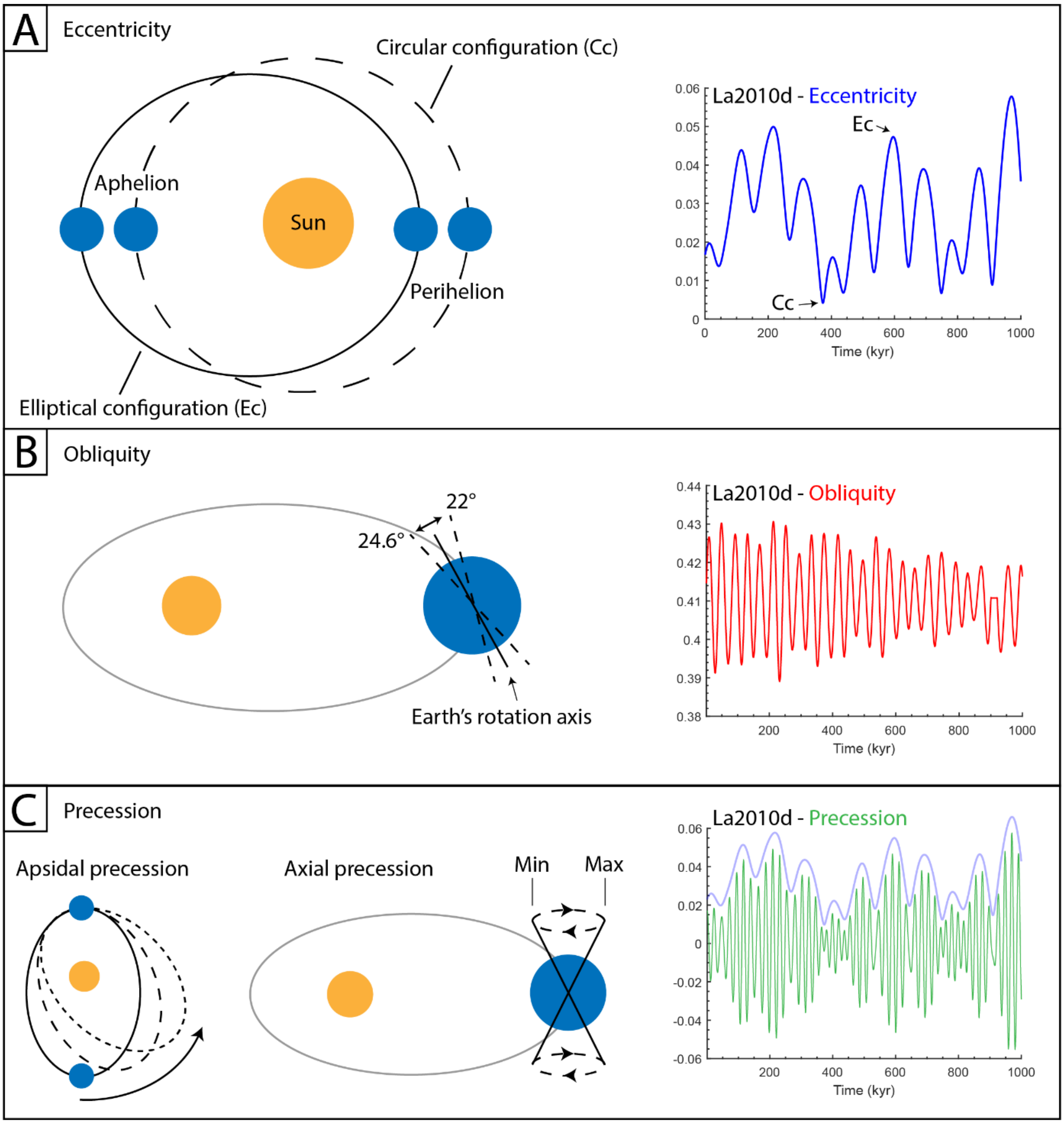

__Figure 5__: Les paramètres orbitaux de la Terre (cycles de Milankovitch). (__A__) Schéma de l'excentricité (gauche) et sa solution La2010d (Laskar et al., 2011) pour le dernier million d'années (droite). (__B__) Schéma de l'obliquité (à gauche) et sa solution La2010d pour le dernier million d'années (à droite). (__C__) Schéma de la précession apsidale (à gauche) et de la précession axiale (au milieu), et sa solution La2010d pour le dernier million d'années. Les valeurs maximales locales de précession représentent les périodes où l'hémisphère sud connaît une saisonnalité accrue. La courbe bleue est la courbe d'excentricité qui montre comment la précession est modulée par l'excentricité. Les solutions La2010d ont été produites à l'aide du logiciel Acycle (v.2.3.1) (Li et al., 2019).

Les changements de la distance Terre-Soleil en raison de la trajectoire elliptique et de l'inclinaison de l'axe terrestre induits par les cycles orbitaux influencent la quantité d'insolation perçue au sommet de l'atmosphère, ce qui se traduit ensuite par des changements climatiques à travers la modification de plusieurs paramètres terrestres (Berger, 1978 ; Schwarzacher, 1993). Ces changements climatiques contrôlent directement ou indirectement la production, le transport et l'accumulation des sédiments et peuvent donc être enregistrés par les environnements sédimentaires sous de bonnes conditions (Strasser et al., 2006). La position des cellules de circulation atmosphérique est influencée par les changements d'insolation, qui peuvent provoquer le déplacement latitudinal des ceintures climatiques (Matthews & Pelmutter, 1994). Ces changements influencent les schémas et la disposition des océans, des lacs, des rivières, des vents, des glaciers et de la végétation, ce qui entraîne des changements dans le dépôt de sédiments. Ils provoquent des variations dans l'apport d'eau douce et de nutriments par les rivières, les processus d'évaporation et la circulation de l'eau dans les lacs et les océans, qui sont des contrôles directs de la production de sédiments organiques et inorganiques, des lithologies et de la chimie de l'eau. Ces changements peuvent être enregistrés par divers indicateurs utilisés par les scientifiques pour reconstituer le passé climatique de la Terre.

Chapitre III : Matériels & Méthodes

Les matériels utilisés au cours de cette thèse sont d’origines diverses. Il y a en premier lieux les données bibliographiques, notamment celles des grands travaux effectués à la fin du 20ème siècle sur le Fossé Rhénan. Ce sont notamment les investigations palynologiques de Schuler (1988), les investigations sur le bassin de Mulhouse de Blanc-Valleron (1990), et les investigations sédimentologiques des conglomérats côtiers de Duringer (1988). Il y a ensuite les données de subsurface. Dans le bassin de Mulhouse, ces données sont des diagraphies issues de différents sondages, et des échantillons de carottes issus des sondages DP-XXVIII et DP-95. Dans le bassin de Pechelbronn, ces données sont des cuttings et données diagraphiques issus des puits GRT-1 et GPK-2 mises à disposition par ES Géothermie. Viennent ensuite les données de surfaces, qui sont les observations effectuées sur divers affleurements et les échantillons de roches qui y ont été prélevés.

Cinq grandes disciplines ont été utilisées au cours de cette thèse, qui sont la sédimentologie, la cyclostratigraphie, la palynologie, le paléomagnétisme, et la géochimie.

La sédimentologie (ou pétrologie sédimentaire) est une discipline de la géologie qui traite de la nature et de l'origine des dépôts sédimentaires (actuels et anciens) et dont l'objectif principal est l'interprétation des processus qui ont abouti à leur formation. Les méthodes utilisées sont la pétrographie, l’interprétation des structures et faciès sédimentaires, et la stratigraphie séquentielle.

La cyclostratigraphie est l'étude des enregistrements stratigraphiques des changements environnementaux cycliques (Fischer et al., 1990). La sédimentation peut être influencée par divers facteurs, notamment les variations climatiques induites par le forçage astronomique. Les deux principales méthodes utilisées sont l’analyse du signal et l’ancrage orbital. La première permet d’identifier le cycle orbital auquel un cycle sédimentaire est associé. Le second permet d’ancrer une suite de cycles sédimentaires associés à des cycle sorbitaux sur l’échelle des temps géologiques à l’aide des solutions orbitales (= mouvements orbitaux calculés à travers le passé) (Laskar et al., 2011).

La palynologie englobe l'étude des microfossiles à parois organiques appelés palynomorphes et constitue une science interdisciplinaire entre les sciences de la terre et les sciences biologiques. Les palynomorphes comprennent notamment les grains de pollen, les spores et les kystes de dinoflagellés. Dans cette thèse, l’identification et le comptage de grains de pollen et kystes de dinoflagellés ont été utilisés afin de déduire des informations sur le climat et les environnements de dépôts.

Le paléomagnétisme est l'étude du champ magnétique terrestre passé conservé dans les roches et les découvertes archéologiques (Kodama, 2012 ; Chree, 1911). Le principe de base du paléomagnétisme est que certains minéraux sont magnétisés parallèlement au champ magnétique terrestre et que cette magnétisation est conservée une fois que le matériau dont ils font partie durcit (par exemple, la roche, la poterie). Dans le cas des sédiments, les minéraux magnétiques sont remaniés à partir de formations rocheuses préexistantes et sont déposés ailleurs. Ils s'alignent alors sur le magnétisme terrestre pendant et/ou peu après leur dépôt. De petites carottes ont été prélevées sur plusieurs affleurements à l'aide d'une perceuse électrique à main, puis ils ont été démagnétisés en laboratoire pour déduire l'orientation du champ magnétique lors de leur dépôt.

La géochimie est la science utilisée pour expliquer les mécanismes qui sous-tendent les systèmes géologiques primaires de la Terre à l'aide des outils et des principes de la chimie. Elle a principalement été utilisée sur les échantillons de cuttings des forages GRT-1 et GPK-2 afin de mesurer les proportions de carbone organique et inorganique, d'azote et de sulfure. Ces données ont ensuite été utilisées pour calculer les ratios C/N (carbone organique sur azote) et C/S (carbone organique sur sulfure) des échantillons. Les valeurs du ratio C/N informent sur l'origine de la matière organique et celles du ratio C/S sur la nature marine, saumâtre, ou d'eau douce de l'eau dans laquelle les sédiments ont été déposés.

Chapitre IV : Investigation des enregistrements sédimentaires accessibles du Fossé Rhénan

Une partie importante de ce travail de thèse a porté sur l'analyse des fragments de carottes géologiques issues du sondage DP-XXVIII du bassin de Mulhouse. Des fragments datant du Jurassique jusqu'à la « Série Grise » ont été étudiés, avec une attention particulière portée sur ceux appartenant à l' « Éocène basal », à la « Zone Salifère Inférieure », et à la « Zone Salifère Moyenne ». Un log sédimentologique détaillé a été produit en utilisant les descriptions effectuées par les géologues lors de l'extraction des carottes au milieu du 20ème siècle, ainsi que par l'apport de mes observations (**Figure 6**). Dans le puits DP-XXVIII, les dépôts de la formation "Eocène basal" consistent principalement en des calcaires argileux rouges fortement bioturbés. Dans la plupart des échantillons, lorsque des laminations sont présentes, leurs limites sont indistinctes en raison d'une forte bioturbation. Quelques échantillons de cette formation sont des conglomérats et des grès, dans lesquels les clastes sont principalement constitués de fragments de calcaire jurassique. Alors que les calcaires argileux suggèrent un dépôt dans un environnement lacustre relativement calme, la présence de grès et de conglomérats implique que certains processus ont permis l'apport de matériaux plus épais loin dans le lac. Les observations effectuées sur les échantillons de la « Zone Salifère Inférieure » ont permis de montrer que les intervalles marneux présentent un faciès massif et homogène, à cassure conchoïdale. Bien que des fragments de halite ont été conservés, leur état n'a pas permis d'interpréter leur faciès, à cause de reprécipitations liée à leur préservation au cours du 20ème siècle. Un changement de faciès important a été observé à la base de la « Zone Salifère Moyenne » où les marnes massives ont laissé place a des marnes finement laminées. Au même moment, des alternations marne-évaporite décamétriques apparaissent dans le log sédimentaire. Ces changements ont été interprétés et ont fait l'objet d'une publication (Chapitre V). Aucun échantillon de la « Zone Salifère Supérieure » n'a été préservés, à l'exception de quelques morceaux de carottes tout au sommet de la formation.

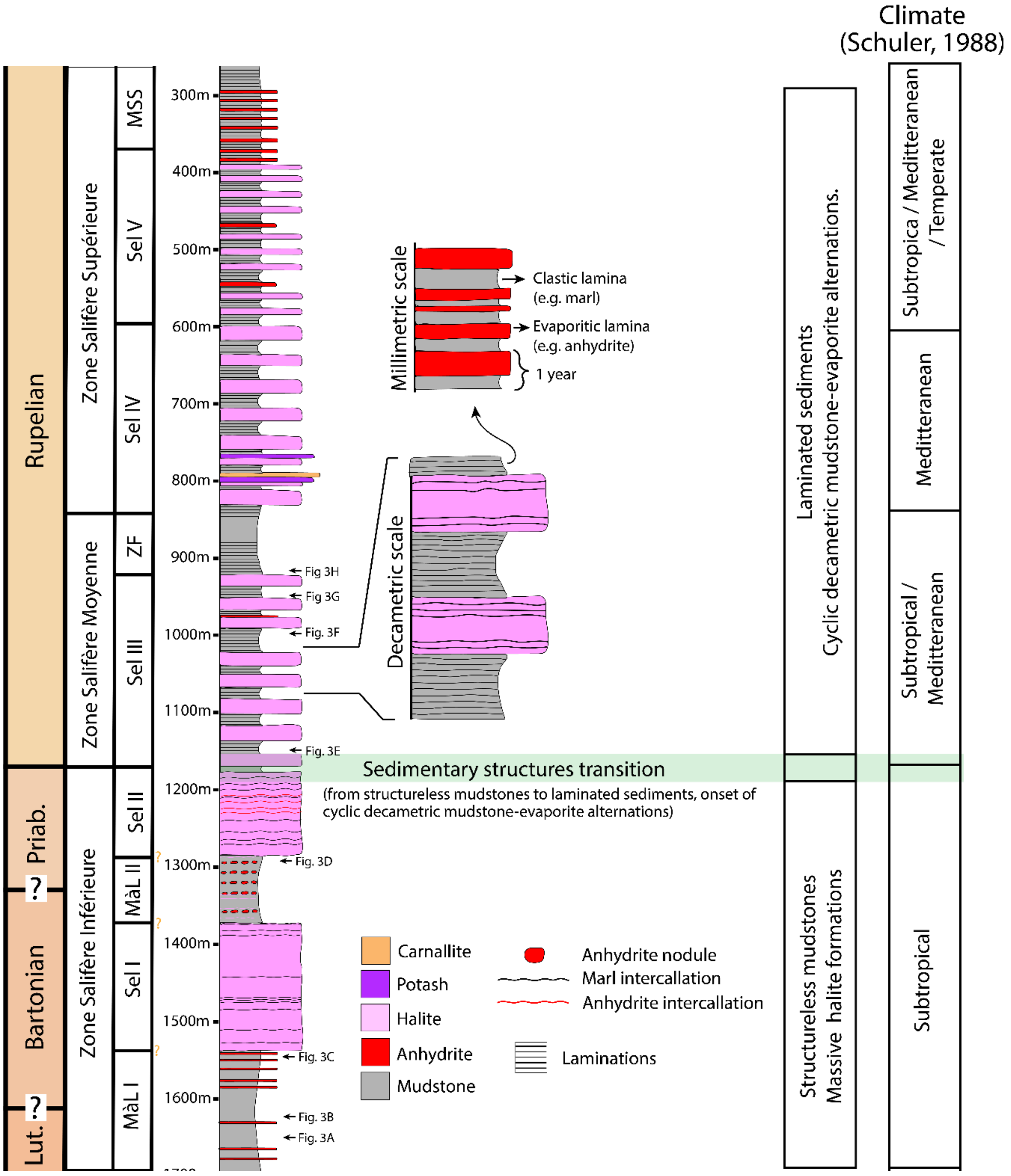

***Figure 6**: Log synthétique de la succession sédimentaire des formations du bassin de Mulhouse à travers un segment du puits DP-XXVIII, avec les observations paléoclimatiques déduites de la palynologie (Schuler, 1988). La chronostratigraphie est basée sur Grimm et al. (2011) et Châteauneuf & Ménillet (2014), et la limite Eocène-Oligocène est placée selon les corrélations présentées dans cette thèse. La taille des alternances mudstone-évaporite du "Sel III" et de la "Zone Salifère Supérieure" est exagérée. MàL I = Marnes à Limnées I, MàL II = Marnes à Limnées II, MSS = Marnes sans Sel. La version détaillée de ce log est disponible en annexe.*

Cependant, des carottes des couches de Potasse ont pu être étudiées au musée des mines de potasses (Kalivie, Wittelsheim) ainsi que via des carottes du sondage DP-95. Une fraction du « Sel IV », sous la couche de Potasse inférieure, a également pu être étudiée via l'étude d'une paroi de galerie de mine (puits Joseph-Else). J'ai pu y observer des bancs de halite composés de cristaux centimétriques, formant des structures en chevrons, intercalés de petits horizons marneux. Ces marnes présentent un faciès finement laminé, montrant alternance de marnes et d'anhydrite. Les filons de potasse du bassin de Mulhouse sont généralement constitués d'une alternance de fines couches de marne, de halite cristalline et de sylvite cristalline. Les couches marneuses sont généralement de couleur gris foncé à gris brillant et forment des lamines millimétriques singulières. L'halite forme généralement des structures en chevron ("chou-fleur") et est constituée de cristaux millimétriques à centimétriques d'épaisseur avec des inclusions fluides. La couleur de ces lits de halite oscille entre le gris brillant et le gris foncé, les lits gris foncé contenant très probablement une partie des taches marneuses interstitielles. Les lits de sylvite sont parfois très semblables aux lits de halite, formant de gros cristaux rouges de croissance de fond. Ce sont potentiellement des cristaux de halite avec de la sylvite interstitielle. La sylvite se présente également sous forme de cristaux millimétriques (cumulas) drapés ou déposés entre les chevrons de halite sous-jacents. La couleur de ces lits de sylvite oscille entre le rouge foncé et le rouge vif, ce qui indique sa pureté. Différents types d'alternances de potasses ont été observées et interprétées.

Les principaux affleurements étudiés au cours de cette thèse sont localisés à Turckheim (Letzenberg), Westhalten (Strangenberg), Tagolsheim, et Altkirch. Des logs stratigraphiques détaillés ont été produits, basés sur l'observation des lithologies et des structures et faciès sédimentaire.

J'ai observé au Letzenberg des alternances de conglomérats, de grès, et de marnes. Les conglomérats sont soutenus par des clastes, et les clastes sont hétérolithiques, arrondis et globalement non triés (sauf à de rares endroits). La rondeur des clastes suggère qu'ils ont parcouru une distance suffisante pour être arrondis soit par l'eau, soit par des impacts répétés. Sur cet affleurement, le faciès des conglomérats est caractéristique de dépôts de fan-delta. Par endroits sont présents des petits ensembles de clastes triés, interprétés par Duringer (1988) comme étant le résultat d'un tri par les vagues, impliquant une dynamique côtière (lacustre). Au premier ordre, j'interprète les alternances de marnes, grès, et conglomérats comme induites par des variations du niveau du lac.

Le Strangenberg est similaire au Letzenberg dans le sens où des alternances de marnes, grès et conglomérats sont observés. La proportion de grès y est cependant plus importante et les conglomérats moins imposants. Des structures sédimentaires telles que des laminations, des rides d'oscillations, des gouttières d'érosions et autres structures érosives y sont présentes. Les caractéristiques de cet affleurement suggèrent un environnement de cône alluvial distal. Une succession sédimentaire caractéristique d'un dépôt de tempête y est observé.

La base de la carrière de Tagolsheim contient des floatstones, boundstones, brèches et marnes. Des fossiles peuvent y être observés, notamment des roseaux fossiles en positions de vie, et des coquilles des familles Lymnaea, Cerithiidae, et Melanoides. La présence de ce type de fossile suggère un environnement d'eau douce peu profonde.

La base de la carrière d'Altkirch présente des alternances de marnes laminées et de d'argiles calcaires laminées. L'étude du microfaciès de ces sédiments finement laminés a été effectué dans le Chapitre V, indiquant la présence de varves (dépôts saisonniers).

<u>Chapitre V</u> : Les rythmites lacustres du bassin de Mulhouse (Fossé Rhénan, France) : un enregistrement d'une augmentation du contraste climatique saisonnier et de la sensibilité du climat aux variations orbitales à travers la transition Éocène-Oligocène ?

La transition Éocène-Oligocène (TEO) marque le passage des conditions « greenhouse » de l'Éocène aux conditions « icehouse » de l'Oligocène. Elle nous permet de mieux comprendre le comportement des systèmes climatiques en cas de variations importantes de la teneur en pCO_2. Si l'impact environnemental de la TEO est plutôt homogène dans les océans, il est beaucoup plus hétérogène sur les continents. Bien que des changements faibles ou nuls soient enregistrés dans certaines régions, plusieurs études sur la TEO dans l'ouest de l'Eurasie suggèrent une augmentation du contraste climatique saisonnier (par exemple, une plus grande amplitude des changements de la température moyenne ou des précipitations), ainsi qu'une plus grande sensibilité du climat aux variations orbitales. Toutefois, ces variations doivent encore être correctement documentées par des changements dans les faciès et les structures sédimentaires, et par l'identification des mécanismes de forçage. Nous étudions ici le dépocentre du bassin de Mulhouse (Fossé Rhénan), qui révèle une transition importante entre les mudstones massives et les sédiments laminés et varvés, ainsi que l'émergence d'alternances mudstone-évaporite soumises à un forçage astronomique. Ces changements sont identifiés dans les parties distales et proximales du Fossé Rhénan méridional, où ils consistent en des couplets mudstone-évaporite d'épaisseur millimétrique et des couplets siliciclastic-carbonates. La composition élémentaire et l'analyse des microfaciès des lamines montrent un schéma de dépôt récurrent compatible avec un processus de dépôt saisonnier, ce qui suggère qu'il s'agit de varves. Nous proposons que le développement de sédiments varvés et de l'enregistrement de la cyclicité orbitale dans le sud du Fossé Rhénan reflètent une augmentation du contraste climatique saisonnier et de la sensibilité du climat aux variations orbitales à travers la TEO. Nous montrons que des changements similaires ont été observés dans les bassins de Rennes et de Bourg-en-Bresse (**Figure 7**), et que d'autres enregistrements Eurasiens témoignent de conditions climatiques similaires. Ce travail souligne le potentiel des structures sédimentaires à haute résolution pour servir de marqueurs des changements climatiques à travers la TEO.

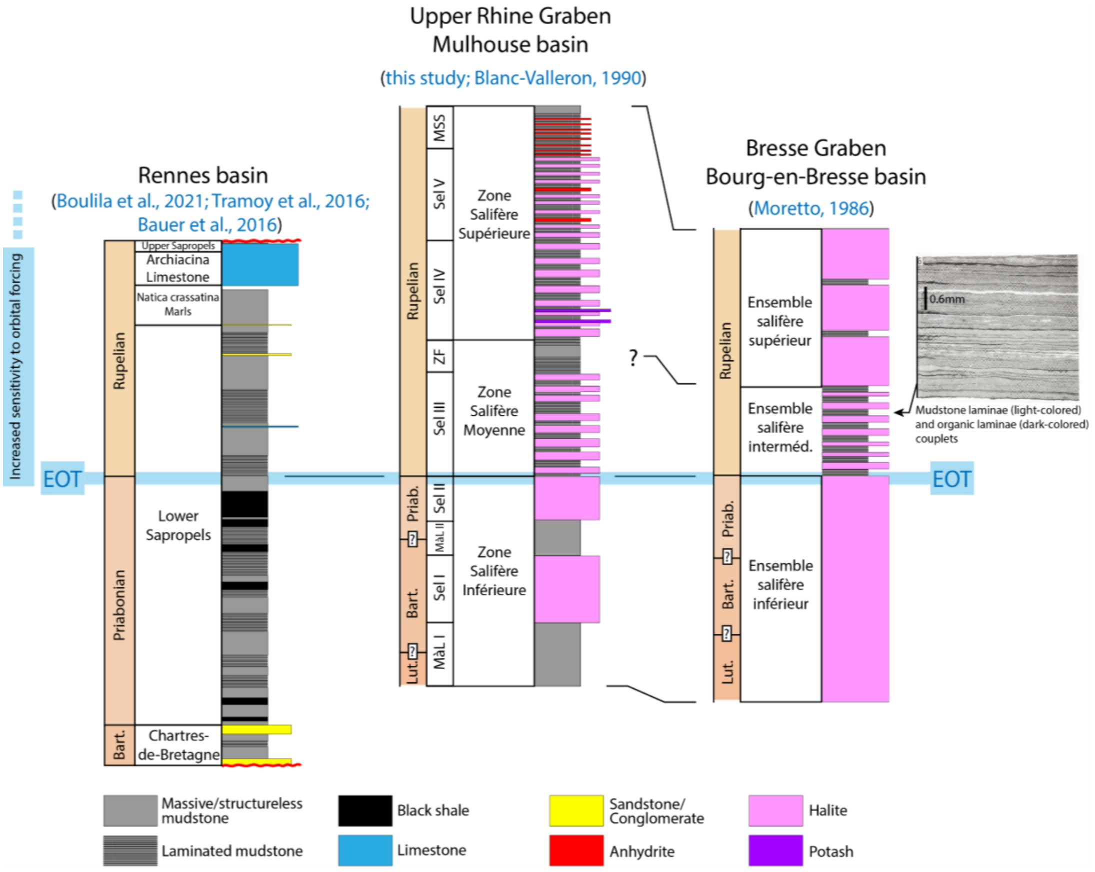

Figure 7: Comparaison et corrélations entre les enregistrements sédimentaires des bassins de Rennes, Mulhouse et Bourg-en-Bresse. Des changements similaires sont observés dans les trois bassins et sont interprétés comme résultants des impacts de la Transition Éocène-Oligocène sur le climat et l'environnement.

Chapitre VI : Cyclostratigraphie du Fossé Rhénan

Dans le bassin de Mulhouse, les investigations cyclostratigraphiques effectuées sur les données de diagraphie des sondages DP-206, DP-211, et DP-212 ont permis de démontrer que les alternances mudstone-évaporite du "Sel III" et de la "Zone Salifère Supérieure" (= "Sel IV", "Sel V", et "Marnes sans Sel") ont été induites par les cycles orbitaux, et les durées minimums de ces différentes formations ont pu être estimées. La durée minimale de l'unité "Sel III" est estimée à 556.8 ka, et la durée minimale de la formation "Zone Salifère Supérieure" à 2272.1 ka. La durée de la "Zone Fossilifère" a été estimée à 1.02 Ma après avoir ancré les modèles d'âge du "Sel III" et de la "Zone Salifère Supérieure" à des âges indépendants (le bas du "Sel III" correspond à l'événement Oi-1 (33,65 Ma), et le haut de la "Zone Salifère Supérieure" à la biozone P20 moyenne (~29,80 Ma) (**Figure 8**). L'ancrage orbital de l'enregistrement étudié à l'aide des filtres de la petite eccentricité suggère que le sommet de la "Zone Salifère Supérieure" est daté de 29,62 Ma, ce qui est cohérent avec son attribution à la biozone P20 moyenne. En utilisant cet âge, la durée de la "Zone Fossilifère" serait plus longue de 180,0 kyr, son sommet étant daté de 31.9 Ma. Il est possible que les bancs évaporitiques se soient déposés pendant les périodes froides et arides et que les bancs de mudstone pendant les périodes chaudes et humides, sous l'effet des changements d'insolation imposés par l'astronomie. D'autres études sont nécessaires pour mieux démontrer (ou réfuter) cette hypothèse et déterminer les mécanismes climatiques sous-jacents.

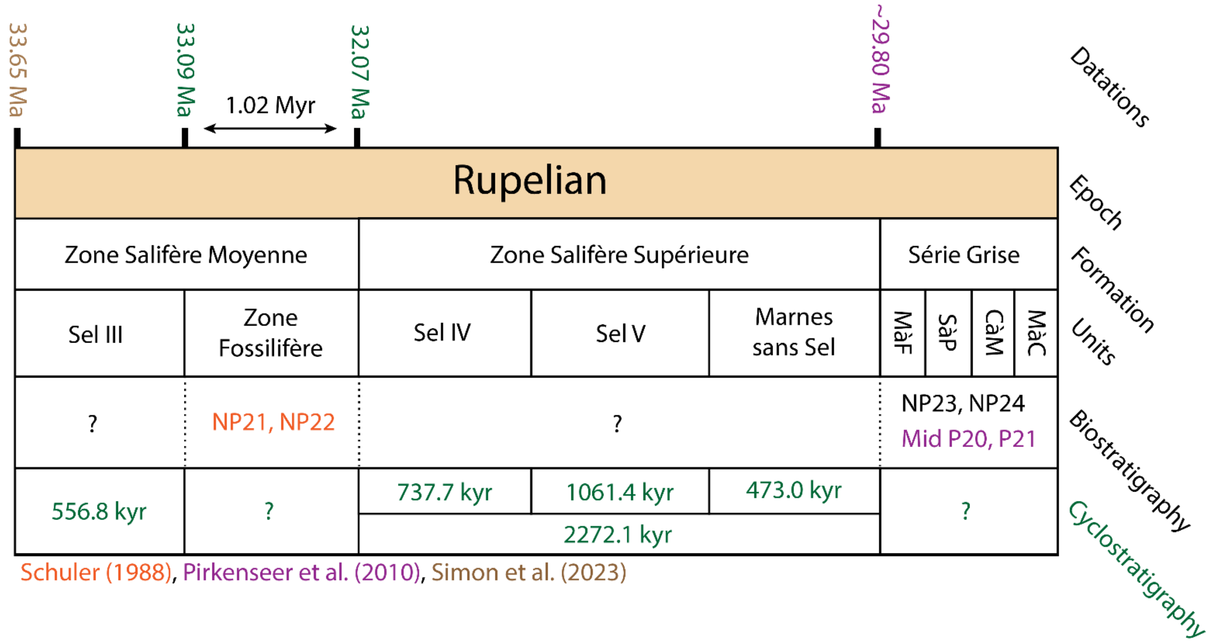

***Figure 8**: Synthèse des données chronologiques, des attributions biostratigraphiques (Schuler, 1988 ; Pirkenseer et al., 2010) et de la durée des intervalles sédimentaires étudiés du bassin de Mulhouse d'après les analyses de cyclostratigraphie effectuées dans cette thèse.*

Les résultats cyclostratigraphiques suggèrent l'empreinte des cycles orbitaux dans le dépôt des alternances mudstone-sandstone/conglomérat du bassin de Pechelbronn dans les "Couches de Pechelbronn". La durée minimale des unités "Couches de Pechelbronn Inférieures" et "Couches de Pechelbronn Supérieures" est de 1440,5 ka, et la durée minimale de l'unité "Couches de Pechelbronn Supérieures" est de 1483,5 ka. Il y a des différences substantielles dans les durées minimales par rapport au bassin de Mulhouse, ce qui implique la présence de hiatus non négligeables. Une discordance est connue au sommet des "

Couches de Pechelbronn Supérieures " (Duringer et al., 2019 ; Aichholzer et al., 2016), et certains lits de grès et de conglomérats pourraient potentiellement être érosifs. En particulier, la "Zone Détritique de Glaswinkel" (lit épais de conglomérat) pourrait être la cause d'un hiatus substantiel entre les "Couches de Pechelbronn Supérieures" et les unités sous-jacentes. En raison de la présence probable de hiatus dans les intervalles étudiés, l'ancrage orbital n'a pas été appliqué dans les forages étudiés. Les lits gréseux/conglomératiques ont peut-être été déposés pendant des périodes arides et les lits de mudstone pendant des périodes humides, sous l'effet des changements d'insolation imposés par l'astronomie. D'autres études sont nécessaires pour mieux démontrer (ou réfuter) cette hypothèse et déterminer les mécanismes climatiques sous-jacents.

Chapitre VII : Changements paléoclimatiques et paléoenvironnementaux dans le bassin de Pechelbronn : aperçu des forages GRT-1 et GPK-2 basé sur la palynologie et la géochimie

Les analyses géochimiques (teneur en carbonate, rapport C/N, rapport C/S) suggèrent que l'environnement était saumâtre à marin sur l'ensemble de l'intervalle étudié ("Zone Dolomitique" à "Série Grise"), et que la matière organique provenait principalement d'un mélange de plantes terrestres et d'algues, à l'exception des échantillons présentant des valeurs élevées de COT, où elle provenait principalement de plantes terrestres.

Les comptages de grains de pollen dans le forage GRT-1 montrent que le spectre pollinique était dominé par les Pinaceae dans les "Couches de Pechelbronn Inférieures" et les "Couches de Pechelbronn Moyennes", et qu'un changement clair s'est produit au bas des "Couches de Pechelbronn Supérieures" où la proportion de Pinaceae a diminué tandis que la proportion de Cupressaceae a augmenté (**Figure 9**). Ce changement est interprété comme étant causé par l'aridification et s'est produit le long du dépôt d'un intervalle conglomératique épais ("Zone Détritique de Glaswinkel"), ce qui suggère que les lits conglomératiques et gréseux sont potentiellement liés à des conditions d’aridité dans le bassin de Pechelbronn.

La présence de kystes de dinoflagellés dans les "Couches de Pechelbronn Inférieures" et les "Couches de Pechelbronn Moyennes" indique des incursions marines, en particulier dans la partie inférieure de cette dernière, qui pourrait être une véritable transgression, en raison de la présence d'espèces acclimatées à la mer sur plusieurs dizaines de mètres. La présence de kystes de dinoflagellés tertiaires dans les "Couches de Pechelbronn Inférieures", même assez près du fond de l'unité (ex. Spiniferites pseudofurcatus dans le forage GRT-1), suggère que la limite Eocène-Oligocène est probablement située en dessous de leur première occurrence, car leur dépôt pendant une période de baisse du niveau marin de 70m semble très improbable, d'autant plus qu'aucun kyste de dinoflagellés tertiaire n'a été trouvé dans des sédiments sous-jacents (Schuler, 1988).

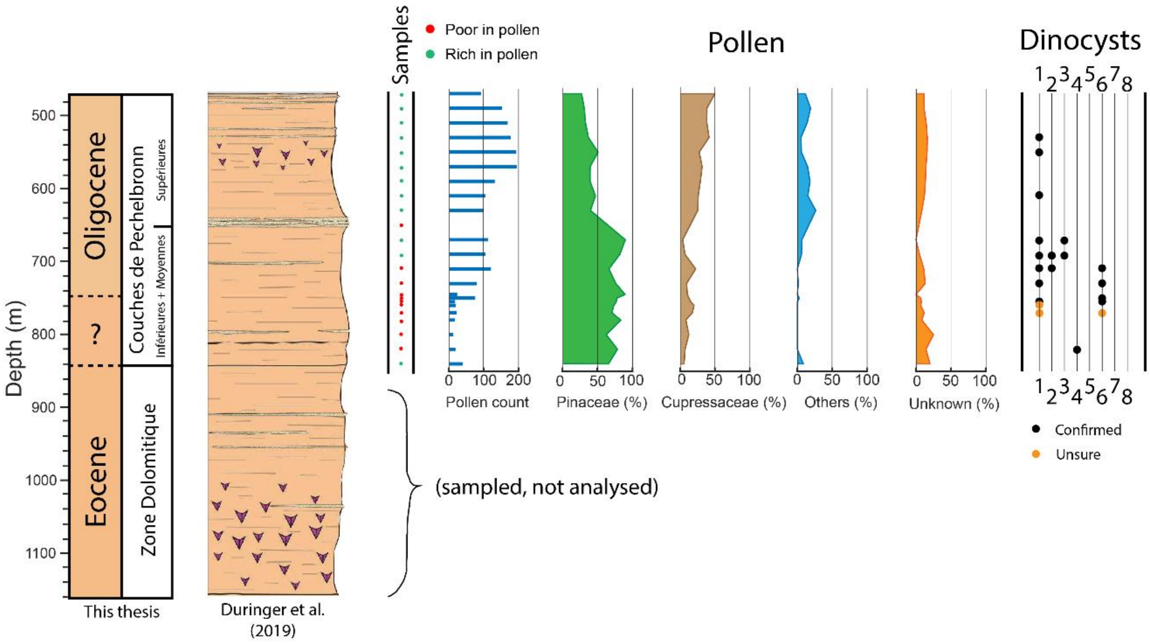

Figure 9: Résultats palynologiques dans le forage GRT-1 tracés le long du log sédimentaire de Duringer et al. (2019). Ils consistent en la numération des pollens, les proportions de Pinaceae et Cupressaceae (aux côtés d'autres familles et de grains indiscernables), et les occurrences de kystes de dinoflagellés spécifiques. Le point d'interrogation entre l'Éocène et l'Oligocène correspond à l'incertitude sur la localisation de la limite Éocène-Oligocène.

Chapitre VIII : Mesures paléomagnétiques

Les mesures paléomagnétiques effectuées sur certains affleurements ont permis de mettre en évidence le fait que certaines lithologies, notamment les marnes, donnent de bons résultats. Dans le cas de la carrière du Strangenberg, les analyses ont montré que les sédiments de l'affleurements avaient sûrement été déposés au cours d'un intervalle magnétique inverse, et comme l'équivalent de la « Zone Fossilifère » est juste en dessous de l'intervalle étudié, il est vraisemblable que ce dernier appartient au chron magnétique C12 daté entre ~33.2 et ~31 Ma. La majorité des échantillons analysés provenant d'autres affleurements ont montré qu'ils ne disposaient pas d'une susceptibilité magnétique suffisante pour en tirer des interprétations à propos de l'orientation du champ magnétique terrestre lors de leur dépôt. Les échantillons prélevés dans une galerie de mine a permis de suggérer que les marnes du bassin de Mulhouse ont une bonne susceptibilité magnétique. Si un nouveau sondage devait être effectué un jour dans ce bassin, je suggère qu'une analyse magnétostratigraphique détaillée y soit effectuée afin de permettre un bon ancrage des formations dans le temps, à l'aide des résultats de cyclostratigraphie.

Conclusions

Les résultats exposés dans cette thèse sont le fruit d'une étude pluridisciplinaire menée sur les enregistrements sédimentaires de l'Éocène et de l'Oligocène du Fossé Rhénan, notamment dans les bassins de Mulhouse et de Pechelbronn, ainsi que sur des affleurements. Les outils et les principes de la sédimentologie, de la cyclostratigraphie, de la palynologie, de la géochimie et du paléomagnétisme ont été utilisés pour élucider l'évolution climatique et environnementale du Fossé Rhénan pendant et à travers le changement climatique de la transition Éocène-Oligocène, ainsi que pour affiner le cadre chronostratigraphique de la région.

Les impacts identifiés de la transition Éocène-Oligocène sur les environnements continentaux du Fossé rhénan supérieur sont les suivants :

- Refroidissement,
- Aridification,
- Augmentation du contraste climatique saisonnier,
- Sensibilité accrue du climat aux variations orbitales.

Cadre sédimentaire et chronostratigraphique

La sédimentation syn-rift a commencé pendant le Lutétien et a conduit au dépôt de mudstones et de conglomérats rouges de l'"Éocène basal" sur le substrat jurassique. Tout au long du processus de rifting, plusieurs sous-bassins se sont différenciés et la nature des remplissages sédimentaires a beaucoup varié du nord au sud, du bassin de Pechelbronn, dominé par les silico-clastiques, au bassin de Mulhouse, dominé par les marnes et les évaporites. Au milieu de ces différences, deux formations connues sous le nom de "Zone Fossilifère" et de "Série Grise" forment des dépôts continus à travers le fossé rhénan supérieur et servent de surfaces de corrélation majeures, signant des périodes de nette élévation du niveau de l'eau. La nature de la "Zone Fossilifère" a suscité un débat au sein de la communauté scientifique. Certains ont interprété l'élévation du niveau de l'eau comme le résultat d'une transgression marine, d'autres comme le résultat d'une transgression lacustre purement isolée. Dans cette thèse, grâce à la synthèse de publications antérieures et de nouvelles recherches palynologiques dans le bassin de Pechelbronn, je propose que la "Zone Fossilifère" ait été influencée par une transgression marine, notamment dans sa partie inférieure, en raison de la présence d'espèces et d'assemblages de dinoflagellés marins spécifiques du Tertiaire. Ceux-ci n'ont pas été trouvés dans les dépôts plus anciens, à l'exception du "Sel III" et des "Couches de Pechelbronn Inférieures" (juste en dessous de la "Zone Fossilifère"), qui sont probablement des précurseurs de la transgression suivante.

Jusqu'à présent, la limite Eocène-Oligocène était placée à la base de la "Zone Fossilifère", mais cette proposition n'avait pas de sens car l'EOT est marquée par une chute du niveau de la mer de ~70 m, ce qui aurait rendu toute transgression marine dans l'URG très improbable. Grâce à la synthèse des publications bio-stratigraphiques, aux comparaisons avec les variations du niveau de la mer et à la production de modèles d'âge déduits de la cyclostratigraphie, je propose que la base de la "Zone Fossilifère" soit très probablement datée à ~33,16 Ma, dans la partie supérieure de la biozone NP21, en corrélation avec l'élévation du niveau de la mer suivant la séquence PaRu1, qui est liée à la fonte partielle de la calotte glaciaire antarctique à la fin de l'EOGM (probablement couplée à une activité tectonique). En outre, je propose que la durée de l'unité "Sel III" soit estimée par cyclostratigraphie à ~556,8 kyr, ce qui suggère que la limite Éocène-Oligocène (33,9 Ma) devrait être située légèrement sous la base du "Sel III" (~33,72 Ma). L'âge estimé pour la base du "Sel III" est presque celui de l'événement Oi-1 (33,65 Ma). Cette attribution d'âge correspond très bien aux changements climatiques et sédimentaires observés à la base du "Sel III".

Impacts de la TEO sur les environnements continentaux du Fossé Rhénan

Dans le bassin de Mulhouse, la base du "Sel III" est marquée par une nette augmentation du contraste climatique saisonnier, par une aridification et par un refroidissement, selon des études palynologiques antérieures (Schuler, 1988), que je corrèle au changement climatique de la transition Éocène-Oligocène sur la base du cadre chronostratigraphique nouvellement proposé. En outre, l'étude du puits DP-XXVIII et les documents miniers originaux montrent que la base du "Sel III" marque la transition entre des mudstones massives vers des varves et sédiments finement laminés, ainsi que l'apparition de cycles sédimentaires induits par les variations orbitales. (Simon et al., 2024) (in press). L'apparition des varves est interprétée comme l'enregistrement sédimentaire d'un contraste climatique saisonnier accrue au cours de l'EOT. L'apparition de cycles sédimentaires induits par les variations (précession, obliquité, courte excentricité) à la base du "Sel III" est cohérente avec une sensibilité accrue du climate aux variations orbitales à travers la TEO (Tardif et al., 2021 ; Westerhold et al., 2020). Ces observations sont comparables à celles effectuées à d'autres endroits, notamment le bassin de Rennes, le bassin de Bourg-en-Bresse, ainsi que dans le nord-est du Tibet.

Palynologie et géochimie

Des espèces de kystes de dinoflagellés tertiaires ont été trouvées dans les "Couches de Pechelbronn Moyennes" (= "Zone Fossilifère") et dans les "Couches de Pechelbronn Inférieures" dans une moindre mesure. Ces espèces sont marines et suggèrent donc l'existence d'une transgression marine et/ou d'incursions marines à cette époque. Le comptage des grains de pollen montre que la famille des Pinaceae est dominante dans les "Couches de Pechelbronn Inférieures" et les "Couches de Pechelbronn Moyennes", et que les "Couches de Pechelbronn Supérieures" sont marquées par une nette augmentation de la famille des Cupressaceae. Ce changement pourrait être lié à une augmentation de l'aridité, comme l'avait déjà suggéré Schuler (1988). Cependant, les profondeurs auxquelles la famille des Pinaceae est dominante sont relativement les mêmes que celles où l'on trouve des espèces de dinoflagellés marins, et des études récentes suggèrent que les types de pollen bissacés (tels que les Pinaceae) sont surreprésentés dans les sédiments marins (Mudie, 1982). Par conséquent, ce changement pourrait résulter en partie d'une modification de l'environnement sédimentaire, mais l'apparition d'un dépôt massif de conglomérat au fond des "Couches de Pechelbronn Supérieures" est cohérente avec une augmentation de l'aridité. De même, la présence de filons de potasse au-dessus de la "Zone Fossilifère" dans le bassin de Mulhouse est un argument supplémentaire en faveur d'une augmentation de l'aridité à cette époque. Ces deux dépôts spécifiques pourraient être synchrones.

L'analyse géochimique de l'ensemble de la succession sédimentaire éocène et oligocène des forages GRT-1 et GPK-2 indique que ces sédiments sont très riches en carbonates et que plusieurs intervalles sont riches en carbone organique total (jusqu'à ~3,8 % dans les "Couches de Pechelbronn Supérieures" les plus basses du forage GRT-1). L'étude des rapports C/S suggère que l'eau était saumâtre ou marine sur l'ensemble de l'intervalle. Je suggère que l'eau est marine là où l'on trouve des kystes de dinoflagellés marins, et saumâtre sinon (et là où l'on trouve Deflandrea phosphorita seul, car il vivait dans des conditions marines restreintes). L'étude des rapports C/N indique que l'origine de la matière organique est principalement liée à un mélange d'algues aquatiques et de plantes terrestres, à l'exception des sédiments avec des valeurs de COT >1% qui sont principalement liés à des plantes terrestres.

Perspectives

Cette thèse fournit la première étude des impacts de la transition Eocène-Oligocène sur les environnements continentaux du Fossé Rhénan (refroidissement, aridification, augmentation du contraste climatique saisonnier, augmentation de la sensibilité du climat aux variations orbitales), qui sera utile à la communauté scientifique pour mieux comprendre comment cet événement a affecté les climats et les environnements dans le monde entier, et comment les changements climatiques globaux en général affectent les environnements continentaux. Ce travail sera également utile aux modélisateurs numériques du climat, car les impacts décrits dans cette thèse peuvent servir de points de référence à atteindre en testant divers paramétrages (par exemple, les niveaux de CO_2, les configurations paléogéographiques). Les changements observés semblent s'être produits relativement rapidement (sur quelques dizaines de mètres dans le bassin de Mulhouse), ce qui suggère l'occurrence d'un point de basculement qui a favorisé les changements climatiques et sédimentaires.

Bien que le cadre chronostratigraphique Éocène et Oligocène du Fossé Rhénan, et en particulier du bassin de Mulhouse, ait été amélioré dans cette thèse, notamment grâce aux investigations cyclostratigraphiques, il pourrait être encore amélioré par l'étude des enregistrements de carottage continus en utilisant conjointement la magnétostratigraphie, la biostratigraphie et la cyclostratigraphie. De nouveaux projets de carottage seront essentiels pour étudier plus en détail l'histoire géologique et climatique du Fossé Rhénan. Un nouveau carottage continu permettrait également l'étude détaillée et continue des intervalles varvés, ce qui permettrait d'étudier les cycles à haute fréquence sur de longues périodes et de documenter l'évolution de la variabilité climatique interannuelle. Un tel projet de carottage devrait être réalisé dans la zone où les isopaques des sédiments de l'Éocène et de l’Oligocène atteignent leur maximum, sans failles et avec des hiatus limités, près du puits DP-XXVIII (partie la plus profonde du bassin à l'époque).

L'étude du bassin de Mulhouse a montré comment les environnements hypersalins peuvent être de riches archives des changements climatiques passés. Je suggère que d'autres environnements de ce type dans d'autres bassins soient étudiés en détail (cyclostratigraphie en particulier), comme le bassin de Bourg-en-Bresse qui contient des alternances mudstone-evaporite similaires à celles du bassin de Mulhouse, ainsi que des sédiments finement laminés (Moretto, 1987).

Comme je me suis principalement concentré sur les bassins de Mulhouse et de Pechelbronn, les autres bassins du Fossé Rhénan doivent encore être étudiés dans le cadre de la TEO, tant du côté français que du côté allemand.

Les enregistrements sédimentaires eurasiens montrent des réponses assez homogènes à travers la TEO, mais les hétérogénéités sont évidentes dans le monde entier. Un nombre conséquent d'enregistrements a été étudié dans l'hémisphère nord, contrairement à l'hémisphère sud, qui devrait faire l'objet d'une plus grande attention afin d'obtenir une vision plus claire des hétérogénéités mondiales. Un effort particulier devrait être fait pour extraire des valeurs numériques de pCO_2, de températures et de précipitations à partir des enregistrements continentaux dans l'ensemble de la TEO.

Chapter I : Introduction

I.1 : Thesis Rationale

The Earth is currently undergoing climate change at rates never seen before in its geological history, almost exclusively because of human-induced greenhouse gases emissions (Foster et al., 2018). Major climate changes have had, have, and will have major consequences on environments (Masson-Delmotte et al., 2018; Zachos et al., 2001). In modern days, observed adverse impacts of climate change on ecosystems include changes in species range, phenology timing, and overall ecosystem structure (Shukla et al., 2019). Observed adverse impacts on human systems include water scarcity, reduced food productivity, degradation of health and well-being, and damage to infrastructures (Shukla et al., 2019).

Broad impacts and mechanisms of climate change are relatively well understood but they are associated with uncertainties. If greenhouse gases emissions continue, adverse impacts will get more frequent and of higher amplitudes (Shukla et al., 2019), but uncertainties remain and prevent models to sufficiently predict the future; for a given pCO^2 increase, will the average temperature increase by 2°C, 6°C, or somewhere in between? How fast will ice sheets melt? Will changes in oceanic currents provoke deep changes in some regions? Not precisely knowing this makes policy-making more complicated, therefore, increasing climate change knowledge is essential. Factors of uncertainty in climate change assessment include natural variability and climate sensitivity.

To better understand climate change, scientists have investigated climate proxies (e.g. temperature, pCO_2) of the past few decades. Others also investigated Earth's past. From the coldness of the Cryogenian period, when grounded ice sheets reached sea-level at all latitudes (Hoffman et al. 2017), to the warmth of the Paleocene-Eocene Thermal Maximum (PETM), when no icesheets were present at the poles and volcanic-induced CO_2 emissions provoked a global temperature increase of 5-8°C (McInerney and Wing, 2011), the Earth underwent many climatic shifts. Studying the sedimentary record of such shifts increases our understanding of the impacts that they had on environments at the time. Even though past warming events seem to be the ideal candidates to study as analogues of modern global warming, cooling events also detain critical keys to our better understanding of climate change processes (Tierney et al., 2020). The Eocene-Oligocene Transition (EOT) signs the switch between the greenhouse state of the early Cenozoic, to the icehouse state of the Oligocene (and onwards), marked by a global temperature cooling of 4-6°C and the glaciation of Antarctica (Lear et al., 2008). Documenting sedimentary records of the EOT is critical to better understand climate change. Pre-EOT records (Paleocene – Eocene) hold information on Earth's climate under high CO_2 and temperature conditions (**Figure 10**), post-EOT records (Oligocene – Holocene) hold information on Earth's climate under lower CO_2 and temperature conditions, considered quasi-modern, and the EOT is the key to understand how we get from one to the other, and especially on how climate systems behave under major pCO_2 shifts. Climate proxies of these periods can help to refine climate models, which in term will produce more accurate predictions.

The Upper Rhine Graben (URG), study area of this project, holds early Cenozoic sedimentary records from the Lutetian to the Chattian, and is thus a perfect area to investigate such climate changes. It also has rich underground resources which include geothermal brines, potash, and hydrocarbons. This area has recently gotten interest again as lithium might be extractable from geothermal brines (Sanjuan et al., 2022), and potentially from potash as well. Such natural resources are important to identify and document, as they could play a role in climate-change mitigation processes and policies.

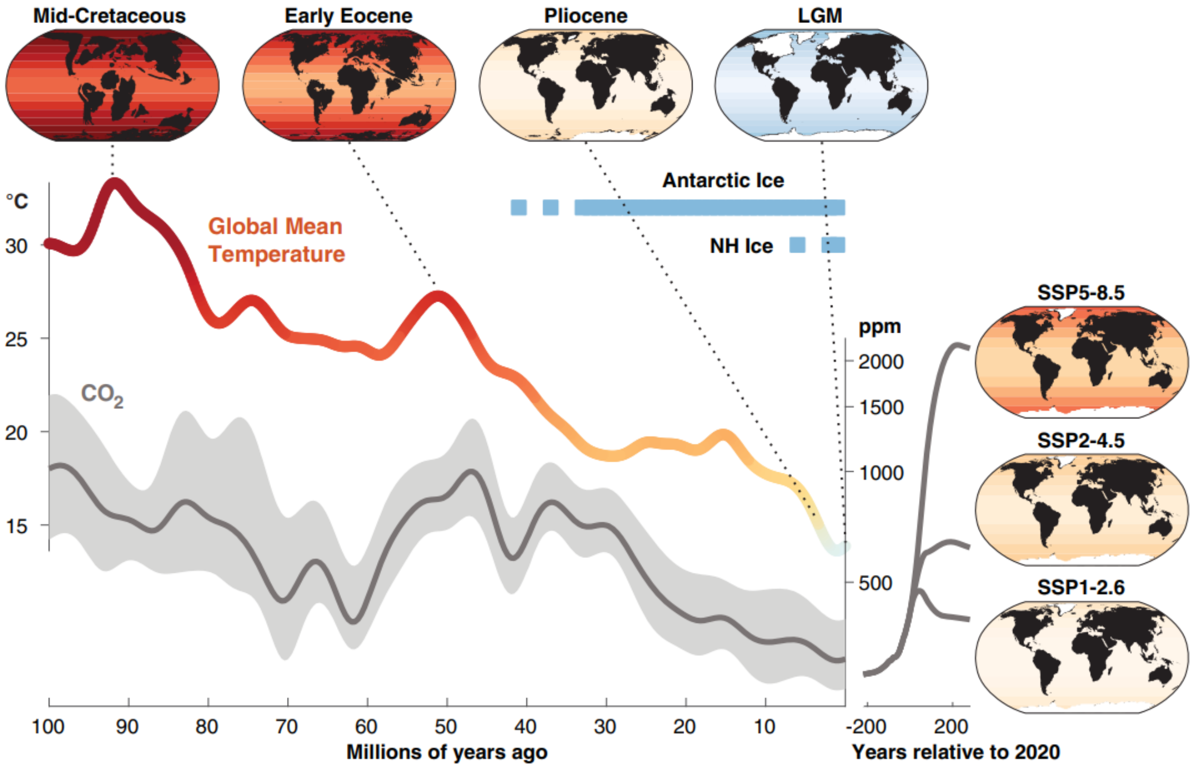

Figure 10: Global mean surface temperatures and CO_2 for the past 100 million years with future climate scenarios, as synthetized by Tierney et al. (2020). The curves were smoothed to highlight long-term trends. LGM = Last Glacial Maximum, NH = Northern Hemisphere. SSP = Shared Socioeconomic Pathways. From Tierney et al. (2020).

I.2 : Objective

Understanding the past is a major step to assess the future of our changing world (Tierney et al., 2020). It is a collective effort driven by scientists from various disciplines, focused on documenting how past environments, ecosystems, and climates were at given places and times, and how they evolved since. **The objective of this PhD is to contribute to this effort by documenting how the continental environments of the Upper Rhine Graben were impacted across the climate shift of the Eocene-Oligocene transition**. To do so, the sedimentary record of the Upper Rhine Graben was investigated through the lens of sedimentology, cyclostratigraphy, geochemistry, palynology, and paleomagnetism, and several sub-objectives were set:

- Synthetizing and improving the Eocene and Oligocene chronostratigraphic framework of the Upper Rhine Graben, notably to locate the Eocene-Oligocene transition in its sedimentary record.

- Documenting the Eocene and Oligocene paleoenvironmental and paleoclimatic evolution of the URG.

- Documenting the impacts that the Eocene-Oligocene transition had on the continental environments of the URG.

While the focus of this thesis is the EOT, which is a ~790 kyr period of accelerated climate change, it is part of a wider framework of long-term climate variations studies of the Cenozoic. Documenting the “before” and “after” of this event is just as important as documenting the “during”. Therefore, this thesis gives a strong emphasis on the whole Eocene and Oligocene epochs, and more specifically from the Lutetian to the late Rupelian, corresponding to the accessible sedimentary records of the Upper Rhine Graben. This work will provide data and information on paleoclimatic and paleoenvironmental change in the URG through the EOT, that can in term be used to better constrain climate models and improve climate predictions.

Chapter II : Scientific and geological contexts

This chapter offers a state-of-the-art synthesis of the scientific and geological context of this thesis. It is divided in four sections which distinctively deal with **II.1 : Modern climate, global warming, and glacial-interglacial cycles**, the definition, causes, and impacts of **II.2 : The Eocene-Oligocene Transition** worldwide, with the **II.3 : Geological Setting** of the European Cenozoic Rift System, and more specifically of the Upper Rhine Graben (URG), and with the theory of orbital cycles and of their impact on climate and sedimentation (**II.4 : Orbital cycles, insolation, and sedimentation**). The review of the literature focused on the EOT and on the URG at the beginning of this PhD resulted in the publication of a synthesis in the French professional journal *Géologues* (Simon et al., 2021).

II.1 : Modern climate, global warming, and glacial-interglacial cycles

II.1.a : Modern climate

Weather characterizes what the conditions of the atmosphere are through short periods of time, predominantly according to temperature, precipitations, and cloud physics. Climate is defined as the long-term weather pattern of a region (Peixoto & Oort, 1992; Schneider & Dickinson, 1974). While “long-term” means ~30 years for modern climatologists, it can sometimes describe several hundred thousand years (if not more) for paleoclimatologists. Climate is currently partially dictated by the arrangement of several characteristics of the Earth. One primary characteristic is the disposition of continents and oceanic gateways that dictate the limits and directions of oceanic currents flows. Ocean currents are continuous and directed movements of sea-water masses generated by several processes (e.g. wind pressure, density flow). They play a major role in the determination of climate in many regions, as they notably influence temperature and precipitation by bringing air with specific temperature and humidity contents to the continents (Clark et al., 2002; Wunsch, 2002; Rahmstorf, 2003). The Thermohaline Circulation (THC), also known as the ocean conveyor belt, is a large-scale oceanic water circulation driven by density gradients determined by freshwater fluxes and surface heat (Wunsch, 2002) (**Figure 11**). The THC forms a worldwide loop of ocean water circulation. Temperature (thermo) and salinity (haline) differences of specific water masses influence their density. Due to dilatation, warm water masses are less dense than cold water masses, provoking upwelling of warm water masses and downwelling of cold ones at specific spots, movement that creates continuous current loops. Similarly, water will get denser the more salt it contains, therefore equatorial waters tend to be saltier due to more evaporation than in higher latitudes. There are tons of parameters influencing oceanic currents, and we can argue that they currently are at an equilibrium on which the modern configuration of oceanic currents depends. Other oceanic currents, such as the Gulf Stream, are primarily driven by surface wind such as the Westerlies, one of the prevailing winds (Seager et al., 2002; Taylor & Stephens, 1998).

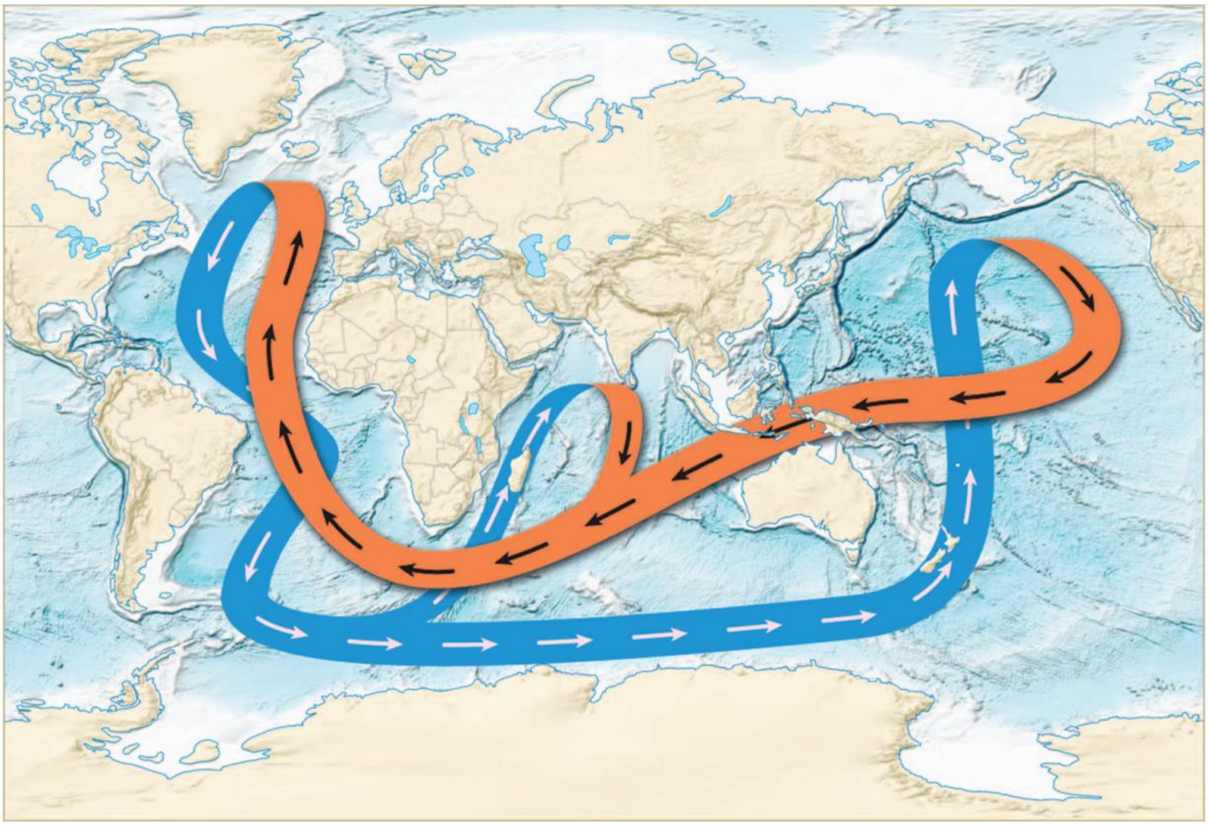

Figure 11: Schematic representation of the thermohaline circulation (or ocean conveyor belt). Arrows indicate the direction of flow. The orange color represents the warm shallow waters (upper part of the conveyor belt), and the blue color represents the cold deep waters (lower part of the ocean conveyor belt). From Lozier (2010).

Prevailing winds designate the major surface wind patterns that blow in particular directions. These patterns are specific to given latitude ranges in both hemispheres that are related to atmospheric cells (Oort, 1983, Budikova, 2009, Kushner et al., 2001). These cells are known as the Hadley, Ferrel, and Polar cells. The Hadley cell occurs between 0 and 30° latitude and is related to the wind patterns known as the Northeasterly Trades (northern hemisphere) and the Southeasterly Trades (southern hemisphere), which surface component blows eastward and towards the Intertropical Convergence Zone (ITCZ). The Ferrel cell occurs between 30 and 60° latitude in both hemispheres and is related to the westerlies, which are wind patterns which surface component blows eastward and towards the poles. The Polar cell occurs between 60 and 90° latitude and is linked to the wind patterns known as the polar easterlies, which surface component blows westwards and towards the ITCZ. In the upper atmosphere, these prevailing winds blow in the opposite directions. The prevailing winds exist due to processes driven by solar insolation. Because of the curvature of Earth, the rays of the Sun directly hit the equator with a 90° angle which result in a great concentration of heat, while much lower heat is delivered to the poles due to the very oblique angles of solar rays there. This is the main reason why the equator is warm and the poles cold. Therefore, the air tends to be denser at the poles and less dense at the equator. The warm equatorial air reaches a certain height before spilling north and south. Then, due to the rotation of the Earth and of the Coriolis force, instead of there being only one major cell exchanging warm and cold air between the equator and the poles, the direction of air is deflected, and several processes induced the existence of the three major cells described (White & Bromley, 1995). While these global trends are true, the real circulations are extremely complex due to the tilt of Earth's axis, the landmass difference between the two hemispheres, the presence of mountains, and the feedback processes with the oceanic currents, among other parameters.

The Gulf Stream, which is the strong oceanic current that transfers warm water from the Gulf of Mexico to the Atlantic Ocean, is an important current that influences climate in western Europe, and more broadly of the whole Northern Hemisphere (Stommel, 2022; Taylor et al., 1998). It specifically carries the warm poleward flow of the North Atlantic subtropical gyre and of the Atlantic Meridional Overturning Circulation (AMOC). While receiving the same amount of solar radiation than other regions of the same latitude, western Europe is milder than its counterparts due to influence of the Gulf Stream, as it continuously brings mild through the movement of warm surface waters (and thus air) through the North Atlantic Ocean (NAO). However, some scientists tend to argue that other processes play major roles in European climate, such as the release of heat accumulated through summers from the shallow surface layer of the North Atlantic (Seager et al., 2006), or that current models lack the knowledge of coupled ocean-atmosphere system processes (Rhines et al., 2008). While more knowledge is needed to better constrain the roles of each process, it is relatively clear that the Gulf Stream has an influence on climate, either major or subordinate (Palter, 2015). In western Europe, the surface air temperatures in winter are up to 10°C higher than the zonal mean at equivalent latitudes. Nowadays, due to anthropogenic-induced climate change, the equilibrium of oceanic currents, and thus of both regional and global climate, is put at risk.

II.1.b : Anthropogenic global warming

While climate changes have occurred over a large range of timescales through geological time, their rates (temperature per time unit) were much lower than those observed currently. Since the industrial revolution in the 18th and 19th centuries, large amounts of greenhouse gases have been injected into the atmosphere, notably through the burning of fossil fuels (**Figure 12**A) and large-scale deforestation (Salam & Noguchi, 2005). Due to the greenhouse effect, the process through which heat is partially absorbed, redirected, and trapped in the atmosphere, the average temperature of the Earth has increased by more than 1°C since the early 1900s (**Figure 12**B). The speed of this warming is unprecedented, even throughout geological time, surpassing any past rate of volcanic-induced emissions of CO_2 such as during the PETM (Mcinerney & Wing, 2011). The impacts of these rapid changes are already being noticed and are expected to get worse if nothing is done (IPCC, 2022). The rise of atmospheric CO_2 concentrations is resulting in increasing ocean acidification, causing huge shifts in seawater carbonate chemistry (Doney et al., 2009). Seawater acidification alters various biogeochemical cycles. It notably lowers calcium carbonate saturation states, known to impact many shell-forming organisms from plankton to corals (Doney et al., 2009; Hoegh-Guldberg et al., 2007), disturbing a huge part of marine ecosystems. Due to the recent warming of the Earth, also observed in the oceans, the equilibrium of ice sheets has broken, causing them to melt at alarming rates (**Figure 12**C), both in the southern and northern poles. Furthermore, because of the melting of ice sheets and the warming-induced dilatation of seawater, the average sea-level is rising (**Figure 12**D) (Alley et al., 2005; Lombard et al., 2005). Various threats emerge from these rapid changes. Extreme natural hazards such as storms, wildfires, and floods are getting more severe and frequent (Van Aalst, 2006). Environmental changes will induce water and food scarcity in several regions (Mancosu et al., 2015). Human health is at risk due to changes in weather and climate patterns that lead to waterborne diseases through increased flooding. Other diseases carried by species such as mosquitoes and ticks are expanding to new areas as they migrate. These fast changes also threaten the existence of species adapted to specific environments and conditions.

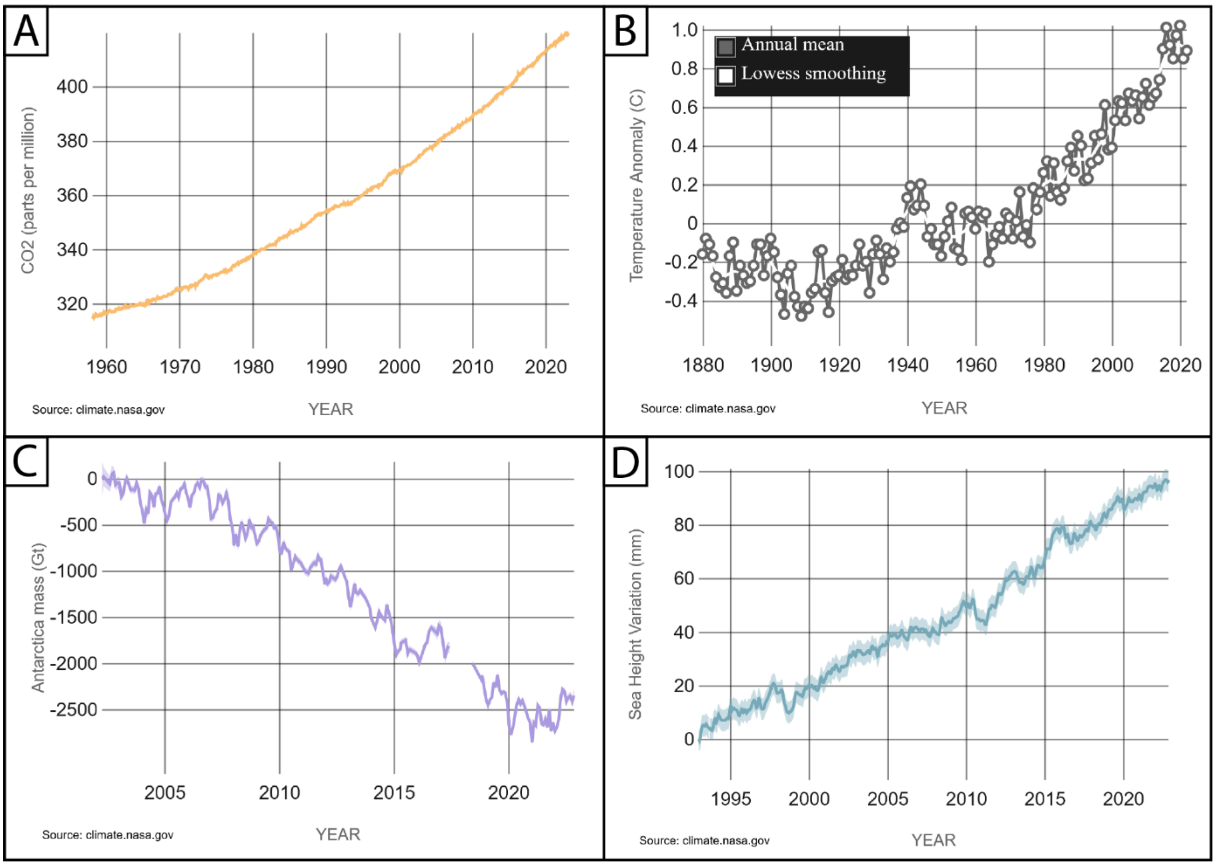

***Figure 12**: Climatic data of the recent past from the National Aeronautics and Space Administration (NASA) and National Oceanic and Atmospheric Administration (NOAA). (A) Atmospheric CO_2 content in parts per million since 1960 (NOAA). (B) Temperature anomaly compared to the pre-industrial temperature since 1880 (NASA). (C) Change in the mass of Antarctica's ice sheets since 2002 according to the data retrieved from the GRACE satellite missions. (D) Sea-level variation since 1993 from NASA's satellite sea-level observations.*

II.1.c : Glacial-interglacial cycles

Throughout Earth's history, and notably across the Quaternary (2.6 Myr), climate changes have been driven by natural processes, especially through the repartition of insolation on Earth due to orbital cycles that induced the glacial-interglacial cycles (**II.4 : Orbital cycles, insolation, and sedimentation**) (Berger, 1988; Berger, 2001; Archer et al., 2020). The glacial-interglacial cycles refer to the observed changes in pCO_2, temperature, aridity, and ice extent through the past few million years. High-resolution data of pCO_2 and temperature is available throughout the past 800 kyr (Lüthi et al., 2008) (**Figure 13**).

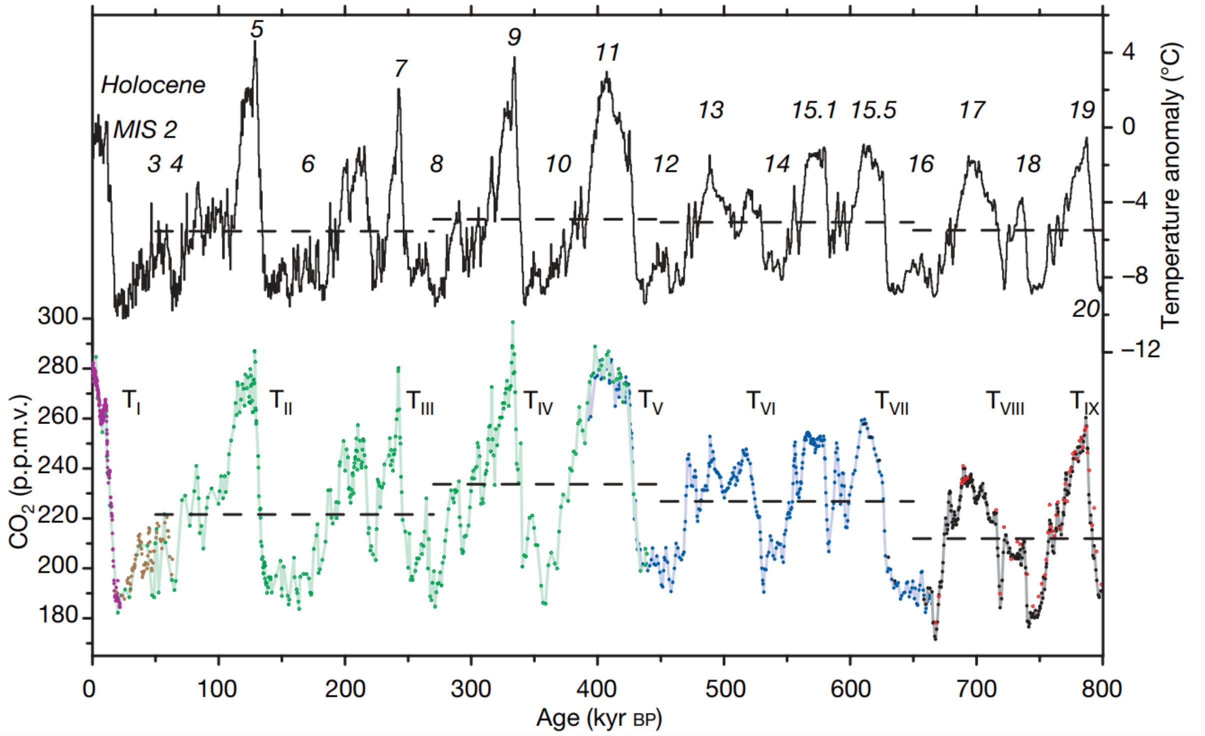

Figure 13*: Evolution of CO_2 levels and temperature anomaly throughout the past 800 kyr as reconstructed from ice cores. These ice cores are from Dome C (purple, blue and black solid circles, and red open circles), Taylor Dome (brown), and Vostok (green). Horizontal lines represent average values for given intervals. The highest historical CO_2 level of the past 800 kyr at least was outmatched in 1950. In modern days, it is almost two times the historical average. From Lüthi et al. (2008).*

Glacial periods are colder and drier than interglacial ones. The investigation of ice cores from Antarctica allowed the study of climate proxies through the past and have shown that changes in the concentration of greenhouse gases correlate well with the variations of Antarctica's temperature through the record. For the past 1.2 Myr, the data shows that glacial-interglacial cycles occurred every 100 kyr, while they seem to have occurred every ~41 kyr from 1.2 Myr to 5.4 Myr (Lisiecki & Raymo, 2005). These observations are confirmed by the spectral analysis of the $\delta^{18}O$ data (**Figure 14**) (see **III.2.b.ii : Signal Analysis**). These findings are very interesting because the cycle that has the most impact on insolation is precession, however the precession cycle (23 kyr) barely appears in the spectral analysis of the data. This is still the subject of active research which specifically focuses on non-linear processes and feedback mechanisms that could have provoked these glacial-interglacial cycles. The insolation variations caused by orbital cycles are too low to explain the observed paleoenvironmental and paleoclimatic changes (Budyko, 1969; Sellers, 1969). These changes are better explained by positive feedbacks responses of mechanisms such as albedo, carbon sinks, atmospheric and oceanic circulations to these insolation variations (Strasser et al., 2006).

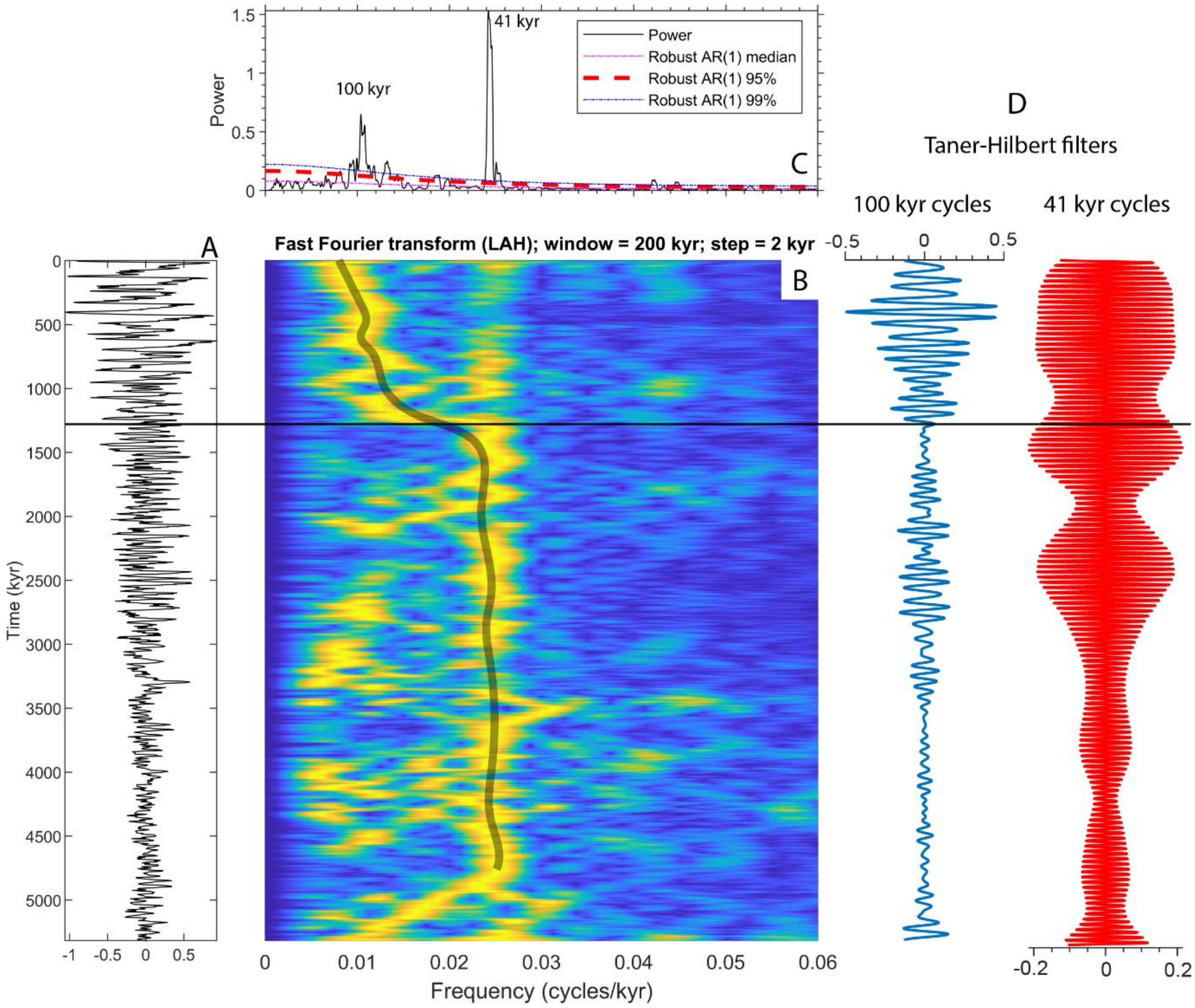

Figure 14: *Spectral analysis of the δ^{18}O stack from Lisieki & Raymo (2005) through the past 5.3 Myr. (A) Detrended (LOESS) δ^{18}O series. (B) Evolutive Fast Fourier Transform of the detrended data. The grey transparent curve shows the main frequencies that emerge from the analysis (100 kyr cycles from 0 to ~1.24 Myr and 41 kyr cycles from ~1.24 Myr to 5.3 Myr). (C) 2π multitaper analysis of the detrended series. (D) Taner-Hilbert filters of the 100 kyr cycle (0.009 cycles/kyr – 0.015 cycles/kyr) and of the 41 kyr cycle (0.023 cycles/kyr – 0.026 cycles/kyr). The black line shows the age at which the glacial-interglacial cycles switched from 100 kyr cycles to 41 kyr cycles (~1.24 Myr).*

The keys to our understanding of the complex interactions between orbital cycles and feedback mechanisms may lie in the deeper past, especially through the Eocene-Oligocene Transition (EOT), which marks the transition between greenhouse and icehouse conditions.

II.1.d : Summary

- Earth's climate system is primarily driven by complex interactions between the repartition of insolation, atmospheric and oceanic circulations, and feedback mechanisms (e.g. albedo, CO_2 sinks), to which our knowledge is currently still limited.

- Global warming currently puts the equilibrium of the climate system at risk through changes in temperature, ice volumes, and sea-level, among other parameters. These changes have impacts on society, biodiversity and ecosystems.

- The past holds keys to our understanding of the impacts of climate changes. The Eocene-Oligocene Transition is especially important to document as it marks the transition from greenhouse to icehouse conditions, with particular implications regarding CO_2 and icesheets.

II.2 : The Eocene-Oligocene Transition (EOT)

The EOT is one of Earth’s major periods of global climate perturbation that marked the transition from Greenhouse to Icehouse conditions. With the topic of this research being the expression of the EOT in the URG, the purpose of this chapter is to provide an updated review of the EOT, including its definition, causes, and consequences around the globe. It is one of the most important climatic events of the Cenozoic among the climatic and thermal maximums (PETM, EECO, MECO, MMCO) and long-term warming and cooling trends (**Figure 15**). These events and trends are marked by increases or decreases of benthic foraminiferal $\delta^{18}O$ which have served as the principal proxy of global and regional climate change since the early 1970s. $\delta^{18}O$ is a proxy of both sea-water temperature and continental ice-volume (Hays et al., 1976; Epstein et al., 1953). When $\delta^{18}O$ values increase, they mark sea-water cooling, or continental glaciation, or both. A recent synthesis of the EOT was published by Hutchinson et al. (2020).

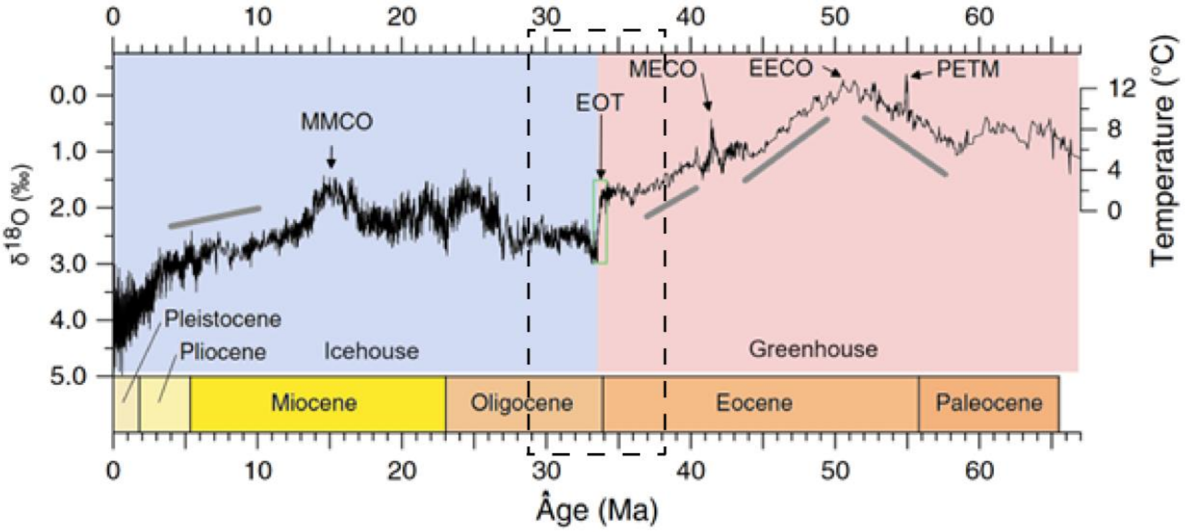

__Figure 15__: Climate’s evolution during the Cenozoic, based on benthic foraminiferal $\delta^{18}O$ data (Zachos et al. 2001). The data is placed on the geologic time scale of Berggren et al. (1995), and the boundaries between different epochs on that of Gradstein et al. (2004). The temperature scale (Zachos et al., 2001) is valid for the greenhouse period and represents benthic temperature changes. For the icehouse period, the $\delta^{18}O$ data represents the change in benthic temperatures and in ice volumes at the poles, as a convoluted signal. Modified from Mudelsee et al., *(2014). PETM: Paleocene-Eocene Thermal Maximum; EECO: Early Eocene Climatic Optimum; MECO: Middle Eocene Climatic Optimum; EOT: Eocene-Oligocene Transition; MMCO: Middle Miocene Climatic Optimum. The solid grey lines represent long-term climate change trends.*

II.2.a : Definition of the EOT

The EOT refers to the transient interval from the Eocene Epoch to the Oligocene Epoch, known as a phase of rapid and important climatic and biotic reorganization of the Earth. This shift happened over a span of ~790 kyr, starting before, and ending after the Eocene-Oligocene Boundary (EOB), dated at 33.9 Ma according to the 2012 Geological Time Scale (Gradstein et al., 2012). This boundary has been stratigraphically defined as the *Hantkeninidae* planktonic foraminiferal family extinction sedimentary horizon in Italy, at the Global Stratotype Section and Point (GSSP) in the Massignano outcrop (Nocchi et al. 1986; Premoli Silva & Jenkins, 1993). The study of various sedimentary, paleontological, and geochemical data-sets support the hypothesis that this relatively short period marked the evolution of Earth's climate from high-CO_2 Cenozoic "greenhouse" conditions (ice-free Earth) to modern-like "icehouse" conditions with the rapid growth of ice-sheets in the Antarctic, event associated with a major and global average cooling of the global temperature of ~4-6°C and eustatic sea-level drop of ~70m (Ao et al. 2020; Colwyn & Hren 2019; Dupont-Nivet et al. 2007; Katz et al. 2008; Ladant et al. 2014; Lear et al. 2008). The Eocene-Oligocene climate transition is defined by benthic foraminiferal $\delta^{18}O$ records from deep-sea sites (Coxall et al., 2005; Zachos et al., 2001), which show a 1.5 ‰ increase on average due to combined terrestrial ice growth and deep-sea cooling (**Figure 16**).

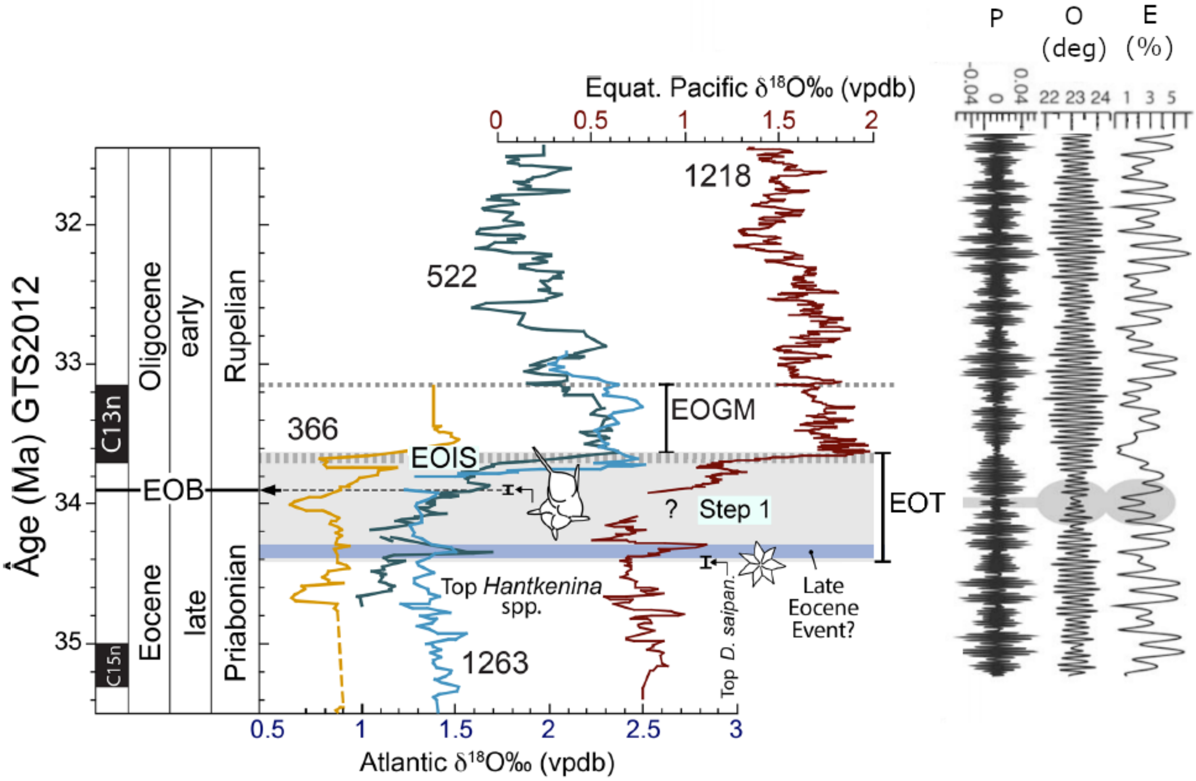

Figure 16: Expression of the EOT through variations of the $\delta^{18}O$ *of foraminifera in oceanic cores, showing the main steps as well as the orbital parameters (P: precession, O: obliquity, E: eccentricity). The "Step 1" is preceded by a short period during which the configuration orbital cycles induced low insolation values in the Southern Hemisphere, causing colder summers. Modified after Hutchinson et al. (2020) and Coxall & Pearson (2007).*

The EOT is defined as a composite event comprising three main stages, respectively named "Late Eocene Event", "Step 1" and "Earliest Oligocene oxygen Isotope Step" (EOIS). Its onset corresponds to the extinction of the foraminiferal species *Discoaster saipanensis* and its end corresponds to the termination of the EOIS. The EOT approximatively lasted from 34.44 Ma to 33.65 Ma. The terminology used, based on a recent synthesis (Hutchinson et al., 2020), is as follows:

- **Late Eocene Event**: It is a short, cold transient event intervening in the upper Priabonian. It corresponds to a $\delta^{18}O$ peak observed in some records, the initiation of which is correlated with the extinction of the foraminiferal species *Discoaster saipanensis* dated at ~34.44 Ma at Site 1218 (equatorial Pacific). This event is sometimes interpreted as an aborted first Antarctic glaciation and may be associated with a significant change in North Atlantic currents (Coxall et al., 2018).

- **Step 1**: It corresponds to the first $\delta^{18}O$ excursion observed shortly before the Eocene-Oligocene boundary in some records. It starts at ~34.15 Ma for a duration of ~40,000 years. The recent consensus suggests that this excursion is predominantly related to deep water and low latitude cooling of ~2°C, while the increase in ice volume at the pole is minor (Bohaty et al., 2012; Peck et al., 2010; Pusz et al., 2011; Lear et al., 2010, 2008, 2004). The Step 1 is also known as the “EOT-1” event (Katz et al., 2008).

- **EOIS**: It is a short second period of rapid $\delta^{18}O$ increase posterior to the Eocene-Oligocene boundary and taken within the lower part of the C13n magnetic episode. The duration of this excursion is ~40,000 yr and the $\delta^{18}O$ maximum is reached at ~33.65 Ma. The appearance of the Antarctic Ice Sheet (**AIS**) at this time appears to be the primary factor controlling the $\delta^{18}O$ excursion, likely coupled with further cooling (Kennedy et al., 2015). The EOIS is also known as the “Oi1” event (Miller et al., 1991) and as the “Oi-1a” event (Zachos et al., 1996).

The termination of the EOT is directly followed by the “**Early Oligocene Glacial Maximum**” (EOGM). This is a ~490,000-year period during which the extent of the newly emerged ice sheet reaches its maximum and temperatures continue to fall. Its extent was possibly equivalent to that of the modern AIS (Lear et al., 2008). Following the EOGM, the $\delta^{18}O$ decreases again and marks partial melting of the newly formed AIS and/or relative deep-sea warming.

II.2.b : Causes of the EOT

The two main causes evoked to explain the EOT are the evolution of **greenhouse gases** and **tectonics**, with a drastic drop in atmospheric CO_2 on one hand, and a change in oceanic gateways and currents on the other (Kennedy et al., 2015; Pearson et al., 2009; Livermore et al, 2007). In addition, variations of insolation perceived by the Earth explained by a particular configuration of orbital parameters, could have allowed ice to persist during the summer in some nucleation points and rapidly spread to the whole Antarctic continent (DeConto & Pollard, 2003; Ladant et al., 2014). The main cause of the Antarctic glaciation has long been explained by the establishment of the Antarctic Circumpolar Current (ACC) because of changes in ocean currents induced by tectonic movements with the deepening of the Drake Passage south of Chile and the opening of the Tasmanian Seaway south of Australia at a time near the EOT (Livermore et al., 2007; Kennedy et al., 2015, Abelson & Erez, 2017). The establishment of such currents would have thermally isolated Antarctica by blocking warm water inflow from the equator (Kenneth, 1977). However, this hypothesis is still debated to this day: the Drake Passage may not have been deep enough at the time of the EOT to allow for significant deep-water circulation. Recent investigations suggest that changes in the Atlantic-Arctic gateways controlled ocean circulation and were a major factor in the growth of continental icesheets alongside CO_2 drawdown (Straume et al., 2022). Specifically, pulsations of the Iceland mantle plume would have modified the bathymetry of the Greenland-Scotland Ridge (GSR), which played a major role in the modification of deep water currents in the North Atlantic. The simulation of Straume et al. (2022) shows that the uplift of the GSR strengthened the AMOC which cooled the southern hemisphere and contributed to the formation of the AIS through the EOT (**Figure 17**). Later, the deepening of the GSR along a shallow seaway to the Arctic Ocean put a stop to the AMOC and caused the cooling of the Northern Hemisphere.

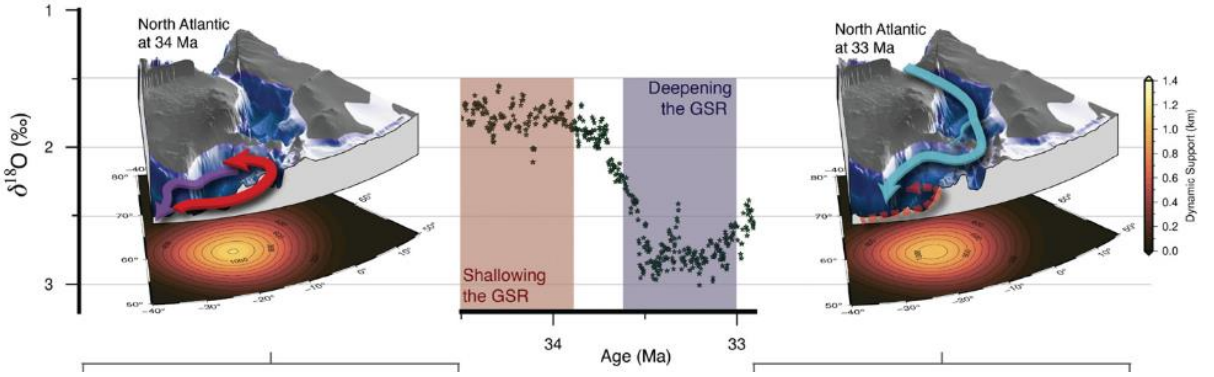

***Figure 17**: Comparison between the $\delta^{18}O$ of benthic foraminifera and the paleogeographic configuration of the Greenland-Scotland Ridge at 34 Ma (left) and 33 Ma (right) along the support of the Iceland plume. From Straume et al. (2022).*

Numerical modelling suggests that the fall in atmospheric CO_2 had a major impact during the EOT (DeConto & Pollard., 2003; Ladant et al., 2014). Atmospheric CO_2 shifted from ~1,100 ppm in the Late Priabonian to ~600 ppm in the Early Rupelian (Pearson et al., 2009). The Antarctic glaciation would have started after a critical value of CO_2 estimated at ~750 ppm was exceeded, which is however still debated (Pearson et al., 2009). According to Ladant et al. (2014), this threshold would rather be around 900 ppm, higher than previously suggested, and according to their modelization, the CO_2 drawdown caused major sea-surface and deep-sea temperatures (**Figure 18**). Through the greenhouse effect, the partial pressure of atmospheric CO_2 has affected temperature since ancient times (Berner & Kothavala, 2001). The proposed causes for the reduction in atmospheric CO_2 around the EOT remain highly debated. They include long-term causes such as increased chemical weathering of silicates (i.e. CO_2 sinks) possibly related to the Himalayan orogeny (Raymo & Ruddiman, 1992; Ruddiman et al., 1997), an increase in the rate of organic carbon burial (i.e. CO_2 sinks) (Diester Haass & Zachos, 2003), and a sharp reduction in volcanic and hydrothermal degassing (i.e. CO_2 sources) in relation to a decrease in the rate of ocean expansion (Berner, 1990). However, numerical models (e.g. DeConto & Pollard, 2003; Ladant et al., 2014) indicate that the fast decrease in atmospheric CO_2 would have occurred in a time interval restricted to the EOT. While the influence of bathymetric changes to the Atlantic-Arctic oceanic gateways suggested by Straume et al. (2022) could be a strong contender, it did not start the CO_2 drawdown, which true cause is still mystery. The modification of oceanic currents might have modified precipitation rates on continents, enhancing CO_2 drawdown through the weathering of silicates, and could have transported nutrient-rich waters to the surface, also enhancing CO_2 drawdown through increased biological productivity (Straume et al., 2022).

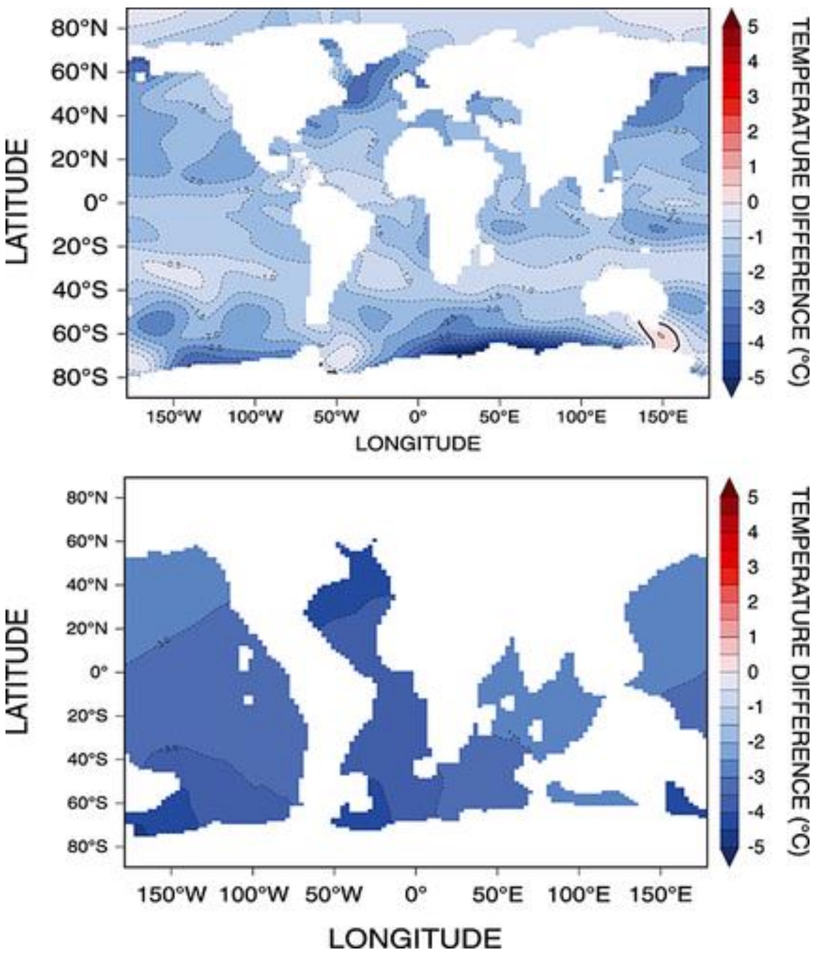

***Figure 18**: Changes in sea surface (top) and deep-sea (bottom) temperature across the EOT due to pCO$_2$ drawdown according to the modelization of Ladant et al. (2014), showing global cooling.*

II.2.c : Consequences of the EOT

The main consequences associated with the EOT are (but are not limited to) (i) a sharp drop in global mean temperature, (ii) the appearance of the AIS and an associated ~70 m drop in absolute eustatic level (Pekar et al., 2002), (iii) major faunal and floristic changes, and (iv) a deepening of the carbonate compensation depth in the oceans related with a change in water chemistry. While the impacts of the EOT are rather homogenous in the marine realm, they are much more heterogenous in the continental realm.

II.2.c.i : Marine realm

In the oceans, temperature falls were observed through the EOT for both the sea-surface and the deep-sea. The planktonic foraminifera Mg/Ca paleothermometer shows drops in sea-surface temperatures of 2.5°C in Tanzania (Lear et al., 2008) and 3-4°C in the Gulf of Mexico (Wade et al., 2012). Other studies using Mg/Ca and other paleothermometers (e.g. $U_{37}^{K'}$, TEX_{86}, Δ_{47}, $\delta^{18}O$) at various paleolatitudes show drop in sea-surface temperatures between 0 and 8°C (Hutchinson et al., 2020; Bohaty et al., 2012; Cramwinckel et al., 2018; Inglis et al., 2015; Kobashi et al., 2004; Lear et al., 2008; Liu et al., 2009, 2018; Pearson et al., 2007., Petersen and Schrag, 2015; Piga, 2020; Sliwinska et al., 2019; Wade et al., 2012; Zhang et al., 2013) (**Figure 19**). In the case of the deep-sea benthic foraminifera $\delta^{18}O$ increase (Coxall et al., 2005; Zachos et al., 2001) suggest cooling and terrestrial glaciation. Mg/Ca investigations suggest deep-sea cooling of 2-3 °C in the Southern Ocean (Bohaty et al., 2012).

In the marine realm, cooling due to the EOT seems relatively homogeneous, especially in the deep-sea.

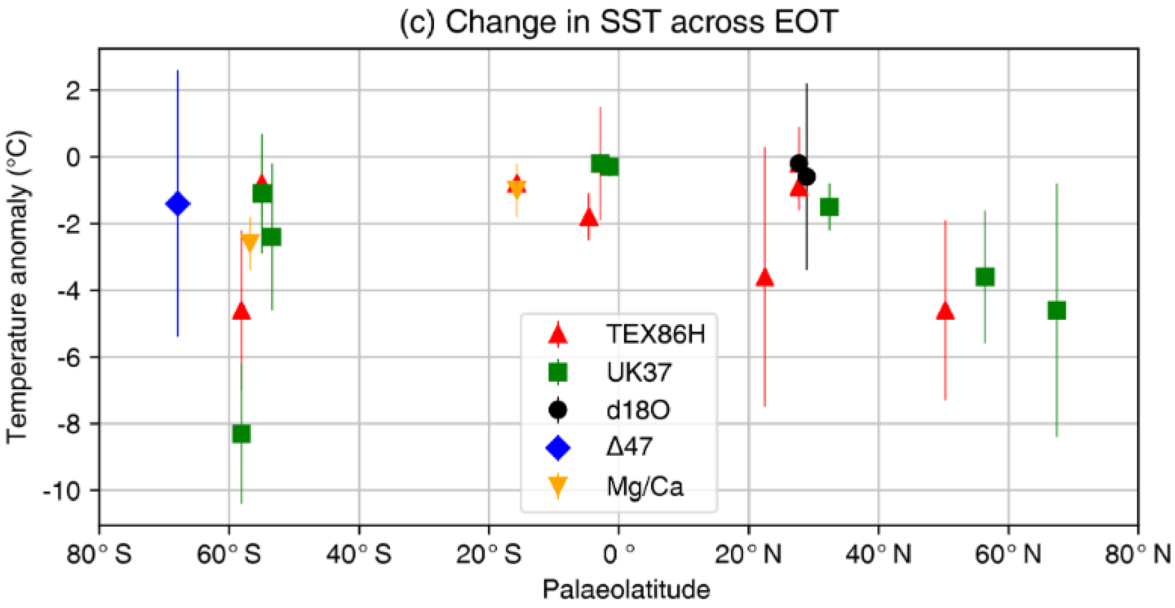

Figure 19: Summary of Sea Surface Temperature (SST) change across the EOT at various sites according to several proxies (from Hutchinson et al., 2020). While there is some heterogeneity (more than in the deep-sea), SST change is approximately -2.5°C through the EOT on average. Cooling seems to be stronger in high northern and southern latitudes while low at the equator.

The study of the EOT-induced sea-level variations is an important part for its global understanding, and it is particularly important in the case of the Upper Rhine Graben (URG), as this rift system was influenced by multiple marine transgression during the Oligocene (Berger et al., 2005a, 2005b). With a major event such as the glaciation of Antarctica, it is assumed that a non-negligeable sea-level fall happened. The modern estimates of this sea-level fall across the EOT are of approximatively 70m (Miller et al., 1991, 2008; Wilson et al., 2013), which are consistent with shelf paleo-environments investigations (Houben et al., 2012) and with the covariance between tropical and benthic planktonic records of $\delta^{18}O$ (Miller et al., 1991). However, this sea-level fall does not appear ubiquitous everywhere; in the Mississippi estuarine records in the USA, a sea-level highstand is correlated to the stratigraphy of the EOB, and the paleo water-depths are believed to be increasing across the whole transition (Echols et al., 2003). In the Hampshire Basin in the UK, the maximum sea-level fall is estimated at 15m only across the transition (Gale et al., 2006). This used to beg the question of the actual extent of the E-O sea-level fall, or if it happened at all (Haye et al., 2005), but considering the advances made since, it is more likely that these contradictory signals were masked by widespread tectonic activity.

The Carbonate Compensation Depth (CCD) refers to the ocean depth at which the supply of carbonate produced in surface waters is balanced by dissolution (which thus greatly affects the benthic foraminifers which sink beneath it). The main parameters that constrain the CCD are ocean fertility, acidity and pCO_2, making it a notion tightly linked to the global climate and its variations. Across the Eocene and Oligocene Epochs, the paleodepth reconstructions on which the distribution of carbonate sediments across the oceans basins were deposited unfold a major and global deepening of the CCD as more carbonated content is found in the Oligocene series compared to the Eocene series (Thunell et Corliss, 1986; Hsü et al., 1984; Van Andel, 1975). The CCD deepened by up to 1200m in the eastern equatorial Pacific (Rea et Lyle, 2005). This major CCD deepening resulted in an effective doubling of sea-floor area where $CaCO_3$ deposition was possible (Rea et Lyle, 2005). Close to the EOB, the sedimentary records of the equatorial Pacific ODP Site 1218 show a very fast increase in $CaCO_3$ mass accumulation rate (MAR) and content (Coxall et al., 2005) (**Figure 20**), and that it happened synchronously with the stepwise increases of the benthic $\delta^{18}O$ (onset of the major Antarctic glaciation) and $\delta^{13}C$ records.

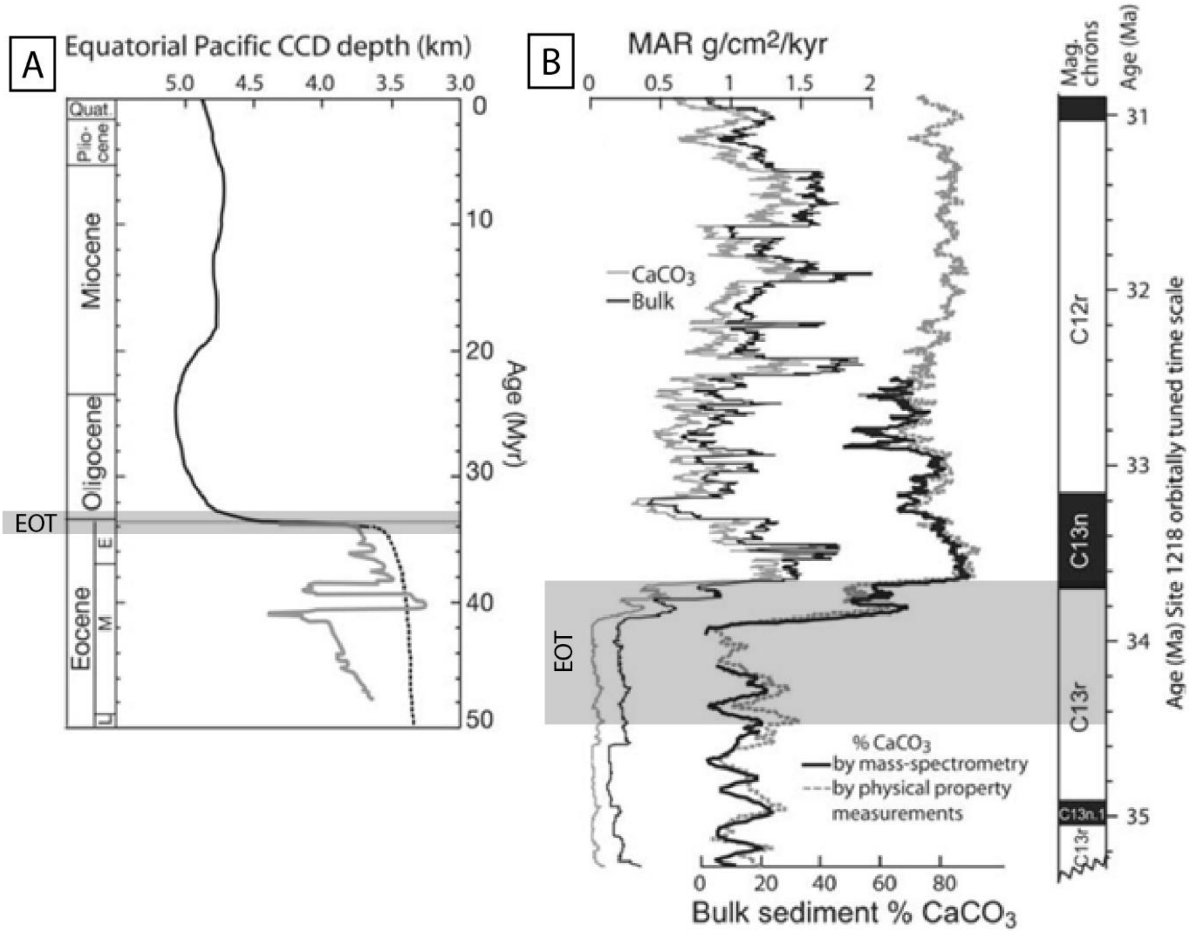

***Figure 20**: Eocene-Oligocene deep-sea records of the equatorial Pacific showing changes in the Calcite Compensation Depth (CCD). (A) Record of the CCD from 50 Ma to present according to carbonate Mass Accumulation Rate (MAR) (Tripati et al., 2005). (B) $CaCO_3$ and %$CaCO_3$ MAR through the EOT from ODP Leg 199 sediments (Coxall et al., 2005). Modified after Coxall and Pearson (2007).*

II.2.c.ii : Continental realm

In contrast to the relative homogeneity of marine records (**Figure 19**), continental sedimentary records show more heterogeneous climate responses during the EOT (**Figure 21**, **Figure 22**) demonstrating the greater climate variability on continents (Hutchinson et al., 2020; Pound & Salzmann, 2017; Toumoulin et al., 2021). In general, climates have become colder and more arid, but there are exceptions. The persistence of some fauna suggests that some regions were less affected than others (e.g. Zanazzi et al., 2007).

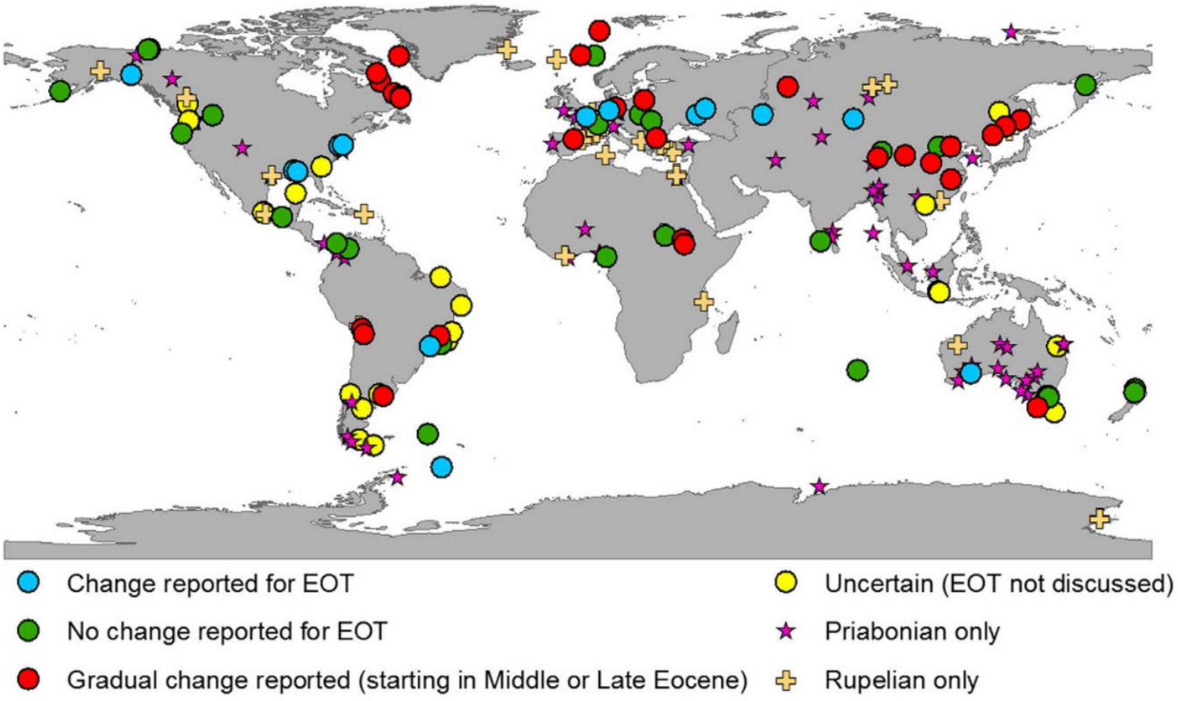

Figure 21: The selected continental palynological sites from the study of Pound and Salzmann (2017). This figure shows the great heterogeneity of climate changes on the continents, with records showing change (blue circles, N = 14), no change (green circles, N = 27), gradual change (red circles, N = 29), and uncertain change (yellow circle, N = 24) through the EOT.

Europe: In the Paris (France) and Hampshire (United Kingdom) basins, Stehlin's (1910) observations of the "Grande Coupure", expressed by the disappearance and replacement of endemic European mammals by Asian species better adapted to a colder climate, suggest aggravated cooling. More recently, in the Hampshire Basin, Hooker et al. (2004) confirmed Stehlin's observations of the "Grande Coupure" and demonstrate that it coincides with the first Oligocene oxygen isotope excursion (the EOIS). In the same basin, geochemical analysis of freshwater gastropod *Viviparus lentus* shells allowed the reconstruction of paleo-temperatures, revealing a 10°C cooling of surface water temperature in the growing season, corresponding to a 4-6°C cooling of the mean annual air temperature during the EOT (Hren et al., 2013). In the Rennes Basin, the warm, humid climate of the upper Eocene deteriorated until the lower Oligocene when conditions got colder and more arid (Tramoy et al., 2016). In the same basin, the completion of a high-definition age model based on cyclostratigraphy and magnetostratigraphy has confirmed these observations and correlated sedimentary facies changes with the “Step 1” (EOT-1) and “EOIS” (Oi-1) (Boulila et al., 2021).

In the **URG** (France), palynology studies revealed long-term cooling from the Lutetian to the uppermost lower Rupelian, with a **phase of rapid cooling, drying,** and **increased seasonality** in the “Sel III” unit (Schuler, 1988) inside which the EOB is most likely positioned (Grimm et al., 2011) (see **I.4.b.iii**). Other investigations related to the EOT in the Cenozoic basins of France are detailed in **II.3 : Geological Setting**.

Antarctica: Plant diversity has progressively declined since the middle Eocene from evergreen forests to low-lying vegetation (Pound & Salzmann, 2017; Francis et al., 2008). In the eastern part of the continent, the lower Eocene consisted of a warm climate that favored the growth of highly diverse subtropical forests, characterized by mesothermic and megathermic taxa, including palms and Bombacoideae (Pross et al., 2012). The climate there degraded from the middle Eocene to the early Oligocene, indicating cooling that induced the development of cool temperate forests (Strother et al., 2017; Pross et al., 2012).

Asia: Continental aridification and monsoon amplification determined from sedimentary records, initially interpreted as resulting from the uplift of the Tibetan Plateau, have since been correlated to the EOT, thanks to the establishment of a precise chronostratigraphy in the Xining Basin (Dupont-Nivet et al., 2007). In Mongolia and northwest China, Sun et al. (2014) report a large faunal change synchronous with the "Grande Coupure". In southwestern Mongolia, the occurrence of eolian dust through the late Eocene has been interpreted as resulting from increased aridity through the EOT.

Australia: The transition from warm to temperate tropical forests is observed and indicates change in mean annual temperatures from 14-20°C in the upper Eocene to 10-14°C in the lower Oligocene (Korasidis et al., 2019). Other floristic studies appear to show a loss of diversity rather than a major change (Macphail, 2007; Martin, 2006). Recent investigations support the proposition of temperature cooling in southeastern Australia based on vegetation changes (Sluiter et al., 2022). The mean annual temperature would have dropped from 16°C to 13°C, before warming again through the Oligocene.

North America: In the Rocky Mountain region, from the middle Eocene to the end of the Oligocene, cooling and aridification are expressed by the disappearance of typical Cretaceous-Paleocene flora and by the preponderance of temperate species (Wing, 1987). In northern Yukon, a transition from angiosperm to gymnosperm forests from the upper Eocene to the lower Oligocene also reveals cooling (Ridgway & Sweet, 1995). Isotopic analyses in the north-central United States of America indicate cooling of ~7°C in air temperatures (Fan et al., 2018) and ~8°C in mean annual temperatures (Zanazzi et al., 2007). In Oregon, the study of paleosols indicates cooling of ~2.8°C across the EOT (Gallagher & Sheldon, 2013). Longer-term cooling and aridification trends are observed in sedimentary records of western Washington (Breedlovestrout et al., 2013) and Texas (Yancey et al., 2003).

South America: The impacts of the EOT on sedimentary records appear to be heterogeneous in South America. In Patagonia, while vegetation appears to be unchanged across the EOT (Kohn et al., 2004, 2015; Strömberg et al, 2013), or only show long-term cooling (Quattrocchio et al., 2013), rapid cooling of ~5°C of mean annual temperatures is suggested by isotopic analysis of hydrated volcanic glasses (Colwyn & Hren, 2019). Barreda & Palazzesi (2010) studied vegetation change in central Patagonia from the Eocene to the Miocene and show that the temperate to warm-temperate taxa of the Eocene were replaced by temperate to cold-temperate taxa in the early Oligocene. Remodeling in the metatherian faunas in South America is believed to have happened simultaneously with vegetation changes (Abello et al., 2018).

Africa: There is little data related to the EOT in Africa due to significant gaps in palaeobotanical records across this time interval (Pound & Salzmann, 2017). Pan et al. (2006) suggested that the extinction of African palms was related to the EOT.

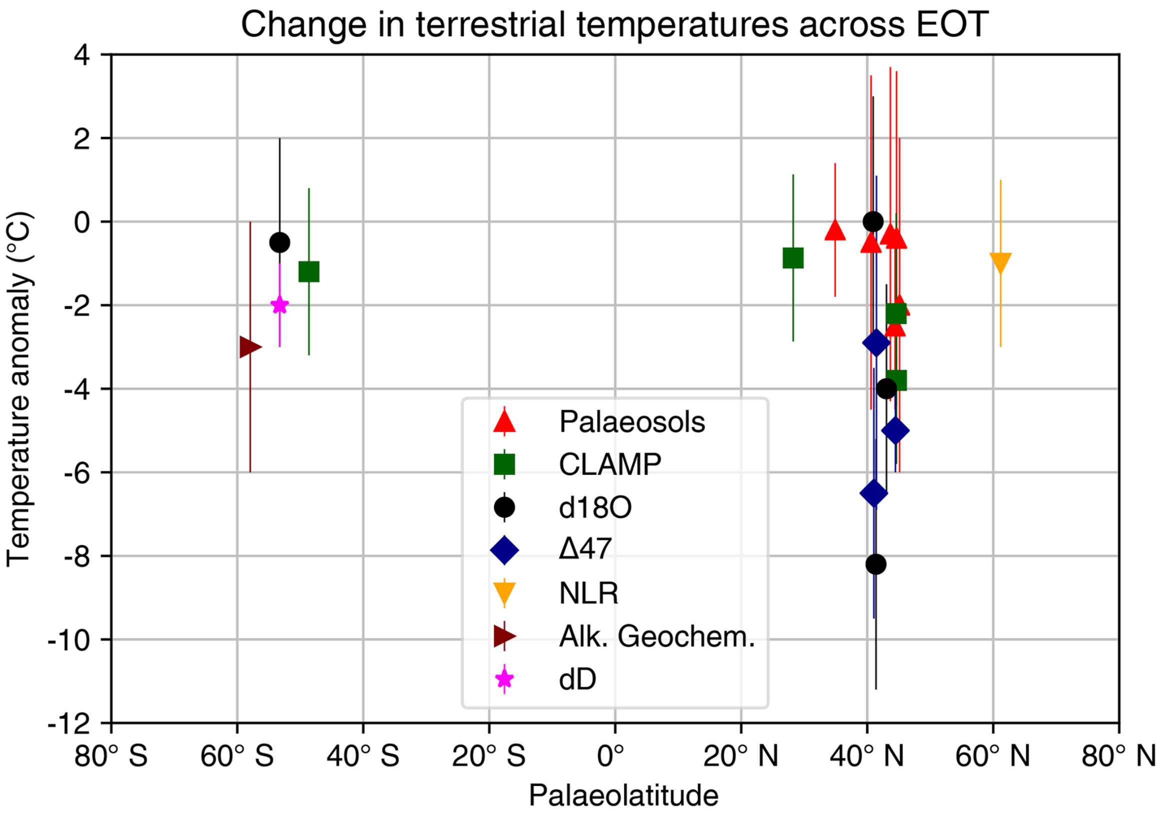

***Figure 22**: Summary of change in terrestrial temperature across the EOT at various sites according to several proxies. From Hutchinson et al., 2020.*

Overall, global climate forcing at the EOT is variably expressed in different regions. While many records show cooling, aridification, and/or increased seasonality near the EOT, several others show no major changes. Furthermore, some climatic changes occurred prior to the EOT in some places as a response of long-term pCO_2 decrease, and some records show changes after the EOT, therefore indicating the possibility of a time-lag between pCO_2 decrease and climatic repercussions. These processes are very important to document to better our understanding of climate variability on the continents under major pCO_2 variations. A clear problem that emerges from continental studies of the EOT is the lack a high-resolution age models, which complicates the correlation of observed events with the rapid $\delta^{18}O$ steps observed in marine records.

II.2.d : Continental seasonality near the Eocene-Oligocene Transition

When studying climate change, a very important notion to document is seasonality. Seasonality is defined as the seasonal variations of temperature and precipitations (Kwiecien et al., 2022). Changes in seasonality can have immense impacts on the fauna and flora, as some species are accustomed to specific ranges of temperature and/or precipitation, so changes in seasonality can cause their extinction or migration (Lindström & McLoughlin, 2007; Willis et al., 2008). Moreover, recent studies argue that the biotic turnovers of the EOT might have been primarily driven by an increase of seasonality expressed by colder winters (Page et al., 2019; Eldrett et al., 2009). The continental records displaying increased seasonality through the EOT are mostly from mid to high latitudes and are relatively few. They include the Hampshire basin in the United Kingdoms (Hren et al., 2013), the US Gulf coastal plain (Ivany et al., 2000), the Norwegian-Greenland Sea (pollen and spores derived from the continent)

(Eldrett et al., 2009), and the Rennes basin (Boulila et al., 2021; Bauer et al., 2016). In the URG, the palynological investigations of Schuler (1988) show a clear change from a subtropical climate with a short or inexistant dry season ("Zone Salifère Inférieure") to a subtropical/Mediterranean climate with a long dry season ("Zone Salifère Moyenne") at the base of the "Sel III", suggesting a strong increase of seasonality prior to and/or through the EOT. Furthermore, Schuler (1988) has shown similar trends in the Hessian and Bresse grabens. While southern latitudes studies of seasonality through the EOT are rare. Selkin et al. (2015) observed the disappearance of fire-related characteristics (e.g., burnt palm phytoliths) through the EOT and suggests that it is related to changes in seasonal precipitation. Therefore, seasonality changes seem to have affected high latitudes in both hemispheres, but other records show no changes (Kohn et al., 2004) and more investigations are needed to provide a clear global trend. In this thesis, I propose that some sedimentary structures could be used to study seasonality changes across the EOT (**Chapter V :**).

II.2.e : Numerical simulations of paleoclimatic change

Various numerical simulations studies have been conducted to investigate the processes that could have led to the EOT and to better understand the consequences of that event.

II.2.e.i : Atmospheric pCO_2 decrease

Based on the numerical simulation study of DeConto & Pollard (2003), the mainspring of the EOT seems to be a decrease in atmospheric pCO_2. This decrease led to the formation of small ice caps on elevated Antarctic uplands, followed by feedback mechanisms once a pCO_2 threshold was exceeded, causing the ice caps to rapidly grow along orbital variations, resulting in the continental-scale **East Antarctic Ice Sheet** (**EAIS**). However, Eocene climate models using proxy-data usually fail to reproduce the recorded low meridional temperature gradient, potentially because of the insufficient sensitivity in coupled models and the inaccurate model representation of feedback processes (Roberts et al., 2009). Interestingly, models that have a better match to temperature gradients and high-latitude temperature proxies are those that used extremely high atmospheric CO_2 values of 2240 or 4480 ppm (Cramwinckel et al., 2018; Hubert & Caballero, 2011; Eldrett et al, 2009). These results suggest that models are not yet able to sufficiently reproduce observations of the sedimentary records, meaning that they possibly underestimate forcing of CO_2 on climate sensitivity through inaccurate or missing feedback mechanisms (Hutchinson et al., 2020). More recently, the numerical simulations of Tardif et al. (2021) suggest that orbital variations were crucial, along with the pCO_2 decrease, in the major biotic event around the EOT such as the "Grande Coupure". The numerical simulations of Toumoulin et al. (2022) suggest that pCO_2 decrease alone was not sufficient to explain the seasonality changes observed across the EOT, but a combined effect of it along with the AIS formation and increased continentality. They also suggest that areas of increased continentality due to sea-level lowering are the areas with most increased seasonality, giving an answer for most of the heterogeneity in temperature changes on continents.

II.2.e.ii : Oceanic gateways

Even though the opening of the Southern Ocean gateways has long been considered the main driver for the onset on the **Atlantic Meridional Overturning Circulation** (AMOC) and glaciation of Antarctica, numerical simulation studies using Eocene boundary conditions show otherwise. They show that the **opening of these gateways only had a modest impact on ocean poleward heat transport**, meaning that it is not directly responsible for the onset of the AIS (Goldner et al., 2014). Furthermore, another study showed that even if the Southern Ocean gateways allowed deep-water connections, a strong-enough **Antarctic Circumpolar Current** (ACC) could not have developed until Australia had sufficiently shifted northward to no longer stop strong zonal flow in the Southern Ocean (Hill et al., 2013). However, the long-term evolution of these gateways could explain local benthic temperature observations, as it may have caused ~3°C cooling of bottom waters (Sijp et al., 2014). Ocean circulation changes are more likely to be a consequence of glaciation rather than a cause, as the presence of the AIS seem to have enhanced Southern Ocean deep-water circulations and benthic cooling (Goldner et al., 2014). However, bathymetry changes of the GSR might have been a prime driver of the EOT through the strengthening of the AMOC (Straume et al., 2022).

II.2.f : Summary

- The Eocene-Oligocene Transition (EOT, 34.44 – 33.65 Ma) is globally characterized by cooling, aridification, and increased seasonality, the glaciation of Antarctica (and induced ~70 m sea-level drop), changes in oceanic water-circulations, and important changes in the fauna, flora, and sea-water chemistry (e.g. CCD).

- The main causes of the Eocene-Oligocene Transition (EOT) are the fall in atmospheric CO_2 and changes in oceanic gateways, along the influence of astronomical forcing. The precise cause of the CO_2 drawdown is still unknown.

- While the impacts of the EOT are rather homogenous in the marine realm, they are much more heterogenous in the continental realm. This heterogeneity is important to document in order to better assess the climate systems' responses to major pCO_2 shifts.

- In comparison with the marine realm, continental records usually lack high-resolution age models, making it difficult to correlate continental climate changes with oceanic $\delta^{18}O$ steps.

- The lack of knowledge on feedback mechanisms and how they interact with CO_2 changes and oceanic currents modification might cause underestimations or overestimations of changes observed in modelization studies.

II.3 : Geological Setting

II.3.a : European Cenozoic Rift System

The European Cenozoic Rift System (ECRS) extends across ~1100km from the Mediterranean Sea to the North Sea and contains several intracontinental rifts (Ziegler, 1992; Bergerat, 1985; Illies et al., 1967). The localizations of these rifts are correlated with the positions of fracture systems inherited from the Hercynian orogeny (Edel et al., 2007). The formation of the ECRS is explained by the reactivation of these fracture systems due to north striking transpressional stresses induced by the continental collisions of the Pyrenean and Alpine orogens (Dèzes et al., 2004; Schumacher, 2002; Bergerat, 1987). The rift valleys of the ECRS are the Upper Rhine Graben (URG), Lower Rhine Graben (LRG), Hessian Graben (HG), Eger Graben (EG) (also known as the Ohre Graben), Bresse Graben (BG), and Limagne Graben (LG) (**Figure 23**). There are also several other Cenozoic grabens and basins near the Mediterranean Sea related to the ECRS.

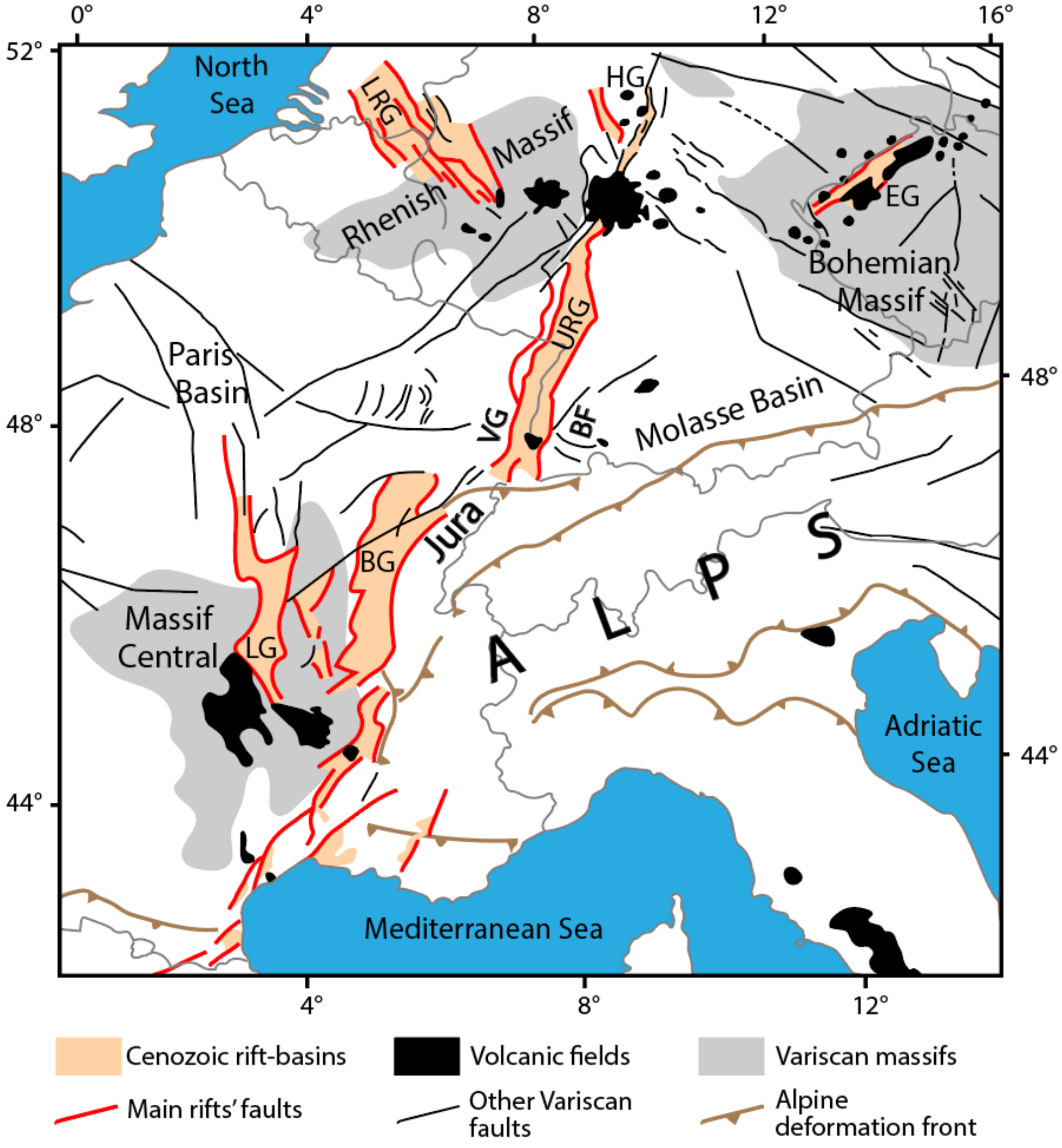

***Figure 23**: Location map and main structures of the European Cenozoic Rift System. URG = Upper Rhine Graben, LRG = Lower Rhine (Roer Valley) Graben, HG = Hessian Graben, EG = Eger (Ohre) Graben, BG = Bresse Graben, LG = Limagne Graben, VG = Vosges, BF = Black Forest. Modified after Dèzes et al. (2004).*

II.3.a.i : Lower Rhine Graben

The LRG is a marine rift basin located in the southern part of the Dutch German Central Graben. It morphologically resembles an embayment which cuts through the Rhenish Massif. On the German side, this basin contains close to 1300 m of siliciclastic sediments with brown coal intercalations, ranging from the Oligocene to the Pleistocene (Hager, 1986). These coal layers have been exploited since the 19th century in open-cast mines. This basin contains three units which are marine beds in the deepest part of the basin, marine deposits with coal seams in the middle, and fluvial and lacustrine sediments in the upper part of the basin (Schäfer et al., 2005). Most of the clastic material originates from the Rhenish Massif. The sedimentary record of the LRG shows several base level cycles related to tectonics and sea-level changes. Due to the absence of Eocene sediments in the LRG, no investigations were conducted in this graben with regards to the EOT. Also, there seems to be no publications regarding the Oligocene paleoclimate of the LRG.

II.3.a.ii : Hessian Graben

The HG is considered as the north-east prolongation of the URG. It contains fluvial, lacustrine, and marine sediments ranging from the middle Eocene to the Miocene which have different facies in the Kassel Basin than in the area north to the Vogelsberg. They form an unconformity on the underlying Buntsandstein (Triassic).

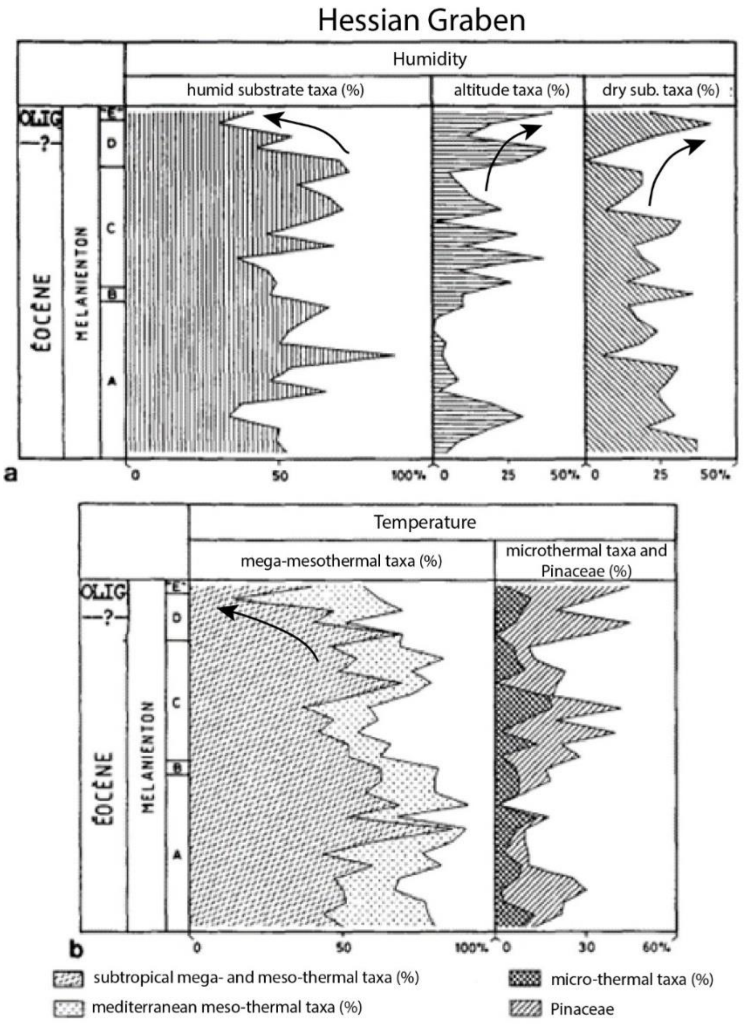

***Figure 24**: Humidity and temperature results of Schuler (1988) in the Hessian Graben based on palynological observations. The black arrows show notable positive or negative changes. Modified after Schuler (1988).*

In the Kassel basin, the Eocene sediments, ranging from the Lutetian to (possibly) the Priabonian (Schuler, 1988; Ritzkowski, 1969; Brosius & Gramann, 1959), consist of the fluvial/lacustrine “Lignites de Borken” and “Weissblauer Ton”, mainly made of marls, and of the brackish “Melanienton”, also mainly consisting of marls with *Melania*. The Rupelian corresponds to the marine sediments of the “Rupelton” attributed to the main marine transgression of the Rupelian, which is the equivalent of the “Marnes à Foraminifères” and “Schistes à Poissons” of the Upper Rhine Graben. During the Chattian, the marine to fluvial/lacustrine “Oberer Quartzitsand” unit was deposited and consisted of sandstones, quartzites containing *Ophtomorpha nodosa* tubes, and conglomerates with Cretaceous clasts. In the area north of the Vogelsberg, the Eocene sediments consists of the fluvial/lacustrine “Ältere Sand- und Ton-Serie” made of sandy marls, and of the brackish “Melanienton” similar to the Kassel basin. The Oligocene sediments consist of the marine “Rupelton”, similar to the Kassel basin, of the marine “Schleichsand” made of sandstones and marls, both attributed to the Rupelian. The marine to fluvial/lacustrine “Jüngere Sand- und Ton-Serie”, attributed to the Chattian, consists of sandstones and marls.

The palynological investigations of Schuler (1988) in the Hessian Graben unveils tropical to subtropical climatic conditions with very little temperature and humidity variations through the Eocene (**Figure 24**). In the lowermost Oligocene, the decline of wet substrate taxa and the rise of dry substrate taxa, along the decline of mega-mesothermal taxa indicates aridification and cooling, but Schuler (1988) suggests that it could be attributed to tectonic forcing rather than to climatic changes.

II.3.a.iii : Bresse Graben

The Bresse Graben is a tectonic depression that is 200 km long and 30 to 60 km wide. It is confined by the Jura to the east and by the Massif Central to the West and located southwest of the URG (Gelard, 1978). This graben contains three distinct sub-basins known from north to south as the Chalon basin, the Louhans basin, and the Bourg-en-Bresse basin. The Bourg-en-Bresse basin, the deepest of the three, contains up to 1600m of Cenozoic sediments, 1400m of which are evaporitic formations (Moretto, 1986). In these 1400m, it is estimated that that cumulated thickness of halite reaches up to 1200m (Blanc-Valleron, 1990). Going northward to the Louhans and Chalon basins, halite deposits become more and more rare and let place to sulfates and carbonates. These formations range from the Priabonian to the Rupelian and have been correlated to the salt formations of the Mulhouse basin (URG) based on palynological comparisons (Schuler, 1988).

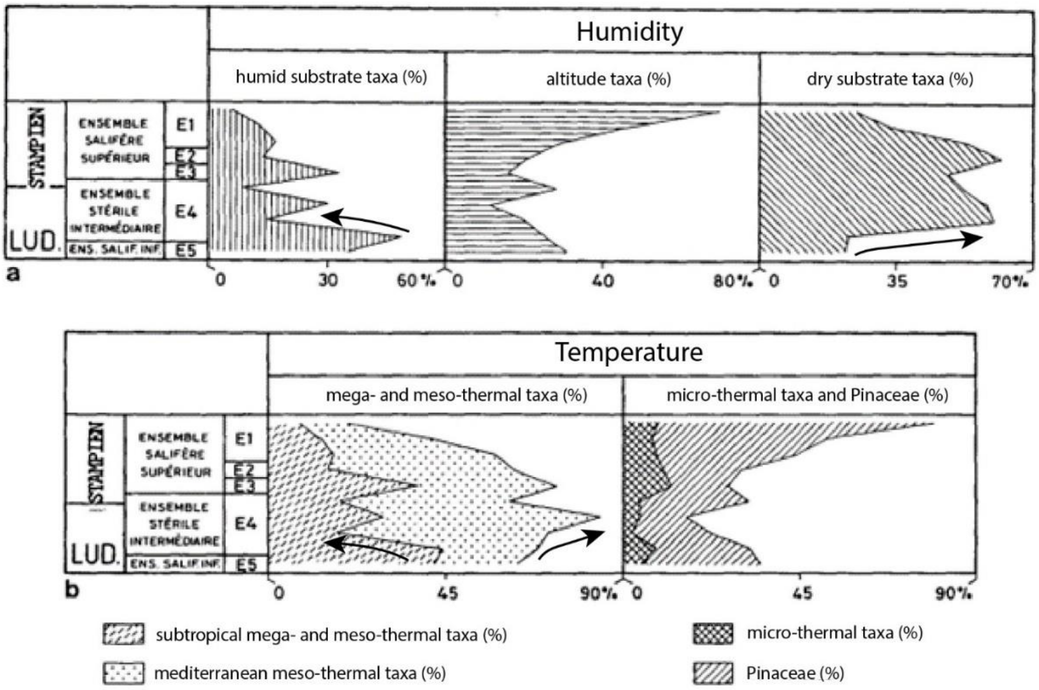

__Figure 25__: Humidity and temperature results of Schuler (1988) in the Bresse Graben based on palynological observations, which suggest rapid aridification and cooling in the “Ensemble Stérile Intermédiaire” formation. LUD. = Priabonian, STAMPIEN = Rupelian. The black arrows show notable positive or negative changes. Modified after Schuler (1988).

An interesting observation is the fact that both the ”Sel III” unit of the Mulhouse basin and the “E4” unit of the Bourg-en-Bresse basin display similar decametric marl-evaporite alternations, that could potentially be astronomically forced (see **Chapter I :**). The palynological investigations of Schuler (1988) suggest that the climates changes observed in the Bresse graben were similar to those observed in the Upper Rhine Graben, notably in the

"Ensemble Stérile Intermédiaire" (equivalent of the "Zone Salifère Moyenne" of the URG). They show the rapid diminution of wet substrate taxa and the rapid increase of dry substrate taxa suggesting increased aridity, along with the rapid decline of mega-mesothermal taxa suggesting cooling (**Figure 25**). Moreover, the spread of Mediterranean taxa suggests an increase in seasonality.

II.3.a.iv : Eger Graben (Ohre Graben)

The Eger graben contains five sub-basins known as the Cheb basin, the Sokolov basin, the Most basin, the Zittau basin, and the Berdzdorf-Radomierzyce basin (Rajchl et al., 2009). The Most basin is the largest preserved sedimentary record of the Eger Graben with sediments ranging from the late Eocene to the Miocene. The Eocene sediments consist of pre-rift fluvial clastics, while the syn-rift fill consists of up to 500m thick sequence of continental fluvial, pyroclastic, swampy, deltaic, lacustrine sediments (Havelcová et al., 2015). This basin is the largest and economically most important lignite basin of the Czech Republic, with several occurrences of coal seams. The only climate investigations pursued in the Most basin were focused on the Miocene sediments, with a particular emphasis on the Miocene Climatic Optimum (Grygar et al., 2019; Grygar et al., 2014). There seems to have been no emphasis given on the Eocene-Oligocene transition in this basin, possibly due to the nature of the pre-rift Eocene fluvial sediments that are hardly usable for paleoclimate investigations. There could however be relevant data in the Czech literature.

II.3.a.v : Limagne Graben

The Limagne graben, which actually is a half-graben, is classically divided into the Limagne centrale, the Grande Limagne, the Limagne d'Issoire, and the Limagne de Brioude (Wattinne et al., 2018). It is bounded by a major north-south normal fault to the west known as the Limagne fault (Michon, 2000). Due to this fault, the sedimentary record of the western part of the Limagne graben reaches 2500m, while thinner deposits were deposited to the east (Pelletier, 1972). The sediments of these basins date back as far as the Lutetian in the eastern part of the Limagne graben, and as far as the Bartonian in the western part (Riveline et al., 1988). The Eocene sedimentary successions of the Limagne Graben consist of fluvio-lacustrine sands, marls, clays, and calcareous sediments deposited under warm and humid conditions (Gorin, 1974). Accelerated subsidence at the end of the Eocene led to the wide deposition of lacustrine carbonates and clays (Hugueney, 1984). The Rupelian sediments are characterized by the presence of evaporites as well as several palynomorphs that indicated a progressively drier climate (Hugueney, 1984; Giot et al., 1976; Gorin, 1974), likely due to the Eocene-Oligocene transition. It is uncertain if the evaporites were the result of marine incursions and/or remobilization of older evaporites (Gaudant, 2012). During the Chattian, a widespread cooling episode is reflected by the deposition of marls and concreted freshwater limestones (Gorin, 1974). Deposition of sediments, mainly lacustrine, continued until the Middle Miocene (Merle et al., 1998).

II.3.a.vi : The basins from southeastern France

There are numerous Cenozoic basins in southeastern France. They are known as the Alès Basin, Aix Basin, Central Graben, Grand Faraman Basin, Hérault Basin, Issirac Basin, Manosque Basin, Mormoiron Basin, Offshore Vistrenque Graben, Roussillon Basin, Sommières Basin, Saint-Chaptes Basin, and Vistrenque Graben (Semmani et al., 2023). These basins contain Upper Eocene and to late Oligocene lacustrine sediments characterized by thick siliciclastic, carbonate and evaporitic rocks (Rouchy, 1997). While the Vistrenque Basin is considered as the deepest of the Cenozoic southeastern basins of France with up to 5km of sediment accumulation, it is relatively poorly known due to the lack of continuous data such as cores. However, recent investigations in several SE France basins unveiled answers to their Eocene to Oligocene paleogeographic and paleoclimatic evolution (Semmani et al., 2023; Létteron et al., 2022; Létteron et al., 2018). Létteron et al. (2022) studied the Alès, Saint-Chaptes, and Issirac basins and provided models of their sedimentary profiles and stratigraphic architecture, as well as their evolution over time. They have shown that these lacustrine systems are characterized by a freshwater to oligohaline open-lake through the earliest middle Priabonian, by an oligohaline to mesohaline closed-lake through the middle Priabonian, and by a hypersaline lake restricted to the depocenter area (Alès basin) in the middle-late Priabonian. They suggest that the degradation of climate through the EOT influenced the evolution of these lake systems. More recently, Semmani et al. (2023) studied cores, cuttings, and well-logs from the Vistrenque, Alès, Saint-Chaptes, Issirac, and Roussillon basin and provided new insights of their chronostratigraphy and paleogeographical, paleoenvironmental, and paleoclimatic evolution. They suggest that the significant stage of climate cooling and aridification that they observed in the early Rupelian could be the result of the EOT.

II.3.b : The Upper Rhine Graben

II.3.b.i : *Paleogeography*

To study the evolution of paleoclimates and environments in a basin, it is important to know its paleogeography, as it might have shifted since the deposition of its sedimentary record. A different paleogeography means that the basin could have been under a different atmospheric circulation zone due to a difference in latitude, and not receiving the same amount of insolation as prior (see **Orbital cycles**). According to paleogeographic reconstructions at 36 Ma by Scotese and Wright (2018) (**Figure 26**) and comparisons with modern geography, the paleogeography of the URG have remained relatively stable throughout the Cenozoic. The URG was therefore located under the Ferrel cell through the EOT.

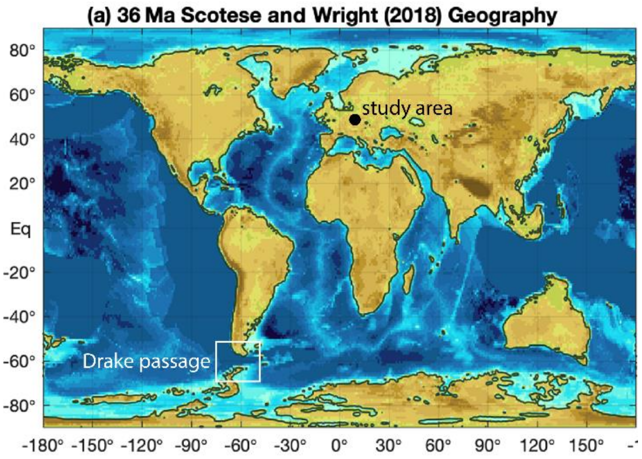

(a) 36 Ma Scotese and Wright (2018) Geography

Figure 26*: Earth's paleogeography and sea distribution reconstruction at 36 Ma (Scotese & Wright, 2018). Modified after Hutchinson et al. (2020)*

II.3.b.ii : *Pre-rift setting*

Schumacher (2002) provides a detailed overview of the tectonic inheritance and evolution of the URG. However, the chronostratigraphy of his paper is outdated (**II.3.c.iv : Overview of the chrono-stratigraphy**).

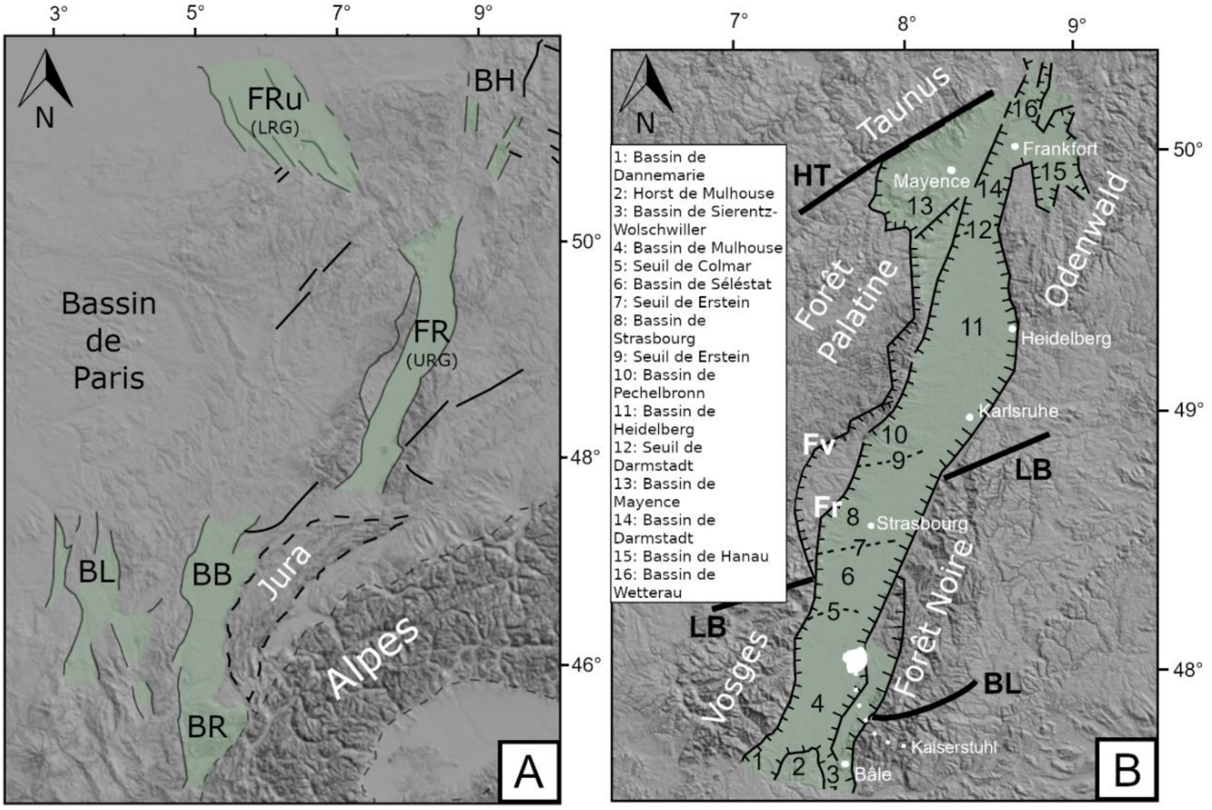

***Figure 27**: Localization map of the study area with a Digital Elevation Model (DEM). (A) Western part of the European Cenozoic Rift System (ECRS) according to Schumacher (2002). The green surfaces represent basins with tertiary deposits. LRG: Lower Rhine Graben FRu: Ruhr Graben, BB: Bresse Basin, BR: Rhône Basin, BL: Limagne Basin, BH: Hesse Basin (B) Localization of the various highs and sub-basins of the URG according to Sissingh (2006). HT: Hunsrück-Taunus fault, LLBB: Lalaye-Lubine-Baden-Baden fault, BL: Badenweiler-Lenzkirch (Todnau) fault, Fv: vosgienne fault, Fr: western rhénane fault.*

Paleozoic

The long and complex structural history of the Upper Rhine Graben (URG) began with the Hercynian (or Variscan) orogeny and particularly with the Permian-Carboniferous phase of wrench tectonics (Ziegler, 1990) (**Figure 28**), from which it inherited its main structural trends. At the end of the Carboniferous, a large mountain belt, part of the western European Hercynian belt, extended from the Caucasus to the East, to the southern Ouachitas and Appalachians of North America, to the West (Matte, 2001). The Hercynian belt is the result of the collision and accretion of two continents, Laurussia to the North and Gondwana to the South (Ziegler, 1990) (**Figure 28**). Structures that the URG inherited from the Hercynian orogeny are the NE to ENE trending dislocation zones. They represent, from the north to the south of the URG; the Hunsrück-Taunus border fault, which highlights the limit between the inherited Rhenohercynian and Saxothuringian domains which was back-folded to the south as the Hercynian orogeny was close to its end (Anderle, 1987); the Lalaye-Lubine-Baden-Baden NW vergent and sheared dextrally, which highlights the limit between the inherited Saxothuringian and Moldanubian domains (Wickert & Eisbacher, 1988); and the Badenweiler-Lenzkirch zone (Todtnau fault), SE vergent and sheared dextrally, which is inside the Moldanubian domain (Krohe & Eisbacher, 1988) (**Figure 27**). Other comparable lineaments, ENE oriented and located along the southern margin of the Vosges and in the western Badenweiler-Lenzkirch zone prolongation, were highlighted in the southernmost subsurface of the URG by gravity and magnetic data (Edel & Fluck, 1989). Other inherited structures are the NNE oriented sinistral fault zones associated with intrusive dyke swarm and bodies from the Lower Carboniferous to the Permian. These fault systems are interpreted as the precursors of the Cenozoic URG (Illies, 1962). They outcrop in the basement of the Vosges, Black Forest and Odenwald

Mountains and were further documented by geophysical data and kinematic analyses (Edel & Weber, 1995). The inherited structures that greatly modified the tertiary deposition in the URG, along with the syn-rift events, are the Hercynian Highs and Lows, which can be correlated to the limits of the main sub-basins (Schumacher, 2002).

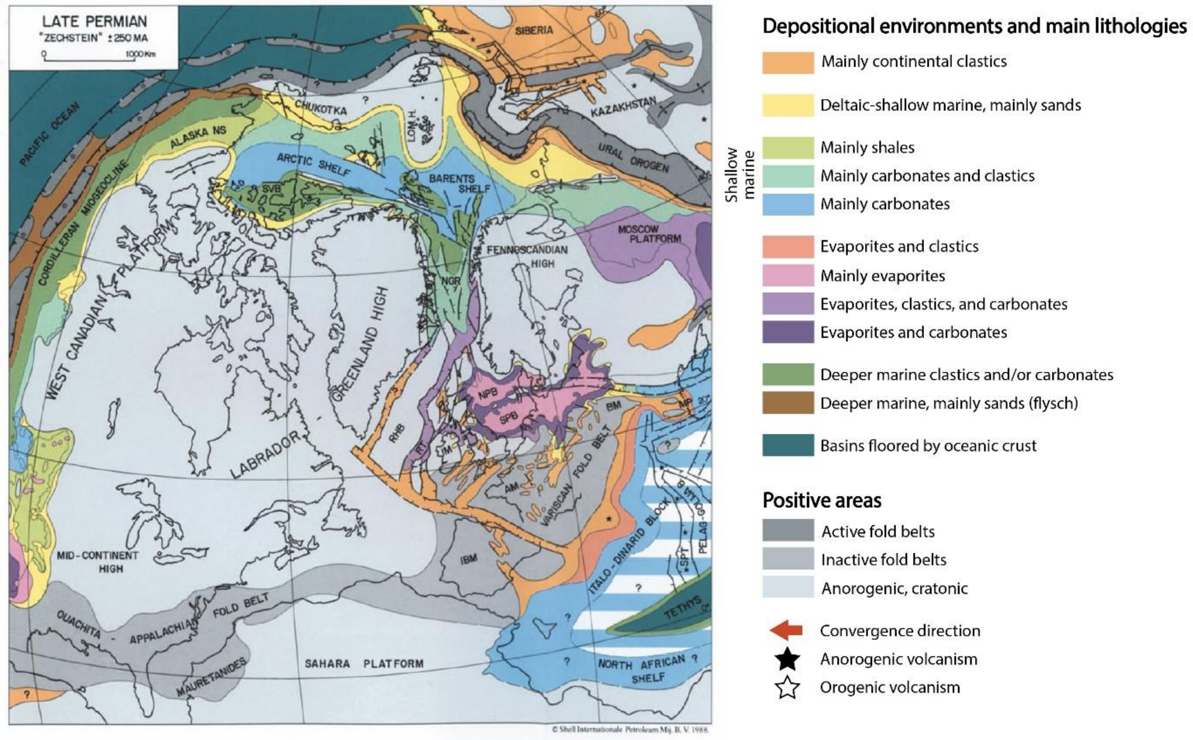

__Figure 28__: Late Permian paleogeography, geological structures, and sedimentary basins near what became western modern Europe (Ziegler, 1990). The Late Permian marks the beginning of continental clastic sedimentation in the Germanic basin. AM = Armorican Massif, IBM = Iberia Meseta, IM = Irish Massif, MP = Moesian Platform, NGR = Norwegian-Greenland Sea Rift, NPB = Northern Permian Basin, RHB = Rockall-Hatton Bank, RT = Rockall Trough, SPB = Southern Permian Basin, SVB = Sverdrup Basin. Modified after Ziegler (1990).

Mesozoic

From the late Permian to the Triassic, the formation of Mesozoic basins is associated with the initiation of Pangea's break-up. To the west of the Tethys, Mesozoic basins such as the intracratonic Germanic basin started to subside and allowed the deposition of sediments, extending from modern England to Poland. From the west to the east, structural heterogeneities probably inherited from the Hercynian orogeny influenced sedimentation, resulting in a deposition delay for the first formation known as the "Buntsandstein". In France, a part of this formation is attributed to the late Permian (Bourquin et al., 2007), while it is only attributed to the Triassic in other places. In the Upper Rhine Graben, sediments of the Germanic basin date from the late Permian to the late Jurassic and consist in the stacked formations of the "Buntsandstein", "Muschelkalk", "Keuper", "Lias", and "Dogger" (**Figure 29**). For detailed description of these formations through drill wells, see the publication of Aichholzer et al. (2016), Duringer et al. (2019), and Aichholzer (2019).

The "Buntsandstein" (~450 m), attributed to the late Permian and early Triassic (Ménillet et al., 2015; Mader, 1985; Gall, 1985; Gall, 1972; Gall, 1971; Durand, 1972), consists of continental red sandstones (fine to coarse) and conglomerates. These deposits are of fluviatile and aeolian origin, with the sediments' source being the Paleozoic basement on which it lays. The top of this unit marks increasing marine influences and the apparition of clays. The "Muschelkalk" (~150 m), assigned to the middle Triassic (Ménillet et al., 2015), corresponds to a marine episode that flooded the whole Germanic basin. This unit is mainly composed of fossil rich limestones, marls-limestones alternations, and dolomites (Duringer et al., 2019; Aichholzer et al., 2016). Anhydrite layers were found in the middle of this unit, suggesting evaporitic episodes. The “Keuper” (~190 m), attributed to the late Triassic (Ménillet et al., 2015), mainly contains clays, marls, dolomites, and anhydrites (Duringer et al., 2019; Aichholzer et al., 2016). Some sandstone layers are found in the unit and were deposited under fluviatile and shallow marine conditions. The “Lias” (~160 m), assigned to the lower Jurassic, mainly consists of monotonous clays with some limestone layers (Duringer et al., 2019; Aichholzer et al., 2016). The “Dogger” (~220 m), attributed to the upper Jurassic, contains monotonous clays, sandstones, and limestones (Duringer et al., 2019; Aichholzer et al., 2016). One of the limestone units of the “Dogger” is known as the “Grande Oolithe”, which is a widely known unit, almost completely made of oolites. It is found in several outcrops of the URG, such as in the Turckheim outcrop (**Figure 66**, **Figure 67**).

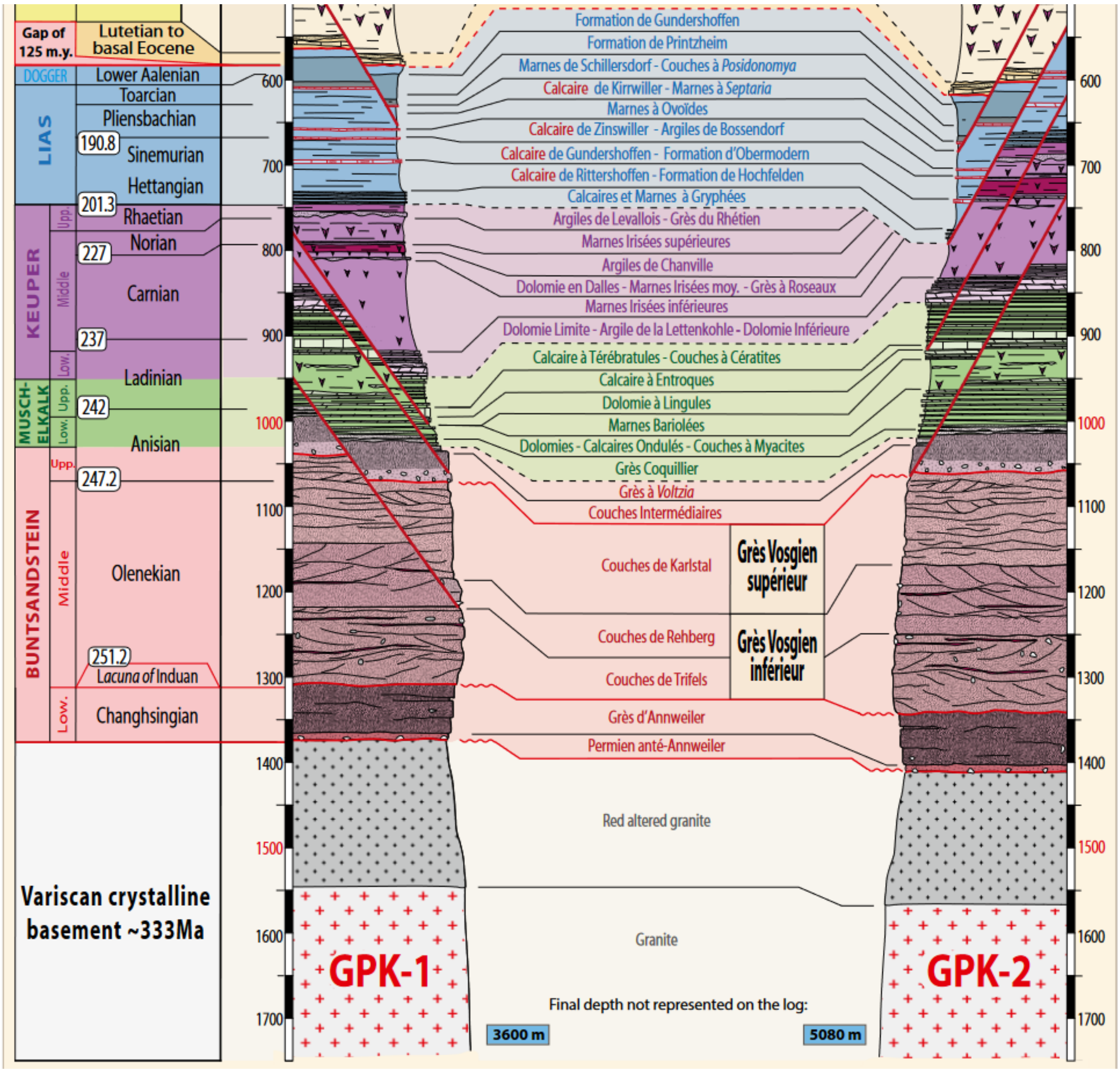

Figure 29: Sedimentary log of the Paleozoic and Mesozoic pre-rift series in the GPK-1 and GPK-2 borehole of the Pechelbronn basin according to Aichhozler et al. (2016).

Cretaceous sediments are totally absent from the URG’s sedimentary record. Active extension in the North Sea and Atlantic margin caused the uplifting of areas near the position where the URG later formed. This uplift might have been sustained via a mantle plume or by buckling of the lithosphere (Bourgeois et al., 2007). Uplifting of the area caused the non-deposition and/or erosion of Cretaceous units. Several Cretaceous volcanic episodes strengthen the thesis of lithospheric-scale mechanisms of uplift sustenance (Sittler, 1965).

II.3.b.iii : Syn-rift setting

Tectonics

The URG's evolution has been primarily driven by stresses induced on the Alpine foreland through collisions caused by the Alpine and Pyrenean orogens, in possible combination with forces exerted by the Artic-North Atlantic Ridge (Schumacher, 2002; Müller et al., 1997). It is described as a polyphasic rift evolution.

Prior to the rifting, tectonic subsidence started during the Lutetian and resulted in the karstic weathering of the "Dogger" limestones, followed by the occurrence of small lakes superimposed on Paleozoic structural depressions. The first main subsidence phase, which most likely began during the late Lutetian or early Bartonian, is associated with WNW-ESE trending extension. A few decades ago, due to the lack of age constraints, some authors suggested generalized uplift which led to the erosion and/or non-deposition of Bartonian sediments (Schumacher, 2002; Sissingh, 1998), but recent investigations confirmed the presence of Bartonian formations (Châteauneuf & Ménillet, 2014, Berger et al., 2005), suggesting that sedimentation was continuous during this interval. Subsidence increased from the Priabonian to the early Rupelian, inducing intense fracturing and development of tilted blocks. At that point, while the rift's basin subsided, the rift's shoulders uplifted, resulting in the deposition of alluvial fans along the southern, western, and eastern margins of the southern URG (Duringer, 1988), governed by WNW-ESE trending extensional stress regime (Illies, 1977). The master faults segregating the basin from the rift shoulders became evident by that time (Schumacher, 2002). A tectonically and/or climatically induced and marine influenced (Lavoyer, 2013) transgression resulted in the deposition of a uniform marl formation across the whole URG known as the "***Zone Fossilifère***". This formation is possibly linked with eustatic sea-level rise between the PaRu1 and PaRu2 sequences (Berger, 2005; Haq et al., 1998) corresponding to the end of the EOGM. Connection with the marine realm was stopped until the Upper Rupelian. During the Upper Rupelian, the Hessian depression to the north and the Raurachian depression to the south connected the URG with the North Sea basin and the eastern part of the Alpine foreland basin (Berger, 1996; Martini, 1990) due to eustatic sea-level increase between the PaRu2 and PaRu3 sequences. The URG thus became a marine channel which shale deposits ("***Série Grise***") show uniform thickness and facies evolution across the whole rift basin (Roussé, 2006). Towards the Rupelian-Chattian boundary, sea-level fall caused isolation of the URG from marine realms, marking the shift from Upper Rupelian marine shales to Chattian fluvio-lacustrine brackish to freshwater deposits. During the Chattian, the middle segment of the URG continued to subside while the northern and southern segments were temporarily uplifted, resulting in an intra-Chattian unconformity (Rothausen and Sonne, 1984). Across the Miocene, subsidence continued in the northern URG, while the southern URG underwent uplift and erosion which erased the record of the late Chattian subsidence (Villemin et al., 1986), and was likely accompanied by the Kaiserstuhl volcanism. By the end of the Miocene, a compressive regime comes into play and marks the end of the Upper Rhine Graben extension. Since the uppermost Pliocene, the URG is affected by trans-tension deformation and strike-slip faulting. Differential Quaternary uplift of the rift shoulders signed the modern morphology of the URG (Lutz & Cleintuar, 1999).

Sedimentary infill

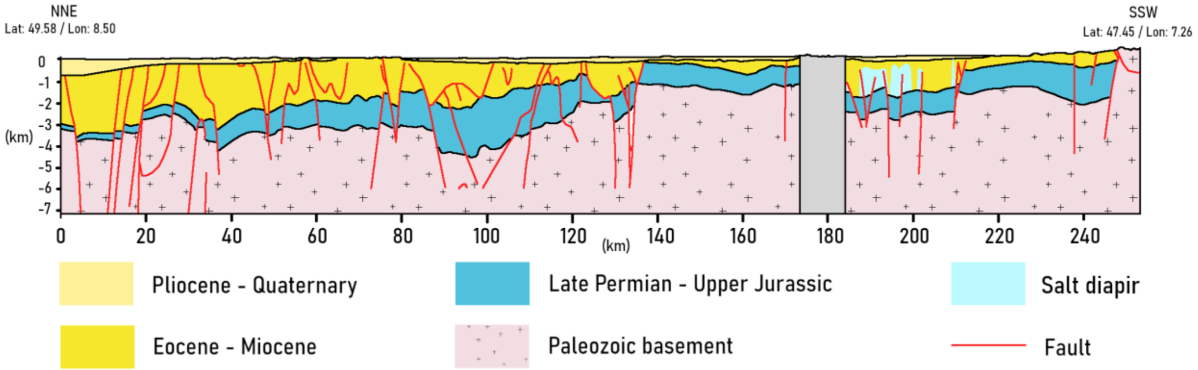

Figure 30: Geological cross section across the whole URG. Sedimentary formations are undifferentiated. Modified after publications of the GeORG project.

In the URG, the Tertiary sedimentary infill reaches up to 3.5 km of thickness in the north near Karlsruhe, while in the south, it reaches 2.5 km at most (Figure 30). This difference is linked to the Miocene uplift of the southern URG. The tertiary sedimentary environments of the URG are very varied, and include terrestrial, fluviatile, freshwater lacustrine, brackish lacustrine, and marine channel environments. There are various throughs and highs due to the Paleozoic basement structure.

Regional paleoclimate

The evolution of the regional paleoclimate through the Eocene and Oligocene in the URG is relatively well known thanks to the palynological investigations of Schuler (1988). These investigations were done in various localities and wells through the URG allowing a great overview of main climate trends (Figure 31).

after Schuler (1988)

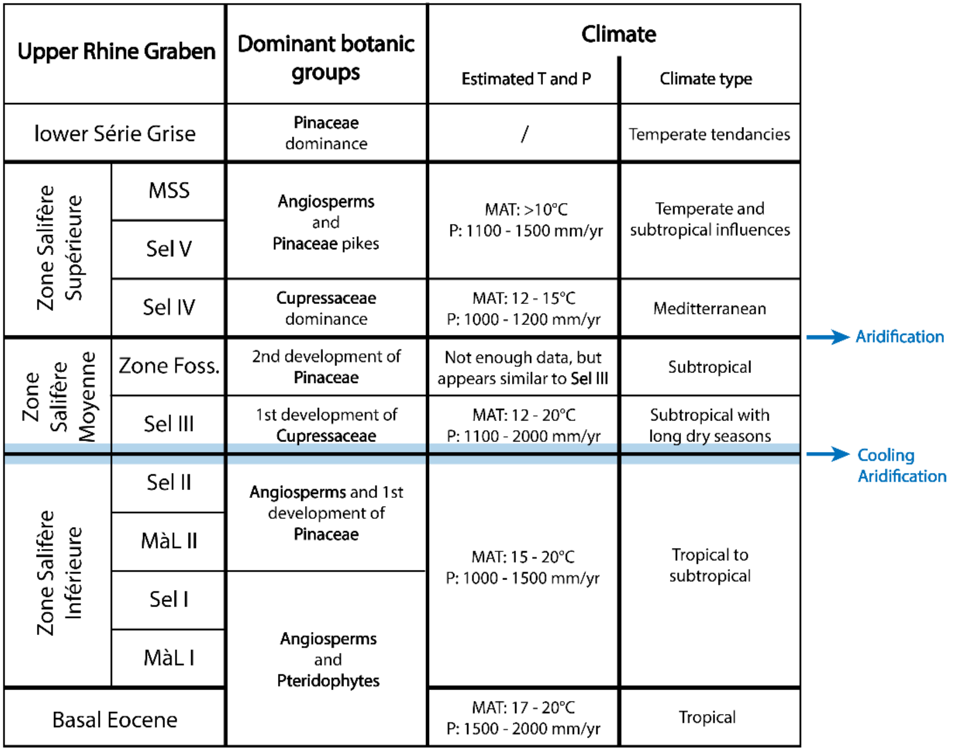

Upper Rhine Graben		Dominant botanic groups	Climate	
			Estimated T and P	Climate type
lower Série Grise		Pinaceae dominance	/	Temperate tendancies
Zone Salifère Supérieure	MSS	Angiosperms and Pinaceae pikes	MAT: >10°C P: 1100 - 1500 mm/yr	Temperate and subtropical influences
	Sel V			
	Sel IV	Cupressaceae dominance	MAT: 12 - 15°C P: 1000 - 1200 mm/yr	Meditterranean
Zone Salifère Moyenne	Zone Foss.	2nd development of Pinaceae	Not enough data, but appears similar to Sel III	Subtropical
	Sel III	1st development of Cupressaceae	MAT: 12 - 20°C P: 1100 - 2000 mm/yr	Subtropical with long dry seasons
Zone Salifère Inférieure	Sel II	Angiosperms and 1st development of Pinaceae	MAT: 15 - 20°C P: 1000 - 1500 mm/yr	Tropical to subtropical
	MàL II			
	Sel I	Angiosperms and Pteridophytes		
	MàL I			
Basal Eocene			MAT: 17 - 20°C P: 1500 - 2000 mm/yr	Tropical

Figure 31: Synthesis of the palynology results of Schuler (1988) for the Upper Rhine Graben.

The **Lutetian** (“**Basal Eocene**”), based on the palynology of the Bouxwiller deposits, is characterized by a large majority of wet substrate- and tropical megathermal-mesothermal taxa, with a few dry-substrate and mesothermal taxa. The climate can be considered tropical, hot, and wet, with mean annual temperatures of 17 - 20 °C and a pluviometry of 1500 – 2000 mm/year. The **upper Lutetian**, **Bartonian** and **lower Priabonian** (“**Marnes à Limnées I**”, “**Sel I**”, “**Marnes à Limnées II**”, “**Sel II**”) are dominated by megathermal-mesothermal taxa that indicate a humid tropical to subtropical climate, which is a little bit colder and drier than the Lutetian, with mean annual temperatures of 15 – 20 °C and a pluviometry of 1000 – 1500 mm/year. The presence of a few Mediterranean taxa suggests the possible occurrence of a very short dry season.

The **uppermost Priabonian to lowermost Rupelian** (lowermost “**Sel III**”) is a period of marked cooling, drying and increased seasonality, which I **correlate to the EOT**. The climate of the “**Sel III**” appears to be intermediary between a subtropical climate characterized by a pluviometry of 1500 – 2000 mm/year and mean annual temperatures of 15 – 20°C, and a Mediterranean climate with a long dry season, a pluviometry of 1100 – 1500 mm/year, and mean annual temperatures of 12 – 15°C.

The palynology of the “**Zone Fossilifère**” (**Lower Rupelian**) is not well defined due to few taxa found but seems to be identical as that of the uppermost “**Sel III**”, while maybe a bit more moist, due to the marine-influenced transgression. The **Lower Rupelian** (“**Sel IV**”, “**Sel V**”, “**Marnes sans sel**”) is characterized by a large majority of mesothermal taxa and an increase in microthermal taxa. The climate is considered Mediterranean with a relatively long dry season, mean annual temperatures of 12-15 °C, and a pluviometry of 1000-1200 mm/year for the “**Sel IV**”, unveiling a marked period of aridification. For the “**Sel V**” and “**Marnes sans sel**”, the climate is wetter and colder. The **Upper Rupelian** (“Série Grise”) is characterized by a large majority of Pinaceae. Compared to the Lower Rupelian, the pluviometry might have been a bit higher and the temperature a bit lower. The taxa diversity was not high enough to determine precise mean annual temperatures and pluviometry estimates.

II.3.b.iv : Summary

- The Upper Rhine Graben (URG) is a complex intra-continental rift system with several sub-basins which was initiated during the middle Eocene.
- The formation of the URG was greatly influenced by the structure of the Paleozoic crystalline basement.
- The Cenozoic sediments of the URG form an unconformity on the Jurassic deposits of the Germanic basin. There are no cretaceous sediments in the URG.
- The URG evolved through multiple tectonic phases and was sometimes influenced by marine connections and/or incursions.
- The Eocene-Oligocene Transition (EOT) is likely recorded in the URG and is characterized by cooling, aridification, and increased seasonality in the “***Sel III***” unit according to the palynology investigations of Schuler (1988) (**Figure 31**). Other Cenozoic basins of the European Cenozoic Rift System show paleoclimatic change related to the EOT.
- Several rift-basins of the European Cenozoic Rift System recorded the cooling and aridification of climate through the EOT.

II.3.c : Sub-basins: chrono-stratigraphy, structure, paleontology

This chapter is a literature review of the sub-basins of the URG, specifically focused on both the Mulhouse and Pechelbronn basins. Correlations between the different formations of the sub-basins of the URG, Mainz basin and Jura mountains are relatively well known (Pirkenseer et al., 2018) (**Figure 31**). The Upper Rhine Graben contains several sub-basins known, from south to north and from west to east as the Dannemarie Basin, Mulhouse Horst, Sierentz-Wolschwiller Basin, Mulhouse Basin, Séléstat Basin, Strasbourg Basin, Pechelbronn Basin, Heidelberg Basin, Mainz Basin, Darmstadt Basin, Hanau Basin, and Wetterau Basin (Sissingh, 2006) (**Figure 27**). Each sub-basin has specific sedimentary accumulations. However, the southern Upper Rhine Graben is particularly characterized by the large accumulation of evaporites, while the northern Upper Rhine Graben is rather constituted of lacustrine and marine siliciclastics.

II.3.c.i : Mulhouse basin

The Mulhouse basin (also known as the Potash basin) has been extensively studied by Blanc-Valleron (1990) and Maikovsky (1941). In the URG, this basin is characterized by its important volume of Eocene-Oligocene evaporites (e.g. anhydrite, gypsum, halite, sylvite, carnallite), and is the only one which contains potash seams. The following paragraphs are based on literature. For the detailed description of the DP-XXVIII well, which gives an overview of the sedimentary record in the center of the Mulhouse basin, see **Chapter I :** .

Lithostratigraphy, paleontology

II.3.c.i..1 Basal Eocene

In this thesis, I refer to the Lutetian formations that formed above the Jurassic substratum as “**Basal Eocene**”. This term includes appellations such as : “***Sidérolithique***”, “***Zone de Transition***”, “***Calcaire à Planorbe***“, “***Bouxwiller Formation***”, and “***Calcaires d’eau douce Lutétiens***”. The “*Sidérolithique*” classically refers to the Jurassic limestones’ karstic infills. In the Mulhouse basin, the “**Basal Eocene**” consists of carbonated and detrital sediments that formed above the Jurassic substratum, as well as laterites, and karsts that formed inside it. In the DP-III well, this formation consists of marls, clays, limestones, sandstones, and conglomerates. This diversity of lithologies is probably linked with the initiation of the rifting phase. Maïkovsky (1941) found the remains of *Planorbis pseudoammonius* in the DP-III well. By correlation with the lacustrine limestones of Bouxwiller documented by charophyte and mammal remains, the “**Basal Eocene**” can be partly attributed to the MP13b European mammal biozone in the Lutetian (Schmidt-Kittler et al., 1997; Jaeger, 1971).

II.3.c.i..2 Zone Salifère Inférieure

The “**Zone Salifère Inférieure**” formation is subdivided in four distinct units known as the “***Marnes à Limnées I***”, “***Sel I***”, “***Marnes à Limnées II***”, and “***Sel II***”. The “**Lower Salt Formation**” could extend from the late Lutetian to the end of the Bartonian (or early Priabonian), from NP16 to NP17 (Berger et al., 2005; Schuler, 1983, 1988, 1990; Châteauneuf, 1983; Sittler, 1965).

The “***Marnes à Limnées I***” unit (> ~160m) is characterized by its vertically and horizontally homogeneous marly facies, which suggests a relatively deep-water environment during their deposition. The name of this unit is linked to the discovery of few *Lymnaea* remains (Maïkovsky, 1941) which indicate a lacustrine setting. Rare unidentified plant and shell remains were also found. Organic geochemistry investigations revealed that the Hydrogen Index (HI) is coherent with type III kerogen, derived from land plants (Blanc-Valleron, 1990). This unit is partly attributed to the Bartonian based on floral assemblage correlation with other basins (Châteauneuf & Ménillet, 2014). According to the detailed sedimentary log of the DP-XXVIII well (**Figure S2**), there are several anhydrite beds and bedded anhydrite nodules which indicate the input and saturation of sulfates. They seem to form 5 deepening-up (brine recharge) and shallowing up (brine saturation) cycles, that could potentially have an orbital print.

The "***Sel I***" unit (~400m) is characterized by a thick halite section with few interstratified marls (up to 200 m) in its lower half, and by a thick marl section with few halite layers in its upper half. Important recrystallization of the halite is suggested by its glassy aspect which indicates the absence of fluid inclusion-rich layers, and by the absence of primary structures (Blanc-Valleron, 1990). The marly layers are comparable to those of the "***Marnes à Limnées I***" with type III kerogen. Bromine values in halite show low values of 30 – 40 ppm (Blanc-Valleron, 1990). Maïkovsky (1941) observed remains of *Lymnaea marginate, Lymnaea sp., Hydrobia?*, and possibly *Nystia* and *Melania* in this unit.

The "***Marnes à Limnées II***" unit (> ~150 m) show facies, organic geochemistry, and paleontology observations almost identical to those of the "***Marnes à Limnées I***". It is in this unit that the large presence of *Pinaceae* is observed and possibly indicates their spread on the uplifted rift's margins (Schuler, 1988). According to Maïkovsky (1941) and documents of the MDPA (MDPA, 1960), this unit contains remains of *Lymnaea crassula, Lymnaea margniata, Lymnaea sp., Melania (Brotia) albigensis, Nystia polita,* along vegetal remains including *Phragmites oeningensis* and unidentified algae.

The "***Sel II***" unit (~160 m) consists in halite, anhydrite, and marls alternations. The marls, like in the previous sub-units, show type III kerogen (Blanc-Valleron, 1990). Bromine values in halite are of 50 – 70 ppm, higher than those of the "***Sel I***". The species diversity obtained in the "Marnes à Limnées II" unit have persisted through the "Sel II", as Maïkovsky (1941) and others (MDPA, 1960) documented the presence of *Melania (Brotia) albigensis, Auricula, Hydrobia?, Lymnaea crassula, Lymnaea marginata, Nystia polita,* along plant remains.

II.3.c.i..3 Zone Salifère Moyenne

The "**Zone Salifère Moyenne**" formation is subdivided in two distinct units known as "***Sel III***" and "***Zone Fossilifère***". The "***Zone Fossilifère***" itself is subdivided in three distinct sub-units known as the "*Zone à Mytilus*", "*Zone à Bryozoaires*", and "*Zone à Hydrobies*".

The "***Sel III***" unit (~ 220 m) consists of halite, anhydrite, and marls alternations. The bromine values of the halite are of 90 – 150 ppm, all higher than those of the "**Sel I**" *and* "***Sel II***". Blanc-Valleron (1990) synthetized the paleontology of the marl layers of the "***Sel III***" after Förster (1911), Maïkovsky (1941), Stchepinsky (1960), Gaudant (1981), and after the archived MDPA documents, which include: **foraminifera** (*Nodosaria, Quinqueloculina*), **fishes** (*Prolebias rhenanus, Pomatoschistus bleicheri*), **lamellibranches** (*Cyrena semistriata, Mytilus socialis*), **gastropods** (*Hydrobia, Planorbis, Tympanotonos labyrinthus, Nystia (Euchilis) chastelii*), **ostracods** (*Haplocytheridea gilletae*), **gammarids** (*Melita palmata*), **isopods** (*Eosphaeroma margarum*), **plants** (*Sequoia, Cinnamomum, Equisetum, Graminophyllum ?,* and Conifers), **algae**, **charophytes**, and **insects**. Blanc-Valleron (1990) also found tertiary **dinocysts** (*Phtanoperidinium*), **coccoliths** (*Coccolithus* cf *pelagicus, Reticulofenestra* cf *umbilica*), and **acritarches** (*Mirchystidium*). The development of brackish organisms and marine phytoplankton (dinocysts, coccoliths, acritarches) in the "***Sel III***" potentially marks early communications with the North Sea. The mudstone-evaporite alternations (metric to decametric) of the "Sel III" are very similar to those of the "Zone Salifère Supérieure". According to Blanc-Valleron (1989), at the bottom of the "Zone Salifère Supérieure", these alternations are astronomically forced. In **Chapter I :** , the cyclostratigraphy of the Mulhouse basin is investigated, and the orbital forcing on these alternations is demonstrated, with implications on the impact of the Eocene-Oligocene transition (see **Chapter I :**).

The "***Zone Fossilifère***" unit (~70 m) consists of marls with some anhydrite layers and is found everywhere in the URG with good continuity. The kerogen of the marls seems to be of type II (Blanc-Valleron, 1990), classically interpreted as deposited in a marine environment. The fauna of the "***Zone Fossilifère***" is similar to the one of the "***Sel III***" but is marked by a strong development of benthic organisms such as **ostracods** (*Haplocytheridea gilletae, Candona [Typhlocypris] pechelbronnensis, Eucypris entzheimensis, Schuleridea sp.*), **foraminifera** (*Bolivina sp., Eponides sp., Bulimina coprolithoides, Bulimina sp., Discorbis sp.,* and miliolids), and **dinocysts** (*Adnatosphaeridium reticulense, Hystrichokolpoma rigaudae, Deflandrea phosphoritica, Cordosphaeridium inodes, C. microtriana, Gonyaulacysta type guiseppei, Glaphyrocys cf. exuberans, Apteodinium sp., Rottnestia borussica, Operculodinium microtriainum, O. tiara, Spiniferites sp., Deflandrea sp., Heteraulacacysta campanula, Hystrichosphaeropsis sp., Polysphaeridium sp.,* and *Thallassiphora sp)* (Pirkenseer et al., 2010; Schuler, 1988; Maïkovsky, 1941). Compared to the "***Sel III***", there seems to be more ostracods, but less fish and Cyrena. The "***Zone Fossilifère***" likely marks a communication(s) with the sea, and various authors interpret it as a marine transgression (Berger, 2005; Pirkenseer et al., 2010, 2011). This unit ranges from NP21 to NP22 according to Schuler (1988, 1990) and is also attributed to MP21 according to Storni (2002). The "**Zone Fossilifère**" can be tentatively correlated to the $\delta^{18}O$ drop following the EOGM, linked to the partial melting of the newly formed AIS and increased sea-level (Zachos et al., 2001). This correlation is coherent as the $\delta^{18}O$ drop happens in the upper part of the NP21 biozone. However, Duringer (1988) and Gaudant (1981) advocated for a purely brackish/freshwater nature of the "Zone Fossilifère". This controversy is discussed in **II.3.c.iii : About the "Zone Fossilifère"**.

II.3.c.i..4 Zone Salifère Supérieure

The "**Zone Salifère Supérieure**" formation is subdivided in three distinct units known as the "***Sel IV***", "***Sel V***", and "***Marnes sans sel***".

The "***Sel IV***" unit is characterized by cyclic alternations of marls and halite or anhydrite, as well as by two potash seams in the center of the Mulhouse basin. Both the marls-evaporite alternations and potash seams show impressive continuity across the basin; centimetric layers in the potash seams can be correlated across multiple kilometers. Studies on the lower part of the "***Sel IV***" show that the marls-evaporite alternations are forced by precession (**Chapter I :** ; Blanc-Valleron, 1989). Before the potash seams, halite bromine levels are around 70 ppm, coherent with marine values (even though non-marine evaporites can have similar values). Across the potash seams, bromine values are of 200 – 340 for the halite, 2800 – 3900 for the sylvite, and ~2000 for the carnallite. After the potash seams, bromine levels in halite drop around 100 ppm. Organisms remains suggest aeolian (insects, pollen, spores) and fluviatile (Lymnea, freshwater turtle) inputs in the basin. Compared to the "**Zone Salifère Moyenne**", there is a decrease in mollusks, ostracods, and gammarids (Blanc-Valleron, 1990). The presence of dinocysts, *Tytthodiscus*, *Botryococcus*, calcareous nanoplanktons, and evaporites suggest a brackish to marine depositional environment. Geochemistry investigations showed that the "***Sel IV***" unit might have started as mostly marine but drifted to non-marine inputs (Cendon et al., 2008).

The "***Sel V***" unit consists of marl and halite alternations. The bromine values decrease from ~100 ppm at the bottom of the unit to ~50 ppm at its top. The organisms found suggest variations between freshwater and brackish environments (Blanc-Valleron, 1990). Marine influences seem unlikely in this unit but cannot be excluded due to the persistence of dinocysts and acritarches. The halite/anhydrite beds of the "Sel IV" and "Sel V" units are nicely correlable across multiple kilometers in the Mulhouse basin, so much so that the MDPA made a type-log and gave a name to each bed (**Figure 32**).

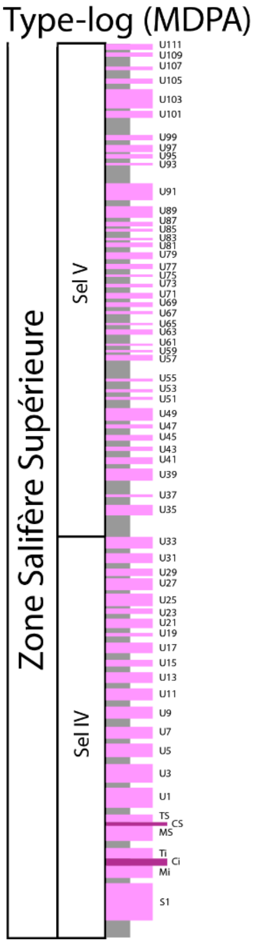

***Figure 32**: Type-log of the “Sel IV” and “Sel V” units of the Mulhouse basin according to the MDPA (Blanc-Valleron, 1990; original documents), with the names of the halite beds. Grey = marlstones, pink = halite, purple = potash.*

The ”***Marnes sans sel***” unit is characterized by alternations of thick marl and anhydrite beds, and by the absence of halite. The freshwater to brackish influences seems to persist in this unit, until its top where a rich assemblage of dinocysts announce the initiation of the marine transgression of the “**Série Grise**”.

II.3.c.i..5 Série Grise

The “**Série Grise**” formation (~450 m) is composed of four distinct units known as the “***Marnes à Foraminifères***”, “***Schistes à Poissons***”, “***Couches à Mélettes***”, and “***Marnes à Cyrènes***”.

The “***Marnes à Foraminifères***” unit, characterized by a rich diversity of foraminifera, marks the marine transgression that flooded the whole basin in the middle Rupelian. The “***Marnes à Foraminifères***” and “***Schistes à Poissons***” units are attributed to the NP23 and P20 biozones thanks to their rich micropaleontological content (foraminifera, calcareous nannoplankton, ostracods, fish otoliths, charophytes, phytoplankton, spores, and pollen) (Schuler, 1988; Grimm, 2002; Martini & Reichenbacher, 2007; Pirkenseer et al., 2010, 2011). The URG likely remained a marine channel linking the Northern Sea and the Paratethys sea during the length of the “**Série Grise**” (Berger et al., 2005).

Evaporite sequence of precipitation

When a brine evaporates, different depositional sequences of evaporites can be found based on its chemistry. Brines can either be marine or non-marine, and the study of the resulting evaporites can help to decipher their origin.

II.3.c.i..1 Marine brines

The chemistry of modern marine brines is very well-known, being dominated by Na and Cl, and containing lesser proportions of SO_4, Mg, Ca, K, CO_3, and HCO_3 (Warren, 2016). When marine brines concentrate, $CaCO_3$ is precipitated first, when the brine reaches twice its original concentration at a density of ~1.10 g/cc (Warren, 2016; Usiglio, 1849; Carpenter, 1978; McCaffrey et al., 1987) (**Figure 33**). At four times its original concentration, the brine gives way to the precipitation of gypsum at a density of ~1.13 g/cc. Starting from 10 times the original concentration of seawater, and densities of ~1.22 g/cc, halite is precipitated. Once the brine reaches more than 60 times its original concentration, the evaporites known as bittern salts (K-Mg salts) start to precipitate.

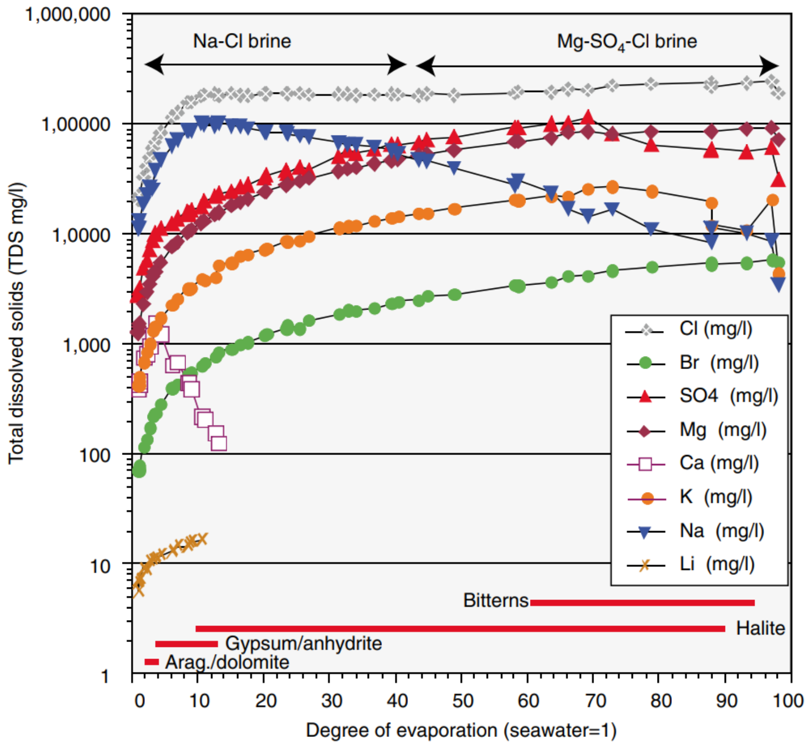

Figure 33: *Changes in ionic proportions related to the concentration of marine brines as aragonite, gypsum, halite, and bittern salts are sequentially precipitated. Aragonite and dolomite are precipitated very early in the sequence. Gypsum and anhydrite are precipitated during a degree of evaporation between 2 and 4. These values are from 10 to 90 for halite, and from 60 to 94 for bittern salts. From Warren (2016).*

II.3.c.i..2 Non-marine brines

On continents, as the chemistry of brines usually highly differ from marine ones, the sequence of precipitated evaporites is less predictable and can be more diverse. In hydrologically closed systems, the chemistry of the brine will depend on the lithologies that are leached into the basin from river and groundwater inputs (Eugster & Hardie, 1978). Five major brine types were distinguished by Eugster and Hardie (1978) that are (1) Ca-Mg-Na(K)-Cl, (2) Na-(Ca)-SO_4-Cl, (3) Mg-Na-(Ca)-SO_4-Cl, (4) Na-CO_3-Cl, and (5) Na-CO_3-SO_4- Cl waters. The concentration on any of these brine types will lead to the precipitation of characteristic sequences of evaporites (Warren, 2016; Eugster & Hardie, 1978).

II.3.c.i..3 Mulhouse basin: marine or non-marine brines?

Several authors have investigated on the marine or non-marine origin of brines that led to the precipitation of the evaporites of the Mulhouse basin (carbonates, gypsum, anhydrite, halite, sylvite). Cendón et al. (2008) studied the lowermost part of the “Sel IV”, from the S2 to Ci beds. Based on their isotopic analyses of fluid inclusions in primary textures, they suggest that the basin was influenced by hydrothermal inputs and recycling of Permian evaporites, and that the lower part of the “Sel IV” evolved from an originally marine input. These results fit well with the interpretation of the “Zone Fossilifère” as the result of a marine transgression (see **II.3.c.iii** : **Chapter VII** : Blanc-Valleron (1990) synthetized data in relation with the origin of the evaporites, which contain arguments for both the remobilization of ancient evaporites (for the “Zone Salifère Inférieure” in particular) and for the input of marine water (for the “Zone Fossilifère” and uppermost “Zone Salifère Supérieure” in particular). Tertiary marine biomarkers (i.e. dinoflagellate cysts, foraminifera) are only found in the “Zone Fossilifère” (and few meters underneath) and “Série Grise” (this thesis; Schuler, 1988; Blanc-Valleron, 1990; Prikenseer et al., 2010). This suggests that the evaporites of the Mulhouse basin mostly originated from reworking of ancient evaporites but were influenced by the input of marine seawater at the time of the “Zone Fossilifère”.

Structure

The Mulhouse basin displays a central downfaulted depression which appears to be a typical and relatively symmetrical graben which formed along the main structural faults of the URG (**Figure 34**). Several faults breach the sedimentary record from the late Miocene down to the Paleozoic basement which implies important tectonism near the time of deposition of these formations. Several salt diapirs were discovered and can be up to 2 km of height and diameter. However, the isopach maps of Blanc-Valleron (1990) suggest that the southwestern part of the Mulhouse basin was the depocenter and underwent subsidence rates higher than in its other parts.

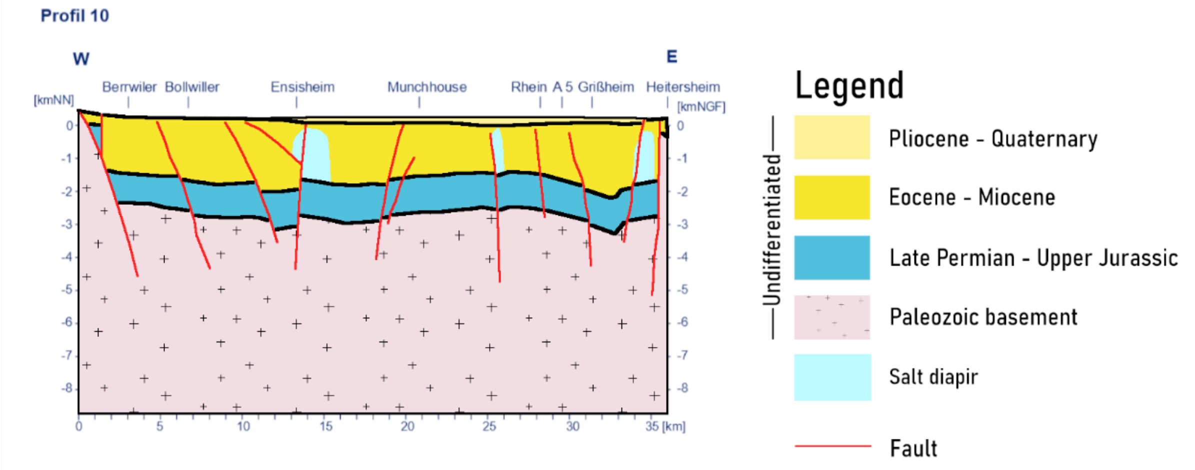

Figure 34*: Geological cross-section in the Mulhouse basin showing a relatively typical and symmetrical graben structure with several salt diapirs. Modified after publications of the GeORG project (Équipe du projet GeORG, 2013).*

II.3.c.ii : Pechelbronn basin

The Pechelbronn basin, which is also referred to as the Pechelbronn – Haguenau – Rastatt basin due to its geographical extent (Blanc-Valleron, 1990), is the northernmost basin of the French part of the URG and extends in the German part of the URG between Rastatt, Karlsruhe, Speyer, and Manheim. To the south, the Pechelbronn basin is delimited by the Brumath high. Several lithostratigraphic nomenclatures were introduced through the several drilling and coring projects of the basin, notably in the locality of Merkwiller-Pechelbronn where most were done for the exploration and exploitation of oil (Sittler, 1965; Schnaebele, 1948; Hoehne, 1916; Gignoux & Hoffmann, 1920; Van Werveke, 1913). Note that this location is located on the western margin of the basin; the center of the basin is located eastward in Germany. The publication of Schnaebele (1948) contains the literal description of the sedimentary formations of the Pechelbronn basin, garmented with descriptions of core segments from several wells.

Lithostratigraphy, paleontology

While the Pechelbronn basin is characterized in the URG by its siliciclastic sedimentary record and oil-bearing sandstones and conglomerates, it still contains a decent amount of evaporites, most notably gypsum, anhydrite, and halite. The following lithostratigraphic descriptions are based on the work of Schaebele (1948), Sittler (1965), Blanc-Valleron (1990), and Duringer et al. (2019).

II.3.c.ii..1 Basal Eocene

In the Pechelbronn basin, the "***Basal Eocene***" is subdivided in the "***Zone de Transition***" and "***Calcaire à Planorbes***" units.

The "***Zone de Transition***" mostly consists of continental fluvial-lacustrine deposits of Lutetian age and forms an unconformity on the Jurassic substratum. Its thickness is highly variable depending on the site (0m to 20m), as well as its sedimentary infill (e.g. marls, calcareous clays, conglomerates, laterites).

Just as the latter, the thickness of the "***Calcaire à Planorbes***" (or "***Calcaire de Bouxwiller***") is highly variable and lurches between a few meters up to 30m in the Bouxwiller area. This unit consists of limestones which contain fossils of *Planorbis*.

II.3.c.ii..2 Zone Dolomitique

The "***Zone Dolomitique***" formation (~150m) was divided by Schnaebele (1948) in two marl units known as the "***Zone des Marnes à Anhydrite***" in the lower half and as the "***Zones des Marnes Dolomitiques***" in the upper half. This distinction was done to emphasize the richer proportion of anhydrite in the lower half, in comparison with the upper half believed to be dolomitic, which is apparently not always the case (or sufficiently enough to deserve that name) (Duringer et al., 2019).

The "***Zone des Marnes à Anhydrite***" mainly consists of dark grey to black marls, sometimes greenish, poorly dolomitic, inside which anhydrite is abundant and deposited as either beds, interstratified layers, or nodules. The presence of layered anhydrite suggests that the depositional environment consisted of a shallow-water brackish lake. The alternating occurrence of halite pseudomorphs, brackish organisms, and freshwater organisms seem to indicate clear salinity variations. While the only evaporites on the margin of the basin are anhydrites, a thick halitic formation reveals itself when investigating closer to the center of the basin.

The "***Zone des Marnes Dolomitiques***" mainly consists of grey-green marls, variegated marls, and conglomeratic sandstones, marking the interruption of the lake's important salinity, and the onset of a brackish to freshwater lake. These marls contain fossils of *Lymnea, Planorbis, Cypris,* and *Helix*. Often, they are dolomitic and display conchoidal fractures, which suggests that they are homogeneous, massive, and lack bedding.

While these descriptions are a good average representation of the "***Zone Dolomitique***" of the Merkwiller-Pechelbronn localy, there are several areas that show variants of this sedimentary succession. Notably, going eastward, these marls become strictly green and rich in *Lymnea*. This is the same facies described as "***Grüne Lymnäenmergel***" (or "***Lymneenmergel***") in Germany. According to the Deutsche Stratigraphische Kommission (2016), the Lymneenmergel extend from the late Lutetian to the middle Priabonian.

II.3.c.ii..3 Couche Rouge

The "***Couche Rouge***" formation consists of a monotonous of red dolomitic marls and red clayey marls. The red color gave the name to the formation and served as an important marker at the time of the oil exploitation. On the German side, the "***Couche Rouge***" is known as the "***Rote Leitschicht***". It contains an abundance of relatively small anhydrite nodules (3cm maximum), but across the basin, these anhydrite nodules sometime disappear. The marls are mostly homogeneous and lack laminations. Very rare sandy marls and/or sandstones are sometimes present depending on the locality. Duringer et al. (2019) noticed some hues amongst clayey marls made of almost pure clay in Rittershoffen. While there are almost no fossils in this formation, rare *Lymnea* were found in some wells. The "***Couche Rouge***" is also limited spatially and only found in the Merkwiller-Pechelbronn area and nearby Palatinat.

II.3.c.ii..4 Couches de Pechelbronn Inférieures

The "***Couches de Pechelbronn Inférieures***" (also known as "***Zone Bitumineuse Inférieure***") formation consists of alternations of grey, black, green, and red marls with intercalations of dolomitic marls, sandstones, and rarer dolomites and limestones. The marls are described as laminated (or variegated) (Schaebele, 1948). Also, it is in this formation that most of the oil was exploited, notably in the marls.

Fossils found in this formation mainly consist of *Lymnea, Cypris,* and *Hydrobia*, along other Gastropods, as well as *Mytilus* and *Eosphaeroma*. In the upper part of the formation Cyrena and *Mytilus* fossils gradually appear and get more numerous getting close to the "***Zone Fossilifère***", along with fossils of Cerithiidae, Melania, Foraminifera, and insects.

II.3.c.ii..5 Couches de Pechelbronn Moyennes

The "***Couches de Pechelbronn Moyennes***" (equivalent of the "***Zone Fossilifère***") is characterized in the Pechelbronn basin by its rich number of fossils. Just like in the Mulhouse basin (and in the whole URG), this formation is divided in three sub-units known as "***Zone à Mytilus***", "***Zone à Bryozoaires***", and "***Zone à Hydrobies***". A great variety of fauna was found in this unit and led to various assumptions regarding de salinity of the depositional water (marine, brackish, freshwater).

The "***Zone à Mytilus***" is characterized by grey to dark-gray laminated marls in which *Mytilus* fossils are very abundant, so much so that they sometime form shelly limestones over multiple meters (Schnaebele, 1948). This sub-unit also contains limey sandstones, grey-brownish to grey-greenish marls with Hydrobia and Cyrena, and variegated marls with the Crustaceans *Eosphaeroma* and *Gammarus*. A strong marine influence is suspected in this sub-unit (Lavoyer, 2013; Schanebele, 1948).

The "***Zone à Bryozoaires***" consists of compact to laminated grey marls which contain colonies of Bryozoans, usually floating in the marls, and sometimes encrusted on various shells. They are found along Cyrena, *Mytilus*, Ostracods, and Gastropods. According to Schnaebele (1941), in the Pechelbronn basin, bryozoans only exist in this unit, which therefore makes it and great correlation horizon. At the base of the unit, sandstone beds are intercalated in the marls.

The "**Zone à Hydrobies**" is characterized by compact, or slightly laminated, homogeneous grey marls, in which mussels are abundant and often pyritized, as well as many species of the *Hydrobia* genre, such as *H. hassiaca, Stenothyra, Nystia,* and *Bynthinella.* Other fossils are found in abundance and consist of Melanidae, Planorbs, Ostracods (e.g. *Cytheridea*) and algae remains which are often pyritized.

II.3.c.ii..6 Couches de Pechelbronn Supérieures

Unlike the previous formation, the “Couches de Pechelbronn Supérieures” show strong facies variations from the south to the north of the basin. Schnaebele (1948) distinguished two main facies that he called “normal” and “freshwater”, their main difference being the presence or absence of gypsum and anhydrite. The northern “freshwater” facies was described as mainly freshwater lacustrine, while the southern “**normal facies**” was described as brackish with possible marine influences. The northern facies consists of coastal sediments with frequent intercalations of conglomerates, sandstones and lacustrine limestones, in which only freshwater fossils where found: *Paludina* cf. *splendida*, *Melania fasciata*?, *Melania* cf. *muricata*, *Planorbis* cf. *goniobasis*, *Chara variabilis*, etc. The southern facies displays marly sediments where conglomerates, sandstones and lacustrine sediments are almost absent. Intercalations of fibrous gypsum and anhydrite nodules appear, and lots of Foraminifera are found.

Northern facies - The Northern facies is described as a massive unit where no subdivisions were made. It can reach up to 280 meters of thickness and mainly consists of freshwater marls with *Lymnaea*, *Anodonta* and *Planorbis* fossils. These marls are variegated, alternatively reddish and greenish, and contain numerous intercalations of sandstones and conglomerates.

Southern facies - The Southern facies is subdivided in six sub-units. The (1) “Zone de Glaswinkel” (8m to 14m) is a detrital interval made of sandstones and conglomerates, but depending on the localization in the basin, there are only marls. (2) “Zone Intermédiaire Inférieure” (~46m) consists of grey ribboned marls with *Ecaphaeroma*, which also contain rare intercalations of sandy marls. The (3) “Zone à Nodules d’anhydrite” (25m to 31m) is made of reddish brackish marls containing numerous anhydrite nodules, which are intercalated with rare freshwater layers consisting of greenish sandy marls with *Lymnaea* fossils. This unit is hard to distinguish from the **“Couche Rouge”** described previously. The (4) “Zone Intermédiaire supérieure**“** (~21m) consists of alternations of brackish laminated marls and sandy greenish freshwater marls containing *Lymnaea* fossils. The (5) Zone à Pseudomorphoses de sel gemme” (~29m) only differs from the following sub-unit by the fact that the gypsum is totally or partially replaced by halite pseudomorphs. The (6) “Zone à Gypse fibreux” (80m to 88m) is made of brackish and freshwater marls alternations. The brackish marls are laminated, dark greenish-brownish, and contain fibrous gypsum. The freshwater marls are greenish, more or less sandy, and contain *Lymnaea* fossils.

Following the “Couches de Pechelbronn Supérieures“ is the “Série Grise”, which is the same formation as described for the Mulhouse basin (see **Série Grise**).

Structure

In contrast with the Mulhouse basin, the Pechelbronn basin (and its eastern counterparts) resembles a half-graben more than a classic graben. Maximum accommodation was reached on the eastern side of the area, under the modern Rhine River, with Tertiary sediments reaching more than 3 km of thickness (**Figure 35**).

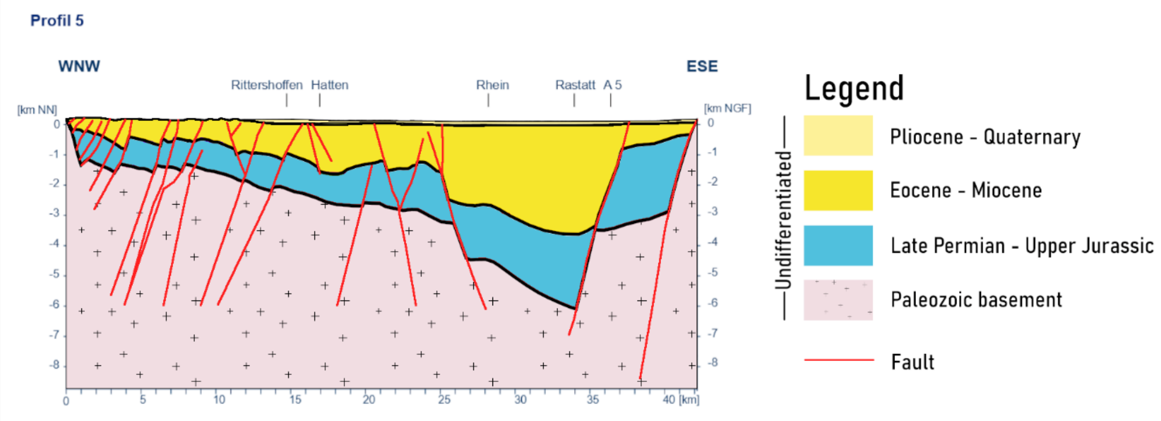

***Figure 35**: Geological cross-section in the Pechelbronn basin and of its eastern counterparts, showing the half-graben structure of the area. Modified after publications of the GeORG project (Équipe du projet GeORG, 2013).*

II.3.c.iii : About the "Zone Fossilifère"

Water chemistry : Marine, brackish, or freshwater?

There has been much debate of the influence of marine incursions in the Upper Rhine Graben before the "Série Grise", notably in the case of the "Zone Fossilifère". There are two main views; the "Zone Fossilifère" either corresponds to a (1) prolonged connection with the North Sea or was deposited in a purely (2) lacustrine setting.

II.3.c.iii..1 Brackish and freshwater arguments

For Duringer (1988), at the time of the "Zone Fossilifère" deposition, the URG was a closed lacustrine basin according to the following arguments:

- **Paleontology**: The macro-fauna of the "Zone Fossilifère" mainly consists of brackish and freshwater organisms. Across ~60 represented species, only the gastropod **Auricula** and the fish **Notogoenous** and **Trichiurides** are candidates for marine influences, only representing up to 2% of the found species, and found along freshwater and brackish species.
- **Sedimentology**: The presence of varves and the absence of tidalites suggests a pure lacustrine setting (Altkirch quarry).
- **Geochemistry**: Isotopic analysis of stromatolites (O^{18} and C^{13}) suggest that they were formed in continental freshwater or slightly brackish lacustrine settings (Altkirch quarry).
- **Paleogeography**: (a) The western, eastern, and southern borders of the URG are limited by a continuous belt of continental conglomerates which paleocurrents were all directed towards the basin, therefore refuting marine connection with the para-Tethys. (b) The unproven continuity of marine sediments from the North Sea to the URG.

For Gaudant (1981, 1984), the fauna of the Zone Fossilifère in the URG mainly consist of brackish to freshwater organisms. In three very specific beds of the Altkrich quarry, he found fish fossils of *Enoplophtalmus alsaticus* nov. sp., *Notogoneus* cf. *cuvieri* (Agassiz), and *Dapaloides* (?) sp, which he argues were species most likely living in slightly brackish conditions. He also references isotopic analyses performed on gypsum layers at the bottom of the quarry which results suggests that they could not have been deposited in marine conditions, and therefore arguing for a continental origin of these evaporites.

The arguments of Duringer (1988) and Gaudant (1981, 1984) mostly rely on macro-paleontological data and observations done in the Altkirch quarry. The argument of Duringer (1988) that varves account for a purely lacustrine setting holds no value as varves are known to also form in marine settings (Schimmelmann et al., 2016).

II.3.c.iii..2 Marine arguments

While the arguments for a purely lacustrine and/or brackish origin of the “Zone Fossilifère” mostly rely on macro-paleontological data, the arguments for marine influences mostly rely on micro-paleontological data.

Schuler (1988), who studied the palynology of the URG, provides several arguments for a strong marine influence in the “Zone Fossilifère” unit. In several wells of the Mulhouse basin, she documented multiple horizons in the “Zone Fossilifère” characterized by rich dinocysts associations that imply strong marine influences. For example, in the DP-XXII well, at depths of 1070m and 1101.2m, she found the association of *Adnatosphaeridium reticulense, Hystrichokolpoma rigaudae, Deflandrea phosphoritica, Cordosphaeridium inodes, C. microtriana, Gonyaulacysta type guiseppei, Glaphyrocys cf. exuberans, Apteodinium sp., Rottnestia borussica, Operculodinium microtriainum, O. tiara, Spiniferites sp., Deflandrea sp., Heteraulacacysta campanula, Hystrichosphaeropsis sp., Polysphaeridium sp.,* and *Thallassiphora sp.* It is hard to find an explanation for the sudden surge of this association that makes more sense than the inflow of marine water into the URG. Furthermore, Tertiary dinoflagellate cysts were only found in the uppermost “Sel III” (low diversity) and in the “Zone Fossilifère” (high diversity), and not further below. Similarly, the palynology investigations performed in this thesis in the Pechelbronn basin are in agreement with these interpretations (see **Chapter VII : Paleoclimatic and paleoenvironmental change in the Pechelbronn**).

Pirkenseer et al. (2010) also studied the micro-paleontology of the Mulhouse basin through cores and outcrops, specifically focusing on the “Série grise”, and a bit on the “Zone Fossilifère”. They show that both formations are characterized by fully marine outer shelf to upper bathyal Foraminifera assemblages, with maximum flooding being reached early in the sequence. However, in the case of the “Zone Fossilifère”, their data is relatively scarce and does not represent the whole formation.

II.3.c.iii..3 Synthesis and interpretation

While there are both arguments for marine and non-marine influences in the “Zone Fossilifère”, the data scarcity for both cases seem to indicate that rather than being purely marine or lacustrine, the “Zone Fossilifère” started with almost purely marine tendencies and became gradually more brackish/freshwater upwars. More specifically, the rich marine assemblages of dinocysts and foraminifera found at the bottom of the unit are a strong argument for an initial marine pulse(s), which became less prevalent going upward, where brackish/freshwater species seem to become the majority. The work from Lavoyer (2013) (**Figure 36**) provides a great continuous overview of the salinity variations through the “Zone Fossilifère” in the Pechelbronn basin. Through his paleontological observations, he shows that the unit starts as marine, and then tends towards brackish and freshwater conditions. Therefore, the “Zone Fossilifère” could be considered as marine at the bottom and brackish/freshwater upward. According to Berger et al. (2005), the “Zone Fossilifère” is related to the sea-level rise following the PaRu1 sequence, which is coherent with its attribution to the NP21 and NP22 calcareous nannoplankton zones (Storni, 2002; Schuler, 1988). Furthermore, the “Zone Fossilifère” is known to have been deposited after the Eocene-Oligocene Boundary due to stratigraphic markers of the Rupelian found in the underlying units (Schuler, 1988). All these arguments are coherent with a sea-level rise linked with the partial melting of the AIS at the end of the EOGM, causing the inflow of marine water into the URG. However, the tectonics conditions and the paleogeography of the URG are not perfectly constrained, so it is not impossible that these marine inflows were forced by tectonic activity rather than sea-level variations. Furthermore, due to the structural highs and throughs of the URG, these marine inputs might not have impacted all the sub-basins the same way in time. Very detailed paleontological and well-log/cores interpretation studies are required to propose a satisfying answer.

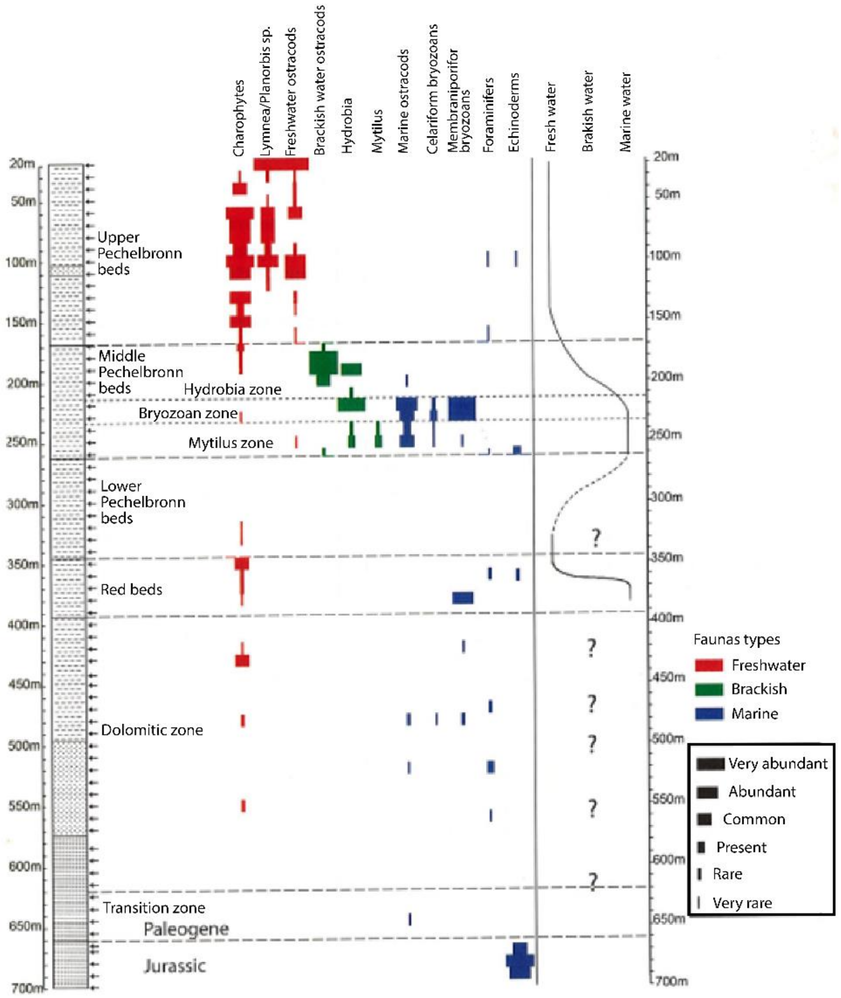

Figure 36: Salinity curve of the GPK-4 borehole from the Jurassic to the "Upper Pechelbronn Beds" according to paleontological data (Lavoyer, 2013). Modified after Lavoyer (2013).

II.3.c.iv : Overview of the chrono-stratigraphy

Prior to the cyclostratigraphic and paleomagnetic investigations performed in this thesis, the chronostratigraphy of the URG was primarily based on biostratigraphy (e.g. calcareous nannofossils, European mammals) and sea-level sequences (e.g. PaRu1, PaRu2) (**Figure 37**). The biostratigraphic zones are relatively long (several million years on average) and are primarily used as relative indicators of sediments ages. It takes very specific species and species assemblages to precisely determine the age of sediments or the location of an epoch boundary in the sedimentary record.

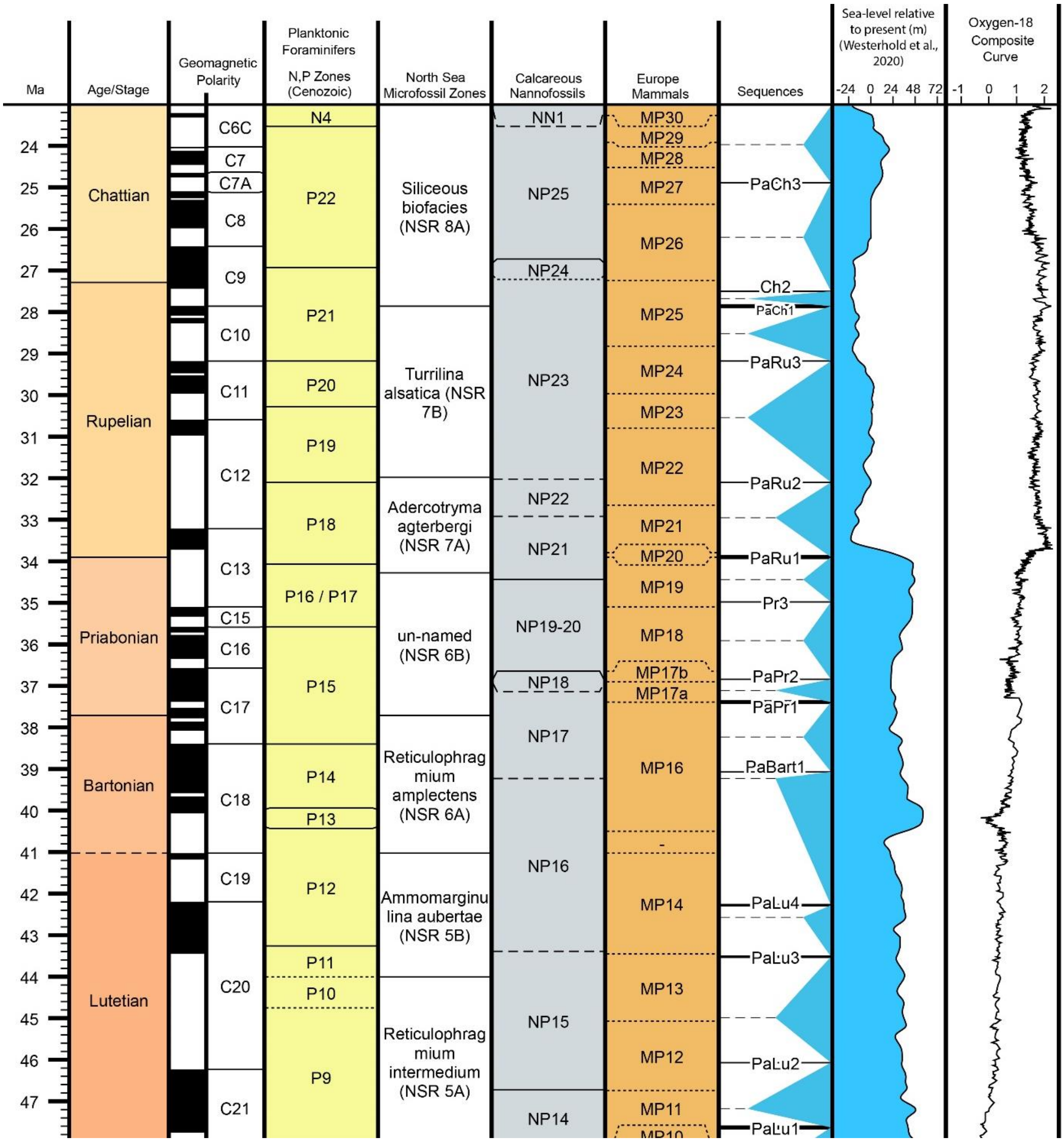

Figure 37: Lutetian-Chattian Geological Time Scale (Gradstein et al., 2012) with corresponding magnetic chrons, planktonic foraminifers' zones, North Sea Microfossil zones, calcareous nannofossils zones, European mammals zones, sea-level sequences, eustasy variations, and oceanic δ^{18}O curve. Made with TimeScaleCreator.

The chronostratigraphy of the Upper Rhine Graben is a rather complex topic. Most of the chronostratigraphic ages rely on biostratigraphic markers found across various wells and outcrops of the URG (for which correlations are not set in stone) and time. While biostratigraphic ages propose an attribution of epochs to sediments, they often do not allow the precise determination of the position of given epoch boundaries in the sedimentary record, such as the EOB. However, the synthesis of Berger et al. (2005), and more recently the one of Grimm et al. (2011) give precious information on the chronostratigraphy of the URG (**Figure 38**).

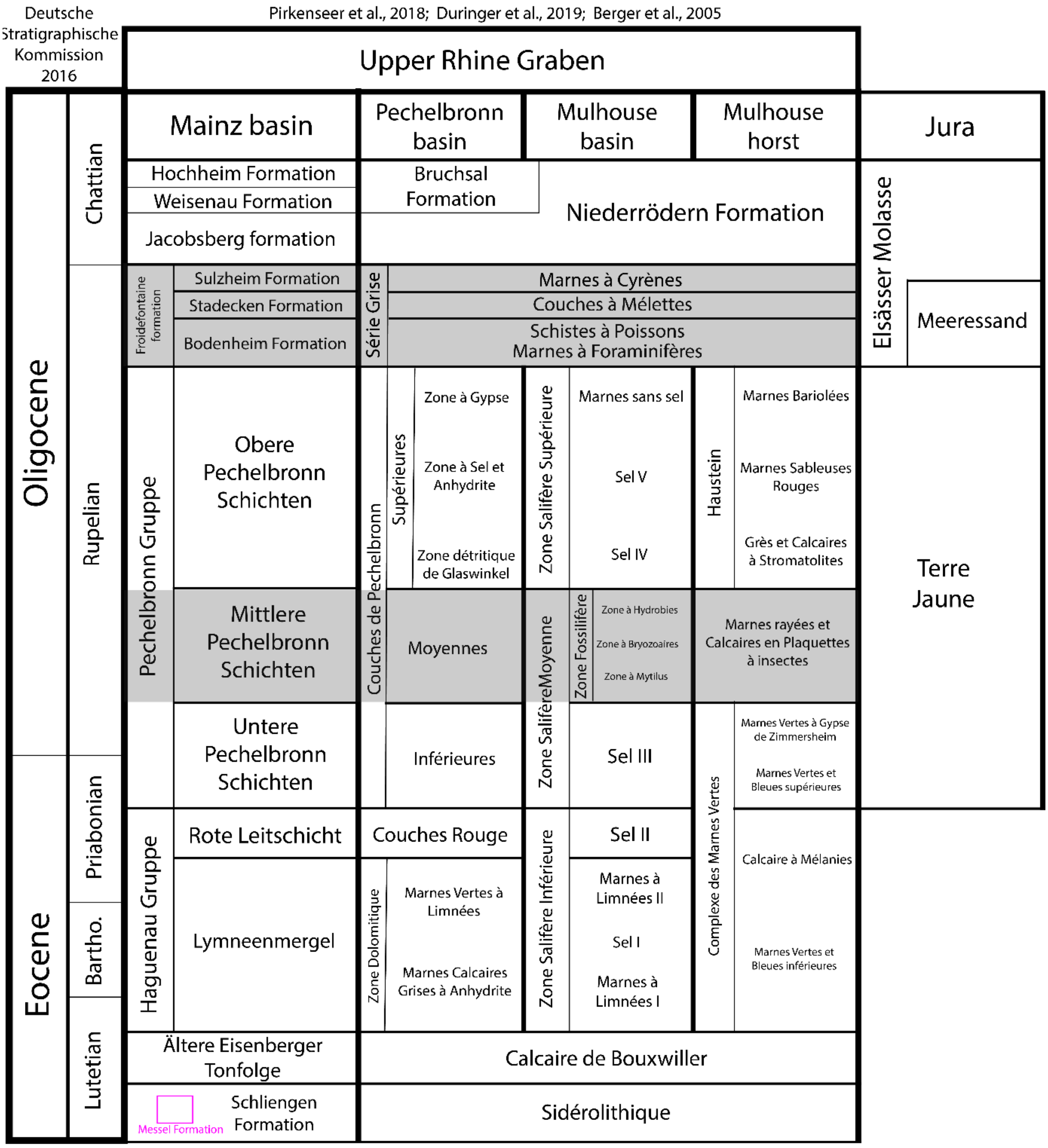

Figure 38: Chronology and correlation of lithostratigraphic concepts and corresponding depositional environments across the Upper Rhine Graben according to the biostratigraphic synthesis of Grimm et al. (2011), the Deutsche Stratigraphische Kommission (2016), Pirkenseer et al. (2018), Duringer et al. (2019), and Berger et al. (2005). The dark grey bands correspond to marine influenced sediments, related to the PaRu1 and PaRu2 sequences.

According to these authors, the EOB is likely to be positioned in the upper part of the "Untere Pechelbronn Schichten" in the northern URG. By stratigraphic correlation, the "Sel III" of the Mulhouse basin is considered as the equivalent of the "Untere Pechelbronn Schichten", so the EOB is therefore suggested to be positioned in the upper part of this unit as well. Nonetheless, the only sedimentary intervals clearly correlable across the URG are the "Zone Fossilifère" and the "Série Grise", so the correlations between the other units could be different. Work done in the scope of this thesis suggests that the EOB might be positioned at the lowermost part of the "Sel III" (**Chapter V :**). Therefore, several possibilities emerge:

- The “Untere Pechelbronn Schichten” and “Sel III” units are not perfect temporal equivalents, making the proposition that the EOB is positioned at the bottom of the “Sel III” coherent.
- Biostratigraphic ages are not precise enough and overestimate the position of the EOB in the sedimentary record, making our proposition that the EOB is positioned at the bottom of the “Sel III” coherent.
- Biostratigraphic ages are correct and the “Untere Pechelbronn Schichten” and “Sel III” units are temporal equivalent, invalidating our proposition that the EOB is positioned at the bottom of the “Sel III”.

To propose a better age model, a multidisciplinary study of continuous cores in the URG using magnetostratigraphy, biostratigraphy, cyclostratigraphy, and sedimentary facies analysis would be required. However, such continuous core records do not exist anymore. Therefore, new coring projects would be required to improve chronological framework of the Cenozoic sub-basins of the URG. However, several propositions are made in this thesis, notably regarding the age and minimum durations of the “Zone Salifère Moyenne” and “Zone Salifère Supérieure” using cyclostratigraphy (**Chapter I :**).

II.4 : Orbital cycles, insolation, and sedimentation

II.4.a : Orbital cycles and their impact on insolation

Earth’s orbit around the sun is affected by cyclic motions which modify the repartition of insolation around the globe through time. Insolation designates the amount of solar radiation perceived at a given locality and is usually measured in W.m². This modification modulates seasonal contrasts which induce climatic and environmental changes at timescales of 10^1 kyr to 10^3 kyr (Berger, 1978; Milankovitch, 1941, 1920). Some sedimentary environments are particularly sensitive to such changes and form regular sedimentary alternations that are literal archives of these past climatic changes. Therefore, regular sedimentary alternations are often investigated to study past climatic changes through the discipline of cyclostratigraphy (**III.2.b : Cyclostratigraphy**). The three main orbital cycles that induce such climatic changes are known as eccentricity, obliquity, and precession.

Eccentricity – Eccentricity is related to the shape of Earth’s orbit around the sun; it oscillates between an almost perfect circle and an elongated ellipse (**Figure 39**A). Its measured as an elongation ratio between the long and half-axis of Earth’s orbit. It oscillates between 0 and 7% with periods of 95 and 124 kyr for small eccentricity, and of 405 kyr for big eccentricity. This oscillation is caused by interactions of Earth with Jupiter and Saturn. Eccentricity is the reason why Earth’s seasons are of slightly different lengths. Eccentricity is also modulated by a 2.4 Myr cycle. The distance between the Earth and the sun affects the amount of solar radiation captured by Earth.

Obliquity - The **obliquity** is the angle between Earth’s rotation axis and the normal to the ecliptic plane (**Figure 39**B). This angle oscillates between 22 and 24.6 degrees with a main modern period of 41 kyr and sub-periods of 29 and 53 kyr. Obliquity is also modulated by a 1.2 Myr cycle. This cycle also impacts the amount of insolation perceived by hemispheres; it makes each hemisphere receive more insolation in their respective summer and less in their respective winter, therefore influencing seasonality. Nowadays, obliquity is at 23.44 degrees.

Precession - Precession consists of the combination of two movements. The main movement is known as **axial precession** which is the rotation of Earth’s rotation axis on a conical orbit, movement usually depicted as the motion of a spinning top near the end of its course (**Figure 39**C). In recent times, the period of this movement according to the stars' frame of reference, is near 25.8 kyr. The second movement is known as **apsidal precession** which changes the orientation of Earth's orbit relative to the elliptical plane due to interactions with Jupiter and Saturn (**Figure 39**C). This movement causes the **axial precession** in the frame of reference of the orbital plane to lurch between superpositions of several periods, around 19, 22, and 24 kyr (recent times). **Precession**, or **climatic precession**, affects the timing of seasons and makes seasonal contrasts more extreme in one hemisphere and less extreme in the other depending on the timing of perihelion (when Earth is the closest from the sun) and aphelion (when Earth is the furthest away from the sun).

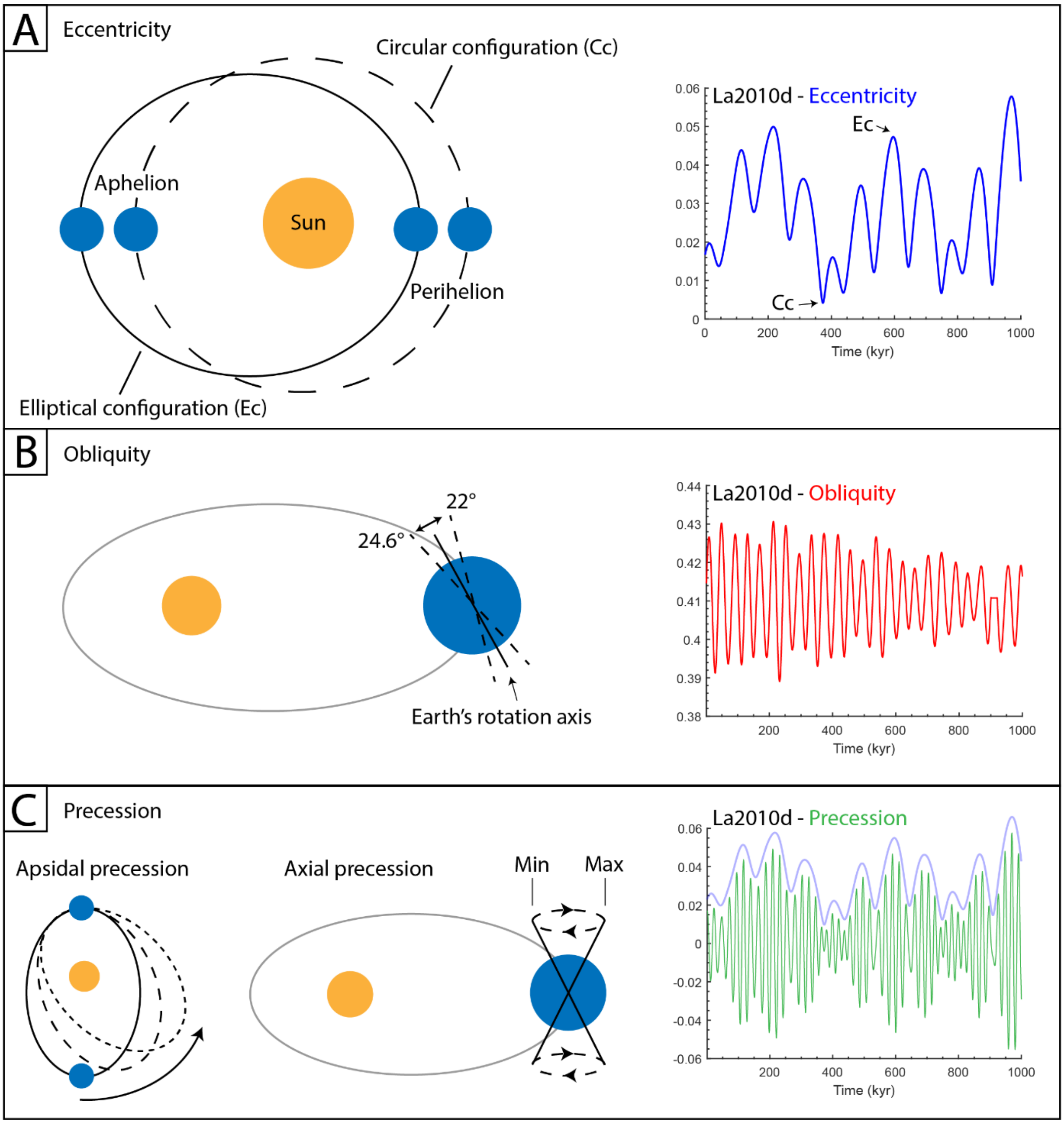

Figure 39: *The orbital parameters of the Earth (Milankovitch cycles). (A) Schema of the eccentricity (left) and its La2010d solution (Laskar et al., 2011) for the past million year (right). (B) Schema of obliquity (left) and its La2010d solution for the past million year (right). (C) Schema of the apsidal precession (left) and of the axial precession (middle), and its La2010d solution for the past million year. Local maximum precession values represent periods where the southern hemisphere experiences increased seasonality. The blue curve is the eccentricity curve*

showing how precession is modulated by eccentricity. The La2010d solutions were produced using the Acycle software (v.2.3.1) (Li et al., 2019).

This happens since precession causes a hemisphere to receive more insolation than the other during perihelion and less during aphelion. Currently, perihelion happens during winter in the Northern Hemisphere and during summer In the Southern Hemisphere. In the current orbital configuration (near precession maximum), the Southern Hemisphere gets hotter summers and colder winters, as it receives more insolation during perihelion and less during aphelion compared to the Northern Hemisphere. In ~13 kyr, it will be the opposite.

II.4.b : Astronomical solutions

The solar radiation perceived at a given point on the Earth depends on its position in space and on its orientation with respect to the Sun. Therefore, to accurately calculate Earth's past climatic evolution, a precise solution for the Earth's orbital movements through time needs to be obtained. Such calculations are complicated due to the perturbation of Earth’s motion in space by the other planets of the Solar System in particular (Laskar, 1999).

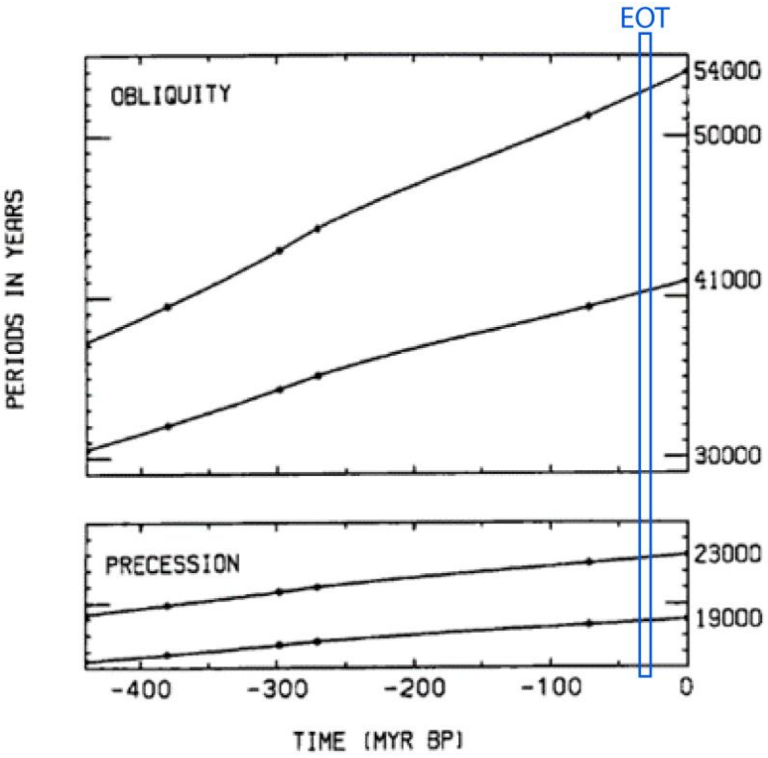

***Figure 40**: Estimations of obliquity and precession periods evolution during the past 450 Myr (Berger et al., 1989), showing the changes of obliquity and precession periods through time.*

The knowledge developed on orbital cycles allowed researchers to estimate the periodicity of orbital cycles through geological time. Although orbital motions are not truly cyclical but rather quasi-periodic, they are commonly accepted as “orbital cycles” or “Milankovitch cycles” by the scientific community. Le Verrier (1856) was the first to estimate the solution of Earth’s motion using linearized equations for planets orbits’ evolution. The first one to propose a theory of astronomically forced climate change was Milankovitch (1920, 1941), who quantified variations of insolation caused by orbital cycles through the past 600 kyr using Le Verrier’s (1856) solutions. His theory remained controversial to other climate modelers (Budyko, 1969; Sellers, 1969) before being correlated with cyclic variations observed in marine Pleistocene records of benthic foraminifera $\delta^{18}O$ (Hays et al., 1976; Imbrie et al., 1984), thus proving the legitimacy of his theory. After this discovery, other researchers started investigating astronomical solutions of the deeper past through calculation of trigonometric equations integrating gravitational interactions of high orders (Berger, 1978; Bretagnon, 1974). Berger et al. (1989) have shown that obliquity and precession periods have gradually increased in the past 450 Myr due to the increase of the Earth-Moon distance (**Figure 40**).

These solutions were based of the hypothesis of a steady Solar System, which has been proven untrue by Laskar (1989), even though they give good results for relatively short timescales (<1 Myr). Laskar (1999) showed that the solutions are divergent, notably because of the chaotic secular variations of telluric planets' orbits due to their low mass compared with gaseous planets. Other parameters are involved in the difficulty of establishing perfect solutions, such as the uncertainties on planetary masses, planetary positions, and effect of satellites. Overall, he estimated that the incertitude of astronomical solutions is multiplied by 10 for every 10 million years (Laskar, 1990). Over the past three decades, Laskar et al. (2011) worked to increase the precision of astronomical solutions and proposed the La2010 solution which gives precisely reconstituted movements precession and obliquity for the past 40 Myr, as well as for eccentricity for the past 50 Myr (**Figure 41**). However, the long eccentricity specifically has been stable for at least 215 Myr (Kent et al., 2018) and maybe even longer.

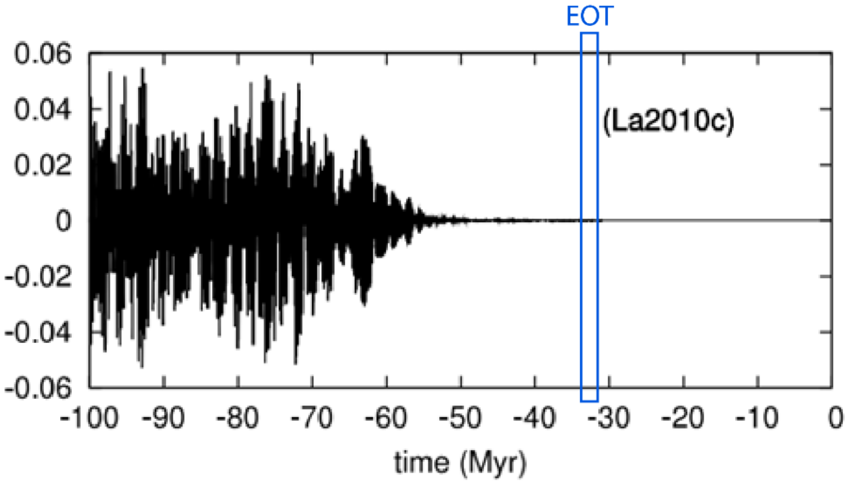

***Figure 41**: Estimate of the incertitude of the La2010c eccentricity solution (Laskar et al., 2011). This shows that the incertitude of the solution of eccentricity is negligeable before ~50 Ma, allowing for high-certitude astrochronology studies in this time interval.*

La2010 solutions can now be used to accurately investigate insolation variations through the Cenozoic at any given latitude. Where cyclic sedimentary alternations are continuously preserved (e.g. no major hiatus, stable SAR), their cyclostratigraphic investigation (**III.2.b : Cyclostratigraphy**) can provide precise dating of the sedimentary succession by correlating sedimentary patterns to orbital parameters, as well as providing insights on the paleoclimate and how it could have impacted the environment. In our period of interest, at the Eocene-Oligocene Transition, La2010a solutions show values of 400.2, 129.1, and 97.4 kyr for eccentricity, 52 and 39.6 kyr for obliquity, and 23.4, 22.1, and 18.9 kyr for precession (Laskar et al., 2011) (**Figure 42**). Therefore, the periods of the orbital cycles used to perform the interpretation of sedimentary cycles in this thesis are 400.2 kyr (long eccentricity), 97.4 kyr (main component of the short eccentricity), 39.6 kyr (main component of obliquity), and 21.5 kyr (average value of precession) (see **III.2.b : Cyclostratigraphy**). These periods give ratios in the time domain of 18.6 : 4.5 : 1.8 : 1. Knowing the precise durations of these cycles is important for the reliability of age models inferred from cyclostratigraphic investigations (**see III.2.b.iv : Orbital tuning**).

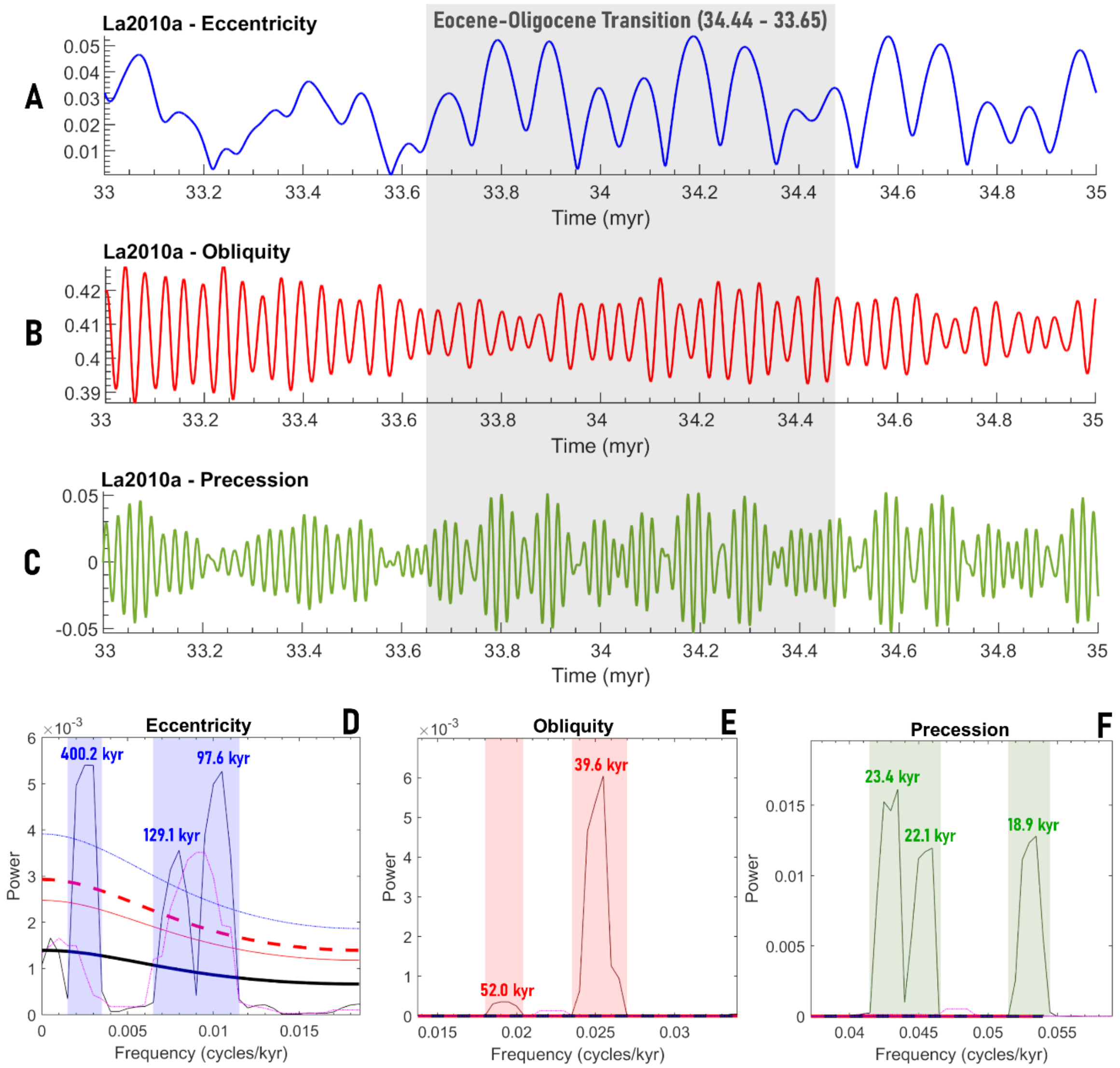

Figure 42*: (A, B, C) La2010a solutions of eccentricity, obliquity, and precession between 35 and 33 Myr (Laskar et al., 2011). (D, E, F) Spectral analysis (2piMTM) of the La2010a solutions between 35 and 33 Myr.*

II.4.c : The impacts of the astronomical forcing of insolation on climate and sedimentation

Changes in the Earth-Sun distance and in the inclination of the Earth's axis induced by orbital cycles influence the amount of insolation perceived at the top of the atmosphere, which then translate into climate change through the modification of several Earthen parameters (Berger, 1978; Schwarzacher, 1993) (**Figure 43**). Such climatic changes directly or indirectly control sediment production, transport, and accumulation, and can therefore be recorded by sedimentary environments under the right conditions (Strasser et al., 2006). They can also provoke vegetation cycles that can be observed through palynological investigations (Suc & Popescu, 2005). The position of the atmospheric circulation cells is influenced by insolation changes, which can provoke the latitudinal shifting of climatic belts (Matthews & Pelmutter, 1994). These changes influence the patterns and disposition of oceans, lakes, rivers, wind, glaciers, and vegetation, resulting in changes in sediment deposition. These changes provoke variations in freshwater and nutrient input through rivers, evaporation patterns, and water circulation in lakes and oceans, that are direct controls of organic and inorganic sediment production, lithologies, and water chemistry. These changes can be recorded by various proxies that are used by scientists to unravel Earth's climate past.

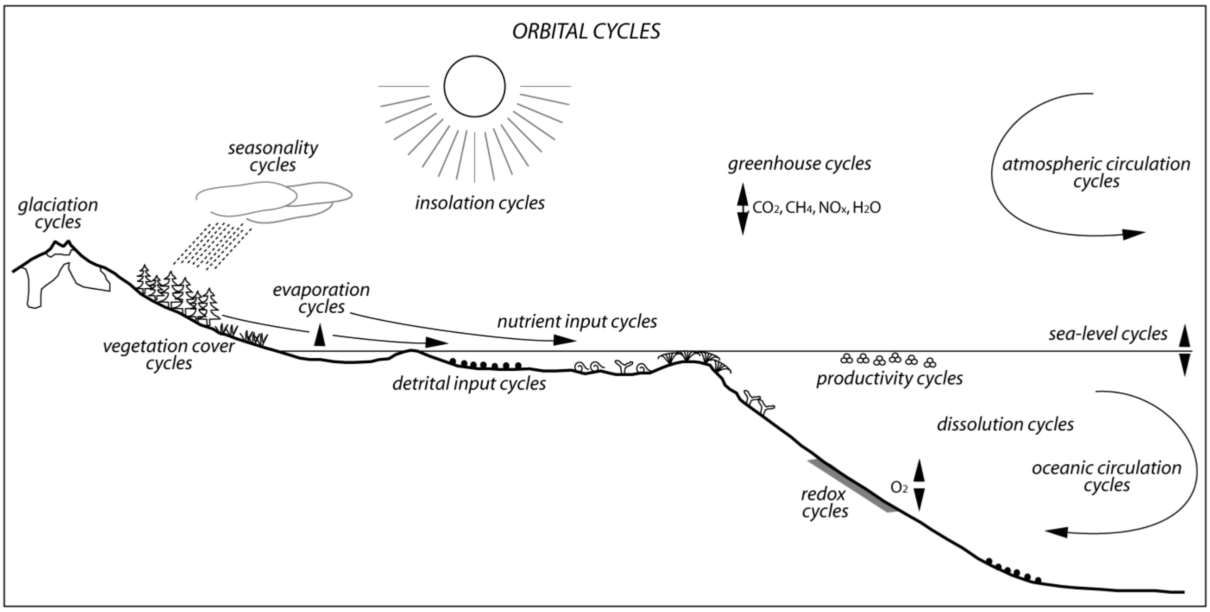

***Figure 43**: Schematic representation of Earth's systems and cycles influenced by orbitally induced insolation changes. Their modifications can be recorded by sedimentary environments. From Strasser et al. (2006).*

Due to the sedimentary nature of the URG through the Eocene and Oligocene, its sedimentary records are promising archives of orbital control on climate and sedimentary processes, particularly in the Mulhouse basin. They have been investigated using the tools and principles of cyclostratigraphy in order to study the impact of orbitally controlled climate change on continental environments, and to produce chronostratigraphic frameworks.

Chapter III : Material & Methods

III.1 : Material

The material used in this thesis consist of data from the literature, well-logs, core-samples, cuttings, mining documents, outcrops, and rock samples. The original geographical locations of the outcrops and boreholes from which materials originated are shown in Figure 44.

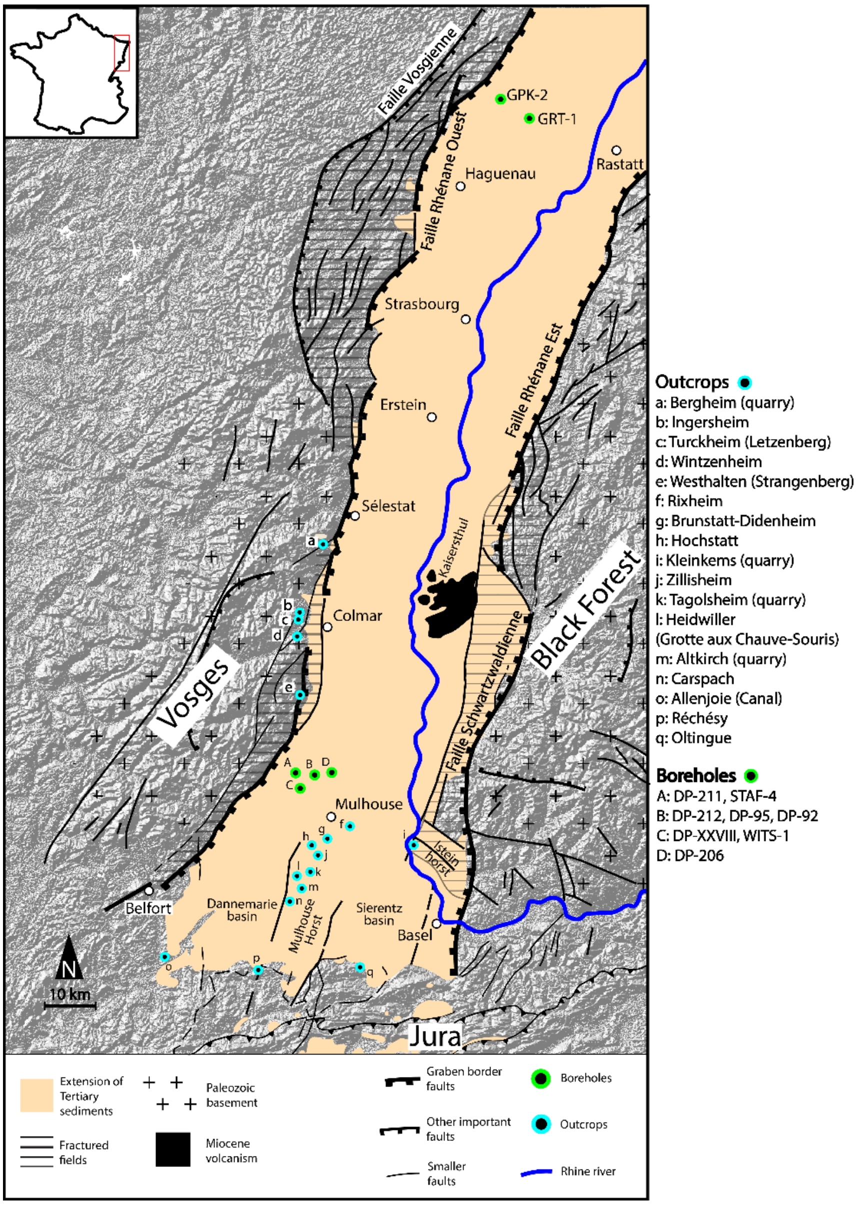

Figure 44: Location of the investigated outcrops and boreholes according to the structure of the Upper Rhine Graben, alongside structural faults.

III.1.a : Literature

Thanks to the exploration done in the URG through the past century, many scientists have been able to dwell into its sedimentology, geochemistry, and paleoclimatology. Several works, and in particular French state thesis, contain a lot of precious information on those topics. The main ones are the palynological investigations of Schuler (1988) (paleoclimate, paleoenvironments), the study of the Mulhouse basin of Blanc-Valleron (1990) (sedimentology, geochemistry), and the sedimentological investigations of the coastal conglomerates of Duringer (1988) (sedimentology, paleoenvironments).

III.1.b : Sub-surface data

III.1.b.i : Well-logs

Several well-logs have been investigated in the Mulhouse and Pechelbronn basins to investigate the sedimentology and the cyclostratigraphy of their sedimentary records. The main ones presented throughout this thesis are the well-logs of the DP-206, DP-211, and DP-212 wells of the Mulhouse basin (gamma-ray, neutron, sonic), and the well-logs of the GRT-1 and GPK-2 boreholes of the Pechelbronn basin (gamma-ray only) (**Figure 44**). Other well-logs available in the database of the BRGM (Bureau de Recherches Géologiques et Minières) were investigated, but not studied in great depths. Some well-logs from the Mulhouse basin were made available by the KALIVIE museum in Wittelsheim (France) and scanned at the Institut Terre et Environnement de Strasbourg. Numerical data was extracted from these scans using MATLAB scripts developed throughout the thesis (see Error! Reference source not found.Error! Reference source not found.).

III.1.b.ii : Core samples

Core samples from the DP-XXVIII borehole (**Figure 44**) of the Mulhouse basin were lent by the Musée d'Histoire Naturelle et d'Ethnographie de Colmar. They consist of a fragmentary record of the sedimentary history of the Mulhouse basin, with samples from the Jurassic, "basal Eocene", "Zone Salifère Inférieure", "Zone Salifère Moyenne", and "Série Grise" formations. Overall, around 356 core samples from the DP-XXVIII borehole were investigated. No samples from the "Zone Salifère Supérieure" have been saved from this borehole. Other core samples from the DP-95 borehole (**Figure 44**) were lent by the same museum, which consist of parts of the potash beds of the "Zone Salifère Supérieure" and nearby beds.

III.1.b.iii : Cuttings

Portions of cuttings from the GRT-1 and GPK-2 boreholes (**Figure 44**) of the Pechelbronn basin were given by ES Géothermie. These cuttings range from the "Couche Rouge" to the "Série Grise". There are 112 samples from the GRT-1 borehole and 66 samples from the GPK-2 borehole. Cuttings were sampled every 5 meters in the "Couches de Pechelbronn" and every 20 meters in the underlying and overlying formations. They were primarily used for geochemistry, palynology, and to make smear slides.

III.1.c : Outcrops

There are several outcrops still accessible at the time of writing this manuscript. Most of the accessible outcrops of the Haut-Rhin are ancient (or still active) quarries. A good portion of those outcrops are coastal alluvial fan deposits, also known as coastal conglomerates, which were extensively described by Duringer (1988). A substantial number of outcrops that were studied in the past are no longer accessible due to quarry resealing, revitalization, or privatization. The main investigated outcrops are the Altkirch quarry, Strangenberg quarry, Turckheim quarry, Tagolsheim quarry, and Kleinkems quarry (**Figure 44**). I was also able to study a mine gallery in Wittelsheim (~500m underground) to produce a sedimentary log and to collect samples. Several other outcrops were visited (**Figure 44**).

III.2 : Methods with emphasis on cyclostratigraphy

III.2.a : Sedimentology

Sedimentology (or sedimentary petrology) is a discipline of geology that deals with the nature and origin of sedimentary deposits (both present and ancient), the main objectives of which is the interpretation of the processes that resulted in their formation. Sedimentology is tightly related to other disciplines of geology such as geochemistry, paleontology, mineralogy, and to other sciences such as climatology, biology, and physics.

III.2.a.i : Petrography

Petrography is a discipline of petrology that deals with the detailed description of rocks, ranging from macroscopic descriptions of outcrops and rock/core samples to their microscopic descriptions, usually using a microscope.

Outcrops, core samples, and rock samples, were all investigated by performing macroscopic descriptions. Some core samples were investigated using a binocular magnifier. In the case of outcrops, when possible, a detailed sedimentary log was produced after the sedimentary successions were observed and measured. Clastic successions were logged using a granulometry scale (e.g. **Figure 66**), while carbonate successions were logged using a weathering scale (e.g. **Figure 71**).

Several thin sections of rock and core samples were made at the Institut Terre & Environnement de Strasbourg to study their microscopic features using a polarizing microscope. Cuttings from the GRT-1 and GPK-2 boreholes were used to make smear slides in order to measure their granulometry using the comparison chart for visual percentage estimation at different scales (sand, silt, clay) (Terry & Chilingar, 1955) (**Error! Reference s ource not found.**), and to document other possible observations (e.g. fossils). Smear slides were made using the classical protocol (Schnurrenberger et al., 2003).

III.2.a.ii : Interpretation of sedimentary structures and facies

A good part of the sedimentology work performed in this thesis deals with the identification of sedimentary structures, facies, and of their interpretation. Depending on many factors, including depositional environment and climate, sediments get deposited in all sorts of ways, forming sedimentary structures, the study which give information on said factors. As such, sediments deposited in aeolian, fluvial, lacustrine, and marine settings will tend to exhibit characteristic structures which allow their distinction from each other's. This is however not always true, and other investigations might be required to characterize them, such as geochemistry, paleontology, and palynology. For example, lacustrine and marine sediments can exhibit very similar sedimentary structures such as laminated mudstones, and only the presence of particular biomarkers, such as marine-acclimated dinoflagellate species, can help distinguish the original depositional environment. Primary sedimentary structures relate to transport and depositional processes that are used to identify depositional environments. The book "Sedimentary Structures" (fourth edition) of Collinson & Mountney (2019) served as a reference for the field observations, along with papers from the literature cited throughout **Chapter I** : In addition to sedimentary structures, the investigated sedimentary records were also studied to detail their compositional and textural features. They were grouped as lithofacies (commonly just "facies") with the idea that specific lithofacies or lithofacies successions are associated with specific environments (Reading, 2009).

III.2.a.iii : Sequence stratigraphy

Sequence stratigraphy is a branch of sedimentary stratigraphy that deals with the study of repetitive and genetically related strata within a chronostratigraphic framework, with particular emphasis on bounding surfaces. In the case of the Upper Rhine Graben, which used to be a mega-lake (or made of several lakes) throughout its Eocene and Oligocene history, sequence stratigraphy principles were notably used to interpret changes in sedimentary deposits in terms lake-level variations, sediment availability, and accommodation (Catuneanu, 2020). As such, the concept of transgressive-regressive sequences ("T-R Sequences") (Catuneanu, 2020; Johnson & Murphy, 1984; Embry & Johannessen, 1993) was applied to explain observations such as the mudstone-evaporite alternations of the Mulhouse basin ("Sel III", "Zone Salifère Supérieure") as well as the mudstone-sandstone and mudstone-conglomerate alternations of the Pechelbronn basin ("Couches de Pechelbronn"), along outcrop sequences. While the concepts of sequence stratigraphy are fully applicable to lacustrine sedimentary successions, the characteristics of lacustrine sequences are widely different from the classical marine ones (Bohacs et al., 2000). Rather than eustasy, the water level of lacustrine systems tend to be primarily controlled by climate, tectonics, and sediment supply. Furthermore, hydrologically closed lakes are usually profoundly influenced by climate (Olsen, 1984; Olsen, 1986; Jones et al., 2001). In the case of mudstone-evaporite alternations, mudstones are interpreted as the result of water-level rise related to increased precipitations during humid periods, inside which local maximum flooding surfaces are placed (**Figure 45**). Evaporites are interpreted as the result of water-level fall related to brine saturation during arid periods, inside which local maximum regressive surfaces are placed. In the Pechelbronn basin, local maximum flooding surfaces are placed in mudstones while local maximum regressive surfaces are placed in sandstones and conglomerates, similarly to the model of Duringer (1988).

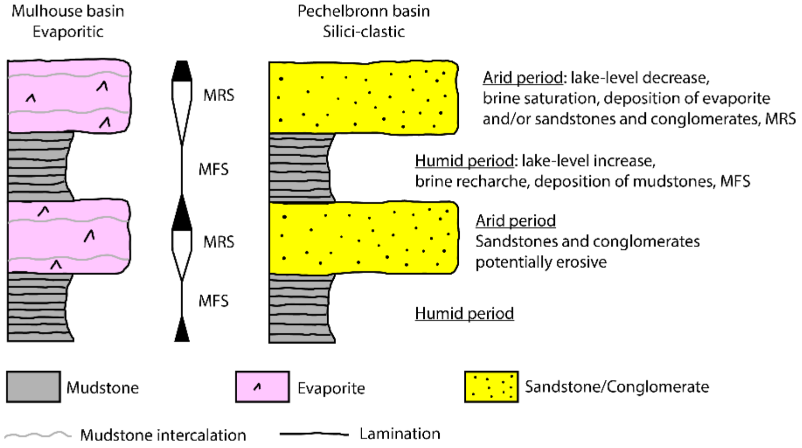

Figure 45: *Interpretation of the mudstone-evaporite alternations of the Mulhouse basin and of the mudstone-sandstone and mudstone-conglomerate alternations of the Pechelbronn basin in terms of sequence stratigraphy.*

III.2.b : Cyclostratigraphy

Cyclostratigraphy is the study of the stratigraphic records of cyclic environmental change (Fischer et al., 1990). Sedimentation can be impacted by various factors, including climate variations induced by astronomical forcing. Various methods, tools, and rules are used in cyclostratigraphy studies.

Since the first cyclostratigraphy studies, it has become clear that this subdiscipline can be rather subjective, due to the subjective aspects of signal manipulation and to certain quantitative approaches remaining debated (Hilgen et al., 2015). The Cyclostratigraphy

Intercomparison Project (CIP) (Sinnesael et al., 2019) has been launched to evaluate the robustness of the cyclostratigraphy methodologies and their dependance on the investigator using artificial cyclostratigraphic case studies. It has been noticed that no participant achieved the perfect solutions, but that the median solutions submitted by the investigators were very close to the correct result. The results differences are explained by the differences in the investigators' tools, experiences, and time dedicated to the project. The authors proposed flexible guidelines on what a good cyclostratigraphy should include, which are, in order: (1) a stratigraphic description, (2) an independent age model, (3) a paleoclimate proxy record, (4) an initial astronomical interpretation including data-series analysis in the depth-domain, (5) a conversion of the proxy data to the time-domain and its data-series analysis, (6) an astronomical forcing model, (7) an astronomical tuning, (8) a concluding astronomical interpretation, (9) an age model, (10) and an open access reporting for other researchers to reproduce and check the results and interpretations.

In this thesis, all low-frequency (= "Milankovitch") cycles were investigated through the signal analysis of gamma-ray depth-series. It is the measure of the natural radioactivity of rocks based on their potassium, thorium, and uranium content (gamma radiation) (Howell & Frosch, 1939). Based on their lithology and composition, different rocks will have different gamma-ray signatures, and the gamma-ray depth-series will therefore sometimes be enough to differentiate lithologies through depth. Shales tend to be more radioactive than other common lithologies such as sandstone (mature), gypsum, halite, dolomite, and limestone, due to potassium and thorium being important components of most shales. In the Mulhouse basin, gamma-ray depth-series are useful to differentiate shales and marlstones (high-value) from halite and gypsum (low-value), with potash seams having very high values.

III.2.b.i : Preliminary investigations for a cyclostratigraphy study

Not all sedimentary records are appropriate for cyclostratigraphy studies, therefore it is important to perform preliminary investigations to assess their suitability. One needs to make sure that the sedimentary record he wishes to perform a cyclostratigraphy analysis on respects the following criteria: decent (1) **completeness** and (2) **continuity**. Decent **completeness** implies that the record should not contain important hiatuses. While small hiatuses might not impact the cyclostratigraphy analysis too much (one might lose some small cycles signals but keep the longer ones), important hiatuses could completely erase some of the bigger orbital cycles from the record and falsify the age model. If an important hiatus is known, it is required to perform two separate cyclostratigraphy investigations under and above the hiatus. Therefore, some sedimentary environments such as proximal systems are not ideal for such investigations. Also, it is very important to be careful about faults, which are not always known and can greatly impact the cyclostratigraphy analysis as one might half or double a sedimentary succession in the record. A decent **continuity** implies that the Sediment Accumulation Rate (SAR) should stay relatively constant across the investigated record. The SAR can be impacted by various factors, including tectonic activity which usually is the biggest one. For example, important changes in SAR can cause the merging of the orbital cycles frequency bands in a periodogram. If the SAR change is sharp at a given depth, but globally continuous below and above that depth, two separate cyclostratigraphy investigations are required above and below that depth, and if there are no hiatuses, the two ensuing age models can be merged. It is not always possible to assess the completeness and continuity of a sedimentary record. For example, singular boreholes might not always have a detailed sedimentary description, and undetected faults and hiatuses could impact the completeness of the record. If a cyclostratigraphy analysis is performed on such boreholes, it is important to state what the potential issues are.

To produce the best cyclostratigraphy analysis possible, before getting into the signal processing, it is important to provide a detailed stratigraphic description of the sedimentary record, including its variations and patterns, and gather as much independent information about the age and duration of this record (e.g. biostratigraphy, radio-isotopic geochronology, magnetostratigraphy). Even if the available chrono-stratigraphy is not particularly precise, it can still give precious information to simplify the tuning of the record (see **III.2.b.iv : Orbital tuning**) and to avoid circular reasoning by providing and order of magnitude of the record's duration. It is also important to make sure that at least one decent paleoclimate proxy record is available for the studied sedimentary succession, and that its variations through depths coincide with the sedimentary patterns.

III.2.b.ii : Signal Analysis

There are multiple signal processing tools classically used in cyclostratigraphy studies. They include but are not limited to: (1) Multi-Taper Method (MTM), (2) evolutive Fast-Fourier Transform (eFFT), (3) Wavelet Transform, (4) Correlation Coefficient approach, and (5) Taner-Hilbert filter. In this thesis, I mostly used methods (1), (2), and (5). These tools are used at the various stages of cyclostratigraphy analysis and provide crucial results for the creation of an astronomical interpretation and age model. These signal processing tools and steps are demonstrated in the following simple artificial cyclostratigraphy case study. The artificial cyclostratigraphy case study corresponds to a simple record of marl-limestone alternations forced by precession (20 kyr) and modulated by obliquity (40 kyr) and short eccentricity (100 kyr). In the depth domain, the precession cycle corresponds to the 5m thick marl-limestone couplets (y_P), and the obliquity and short eccentricity cycles will correspond to the 10m (y_O) and 25m (y_e) cyclic trends (**Figure 46**).

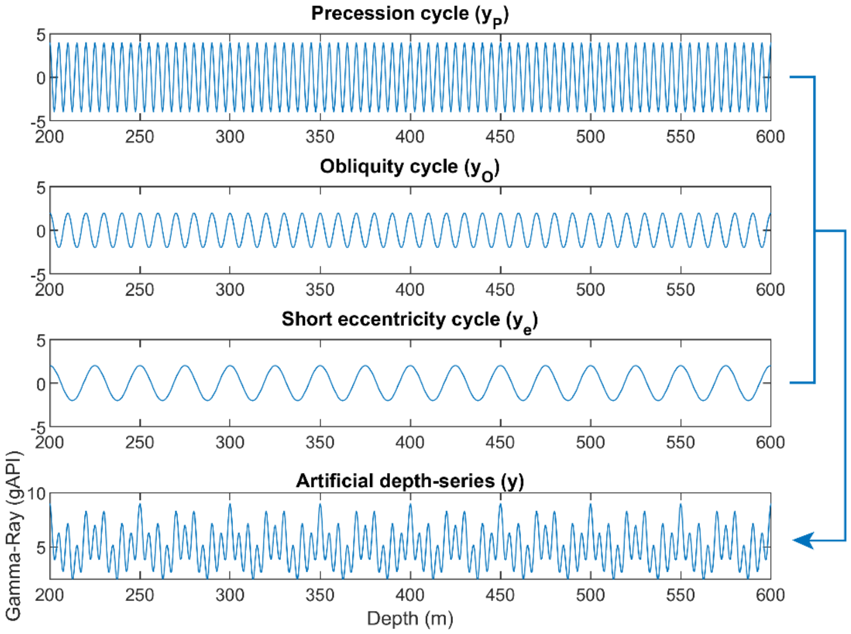

***Figure 46**: The components of the artificial depth-series (y), which will be considered as a gamma-ray well-log in a sedimentary succession made of marls (high gamma-ray signal) and limestones (low gamma-ray signal) alternations.*

$$x = 200:0.5:600$$

$$y_P(x) = 4\cos\left(x * \left(\frac{2\pi}{5}\right)\right)$$

$$y_O(x) = 2\cos\left(x * \left(\frac{2\pi}{10}\right)\right)$$

$$y_e(x) = 2\cos\left(x * \left(\frac{2\pi}{25}\right)\right)$$

$$y(x) = ((y_P + y_O + y_e) + 10)/2$$

Random noise is added to the y depth-series to make it more realistic and to show the importance of the signal processing tools to decipher cyclic components from noise (**Figure 47**). Visually, it is much harder to decipher noise from cyclic components in the noisy series.

$$y_{noise} = \left(y + \frac{50 * rand\big(1, length(y)\big) - 25}{4}\right) + 2$$

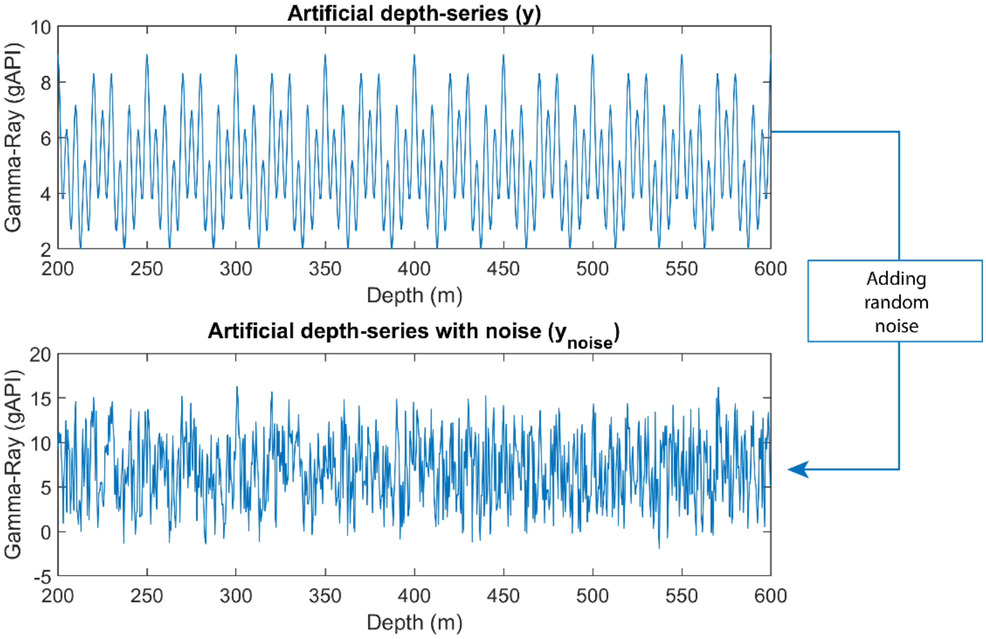

***Figure 47**: The upper graph shows the basic artificial depth-series (y) with the cyclic components only. The lower one shows the depth-series with noise added (y_{noise}).*

Prior to performing spectral analyses, the investigated series interpolated (generation of a uniformly spaced series from the original signal) and detrended using the tools made available in Acycle (Li et al., 2019). Paleoclimatic data-series can have secular trends that are of high amplitude and irregular, which cause the bulk of the data variability to be above or below the overall mean value (Rodionov, 2006). Detrending is used to remove such trends to ensure that the variability of the data oscillates around a zero mean, as well as avoiding power leakage from low-frequency components to high-frequency broadbands (Kodama & Hinnov, 2014). The artificial depth-series was detrended using the LOWESS method (35%).

Multi-Taper Method (MTM)

The Multi-Taper Method can be considered an amelioration of the Fourier Transform, as it overcomes its non-parametric limitations (Kodama & Hinnov, 2014; Weedon, 2003). While other spectral methods exist, such as the smoothed periodogram and Blackman-Tukey correlogram, the MTM method achieves the best trade-off between frequency resolution and statistical confidence (Thompson, 1982), and is therefore one of the most used tools in cyclostratigraphy. The Fourier Transform is a mathematical operation which consists in decomposing a signal in multiple sinusoids of given frequency and amplitude, in such a way that summing these sinusoids recreate the original signal. This operation only works for continuous signals that are sampled evenly (hence the use of interpolation). The MTM method outputs the frequencies of the investigated signal, and their powers. Red-noise modelling is used to detect the statistically significant cycles of the investigated signal using the robust AR(1) test (Mann & Lees, 1996; Thompson, 1982). The MTM analysis of the artificial noisy depth-series displays three main cycles with high statistical significance (>99% CL) of 26.7 m, 10.1 m, and 5.0 m (**Figure 48**). These are the three main cyclicities (y_e, y_O, y_P) of the artificial depth-series, with minor differences induced by noise. Other frequency peaks can be observed on the MTM plot and show one of the limits of the method; some peaks may originate from random noise and can lead to wrongful interpretations. To avoid making such wrongful interpretations, other methods, described throughout this section, are used (see **III.2.b.iii : Interpretation**).

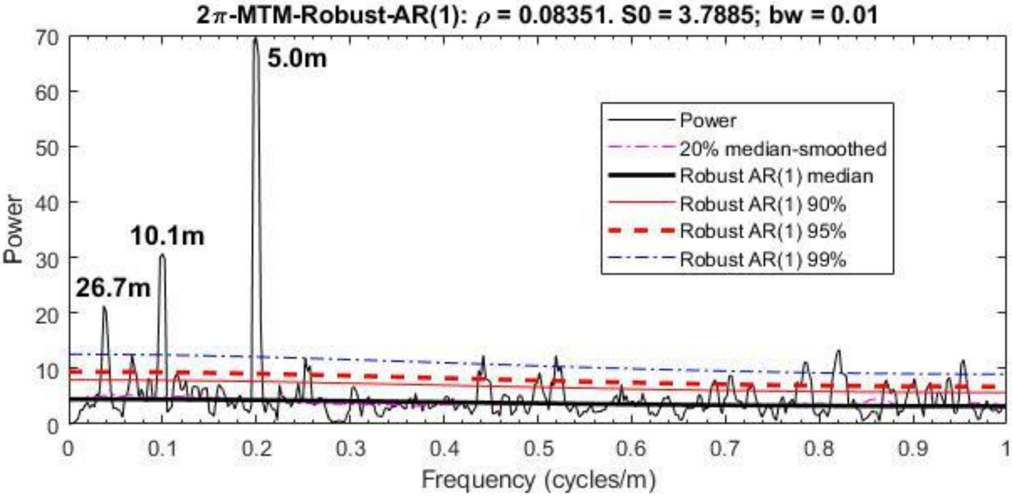

***Figure 48**: Multi-Taper Method (MTM) used on the artificial noisy depth-series using the Acycle software (Li et al., 2019). The three main cyclicities of the noisy depth-series are found with slight differences due to the noise. Some statistically significant cycles appeared, purely generated by the noise.*

Evolutive Fast Fourier Transform

The spectral power of a signal can very well vary with depth or time due to several factors, especially in the case of paleoclimatic data-series. Very often, part of the noise of a data-series is caused by variations of Sediment Accumulation Rates (SAR), which induces the smearing of the spectral power of a given cycle over several frequencies (Weedon, 2003). The Evolutive Fast Fourier Transform (EFFT) is a method that consists of producing a succession of Fast Fourier Transforms over short intervals. This is commonly known as a sliding window spectral analysis (Kodama & Hinnov, 2014). This method is used to visualize the evolution of frequencies across the whole investigated interval. As such, it allows to visualize the evolution of SARs across the investigated interval, as well as the presence of potential hiatuses, when they erase part of a cycle (and not the whole cycle). To visualize this, an artificial cyclic signal was made with an interval of decreased SARs, an interval of increased SARs, and a hiatus, and the EFFT was performed on it (**Figure 49**). The sliding window is a key tool of the EFFT and has to be carefully set. If it is too small, low-frequencies will not be detected, and if it is too long, high-frequencies will be overly smoothed.

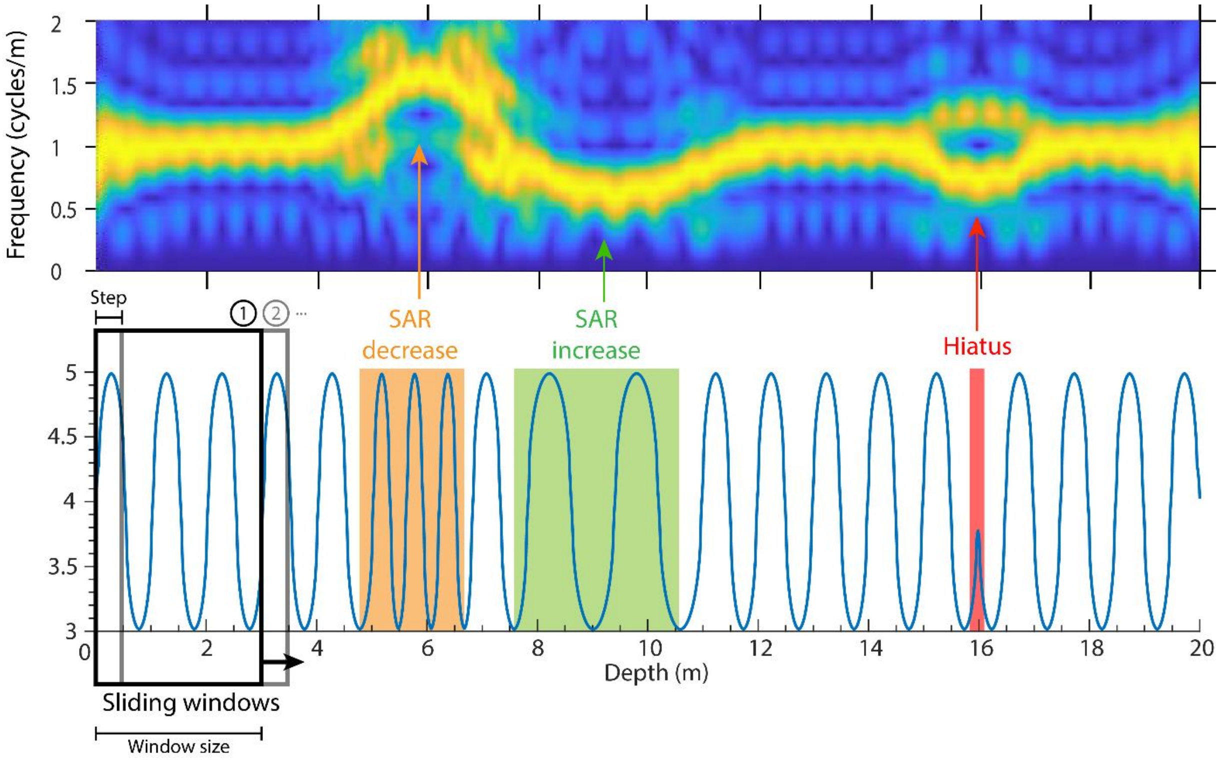

***Figure 49**: Evolutive Fast Fourier Transform (EFFT) performed on an artificial signal (lower part) to visualize the effect of SARs changes and hiatuses of the resulting plot (upper part). The sliding window has a size of 3 m and a step of 0.5 m.*

Filtering

Filtering is the process through which specific frequencies of a signal's spectrum get isolated. It is primarily used to isolate a cyclicity of interest from the surrounding noise, once the interpretation of said cyclicities are performed (see **III.2.b.iii : Interpretation**). There are three main types of filters which are the:

- Low-pass filter; used to isolate the low frequencies of a signal.
- High-pass filter; used to isolate the high frequencies of a signal.
- Band-pass filter; used to isolate a specific frequency bandwidth (e.g., isolating a Milankovitch cycle).

There are several band-pass filtering methods that are available, but the one used throughout this thesis is known as the Taner-Hilbert filter (Taner, 2000; Kodama & Hinnov, 2014), which is available in the Acycle software (Li et al., 2019). This filter is known as a frequency-domain filter, which are considered as the best-fitted for cyclostratigraphy investigations as they impose no time delay is the filtered output ("zero-phase"). The data are Fourier transformed to the frequency domain, multiplied by the filter, and inverse-Fourier transformed back to the original domain (usually either depth or time) (Kodama & Hinnov, 2014). To visualize this process, it was performed on the artificial noisy depth-series y_{noise} to extract the three original cycles (**Figure 50**). After filtering the three main components of the artificial noisy depth-series, the same number of cycles is found as those from the original depth-series without noise, but with varying amplitudes, due to the noise partially affecting the amplitude at the original cycles' frequencies (**Figure 50**).

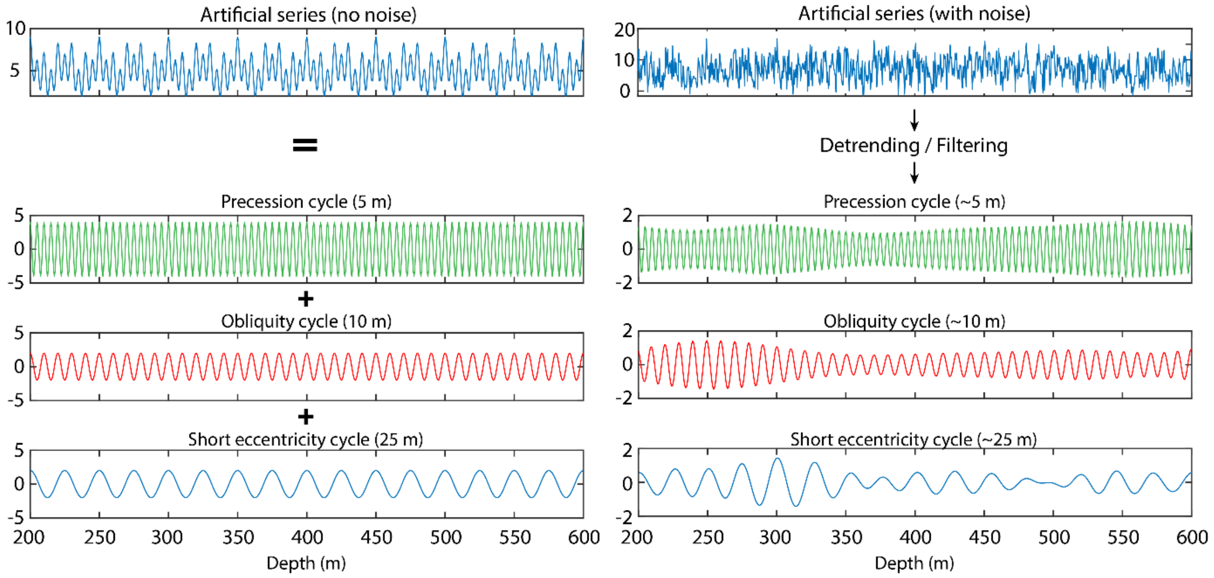

***Figure 50**: (Left) Artificial depth-series without noise with its three main components and (Right) artificial depth-series with considerable noise and the filters of the three main cycles that appeared on the MTM plot (**Figure 48**). The amplitudes of the filtered cycles variates through depth due to the noise.*

III.2.b.iii : Interpretation

The interpretation of spectral analysis results is the most crucial part of the cyclostratigraphy process, and precautions must be taken when doing so because of some phenomena. Firstly, any signal, even if made of totally random numbers, will show some sort of cyclic component once analyzed. This phenomenon can be observed on MTM analysis of the artificial depth-series (y_{noise}), on which frequency peaks appear that are not related to the three main cycles (**Figure 48**). With real data, the investigator must make sure not to wrongfully interpret such peaks induced by noise, even more so that in the real world, noise can be much more prevalent. Secondly, changes in SARs can cause frequency peaks to potentially spread and merge with one-another, it is therefore very important to perform an EFFT (or equivalent) to document the evolution of SARs through depth or time. If such a shift is observed, it might be necessary to divide the section into two parts to investigate separately.

Several methods have been proposed to avoid the misinterpretation of spectral analysis results (Weedon, 2003; Kodama & Hinnov, 2015). In the case of depth-series, the spectral analysis results will consist in sedimentary cycles (in meters) with varying confidence levels (robust AR(1) test curves). It is not possible to directly attribute sedimentary cycles to climatic cycles due to the imprecision of geological timescales. The main method consists in comparing the ratios of sedimentary cycles in the depth-domain with climatic cycles in the time-domain. Milankovitch cycles have a known period in the time-domain, and their evolution through time is known for a relatively small portion of Earth's history. The movements of precession and obliquity are well known for the past 40 Myr, and that of short eccentricity for the past 50 Myr, while that of the long eccentricity has been stable for me than at least 215 myr (Kent et al., 2018; Waltham, 2015; Laskar et al., 2011) (see **II.4.b : Astronomical solutions**). Across the Eocene and Oligocene, the average values of the Milankovitch cycles are 400.2 kyr (long eccentricity), 97.4 kyr (main component of the short eccentricity), 39.6 kyr (main component of obliquity), and 21.5 kyr (average value of precession), resulting in ratios in the time domain of 18.6 : 4.5 : 1.8 : 1 (Laskar et al., 2011). Therefore, if the ratios between the investigated sedimentary cycles are equal (or close enough) to these ratios, they can be attributed to the Milankitch cycles. When there is little to no noise, this can be done directly by the investigator. However, when noise is too important, it can be useful to use automated methods such as the

Correlation Coefficient (COCO) and its evolutionary counterpart (eCOCO). These methods can be used to test for astronomical forcing in paleoclimate data-series, as well as the average sedimentation rates (Li et al., 2018; Li et al., 2019).

III.2.b.iv : Orbital tuning

Orbital tuning is the process through which thicknesses are converted to timescales. Once the sedimentary cycles are attributed to Milankovitch cycles (or any other climatic cycle of known duration), orbital tuning is possible. The sedimentary cycle is filtered, and each of its repetitions are attributed to a given duration. For example, if a sedimentary cycle of 40 m is attributed to the long eccentricity, each repetition of this 40 m cycle will be counted as 400.2 kyr. This method creates anchor points in the depth-series that are attributed to durations, which allow for its conversion in the time domain (the data-series can be plotted through time instead of depth). Once the conversion is done, spectral analysis is performed again on the now time-series to check for its quality, as the Milankovitch cycles are expected to appear clearly on the MTM and EFFT. This creates what is known as a flying age model, which duration is known but which position in the geological timescale is not anchored. When the climate signal is nicely recorded in a paleoclimatic data-series, it is sometimes possible to directly correlate sedimentary (or time) cycles with the astronomical solutions' curves (Laskar et al., 2011), which can be done visually. Alternatively, if absolute ages, or bio-stratigraphic ages are known in the data-series, it is possible to anchor the flying age model on it.

III.2.c : Palynology

Palynology encompasses the study of organic-walled microfossils known as palynomorphs and is an interdisciplinary science between earth sciences and biological sciences. Palynomorphs notably include pollen grains, spores, and dinoflagellate cysts, amongst other groups. In geology, palynology can be used to document the depositional paleoenvironment of sediments, as well as the regional paleoclimate along which they were deposited. Several species can also be used as age indicators. In this thesis, pollen grains and dinoflagellate cysts were investigated. Pollen grains give insights on the regional continental paleoclimates and paleoenvironments, while dinoflagellate cysts, being mostly marine species, give insights on the paleoenvironment (notably on the occurrence of marine incursions and transgressions in intra-continental settings).

Pollen is the microspore wall of seed plants, plus the gametophyte that develops inside of it (Traverse, 1988). As such, its definition is functional rather than morphological. It is the male mobile element produced by flowers, eventually let loose and transported by wind, some of which ending up in sediments. The outer microspore wall is what survives as a fossil. There are many different morphologies of pollen grains, which can be attributed to specific families and species. On the assumption that Tertiary plant taxa lived under similar conditions than their nearest living relatives, paleoclimatic reconstructions are sometimes possible (Mosbrugger & Utescher, 1997). **Dinoflagellate cysts** are produced by single-celled algae classified as Pyrrhophyta, and form a large part of microphytoplankton, mostly found in marine environments, but also less commonly in brackish and freshwater environments. Due to their rapid evolution starting from the Jurassic, many species have been attributed to very specific time intervals, making them valuable tools for the age dating of strata (Williams et al., 2004). Furthermore, they also are valuable tools for the interpretation of depositional environments, as several families are known to live under specific conditions (Pross & Brinkhuis, 2005; Sluijs et al. 2005).

Rock and cutting samples were processed at the Institute of Earth Sciences at the University of Heidelberg. 1 to 5 grams of rock were processed through standard palynological preparation techniques, including HCl, NaOH, and HF treatment, sieving (10 µm), and mounting on glass slides using glycerol gelatin. Furthermore, the samples were spiked with established quantities of *Lycopodium* spores (Batch No. 050220211) to allow the calculation of absolute concentrations. Also, a few samples were treated through acetolysis.

Different families and species of pollen grains (**Figure 104**) and dinoflagellate cysts (**Figure 105**) were photographed and identified by comparing their characteristics with those from the palynomorphs plates of Schuler (1988), photographs from the palynological database (PalDat) (Weber & Ulrich, 2017), dinoflagellate cysts photographs and drawings from the synthesis of Williams et al. (2004), amongst other photographs and drawings of palynomorphs from papers cited throughout this manuscript.

At least 100 pollen grains were counted per slide, when possible, alongside *Lycopodium* spores. Some slides were very poor in pollen, and in such cases the whole slide was investigated to get as much as possible. *Lycopodium* spores where not counted is such cases. The results are plotted as percentages of the main botanic families. Once a good enough number of pollen grains were counted, the whole slide was investigated for the presence of dinoflagellate cysts.

Dinoflagellate cysts were only present as very few individuals in each slide, apart from one slide with >20 counts of *Deflandrea phosphoritica* specifically. As such, statistics of dinoflagellate cysts proportions were not possible to do, so their occurrences only were acknowledged. A table synthetizing the time ranges and living environments of the identified dinoflagellate species was produced to document depositional environments and occurrence of marine incursions and/or transgressions based on their occurrences (**Table 6**).

III.2.d : Paleomagnetism

Paleomagnetism is the study of the Earth's past magnetic field preserved in rocks, sediments, as well as in archeological findings (Kodama, 2012; Chree, 1911). The basic principle of paleomagnetism is that some minerals become magnetized parallel to the Earth's magnetic field, and that this magnetization is preserved once the material in which they are a part of hardens (e.g. rock, pottery). In the case of sediments, magnetic minerals are reworked from pre-existing rock formations and are deposited elsewhere. They then become aligned with Earth's magnetic during and/or soon after deposition. Earth's magnetic field is dipolar, which means that it possesses two poles, and approximately forms what is known as a magnetic dipole. It exists due to convection currents occurring in Earth's outer core (containing molten iron and nickel) which generate electric currents (Elsasser, 1956; Cowling, 1981). Throughout Earth's history, the dipole field has been reversed many times, causing flips between the magnetic North and South, due to complex changes in the outer core's convection movements. These polarity reversals are (1) rapid and globally synchronous, and are (2) not predictable, meaning that they yield unique reversal patterns (Langereis et al., 2010). These characteristics make paleomagnetism a robust tool for geochronology, as many of those past reversals are known and dated. When such reversals are found in a sedimentary record, they can be used to date these sediments, usually paired with other age estimates (e.g. biostratigraphy, radiometric dating). I attempted to find such reversals in sedimentary outcrops of the Upper Rhine Graben to attempt to locate the Eocene-Oligocene boundary, as an inversion (from inverse to normal) occurs slightly before the end on the EOT in the C13 chron, after the Eocene-Oligocene boundary (**Figure 37**).

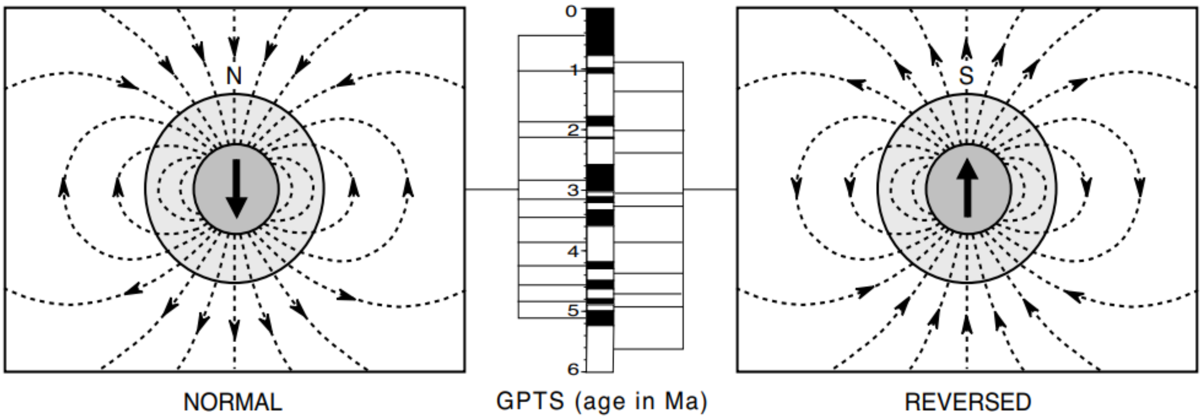

Figure 51: Schematic representation of Earth's axial dipole and of its geomagnetic field. Normal refers to modern-like polarity where the North and South magnetic poles are located near the geographic poles. During reversed intervals, the North magnetic pole is at the geographic South pole, and the South magnetic pole at the geographic North pole. On the geologic timescale, normal intervals are represented as black rectangles, and reversed intervals as white rectangles. From Langereis et al. (2010).

Small cores were sampled from several outcrops using an electric hand drill. The orientation of each sample was measured using a compass mounted on an orientation stage. The position of each core samples are detailed on sedimentary logs in **Chapter I :**

Investigation of the accessible sedimentary records of the Upper Rhine Graben and in **Chapter VIII : Paleomagnetism measurements**. Core samples were analyzed at the Archeo-Paleomagnetic laboratory of Géosciences Rennes. They were gradually heated to thermally demagnetize them using an MMTD-48 oven, and their magnetic susceptibilities were measured using a Bartington MS2. The results were reported on orthogonal plots (also known as Zijderveld diagrams) (Zijderveld, 2013; Zijderveld, 1967), on which the inclination and declination of the samples are shown at the different steps of the demagnetization process. Such diagrams allow for a clear visualization of the demagnetization path of the sample, which ultimately gives the orientation of the magnetic field at the time of deposition. However, rocks to not always record the orientation of the magnetic field in which their where deposited in. Throughout diagenesis, depending on the depth and geothermal gradient, rocks can reach relatively high temperatures, which can cause the partial melting of some of their parts, causing the magnetic minerals to re-align according to the actual field.

III.2.e : Geochemistry

Geochemistry is the science used to explain the mechanisms underlying Earth's primary geological systems using the tools and principles of chemistry. All measurements were done at the Institut für Geologie at the University of Bern.

III.2.e.i : Total Organic Carbon

Total Organic Carbon (TOC) refers to the amount of carbon found in the organic compounds of a rock sample expressed as a weight percent. It is a proxy for the total amount of organic matter found in a rock sample. Values above 2% are considered interesting in terms of petroleum exploration, but not all organic matter will be capable of generating hydrocarbons. TOC is an important element to document for the reconstruction of paleoenvironments and paleoclimates, and is notably used along with nitrogen and sulfur to investigate the organic matter source and the salinity of the water environment it was deposited in.

III.2.e.ii : Total Inorganic Carbon

Total Inorganic Carbon (TIC), in geology, refers to the amount of non-organic carbon found in a rock sample. It usually derives from simple compounds such as carbonates (CO_3^{2-}) and can thus be used as a proxy of carbonate content. In lacustrine environments, the deposition of carbonates is often associated with semi-arid conditions, as carbonate concentration could be too dilute in humid conditions, and overly dry conditions could cause the inability to maintain perennial water bodies (Tanner, 2010). In the geological record, lacustrine carbonates can be associated with evaporites (Warren, 2016). However, the presence of carbonates in lacustrine settings is not an indicator of climate by itself, as lakes are also controlled by very local parameters, and pre-existing carbonates could easily be reworked from the nearby topography. In the Upper Rhine Graben for example, Jurassic limestones that were on the rift shoulders were one source of carbonated material for the basins, and fragments of these limestones are found as clasts in coastal conglomerates and sandstones (Duringer, 1988). Some lacustrine carbonates of the Upper Rhine Graben were deposited under tropical conditions (Schuler, 1988).

III.2.e.iii : C/N ratio

The ratio of total organic carbon over total nitrogen (C/N) is a geochemistry method which can be used to decipher the origin of the organic matter between a terrigenous source (vascular land plants, $C/N > 20$) and in situ lacustrine/marine production (aquatic algae, $4 < C/N < 10$) (Lamb et al., 2004; Thornton & McManus, 1994; Prahl et al., 1980; Bordovskiy, 1965). This significant difference in C/N ratios is mainly the cause of the lack of cellulose $(C_6H_{10}O_5)_n$ and of the greater number of proteins in algae in comparison with vascular land plants. Some precautions should be acknowledged when interpreting C/N results. (1) Materials from all sources are subject to decomposition processes, which can result in the convergence of the C/N ratios, thus making the sources undistinguishable in some cases. (2) There might be a granulometric control on the C/N ratios, with coarse grain sediments having higher C/N ratio and fine grain sediments having lower C/N ratios (Bordovskiy, 1965). (3) Other organic matter sources might impact the C/N ratio (Roman, 1980; Bordovskiy, 1965).

III.2.e.iv : C/S ratio

The ratio of total organic carbon over total sulfur (C/S) is a geochemistry method used to distinguish marine/brackish sedimentary rocks from freshwater sedimentary rocks (Berner & Raiswell, 1984). This method is based on the principle that much more diagenetic pyrite is formed in organic rich marine/brackish sediments compared to organic rich freshwater sediments as higher concentrations of dissolved sulfates are found in marine/brackish waters. H_2S is derived from the bacterial reduction of dissolved sulfate under anoxic conditions (Berner & Raiswell, 1983).

$$2CH_2O + SO_4^{=} \rightarrow H_2S + 2HCO_3^{-} \#(\quad)$$

Sedimentary pyrite forms from the reaction of H_2S with detrital iron minerals during early diagenesis.

$$FeS + H_2S \rightarrow FeS_2 + H_2 \#(\quad)$$

Berner & Raiswell (1984) tested the C/S method on marine and freshwater sedimentary rocks and showed that marine rocks are characterized by low C/S values (0.5 – 5) while freshwater rocks are characterized by high C/S values (>10). The C/S ratio could be used to distinguish marine from brackish sedimentary rocks when the brackish water salinity is lower than half the salinity of marine water. When above half the salinity of marine water, pyrite formation is no longer limited by sulfates, thus making the C/S ratio independent from salinity. Several precautions are to be considered before using the C/S method (Berner & Raiswell, 1984). (1) It should not be applied to rocks low in organic carbon (<1%) or too rich in organic carbon (>15%). (2) It should not be applied to nearly pure limestones as they won't contain enough detrital iron minerals. (3) Total sulfur should represent mainly pyrite. (4) Analyzed rocks should have undergone little to no weathering.

Chapter IV : Investigation of the accessible sedimentary records of the Upper Rhine Graben

This chapter provides details on the sedimentology of the Upper Rhine Graben through the lens of cores samples, well-logs, outcrops, and of a mine gallery, which are mostly located in the southern URG. Core samples are from the DP-XXVIII and DP-95 exploration wells. The well-logs presented here are from the STA-4 and WIL-1 boreholes. The main investigated outcrops are located in Turckheim (Letzenberg), Westhalten (Strangenberg), Altkirch (quarry) and Tagolsheim (quarry). The visited and studied mine gallery is located ~500m underground at the Joseph-Else well in Wittelsheim. Other core samples from various boreholes presented here are displayed at the KALIVIE museum in Wittelsheim.

IV.1 : Investigation of the Mulhouse basin through the study of core samples, well-logs, and of a mine gallery

IV.1.a : Localization and history of the boreholes

The DP-XXVIII borehole, located in Wittelsheim (47° 48' 22'' N, 7° 15' 29'' E) (**Figure 44**) was drilled between the 13th of October 1949 and the 24th of November 1951 by the Mines Domaniales de Potasse d'Alsace (MDPA). This 1948.6m deep borehole was made to investigate the oil potential of the Jurassic limestones and was completely cored. Back then, and for many boreholes, geologists described the whole sedimentary successions as the cores were being extracted, and these descriptions are nowadays available in textbooks saved by the Kalivie Museum, or sometimes as digital files on the website of the Bureau de Recherches Géologiques et Minières (BRGM). The core samples of the DP-XXVIII borehole were wrapped in plastic and paper sheets and stored in wooden boxes. Before being partially saved by the Musée d'Histoire Naturelle et d'Ethnographie de Colmar, these boxes were most likely stored in a shed without temperature and moisture management, which damages the samples through time. Some samples such as halite are very damaged (almost completely reprecipitated), while others such as limestones are almost completely intact. These samples are fragmentary.

The DP-95 borehole, located in Wittenheim (47° 49' 11'' N, 7° 17' 16'' E) (**Figure 44**) was made between the 13th of November 1962 and the 28th of November 1962 by the MDPA. This borehole was 816.00m deep and reached the "Zone Salifère Moyenne". The goal of this borehole was to reach the potash seams. The only cores left of this borehole are those of the potash seams.

The well-logs of the STAF-4 and WITS-1 boreholes (**Figure 44**) were used to perform correlations with the DP-XXVIII borehole in order to provide additional details on the sedimentary succession of the Mulhouse basin. These correlations are available in the Supplementary Material (**Figure S1**).

IV.1.b : Study of core samples, well-logs, and mine gallery

Most of the samples described here are from the DP-XXVIII well, for which I made a detailed sedimentary log of the whole succession based on my observations and on the original descriptions of the MDPA (**Figure S2**). In the resistivity column of the presented well-logs, the three curves likely represent, from left to right, the Micro Focused Log, Laterolog shallow, and Laterolog deep, even though it is not clearly depicted on the original documents (**Figure S1**). Lithofacies descriptions, interpretations, and associations are documented in **Table 1**.

IV.1.b.i : Jurassic

Cores of the Jurassic formations recovered from the DP-XXVIII borehole were located between depths of 1893.5m and 1939.9m. According to the original documents, they are attributed to the upper Bathonian (1937.3m – 1948.6m), Callovian and Oxfordian (1793.6m – 1937.3m). Most of the retrieved core samples from the DP-XXVIII well consist of dark-grey limestones and dolomites (**Figure 52**). Their dark taints are due to their rich content in organic matter. Across the URG, several coring projects were dedicated to the investigation of the oil-potential of these formations: while they sometime produced oil, it was never enough for industrial exploitation. The DP-XXVIII well was initially cored to assess the oil potential of the Jurassic (Sittler, 1972).

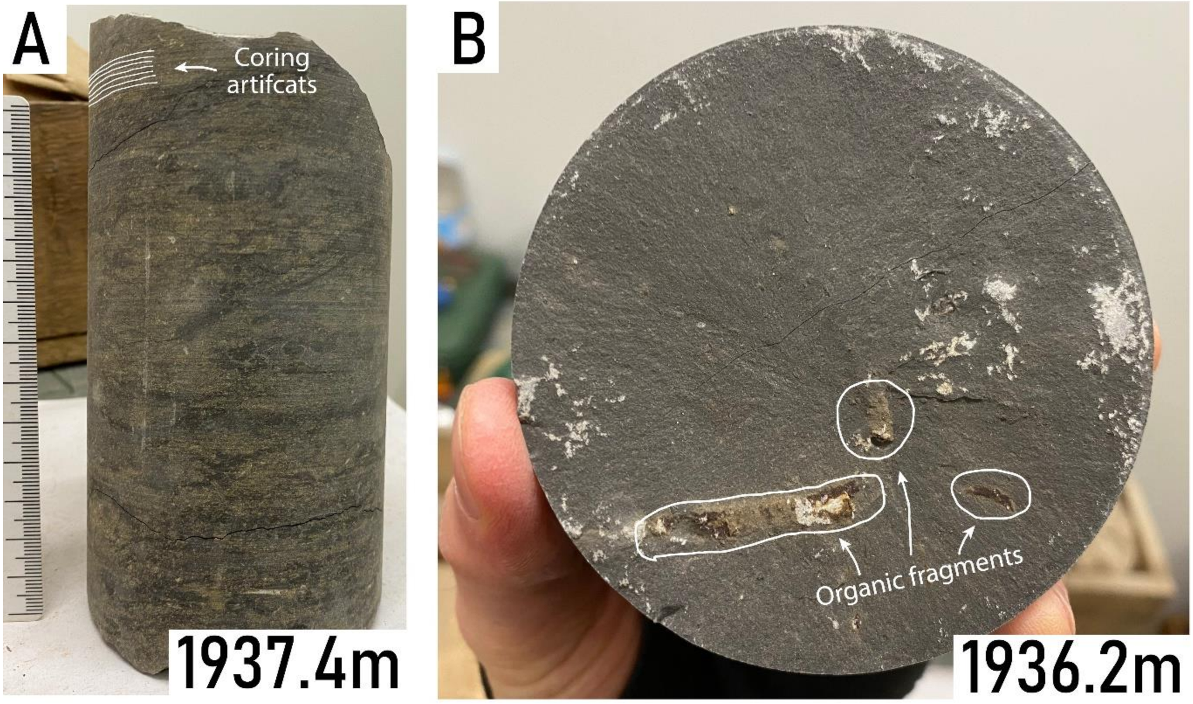

***Figure 52**: Representative selection of retrieved core samples from the Jurassic. (A) Dark-gray clayey dolomite. (B) Dark-gray clayey dolomite with organic fragments.*

While missing from the retrieved cores, the original document assesses the presence of Malm (1764.6m – 1793.6m) under the first Tertiary sediments. In other localities, Tertiary sediment can be in contact with other units of the Jurassic units such as the “Grande Oolithe” in Turckheim (**Figure 66**). The “Grande Oolithe” is a very characteristic unit in the URG, consisting of a limestone made of oolites, which is attributed to the Dogger.

The STA-4 and WIL-1 wells reached slightly deeper than the DP-XXVIII well and reached the “Grande Oolithe” which is described as dolomitic. In these same wells, the upper Bathonian is described as mostly made of marly fossiliferous limestones with grey marls in its lowermost part. The Callovian consists of dark-grey clayey marls in the lower-half, and of gray marl-limestones alternations in the upper-half. The Oxfordian is described as a massive homogenous unit made of dark-grey and slightly micaceous marls (**Figure S1**).

While the transition between the Jurassic and Eocene is missing from the recovered cores, the original core description accounts for a clear limit between a grey limestone with corals (Jurassic) and colorful marls and clays with detrital elements (Lutetian).

IV.1.b.ii : Basal Eocene

The “Basal Eocene” is 72.25m thick in the DP-XXVIII borehole, 81m thick in the STA-4 borehole, and 105m thick in the WIL-1 borehole. The “Basal Eocene” is classically described as red lateritic and karstic marls and clays. They form an unconformity on the Jurassic basement and can be found in karsts, such as it can be seen in the Kleinkems quarry in Germany (Duringer, 1988).

In the DP-XXVIII well, the deposits of this formation mostly consist of highly bioturbated red clayey limestones. According to Dunham’s classification of carbonate rocks (Dunham, 1962), the studied samples are mostly mudstones (**Figure 53**: A, B, C), which implies a low-energy depositional setting of calm water and inhibition of grain-producing organisms. Most samples are very bioturbated, and several contain deformed laminations and/or anhydride nodules. In most samples, when laminations are present, their boundaries are indistinct due to strong bioturbation. Bioturbation structures mainly consist of galleries, shafts, and trails (vertical and horizontal) (**Figure 53**: A, B, C). The intense bioturbation observed through all the “Basal Eocene” suggests that the lake was holomictic and/or shallow as a lot of oxygen must have been available at the sediment-water interface to allow the trace makers to survive and disturb the sediments over a long period of time. A few samples from this formation are conglomerates and sandstones, in which clasts mostly consist of Jurassic limestone fragments. There are ortho-conglomerates (**Figure 53**: F, G) and pebbly mudstones (or para-conglomerates) (**Figure 53**: D, E), with clasts of various sizes. All the clasts seem to originate from Jurassic limestone formations. While clayey limestones suggest deposition in a relatively calm lacustrine environment, the presence of sandstones and conglomerates implies that some processes enabled the input of thicker material far into the lake, which could have been forced by climate changes and/or tectonic activity. An interesting succession of ortho-conglomerates, pebbly mudstones, sandstones, and mudstones is contained between 1710.1m and 1709.3m (Figure S2). This interval starts with a pebbly mudstone (~50% mud matrix) containing thick and rounded limestone clasts (~50%) (**Figure 53**: D) (deposited through gravity processes) which is fining up towards a clayey mudstone. This clayey mudstone is eroded by an orthoconglomerate which is followed by a complex stack of stratified ortho-conglomerate and coarse sandstone layers (deposited through sub-aqueous fluid processes) (**Figure 53**: F), which is fining up towards a mudstone (**Figure 53**: G). This mudstone is also eroded by an ortho-conglomerate which is fining up towards a laminated and bioturbated mudstone. While there appear to be three distinct fining up sequences, the core is not continuous so there could be more sequences in the missing sections. Some other sandy and pebbly samples are found close to this interval (**Figure S2**). Also, some samples are dolomitic, but they display the same bioturbated facies as most samples of this formation.

Due to the relative roundness of the clasts, along with the high proportion of bioturbated clayey limestones, the depositional environment of the “Basal Eocene” formation in this area is interpreted as consisting of a persistent shallow-water and/or holomictic lake with active axial rivers and/or alluvial-fans which sometimes reached into the basin, and mostly only reworked Jurassic formations' rocks at that time. In particular, the stratified sandstones and orthoconglomerates of sample 1709.4m appear to be typical river channel deposits, while the pebbly mudstones (**Figure 53**: D, E) could be indicators of debris flows, potentially driven by floods and/or gravity processes. Therefore, it is possible that the rifting phase (or preliminary subsidence) started during the Lutetian as there likely was a non-negligeable altitude difference between the basin and the nearby Jurassic formations. Furthermore, the exclusive presence of Jurassic limestone clasts suggests that the rifting was young enough that surrounding rivers did not form valleys cutting through the whole Jurassic and reaching underlying formations.

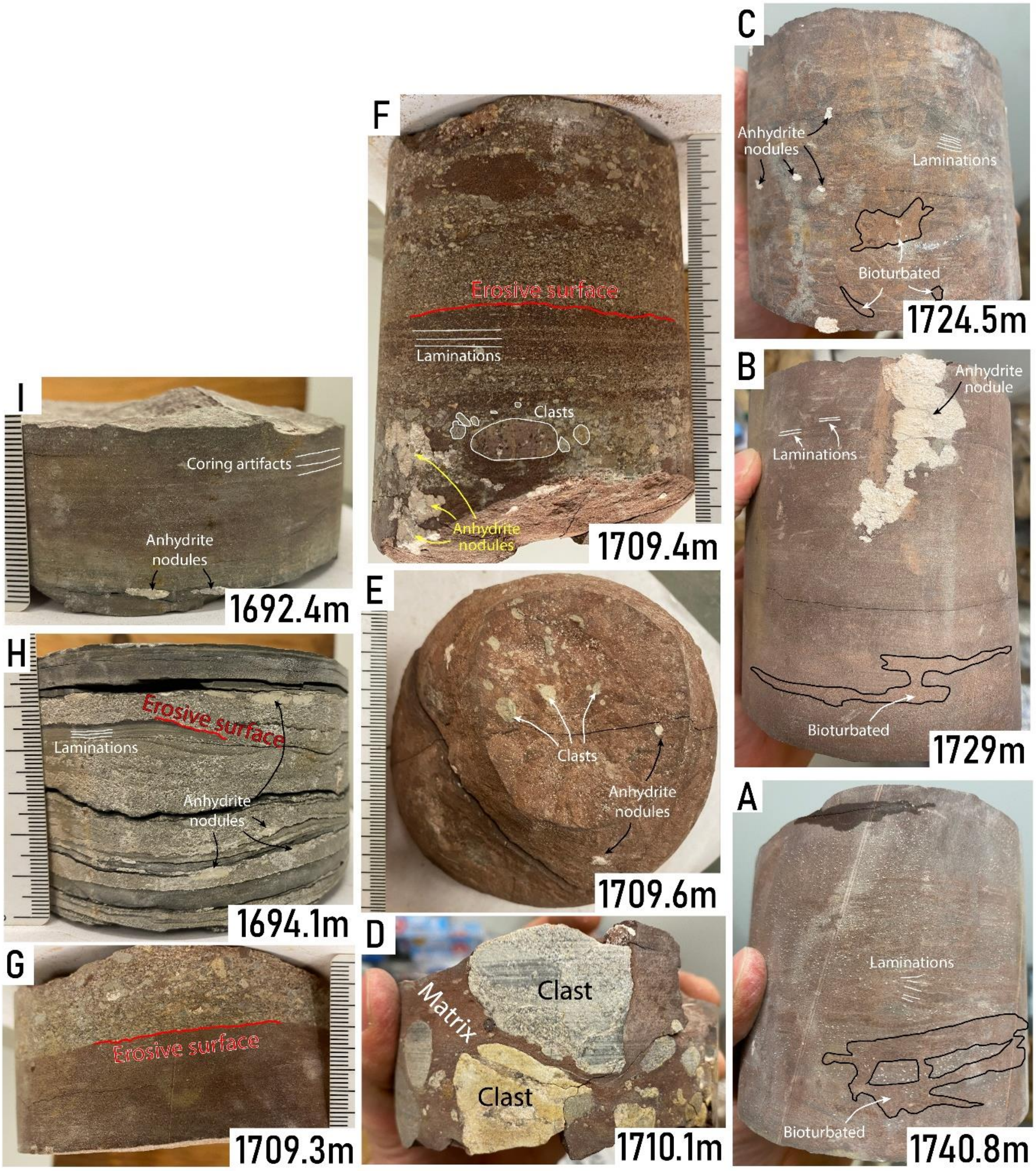

***Figure 53**: Representative selection of retrieved core samples from the "Éocène basal". (A) Intensely bioturbated red clayey limestone with burrows and deformed laminations). (B, C) Similar to (A), but with anhydrite nodules. (D) Pebbly mudstone with sub-angular to sub-rounded Jurassic limestone clasts. (E) Pebbly mudstone with small and*

mostly rounded Jurassic limestone clasts. (F) Successions of ortho-conglomerate beds and coarse stratified sandstone beds, both mainly containing Jurassic limestone clasts, and sometimes interbedded with mud, with occasional anhydrite nodules. (G) Erosional contact between a mudstone and a sandy orthoconglomerate. (H) Laminated grey marl with few anhydrite laminations and nodules. The seem to be deformation and erosional contacts. (I) Grey-red clayey limestone marking the transition from the "Sidérolithique" to the "Marnes à Limnées I".

Well-log interpretation of the STA-4 well indicates high gamma-ray and low resistivity values with little variations. The operators described the rocks of the "Basal Eocene" as red marls with occasional anhydrite, with the marls being slightly dolomitic at the bottom. In the WIL-1 well, the operators described it as starting off with a conglomeratic interval (~20m) with limestone clasts amongst a green to red cement (low gamma-ray and high resistivity), followed by slightly sandy red micaceous marls up to the top of the formation (high gamma-ray and low resistivity) (**Figure S1**). As conglomeratic intervals are not present everywhere in the basal Eocene, early alluvial fans were likely restricted to specific areas.

The transition between the "Basal Eocene" and the "Zone Salifère Inférieure" is expressed in the DP-XXVIII well by the gradual change of the samples colors (from red to grey), by the gradual decrease in bioturbation, and by the occurrence of very few laminated marls and syn-depositional anhydrite layers.

IV.1.b.iii : Zone Salifère Inférieure

The "Zone Salifère Inférieure" is 521.5m thick in the DP-XXVIII well, 582m thick in the STA-4 well, and 580m thick in the WIL-1 well. It is subdivided into four distinct units called "Marnes à Limnées I", "Sel I", Marnes à Limnées II", and "Sel II", from bottom to top. These units range from the late Lutetian/early Bartonian to the middle Priabonian (Châteauneuf et Ménillet, 2014; Pirkenseer et al., 2011, 2010; Berger et al., 2005a, Schuler 1988).

Marnes à Limnées I

The core samples of the "Marnes à Limnées I" unit of the DP-XXVIII well mostly consist of grey limey marls to clayey limestones, with or without anhydrite layers and/or anhydrite nodules (**Figure 54**: A, B). Some samples consist of nodular anhydrites, which were the result of anhydritisation of gypsum pseudomorphs (**Figure 54**: C). The gypsum was syn-depositional and formed as bottom-growing crystals, that were likely anhydritised during diagenesis. Mud is present between the crystals. Other anhydrite nodules are displacive and could be the result of gypsum dehydration after burial.

The well-logs of the STA-4 and WIL-1 wells and their interpretation account for a massive homogeneous marl formation with occasional anhydrite nodules (**Figure S1**).

Sel I

All the core samples from the "Sel I" unit of the DP-XXVIII well consist of massive halite. More precisely, they seem to consist of coarse inclusion-rich growth-aligned halite crystals (**Figure 54**: D), which suggest bottom nucleation in a shallow holomictic lake (Warren, 2016). Their colors range from white to grey, most-likely due to varying percentages of mud located between and/or inside the halite crystals, which contain fluid inclusions. While there seem to be recrystallisation in some samples, it is most likely due to the poor initial packaging and management of the core samples. It is hard to assess the presence or absence of dissolution surfaces. The halite could also be reprecipitated but was originally described as made-up of thick crystals (MDPA, 1960).

Well-log interpretation of the STA-4 and WIL-1 wells show that the "Sel I" unit is a massive halite formation with rare interbedded marls that can be up to ~10m thick. The original reports also account for the presence of rare anhydrite nodules (**Figure S1**).

Marnes à Limnées II

No core samples of the "Marnes à Limnées II" unit was retrieved from the DP-XXVIII well. According to the original description of the DP-XXVIII borehole (MDPA, 1960), this interval mainly consists of structureless marls with occurrences of bedded anhydrite nodules all across, and of few halite beds at the bottom. Some marls contain small limestone clasts.

In the STA-4 well, well-log correlations and original reports account for dolomitic marls in the lower half of the unit, and for marls with occasional anhydrite nodules in the upper half of the unit. In the WIL-1 well, the whole unit consists of marls with occasional anhydrite nodules (**Figure S1**).

Sel II

The core samples from the "Sel II" unit of the DP-XXVIII well mostly consist of massive halite beds that are identical to those found in the "Sel I" unit. The uppermost part of the "Sel II" mostly contains laminated marls with occasional anhydrite nodules (**Figure 54**: F). While most of the halite samples are white and/or translucent, there is an orange halite sample (**Figure 54**: E). Compared with the "Sel I", the "Sel II" interval contains more intercalated marlstone beds.

In the WIL-1 well, parts of the "Sel II" and "Sel III" units are lost due to a fault which seems to reject ~135m of sediments according to correlations with the STA-1 well, against ~320m as stated in the original report, which seems very unlikely due to the almost identical formations' thicknesses across the two wells (**Figure S1**).

IV.1.b.iv : Zone Salifère Moyenne

The "Zone Salifère Moyenne" is divided into two units known as the "Sel III" followed by the "Zone Fossilifère". This formation ranges from the late Priabonian to the early Rupelian (Pirkenseer et al., 2011, 2010; Berger et al., 2005a; Schuler, 1988). However, according to investigations presented in **Chapter V :** and **Chapter I :** , the Eocene-Oligocene Transition is likely to be positioned at the bottom of the "Sel III".

Sel III

The core samples of the "Sel III" unit retrieved from the DP-XXVIII well mostly consist of gray laminated dolomites and marls (**Figure 55**, **Figure 56**). The laminated marls are often associated with anhydrite nodules and layers, also many samples contain plant remains suggesting a relatively rich organic matter content (**Figure 56**: B, C). Others contain shell imprints and remains (**Figure 56**: A). In this unit, there are many samples showing seemingly cyclic millimetric to centimetric alternations of marly and evaporitic layers (**Figure 55**: B, C, E, F). The study of thin sections from the "Sel III" through microfacies analysis and µ-XRF scans suggest that these millimetric alternations are varves (**Chapter V :**) While no massive halite samples were recovered, their presence in the sedimentary record of the "Sel III" in the DP-XXVIII well is confirmed by the simplified lithostratigraphy of the original document, which shows several halite formations. Furthermore, they form cyclic alternations along with marl beds (see **Chapter V :**). One sample, relatively close to the "Zone Fossilifère", contains remains of *Mytilus faujasi*. While this fossil is classically attributed to the "Zone Fossilifère", it has been documented in older sediments.

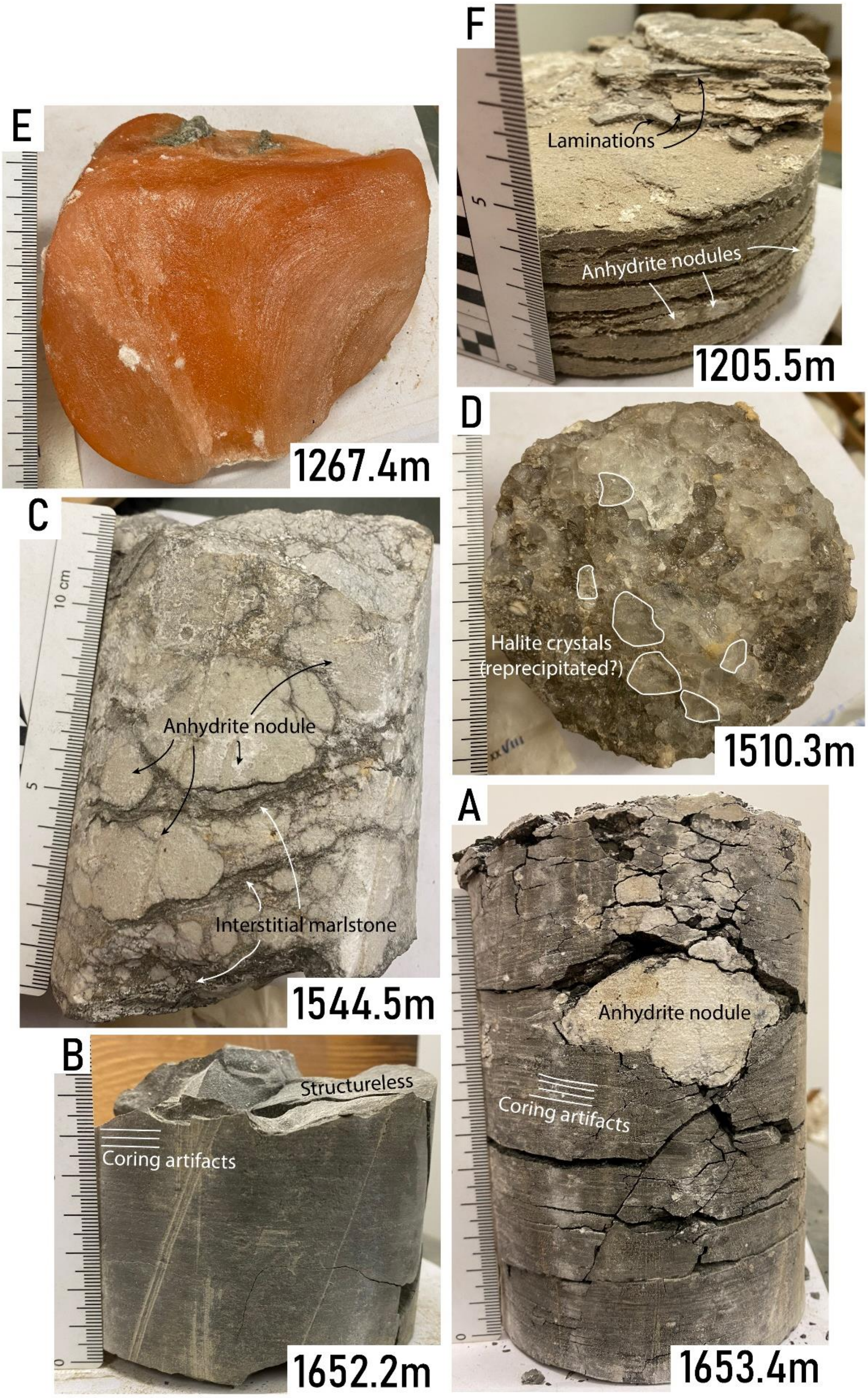

Figure 54: Representative selection of retrieved core samples from the "Zone Salifère Inférieure". (A) Greyish clayey limestone with thick anhydrite nodules. (B) Massive greyish clayey limestone with conchoidal fractures. (C) Thick anhydrite nodules with interstitial marls (anhydritised gypsum pseudomorphs) (D) Massive halite with thick crystals. (E) Orange deformed halite. (F) Laminated marl with small anhydrite nodules.

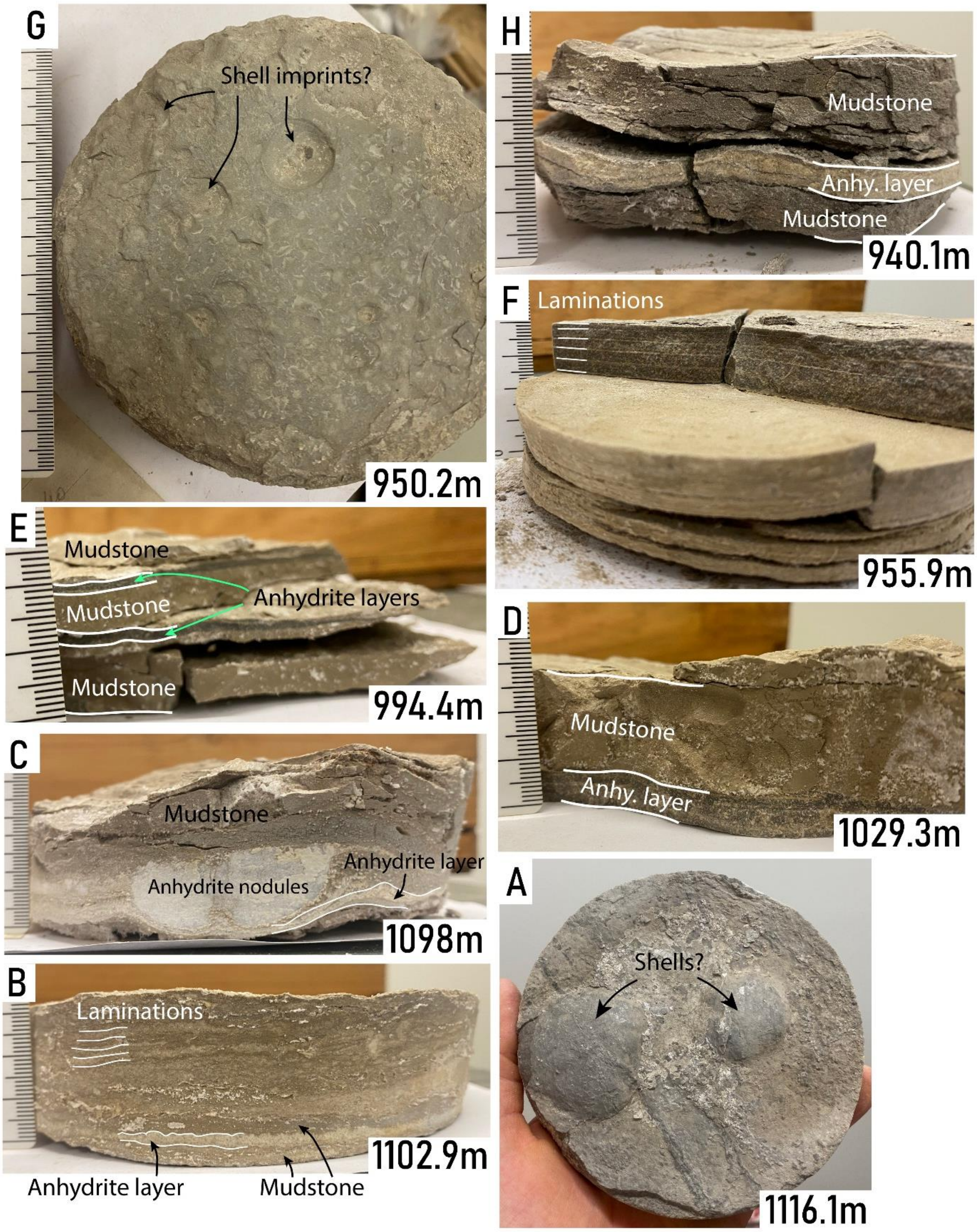

***Figure 55**: Representative selection of retrieved core samples from the “Sel III” unit. (A) Upper view of a laminated marl with either shell imprints or sedimentary concretions. (B) Alternations of millimetric marl and evaporite layers. (C) Anhydritic marl with alternations of marl and evaporite layers with two anhydrite nodules in the lower half, and homogenous marl in the upper half. (D) Similar to the previous sample but without anhydrite nodules and different evaporite layers. (E, F) Alternations of millimetric to centimetric marl and evaporite layers. (G) Upper view of a laminated marl with potential shell imprints. (H) Marl interbedded with a thick anhydrite layer.*

On the well-logs of the STA-4 and WIL-1 wells, while previous units consisted of massive and relatively homogeneous formations of marls or halite, the “Sel III” unit is characterized by the apparition and presence of seemingly cyclic and low amplitude (~15m) marl-evaporite alternations. The apparition of such cyclic features in the unit which contains the Eocene-Oligocene Transition is very interesting, as climate change during this period is congruent with the strengthening of seasonality in the northern high hemisphere (Toumoulin et al., 2022). The onset of orbitally induced sedimentary cycles and of varves at the bottom of the "Sel III" is interpreted as the results of increased sensitivity to orbital forcing and increased seasonality through the Eocene-Oligocene Transition (see **Chapter V :**).

Zone Fossilifère

In the Upper Rhine Graben, the "Zone Fossilifère" is a basin-scale unit which formed after a lacustrine transgression related to marine incursions which likely came from the North Sea through the Hessian Depression (Berger et al., 2005a; Berger et al., 2005b; Pirkenseer et al., 2010). This unit is classically subdivided into three sub-units known as, from older to younger, "Zone à Mytilus", "Zone à Bryozoaires", and "Zone à Hydrobies". In the Pechelbronn basin, the "Zone à Mytilus" and "Zone à Bryozoaires" are dominated by marine faunas, and the "Zone à Hydrobies" is dominated by brackish faunas, possibly revealing a gradual salinity change from bottom to top (Lavoyer, 2013) (**Chapter VII :**).

In the DP-XXVIII well, the "Zone Fossilifère" mostly consists of grey fossiliferous laminated marls (**Figure 56**). While the average thickness of this unit is ~70 m in the Upper Rhine Graben (Duringer et al., 2019), it is a bit thicker in the DP-XXVIII well, reaching ~80m in the WIL-1 and STA-4 wells based on the well-logs correlations (**Figure S1**). Based on the original document of the DP-XXVIII well, the top of the "Zone Salifère Moyenne", which is the top of the "Zone Fossilifère", is located at 842m of depth. While the depth of the limit between the "Sel III" and "Zone Fossilifère" is not given, the simplified lithostratigraphic description shows a thick halite deposit (~10m) below 921m, suggesting that the base of the "Zone Fossilifère" is at 921m and that it therefore is 79m thick, which is more coherent with well-log observations from the nearby wells.

Only 3 samples of the "Zone Fossilifère" have been recovered from the DP-XXVIII borehole. While most of the samples are grey laminated marls and marly limestones, they differ from one another based on their fossil content and sedimentary facies. One is a laminated sandstone rich in organic matter with coal and plant remains (**Figure 56**: F), and the two others are finely laminated and display varve-like alternations of dark and bright laminations (**Figure 56**: D, E). The laminated marls indicate a relatively calm and deep-water environment, and the laminated sandstone with vegetal remains (**Figure 56**: F) potentially marks a flood deposit. The presence of this sandstone could suggest that the coastal fan-deltas could have sometimes reached far into the basin during the period of the "Zone Fossilifère".

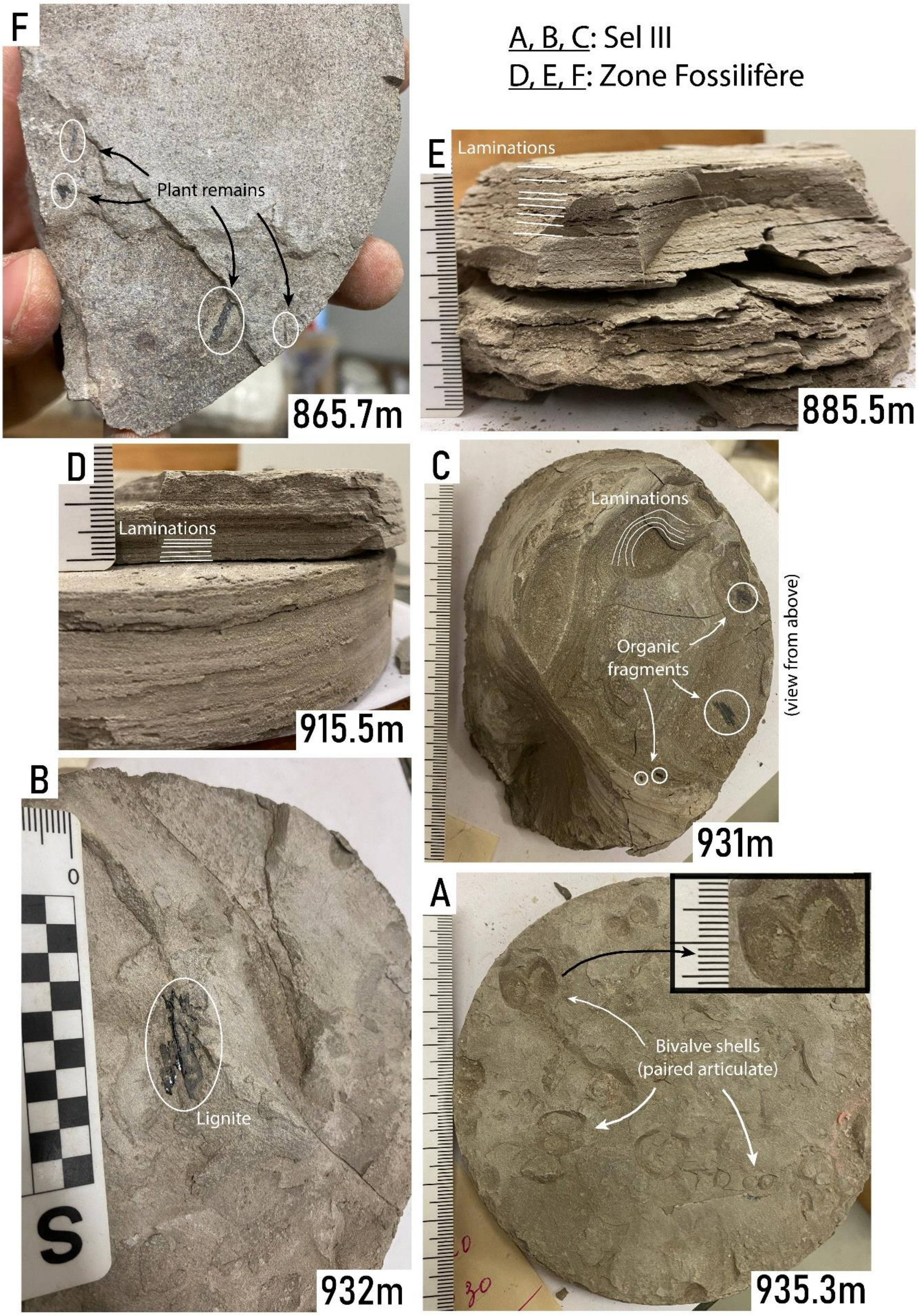

***Figure 56**: Representative selection of the retrieved core samples from the "Sel III" (A, B, C) and "Zone Fossilifère" (D, E, F) units. (A) Laminated marl with Mytilus faujasi imprints. (B, C) Laminated marls with coal fragments. (D) Laminated marl with varve-like alternations. (E) Laminated marl. (F) Laminated marly sandstone with vegetal remains.*

IV.1.b.v : Zone Salifère Supérieure

The “Zone Salifère Supérieure” formation is divided in three units known as “Sel IV”, “Sel V”, and “Marnes sans Sel”, which are characterized by cyclic marl-evaporite alternations. Two potash seams are present at the lowermost part of the formation (« Sel IV ») (Blanc-Valleron, 1990). The “Sel IV” and ‘Sel V” units are missing from the recovered cores of the DP-XXVIII well, with only the uppermost part of the « Marnes sans Sel » being available as samples (**Figure 64**). However, thanks to the potash exploitation by the MDPA during the 20th century, the lithostratigraphy of the “Zone Salifère Supérieure”, and specifically of the “Sel IV” are well-known, so much so that individual beds have specific names (e.g. S2, CS, U33) (**Figure 64**) and were correlated across the basin (Blanc-Valleron, 1990). Also, blocks from the potash seams are currently exposed in Strasbourg (Blessig; **Figure 59**) and Wittelsheim (Kalivie museum; **Figure 60**), and cores of sylvinite occurrences were recovered from the DP-95 borehole (**Figure 62**).

Sel IV

In the DP-XXVIII, STA-4 and WIL-1 boreholes (and pretty much across the entire potash basin), the “Sel IV” unit is made of alternating beds of halite and marl, with sylvinite occurences, classically called from bottom to top: S2, S1, S, Mi, Ci, Ti, T, MS, CS, TS, U, then from U1 to U32, with the even U numbers corresponding to halite beds and the odd U numbers corresponding to marl beds. The other terms correspond to marls (S2, S, Ti, TS), halite (S1, Mi, MS), and potash (Ci, CS) beds. Rare anhydrite occurrences are described in the wells. The cyclostratigraphy of these marl-evaporite alternations is treated in **Chapter V :** . The potash deposits consist of thin marl, halite, and sylvite alternations, which appear to be cyclic (**Figure 59**, **Figure 60**). A very intriguing observation is the fact that the millimetric to centimetric sedimentary layers of the potash seams can be almost perfectly correlated across multiple tens of kilometers in the Mulhouse basin (Blanc-Valleron, 1988). Such a continuity of small layers across such an area is a strong argument for the good continuity of the record, with little to no dissolution surfaces. The end of the “Sel IV” is classically positioned at the top of the U33 halite bed.

IV.1.b.v..1 Mine gallery

The investigated mine gallery is located ~500m underground at the Joseph-Else well location in Wittelsheim. In the stratigraphy, the sedimentary record accessible in the mine gallery (~2.8m) is localized somewhere between the “Zone Fossilifère” and the lower potash seam. By correlation with the synthetic sedimentary logs of the intervals below and above the potash seams (from S2 to U2) (Rybka, 1981), the sedimentary succession of the investigated mine gallery is interpretated as being part of the M1 interval (**Figure 57**, **Figure 58**). It mainly consists of halite beds with intercalated marls, forming centimeter- to millimeter-thick beds and layers (**Figure 57**). This small portion gives a good overview of how the halite intervals of the DP-XXVIII log (**Figure S2**) look like. The alternations between marl and halite beds is interpreted in terms of sequence stratigraphy as lake-level variations, potentially linked to alternating period characterized by humid and arid conditions. Such alternating periods characterized by humid and arid conditions are observed across at least 3 orders of magnitude, with varves at the third order (see **Chapter V :**), orbital cycles at the first order (**Chapter V :**), and the in-between observed in the mine gallery at the second order. While the varves and orbital cycles are of clear climatic origin, such an interpretation is harder to assess for the alternations of the mine gallery. Even though they have a “cyclic look”, they could very well be related to stochastic events.

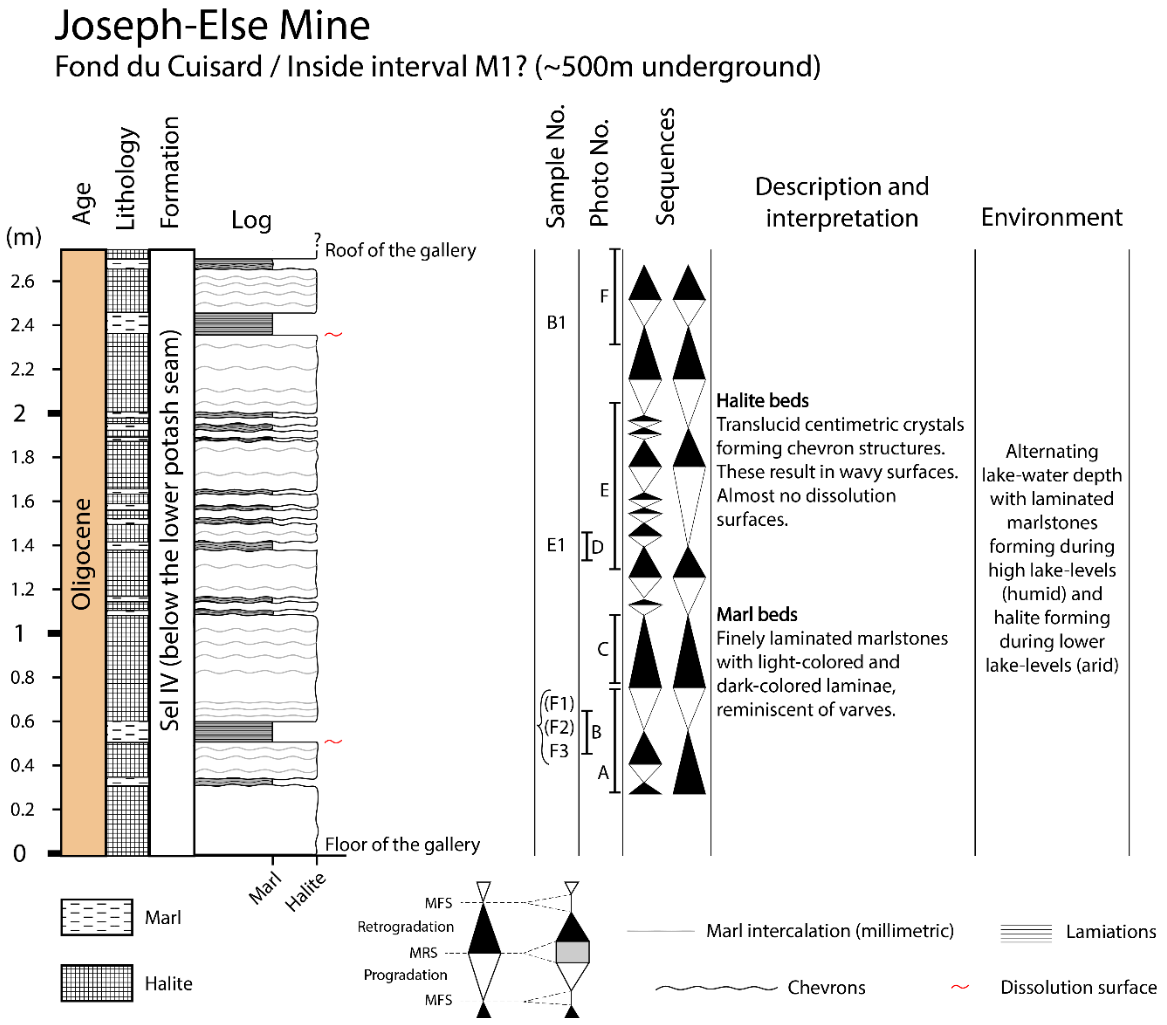

***Figure 57**: Sedimentary log of the mine gallery in the Joseph-Else well.*

In this gallery, the halite beds consist of bottom-nucleated and growth-aligned crystals forming chevron structures (**Figure 58** A, C, E, F). The crystals are coarse, reaching lengths of up to ~2cm (**Figure 58** B, D). The marlstones are either present as fine layers (up to 1 cm) (**Figure 58** A, C, E) draping the halite chevrons, or as thicker beds (up to 10cm) that mark dissolution surfaces, erasing the chevron domes of the underlying halite (**Figure 58** A, B, F). These laminated marlstones seemingly consist of reoccurring alternations of dark- and light-colored laminae (**Figure 58** B), similar to those described in the “Sel III” (see **Chapter V :**) and described by Blanc-Valleron (1990).

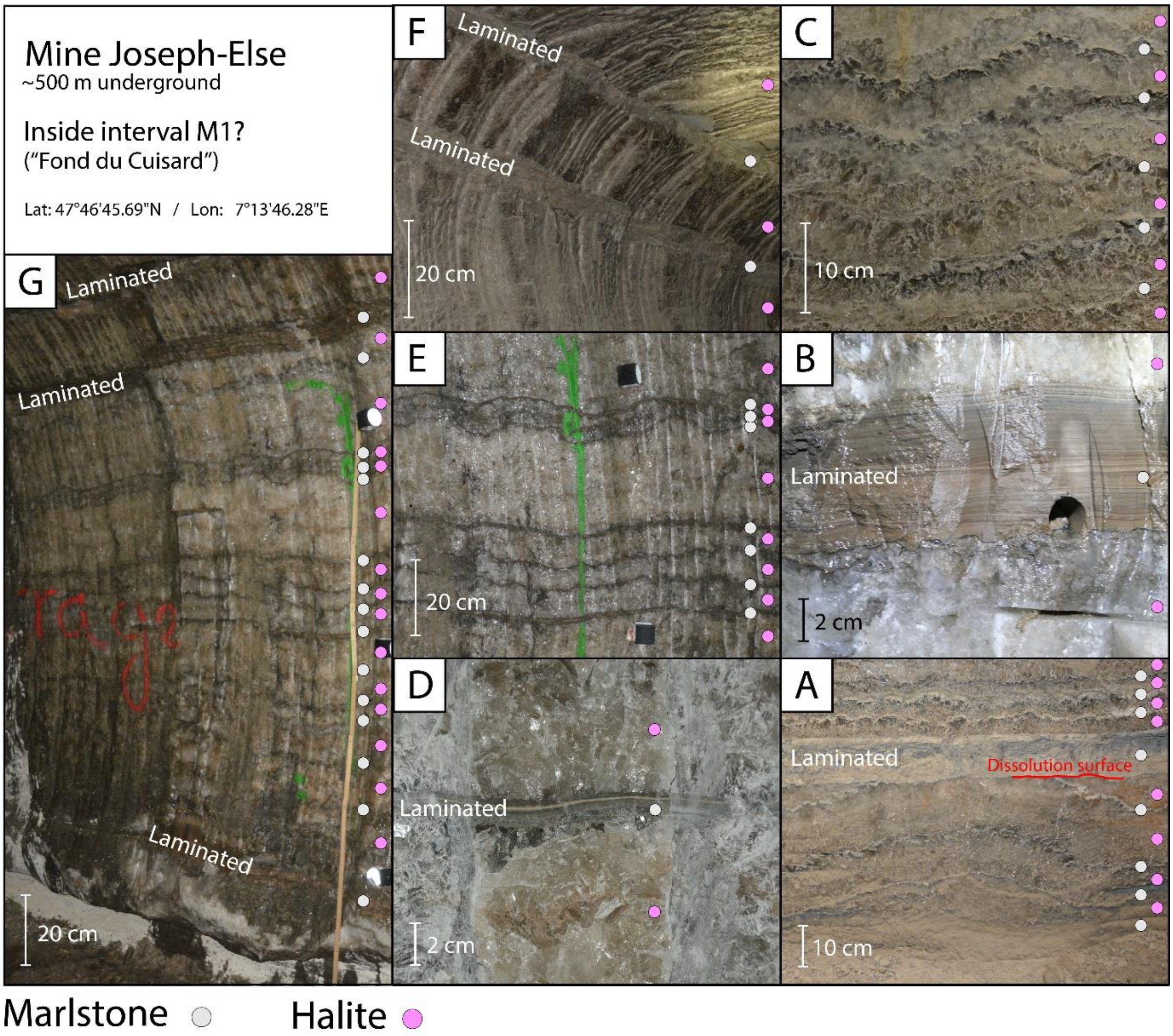

***Figure 58**: Photographs of sedimentary structures in the mine gallery of the Joseph-Else well. (A) Alternations of halite beds and marl layers, with an intercalated marl bed marking a dissolution surface, erasing the top of the underlying halite chevron. (B) Laminated marlstone made of dark- and light-colored laminae, located between two halite beds with coarse crystals. (C, E) Alternations of halite beds forming chevron structures with marlstone layers that drape the chevrons. (D) Laminated marlstone located between two halite beds with coarse crystals. (F) Uppermost part of the gallery, composed of three halite beds with two intercalated laminated marlstone beds, with the first one marking a dissolution surface. (G) Overview of the sedimentary record of the gallery.*

IV.1.b.v..2 Potash seams

The potash seams of the Mulhouse basin generally consist of alternations of thin marl layers, crystalline halite, and crystalline sylvite (**Figure 59**, **Figure 60**). The marl layers are generally dark to bright gray, forming a singular millimetric laminae. The halite generally forms chevron ("cauliflower") structures and is constituted by millimeter to centimeter thick crystals with fluid inclusions. The color of these halite beds oscillate between bright gray and dark gray, with dark gray ones most-likely containing some portion of interstitial marl patches. The sylvite beds are sometimes very similar to the halite ones, forming big red bottom-growth crystals. Sylvite also occurs as millimetric crystals (cumulates) draping or depositing between underlying halite chevrons. The color of these sylvite beds oscillate between dark red and bright red, indicative of its purity. In the depocenter of the Mulhouse basin, the lower potash seam (= "Couche Inférieure de Potasse") reaches close to 5 m in thickness, while the upper potash seam (="Couche Supérieure de Potasse") reaches approximately 1.5 m. The lower potash seam exposed in Strasbourg (Blessig) (**Figure 59**) and the upper potash seam exposed in Wittesheim (Kalivie museum) (**Figure 60**) were logged. The lower potash seam exposed in

Strasbourg is not complete (**Figure 59**), while the upper potash seam exposed in the Kalivie museum is (**Figure 60**).

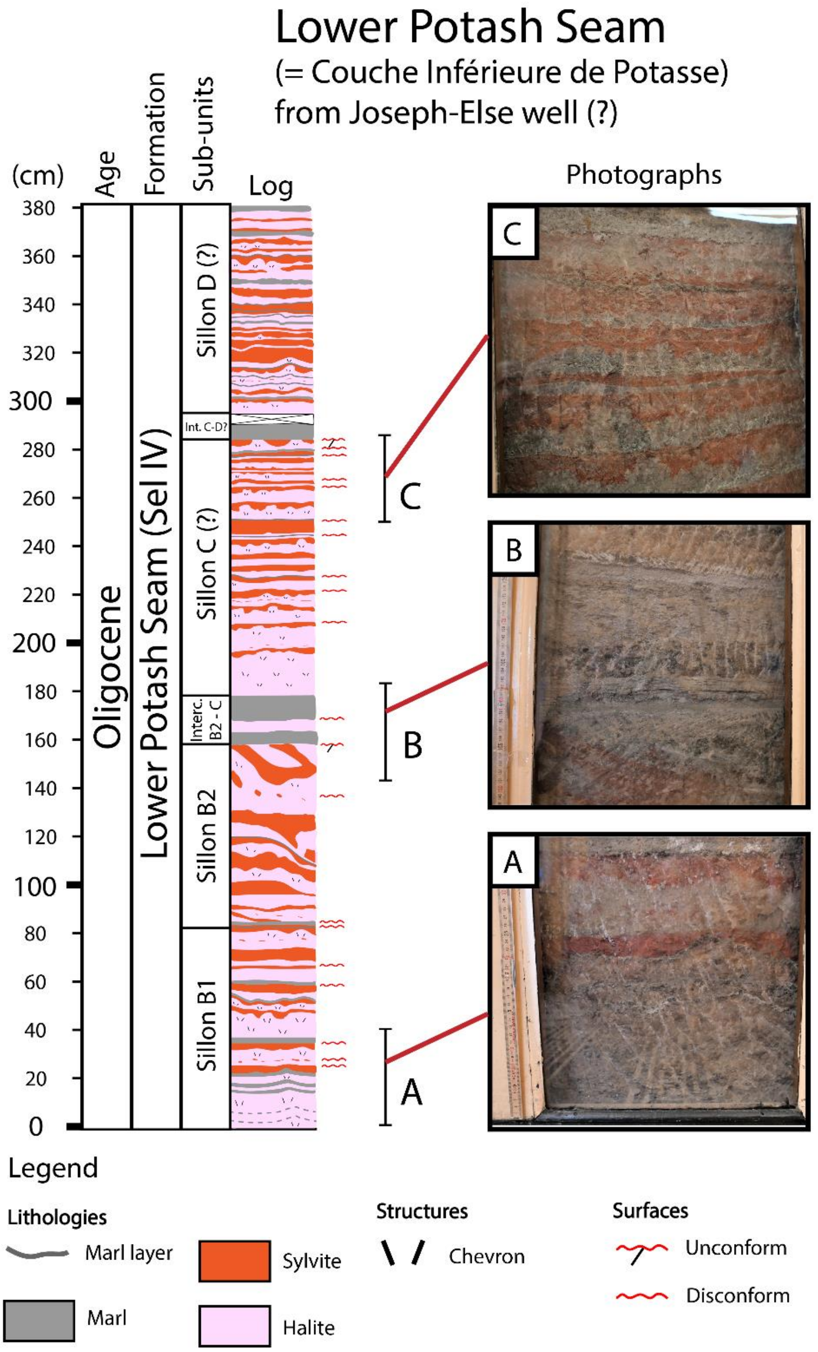

Figure 59: Sedimentary log and photographs of the lower potash seam from the Joseph-Else (?) well of the Mulhouse basin. This seam is currently displayed at the old geology building in Strasbourg (1 rue Blessig).

The lower potash seam contrasts from the upper one by the presence of thicker marl beds that indicate prolongated periods of lake-level rise and represent unconformities through important dissolution surfaces. The apparent reoccurrence of halite, sylvite, and/or marls potentially suggest the cyclic nature of their depositional processes. The investigation of the cyclicity of these alternations in the upper potash seam through spectral analysis is detailed in **VI.2 : Spectral analysis of the Upper Potash seam**.

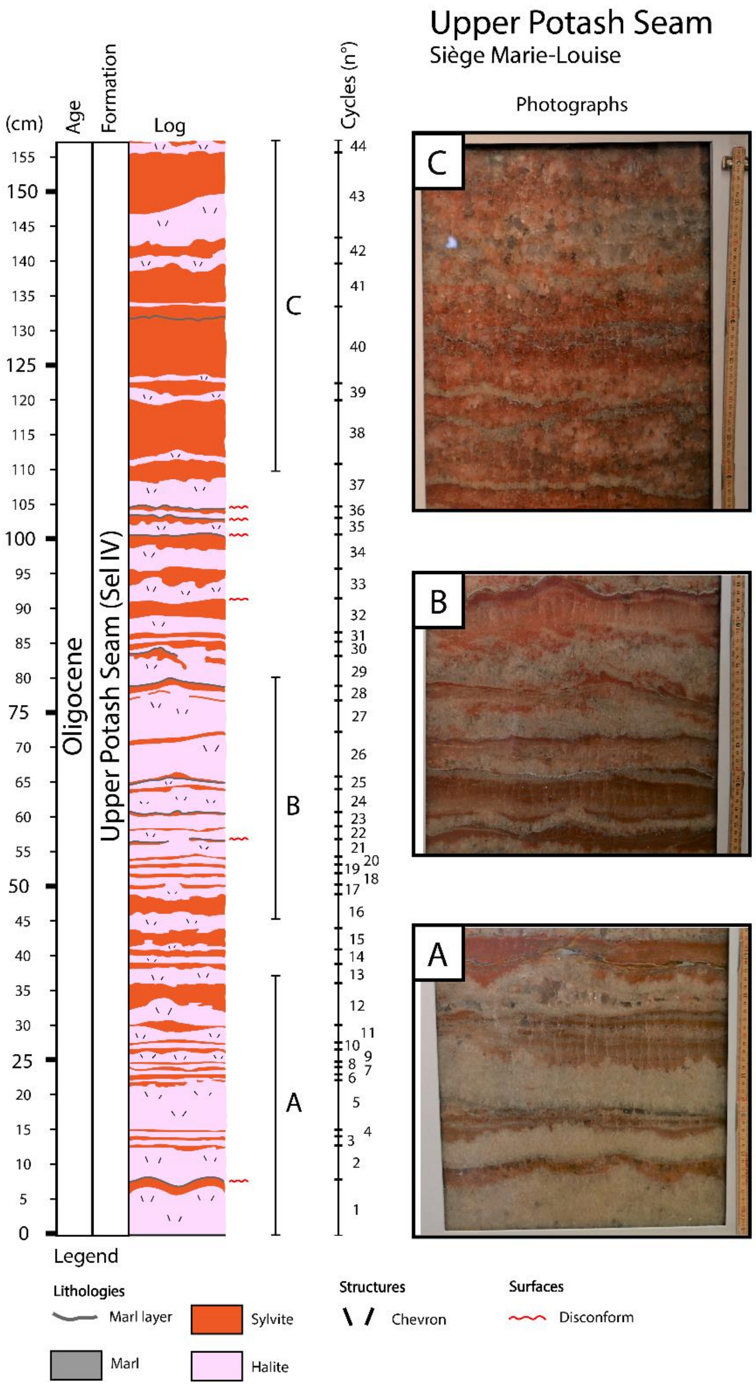

***Figure 60**: Sedimentary log and photographs of the upper potash seam from the Marie-Louise well of the Mulhouse basin. This seam is currently displayed at the Kalivie museum (Wittelsheim).*

To my knowledge, the interpretation of potash alternations (halite, sylvite, marl) as cyclic deposits has never been demonstrated. There could be several parameters and temporalities that could serve as plausible explanations for the depositions of these alternations. One of them is that they could be varve, with seasonal changes in temperature and/or humidity forcing their deposition. However, they are similar to evaporitic alternations found in the Dead Sea (Dor et al., 2019), even though there are no sylvite layers. There, several types of varves are described in the relation to the water balance of the lake. During negative water balance, laminated halite alternations consisting in large bottom-growth crystals, small cumulate crystals, and discrete detrital layers were deposited (up to ~3 cm thick). While originally interpreted as the result of distinct summer/winter precipitation regimes (Kiro et al., 2016;

Neugebauer et al., 2014), these alternations actually seam to originate from temperature variations rather than seasonal evaporation, described as relatively uniform throughout the year (Dor et al., 2019; Hamdani et al., 2018). By comparison with this recent analog, I propose that the halite, sylvite, and marl alternations of the potash seams are of annual nature. Marl layers would have been deposited during the humid season through clay-sized clastic inputs reaching far into the lake, with halite and sylvite beds being deposited during the dry season through evaporation and/or driven by temperature changes. However, marl layers are not present in every alternation, suggesting that the sedimentary output of the axial rivers of the lake were not always enough for clay to reach the depocenter. Therefore halite and sylvite couplets are also interpreted as varves. Several disconformities (dissolution surfaces) can be observed in the lower and upper potash seams. These dissolution surfaces consist of smoothed surfaces instead of irregular surfaces related to crystal fabrics. They usually occur at the top of sylvite beds, forming smooth marl layers (**Figure 61**). These disconformities are interpreted as being relatively minor, as the small marl layers still somewhat drape the underlying smoothed surface, rather than forming perfectly straight erosive surface such as those at the bottom of the thick marl beds of the lower potash seam (**Figure 59**). Such dissolution surfaces are commonly interpreted as being the result of marked freshening episodes (Warren, 2016 ; Gindre-Chanu et al., 2022).

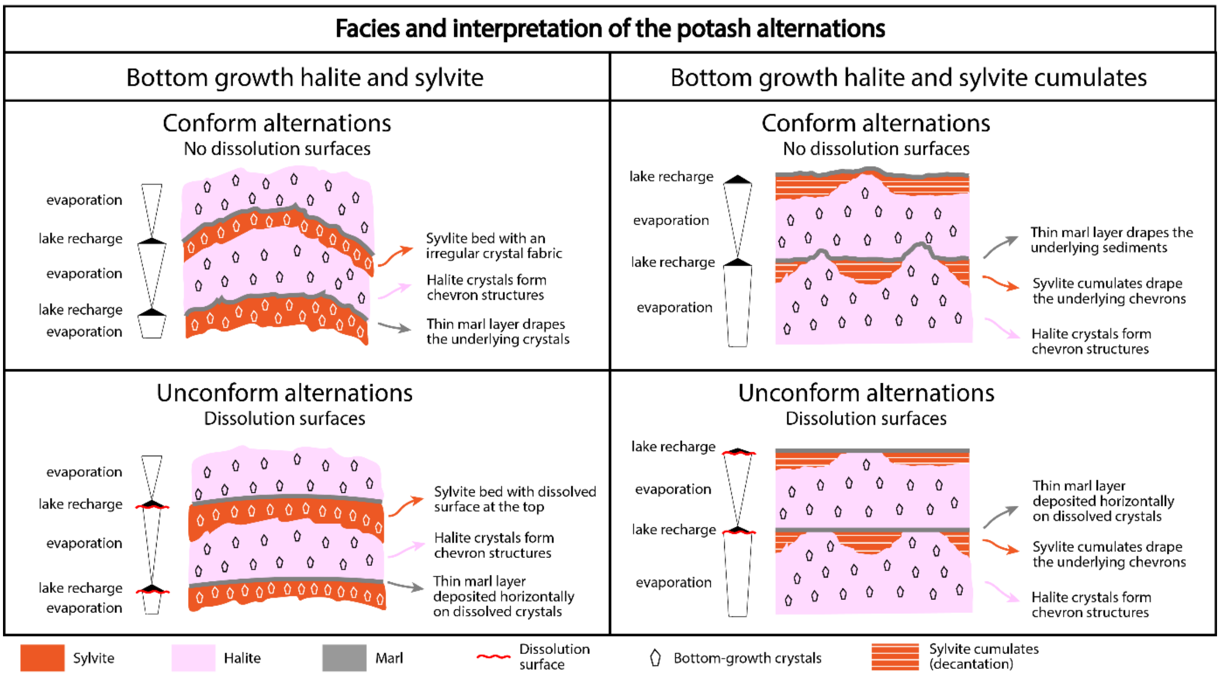

Figure 61: Facies and interpretation of the potash alternations of the lower and upper potash seams of the Mulhouse basin. Marlstone layers can sometimes be missing.

IV.1.b.v..3 Other sylvinite intervals

While the lower and upper potash seam represent the main occurrences of sylvite in the Mulhouse basin, a few other intervals with some sylvinite occurrences exist. In the recovered core of the DP-95 borehole, such occurrences are found in the Ti (“toit Inférieure”) and TS (“toit supérieur”) intervals (**Figure 62**). The sylvinite occurrences in these intervals are similar in facies to the sylvinite beds described in the lower and upper potash seams (**Figure 59**, **Figure 60**). The transition from the upper potash seam to the TS interval is marked by a thick marlstone bed and by the disappearance of sylvinite beds.

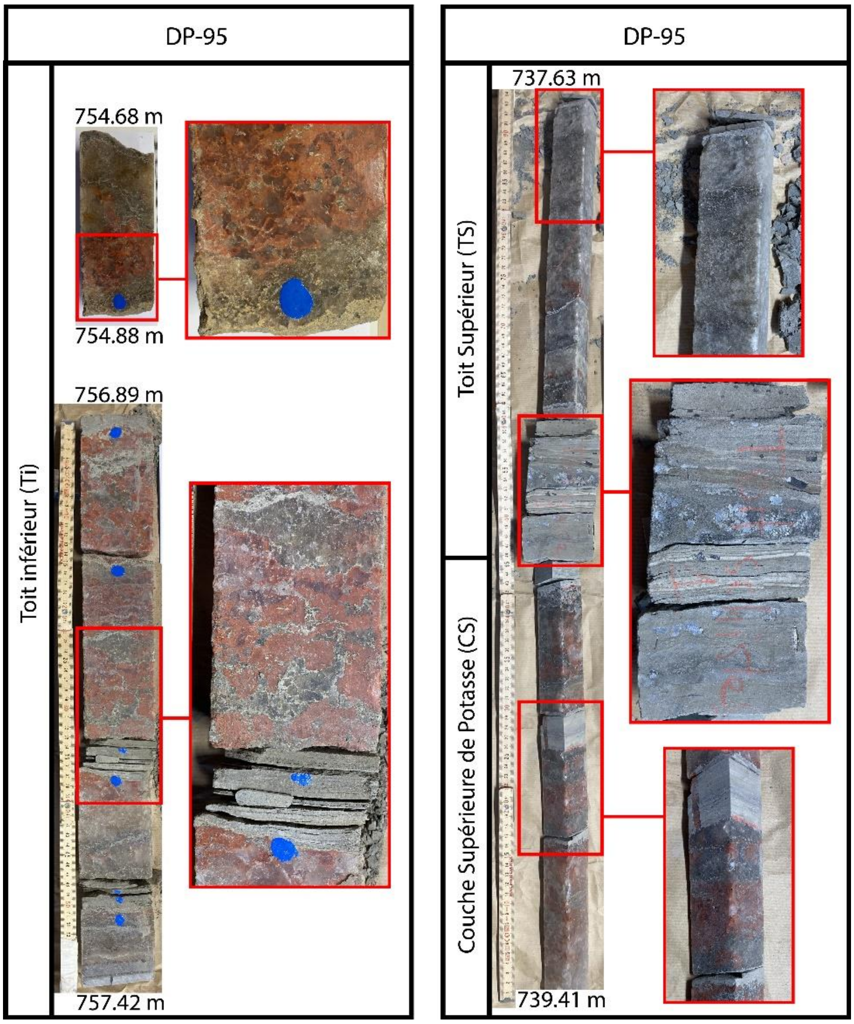

***Figure 62**: Photographs of sylvinite occurrences in the DP-95 borehole. Cores from the "Toit inférieur" (Ti) (left) and from the "Couche Supérieure de Potasse" (CS) and "Toit Supérieur" (TS) (right).*

IV.1.b.v..4 Depositional model

The following depositional model is proposed based on the facies observations of the potash deposits and on the climate knowledge from past palynology studies. According to Schuler (1988), the "Sel IV" is marked by a clear aridity phase. The climate is of "Mediterranean" type with a long dry season (half the year), a pluviometry of 1000-1200 mm/year, and an average annual temperature of 12-15°C. Based on this information, it can be inferred that half the year was dry and hot (including summer), and the other half was more humid and colder (including winter). These characteristics fit well with the proposition that the potash alternations could be of seasonal origin. As such, the marl layer would preferentially be deposited during the humid season during which fluvial inputs were increased, while the halite and sylvite beds would be deposited during the dry season through evaporation and/or temperature-induced saturation (**Figure 63**). However, these potash alternations (~2 to 6 cm) are way thicker than the varves described in the "Sel III" (~2 mm) (see **Chapter V :**), which suggest that they could potentially represent longer periods. Nevertheless, the varves of the "Sel III" consist of marl and anhydrite, while the potash alternations consist of marl, halite and sylvite. Halite is known to have sediment accumulation rates way higher than anhydrite, and past studies suggest that halite deposition was almost 19 times faster than anhydrite deposition in the Mulhouse basin (Kühn and Roth, 1979; Blanc-Valleron, 1990). Therefore, the interpretation of potash alternations as varves is coherent. However, another question remains to be answered: what fostered the deposition of potash? While it is a tricky question, my simple but coherent answer is that they mark two periods of extreme aridity, as partially shown by the palynological investigations of Schuler (1988). Such aridity likely caused the lake-level to significantly drop, causing the hyper-saturation of the brine and preferential precipitation of halite and sylvite. For more precise answers, specific studies would be required to get more details on the lake's hydrological system.

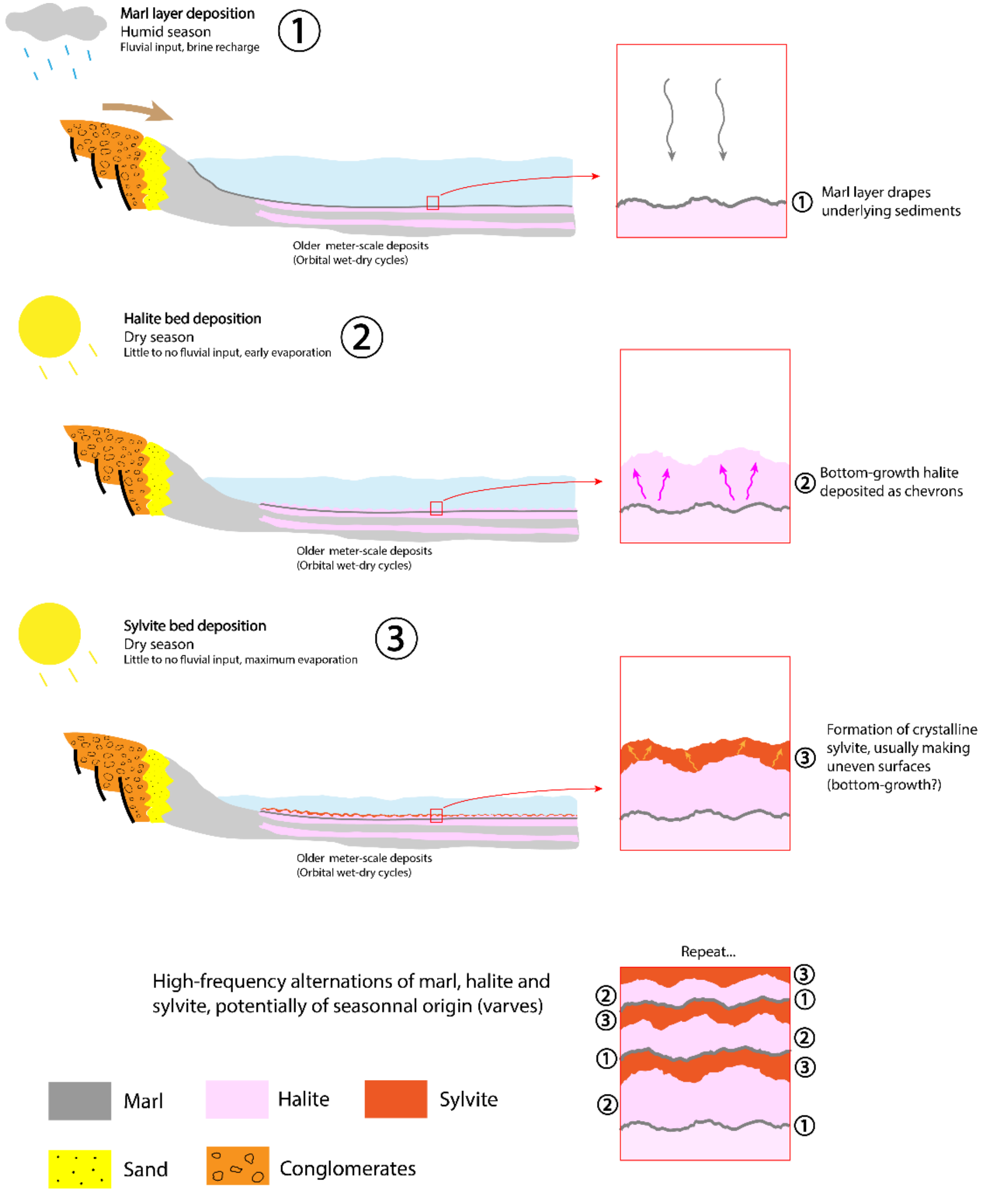

Figure 63: *Simple depositional model of the potash alternations of the Mulhouse basin (not to scale).*

Sel V

In the STA-4 and WIL-1 wells (and even across the entire potash basin), the "Sel V" unit is made of alternating beds of halite and marl beds, with some anhydrite occurrences (**Figure S1**). The end on the "Sel V" is classically defined as the last occurrence of halite. In the MDPA concession, the last halite bed is numerated U111, but going northward, up to 4 additional halite beds have been described in the DP-207, DP-208, and DP-210 wells (Blanc-Valleron, 1990). Overall, the marl-evaporite alternations of the Mulhouse basin display impressive continuity.

Marnes sans sel

The uppermost part of the “Marnes sans sel**”** mostly consist of massive greyish clayey limestones (**Figure 64**). Most samples display conchoidal fractures which reflects very homogenous and isotrope sediments (i.e. no laminations). This is an interesting observation as the rocks of this formation were classically mostly described as marls, while they seem to mostly consist of clayey limestones (in this location at least). Still, a few samples are marls that show horizontal fractures and layers. Also, some samples contain organic matter in the form of small coal fragments. All in all, the studied samples mostly consist of mudstones (**Figure 64**), which implies a low-energy depositional setting of calm water and inhibition of grain-producing organisms.

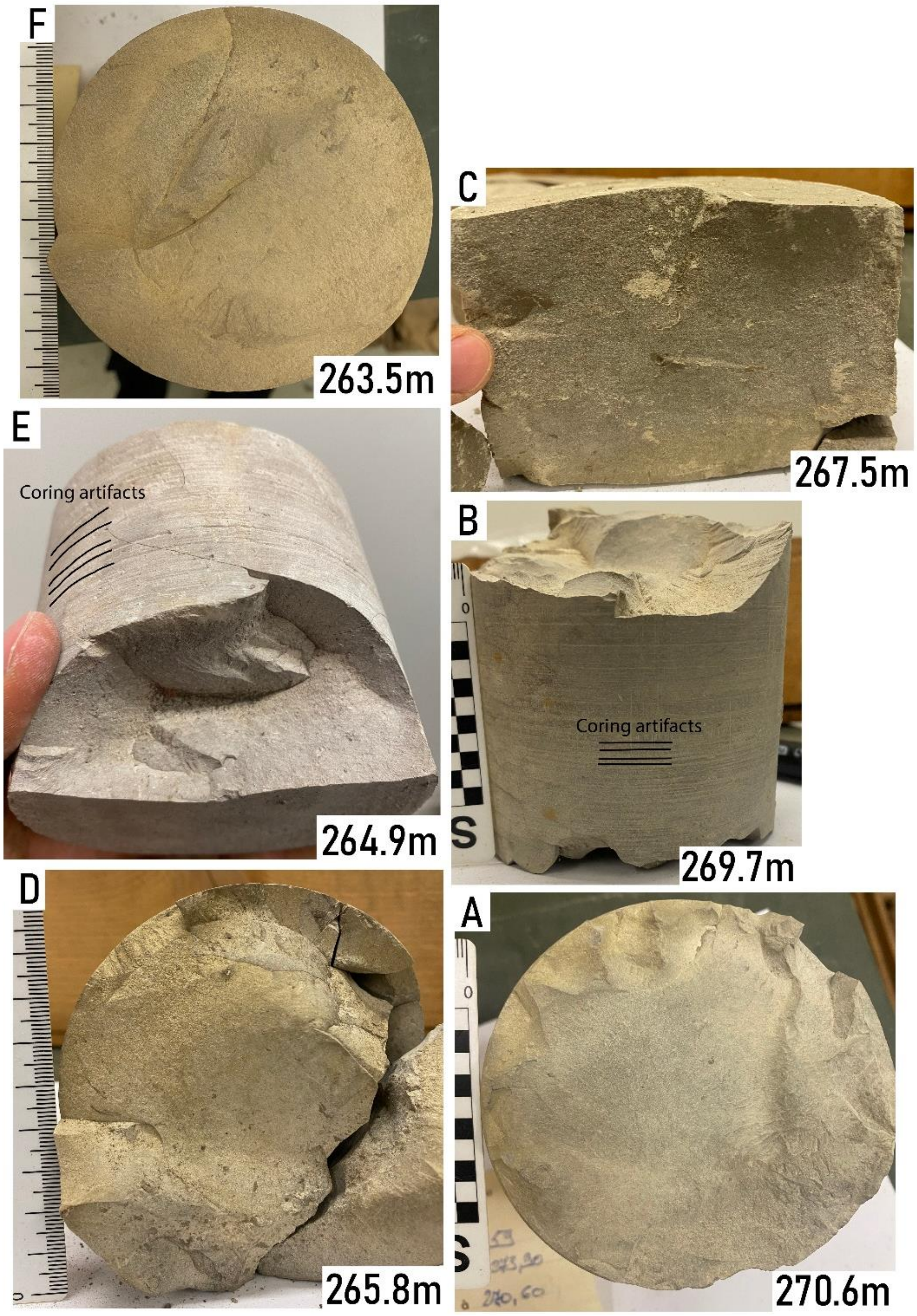

Figure 64*: Representative selection of core samples from the uppermost “Marnes sans sel”. Almost all the core samples consist of (A, B, C, D E, F) massive greyish clayey limestones with conchoidal fractures. Note that the horizontal features seen on photographs B and E are coring artifacts and not laminations.*

In the STA-4 and WIL-1 wells, the “Marnes sans sel” is characterized by cyclic alternations of thick marl and anhydritic marl beds alternations (**Figure S1**). Cyclicity is lost in the uppermost part of the unit just before the “Série Grise”, where only marlstones are left.

IV.1.b.vi : Série Grise

The “Série Grise” formation is classically divided into four units known as “Marnes à Foraminifères”, “Schistes à Poissons” (also known as “Couches à Amphisiles”), “Couches à Mélettes”, and “Marnes à Cyrènes”. This formation has been extensively studied by Roussé (2006) in outcrops and well-logs. It marks the perennial connection of the URG with nearby oceans. The four units are characterized by their fossil content.

Marnes à Foraminifères

In the DP-XXVIII well, the “Marnes à Foraminifères” unit is 8m thick and only two core samples were retrieved from it. The first one at 262.5m is a massive grey-reddish clayey limestone, and the second one at 254.7m is a grey clayey limestone with coal and/or fish bone fragments (**Figure 65**: A).

In other localities, paleontological investigations revealed the presence of rares bivalves, fish scales and remains (Fischer, 1965), as well as marine nannoplankton, planktonic and benthic foraminifera (Pirkenseer et al., 2010), signing an open marine depositional environment.

Schistes à Poissons (or Couches à Amphisiles)

In the DP-XXVIII well, the “Schistes à Poissons” unit is 8.5m thick and only two core sample were retrieved from it. The first one at 254m consists of a grey-yellowish sandy limestone with biological remains. The second one at 253.2m consists of a varve-like laminated fine-grain limey sandstone with few biological remains (**Figure 65**: B).

In the WIL-1 well-logs (and most well-logs of the URG), the “Schistes à Poissons” unit, in comparison with the other units of the “Série Grise”, is characterized by a high gamma-ray value which discloses its high amount of organic matter. This makes it a very good unit for rift-scale correlations as well as seismic-profiles marker (Blanc-Valleron, 1990).

Couches à Mélettes

In the DP-XXVIII well, the “Couches à Mélettes” unit is 170.85m thick. It mostly consists of grey clayey limestone (**Figure 65**: E, F) and grey marly sandstones (**Figure 65**: C, D, F), but there are several in between (e.g. sandy, micaceous, marly limestones). Several samples are rich in biological remains such as lignite fragments and fish bones and/or scales (**Figure 65**: C, D). The grey marly sandstones are often micaceous.

IV.1.c : Lithofacies associations

Facies associations have been distinguished for the “Sidérolithique”, “Zone Salifère Inférieure” and “Zone Salifère Moyenne“, and “Zone Salifère Supérieure” based on the study of core samples, potash blocks, and observations in the mine gallery (**Table 1**). On the detailed log of the sedimentary succession of the DP-XXVIII borehole (**Figure S2**), the lithofacies of each sample is detailed next to the log. The successions of these lithofacies is interpreted in terms of paleoenvironments, and used to reconstruct the history of the Mulhouse basin in a proposed depositional model (see **IV.3 : Depositional model of the Mulhouse basin through the Eocene and Oligocene**).

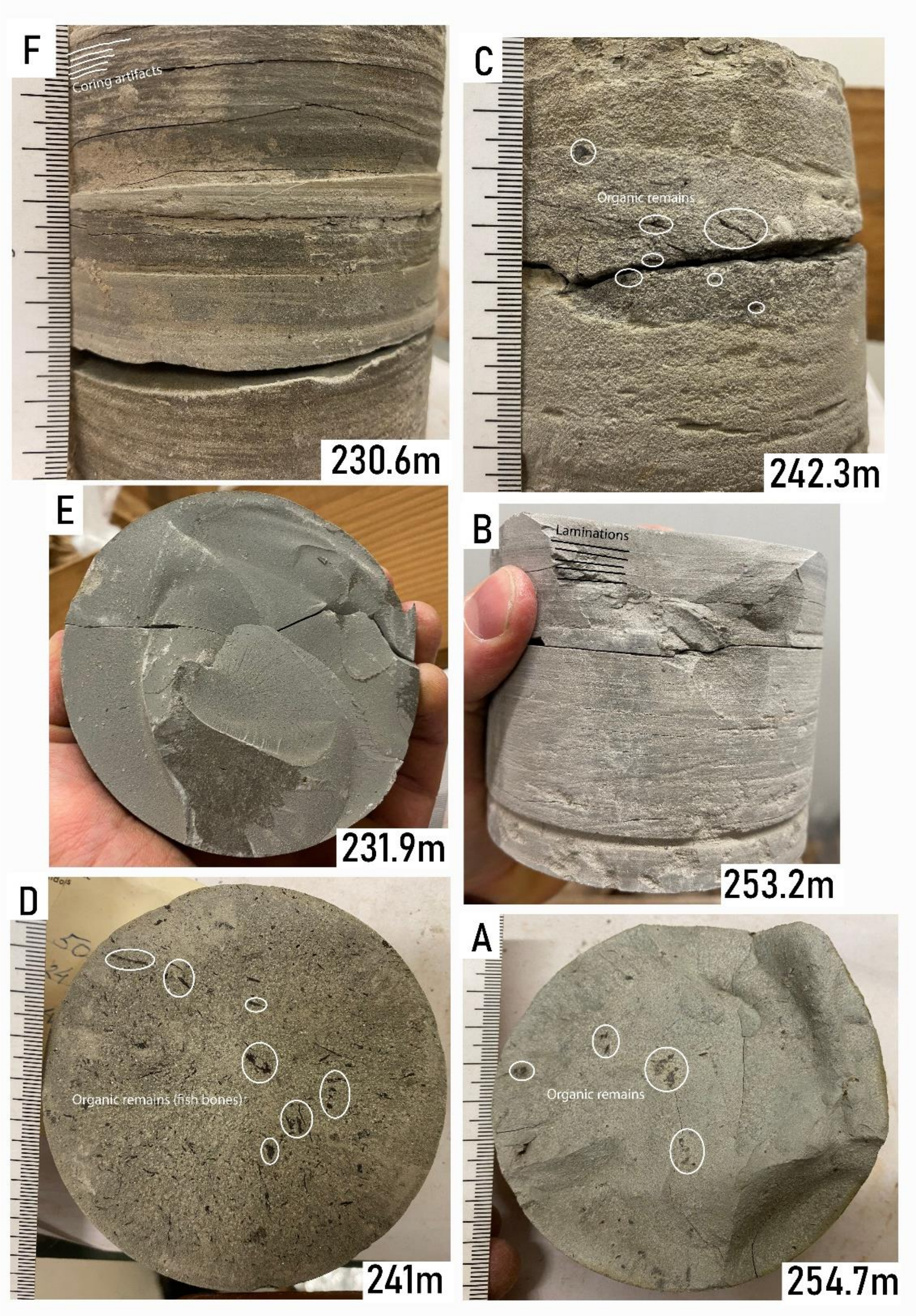

Figure 65: Representative selection of core samples from the "Série Grise". (A) Grey clayey limestone with coal and/or fish bones fragments. (B) Varve-like laminated sandstone with biological remains. (C) Fossiliferous marly sandstone. (D) Fossiliferous marly sandstone with plant remains and fish bone fragments. (E) Grey homogeneous micrite. (F) Grey marly sandstone and marly limestone layers, with small coal fragments. Samples are from the "Couches à Foraminifères" (A), "Couches à Amphisiles" (B), and "Couches à Meletta" (C, D, E, F).

Table 1: Lithofacies associations, descriptions, and interpretations of samples of the "Basal Eocene", "Zone Salifère Inférieure", "Zone Salifère Moyenne", and "Zone Salifère Supérieure" from the DP-XXVIII, DP-95, Marie-Louise, and Joseph-Else boreholes and wells.

Lithofacies	Description	Depositional process	Environment	Photographs
Evaporite				
(A1) Layered anhydrite	Millimeter- to centimeter-scale layers of white fibrous anhydrite. Associated with structureless and/or laminated mudstones.	Occurrences of humid periods (deposition of marl through increased river inputs) and arid period (precipitation of evaporites through evaporation and/or driven by temperature changes)	"Deep" lake with periodically meromictic brine column	**Figure 55** B, C, H
(A2) Nodular anhydrite	Centimeter-scale anhydrite nodules, usually associated with mudstones. Either disposed as beds of nodules, or singular nodules.	Syn-depositional Displacive nodules formed in soil through capillary evaporation Diagenetic Dehydration of gypsum crystals during burial	Either syn-depositional in a sabkha environment, or diagenetic.	Bedded: **Figure 54** C Singular: **Figure 54** A
(H) Bottom-growth halite	Millimeter- to centimeter-scale bottom-growth halite crystals, usually forming chevron structures, apparent fluid inclusions	Precipitation through evaporation of hypersaline brine in a shallow lake	"Shallow" lake with long-term holomictic brine column	**Figure 54** D, **Figure 59**, **Figure 60**, **Figure 62**
(P) Potash alternations	Centimeter-scale alternations of seasonal thin marl layers, halite chevrons, and crystalline sylvite.	Depositional processes controlled by seasons. Marls deposited during the humid season (increased river inputs) and evaporites formed during the arid season (precipitation through evaporation and/or driven by temperature changes)	Successions of relatively humid and arid seasons during a period marked by overall increased aridity in a "shallow" lake.	**Figure 59**, **Figure 60**, **Figure 62**
Sub-aerial, fluvial, alluvial-fan, shallow lacustrine				
(C1) Paraconglomerate / Pebbly mudstone	Red mudstone matrix with ungraded and rounded Jurassic limestone clasts. Disorganized fabric.	Debris-flow of mud and pebbles during floods	Alluvial fan	**Figure 53** D, E
(C2) Ortho-conglomerate	Clast-supported conglomerate with rounded Jurassic limestone clasts. Associated with sandstones and red mudstones. Erosive base.	Bedload transport of gravel to pebble size clasts in a channel	River channel and/or braided stream environment	**Figure 53** F, G
(S1) Structureless sandstone	Sandstone with no clear structure. Associated with stratified orthoconglomerates.	Rapid deposition of sand, most probably through the deceleration of sediment-rich currents	Fluvial and/or alluvial-fan	1735.8 m (supplementary material, DP-XXVIII pictures)
(S2) Stratified sandstone	Sandstone with distinguishable layers.	Upper flow-regime flat bed	Fluvial and/or alluvial-fan	**Figure 53** F

(M1) Bioturbated red mudstone	Red mudstone with traces of tunnels, shafts, and/or trails. Sometimes contains deformed laminations and/or floating pebbles.	Decantation of very fine material perturbated by digging organisms.	Sub-aerial to shallow holomictic lake	**Figure 53** A, B, C
“Deep” lacustrine				
(M2) Structureless mudstone	Mudstone with no clear structure, displaying clear conchoidal fractures	Continual, homogeneous, and steady decantation of very fine material	Shallow to deep lake	**Figure 54** A, B
(M3) Laminated mudstone	Mudstone with clearly distinguishable laminations, which often consist of alternations of marl and anhydritised gypsum. These tend to be thicker than the laminations of varved mudstones.	Occurrences of humid periods (deposition of marl through increased river inputs) and arid period (precipitation of evaporites through evaporation and/or driven by temperature changes)	“Deep” lake with periodically meromictic brine column.	**Figure 54** F, **Figure 55** A, F, E, G **Figure 56** A, B, C, D, E
(M4) Varved mudstones	Mudstone with clearly distinguishable laminations which form reoccurring patterns of dark-colored (marls) and light-colored (anhydrite) laminae	Depositional processes controlled by seasons. Marls deposited during the humid season (increased river inputs) and evaporites formed during the arid season (precipitation through evaporation and/or driven by temperature changes)	“Deep” lake with seasonally meromictic brine column.	See **Chapter V :**

IV.2 : Sedimentological study of the tertiary outcrops of the Upper Rhine Graben

Outcrops localizations (**Figure 44**) were found through two main means: the (1) work of Duringer (1988) on axial conglomerates which contains the localizations of many outcrops, and (2) by superposing the geological map of the Upper Rhine Graben with a map of old quarries. Former quarries localized in Eocene-Oligocene sediments were visited. Many ancient outcrops are not accessible anymore due to vegetation growth, resealing, security reasons and/or constructions. Others are remnants of what they used to be according to their formal descriptions. Despite that, the remaining ones still allow for a nice overview of the stratigraphy and sedimentary structures. The main outcrops that have been studied are located in Turckheim (Letzenberg), Westhalten (Strangenberg), Tagolsheim (quarry), and Altkirch (quarry).

IV.2.a : Turckheim

The investigated outcrop located in Turckheim is found on the southwestern side of the Letzenberg hill. It consists of alternating beds of conglomerates, sandstones, and mudstones. This outcrop is located particularly close to the rift’s western shoulder (**Figure 44**). The first 20 meters were logged (**Figure 66**), but the sediments above those were hard to access. A full log made by Duringer (1988) was made when the section was fresh (~41 meters).

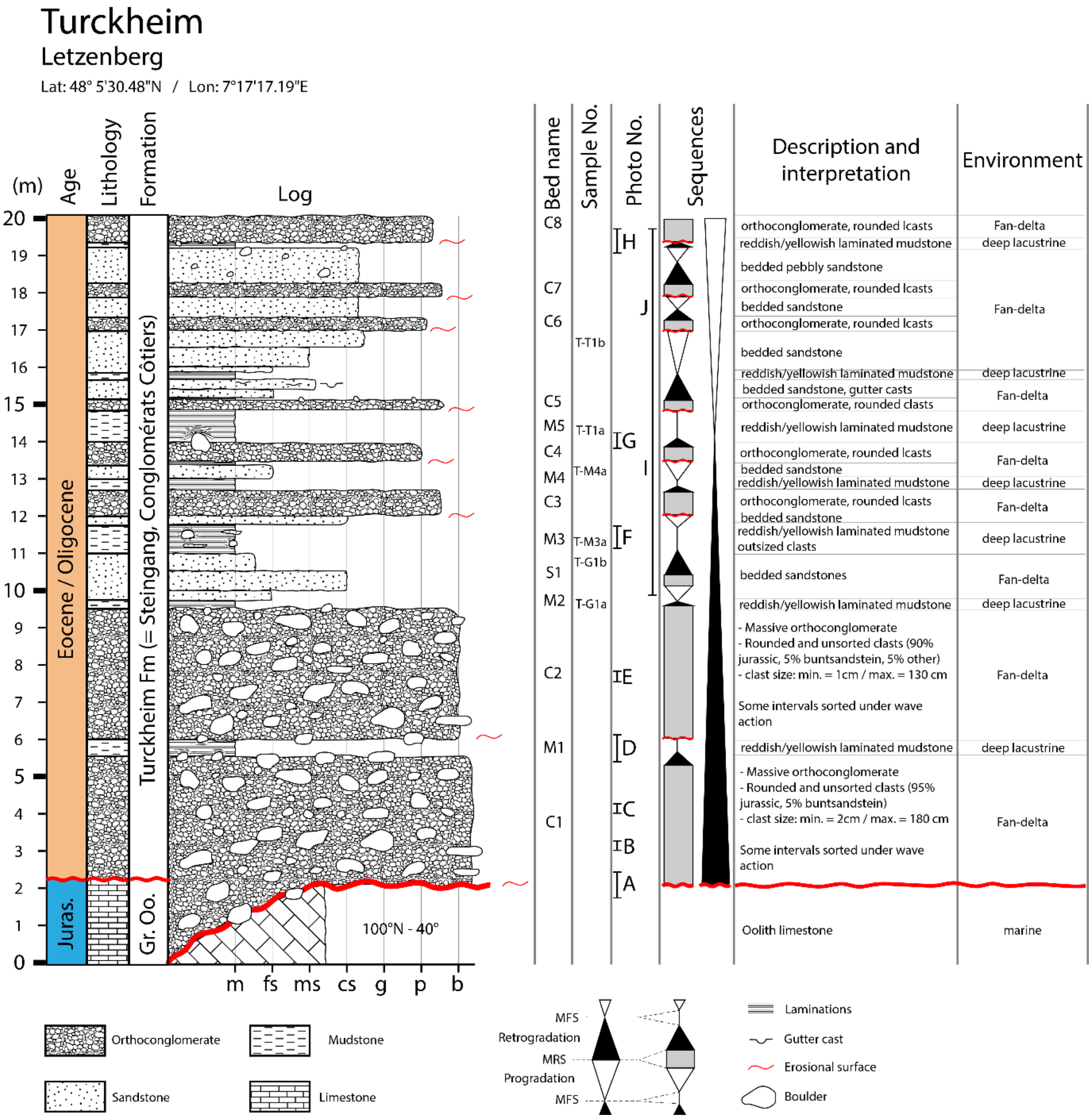

Figure 66: Sedimentary log of the Letzenberg outcrop in Turckheim.

IV.2.a.i : Description

The section begins with an exposed succession of oolithic limestone beds attributed to the "Grande Oolithe" formation of the Jurassic. These beds are eroded by a thick orthoconglomerate unit (~4 to 6m) made of rounded and unsorted clasts with sizes ranging from 2 cm to 180 cm in diameter (Figure 67A, B). These clasts mainly consist of oolithic limestones (95%, Jurassic) and red sandstones (5%, Buntsandstein and/or Aalenian) (Figure 67C). Its upper surface displays washed pebbles (Figure 67D). This orthoconglomerate is topped by a reddish/yellowish laminated mudstone bed, which is itself truncated by a second orthoconglomerate unit similar to the first one. It only differs from the first one by the size of the clasts (1 cm to 130 cm in diameter) and by their origin; there are 90% oolithic limestone clasts (Jurassic), 5% red sandstone clasts (Buntsandstein?), and 5% pure quartz clasts (?) (Figure 67E). On top of it is a thin laminated mudstone bed with overlying structureless sandstone beds. On top of those is a laminated mudstone bed in which outsized clasts are found (Figure 67F). These outsized clasts caused the deformation of the underlying laminations. Above are found, in sequence, a coarse sandstone bed, a pebble-sized orthoconglomerate with an erosive base, a laminated mudstone bed, a fine sandstone bed, and a thin laminated mudstone layer truncated by a pebble-sized orthoconglomerate. At the top of the orthoconglomerate lays a washed boulder followed by draping laminated mudstones (**Figure 67**G). This mudstone bed is truncated by a pebble-sized orthoconglomerate followed by fine to medium grain sandstones with gutter cast structures. Then are found in sequence a thin laminated mudstone bed, a fining upward sequence of fine to coarse size sandstones truncated by a pebble-sized orthoconglomerate. There are then two alternations of coarse grain sandstone truncated by pebble-sized orthoconglomerates, with the presence of a small, laminated mudstone bed between the sandstone and conglomerate of the second alternation.

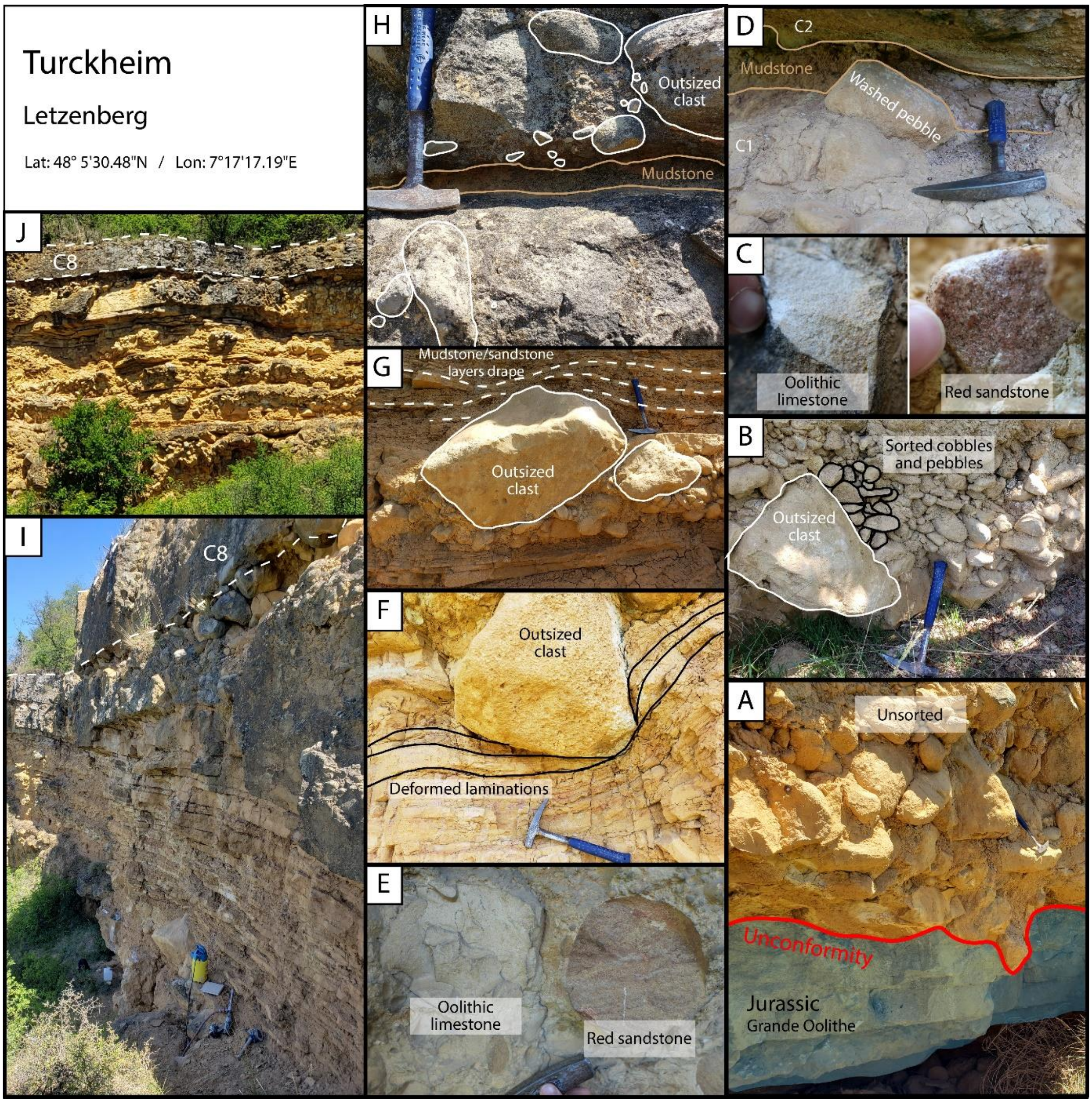

Figure 67*: Photographs of sedimentary structures of the Turckheim outcrop. (A) Unconformity between the Jurassic limestone and truncating Eocene conglomerate. (B) Orthoconglomerate with rounded clasts and lack of stratification. Cobbles and pebbles are sorted between outsized clasts, suggesting sorting under wave action as previously proposed by Duringer (1988). (C) Composition of the constituent clasts of the first conglomerate bed with (left) oolithic limestone and (right) red sandstones. (D) Laminated mudstone interval positioned between the first two conglomerate beds. Note the truncating nature of the overlying conglomerate and the presence of washed pebbles at the top of the underlying one. (E) Composition of the constituent clasts of the second conglomerate bed with oolithic limestone and red sandstones. (F) Outsized clast which deformed the underlying mudstone laminations.*

(G) Outsized clast in a conglomeratic bed. Note how the overlying mudstone drapes the clast. (H) Small, laminated mudstone bed localized between the overlying conglomerate with an erosive base and the underlying bedded pebbly sandstone. (I, J) Overview of the upper part of the log.

IV.2.a.ii : Interpretation

In this outcrop, the laminated mudstones are interpreted as being the result of the settling of fine sediments (clay to silt) in a relatively deep subaqueous setting (below the wave-base). These mudstone beds sometime contain small siltstone to sandstone beds which indicate the input of thicker material, possibly linked to short variations in lake level or sediment flux. Most of the sandstones of this outcrop appear to be structureless, with sharp bases and tops, and displaying rather good lateral continuity. Such beds could be the result of rapid deposition, or specific processes could have destroyed the original laminations. It is also possible that I did not notice laminated or cross stratification structures.

The conglomerates are clast-supported, and the clasts are heterolithic, rounded, and at first glance unsorted. The roundness of the clasts suggests that they travelled enough distance to be rounded either by water or through repeated impacts. They are either the result of a debris flow or of fluvial processes. As such, and according to the position of the outcrop (next to the rift's shoulder), these deposits are interpreted as alluvial fan deposits. Coarse alluvial fan deposits are classically divided into two main categories: (1) braided stream conglomerates and (2) mass-flow (or debris-flow) conglomerates (Nemec and Steel, 1984). Braided stream conglomerates are characterized by their clast-supported nature and crude to well-developed stratification (grain size, sorting), and tend to be associated with well laminated sandstones (Nemec and Steel, 1984). In contrast, because of the potential variability of mass flows, the characteristics of their deposits such as matrix percentage and clast grading are not diagnostic. There however are features generally characteristic of mass flows such as the lack of stratification, clast-supported to matrix-supported deposits often containing "outsized" cobbles or boulders, and beds commonly displaying a positive correlation between their thicknesses and maximum clast sizes (Nemec and Steel, 1984). As such, the conglomerate beds of the Turckheim outcrop seem to be characteristic of mass-flow deposits due to the lack of stratification and presence of many "outsized" boulders. Such deposits can occur either in subaerial or subaqueous settings. While it can be hard to decipher between the two, subaqueous debris-flow often display mudstone interbeds (Nemec and Steel, 1984), similar to those observed in Turckheim. Based on those observations, the sedimentary record of the Turckheim outcrop is coherent with fan-delta deposits. It is however not impossible that some parts of the recorded were deposited subaerially. In the first two big conglomeratic interval at the base of the outcrop, several intervals consist of sorted cobbles and pebbles localized between outsized blocks (**Figure 67** B). These structures have been interpreted as being the result of sorting under wave action by Duringer (1988).

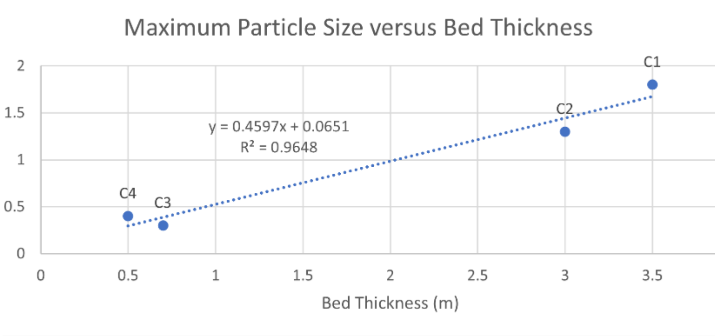

__Figure 68__: Maximum Particle Size versus Bed Thickness of the first four conglomerate beds of the Turckheim outcrops (C1 to C4).

Measurements were performed on the first four conglomerate beds to document the relation between their thickness and the maximum size of their clasts. These measurements suggest a linear correlation which goes through the origin (**Figure 68**). According to the empirical evidence of Nemec and Steel (1984), such results are indicative of cohesionless behavior in fan-deltas.

IV.2.b : Westhalten

Similarly to the Turckheim outcrop, the Strangenberg outcrop mainly contains conglomerates, sandstones, and mudstones (**Figure 69**). Here however, sandstones are predominant. Nowadays, similarly to the Turckheim outcrop, the Strangenberg outcrop is not as fresh as back when scientists first studied them (Duringer, 1988; Gaudant, 1979). The lower part of the section cannot be accessed anymore due to the growth of vegetation and the presence of a pond. By comparison with the log of Duringer (1988), it appears that the mudstone bed attributed to the “Zone Fossilifère” is no longer accessible. As such, the investigated interval is likely to be the time-equivalent of parts of the “Zone Salifère Supérieure”.

IV.2.b.i : Description

The section begins with two alternations of structureless sandstone and thin paraconglomerate with rounded clasts. The paraconglomerates of the section could also be referred to as gravely to pebbly sandstones. The clasts consist of oolithic limestones, red sandstones (**Figure 70**B), pure quartz, and pure micrite. A reddish/yellowish laminated mudstone is found on the top of these beds, and washed pebbles are disposed on the surface between them (**Figure 70**A). This mudstone bed is truncated by a mudstone bed, which even erode down to the underlying paraconglomerate in some parts of the outcrop. There are two small alternations of paraconglomerate and sandstone on top, with the last sandstone bed displaying relatively large oscillations ripples (4 cm in height, 34 cm in wave-length) at the very top, with their crests oriented N180 (almost parallel to the rift’s shoulder fault) (**Figure 70**C). On this surface lay washed pebbles. On top lay a reddish/yellowish laminated mudstone bed (**Figure 70**D) which is truncated at the top by a thin paraconglomerate bed. In sequence are then found a structureless sandstone bed, a thin paraconglomerate, another structureless sandstone bed, and a laminated mudstone bed (**Figure 70**E). On top of the mudstone is found a massive sandstone bed with two thin gravely layers in the lower half. The surface between the mudstone and the sandstone is very planar. On top of the sandstone lays a laminated mudstone bed, truncated by and overlying sandstone bed. This bed is a coarsening up sequence of silt to very fine sand at the bottom to medium sand at the top, with many laminations and several gutter casts and oscillation ripples (**Figure 70**F). Measured oscillation ripples display heights of 1 cm, lengths of 10 cm, with their crests oriented N170. The top surface of the succession consists of oscillation ripples. On top lays a laminated mudstone bed, truncated by a sandstone bed which lower half is laminated and upper half structureless. On top lays a laminated mudstone bed, truncated by a gutter cast from the overlying sandstone bed (**Figure 70**G) which lower half is structureless and upper half laminated with oscillation ripples and erosive surfaces. The gutter cast (7 cm in height, 15 cm in length) at the bottom cuts through the underlying mudstone down to the upper part of the underlying sandstone. Then are found is sequence a laminated mudstone bed, a structureless sandstone, another laminated mudstone bed, and a laminated sandstone bed.

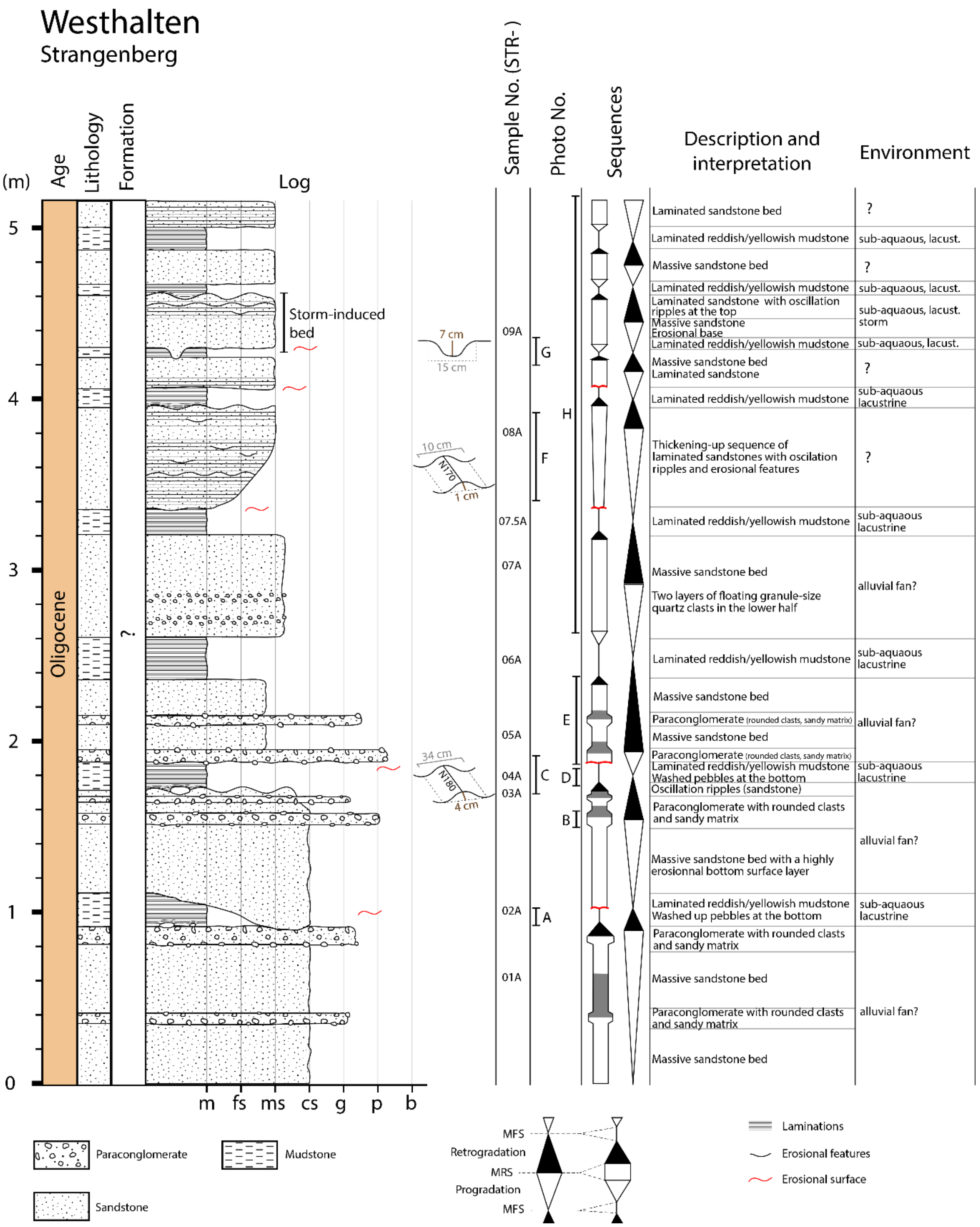

Figure 69: Sedimentary log of the Strangenberg outcrop (ancient quarry) in Westhalten.

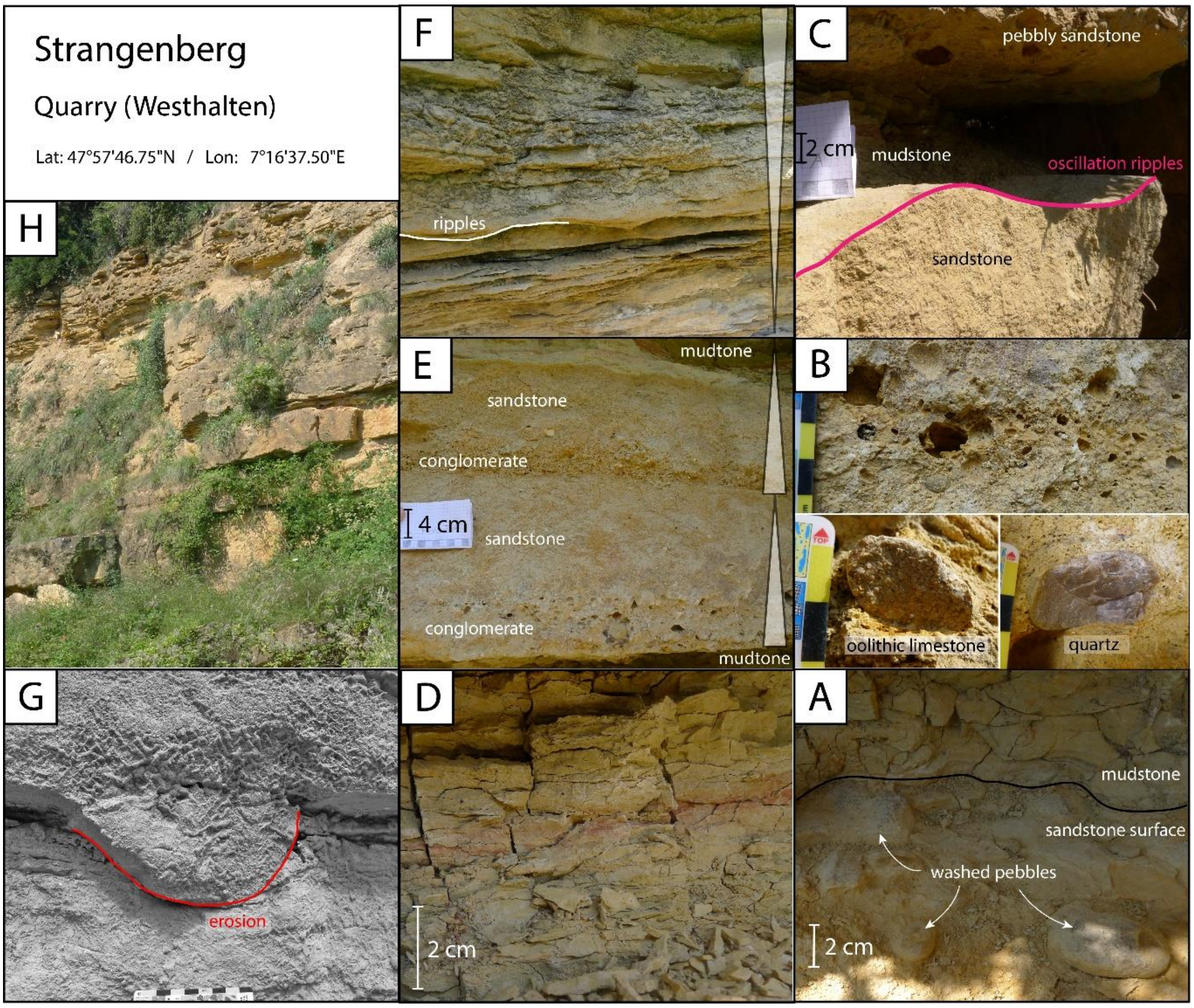

Figure 70: Photographs of sedimentary structures of the Strangenberg outcrop. (A) Wash pebbles of top of a sandstone bed with overlying laminated mudstones. (B) Paraconglomerate (upper half) with oolithic limestone (bottom left) and pure quartz (bottom right). (C) Oscillation ripples on top of a sandstone bed, with overlying laminated mudstone truncated by a pebbly sandstone. (D) Reddish/yellowish laminated mudstone. (E) Two paraconglomerate/sandstone alternations, with laminated mudstones bellow and above. (F) Details of the coarsening up sandstone sequence, with laminated sandstone and oscillation ripples. (G) Erosive feature (gutter cast) truncating through laminated mudstones and sandstone. (H) Overview of the outcrop.

IV.2.b.ii : Interpretation

Similarly to the Turckheim outcrop, the laminated mudstones of the Strangenberg quarry are interpreted as being the result of the decantation of fine sediments (clay to silt) in a relatively deep subaqueous setting. The sandstones however contrast with those of the Turckheim outcrop as several sedimentary structures such as lamination, oscillations ripples, gutter casts, and erosional features were found. The presence of oscillation ripples suggests that they were formed by the action of waves (below lake-level).

In the lower half of the section, the presence of coarse sandstone beds and paraconglomerate beds, as well as washed pebbles (up to 15cm) suggests that processes related to alluvial fans were at work. As such, the sedimentary record described here is interpreted as being part of an ancient alluvial fan, which was probably very close to the shore, sometimes underwater as suggested by the presence of oscillation ripples.

In the upper half of the section, the sediments are finer, suggesting deposition further away from the apex of the alluvial fan. The sedimentary succession of the third sandstone bed starting from the top of the log (**Figure 69**) is particularly reminiscent of a storm induced bed

(Brenchley, 1989). The idealized sequence contains, from bottom to top, an erosive surface, a graded structureless sandstone, parallel or low angle cross-laminations, hummocky and swaley surfaces, planar laminations, ending with wave ripples and potential erosion (Brenchley, 1989). In practice, some parts of this sequence are missing (Brenchley, 1989), which seems to be the case for the sequence of the Strangenberg outcrop. It is therefore interpreted as the result of storm-induced sedimentation in subaqueous lacustrine settings. Other oscillation-ripples in the upper half of the section

IV.2.c : Tagolsheim

The Tagolsheim quarry is located south of the Mulhouse basin, on the Mulhouse horst. It consists of a ~40 m succession of white limestones with rare mudstone beds. Only the first three meters were logged in details due to the impossibility to reach the rest of the section. When the quarry was exploited, there used to be several levels on top of which machines were digging in the limestone. Since then, these levels almost disappeared and/or are full of vegetation, resulting in the quarry nowadays being a 40m wall. However, through a forest on the eastern side of the quarry, some limestone beds of higher sections were reached and sampled for paleomagnetism tests. According to a previous study carried out in this quarry (Stucky, 2005), a reptile tooth found at the bottom of the quarry could be indicative of the MP17 to MP18 biozones (early to mid-Priabonian), and *Characeae* could be indicative of an early Oligocene age at the top. However, according to the French geological map, the limestones of the Tagolsheim quarry are attributed to the “Calcaires à Mélanies”, which are usually attributed to the Bartonian and early Rupelian. New paleontological studies are required to better date these sediments.

IV.2.c.i : Description

The sedimentary record of the Tagolsheim quarry begins with a white limestone in which grey to black limestone clasts are found, forming what resembles a paraconglomerate (**Figure 72**: Photographs of sedimentary structures and fossils from the Tagolsheim quarry.**Figure 72**A). On top are found reeds fossilized in living position inside a limestone matrix, forming a boundstone (**Figure 72**B). Above it is a small clast-supported breccia made of white limestone clasts with interstitial calcite, which doesn’t seem to truncate through the underlying bed (**Figure 72**C). On top lays a floatstone composed of a white limestone matrix with grey to black micrite clasts disposed across it. This bed is truncated at the top by a breccia bed similar to the previous one (**Figure 72**D) which also contains involute shell fossils (**Figure 72**E). Above it, a small, laminated claystone bed is found (**Figure 72**D). On top lays a floatstone similar to the one described previously, which however contains involute and turriform shell fossils (**Figure 72**F, G). Then, another floatstone similar to the first one is found, above which a massive white limestone bed is located. The rest of the section which I could not log in detail is made of massive limestone beds with rare and thin claystone beds (**Figure 71**).

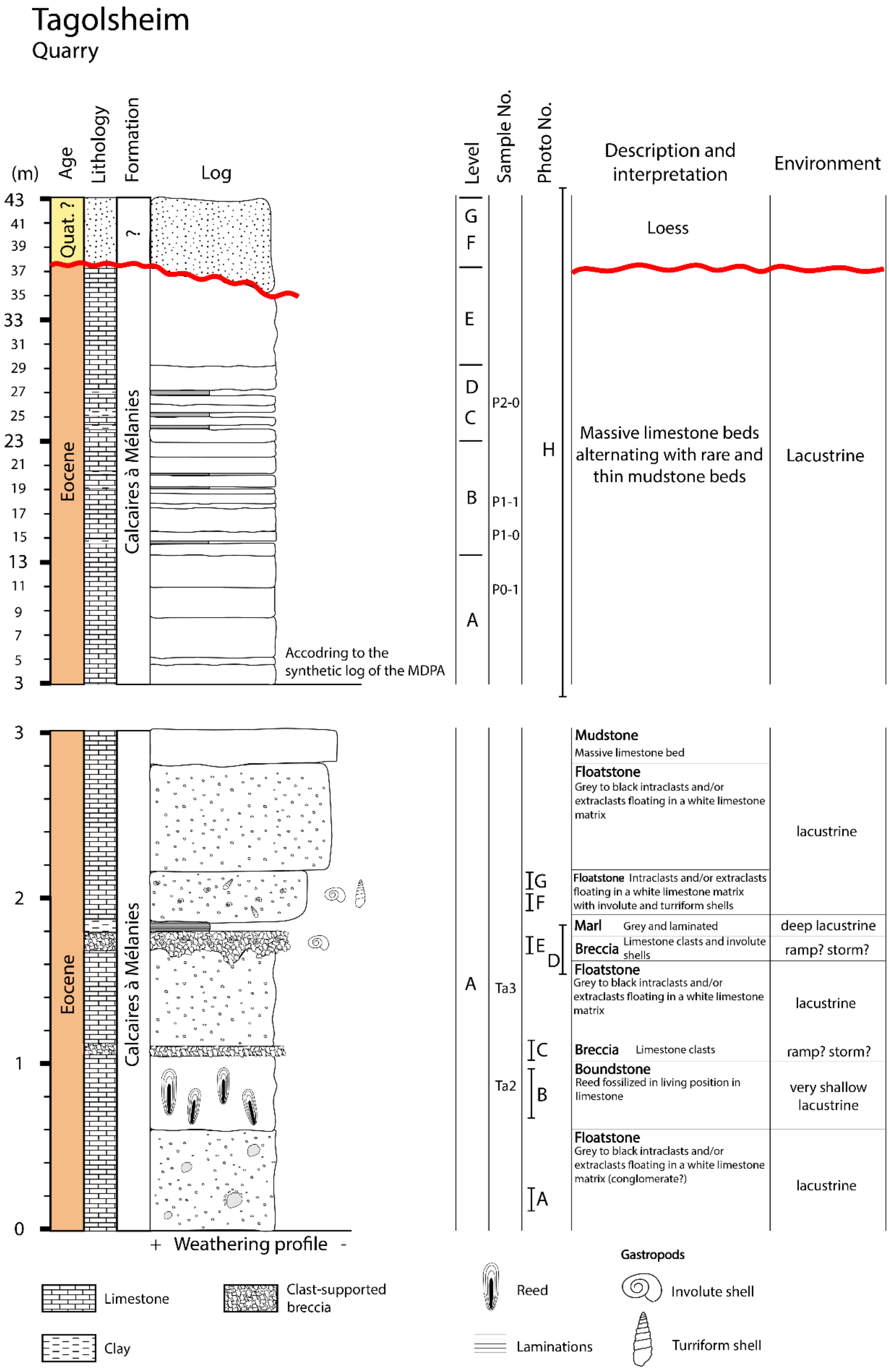

Figure 71: Sedimentary log of the Tagolsheim outcrop (quarry).

IV.2.c.ii : Interpretation

The sedimentary structures and fossils found in the lower part of the Tagolsheim quarry allow the interpretation of their depositional environment. The presence of fossil reeds in living position suggests that the water was shallow enough for the reeds to be slowly encrusted by limestone, likely through a slow by steady increase of the lake water-level. They were potentially living near the shoreline of the lake. The presence of involute and turriform shells, possibly from the *Lymnaea* and *Cerithiidae* families, as well as *Melanoides* genus, suggests that the lake-water was relatively fresh and shallow. However, due to their presence in breccia and in beds with clasts, it is not impossible that they were remobilized. The limestone clasts of the breccias are very similar to the underlying and overlying ones, suggesting the remobilization of limestones from the same formation. As such, the clast-supported breccias and beds with clasts could have been deposited through different processes: either through (1) an alluvial fan remobilizing previously deposited limestones, (2) carbonate slope failure causing the “en masse” deposition of remobilized limestones, or (3) reworked due to storm-induced currents. Due to the absence of sandstone, I argue that the second and third processes are more likely to have forced the deposition of such structures than the first one. Furthermore, due to the observation of a typical storm-deposit in the Westhalten (Strangenberg) outcrop (**Figure 69**), the third option appears to be more-likely, even though a combination of the two is possible. The thin laminated claystone beds are interpreted as being the result of the decantation of fine sediments (clay to silt) in a relatively deep lacustrine setting.

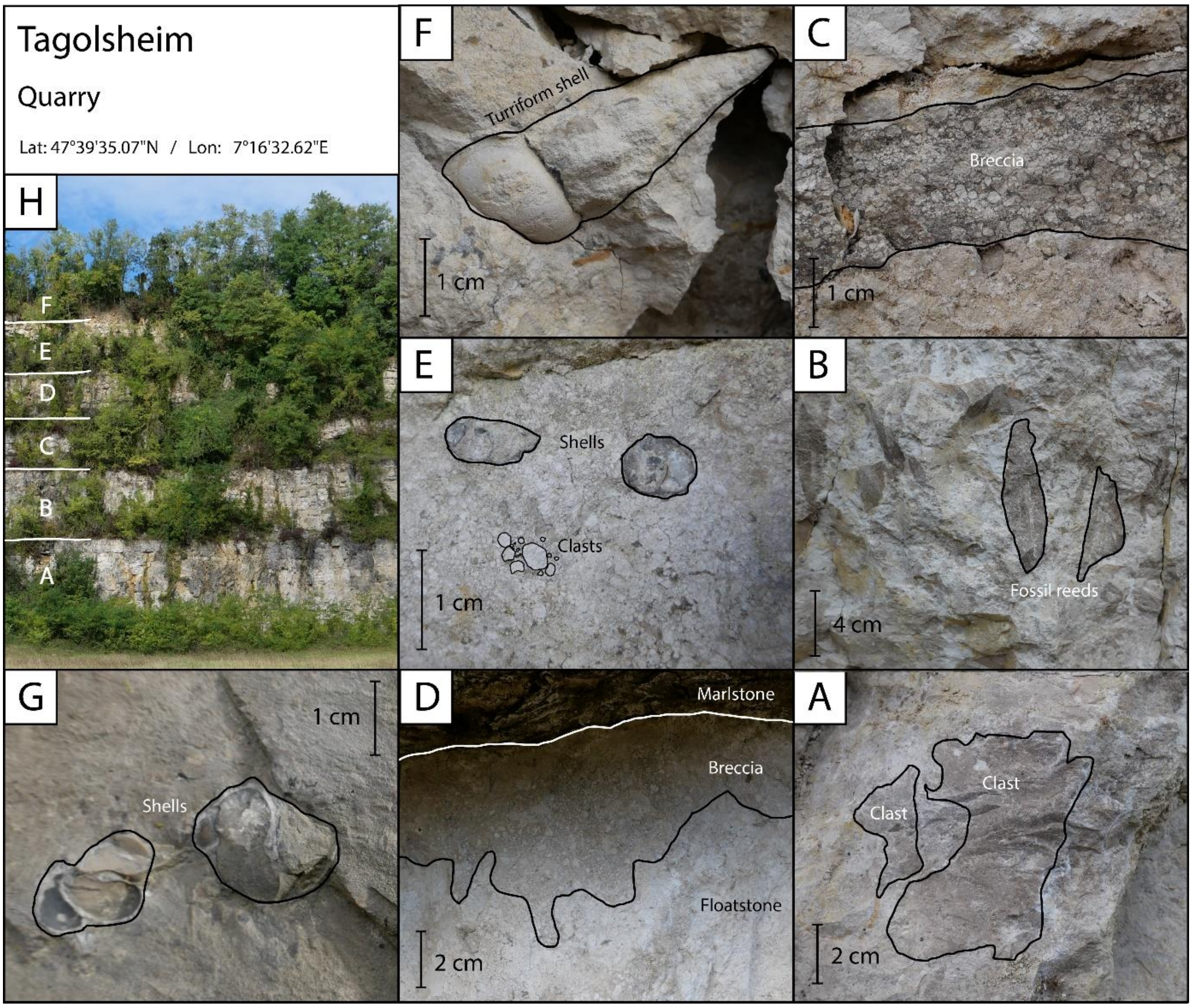

***Figure 72**: Photographs of sedimentary structures and fossils from the Tagolsheim quarry. (A) Gray pebbles and gravels found inside a white limestone matrix. (B) Reeds fossilized in living position inside a white limestone matrix. (C) Clast-supported breccia made of white limestone with interstitial calcite. (D) White limestone truncated by a clast-supported breccia, with laminated claystones on top. (E) Involute shells, likely part of the Lymnaea family, inside the clast-supported breccia. (F) Turriform shell, likely part of the* Cerithiidae *family. (G) Involute shells inside a white limestone matrix, likely from the Melanoides genus. (H) Overview of the whole sedimentary record.*

IV.2.d : Altkirch

The Altkirch quarry is located south of the Tagolsheim quarry, approximately 3.5 km away. While the sedimentary succession of the Tagolsheim quarry is attributed to the “Calcaires à Mélanies”, the lowermost sediments of the Altkirch quarry are attributed to the “Zone Fossilifère” (Duringer, 1988; Gaudant, 1984), which is younger. The Altkirch quarry is still active, and for security reasons (falling boulders), I was not able to log the entire sedimentary succession, but only the lowermost part (**Figure 73**).

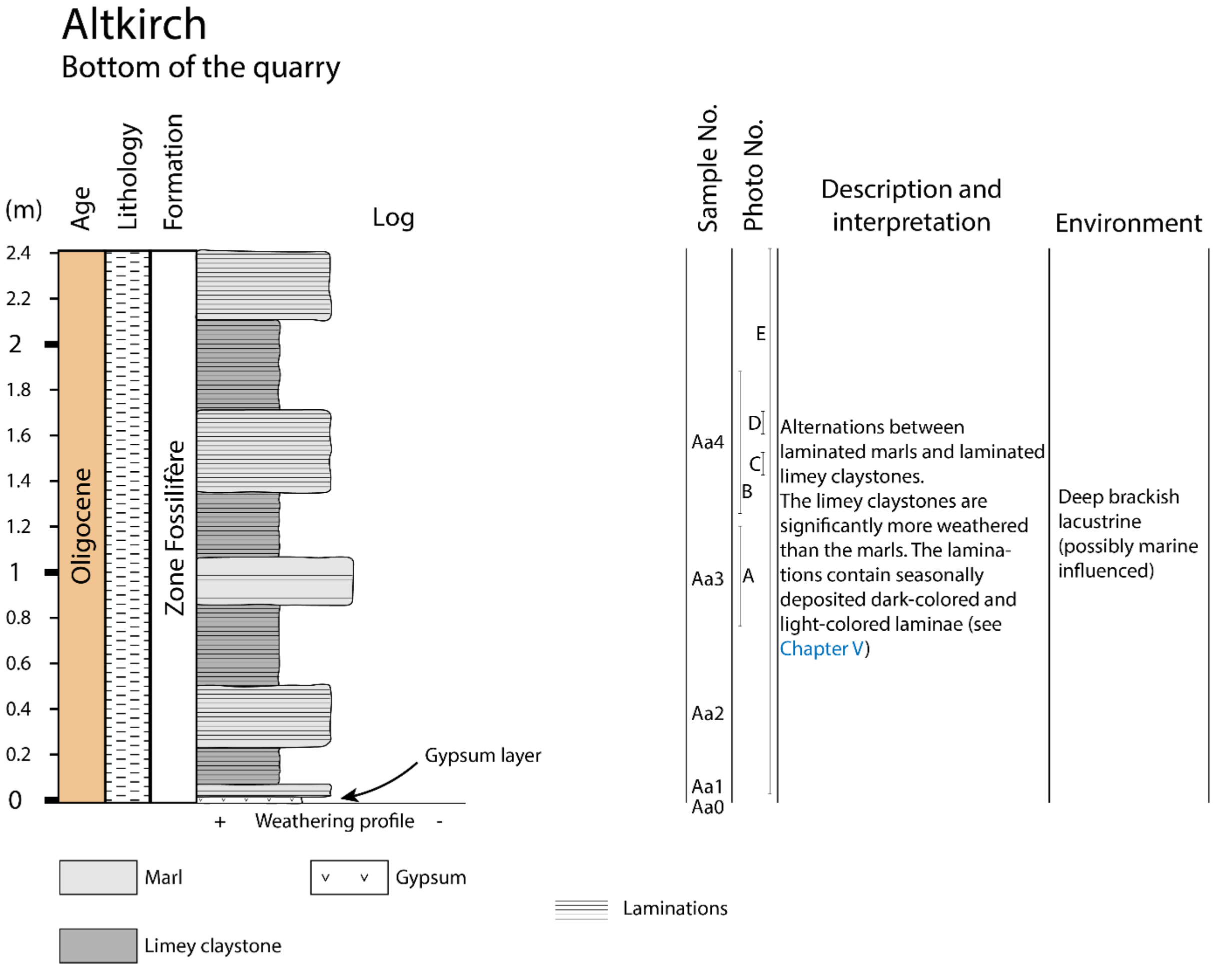

Figure 73: Sedimentary log of the lowermost part of the Altkirch quarry.

IV.2.d.i : Description

The bottom of the quarry, the ground on which the drilling machines drive, consists of anhydrite. The first few meters consists of alternations between laminated marls and laminated limey claystones (**Figure 74**). Thin sections and µ-XRF analyses performed on rock samples from this succession suggest that most of the laminations are of seasonal origin (e.g. varves) (see **Chapter V :**). Other thicker laminations could however originate from floods.

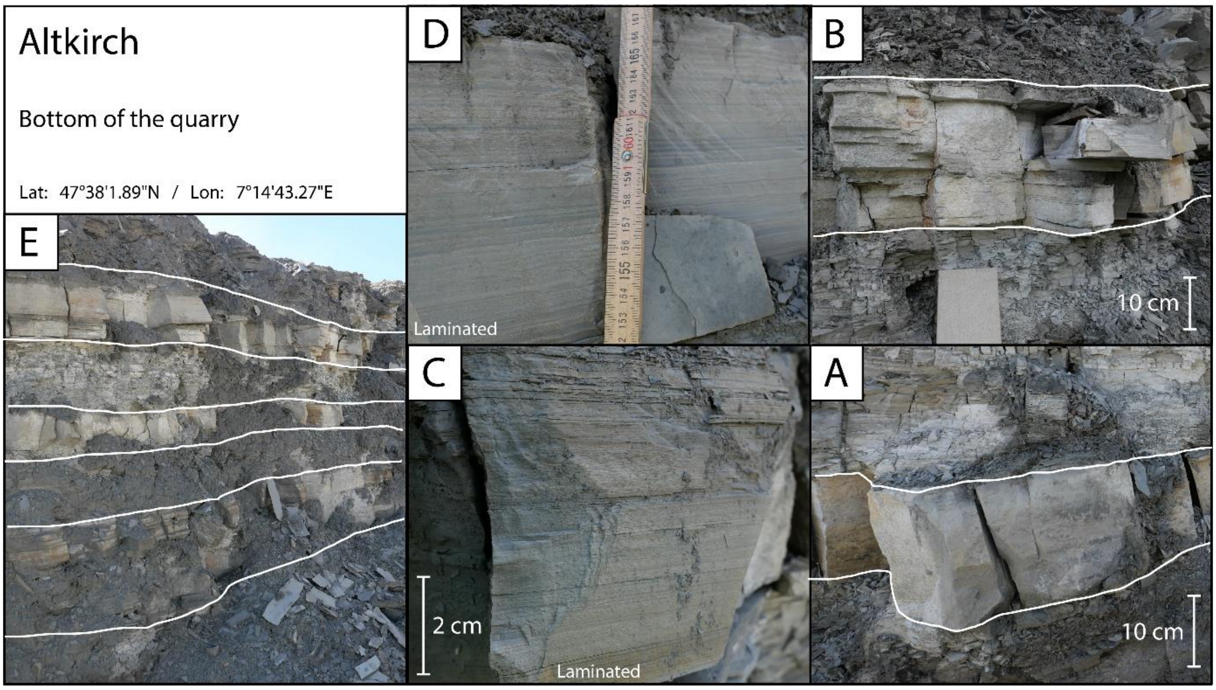

Figure 74: Photographs of sedimentary structures from the Altkirch quarry. (A, B) Laminated marls located between two laminated limey claystones. The marls are more resistant to weathering than the claystones. (C, D) Close photographs of the laminated marls, on which fine laminations of dark-colored and light-colored laminae can be seen. (E) Overview of the investigated section at the bottom of the quarry.

IV.2.d.ii : Interpretation

The presence of varves suggests that the sedimentary processes at work were highly influenced by seasons, with clastic layers deposited during the humid seasons (increased flux of sediments through rain) and carbonate layers deposited during the arid seasons (chemical precipitation through evaporation) (see **Chapter V :**). The environment was lacustrine with potential marine influences. The bottom of the "Zone Fossilifère" in the Mulhouse basin contains clear evidences of marine species (see **II.3.c.iii : About the "Zone Fossilifère"**), but it is not certain if marine pulses coming from the North Sea reached as far as the southernmost Upper Rhine Graben, as structural highs possibly served as barriers.

IV.2.e : Other outcrops

Bergheim

The Bergheim quarry, located a bit further north from the Turckheim outcrop, mainly consists of alternations between clast-supported conglomerates with mostly rounded clasts, and mudstone beds. Only a small part of the section is still visible at the top due to vegetation growth. These sediments are in contact with Jurassic limestones ("Grande Oolithe") due to a fault (**Figure 75**). They are interpreted as fan-delta deposits for similar reasons as those of the section of Turckheim, which are the absence of stratification and grading in conglomerates, presence of "outsized" blocks, as well as the presence of mudstone beds.

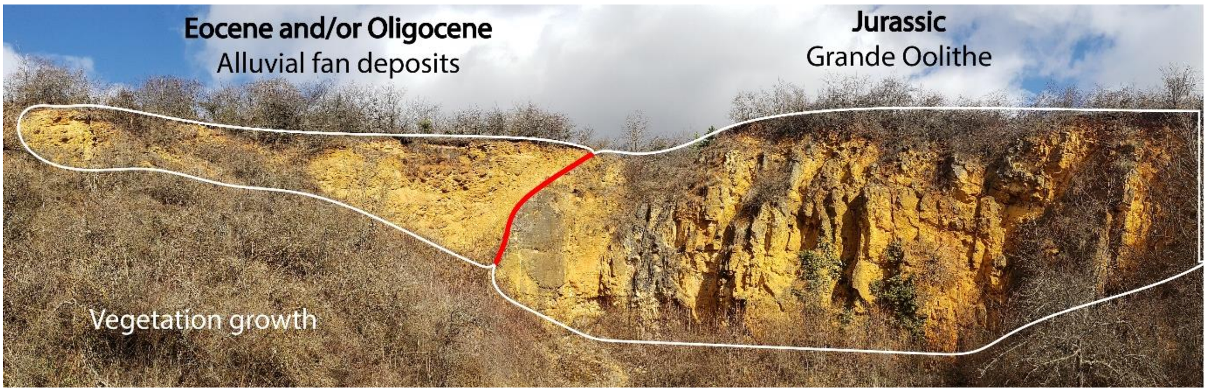

Figure 75: Photograph of the Bergheim quarry, showing the alluvial fan deposits on the left, the Jurassic limestones of the right, and the fault in red between the two.

Réchésy

The Réchésy outcrop is located at the southernmost part of the Upper Rhine Graben, in an ancient quarry. While many parts of this ancient quarry are now covered with vegetation, its main characteristics can be inferred from beds that are still visible. It contains clast-supported conglomerates with mostly rounded clasts which are neither graded nor stratified, with “outsized blocks” (**Figure 76**B, C), slightly indurated sandstones, and red mudstones. These characteristics, similar to those described in Turckheim and Bergheim, strongly suggest that these sediments were part of an ancient alluvial fan system. Paleocurrent measurements done by Duringer (1988) indicate that the flow was going northward.

Rixheim, Hochstatt, Zillisheim

A few ancient quarries located in Rixheim, Hochstatt, and Zillisheim, display a few meters of highly weathered limestones. According to the French geological map, there are attributed to the “Calcaires à Mélanies”. At the Rixheim outcrop, the sedimentary succession consists of centimetric alternations of marls and limestones with meter thick limestone beds in the middle and at the top. Some limestones are rich in *Melanoides* shell fragments and imprints (**Figure 76**Da, Db). The Hochstatt outcrop consists in a 3-meter-thick limestone bed, with breccia containing white limestone clasts, very similar to those described at the bottom of the Tagolsheim quarry (**Figure 72**C, D, E). The Zillisheim outcrop consists in a 2-meter-thick limestone bed which is very weathered (**Figure 76**E).

Heidwiller, Carspach

The two outcrops of the ancient Heidwiller and Carspach quarries are attributed to the “Série Grise” (or “Molasse Alsacienne”) according to the French geological map. They consist of massive gray sandstone beds inside which thin planar and lenticular sandstone beds are intercalated (**Figure 76**G, H).

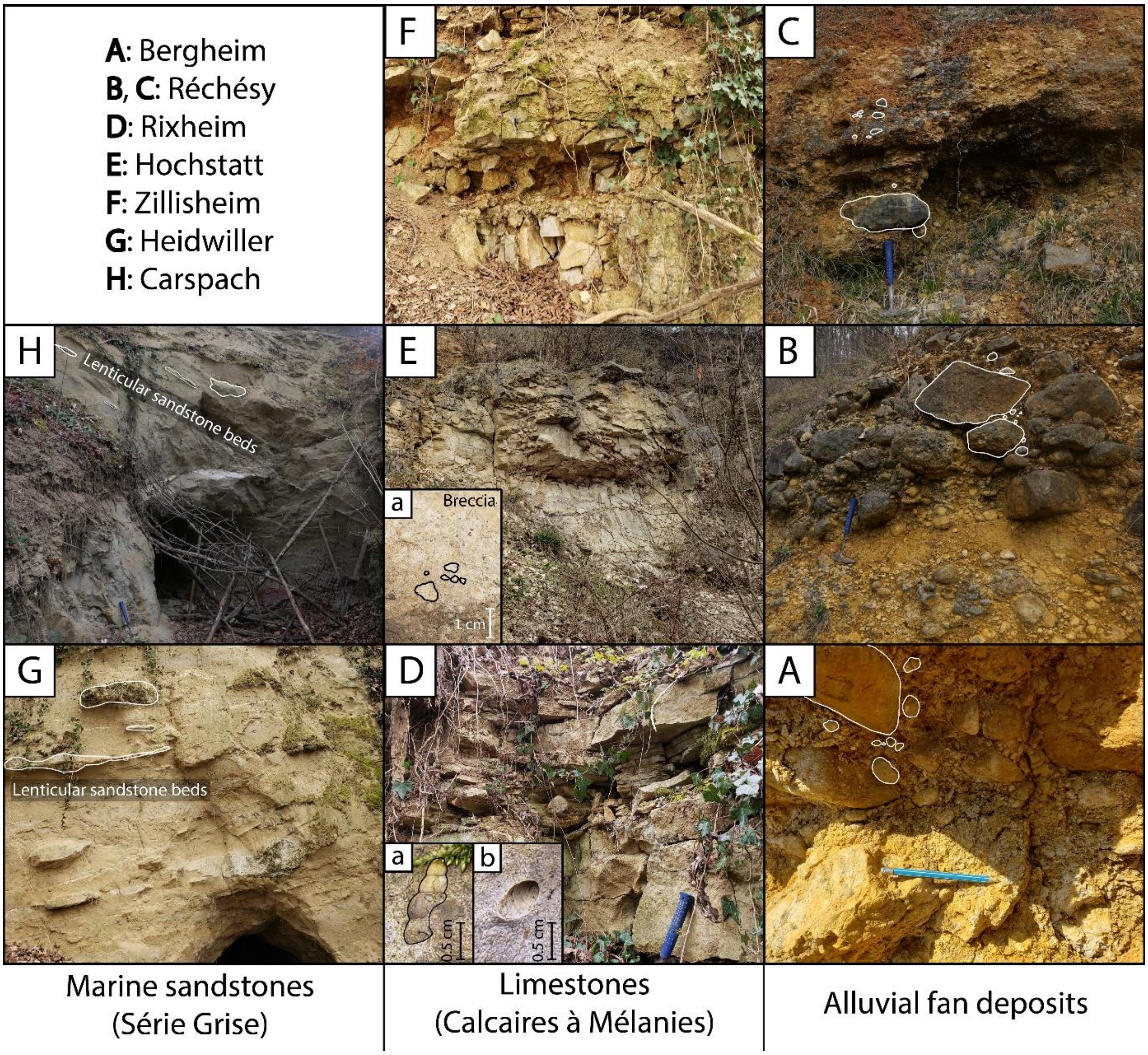

***Figure 76**: Photographs taken in several different outcrops. (A) Clast-supported conglomerate with mostly rounded clasts from the Bergheim quarry (fan-delta). (B, C) Clast-supported conglomerates with mostly rounded clasts alternating with mudstone beds from the Réchésy quarry. (D) Limestones of the Rixheim quarry with Melanoides (Da) shells and (Db) imprints. (E) Limestone of the Hochstatt quarry containing (Ea) breccia with white limestone clasts similar to those found in Tagolsheim. (F) Highly weathered limestone of the Zillisheim quarry. (G, H) Gray sandstones with thin planar and lenticular intercalated sandstone beds.*

IV.2.f : Synthesis

Three main lessons emerge from the sedimentological study of outcrops from the Southern Upper Rhine Graben, which were already detailed by Duringer (1988).

The first one is the presence of transverse alluvial fans issued from the rift shoulders, which fed sediments reworked from the uplifted Mesozoic formations on the rift's shoulders into the rift's basins. The presence of clasts from the Jurassic and Trias in the first conglomerates of the Turckheim outcrop, just above the truncated Jurassic limestones, suggests the presence of deep incised valleys early in the rift's history. Alternations between laminated mudstones, sandstones and conglomerates are interpreted as indicators of lake-level variations, with laminated mudstones deposited during "deep" lake-level intervals, and with sandstones and conglomerates being preferentially deposited during lower lake stands, often truncating through the underlying mudstones (there were also conglomerates deposited during humid periods). Their facies and co-existence suggests that they are fan-delta deposits.

IV.3 : Depositional model of the Mulhouse basin through the Eocene and Oligocene

The following depositional model (**Figure 77**) of the Mulhouse basin is based on the interpretation of core samples, MDPA documents, mine gallery, outcrops, as well as from teachings inferred from the bibliography presented in **II.3 : Geological Setting** (Duringer, 1988; Berger et al., 2005; Roussé, 2006; Blanc-Valleron, 1990; Schuler, 1988; Sittler, 1965).

From the late Jurassic to the early Eocene, the zone in which the URG later formed, was uplifted and formed what was known as the “Rhenish Shield”. The Jurassic limestones were partially eroded and karstified. The filling of these karsts is known as the “Sidérolithique”.

During the middle Eocene (Lutetian, Bartonian?), the zone started subsiding. The occurrence across the URG of very localized lacustrine limestones suggests that small lakes occupied the accommodation space created by structural depressions. In the Mulhouse basin, the occurrence of conglomerates (including pebbly mudstones), sandstones, and red bioturbated mudstones very close to the underlying Jurassic limestones suggests that early rifting started and created a small rift basin in which a shallow-water lake formed, with proto-rift shoulders elevated enough to allow the occurrence of alluvial-fans. The early conglomerates in the middle of the basin appear to be entirely made of Jurassic limestone clasts, suggesting the axial rivers did not cut through the entire Jurassic sedimentary succession at that time.

Across the middle to late Eocene (Bartonian, Priabonian), the main rifting phase started and created a larger and deeper accommodation space in which a “deep”-water lake formed. In the Mulhouse basin, the “Marnes à Limnées I”, “Sel I”, “Marnes à Limnées II”, and “Sel II” were deposited, and are characteristic of an underfilled lake-basin (Bohacs et al., 2000). According to Schuler (1988), the climate was hot and humid all the way through, so the deposition of massive halite intervals was likely induced by tectonics rather than climate, through changes in accommodation rates.

During the Eocene-Oligocene Transition, facies changes from structureless mudstones to laminites and varves occurred (**Chapter V :**), along the appearance of decametric marl-evaporite alternations forced by orbital cycles (**Chapter I :**). These changes are attributed to increased seasonality (**Chapter V :** ; Schuler, 1988) and sensitivity to orbital forcing, events that have been attributed to the EOT in recent studies (Tardif et al., 2021; Wetserhold et al., 2020). The “Sel III”, characterized by these structures, was deposited. Then, the marine transgression of the “Zone Fossilifère” occurred, increasing the lake-level, and resulting in the deposition of a ~80 m thick laminated marlstone interval. The discovery of very specific marine dinocysts assemblages at the bottom of the “Zone Fossilifère” in the Mulhouse basin (Schuler, 1988) strongly suggests the occurrence of an early marine pulse (see **II.3.c.iii : About the “Zone Fossilifère”**).

Across the early to middle Rupelian, the deposition of astronomically forced marl-evaporite alternations happened through the whole “Zone Salifère Supérieure”, suggesting the continued sensitivity of the basin to orbital forcing. Early in the sequence, the occurrence of potash seams marks a period of increased aridity, also suggested by palynological investigations (Schuler, 1988). Climate is however not the sole cause of the deposition of potash seams, as nearby basins do not contain any; the Mulhouse basin’s morphology was particular and closed enough to allow the extreme saturation of brines. From bottom to top, the evaporites of the “Zone Salifère Supérieure”, shifted from halite, to anhydrite, and from anhydrite to gypsum, suggesting changes in accommodations rates and/or climate. According to Schuler (1988), the climate got more humid going upward.

During the middle to late Rupelian, the marine transgression of the "Série Grise" occurred and flooded the whole rift, inducing the deposition of marine sandstones and marlstones.

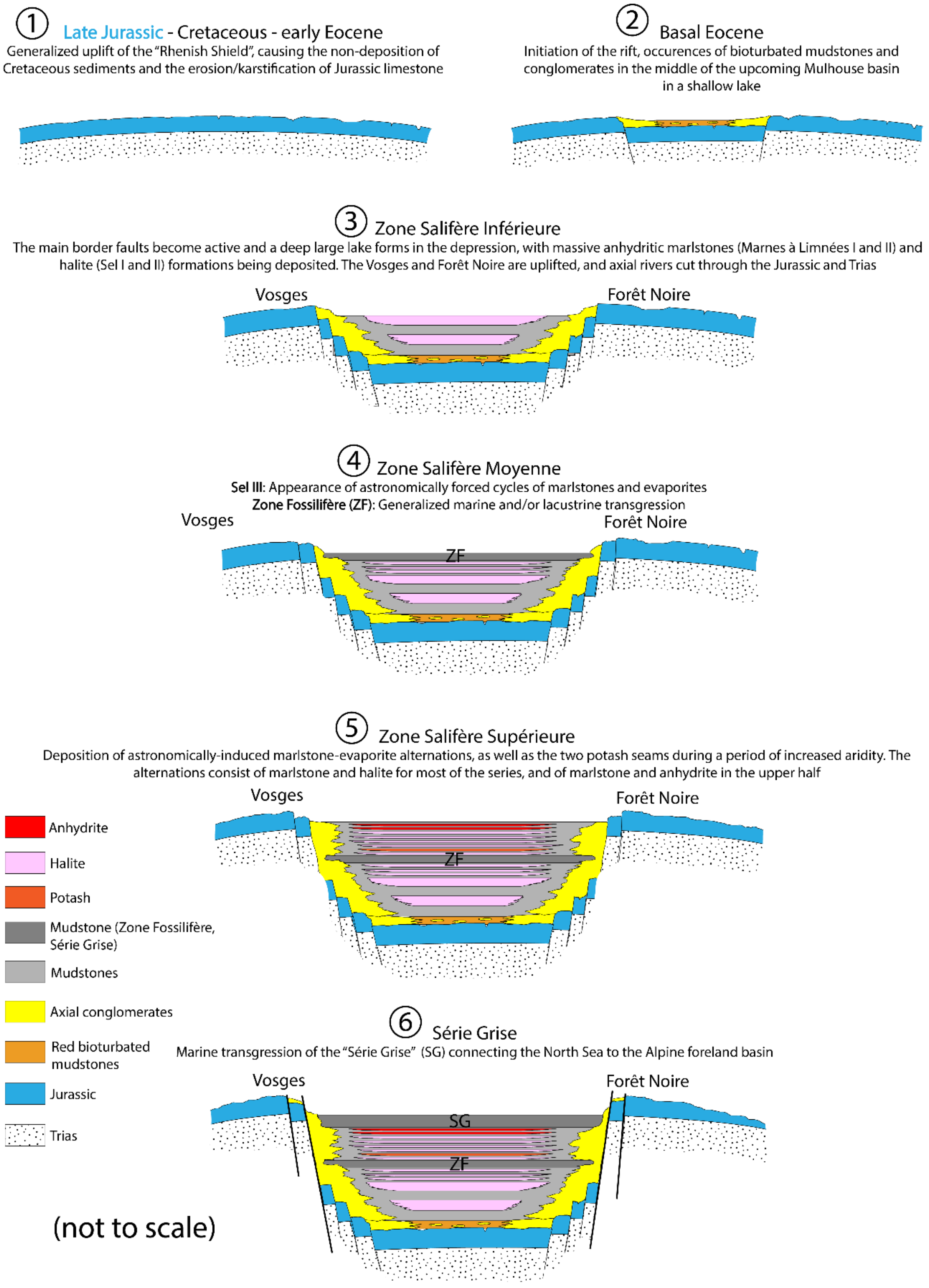

Figure 77: Simplified depositional model of the sedimentary succession of the Mulhouse basin (not to scale).

Chapter V : Lacustrine rhytmites from the Mulhouse basin (Upper Rhine Graben, France): a sedimentological record of increased seasonal climatic contrast and sensitivity of the climate to orbital variations through the Eocene-Oligocene Transition?

This chapter is about the interpretation of the observations performed on the core samples from the DP-XXVIII well. The main result of this article is the identification of the impacts of the Eocene-Oligocene Transition on the sedimentary record of the Mulhouse basin. It is expressed as a sedimentary facies transition from massive mudstones to laminated sediments alongside the onset of decameter-thick mudstone-evaporite alternations induced by orbital cycles. These changes are interpreted as being the result of an increase of the seasonal climatic contrast as well as an increase of the sensitivity of the climate to orbital variations. These observations are compared with those performed in other Eurasian basins, showing strong similitudes.

This study has been submitted to the *Sedimentologika* journal and is under review at the time of publication of this thesis.

Lacustrine rhythmites from the Mulhouse basin (Upper Rhine Graben, France): a sedimentary record of increased seasonal climatic contrast and sensitivity of the climate to orbital variations through the Eocene-Oligocene Transition

Emile SIMON[1], Laurent GINDRE-CHANU[2], Cécile BLANCHET[3], Guillaume DUPONT-NIVET[4,3], Mathieu MARTINEZ[4], François GUILLOCHEAU[4], Marc ULRICH[1], Alexis NUTZ[5], Hendrik VOGEL[6], Mathieu SCHUSTER[1]

Abstract. The Eocene-Oligocene Transition (EOT) marks the passage from the Eocene greenhouse to the Oligocene icehouse conditions. It holds keys to our understanding of the behavior of climate systems under major pCO_2 shifts. While the environmental impact of the EOT is rather homogenous in oceans, it is much more heterogeneous on continents. Although little to no changes are recorded in some regions, several EOT studies in western Eurasia suggest an increase in seasonal climatic contrast (e.g., higher amplitude of changes in mean temperature or precipitation), along with a higher sensitivity of the climate to orbital variations. However, these variations remain to be properly documented through changes in sedimentary facies and structures, and forcing mechanisms identified. We investigate here the depocenter of the Mulhouse basin (Upper Rhine Graben; URG) revealing a prominent transition from massive mudstones to laminated sediments and varves, alongside the emergence of astronomically-forced mudstone-evaporite alternations. These changes are identified in the distal and proximal parts of the southern URG, where they consist of millimeter-thick mudstone-evaporite couplets and siliciclastic-carbonate couplets. The elemental composition and micro-facies analysis of thelaminae show a recurrent depositional pattern consistent with a seasonal depositional process which suggests that they are varves. We propose that the occurrence of varved sediments together with the orbital cyclicity in the southern URG reflects an increase in seasonal climatic contrast and in the sensitivity of climate to orbital variations across the EOT. We show that similar changes were noticed in the Rennes and Bourg-en-Bresse basins, and that other western Eurasian records for similar climatic conditions. This work emphasizes the potential of high-resolution sedimentary structures to serve as markers of climate change across the EOT.

Keywords: Eocene-Oligocene Transition, Seasonality, Varves, Lake, Upper Rhine Graben

2 Introduction

The Eocene-Oligocene Transition (EOT) climatic event (~33.9 Ma) is marked by a strong oxygen isotopic shift globally recorded in oceanic benthic foraminifera and interpreted as a combination of temperature drop and development of the Antarctic ice-sheet (Hutchinson et al., 2021; Miller et al., 2020; Zachos et al., 2001). Data from deep marine carbon and oxygen stable isotope records suggest that the EOT occurred in several steps, with the two major ones being the EOT-1 and the Oi-1 events associated to cooling and to the formation of the Antarctic ice-sheet respectively, the latter resulting in a ca. 70 m eustatic sea-level drop (Hutchinson et al., 2021; Katz et al., 2008; Coxall et al., 2005; Zachos et al., 2001, Miller et al., 1991). Two main mechanisms underpinning the EOT have been proposed: (1) the decrease in atmospheric pCO_2, which likely passed a threshold value (Toumoulin et al., 2022; Pearson et al., 2009, DeConto & Pollard, 2003), and/or (2) changes in oceanic gateways (e.g. Atlantic-Arctic, Southern Ocean, and Mesopotamian), which possibly initiated the Antarctic Circumpolar Current (ACC) (Sarkar et al., 2019; Kennett, 1977).. Initiation and/or strengthening of the ACC could have thermally isolated Antarctica (thus forcing the glaciation) and enhanced CO_2 drawdown through increasing precipitation on land (silicate weathering) (Straume et al., 2022). In addition, the EOT-1 event correspond to a period of low summer insolation, which allowed ice sheets to persist during the summer in some places and eventually spread over the entire Antarctic continent (DeConto & Pollard, 2003; Ladant et al., 2014).

The environmental impacts of climate change at the EOT are well documentedin the marine realm generally showing cooling and increased variability homogenously across the globe (Hutchinson et al., 2021; Bohaty et al., 2012; Liu et al., 2009; Lear et al., 2008; Pearson et al., 2008; Toumoulin et al., 2020). They are a lot more heterogeneous in continental basins, due to the high variability of climate systems affecting continents (Hutchinson et al., 2019; Tardif et al., 2021; Toumoulin et al., 2021). Although various studies report evidence of cooling, aridification, increased seasonal climatic contrast (e.g. decrease in cold month mean temperature, increased aridity) (Hutchinson et al., 2021; Utescher et al., 2015; Eldrett et al., 2009; Dupont-Nivet et al., 2007; Mosbrugger et al., 2005; Ivany et al., 2000), and/or biotic turnovers (e.g. Hooker et al., 2004) on continents during the EOT, some do not show any significant climatic changes (Kohn et al., 2009; Zanazzi et al., 2007). These differences potentially inform us on the mechanisms and impacts of the EOT, but they remain poorly documented and quantified.

We focus here on western Eurasia that is affected by various climate systems at this time. In western Eurasia the westerly-dominated moisture source may have been modulated by a proto-Atlantic Meridional Overturning Circulation (AMOC; Abelson & Erez, 2017) or affected by tectonically driven reorganization of the Arctic circulation associated with the EOT (Coxall et al., 2018; Straume et al., 2022). Several studies across the Eurasia suggested that the decrease in continental temperatures was particularly pronounced in winter, leading to a stronger seasonal temperature contrast that could have driven the well-documented biotic turnovers (Grande Coupure; Tardif et al., 2021; Utescher et al., 2015; Eldrett et al., 2009; Mosbrugger et al., 2005; Hooker et al., 2004). Furthermore, recent studies have suggested an increase in the sensitivity of climate to orbital variations across the EOT. In the Rennes Basin (France), lacustrine deposits record successive facies shifts before and after the EOT with strengthening of the eccentricity and precession expressed in the cyclostratigraphic record (Boulila et al., 2021). This can be compared to cyclostratigraphic investigations in northeastern Tibet affected by westerlies showing the sedimentary cycles were dominated by eccentricity prior to the EOT, and that a clear change occurred at the Oi-1 event after which the cycles were paced by a combination of eccentricity, obliquity, and precession (Ao et al., 2020), suggesting a continental-wide increase of the sensitivity of climate to orbital variations. Increased variability and climatic seasonal contrast needs to be better established and documented across Eurasian regions to better assess potential driving mechanisms such as polar amplifications, increased ICTZ shifts, proto-AMOC and land-sea interactions in response to continentalization and aridification (Abelson & Erez, 2017; Tardif et al., 2021).

More generally, further documenting the impacts of climate change during the EOT in continental settings of western Eurasia is relevant to assess the behavior of climate systems through major atmospheric CO_2 shifts, and to contextualize subsequent environmental changes. An opportunity to study these changes and to investigate climate dynamics through the EOT in a mid-latitude continental setting is provided by the rich sedimentary record of the Upper Rhine Graben (URG) rift system that is the focus of this study.

The URG is composed of several sub-basins that have accumulated continental lacustrine as well as epicontinental marine sediment strata of middle Eocene to late Oligocene age (Berger et al., 2005; Simon et al., 2021). The Mulhouse basin, located in the south of the URG (**Figure 1**), is characterized by the large accumulation of predominantly lacustrine mudstones and evaporites (e.g. gypsum, anhydrite, halite, sylvite, and carnallite) of the “Zone Salifère Inférieure” (Lower Salt Zone), “Zone Salifère Moyenne” (Middle Salt Zone), and “Zone Salifère Supérieure'' (Upper Salt Zone) stratigraphic formations (Blanc-Valleron, 1990; Figure 2, see detailed description in section 4.1). Such evaporitic basins are known to be particularly sensitive to climatic changes (Tanner, 2010). Past investigations in the URG suggested an increase in the seasonal climatic contrast at the base of the “Sel III’’ (Salt III) stratigraphic unit of the Mulhouse basin based on palynological changes (Schuler, 1988). It was also suggested that the Eocene-Oligocene boundary (EOb) is represented at certain depth within the Sel III, based on biostratigraphic studies and stratigraphic correlations (Grimm et al., 2011). However, large uncertainties still remain concerning the chronology, and new constraints are required to improve the chronostratigraphy and to characterize the environmental changes in more detail. So far, most of the information comes from palynological studies that show climate changes across the sedimentary formations (**Figure 2**) (Schuler, 1988). Climatic conditions were subtropical with a short or nonexistent dry season through the “Zone Salifère Inférieure”. They were subtropical/Mediterranean through the “Zone Salifère Moyenne'' (suggesting the appearance of a long dry season and thus increased seasonal climatic contrast).A drastic change into a dry and moderately warm Mediterranean-type climate grading upwards into further temperate conditions occurred throughout the “Zone Salifère Supérieure”. However, interpretations of the rich sedimentary facies expressed in the records remain rudimentary and not directly compared to the climate forcing mechanism attributed to the EOT.

Seasonality refers here to the annual cycles of temperature and precipitation (Kwiecien et al., 2022) and is a key phenomenon to document in the scope of EOT studies. Seasonality of temperature refers to the amplitude between the maxima and minima of temperature, and seasonality of precipitation refers to the amplitude and temporal distribution of precipitation (Kwiecien et al., 2022). While investigations (Eldrett et al., 2009; Ivany et al., 2000) and numerical modeling results (Toumoulin et al., 2022) suggest an increase in seasonal climatic contrast at the EOT marked by a fall in cold month mean temperature and higher aridity, it remains to be documented from specific changes in sedimentary facies and structures, and forcing mechanisms remain to be identified. The URG is therefore an excellent site to investigate the impacts of the EOT as it contains several Eocene-Oligocene lacustrine sequences. Furthermore, prior palynological investigations report an increase in the seasonal climatic contrast in the “Sel III'' unit marked by the onset of a long dry season (Schuler, 1988), reinforcing the need for such a study. In this paper, we investigate the sedimentary record of the URG, aiming to provide clues into potential seasonality contrast changes across the EOT, by identifying the development of thinly bedded cycles and associated sedimentological markers of seasonality.

2 Geological Setting

Thanks to its rich underground resources (e.g. petroleum, potash, and geothermal brines), the structure, stratigraphy, and sedimentary record of the URG have been widely accessed through seismic imaging, drilling, coring, and borehole petrophysical logging already over half a century (Roussé, 2006; Blanc-Valleron, 1990; Schuler, 1988; Sittler, 1965; Maïkovsky, 1941). The URG is an intracontinental rift system that contains several middle Eocene to late Oligocene sub-basins (e.g., Mulhouse, Sélestat, and Strasbourg basins), which are separated by structural swells (e.g. Colmar, and Erstein). It is part of the European Cenozoic Rift System (ECRS), which extends across ~1,100 km from the Mediterranean to the North seas. The ECRS formed through the reactivation of Hercynian fracture systems induced by the continental collisions of the Alpine and Pyrenean orogens (Edel et al., 2007; Dèzes et al., 2004). The Tertiary sediments of the URG uncomformably overlie the Mesozoic Germanic basin sediments (e.g. Buntsandstein, Muschelkalk, Keuper, Lias, and Dogger), which cover the crystalline Paleozoic basement (Aichholzer, 2019).

The Mulhouse basin is located in the southern part of the URG (**Figure 1A**), and is delimited by two border faults, with large salt diapirs present in some localities (**Figure 1C**). The basinal infill is characterized by evaporites (e.g. anhydrite, gypsum, halite, sylvite, and carnallite), which alternate with anhydritic mudstones and carbonates (Blanc-Valleron, 1990). Themudstones primarily consist of marlstones composed of micrite and clay to silt-sized lithogenic grains, sometimes with organic matter (Blanc-Valleron, 1990). The nomenclature of the Mulhouse basin was first defined by Förster (1911), before being revised by Maïkovsky (1941), Courtot et al. (1972), and Blanc-Valleron (1990). The southwestern part of the Mulhouse basin is its depocenter (**Figure 1**A, B). The “Sel III” unit and “Zone Salifère Supérieure" formations, separated by the “Zone Fossilifère” unit, consist of cyclic meter-thick to decameter-thick mudstone-evaporite alternations (**Figure 2**). In the lowermost part of the “Zone Salifère Supérieure”, these alternations have been interpreted as being induced by precession (Blanc-Valleron, 1989) based on Sediment Accumulation Rates (SARs) inferred from fine laminations interpreted as varves (Kühn & Roth, 1979).

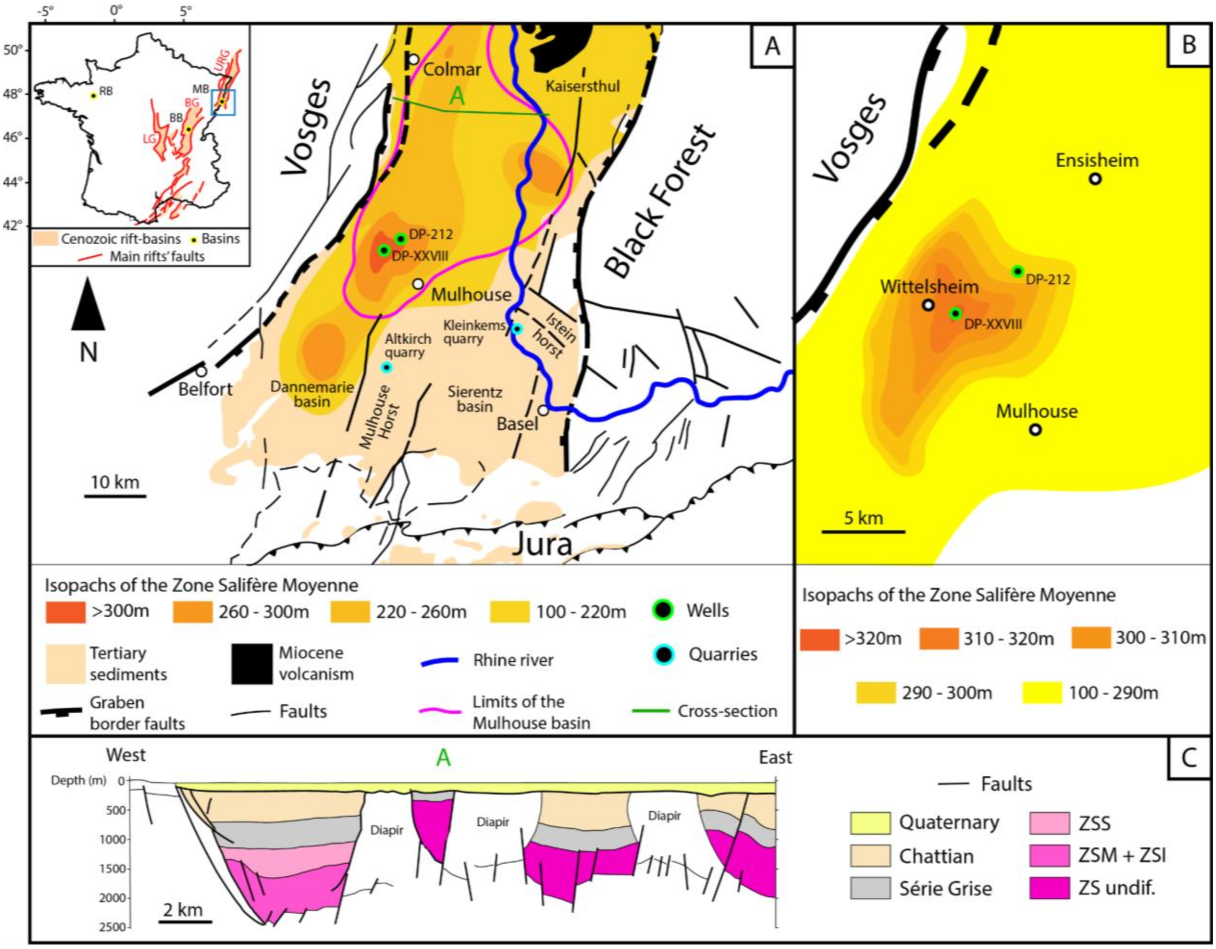

Figure 1: Localization map and geological structure of the southern Upper Rhine Graben. (A) Localization and details of the southern Upper Rhine Graben, with the isopachs of the "Zone Salifère Moyenne", after Blanc-Valleron (1990), Roussé (2006), and the French geological map. (B) Detailed isopachs of the "Zone Salifère Moyenne" in the Mulhouse basin near the DP-XXVIII well, after Blanc-Valleron (1990). (C) Geological cross-section across the upper part of the Mulhouse basin, after Roussé (2006), showing the classical graben structure and the occurrence of huge salt diapirs. URG = Upper Rhine Graben, MB = Mulhouse Basin, BG = Bresse Graben, BB = Bourg-en-Bresse Basin, LG = Limagnes Graben, RB = Rennes Basin, ZSS = Zone Salifère Supérieure, ZSM = Zone Salifère Moyenne, ZSI = Zone Salifère Inférieure, undif. = undifferentiated.

The distance between the border faults of the URG reaches about 60 km towards the South across the Mulhouse basin with relatively complex structures. Two elevated areas known as the Mulhouse and Istein horsts overhang the rift's plain. The exposed sediments of the Altkirch quarry (Mulhouse horst) range from the "Zone Fossilifère" to the "Haustein" (chronological equivalent of the "Zone Salifère Supérieure") (Duringer, 1988). The Kleinkems quarry contains sedimentary series ranging from the Jurassic to the "Zone Fossilifère" (Duringer, 1988). In both quarries, the sedimentary series consist of marlstones, limestones, and sandstones, with occurrences of gypsum. Laminated sediments have been documented earlier by Duringer (1988) from the lowermost geological section exposed in the Altkirch quarry and from the uppermost geological section exposed in the Kleinkems quarry ("Zone Fossilifère"). Duringer (1988) interpreted some of these laminated sediments as varves on the basis of their repetitive millimeter-thick alternations of dark- and light-colored laminae, forming distinct couplets. In the Altkirch quarry, these deposits correspond to the most distal part of a prograding axial river delta, and their counterparts in the Kleinkems quarry are part of a more proximal segment of a fan delta associated to the eastern border fault (Duringer, 1988).

3 Material and methods

3.1 Rock samples and documentation

From 1949 to 1951, a borehole (DP-XXVIII; 1948.6 m) was drilled into Quaternary, Tertiary, and Jurassic sedimentary successions by Mines Domaniales de Potasse d'Alsace (MDPA) for exploration and production objectives. The isopach maps of the "Zone Salifère Moyenne" (**Figure 1**) (Blanc-Valleron, 1990) reveal that the DP-XXVIII well captures the depocenter of the Mulhouse basin, suggesting maximum sedimentary continuity. Core samples from this well (at a scale averaging a sample every few meters) were made accessible by the Musée d'Histoire Naturelle et d'Ethnographie of Colmar for the purposes of the current study (see Figure S1 in Data Availability). The preservation of several samples is rather poor, and almost all halite samples are re-precipitated, however most mudstone samples are in good condition. The original detailed lithological description of the DP-XXVIII well made by the MDPA was made accessible by the KALIVIE museum (Wittelsheim) (MDPA, 1960). The arranged dataset was amalgamated into a sedimentary log of the well (see Figure S1 in Data Availability). In addition, laminated rock samples were collected from the "Zone Fossilifère" unit exposed in both the Altkirch and Kleinkems quarries (**Figure 1**A).

3.2 Sediment macro- and micro-facies analysis

Micro-facies descriptions were performed on both thin and thick sections from selected and suitable samples of the DP-XXVIII well, Altkirch and Kleinkems quarries. Both macro- and micro-facies descriptions, as well as thin and thick section photographs, were realized using a Leica M205 C stereo microscope. A total of 203 core samples have been investigated and their positions in the the sedimentary log of the well are shown in Figure S1.

3.3 Micro X-Ray Fluorescence scanning

Micro X-Ray Fluorescence (µ-XRF) analyses were performed on thin and thick sections using a Bruker M4 Tornado spectrometer at the Institut Terre & Environnement of Strasbourg. The maximum resolution of 20 µm was used in order to achieve the best representative elemental counts for each lamina. The spectrometer settings were set on a voltage of 50 kV, ampere ratings of 400 µA, and the analyses were performed under vacuum conditions (2 mbar). We selected a set of representative elements to determine the relative changes in detrital input (aluminum, silica potassium, titanium, iron – Al, Si, K, Ti, Fe) and chemogenic or diagenetic deposition (calcium, strontium, sulfur – Ca, Sr, S) (Davies et al., 2015; Boës et al., 2011). Elemental contents are reported as log-ratios in order to avoid closed-sum constraints (Weltje et al., 2015).

3.4 Scanning Electron Microscope

Scanning Electron Microscope (SEM) images and local chemical analyses were performed on a thin section and on a rock sample from the DP-XXVIII well to document the chemistry and microstructure of some minerals using a VEGA TESCAN machine.

3.5 Spectral analysis

Spectral analysis was performed on the Gamma-Ray (GR) series from the “Sel V” unit of the DP-212 well to test the hypothesis of orbital forcing of the meter-thick to decameter-thick mudstone-evaporite alternations (we did not find any remaining well-logs from the DP-XXVIII well). The GR was measured by the MDPA through Schlumberger electrical logging and traces the natural radioactivity of the sedimentary record. The GR series was interpolated, linearly detrended, and normalized using Acycle’s “normalize” function (z-scoring, Li et al., 2019). Sedimentary cycles and their evolution were studied using the Multi-Taper Method applying 2π-tapers with red-noise modeling (2π-MTM analysis; robust AR(1) test) to detect statistically significant sedimentary cycles (Mann & Lees, 1996; Thomson, 1982), the Evolutive Fast Fourier Transform (EFFT) to document the evolution of sedimentary cycles through depth (Weedon, 2003), and Taner band-pass filters to isolate specific broadbands (Taner, 2000). These methods were performed using the Acycle software (v2.3.1; Li et al., 2019). The classical AR(1) test was also performed (Priestley, 1981).

4 Results

4.1 DP-XXVIII well

4.1.1 Synthetic sedimentary log

The detailed sedimentary log of the DP-XXVIII well (see Figure S1 in Data Availability) was produced based on the written description of the sedimentary successions made by the MDPA in the mid-20th century (MDPA, 1960), which we then synthetized (**Figure 2**). Here, we focus on the three zones as defined by Blanc-Valleron (1990) to investigate sedimentary changes across the EOT.

The “Zone Salifère Inférieure” is divided into four units (from base to top): the “Marnes à Limnées I” (Limnea Marls I) unit (thickness: 155 m) consists of massive mudstones alternating with centimeter to meter thick bedded to nodular anhydrite layers. The “Sel I” (Salt I) unit (thickness: 165 m) is a massive halite formation with rare intercalations of centimeter-thick mudstone and anhydrite layers. The halite is described as made up of centimeter-thick crystals forming chevrons (MDPA, 1960), which could correspond to bottom nucleated beds of coarse growth-aligned crystals at the sediment/water interface. The lithology of the “Marnes à Limnées II” (Limnea Marls II) unit (thickness: 84 m) is similar to the ”Marnes à Limnées I”, followed by the “Sel II” (Salt II) unit (thickness: 117 m), which has a similar lithology as the “Sel I” unit, which however contains substantially more intercalations of centimeter-thick to meter-thick mudstone and anhydrite beds.

The “Zone Salifère Moyenne’’ comprises two units (from base to top): the “Sel III” unit (thickness: 249 m) consists of cyclic decameter-thick alternations of laminated mudstones and massive halite beds (their average thickness is ~12.6 m). The laminated mudstones of this unit are often described as made up of millimeter-thick laminae (MDPA, 1960). The overlying “Zone Fossilifère” (Fossiliferous Zone) unit (thickness: 80 m) is a thick mudstone formation attributed to a transgression event that flooded the whole URG during the early Rupelian (Pirkenseer et al., 2010, Berger et al., 2005) and consists of laminated mudstones with occasional dolomite and anhydrite layers.

The “Zone Salifère Supérieure” is composed of three units (from base to top): the “Sel IV” (Salt IV) unit (thickness: ~246 m) is made of cyclic decameter-thick mudstone-halite alternations (which thickness average ~12.4 m). The mudstone beds of these alternations are mostly laminated. Two meter-thick intervals of centimeter-thick halite and sylvite alternations (commonly draped by anhydritic marlstones and dolomitic carbonates), with occasionally interbedded centimeter-thick laminated boundstones, are well identified at the bottom of the formation. A 1.2 m thick carnallite bed is located at the top of the lower potash seam. The “Sel V” unit (thickness: ~227 m) is made of cyclic meter-thick alternations of halite (or anhydrite) and mudstone beds which average ~8.3 m in thickness. The following “Marnes sans Sel” (Salt-free Marls) unit (thickness: ~106 m) consists of cyclic meter-thick mudstone-anhydrite alternations (with an average thickness of ~5.6 m). The mudstone beds of these alternations appear mostly laminated, yet the upper ~45 m is composed of a thick mudstone section without any observable sedimentary alternations. Overall, the “Zone Salifère Supérieure” is characterized by its cyclic meter-thick to decameter-thick mudstone-evaporite alternations where the mudstones are mostly laminated, and by the presence of two potash seams in its lowermost part.

Across the three formations, the mudstones can be divided into two main groups according to the absence or presence of sedimentary structures: (1) massive and (2) laminated mudstones. Massive mudstones are common in the “Zone Salifère Inférieure”, where only very few laminated mudstones have been described (MDPA, 1960). In the lowermost “Zone Salifère Moyenne”, a clear facies change occurs with the appearance of laminated mudstones which make most of the mudstones up to the top of the “Zone Salifère Supérieure”. The seemingly cyclic decameter-thick mudstone-evaporite alternations appear at the same depth as the finely laminated mudstones and remain a predominant feature up to the uppermost “Zone Salifère Supérieure”. However, evaporites are scarce in the “Zone Fossilifère”, even though laminated mudstones remain prevalent. To sum up, the study of the original description of the DP-XXVIII well (MDPA, 1960) reveals that both the millimeter-thick laminitae and the recurrent meter-thick to decameter-thick mudstone-evaporite alternations appear at the bottom of the “Sel III” (depth: 1158 m) and are found up to the uppermost part of the “Zone Salifère Supérieure” (depth: 312 m). The mudstone-evaporite alternations become thinner upward in the section, going from ~12.6 m in the “Sel III” to to ~5.6 m in the “Marnes sans Sel”, suggesting a gradual decrease in SARs.

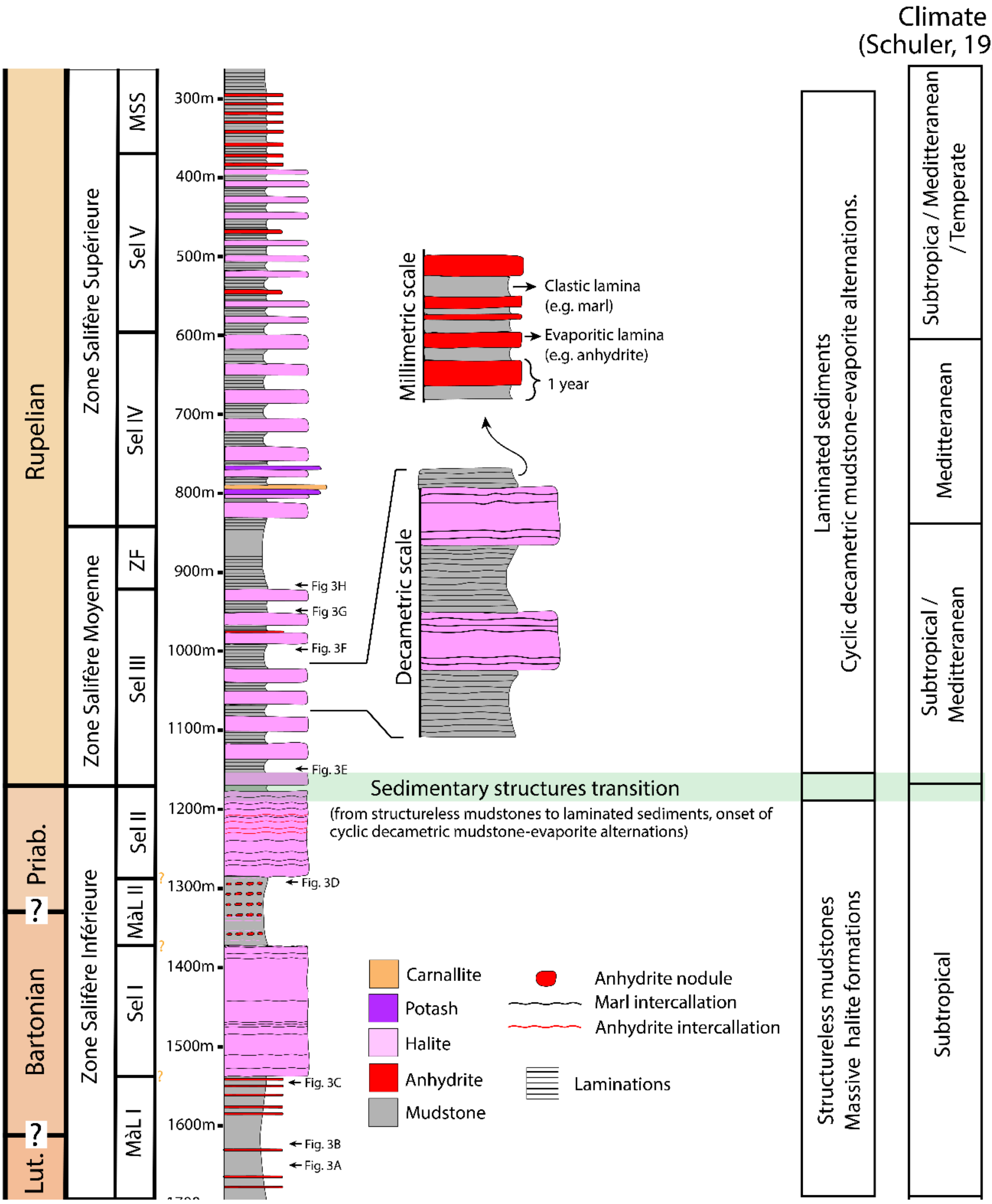

Figure 2: Synthetic log of the sedimentary succession of the Mulhouse basin's formations through a segment of the DP-XXVIII well, along the paleoclimatic observations inferred from palynology (Schuler, 1988). The chronostratigraphy is based after Grimm et al. (2011) and Châteauneuf & Ménillet (2014), and the Eocene-Oligocene boundary is placed according to the correlations presented in this paper. The size of the mudstone-evaporite alternations of the "Sel III" and "Zone Salifère Supérieure" are exaggerated. MàL I = Marnes à Limnées I, MàL II = Marnes à Limnées II, MSS = Marnes sans Sel.

4.1.2 Macro-facies of the core samples

The three main lithologies represented in the DP-XXVIII core are mudstone, halite, and anhydrite. Macro-facies observations of the mudstones are in accordance with the available description (MDPA, 1960) (**Figure 3**).

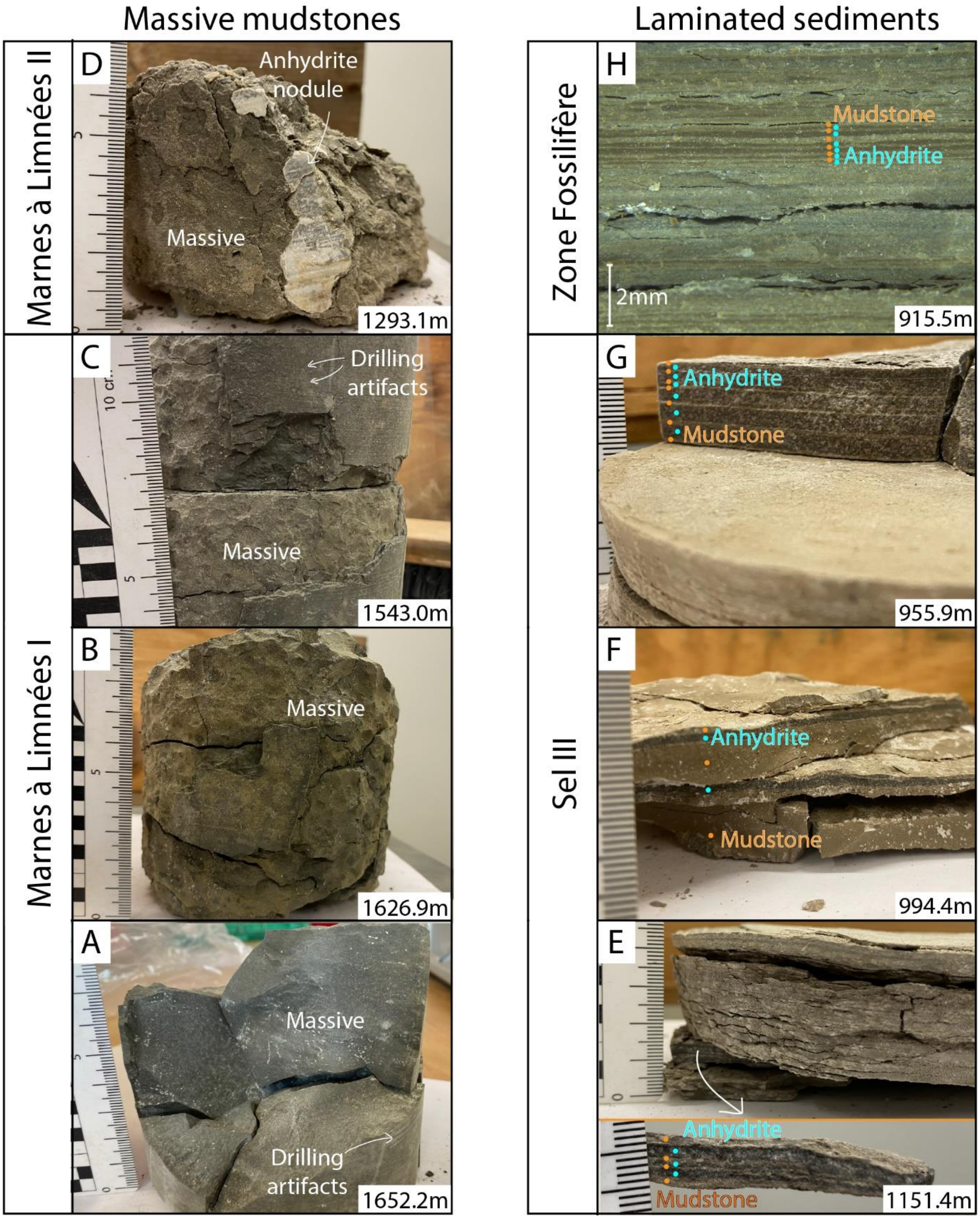

Figure 3: Macro-photographs of core samples from the DP-XXVIII well. (A, B, C, D) Massive mudstones with conchoidal fractures. Coring artifacts from the drill machine are not to be mistaken with laminations. (E, F, G, H) Laminae consisting of mudstone (light-colored laminae) and anhydrite (dark-colored laminae) couplets.

The massive mudstones are predominant in the “Zone Salifère Inférieure”, whereas the laminated mudstones are predominant in the “Zone Salifère Moyenne”. However, a few laminated samples are present in the “Sel II” unit as well. The laminated mudstones consist of millimeter-thick laminae, several of which are made of couplets of dark- and light-colored laminae, especially going upward from the base of the “Sel III” unit. At the macroscopic scale, the dark-colored laminae are primarily composed of anhydrite while the light-colored ones are mainly composed of siliciclastic mud (see 4.2.1 for the detailed description) (**Figure 3**E-H). While some are very finely laminated (e.g., **Figure 3**E, G), others exhibit thicker layers (e.g., **Figure 3**G). At the microscopic (thin section) scale, the color pattern of these laminae is the opposite, with anhydrite laminae being light-colored and mudstone laminae being dark-colored (**Figure 4**).

The halite core samples have been impacted by recrystallization, preventing proper identification of the depositional environment. The anhydrite either forms centimeter-thick elongated to sub-rounded nodule beds with vestigial bottom-growth structures encompassed into marlstone, or layers.

4.2 Laminated sediments of the southern Upper Rhine Graben

4.2.1 Depocenter (DP-XXVIII well)

In the “Zone Salifère Moyenne”, 61 out of 68 mudstone samples are laminated (see Figure S1 in Data Availability). Observation of the samples under the microscope reveals repetitive couplets and triplets of dark- and light-colored laminae (**Figure 4**). The 955.9 m sample consists of repetitive couplets of anhydrite pseudomorphs derived from bottom-growth gypsum (light-colored laminae) and marlstones (dark-colored laminae). The 1151.4 m sample contains an additional fine grained (~30 µm) anhydrite lamina (cumulates). Dark-colored laminae contain very homogenous and massive clay-sized sediments. Some of the laminae are black, suggesting an enrichment in organic matter as indicated by the SEM measurements (see 4.3). In the case of the 1029.3 m sample, the sediments are typified by two couplets of anhydrite pseudomorphs laminae overlaid by draping discontinuous clay without significant dissolution surfaces. Typically, gypsum pseudomorphs are bottom-nucleated crystals that form on the lake floor when brine gets saturated with respect to sulfates (Warren, 2016).

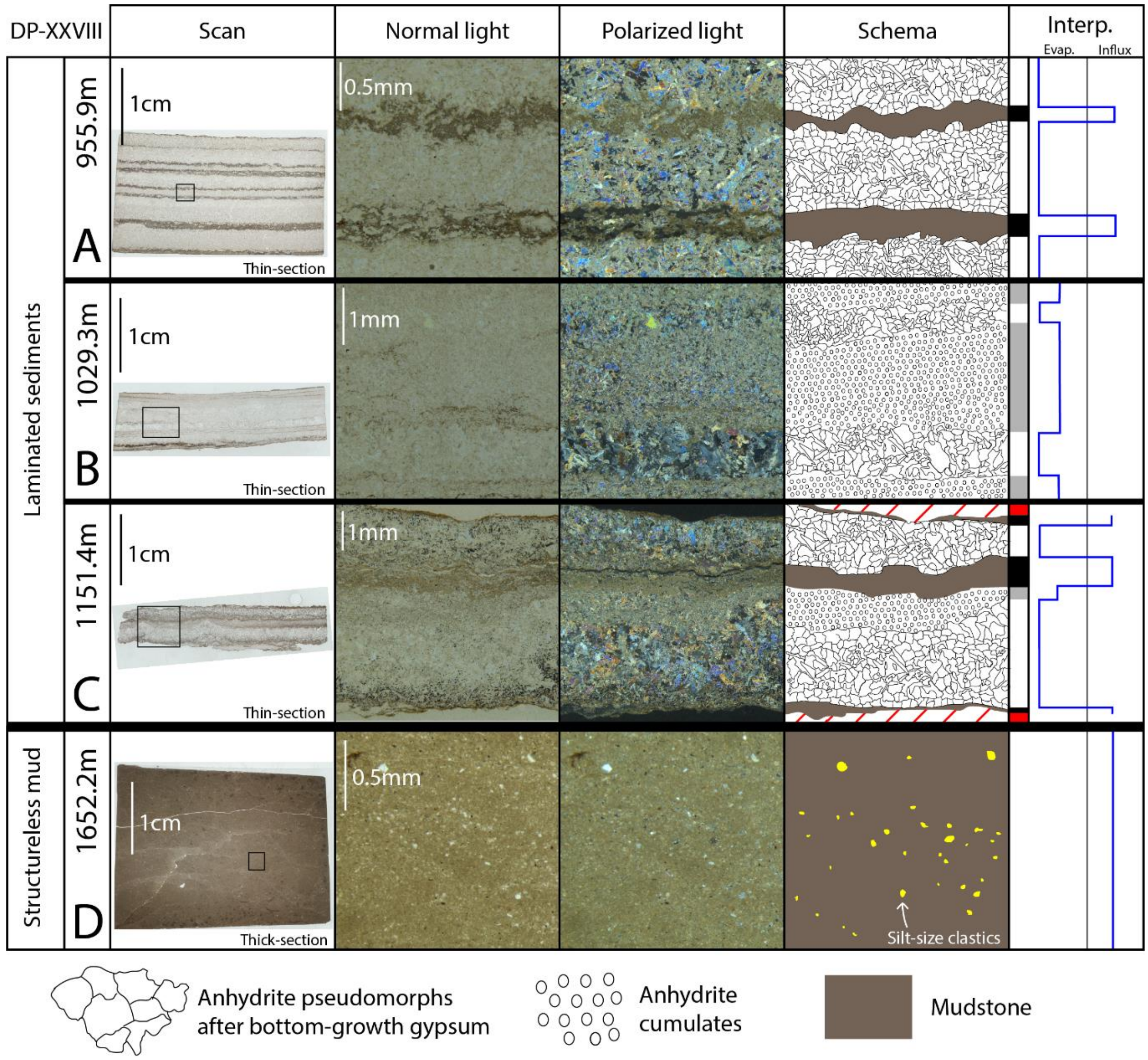

Figure 4: Thin sections of laminated sediments, and thick section of a massive mudstone, from the DP-XXVIII well. A) Laminated sediments made of couplets of mudstones and anhydrite pseudomorphs after bottom-growth gypsum (955.9 m). B) Laminated sediments made of couplets of anhydrite pseudomorphs after bottom-growth gypsum and anhydrite cumulates with some very thin mudstone drapes (1029.3 m). C) Laminated sediments made of couplets of mudstone, anhydrite pseudomorphs overlying bottom-growth gypsum, and anhydrite crystals (1151.4 m). D) Massive mudstone consisting of silt-sized clastic grains in a micrite matrix (1652.2 m).

The elemental geochemistry analysis of the 955.9 m sample shows that the light-colored laminae are enriched in Ca and S, which track the presence of anhydrite as is also inferred from microfacies observations (Figure 5A). The dark-colored laminae are enriched in Fe, Mg, and K, which indicates that they are primarily composed of detrital siliciclastic minerals (clay). The dark-colored laminae are enriched in Mg (high Mg/Ca ratios) and can therefore contain dolomite ((Ca,Mg)CO$_3$), which amount might depend on the presence of Ca (see element maps, Figure 5A). The S content is generally low in dark-colored laminae (low S/Ca ratios), which confirms the absence of anhydrite, but punctual enrichments of S are occasionally observed. This can possibly be attributed to the presence of diagenetic processes that induce precipitation of pyrite (FeS$_2$) (see for instance the third mudstone laminae starting from the bottom, **Figure 5A**). Similar elemental compositions were found for the samples at

1029.3 m and 1151.4 m depth(see **Data Availability**), which suggest similar genesis of the sediments as the one at 955.9 m depth.

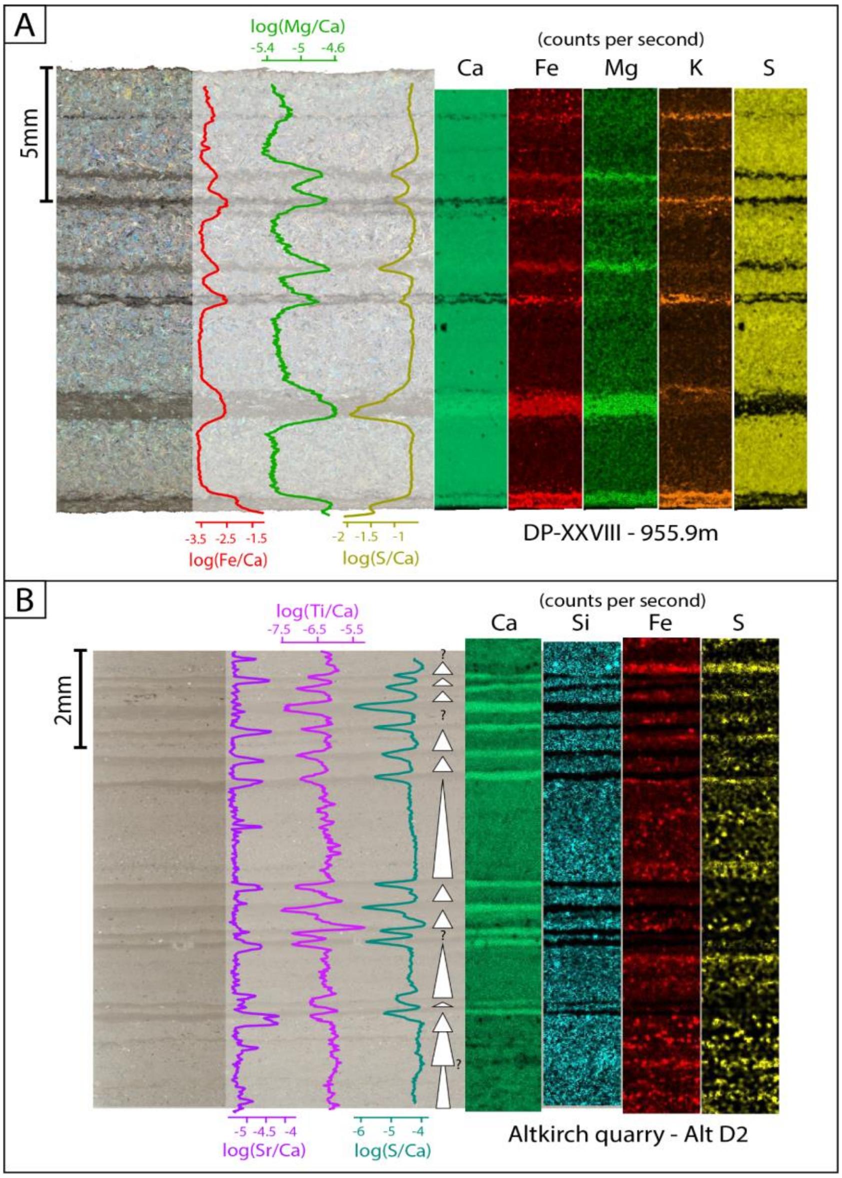

***Figure 5**: µ-XRF analyses consisting of logarithms of specific elemental ratios and elemental mappings of the DP-XXVIII well sample at depth 955.9 m, and of the Alt-D2 sample from the Altkirch quarry. In the case of elemental mappings, black represents no counts per second while the colors represent higher counts per seconds based on the intensity. The white triangles represent fining-up sequences. (A) (DP-XXVIII - 955.9 m) The µ-XRF analyses show that the light-colored laminae are anhydrite (rich in Ca and S) and that the dark-colored laminae range from marls to dolomites due to their varying intensities of Ca and Mg. Furthermore, the elemental mappings show an enrichment in lithogenic elements (e.g. Fe, K) in the dark-colored laminae, suggesting their detrital nature. (B) (Altkirch quarry – Alt D2) The µ-XRF analyses show that the dark-colored laminae are rich in Ca, enriched in Sr, and completely devoid of lithogenic elements, suggesting an evaporitic nature. Inversely, the light-colored laminae are enriched in lithogenic elements (e.g. Si, Ti, Fe), which suggests a detrital nature, further demonstrated by fining-up sequences.*

4.2.2 Altkirch quarry

The laminated sediments from the lowermost part of the Altkirch quarry ("Zone Fossilifère") were first described as varves based on the repetitive nature of their dark- and light-colored laminae (Duringer, 1988; **Figure 6**). The dark-colored laminae are homogenous, have a constant thickness, and consist of very fine micrite crystals (<1 µm). The light-colored laminae (0.15 – 2 mm thick) are composed of larger micrite crystals ~2 µm) and contain clastic grains along with amorphous organic matter (**Figure 6**A). The Altkirch quarry is known for its rich diversity of macrofossil taxons (e.g. fish, insects, and mollusks; Gaudant & Burkhardt, 1984), thus a certain amount of the organic content could also be autochthonous.

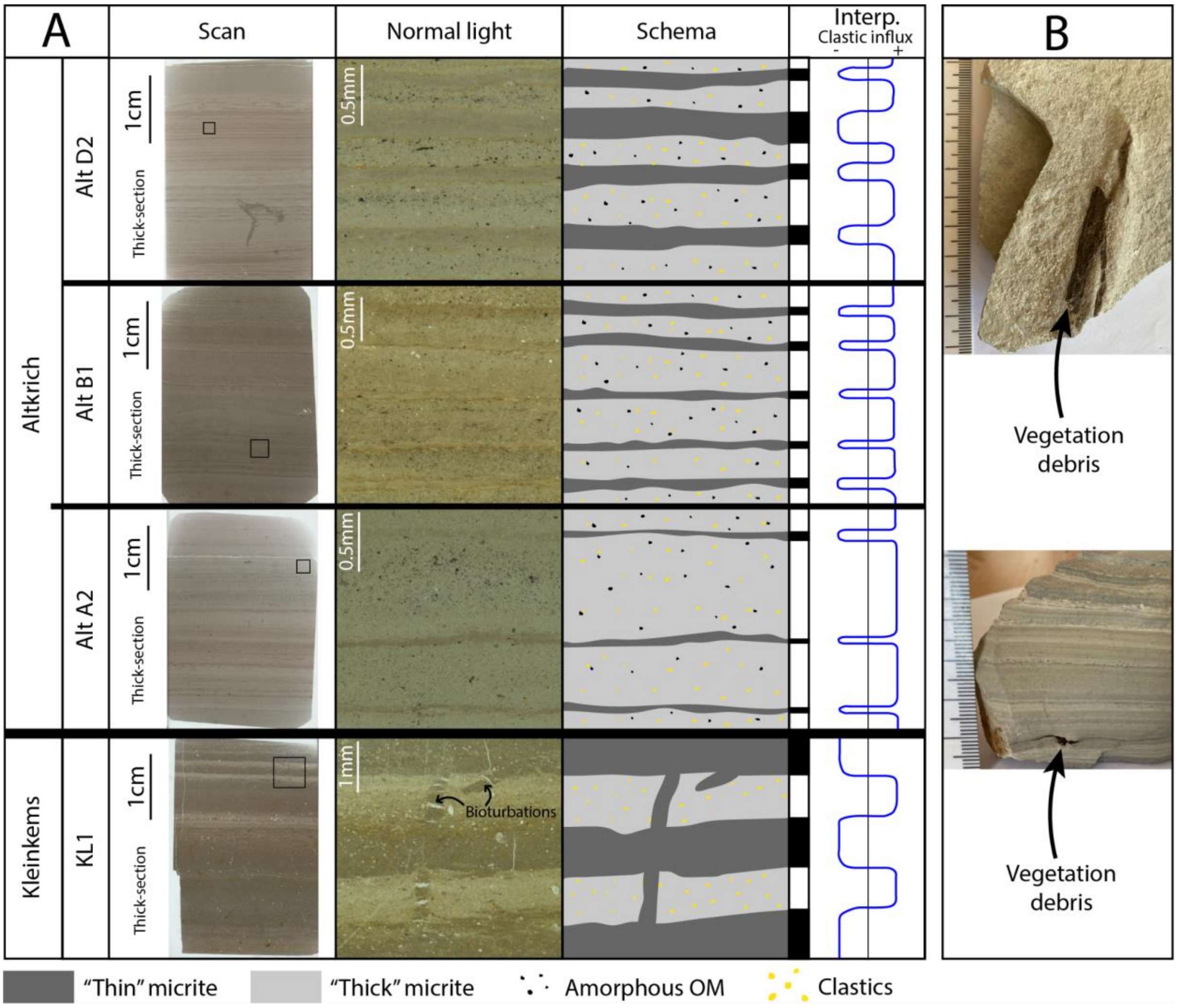

Figure 6: (A) Thick sections of laminated sediments from the Altkirch and Kleinkems quarries ("Zone Fossilifère"). (Alt D2, Alt B-1, Alt-A2) Laminated sediments made of couplets of thin micrite crystals (dark-colored laminae) and thicker micrite crystals, amorphous organic matter, and detrital grains (light-colored laminae). (KL1) Laminated sediments similar to those from the Altkirch quarry, but without amorphous organic matter, and with shells across the laminae. (B) Macro-photographs of laminated sediments from the Altkirch quarry containing macroscopic vegetation debris.

Elemental analyses of the Altkirch laminated sediments (Alt D2 sample, **Figure 5**B) show that the dark-colored laminae are enriched in Ca and Sr, while the Si, Ti, Fe, S, and K values are higher in the light-colored laminae (**Figure 5**B). Several dark-colored layers also contain higher concentrations of Sr (higher Sr/Ca ratios), which potentially indicates the presence of Sr-enriched carbonates, such as aragonite or strontianite. Dark-colored layers are devoid of detrital material (low Si/Ca and Ti/Ca ratios, absence of Si and Fe in element maps), which suggests that the thin micrite crystals of the latter are chemogenic (evaporitic) rather than detrital. In light-colored layers, high levels of lithogenic elements (e.g., Si, Fe, and Ti) track the input of clastic material (e.g., quartz, and feldspars) identified in the micro-facies analysis. The detrital-rich light-colored laminae show distinct fining-upward sequences (**Figure 5**B), which is evidenced by decreasing log-ratio profiles of Si/Ca and Ti/Ca and decreasing grain-size observable on the elemental map of Si. The enrichment in both Fe and S in light-colored laminae suggests the presence of iron sulfides (e.g., pyrite). The clastic grains in the light-colored layers are encased in a micrite matrix (cement). Comparable results were found for the Alt A2 and Alt B1 samples (see **Data Availability**), which suggest that their laminae are similar in nature to those of the Alt D2 sample.

4.2.3 Kleinkems quarry

The laminated sample from the Kleinkems quarry contains several successions of dark- and light-colored calcareous laminae (**Figure 6**). The dark-colored laminae are comparable to those from the Altkirch quarry and are composed of very homogeneous bioclastic fine-grained micrite with randomly distributed shells. The light-colored laminae, similarly to those from the Altkirch quarry, contain a significant amount of clastic grains, but no amorphous organic matter.

The µ-XRF analysis of the KL1 sample shows similar elemental distribution as in the samples from the Altkirch quarry (see **Data Availability**). However, the dark-colored Ca-rich laminae also contains some detrital material, as indicated by the presence of a few lithogenic elements.

4.3 Scanning Electron Microscope

SEM images and localized chemical analyses of a part of the 955.9 m thin section shows the presence of anhydrite (light gray), dolomite (dark gray), and organic matter (black) (**Figure 7A**). Small dolomite patches are encased in the anhydrite. The image of the sample at depth 1009 m shows the presence of anhydrite (light gray) and calcite (dark gray) arranged in layers (upper view) (**Figure 7B**). The anhydrite is characterized by high counts of Ca, S, and O, the dolomite by high counts in Ca, Mg, O, and C, the calcite by high counts in Ca, O, and C, and the organic matter by high counts in C.

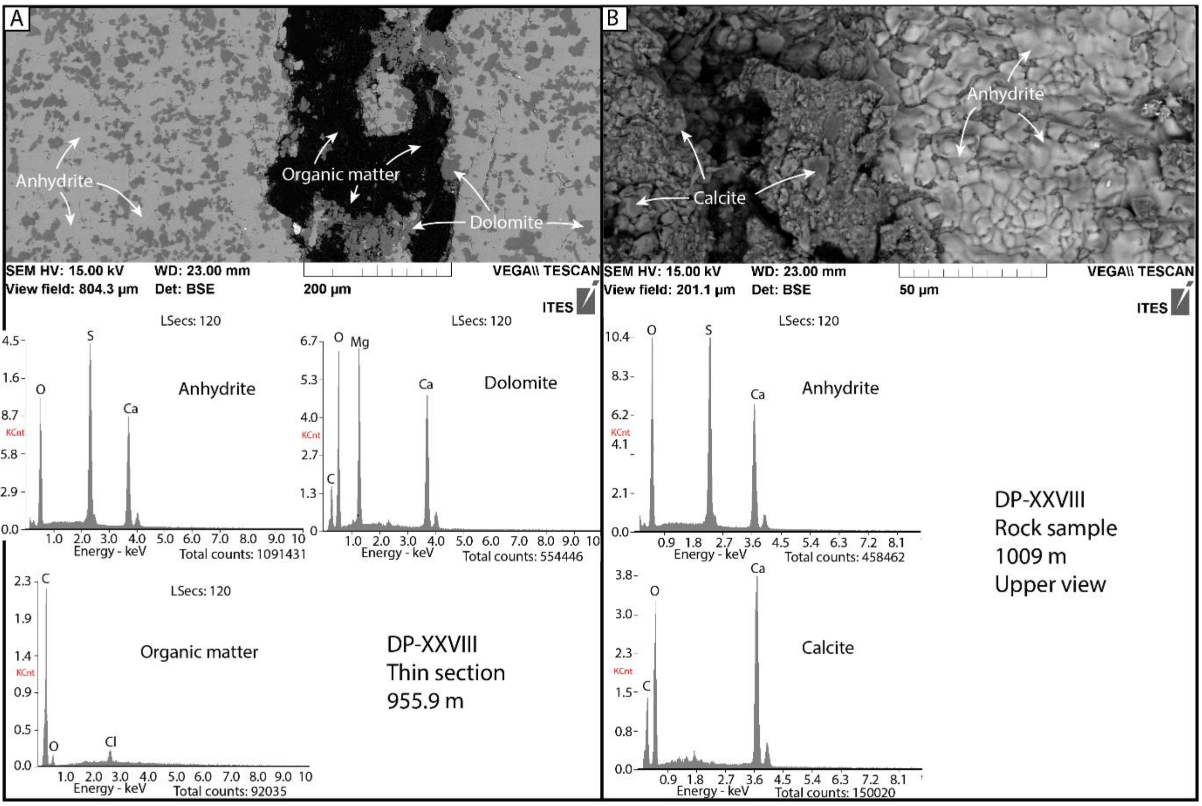

Figure 7: SEM images and localized chemical analyses of a part of the (A) thin section at 955.9 m depth and (B) sample at 1009 m depth.

4.4 Spectral analysis

The 2π-MTM analysis results of the detrended GR series (Figure 8A) of the “Sel V” unit from the DP-212 well reveals statistically significant frequency broadbands related to sedimentary cycles with average thicknesses of 82.3 m, 22.4 m, and 4.5 m (>99% confidence level) and 9 m (> median confidence level) (Figure 8B). The broadband related to the ~4.5 m thick sedimentary cycle shows three distinct peaks. The EFFT shows that the ~22.4 m and the ~4.5 m cycle are prominent throughout the sedimentary record (Figure 8C). The Taner filter of the ~4.5 m cycle is in phase with the large majority of the mudstone-evaporite alternations (Figure 8D, E). The classical AR(1) test shows that almost the whole signal is above the 99.9% confidence level, and that the same frequency peaks appear with the highest amplitudes, except for the ~82.3 m cycle (Figure S2, see Data Availability).

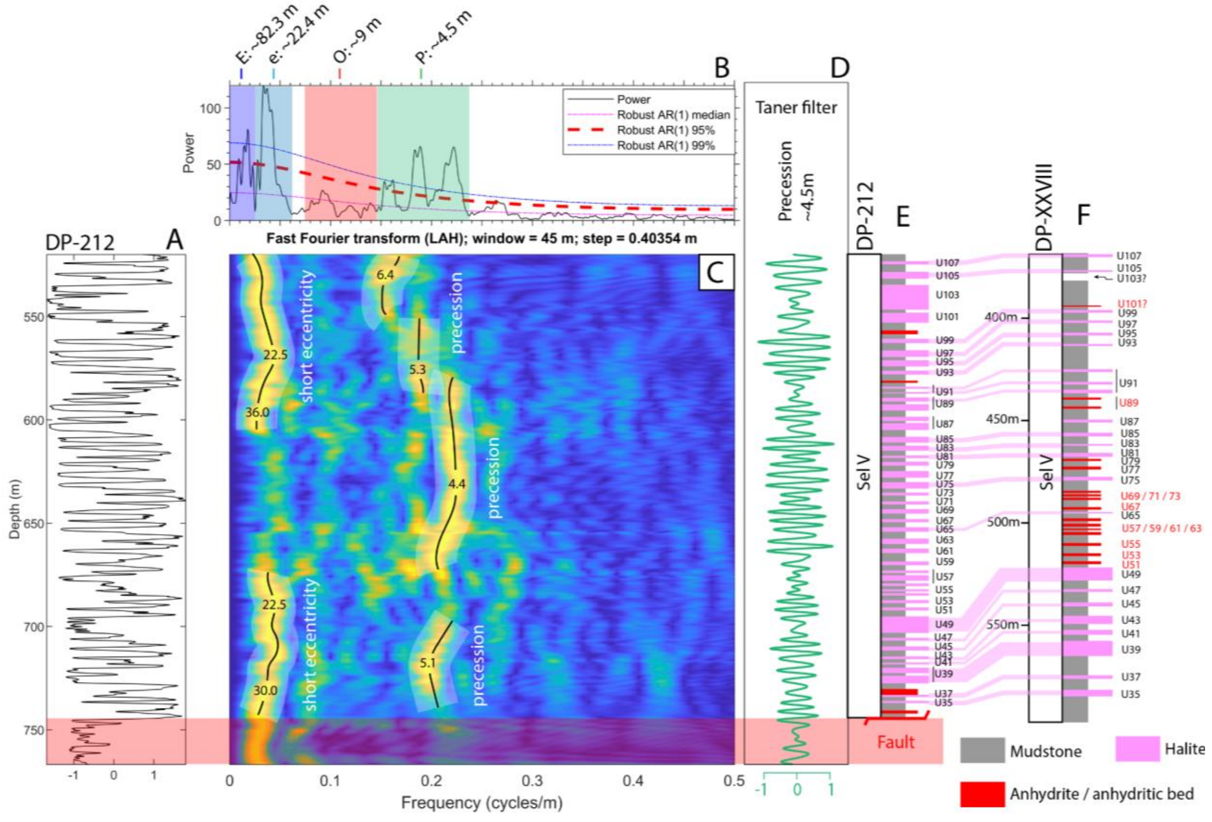

***Figure 8**: Spectral analysis results of the "Sel V" unit of the DP-212 well ("Zone Salifère Supérieure"). (A) Linearly detrended gamma-ray series (DP-212). (B) 2π-multitaper spectrum with linearly fitted red-noise modelling. (C) EFFT with a sliding window of 45m and a step of 0.40354m. (D) Taner filter of the precession (P; 0.1459 – 0.2998 cycles/m) cycles. E = long eccentricity, e= short eccentricity, O = obliquity, P = precession. (E) Sedimentary log of the DP-212 well ("Sel V"). (F) The equivalent sedimentary log of the DP-XXVIII well ("Sel V"). The "U" followed by numbers are the name of each halite bed as initially established by the MDPA (Blanc-Valleron, 1990).*

5 Interpretation and discussion

To achieve the goals of this study we interpret and discuss in the following the results presented above to:

- Estimate whether the observed laminae represent an annually deposited cycle (varves) and if they can thus be used as markers of seasonality.
- Discern the possible mechanisms behind the cyclic sedimentation pattern of the laminae and decameter-thick mudstone-evaporite alternations, with implication to better understanding past environmental changes.
- Place the interpretation of this study in a wider regional scale and to discuss the implications for climatic changes across the EOT

5.1 Laminated sediments and varves: nature and depositional processes

Distinguishing varves from non-annual laminated sediments is challenging for sedimentary archives beyond the radiometric time range. While the annual nature of varves in modern and recent lacustrine and marine environments can be determined using various means (Zolitschka et al. 2015), it can only be hypothesized in older geological (deep-time) records, by interpretating and comparing of petrographic and geochemical data with their modern and recent counterparts (Mingram, 1998; Wilson & Bogen, 1994). For the southern URG, we use the sedimentary records of the Dead Sea, which contain extensive evaporite deposits (Ben Dor et al., 2019), and of the Chatyr Kol lake (Kalanke et al., 2020) as sedimentary analogs, which allow us to propose conceptual models for reconstructing depositional processes.

5.1.1 Distinguishing varves from laminated sediments

Lacustrine sediments, such as laminated sediments and varves, can be categorized as clastic, biogenic, and endogenic (Zolitschka et al., 2015; Brauer et al., 2009). Varves are a particular type of laminated sediments, which are defined as sedimentary layers of distinct composition, occurring as repetitive patterns that represent annual cycles (Zolitschka et al., 2015). The Identification of varves is a strong indicator of local climatic seasonality. Clastic varves are formed when suspended sediment carried by seasonal runoff enters a lake with a stratified water body (Sturm, 1979). They are typically made of laminae with different grain sizes, that results from distinct seasonal runoff regimes. Biogenic varves are formed when seasonality induces changes in the organic productivity of a lake, resulting in the deposition of distinct biogenic laminae (e.g. algal blooms, diatom blooms; e.g. Lake Tiefer See in Germany; Dräger et al., 2017). Endogenic varves, which are often evaporitic, occur when the solubility product of a mineral compound (e.g. anhydrite, halite, and aragonite) is exceeded due to seasonal fluctuations of evaporation and/or precipitations (e.g., the Dead Sea; Ben Dor et al., 2019). It is rare that varves are either purely clastic, biogenic, or endogenic (Zolitchka et al., 2015). An overview of several varve records is available on the PAGES varve database (https://pastglobalchanges.org; Ojala et al., 2012). It should be noted that the presence of laminated sediments and varves indicates that the depositional environment prevented the development of benthic life and bioturbation. It is however beyond the scope of our study to determine whether it has been the lack of oxygen or a specific water chemistry (e.g., hypersaline waters), or a combination of the two that have rendered the lake floor uninhabitable.

5.1.2 Interpretation of the fine laminations as varves and conceptual depositional model

5.1.2.1 Depocenter (DP-XXVIII well)

The samples from the DP-XXVIII core display clear couplets of mudstone and anhydrite pseudomorphs after bottom-growth gypsum with no dissolution surfaces (**Figure 4**, **Figure 5A**). We propose that the evaporites were formed through evaporation-driven brine saturation during the dry season, and that the intercalated mudstone layers (sometimes rich in organic matter) were formed due to enhanced fluvial runoff during the wet season (**Figure 9**). This interpretation is supported by the elemental profiles that clearly allow distinguishing between anhydritic laminae (enriched in Ca and S) and detrital mudstone laminae (enriched in the lithogenic elements Fe and K) (**Figure 5A**). According to the palynological investigations and taking into account the mid-latitudinal position of the site, climatic conditions resembled today's "Mediterranean" type characteristics throughout the "Zone Salifère Moyenne", with distinct wet (winter) and dry (summer) seasons (Schuler, 1988). Furthermore, these mudstone-anhydrite couplets are similar to varves from the late Pleistocene Lisan Formation (Dead Sea, Israel)

(Ben Dor et al., 2019), which are composed of endogenic aragonite and gypsum laminae precipitating during dry summers and detrital-rich laminae deposited during winter runoff. We therefore consider the thin mudstone-anhydrite couplets of the DP-XXVIII well as endogenic-clastic varves comparable to those of the Dead Sea, even though processes might differ following water balance conditions.

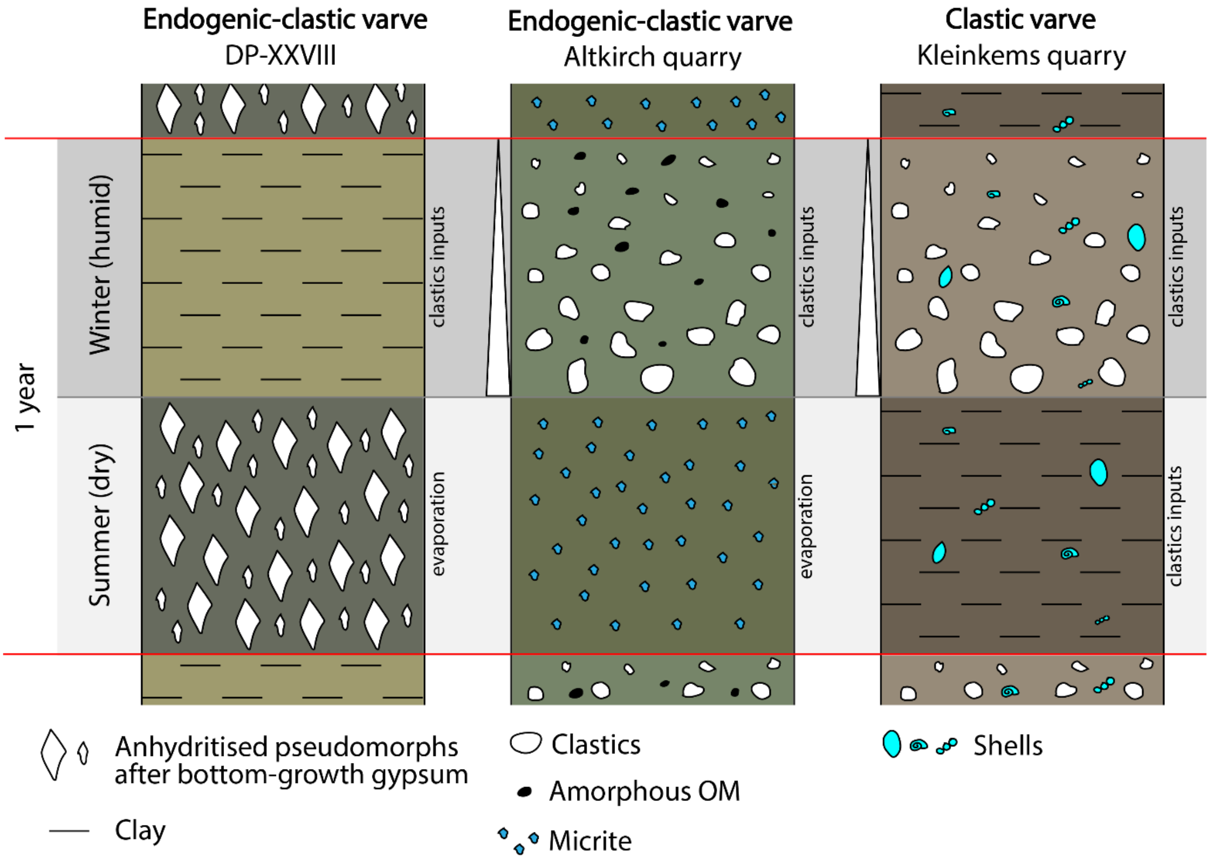

Figure 9: Interpretative deposition model for the formation of three types of varves identified for the southern Upper Rhine Graben through the late Priabonian and Rupelian. The main climate variation causing the seasonality of depositional processes are the changes in precipitations due to dry summers and humid winters.

The anhydrite pseudomorphs overlying bottom-nucleated gypsum and thin crystals (anhydrite cumulates) couplets of the 1029.3 m sample could be varves as well but were deposited under drier conditions than the mudstone-anhydrite ones (**Figure 4**). Those are similar to seasonal temperature-driven couplets described in the Dead Sea, composed of alternations of coarse and fine halite or gypsum crystals (Ben Dor et al., 2019; Sirota et al., 2016).

5.1.2.2 Proximal records (Altkirch and Kleinkems quarries; “Zone Fossilifère”)

The samples from the Altkirch (southern river fan delta) and Kleinkems (fan-delta related to the eastern border fault) (Duringer, 1988) quarries display couplets of dark- and light-colored laminae. The light-colored laminae contain large amounts of detrital silt-sized grains. We propose that they were delivered by fluvial runoff during the wet season. Grains comprise a diverse mineral assemblage with calcite and quartz derived from the erosion of the surrounding uplifted Mesozoic (and Paleozoic) rift shoulders. While quartz grains are clearly detrital, calcite crystals could either be autochthonous or allochthonous (e.g. reworked from Jurassic limestones). In the case of the Altkirch quarry, the presence of organic matter mostly alongside detrital grains suggests that it is of detrital origin. Furthermore, terrestrial macrofossils such as plant debris account for a fluvial sediment source in these deposits (**Figure 6B**; Duringer, 1988; Gaudant & Burkhardt, 1984). The light-colored laminae show fining-up sequences, which suggests that they record a flood (pulse event) during the wet season, rather than a continuous accumulation of sediment through multiple months. The varying thickness of these laminae could reflect year-to-year climatic variability, with the thicker laminae possibly representing winters with more intense precipitation. However, this could also be explained solely by internal fluvial processes, such as channel migration or sediment availability. The dark-colored laminae are homogenous and made of thin micrite (likely aragonite) crystals. The absence of lithogenic elements (Si, Fe, K) in the dark-colored laminae indicates the absence of detrital material, which suggests that the micrite crystals are endogenic (formed in the water column) rather than detrital. These interpretations are supported by the elemental profiles that clearly allow distinguishing between endogenic carbonated laminae (enriched in Ca with no lithogenic elements) and detrital laminae (enriched in lithogenic elements) (**Figure 5**). Furthermore, these couplets are very similar to the Holocene clastic-calcitic varves of Lake Chatyr Kol which annual nature is supported by radiometric dating, even though they contain less sub-layers (Kalanke et al., 2020). These varves exhibit a detrital layer with a sharp basal boundary (runoff) with chrysophytes and/or diatoms occurring after or within it, overlain by a layer of endogenic (evaporation) and fine-grain detrital calcite, and topped by an amorphous organic matter sub-layer. Therefore, by comparison with the varves of Lake Chatyr Kol, and according to petrographic and geochemical evidence presented in this study, we interpret the clastic-endogenic couplets of the Altkirch quarry as varves.

In the case of the Kleinkems quarry, the presence of lithogenic elements in the dark-colored laminae suggests persistent inputs of detrital material even during the dry season. This observation leads us to interpret both the dark- and light-colored laminae couplets of this quarry as purely clastic varves showing seasonal changes in grain-size. However, it is not impossible that the dark-colored laminae are endogenic as well (similarly to the clastic-calcitic varves of Lake Chatyr Kol; Kalanke et al., 2020), and that the proximity of the depositional area with the border fault accounts for occasional detrital inputs.

5.1.2.3 Sediment Accumulation Rates

Considering the ~2 mm varve thickness of the “Sel III” unit (**Figure 4**), the average SAR is estimated at ~2 m/kyr. This SAR would imply that precession cycles would be ~40 m thick, which is much more than the observed ~12.6 m thick mudstone-evaporite alternations of the “Sel III” unit. It would also imply a SAR higher than any observed rift valley (Schwab, 1976). This estimation however does not account for the potential SAR variations across lithologies and when considering the mudstone intervals, as not all mudstone samples are finely laminated (**Figure 3F**; see Figure S1 in Data Availability). Precise estimates cannot be given here due to the fragmentary nature of the retrieved core samples. Further studies are required to provide more details, such as continuous microfacies descriptions (which would require a utilizing a new core). However, in the case of the lowermost “Zone Salifère Supérieure”, SARs from fine laminations interpreted as varves (Kühn & Roth, 1979) have been used to interpret the decameter-thick mudstone-evaporite alternations as induced by precession in the MAX borehole (Blanc-Valleron, 1990; Blanc-Valleron et al., 1989). We performed the spectral analysis of a part of the “Zone Salifère Supérieure” to provide an independent argument for the interpretation of the meter-thick to decameter-thick mudstone-evaporite alternations as astronomically-forced.

5.2 Cycle interpretation

The ratios between the ~82.3 m, ~22.4 m, ~9 m, and ~4.5 sedimentary cycles (DP-212 well, “Sel V”) in the depth domain (18.3 : 5 : 2 : 1) are particularly close to those of the orbital cycles (long eccentricity, short eccentricity, obliquity, precession) in the time domain (20 : 5 : 2 : 1). The ~82.3 m cycle is therefore interpreted as corresponding to the long eccentricity, the ~22.4 m cycle to short eccentricity, the ~9 m cycle to obliquity, and the ~4.5 m cycle to precession. Furthermore, the ~4.5 m sedimentary cycle has three main peaks which can be correlated to the three main periods of precession. The fact that the ~4.5 m cycle is in phase with the large majority of observed mudstone-evaporite alternations suggests that they were primarily induced by precession through the “Sel V” unit (**Figure 8**). By comparison, this interpretation confirms the previous investigation of Blanc-Valleron et al. (1989) and also suggests that the mudstone-evaporite cycles of the “Sel III” were astronomically-forced.

5.3 Facies change across the EOT: a marker of regional climatic change with implications for global climate dynamics

The facies transition from massive mudstones to laminated sediments and varves, along the onset of the meter-thick to decameter-thick mudstone-evaporite alternations, is well documented in the original description of the DP-XXVIII well (MDPA, 1960). Until now, it was neither discussed, nor placed in the perspective of the EOT (**Figure 2**, **Figure 3**). The two main factors classically driving changes in sedimentary facies are climate and tectonics (Carroll & Bohacs, 1999). The climatic evolution of the URG during the Eocene and Oligocene is relatively well-known and reveals a marked increase in the seasonal climatic contrast at the bottom of the “Sel III” unit (Schuler, 1988). Climatic conditions shifted from wet subtropical during the “Zone Salifère Inférieure” with a short or absent dry season, to the drier subtropical/Mediterranean-type conditions of the “Zone Salifère Moyenne” with a pronounced dry season lasting around half the year. This shift is penecontemporaneous with the facies transition, and we therefore argue that this change in sedimentary facies reflects the onset of a pronounced seasonal climatic contrast. In addition, the onset of laminated sediments and varves is also synchronous with the onset of repetitive decameter-thick marl-evaporite alternations. The study of Blanc-Valleron (1989) and the spectral analysis of the DP-212 well presented in this paper suggest that these alternations are forced by precession in the “Zone Salifère Supérieure” (**Figure 2**, **Figure 8**), and in the “Sel III” by comparison.

In paleoenvironmental terms, and with regard to the lake classification of lake-basin types (Carroll & Bohacs, 1999; Bohacs et al., 2000), the deposits of the “Zone Salifère Inférieure”, “Zone Salifère Moyenne”, and “Zone Salifère Supérieure” are characteristic of an underfilled lake. The relative stability of the climate across the deposition of the ”Zone Salifère Inférieure” (Schuler, 1988) suggests that these lithology changes were potentially not driven by climatic changes. Starting from the bottom of the “Sel III”, the decameter-thick mudstone-evaporite cycles were most-likely induced by lake-level variations related to orbital cycles. While we emphasize that the varves resulted from seasonal precipitation changes, with the clastic laminae being deposited during humid winters and chemical laminae deposited during dry summers (potentially associated to seasonal lake-level fluctuations), it is also possible that seasonal temperature changes influenced the saturation of brines.in comparison, facies changes associated with an increase in seasonal climatic contrast have been documented further west in the Rennes Basin across the EOT (Boulila et al., 2021; Tramoy et al., 2016; Bauer et al. 2016). There, a sharp contact between massive, clotted greenish clays and brownish, organic laminated clays is described above the Eocene-Oligocene boundary (Oi-1 event) (Boulila et al., 2021). However, the microfacies of the laminated clays were not analyzed in detail and their depositional processes and potential cyclicity (i.e., as varved deposits) were not assessed. Furthermore, laminated mudstones are also described earlier in the sequence and are attributed to hypoxic lacustrine conditions. Detailed microfacies investigations would be required to assess whether these laminated sediments show significant facies changes before and after the EOT. The detailed cyclostratigraphy of the Rennes basin indicates strengthening of the eccentricity and precession band at the EOT (Boulila et al., 2021). There are therefore strong similarities between the Mulhouse basin and the Rennes basin as both basins display pronounced facies changes with the presence of laminated sediments and astronomically-forced sedimentary alternations. Furthermore, the Bourg-en-Bresse basin (Bresse Graben), similarly to the Mulhouse basin, exhibits the onset of decameter-thick mudstone-evaporite alternations in which mudstones are laminated and display light-colored (carbonated) and dark-colored (organic) sub-millimeter-thick couplets that resemble varves (Moretto, 1986) (**Figure 10**). The bottom of the “Ensemble Salifère Intermédiaire” of the Bourg-en-Bresse basin has been correlated to the bottom of the “Sel III” of the Mulhouse basin (Moretto, 1986; Blanc-Valleron, 1990), and both basins display and increase in seasonal climatic contrast at that time (Schuler, 1988). The combined observations in these three records (which are several hundred of km apart) provide evidence for an increase in seasonal climatic contrast and in sensitivity of the climate to orbital variations over the continental west European mid-latitudes during the EOT. This hypothesis is consistent with recent studies that suggest an increase in sensitivity of the climate to orbital variations across the EOT (Tardif et al., 2021; Westerhold et al., 2020).

This prominent change in sedimentary regime occurs over a short stratigraphic interval and marks a change-point in the evolution of the behavior of the lacustrine systems that occupied the three basins. All these characteristics match well with the definition of a xenoconformity, which describes a stratigraphic surface (or gradational interval) that records an abrupt change in sedimentary facies across regional to global scales (Carroll, 2017). The intra-basinal to inter-basinal recognition of such singular stratigraphic surfaces or intervals is therefore interpreted as diagnostic of major global climate changes such as the Oi-1 event (and EOT) in western Eurasia mid-latitude lacustrine records. We thus propose that the increase in seasonal climatic contrast and in the sensitivity of climate to orbital variations observed in the Mulhouse and Bourg-en-Bresse basin are, similarly, synchronous with the EOT.

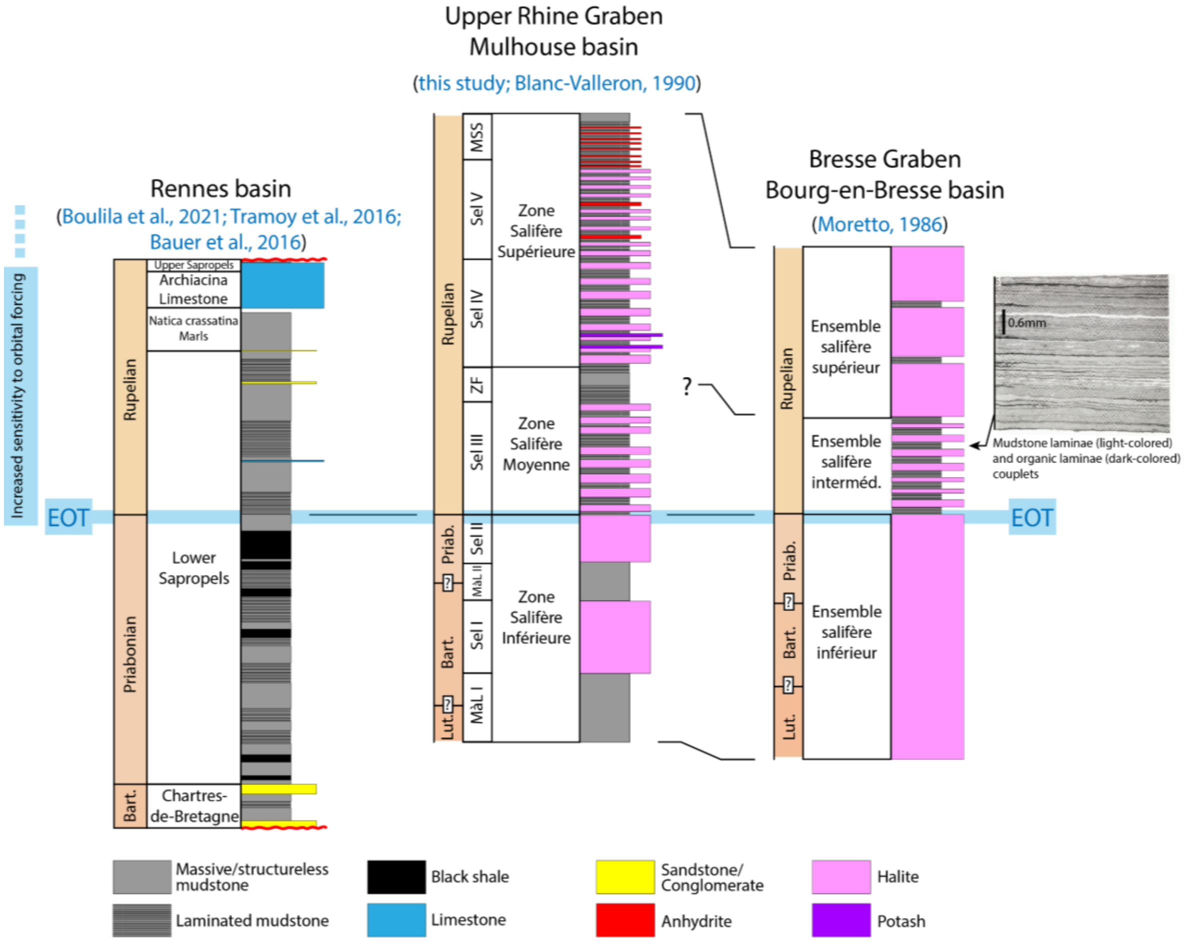

***Figure 10**: Comparison and correlations between the sedimentary records of the Rennes, Mulhouse, and Bourg-en-Bresse basins.*

Our findings compared to investigations performed at other localities enable to better asses their regional and global coherency and therefore potential driving mechanisms of the observed changes. High resolution marine $\delta^{13}C$ and $\delta^{18}O$ benthic records suggest increased sensitivity of the climate to orbital variations across the EOT linked to the formation of the Antarctic ice sheet and resulting increased oceanic circulation dynamics at seasonal and orbital scales (see Westerhold et al., 2020 and references therein). This provides a simple explanation for the increased seasonal climatic contrast observed in western Europe and is substantiated by further studies. The study of North Atlantic sediment cores revealed the change from diverse mixed broadleaved to cooler conifer-dominated pollen, indicative of an increase in seasonal climatic contrast across the EOT (Eldrett et al., 2009). Geochemical analyses performed on shells of freshwater gastropods in the Hampshire basin (United Kingdom) indicate a decrease in growing-season surface temperatures of 4°C across the EOT, indicating that the change in seasonal climatic contrast was likely also expressed by colder winters (Hren et al., 2013). Other studies account for a shift from warm paratropical/temperate to temperate/boreal vegetation in western and central Europe, also indicative of an increase in seasonal climatic contrast across the EOT (Kunzmann et al., 2016; Utescher et al., 2015; Kvaček et al., 2014; Mosbrugger et al., 2005). Continental temperature curves derived from central Europe flora have been correlated to global marine oxygen isotope, suggesting a tight link between continental climate with oceanic changes and Antarctic ice-sheet (Mosbrugger et al., 2005) and the straightforward interpretation that pCO_2 drawdown and associated temperature drop may have simply led to dryer and cooler winters, thus enhancing seasonal climatic contrasts (Eldrett et al., 2009). Furthermore, these observations are similar to a distant record in northeastern Tibet, where a transition from sedimentary cycles dominated by eccentricity to sedimentary cycles paced by a combination of eccentricity, obliquity, and precession is observed across the Oi-1 event (Ao et al., 2020). This suggests increased seasonality extended at least over the Eurasian continent across the EOT. However, this trend does not appear to extent globally as indicated by recent proxy-data reviews across the EOT (Hutchinson et al., 2019) and data-model comparison (Tardif et al., 2021; Toumoulin et al., 2022), notably in North America showing limited variability increases. This implies the EOT affected Eurasia climate patterns differently and led to suggesting increased modulations of the westerlies (Toumoulin et al., 2022) based on several grounds. Most importantly, teleconnections in circulation changes in the North Atlantic following the formation of the Antarctic ice-sheet has been proposed to relate to the onset and/or strengthening of the AMOC (Goldner et al., 2014). Such a mechanism would necessarily affect the seasonal climatic contrast and the sensitivity of local climate to orbital forcing in Eurasian mid-latitude records (Goldner et al., 2014). It should be noted, however, that more recent numerical simulations considering the pCO_2 reduction, the Antarctic ice-sheet development, as well as gateway opening around Antarctica associated with sea-level drop, fail to reproduce strengthening of AMOC-like oceanic dynamics (see Toumoulin et al., 2020 and references therein). Recent studies have also linked the EOT to gateway opening and closing between the Atlantic and the proto-Arctic (Coxall et al., 2018; Straume et al., 2022). These changes may have affected atmospheric and oceanic circulation globally and certainly induced changes in western Europe during the EOT.

Further investigations are required to determine more precisely the links and contributions between global drivers such as pCO_2 drawdown, sea-level drop, and tectonically-forced changes in oceanic circulation (Kennett, 1977; Toumoulin et al., 2020; Pearson et al., 2009; DeConto & Pollard, 2003; Straume et al., 2022; Abelson & Erez, 2017) with European climates across the EOT. This will require to determine the exact timing of the observed changes in seasonality and astronomically-forced cyclicity through the various phases of the EOT (e.g. Boulila e tal., 2021), in combination with numerical model simulations focusing on these particular entities.

6 Conclusion

This paper provides insights into the enhancement of seasonality contrast and sensitivity of the local climate to orbital variationsacross the Eocene-Oligocene Transition in the Upper Rhine Graben. Our new results are based on analyses of sedimentary rock cores and documents from the DP-XXVIII and DP-212 wells, as well as rock samples from the Altkirch and Kleinkems quarries (proximal records; “Zone Fossilifère”). Our investigation provides a new perspective on climate change during the Eocene-Oligocene Transition, how it impacted the lacustrine record of the Upper Rhine Graben and how they relate to global climate dynamics.

1. The presence of varves in the “Sel III” and “Zone Fossilifère” units of the DP-XXVIII well, and in the “Zone Fossilifère” unit of the Altkirch and Kleinkems quarries is

proposed based on microfacies analysis, together with a model combining fabrics formation and depositional hydrology. We compared the lower Oligocene varves of the Mulhouse basin to those from the Dead Sea (Ben Dor et al., 2019), and the varves of the Altkirch and Kleinkems quarries (“Zone Fossilifère”) to those from the Chatyr Kol lake (Kalanke et al., 2020).

2. In the DP-XXVIII well, a strong facies transition, from massive mudstones to laminated and varved mudstones, is documented from the base of the “Sel III” unit. This sedimentary pattern change coincides with the onset decameter-thick mudstone-evaporite cycles which we demonstrated are induced by orbital variations. Palynological studies have shown a penecontemporaneous change in climatic conditions towards a Mediterranean climate with enhanced seasonal contrast (Schuler, 1988). We thus propose that the appearance of the laminated and varved mudstones records a stronger contrast in the sedimentation processes that resulted from the climate change towards a stronger seasonality contrast. We also suggest that the onset of the decameter-thick mudstone-evaporite cycles is related to an increase of the climate’s sensitivity to orbital variations across the EOT.
3. We outlined similarities between our observations in the Upper Rhine Graben and changes in sedimentary facies documented in the Rennes basin during the Eocene-Oligocene Transition (Boulila et al., 2021), and in the Bourg-en-Bresse basin (Moretto, 1986). As such, we suggest that this spatially-transgressive facies transition could be the marker of the Eocene-Oligocene Transition in European mid-latitude lacustrine records. By comparison with similar observations performed in northeastern Tibet, this change could be a marker of the Oi-1 event (Ao et al., 2020). The characterization of such changes in sedimentary facies could help understand climate change during the Eocene-Oligocene Transition and help establish chronological frameworks. In addition, we suggest that the abruptness of this transition in the Mulhouse, Bourg-en-Bresse, and Rennes basins could reflect the crossing of a changepoint that had a major impact on regional climate, possibly through a pCO_2 drop and/or oceanic circulations changes, such as the onset of a proto-AMOC in relation with the formation of the Antarctic icesheet. We also show that these observations are coherent with other coeval paleoclimatic records in Europe.

7 Acknowledgements

We are grateful to the Musée d’Histoire Naturelle et d’Ethnographie de Colmar (Martial BOUTANTIN, Claître PRÊTRE, Manuelle VIGNES) for providing access the core samples from the DP-XXVIII well, and to the Kalivie museum (Chantal VIS, Loïc DEMESY) for providing access to the original written descriptions by MDPA of the DP-XXVIII well. We thank Magalie LINDENMAYER from the Holcim quarry in Altkirch for allowing us to retrieve samples from the quarry. We thank Kirsten GRIMM and Matthias GRIMM for insightful discussions on the biostratigraphy of the Upper Rhine Graben. The PhD of ES is funded by MESRI and Région Grand-Est. Field work and analysis were funded by a research grant from CNRS/INSU (TelluS/SysTer program) attributed to MS. Additional support was provided by the “Geologial Systems” research team at ITES. We are grateful to Ola KWIECIEN and Nicolas WALDMANN for reviewing the manuscript and providing insightful comments.

8 Conflict of Interest

The authors declare no conflict of interest.

9 Data Availability

All the data presented in this publication can be downloaded from the website of *Sedimentologika*.

10 Authors contributions

ES wrote the paper, performed sedimentary facies analysis (with LGC, FG, HV and MS). All authors contributed to interpret and discuss the results. ES and MS worked on the illustrations and collected field samples. ES and LGC worked on the logging and description of the DP-XXVIII well. MU performed the µ-XRF analyses and helped on their interpretation. ES and CB worked on the µ-XRF results and on the interpretation of varves and laminated sediments. MS and HV designed the overall research project dedicated to the EOT in the URG, and group discussions allowed to sharply define the topic of this paper. GDN provided insights and discussions in regard to the EOT. MM provided insights and discussions in regard to cyclostratigraphy and paleoclimates. LGC provided insights and discussions on evaporites, cores, and on the URG. FG provided insights and discussions on the URG and cores. CB, LGC, HV and MS provided expertise on laminated sediments and varves.

Chapter VI : Cyclostratigraphy of the Upper Rhine Graben

In this chapter are presented the cyclostratigraphic investigations of the Mulhouse and Pechelbronn basins using well-log data, notably Gamma-Ray series. They were investigated using the methods and tools detailed in **III.2.b : Cyclostratigraphy**. The ratios between the orbital cycles in the time domain near the Eocene-Oligocene boundary are 18.6 : 4.5 : 1.8 : 1 and correspond to the long eccentricity (400.2 kyr), the short eccentricity (97.4 kyr), obliquity (39.6 kyr), and precession (21.5 kyr). They are the ratios used to correlate sedimentary cycles in the depth domain to the orbital cycle in the time domain (Weedon, 2003).

VI.1 : Mulhouse basin

Thanks to the potash industry of the Mulhouse basin in the 20th century, its sedimentary record has been widely accessed through drilling, coring, and borehole petrophysical logging, even though a consequent amount of data has been lost due to being thrown away by the operators at the end of the potash exploitation in the late 90s. While no continuous core remains, several well-logs have been saved on the BRGM website and at the Kalivie museum (Wittelsheim). These well-logs allow for the study of the sedimentary succession through time by investigating continuous petrophysical measurements such as gamma-ray signals. Three main well-logs have been investigated: DP-206, DP-211, and DP-212 (supplementary material).

VI.1.a : Preliminary investigations

VI.1.a.i : Stratigraphic description

The well-logs of the DP-206, DP-211, and DP-212 wells were revisited to extract the gamma-ray data from the physical documents (see Error! Reference source not found.) and to c reate the synthetic logs of their sedimentary successions (**Figure 78**, “Zone Salifère Supérieure”). There are five main lithologies being mudstone, gypsum, anhydrite, halite, and potash. The well-logs of the DP-206 well are continuous through the whole interval of interest, being the “Zone Salifère Supérieure”, “Zone Salifère Moyenne”, and “Zone Salifère Inférieure”, even though a slight part of the latter might be missing (**Figure 79**). No fault has been detected in this well by the operators, making it the prime record for the cyclostratigraphic investigation of the Mulhouse basin. On the other hand, the well-logs from the DP-211 and DP-212 wells are not continuous due to several faults detected by the operators, below the upper potash seam for DP-211 and above it for DP-212 (**Figure 78**). Also, both end in the “Zone Fossilifère”, and therefore do not allow the investigation of the “Sel III” and “Zone Salifère Inférieure” at these locations. While these records (DP-211, DP-212) are not continuous, they still allow to perform well-log correlations in parts of the “Zone Salifère Supérieure” and to compare cyclostratigraphic results.

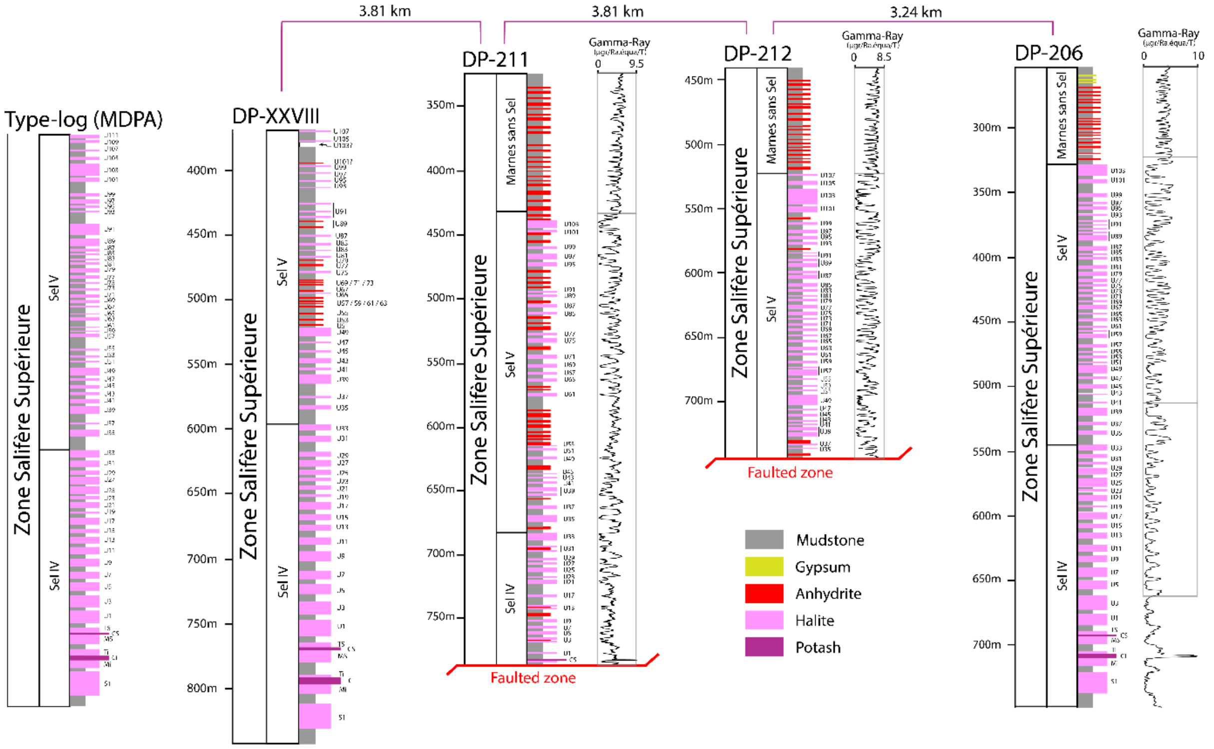

Figure 78: *Synthetic sedimentary logs and gamma-ray signal of the DP-206, DP-211, and DP-212 wells. The grey rectangles represent the several sections that were investigated separately for cyclostratigraphy. By comparison and through well-log correlations, I named the halite beds of the DP-XXVIII, DP-211, DP-212 and DP-206 wells accordingly to the name given by the MDPA in the type-log.*

While all three wells are characterized by sedimentary trends found across the whole Mulhouse basin (**II.3.c.i : Mulhouse basin**), some differences can be observed on the synthetic sedimentary logs. The “Marnes sans Sel” unit is similar in all three wells as characterized by their mudstone-anhydrite alternations, however, gypsum beds appear near the top of the unit in the DP-206 well that are not found in the two others. Furthermore, this unit is thicker in the DP-211 well compared to the two others. The “Sel IV” and “Sel V” units are characterized by their mudstone-evaporite alternation, where the evaporites are mainly halite. However, differences can be observed by looking at the synthetic sedimentary logs, which are the high amount of anhydrite in the DP-211 compared to the two others (**Table 2**). In the case of the DP-206 well, we can observe the gradual decrease of the mudstone-halite alternations’ thicknesses from the bottom to the top (**Figure 79**). This continual decrease is possibly linked with a tectonically driven decrease in Sediment Accumulation Rate (SAR). Because of this, to avoid the mixing of cycles in the cyclostratigraphic investigations, the gamma-ray series of the DP-206 well has been separated in two distinct parts. The relative thicknesses of the mudstone-evaporite alternations at the bottom of the “Sel IV” are very different between the DP-206 and DP-211 wells. While they are pretty thick in the DP-206 well, they seem way thinner in the DP-211 well. This could suggest the presence of dissolution surfaces or small undetected faults, as these alternations are expected to be relatively thick, as described in most wells of the Mulhouse basin by the MDPA (Blanc-Valleron, 1990). Such dissolution surfaces can be quite damaging as they can erase sedimentary alternations or reduce their original thickness, which can lead to the attribution of another orbital cycles, and therefore to the underestimation of the minimum duration of the record. As the same sedimentary units are investigated across multiple wells, the longest minimum duration found for each unit will be the one used for the final age model.

***Table 2**: Thickness and continuity of the investigated sedimentary intervals of the Mulhouse basin.*

	DP-206				DP-211			DP-212	
Unit	Sel III	Sel IV	Sel V	MSS	Sel IV	Sel V	MSS	Sel V	MSS
Thickness	249	202	217	74	103	249	110	247	79
Hiatus	/	/	/	/	Fault	/	/	/	/

Each bed of the “Sel IV” and “Sel V” units have been given a name by the MDPA in some main wells. The beds of the “Sel IV” are named, from bottom to top: S2, S1, S, Mi, Ci, Ti, T, MS, CS, TS, U, then U1, U2, … U33. Mudstone beds are named S2, S, T, U, then U2, U4, … U32. Halite beds are named S1, Mi, Ti, MS, TS, U1, then U3, U5, … U33. Potash beds are named Ci and CS. Then, for the “Sel V”, mudstone beds are named U34, U36, … U110, and halite beds are name U35, U37, … U111. Depending on the location, a few alternations can be missing. I tentatively correlated and named each bed of the DP-206, DP-211, and DP-212 wells by performing diagraphic correlations, as gamma-ray trends can be observed across the three wells.

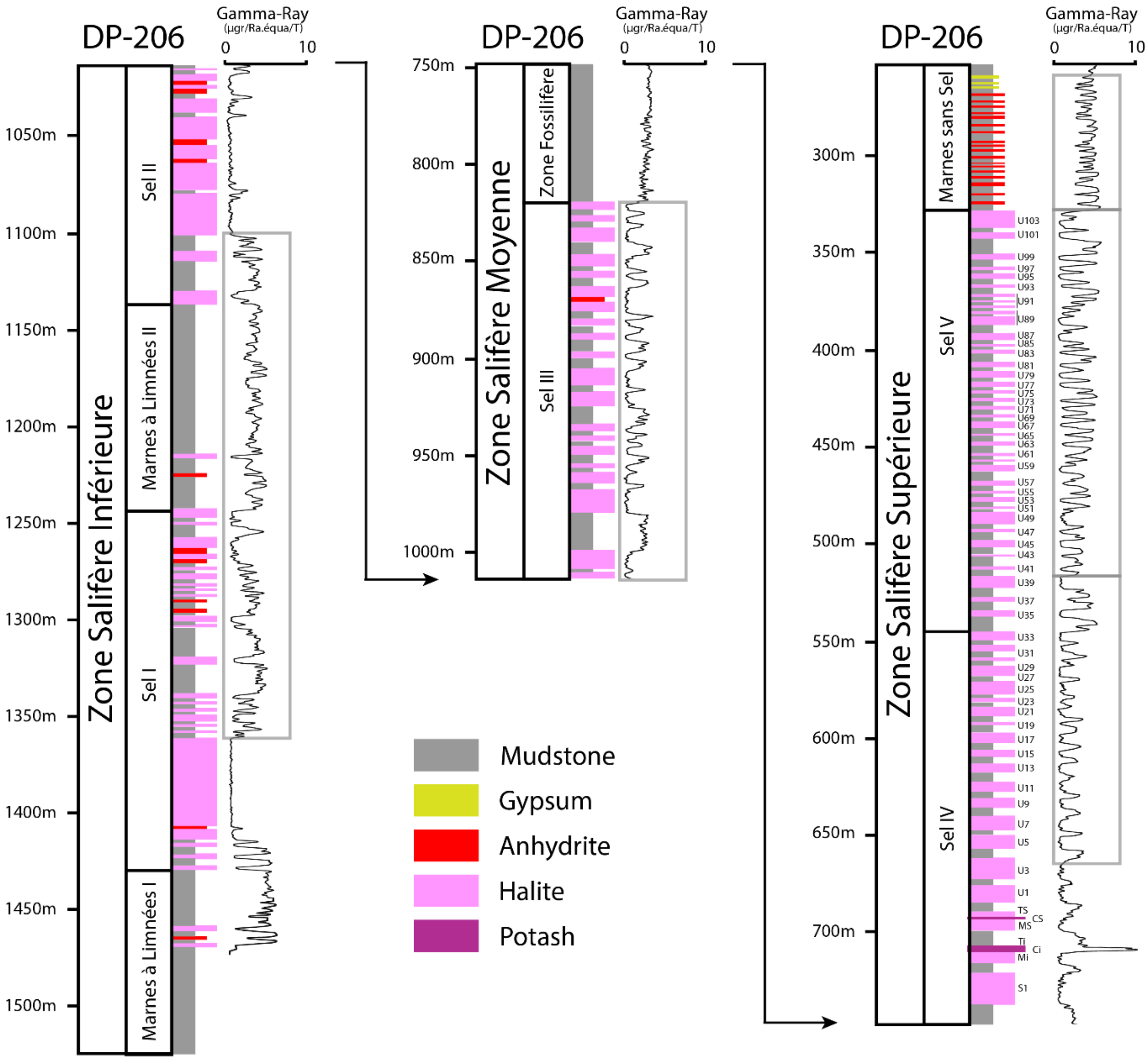

***Figure 79**: Synthetic sedimentary log and gamma-ray signal of the DP-206 well. The grey rectangles represent the sections that were investigated separately through cyclostratigraphy. Not all sections are suitable for cyclostratigraphic investigations due to the absence of alternations (e.g. Zone Salifère Inférieure, Zone Fossilifère). The gray rectangles show which parts of the Gamma-Ray series were used to perform signal analysis.*

In the Mulhouse basin, the use of Gamma-Ray series as a paleoclimatic proxy is particularly strong as it clearly allows to distinguish mudstones from evaporitic beds (**Figure 79**). It is therefore used as a proxy of lake-level variations/precipitations.

VI.1.a.ii : Independent age model

While there is no strong independent age model available for the "Zone Salifère Inférieure", "Zone Salifère Moyenne", and "Zone Salifère Supérieure", an independent age can be estimated based on the assumption that the marine transgression of the "Zone Fossilifère" is related to the PaRu1 sea-level sequence (Berger et al., 2005). Based on this theory, I propose that the bottom of the "Zone Fossilifère" would be dated around ~33.16 Ma as it would corresponds to the end of the EOGM, where the newly formed AIS partially melts and increases the average sea-level. The investigation of the foraminifera of the "Série Grise" by Pirkenseer et al. (2010) suggest that this formation is attributed to the mid P20 to P21 foraminifera biozones. Other studies account for an attribution to the NP23 and NP24 calcareous nannofossils biozone (Doebl et al., 1976; Riveline, 1984). The attribution fn the lowermost part of this formation to the mid P20 zone suggests that the top of the "Zone Salifère Supérieure" (= bottom of the "Série Grise") would be dated around ~29.80 Ma. The "Zone Fossilifère" is partially attributed to the NP21 and NP22 biozones (Schuler, 1988).

Below the "Zone Fossilifère", there are no independent ages that can be inferred from sea-levels sequences as there are no evidence of marine water inputs. However, according to Simon et al. (2024, submitted) (see **Chapter V :**), it is very likely that the facies transition from structureless mudstones to laminites and varves, alongside the apparition of decametric mudstone-evaporite cycles, marks the Oi-1 event at the end of the EOT (= 33.65 Ma). According to this reasoning, the bottom of the "Sel III" unit is dated at ~33.65 Ma. Therefore, using only these independent ages, the duration of the "Sel III" is estimated as being equivalent to the duration of the EOGM, being ~490 kyr.

***Table 3**: Chronostratigraphic elements used to create a low-resolution independent age model for several units and formations of the Mulhouse basin. a: Simon et al. (2024, submitted), b: Pirkenseer et al. (2010), c: this thesis.*

Unit/Formation	Base age (Ma)	Top age (Ma)	Duration (kyr)
Série Grise	~29.80 (mid P20)[b]	?	?
Zone Salifère Supérieure	?	~29.80 (base Série Grise)[b]	?
Zone Fossilifère	~33.16 (end of the EOGM, PaRu1)[c]	?	?
Sel III	~33.65 (Oi-1 event)[a]	~33.16 (base ZF)[c]	~ 490

VI.1.b : Signal analysis, cycle interpretation, minimum durations

VI.1.b.i : DP-206

Zone Salifère Inférieure

The gamma-ray series of the "Zone Salifère Inférieure" formation of the DP-206 well (partial; **Figure 79**) was linearly detrended and standardized. The 2pi-MTM results of the partial gamma-ray signal of the "Zone Salifère Inférieure" formation (thickness: 262m) of the DP-206 well reveal broadbands related to sedimentary cycles with average thicknesses of 50m, 18.5m

(> median CL) and 10.3m (> 95% CL) (**Figure 80**). The ratios between these cycles in the depth domain (4.9 : 1.8 : 1) are particularly close to those of the orbital cycles (short eccentricity, obliquity, precession) in the time domain (4.5 : 1.8 : 1). The ~50m cycle could therefore correspond to the short eccentricity, the ~18.5m cycle to obliquity, and the 10.3m cycle to precession. However, due to the poor statistical significance of the 50m and 18.5m cycles, this interpretation is rather poorly constrained. Furthermore, the synthetic log of the investigated interval does not display clear sedimentary alternations such as those seen in the "Sel III" or "Zone Salifère Supérieure" that could be correlated to the Taner-Hilbert filters of said cycles (see the following sections). For these reasons, and even though the spectral analysis reveals orbital-like ratios, I consider that this interval is not fit for cyclostratigraphic interpretations.

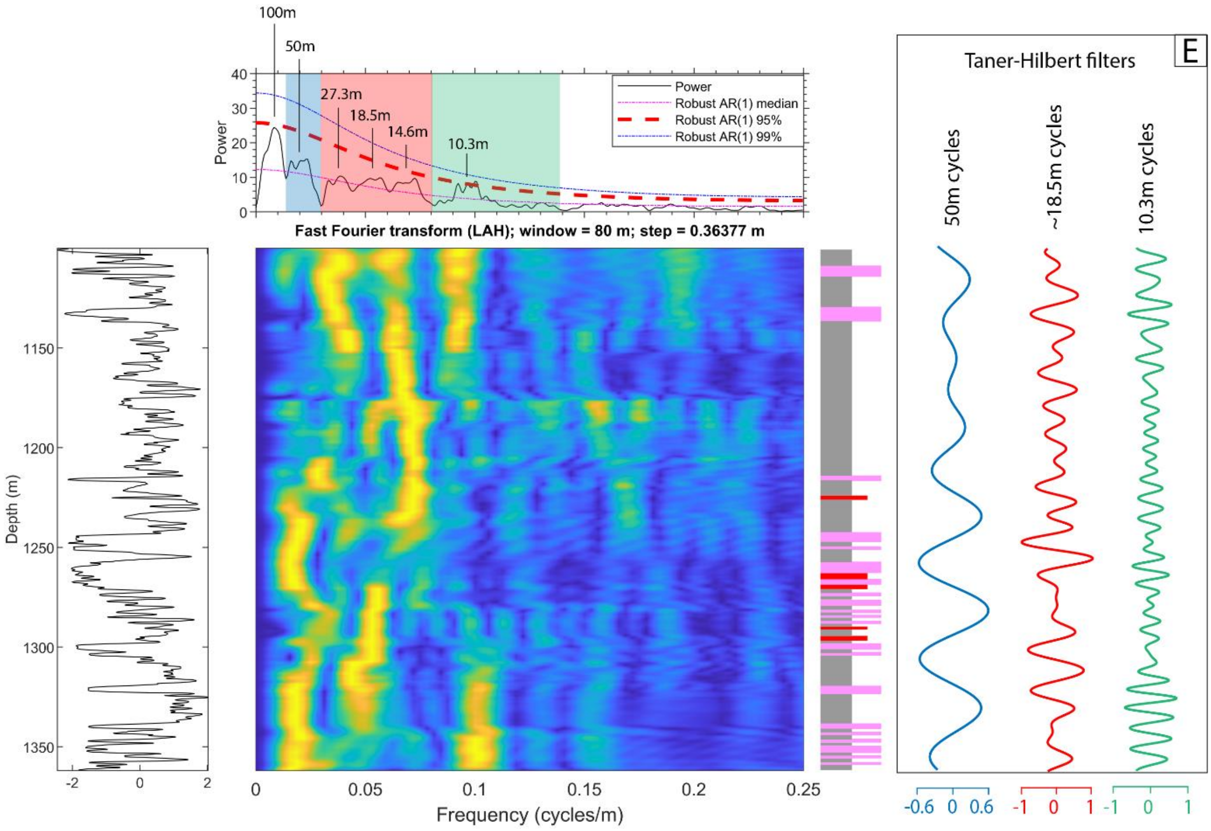

Figure 80: Spectral analysis results of the ZSIm section of the DP-206 well ("Zone Salifère Inférieure"). (A) Linearly detrended gamma-ray series. (B) 2π-multitaper spectrum with linearly fitted red-noise modelling. (C) Evolutive Fast Fourier transform (LAH) with a sliding window of 80m and a step of 0.36377m. (D) Sedimentary log corresponding to the proxy signal with halite in pink, anhydrite in red, and mudstone in grey. (E) Taner-Hilbert filters of the ~50m cycle (0.0137 – 0.0298 cycles/m), ~18.5m cycle (0.0298 – 0.0817 cycles/m), and ~10.3m cycle (0.0817 – 0.1397 cycles/m).

Sel III

The gamma-ray series of the "Sel III" interval was interpolated, linearly detrended, and standardized (**Figure 81**A). The 2π-MTM results of the detrended gamma-ray signal of the "Sel III" unit (thickness: 249m) from the DP-206 well reveals statistically significant frequency broadbands related to sedimentary cycles with average thicknesses of 34.9m, 7.1m (> 95% CL) and 13.2m (> median CL) (**Figure 81**B). The ratios between these cycles in the depth domain (4.9 : 1.9 : 1) are particularly close to those of the orbital cycles (short eccentricity, obliquity, precession) in the time domain (4.5 : 1.8 : 1). The ~34.9m cycle is therefore interpreted as corresponding to the short eccentricity, the ~13.2m cycle to obliquity, and the ~7.1m cycle to precession.

The EFFT plot shows that the ~34.9m cycle is particularly expressed at the bottom of the series through the massive (>10m) mudstone and halite beds between 1012m and 967m (**Figure 81**C). The Taner-Hilbert filter of this same cycle however shows that it is still present upward in the sedimentary record but gets overshadowed by the obliquity and precession cycles as observable on the EFFT plot. The Taner-Hilbert filters of the obliquity and precession cycles, when compared to the sedimentary alternations, show that these alternations are either in tune with obliquity (when their thickness is ~13.2m) or precession (when their thickness is ~7.1m) (**Figure 81**D, E). This observation is a strong argument for the interpretation of the sedimentary alternations as induced by orbital climate fluctuations, with both obliquity and precession having visible impacts on sedimentation (see **VI.1.d : Astronomical forcing model**).

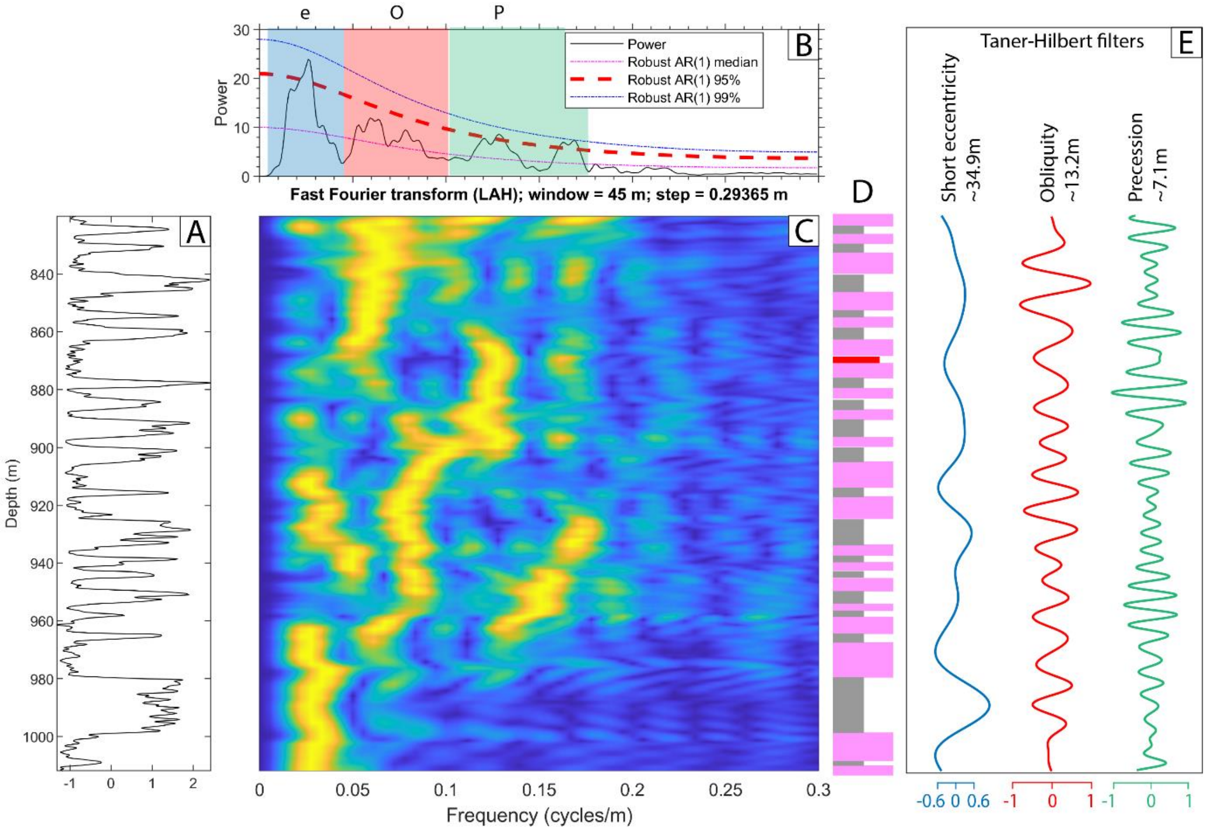

Figure 81: Spectral analysis results of the “Sel III” unit of the DP-206 well (“Zone Salifère Moyenne”). (A) Linearly detrended gamma-ray series. (B) 2π-multitaper spectrum with linearly fitted red-noise modelling. (C) Evolutive Fast Fourier transform (LAH) with a sliding window of 45m and a step of 0.29365m. (D) Sedimentary log corresponding to the proxy signal with halite in pink, anhydrite in red, and mudstone in grey. (E) Taner-Hilbert filters of the interpreted short eccentricity (0.0104 – 0.0469 cycles/m), obliquity (0.0469 – 0.0990 cycles/m), and precession (0.1094 – 0.1771 cycles/m) cycles.

Sel IV (partial)

The gamma-ray series of the “Sel IV” unit (partial) of the DP-206 wellwas interpolated, linearly detrended, and standardized (**Figure 82**A). The 2π-MTM results of the detrended gamma-ray series of the “Sel IV” unit (thickness: 149m) shows statistically significant sedimentary frequency broadbands related to sedimentary cycles with average thicknesses of 15 and 8.6 meters (> 90% CL), and other less significant sedimentary cycles with average thicknesses of 74 and 4.5 meters (> median CL) (**Figure 82**B). The ratios between these cycles in the depth domain (16.3 : 3.3 : 1.9 : 1) are coherent to those of the orbital cycles in the time domain (18.6 : 4.5 : 1.8 : 1) but show significant differences that could be linked to changes in

SAR. The ~74m cycle could correspond to the large eccentricity, the ~15m cycle to the short eccentricity, the ~8.6m cycle to the obliquity, and the ~4.5m cycle to precession.

The change in SAR is apparent in the EFFT plot, where the cycle of the obliquity band shifts from 0.1 cycles/m at 662m depth to 0.16 cycles/m at 570m, before being overshadowed by the short eccentricity cycle upward in the record (**Figure 82**C). The Taner-Hilbert filters of the orbital cycles show that for most of the ZSSI, the mudstone-evaporite alternations are primarily in phase with obliquity (**Figure 82**D, E), meaning that obliquity is very likely to be the primary driver of these alternations. Starting from 570m and upward, the short eccentricity cycles become more apparent in the EFFT, but the sedimentary alternations still seem in phase with the filtered obliquity signal.

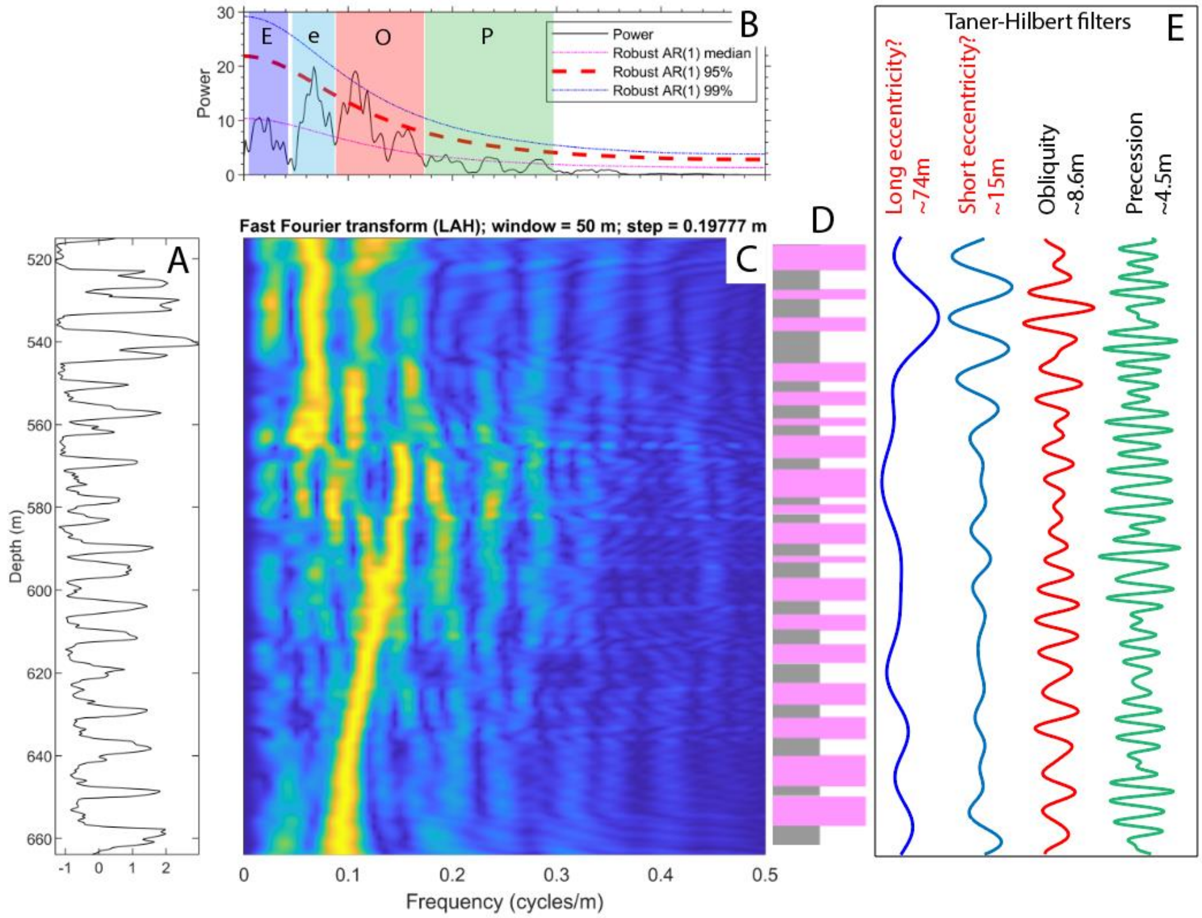

Figure 82: Spectral analysis results of the "Sel IV" unit (partial) of the DP-206 well ("Zone Salifère Supérieure"). (A) Linearly detrended gamma-ray series. (B) 2π-multitaper spectrum with linearly fitted red-noise modelling. (C) Evolutive Fast Fourier transform (LAH) with a sliding window of 50m and a step of 0.19777m. (D) Sedimentary log corresponding to the proxy signal with halite in pink and mudstone in grey. (E) Taner-Hilbert filters of the interpreted long eccentricity (0 – 0.0470 cycles/m), short eccentricity (0.0470 – 0.0873 cycles/m), obliquity (0.0873 – 0.1745 cycles/m), and precession (0.1745 – 0.3088 cycles/m) cycles.

Sel V (+ small part of "Sel IV")

The gamma-ray series of the "Sel V" unit (with a small part of "Sel IV") of the DP-206 well was linearly detrended and standardized (**Figure 83A**). The 2π-MTM results of the "Sel V" unit (187m) shows statistically significant sedimentary cycles with average thicknesses of 25 and 5 meters (>99%), and other significant sedimentary cycles with average thicknesses of 95 and 8 meters (**Figure 83B**). The ratios between these cycles in the depth domain (19 : 5 : 1.6 : 1) are very close to those of the orbital cycles in the time domain (18.6 : 4.5 : 1.8 : 1). The ~95m cycle could therefore correspond to the large eccentricity, the ~25m cycle to the short eccentricity, the ~8m cycle to the obliquity, and the ~5m cycle to precession.

The EFFT plot shows that there could be SAR variations as the frequencies with the highest amplitudes are curved in the precession band rather than straight (**Figure 83C**). The observed sedimentary cycles consisting of mudstone-evaporite alternations are mostly in phase with the Taner-Hilbert filter of precession in this interval, suggesting that precession is the main driver of their deposition (**Figure 83D, E**). However, there still are a few thicker cycles in phase with obliquity, indicating some rare periods where obliquity potentially had more influence than precession on sedimentation.

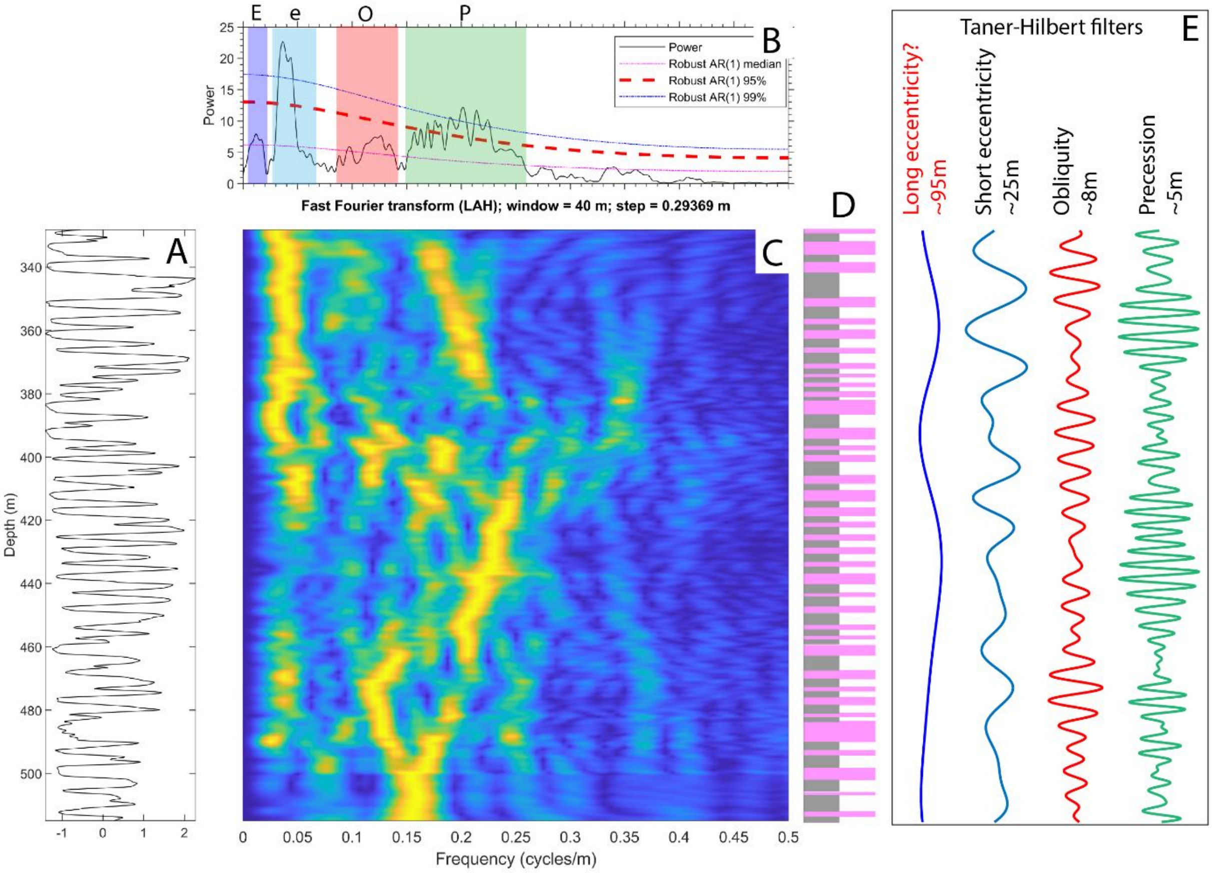

Figure 83: Spectral analysis results of the "Sel V" unit of the DP-206 well ("Zone Salifère Supérieure"). (A) Linearly detrended gamma-ray series. (B) 2π-multitaper spectrum with linearly fitted red-noise modelling. (C) Evolutive Fast Fourier transform (LAH) with a sliding window of 100m and a step of 0.17369m. (D) Sedimentary log corresponding to the proxy signal with halite in pink and mudstone in grey. (E) Taner-Hilbert filters of the interpreted long eccentricity (0.0032099 – 0.021399 cycles/m), short eccentricity (0.026749 – 0.069548 cycles/m), obliquity (0.090948 – 0.14445 cycles/m), and precession (0.1712 – 0.26749 cycles/m) cycles.

Marnes sans Sel

The gamma-ray series of the "Marnes sans Sel" unit of the DP-206 wellwas linearly detrended and standardized (**Figure 84**A). The 2π-MTM results of the gamma-ray signal of the "Marnes sans Sel" unit (thickness: 74m) reveals a significant broadband related to a sedimentary cycle with average thickness of 3.1m (> 99% CL) (**Figure 84**B). Other broadbands, that are however not statistically significant, are related to sedimentary cycles of 16.4m and 6.7m. The ratios between these cycles in the depth domain (5.3 : 2.2 :1) are relatively close to those of the orbital cycles (short eccentricity, obliquity, precession) in the time domain (4.5 : 1.8 : 1). The ~16.4m cycle could therefore correspond to the short eccentricity, the ~6.7m cycle to obliquity, and the ~3.1m cycle to precession. On its own, this proposition would be poorly constrained, but by comparison with what is observed in the series underneath, it is rather logical.

The EFFT plot shows that the sedimentary cycles at the bottom of the unit, between 328m and 313m, are particularly close to the limit between obliquity and precession bands (**Figure 84**C). Furthermore, the Taner-Hilbert filters of both the obliquity and precession bands show similar thicknesses, therefore it looks like there could be some frequency mixing. For the rest of the unit going upward, the EFFT is dominated by the precession band, and the sedimentary alternations are in phase with the precession filter, which suggests that they are induced by precession (**Figure 84**D, E).

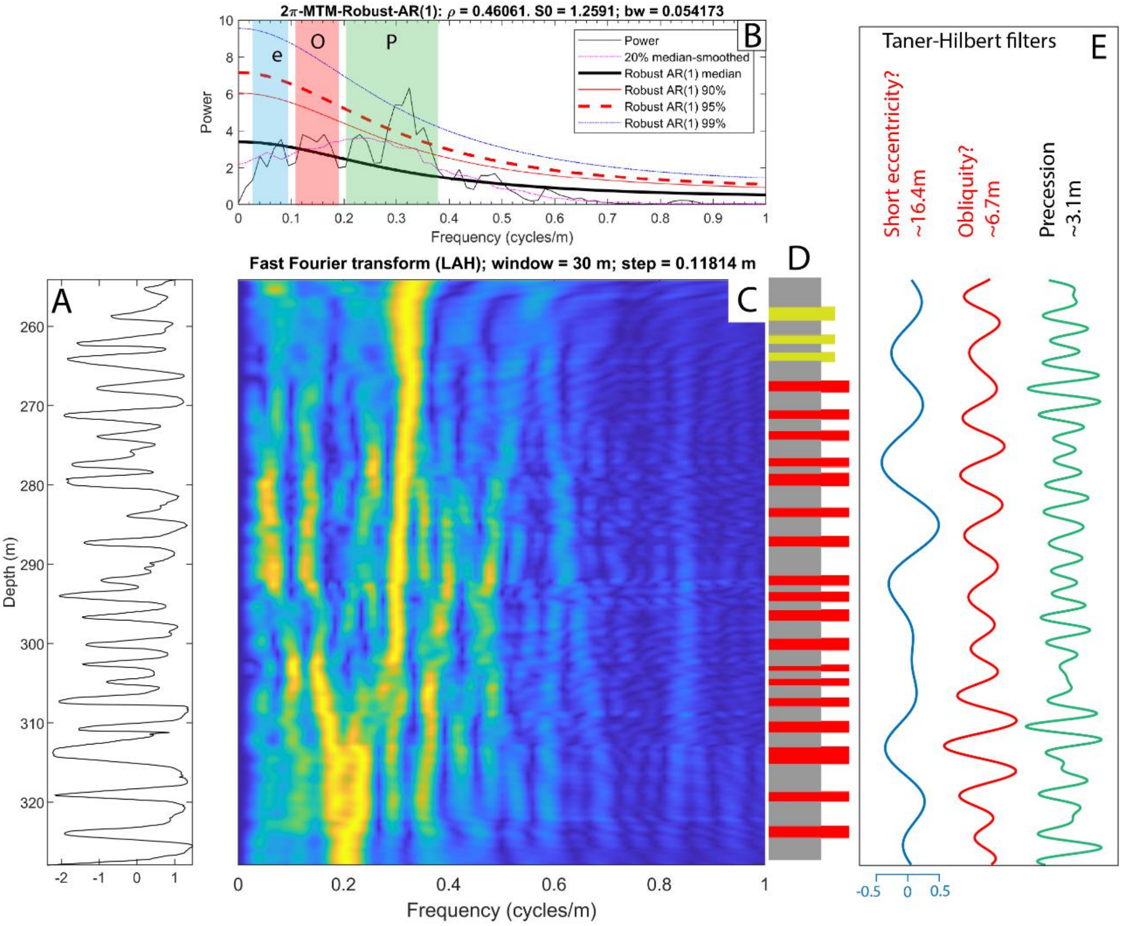

Figure 84: Spectral analysis results of the "Marnes sans Sel" unit of the DP-206 well ("Zone Salifère Supérieure"). (A) Linearly detrended gamma-ray series. (B) 2π-multitaper spectrum with linearly fitted red-noise modelling. (C) Evolutive Fast Fourier transform (LAH) with a sliding window of 30m and a step of 0.11814m. (D) Sedimentary log corresponding to the proxy signal with anhydrite in red, gypsum in yellow, and mudstone in grey. (E) Taner-Hilbert filters of the interpreted short eccentricity (0.0270 – 0.0947 cycles/m), obliquity (0.1082 – 0.1893 cycles/m), and precession (0.2028 – 0.3787 cycles/m) cycles.

Minimum durations

According to the previous results, and by comparing the sedimentary log with the Taner filters of the sedimentary alternations attributed to orbital cycles (**Figure 85**), minimum durations can be estimated for the investigated intervals of the DP-206 well.

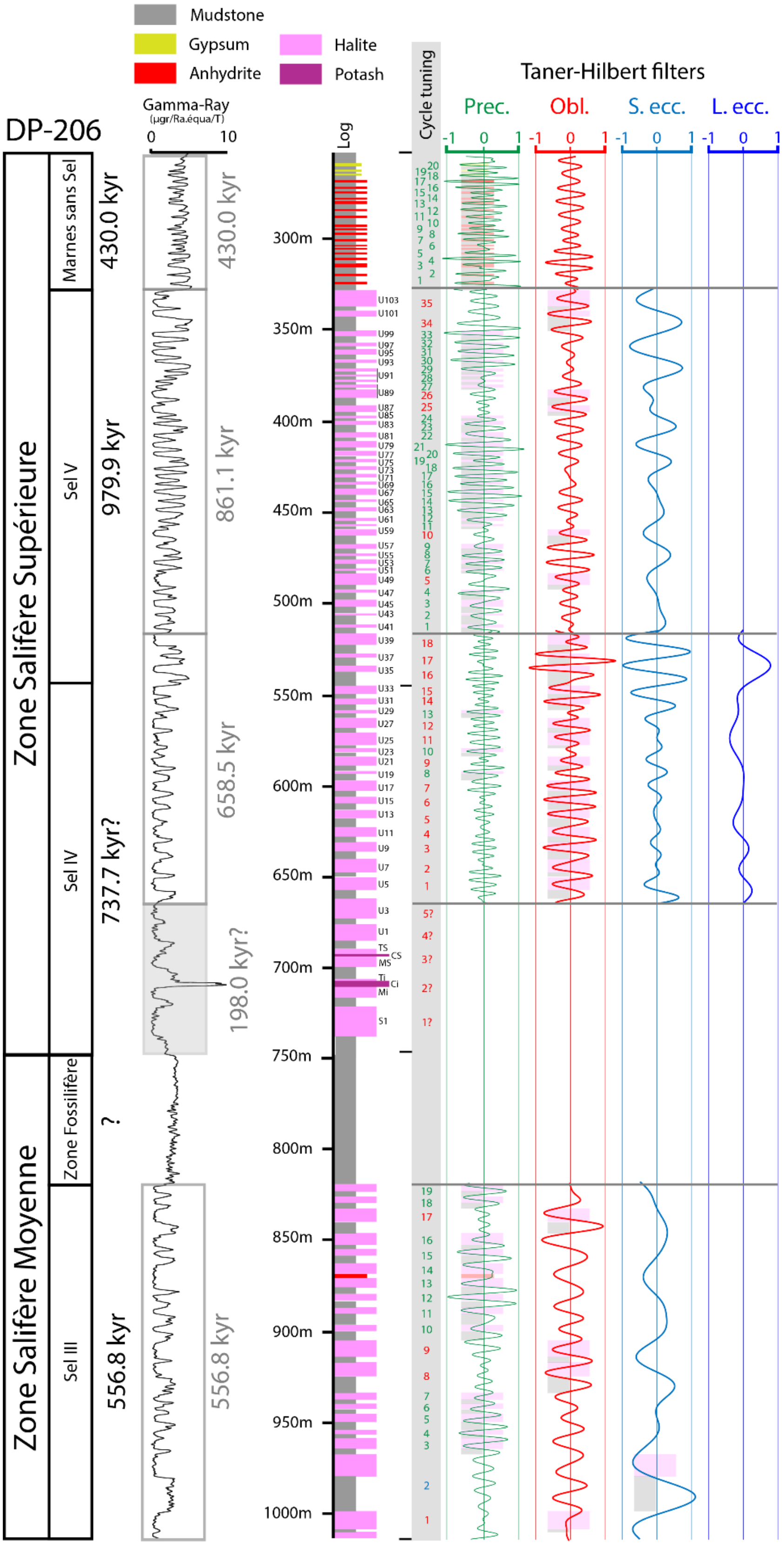

Figure 85: Synthesis of the cyclostratigraphy results from the DP-206 well. The Gamma-Ray series is plotted alongside the sedimentary log and Taner filters of the sedimentary cycles attributed to the orbital cycles. Duration are proposed for each sedimentary alternation based on their correlation with Taner filters. Numbers in the "Cycle tuning" column correspond to each sedimentary cycle and attributed to orbital cycles, with precession in green, obliquity in red, and short eccentricity in pale blue.

The minimum duration of the “Sel III” unit is estimated at 556.8 kyr, with 1 short eccentricity cycle, 4 obliquity cycles, and 14 precession cycles.

The “Sel IV” unit contains 20 sedimentary alternations, with the lowermost 5 being relatively thicker than the rest and showing a thinning trend upward, likely associated with a decrease in SAR. These 5 alternations were excluded from the signal analysis, but by comparison with the following ones, I attributed them to obliquity. Therefore, the minimum duration of the “Sel IV” unit is estimated at 737.7 kyr, with 17 obliquity cycles and 3 precession cycles.

The minimum duration of the “Sel V” unit is estimated at 979.9 kyr, with 9 obliquity cycles and 29 precession cycles.

The minimum duration of the “Marnes sans Sel” unit is estimated at 430.0 kyr with 20 precession cycles. The duration of this unit is probably slightly more as a few meters of mudstones are present above the last mudstone-evaporite alternation.

The minimum duration of the “Zone Salifère Supérieure” formation is therefore estimated at 2147.6 kyr in the DP-206 well.

VI.1.b.ii : DP-211

Sel IV and Sel V

The gamma-ray series of the combined “Sel IV” (thickness: 103 m) and “Sel V” (thickness: 249 m) units of the DP-211 well was linearly detrended and standardized (**Figure 86**A). The 2π-MTM results of the gamma-ray signal of this interval (total thickness: 351 m) reveals significant frequency broadbands related to sedimentary cycles with average thicknesses of 23.9 m, 9.5 m, and 5 m (<99% CL) (**Figure 86**B). The ratios between these cycles in the depth domain (4.8 : 1.9 : 1) are particularly close to those of the orbital cycles (short eccentricity, obliquity, precession) in the time domain (4.5 : 1.8 : 1). The ~23.9 m cycle is therefore attributed to the short eccentricity, the ~ 9.5 m cycle to obliquity, and the ~ 5 m cycle to precession.

The EFFT shows that parts of the interval are dominated either by obliquity, short eccentricity and/or precession (**Figure 86**C). However, the sedimentary alternations are either in phase with the obliquity or precession filters, suggesting that they are mostly driven by these cycles (**Figure 86**D, E).

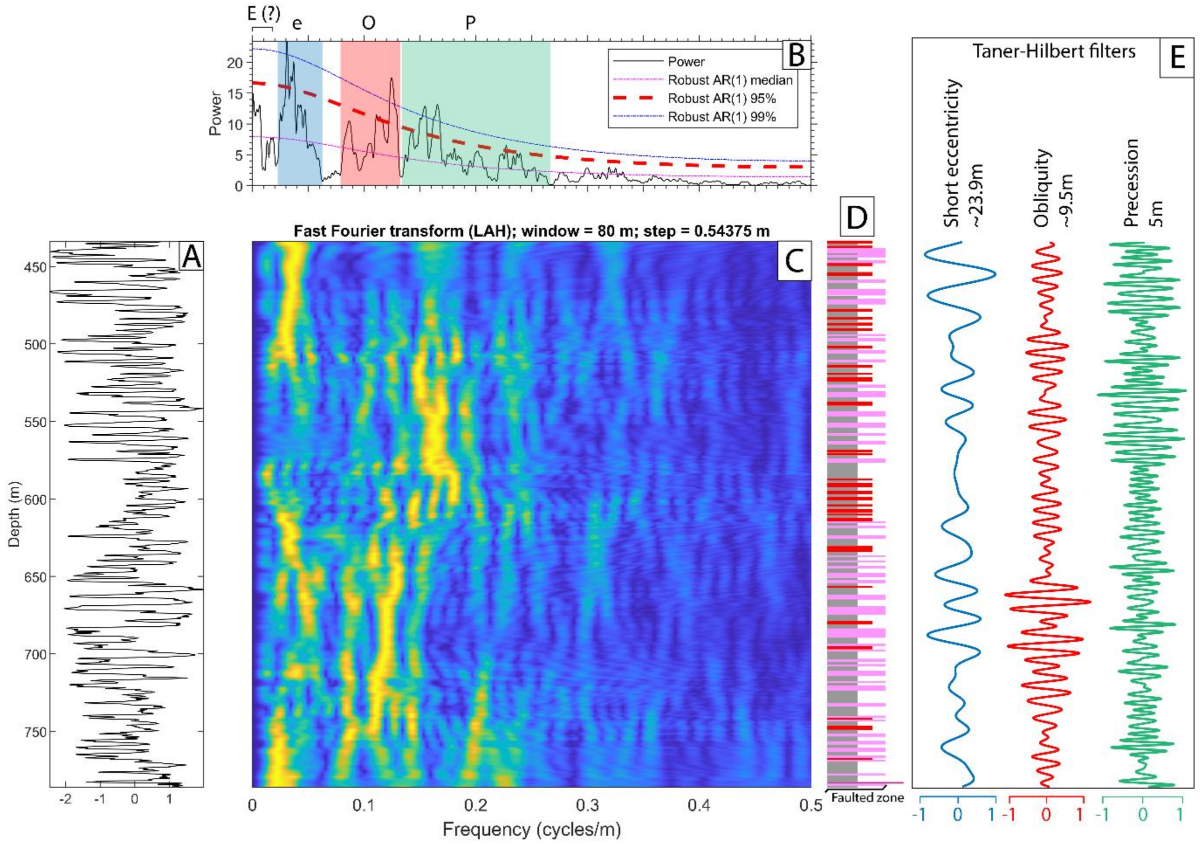

***Figure 86**: Spectral analysis results of the “Sel IV” and “Sel V” units of the DP-211 well (“Zone Salifère Supérieure”). (A) Linearly detrended gamma-ray series. (B) 2π-multitaper spectrum with linearly fitted red-noise modelling. (C) Evolutive Fast Fourier transform (LAH) with a sliding window of 80m and a step of 0.54375m. (D) Sedimentary log corresponding to the proxy signal with halite in pink, anhydrite in red, and mudstone in grey. (E) Taner-Hilbert filters of the interpreted short eccentricity (0.0227 – 0.0625 cycles/m), obliquity (0.0767 – 0.1335 cycles/m), and precession (0.1364 – 0.2671 cycles/m) cycles.*

Marnes sans Sel

The gamma-ray series of the “Marnes sans Sel” unit of the DP-211 well was interpolated, linearly detrended, and standardized (**Figure 87**A). The 2π-MTM results of the detrended gamma-ray signal of the “Marnes sans Sel” unit (thickness: 110m) from the DP-211 well reveals significant frequency broadbands related to sedimentary cycles with average thicknesses of 21.8m, 10m (> median CL) and 4.2m (> 99% CL) (**Figure 87**B). The ratios between these cycles in the depth domain (5.2 : 2.4 : 1) are somewhat close to those of the orbital cycles (short eccentricity, obliquity, precession) in the time domain (4.5 : 1.8 : 1). The ~21.8m cycle is therefore interpreted as corresponding to the short eccentricity, the ~10m cycle to obliquity, and the ~4.2m cycle to precession.

The EFFT shows that the whole interval is dominated either by the precession broadband (**Figure 87**C). Furthermore, the sedimentary alternations are in phase with the precession filter, suggesting that they are driven by precession (**Figure 87**D, E).

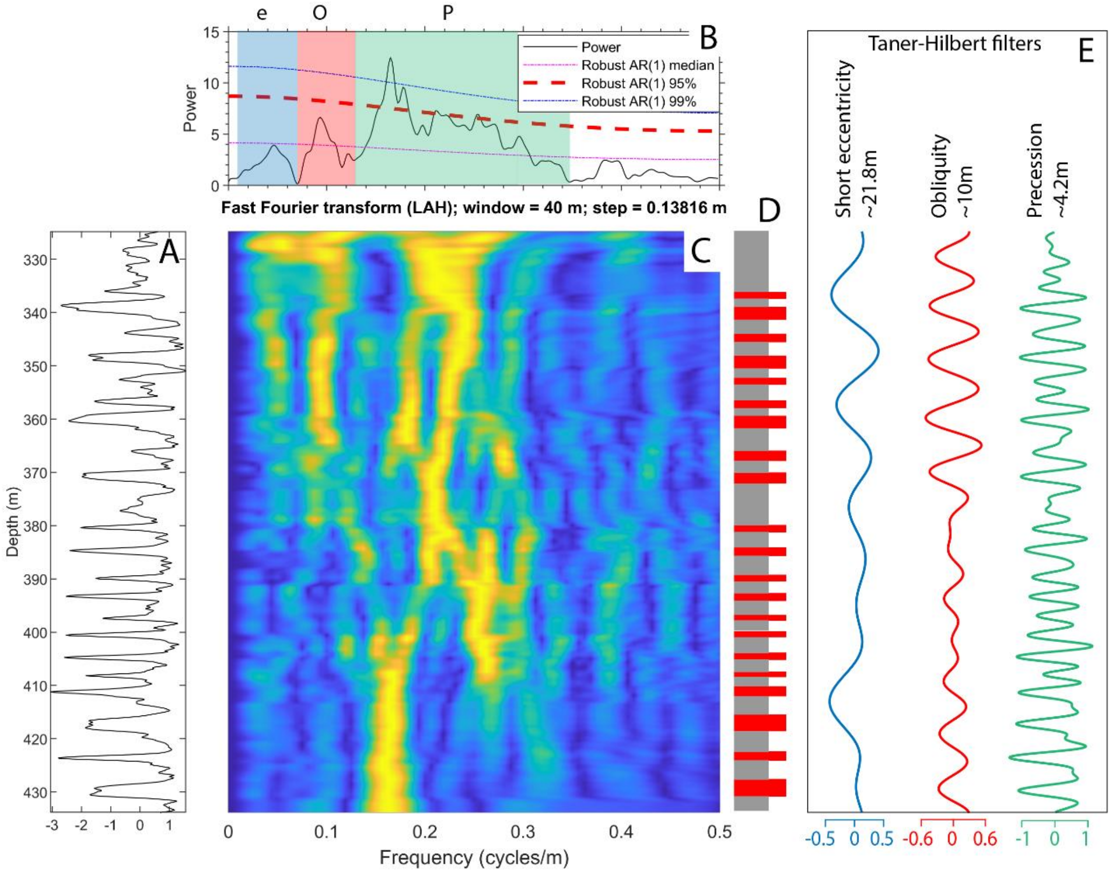

Figure 87: Spectral analysis results of the "Marnes sans Sel" unit of the DP-211 well ("Zone Salifère Supérieure"). (A) Linearly detrended gamma-ray series. (B) 2π-multitaper spectrum with linearly fitted red-noise modelling. (C) Evolutive Fast Fourier transform (LAH) with a sliding window of 40m and a step of 0.13816m. (D) Sedimentary log corresponding to the proxy signal with anhydrite in red and mudstone in grey. (E) Taner-Hilbert filters of the interpreted short eccentricity (0.0183 – 0.0733 cycles/m), obliquity (0.0733 – 0.1282 cycles/m), and precession (0.1282 – 0.3481 cycles/m) cycles.

Minimum durations

According to the previous results, and by comparing the sedimentary log with the Taner filters of the sedimentary alternations attributed to orbital cycles (**Figure 88**), minimum durations can be estimated for the investigated intervals of the DP-211 well.

The minimum duration of the "Sel IV" unit is estimated at 445.8 kyr, with 8 obliquity cycles and 6 precession cycles. However, 2 sedimentary alternations are missing below due to a fault, so up to 2 obliquity cycles are missing by comparison with the DP-206 well. Despite this, the duration is significantly lower than the one found in the "Sel IV" unit of the DP-206 well, as for the same number of sedimentary alternations, more are attributed to obliquity in the DP-206 well. This difference in relative cycle thicknesses at the bottom of the DP-211 well could be attributed to erosional surfaces and/or diminished SAR, inducing the wrongful attribution to some cycles to precession instead of obliquity.

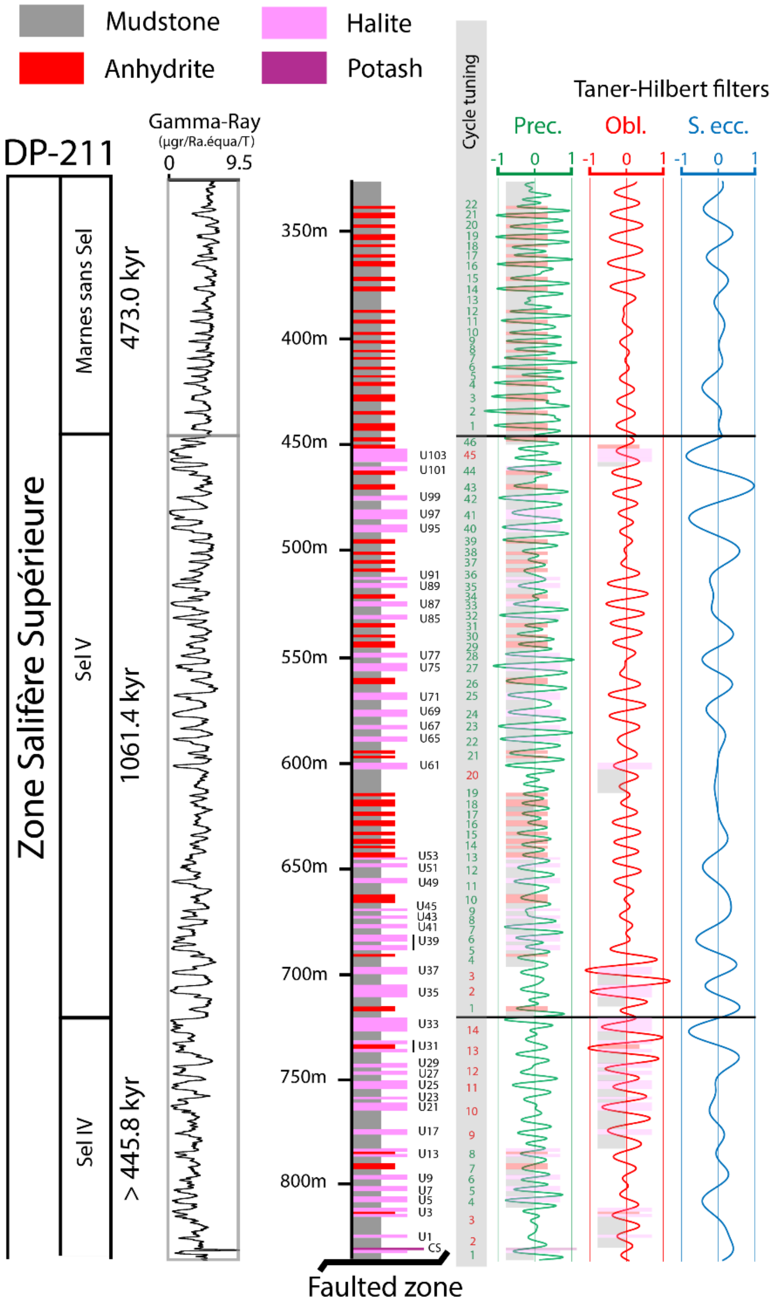

Figure 88: Synthesis of the cyclostratigraphy results from the DP-211 well. The Gamma-Ray series is plotted alongside the sedimentary log and Taner filters of the sedimentary cycles attributed to the orbital cycles. Duration are proposed for each sedimentary alternation based on their correlation with Taner filters. Numbers in the "Cycle tuning" column correspond to each sedimentary cycle and attributed to orbital cycles, with precession in green and obliquity in red.

VI.1.b.iii : DP-212

Sel V

The gamma-ray series of the "Sel V" unit of the DP-212 well was interpolated, linearly detrended, and standardized (**Figure 89**A). The 2π-MTM results of the detrended gamma-ray signal (thickness: 247 m) reveals statistically significant frequency broadbands related to sedimentary cycles with average thicknesses of 82.3m, 22.4m, 4.5m (> 99% CL) and 9m (> median CL) (**Figure 89**B). The ratios between these cycles in the depth domain (18.3 : 5 : 2 : 1) are particularly close to those of the orbital cycles (long eccentricity, short eccentricity, obliquity, precession) in the time domain (18.6 : 4.5 : 1.8 : 1). The ~82.3m cycle is therefore interpreted as corresponding to the long eccentricity, the 22.4m cycle to short eccentricity, the ~9m cycle to obliquity, and the ~4.5m cycle to precession. Three main frequency peaks can be observed in the precession frequency broadband, which can be attributed to the three main periods of precession.

The EFFT shows that the spectrum of the whole interval is dominated by short eccentricity and precession (**Figure 89**C). Furthermore, the sedimentary alternations are in phase with the precession filter, suggesting that they are driven by it (**Figure 89**D, E).

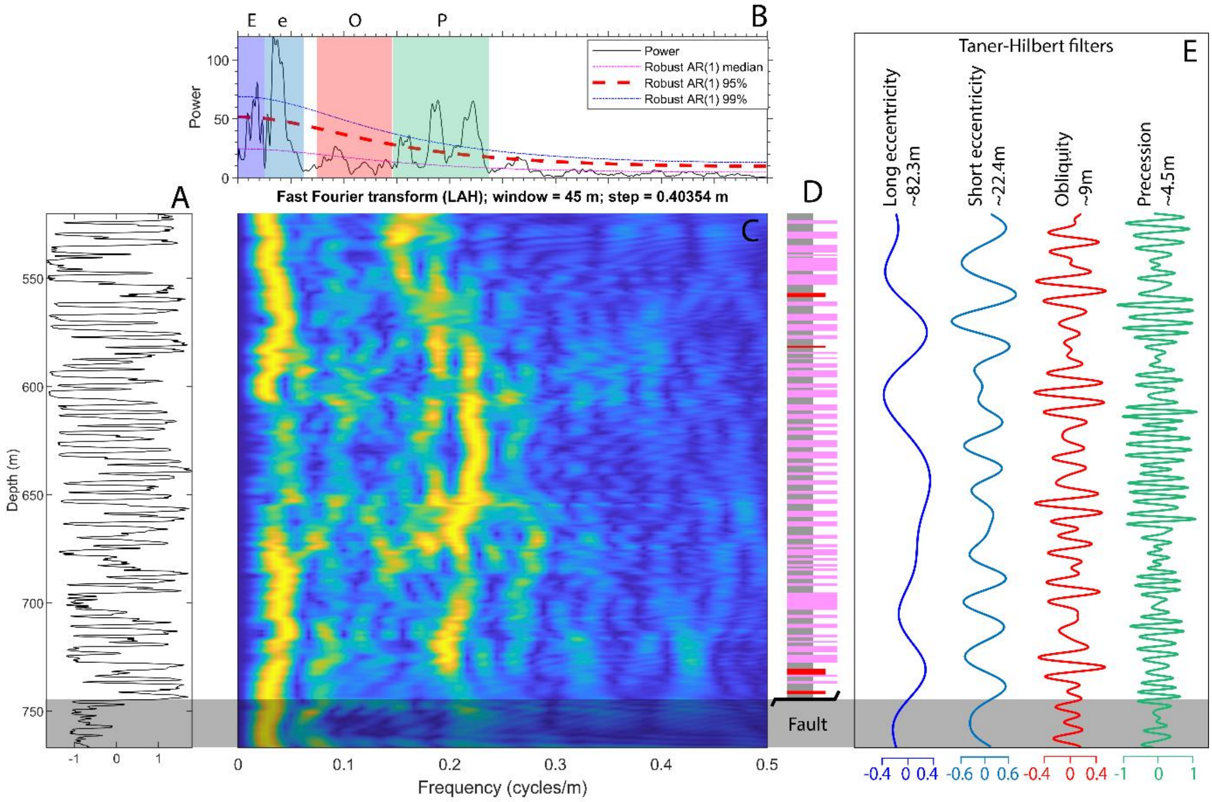

Figure 89: Spectral analysis results of the "Sel V" unit of the DP-212 well ("Zone Salifère Supérieure"). (A) Linearly detrended gamma-ray series. (B) 2π-multitaper spectrum with linearly fitted red-noise modelling. (C) Evolutive Fast Fourier transform (LAH) with a sliding window of 45m and a step of 0.40354m. (D) Sedimentary log corresponding to the proxy signal with halite in pink, anhydrite in red, and mudstone in grey. (E) Taner-Hilbert filters of the interpreted long eccentricity (0.0000 – 0.0243 cycles/m), short eccentricity (0.0243 – 0.0648 cycles/m), obliquity (0.0770 – 0.1459 cycles/m), and precession (0.1459 – 0.2998 cycles/m) cycles.

Marnes sans Sel

The gamma-ray series of the "Marnes sans Sel" unit (thickness: 79 m) of the DP-212 well was linearly detrended and standardized (**Figure 90**A). The 2π-MTM results of the gamma-ray signal reveals one significant broadband related to sedimentary cycles with an average thickness of 3.7m (> 99% CL) (**Figure 90**B). Another less significant broadband related to sedimentary cycles with an average thickness of 10.5m (> median CL) is present. The ratios between these cycles in the depth domain (2.8 : 1) are close to those of the orbital cycles of short eccentricity and obliquity in the time domain (2.5 : 1). However, by comparison with the cyclostratigraphic investigations of the "Marnes sans Sel" unit in the DP-206 and DP-211 well, across which the mudstone-anhydrite alternations can be easily correlated, the 3.7m cycle is attributed to precession rather than obliquity.

The ratio mismatch is likely due to SAR variations that can be observed through the EFFT plot. The EFFT shows that the spectrum of the whole interval is dominated by precession

(**Figure 90**C). Furthermore, the sedimentary alternations are in phase with the precession filter, suggesting that they are driven by it (**Figure 90**D, E).

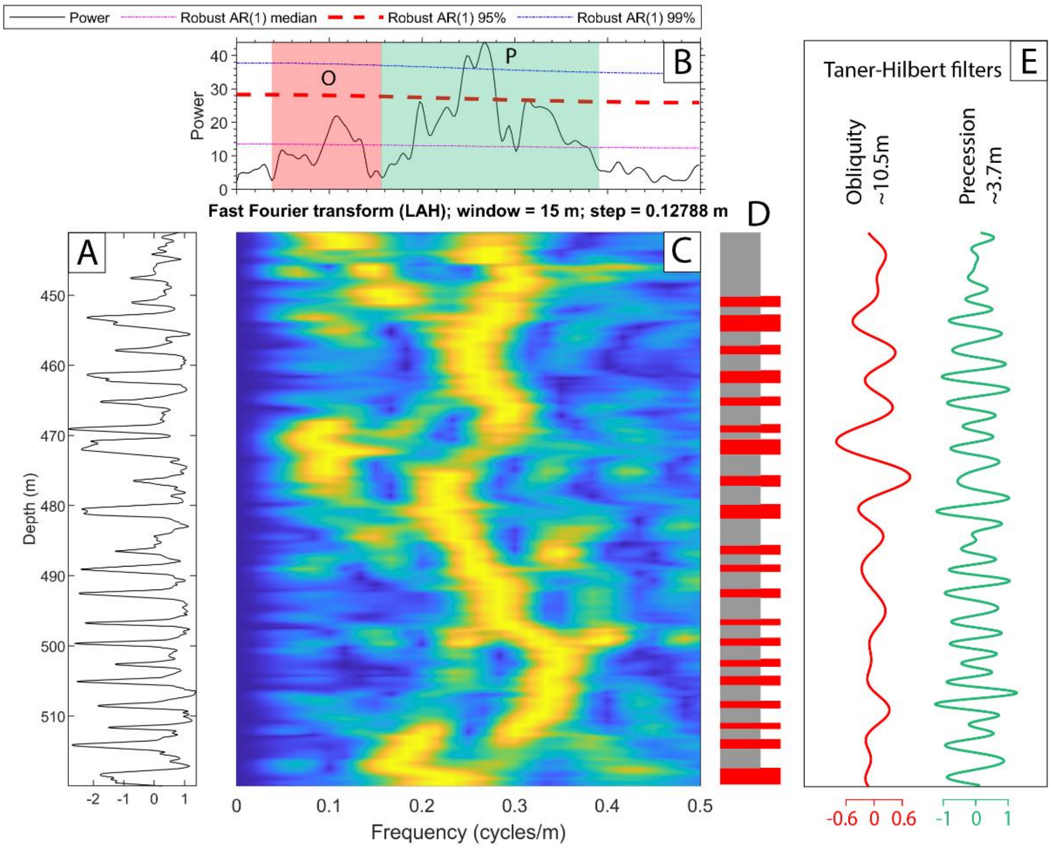

***Figure 90**: Spectral analysis results of the "Marnes sans Sel" unit of the DP-212 well ("Zone Salifère Supérieure"). (A) Linearly detrended gamma-ray series. (B) 2π-multitaper spectrum with linearly fitted red-noise modelling. (C) Evolutive Fast Fourier transform (LAH) with a sliding window of 15m and a step of 0.12788m. (D) Sedimentary log corresponding to the proxy signal with anhydrite in red and mudstone in grey. (E) Taner-Hilbert filters of the interpreted obliquity (0.0380 – 0.1520 cycles/m), and precession (0.1520 – 0.3926 cycles/m) cycles.*

Minimum duration

According to the previous results, and by comparing the sedimentary log with the Taner filters of the sedimentary alternations attributed to orbital cycles (**Figure 91**), minimum durations can be estimated for the investigated intervals of the DP-212 well.

The minimum duration of the "Sel V" unit, which is pretty much complete as the fault is found beneath the U35 halite bed, is estimated to be 1036.5 kyr, with 5 obliquity cycles and 39 precession cycles.

The minimum duration of the "Marnes sans Sel" unit is estimated to be 448.1 kyr with 1 obliquity cycle and 19 precession cycles. The duration of this unit is probably slightly more as a few meters of mudstones are present above the last mudstone-evaporite alternation.

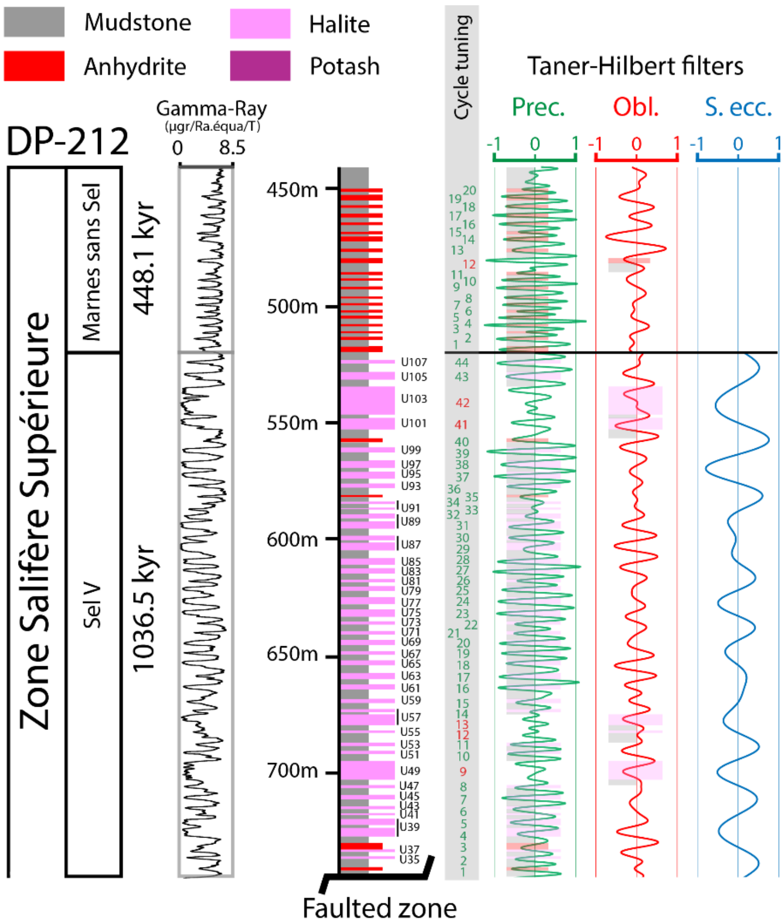

Figure 91: Synthesis of the cyclostratigraphy results from the DP-212 well. The Gamma-Ray series is plotted alongside the sedimentary log and Taner filters of the sedimentary cycles attributed to the orbital cycles. Duration are proposed for each sedimentary alternation based on their correlation with Taner filters. Numbers in the "Cycle tuning" column correspond to each sedimentary cycle and attributed to orbital cycles, with precession in green and obliquity in red.

VI.1.c : Age model and orbital tuning

By synthetizing the cycle interpretations and minimum durations given in **VI.1.b : Signal analysis, cycle interpretation, minimum durations**, along the use of independent ages, an age model and an orbital tuning can be proposer for the investigated intervals. To provide the most precise minimum durations of the investigated sedimentary intervals, the longest durations found in each well are used.

Well-logs from the "Sel III" unit are only available in the DP-206 well, so the value found there of 556.8 kyr is selected as its most conservative minimum duration (**Table 4**). Similarly to the "Sel III", the well-logs of the "Sel IV" units, while found in all three wells, are only complete in the DP-206 well which gives the longest duration. The value of 737.7 kyr is therefore selected as the most conservative minimum duration of the "Sel IV" unit. In the case of the "Sel V", the longest minimum duration has been found in the DP-211 well (1061.4 kyr) but is not too far off from the values found in the DP-212 (1036.5 kyr) and DP-206 (979.9 kyr) wells. Therefore, 1061.4 kyr is selected as the most conservative value of the "Sel V" unit's duration. Just as for the "Sel V", the longest minimum duration found for the "Marnes sans Sel" is from the DP-211 well (473.0 kyr), which is close to the values found in the DP-212 (448.1 kyr) and DP-206 (430.0 kyr) wells. Using these estimates, the minimum duration of the "Zone Salifère Supérieure" formation can be estimated as 2272.1 kyr.

***Table 4**: Minimum durations of units from the Mulhouse basin inferred from cyclostratigraphy.*

Unit	Sel III	Sel IV	Sel V	Marnes sans Sel
Minimum duration	556.8 kyr	737.7 kyr	1061.4 kyr	473.0 kyr

The independent ages suggested that the “Sel III” lasted ~490 kyr. The minimum duration found using cyclostratigraphy is 556.8 kyr, which is pretty close. As I consider that the base of the “Sel III” corresponds to the Oi-1 event (33.65 Ma), the base of the “Zone Fossilifère”, according to the cyclostratigraphic duration would be 33.09 Ma. This is coherent with the biostratigraphic constraints which account for the attribution to a part of the “Zone Fossilifère” to the NP21 biozone. Furthermore, it is very close to the initial assumption that the bottom of the ”Zone Fossilifère” corresponded to the end of the EOGM (33.16 Ma).

The attribution of the bottom of the “Série Grise” to the mid P20 biozone (Pirkenseer et al., 2010) (29.80 Ma), along the minimum duration of 2272.1 kyr of the “Zone Salifère Supérieure”, suggests that the top of the “Zone Fossilifère” is dated at 32.07 Ma, which is in accordance with its attribution to the NP22 biozone. The duration of the “Zone Fossilifère” is therefore estimated to be 1.02 Myr based on these ages (**Figure 92**).

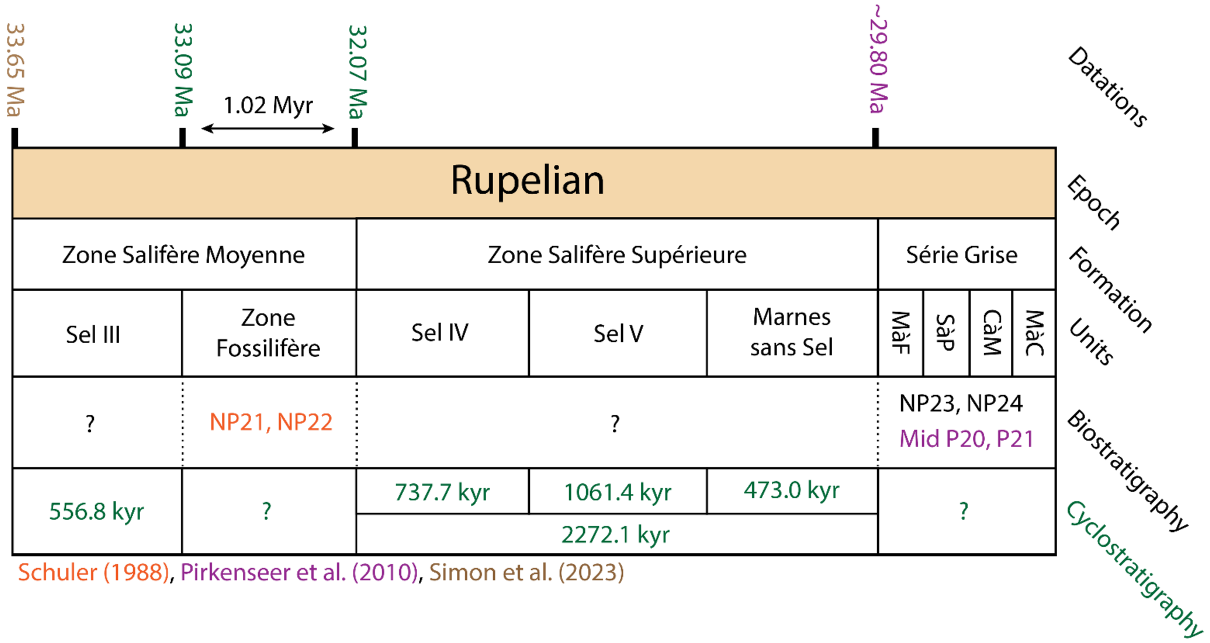

***Figure 92**: Synthesis of the independent ages, biostratigraphic attributions, and cyclostratigraphic duration of the investigated sedimentary intervals of the Mulhouse basin.*

While the two independent ages used to anchor the previous age model are very useful, they are not absolute and can therefore contain uncertainties. To reach more precise age models, cyclostratigraphy investigators usually perform orbital tuning, which consists in correlating the filtered signals of their sedimentary records to the orbital cycles of astronomical forcing models such as those of Laskar et al. (2011). This is usually done using the long eccentricity filter, as long eccentricity has been proven to be the best resolved and most stable orbital cycle through geological time. However, in the case of the Mulhouse basin, long eccentricity cycles, due to the shortness of the investigated intervals, are not well expressed in the signal. Therefore, the orbital tuning of the Mulhouse basin has been attempted by visually correlating the short eccentricity filters to the eccentricity solution of Laskar et al. (2011) (**Figure 93**). Trends in the short eccentricity filters can be visually correlated across all three wells. Furthermore, these correlations are consistent with the well-log correlations as they almost always correspond to specific beds with the same names. These observations further demonstrate the impact of astronomical forcing in the deposition of the mudstone-evaporite alternations of the Mulhouse basin. A trend that is observed across the well is the presence of two very low amplitude short eccentricity local maximums, highlighted in green on **Figure 93**. Two very similar low amplitude local maximum can be observed on the eccentricity solutions of Laskar et al. (2011) at 30.39 Ma and 30.77 Ma and were therefore correlated with them (**Figure 93**). The rest of the short eccentricity cycles were then progressively correlated.

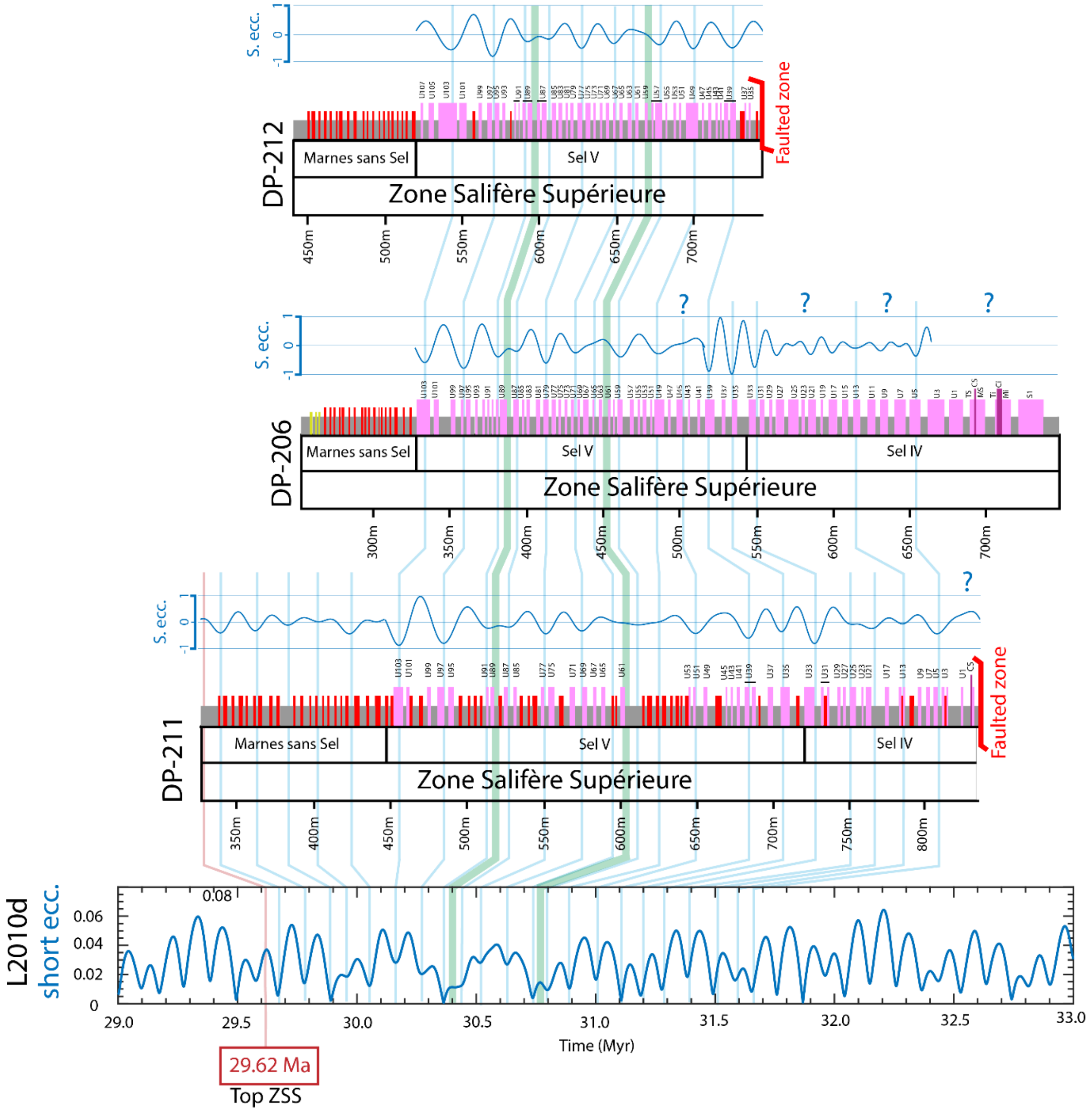

***Figure 93**: Orbital tuning proposition for the "Zone Salifère Supérieure" of the Mulhouse basin using the short eccentricity Taner filters of the DP-206, DP-211, and DP-212 wells. These filters have been visually correlated to the eccentricity solution of Laskar et al. (2011). According to this orbital tuning, the top of the "Zone Salifère Supérieure" is dated at 29.62 Ma.*

According to the orbital tuning of the "Zone Salifère Supérieure", the top of the formation would be dated at 29.62 Ma, which is consistent with its attribution to the mid P20 biozone. Due to the lack of data in the lowermost part of the formation, orbital tuning was not possible there. However, using the minimum durations proposed earlier (2272.1 kyr), and the newly found age of the top of the "Zone Salifère Supérieure" (29.62 Ma), the top of the "Zone

Fossilifère" would be dated at 31.89 Ma, and its duration would therefore be ~ 1.20 Myr. This is still coherent with the biostratigraphy data.

VI.1.d : Astronomical forcing model

The signal analysis and cycle interpretation of the "Sel III" and "Zone Salifère Supérieure" of the DP-206, DP-211, and DP-212 wells suggest that the mudstone-evaporite alternations were primarily induced either by obliquity or precession. The deposition of the metric to decametric mudstone-evaporite alternations of the "Sel III" and "Zone Salifère Supérieure" is interpreted as being the result of alternating periods lake-level and sedimentary input variations, related to relatively dry and humid periods (**Figure 94**). During relatively dry periods, evaporation induced shallowing of the lake-level and saturation of brines, fostering the precipitation of evaporites. During relatively humid periods, precipitations induced relative lake-level rise, major-ion recharge of the brine, and the deposition of mudstones. These humidity changes, as shown by the signal analysis results, were most likely induced by orbital variations. Furthermore, the presence of both obliquity and precession cycles in the sedimentary record is consistent with the fact that both these cycles are expected to have a significant effect on the repartition of insolation at mid-latitudes (**see II.4.c : The impacts of the astronomical forcing of insolation on climate and sedimentation**). The cyclostratigraphy results suggest that the "Sel III", "Sel V", and "Marnes sans Sel" units are dominated by precession, while the "Sel IV" unit is dominated by obliquity. These changes could potentially be related to the evolution of ice-sheets through the early Rupelian, but further investigations are required to demonstrate this.

While attributing such sedimentary alternations to orbital cycles can be quite clear, what is more complicated is to explain how and through which processes the insolation variations affect climate and sedimentation. Such processes can include (but are not limited to) atmospheric and oceanic circulations, carbon sinks, and albedo (Budyko, 1969; Sellers, 1969). As such, it is not obvious if humidity maximums are correlated to insolation maximums or minimums. However, based on the orbital tuning of the "Zone Salifère Supérieure", it seems that short eccentricity minimums are correlated with parts of the sedimentary record particularly rich in thick evaporite beds. As eccentricity modulates precession, it would imply that precession minimums would be attributed to evaporite beds, and that they were deposited during insolation minimums. Assuming that higher insolation means higher temperatures, his implies that orbital cycles forced the alternations of cold arid periods (evaporites) and hot humid periods (mudstone). Further investigations are required to better prove these propositions. Schuler (1988) attempted to perform high-resolution palynological analyses in both mudstone and evaporite beds, but evaporite beds held very few to no palynomorphs.

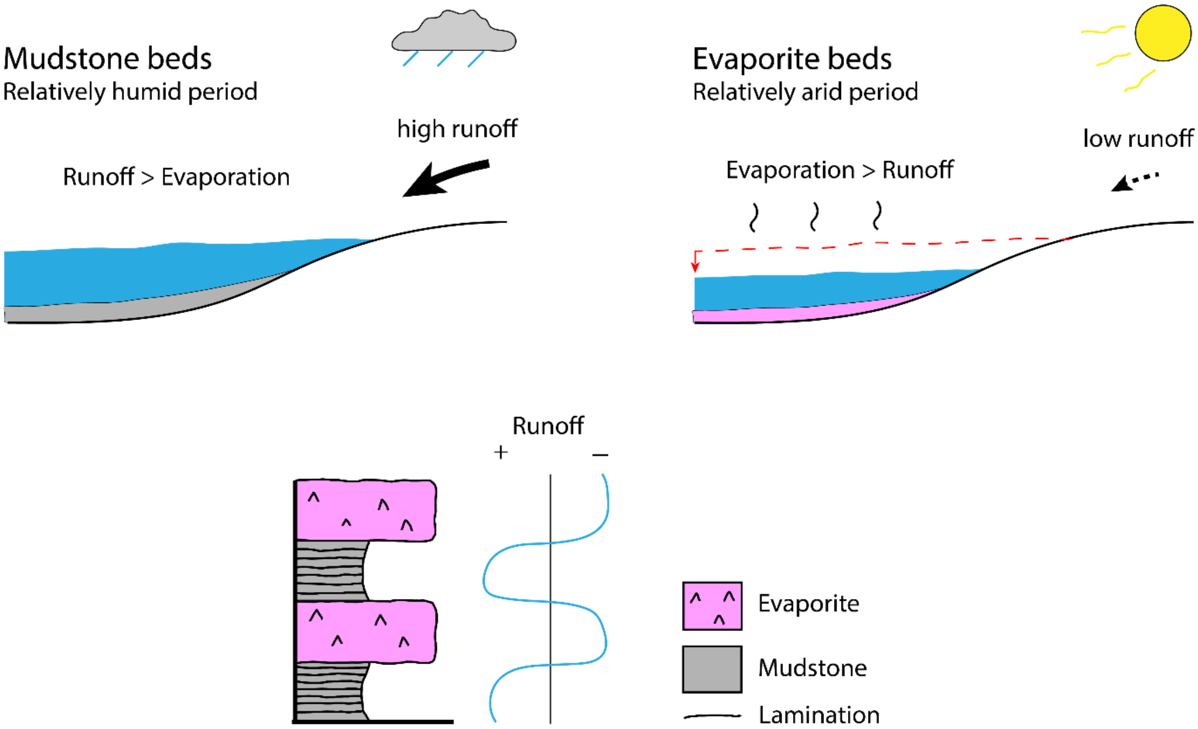

***Figure 94**: Depositional model of the mudstone-evaporite alternations of the Mulhouse basin in the “Sel III” and “Zone Salifère Supérieure”.*

VI.1.e : Summary

- Cyclostratigraphy shows that the mudstone-evaporite alternations of the “Sel III” and “Zone Salifère Supérieure” (= “Sel IV”, “Sel V”, and “Marnes sans Sel”) were induced by orbital cycles.

- The minimum duration of the “Sel III” unit is estimated to be 556.8 kyr, and the minimum duration of the “Zone Salifère Supérieure” formation to be 2272.1 kyr.

- The duration of the “Zone Fossilifère” has been estimated to be 1.02 Myr after anchoring the age models of the “Sel III” and “Zone Salifère Supérieure” to independent ages (the bottom of the “Sel III” corresponds to the Oi-1 event (33.65 Ma), and the top of the “Zone Salifère Supérieure” to the mid P20 biozone (~29.80 Ma)).

- The orbital tuning of the investigated record using the short eccentricity filters suggest that the top of the “Zone Salifère Supérieure” is dated at 29.62 Ma, which is consistent with its attribution to the mid P20 biozone. Using this age, the duration of the “Zone Fossilifère” would be 180.0 kyr longer, with its top dated at 31.9 Ma.

- Evaporitic beds were possibly deposited during cold arid periods and mudstone beds during hot humid periods, dictated by astronomically forced insolation changes. Further investigations are required to better demonstrate (or refute) this hypothesis and what the underlying climatic mechanisms are.

VI.2 : Spectral analysis of the Upper Potash seam

The potash seams of the Mulhouse basin display halite, sylvite, and marl alternations that appear to be cyclic. The upper potash section exposed at the Kalivie museum (Wittelsheim) from the Marie-Louise well has been carefully logged (**Figure 60**). Its alternations are interpreted as the result of seasonal processes similar to those observed in the Dead Sea (Dor et al., 2019). As such, they are considered as varves, and the time-series of their thicknesses and percentage of halite and sylvite have been created and was used to investigate potential cyclicity. The histogram of the number of varves for given thickness intervals shows that most of the varves are between 1 and 6 cm thick (**Figure 95**), which is very similar to those found in the Dead Sea (Dor et al., 2019).

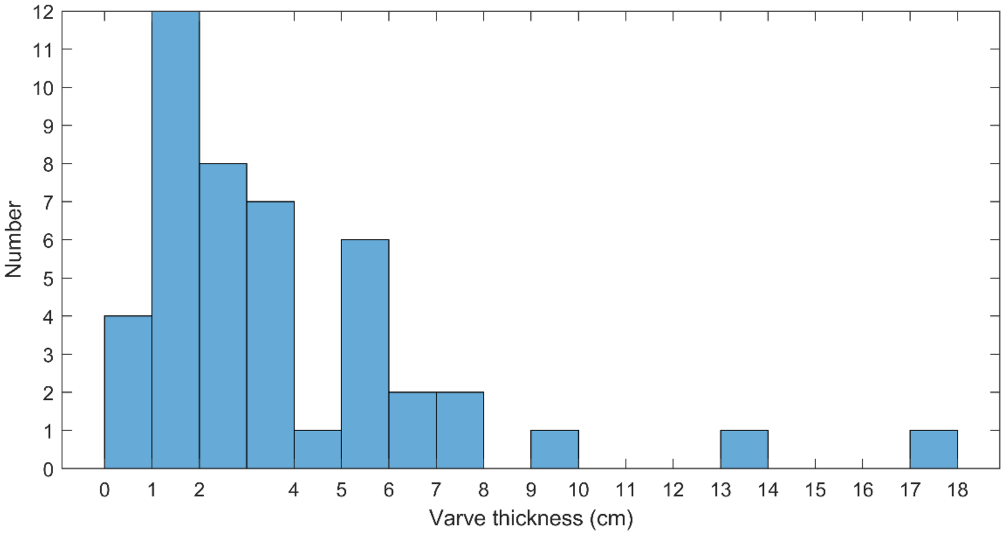

***Figure 95**: Histogram of the number of varves for the investigated section of the Upper Potash seam (157 cm). Most of them are between 1 and 6 cm thick.*

The time-series of varve thicknesses was created by measuring the average thickness of each varve from the Marie-Louise section (**Figure 96**). The time series of halite and sylvite percentages were created by calculating how much of the thickness each lithology made in every varve (**Figure 96**). The first 37 varves are comprised between ~1 and ~6 cm of thickness, while some of the last few ones become significantly thicker. From bottom to top, the proportion of sylvite increases while the proportion of halite decreases.

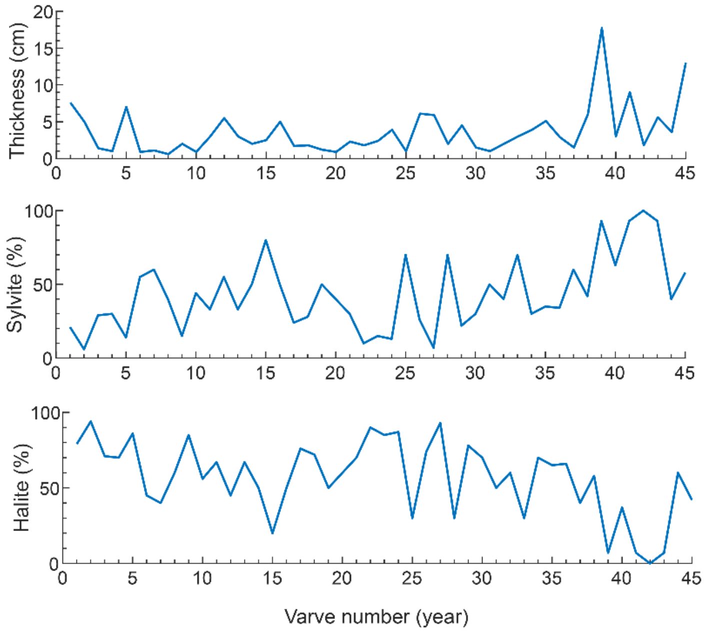

***Figure 96**: Time-series of the varves from the upper potash seam of the Marie-Louise well, with (top) thicknesses, (middle) sylvite percentages, and (bottom) halite percentages.*

The previously presented time-series were detrended using the LOESS method (35%). The 2π-MTM results of the time-series of varve thicknesses shows a statistically significant frequency peak (>99% CL) corresponding to a cycle of 5.6 years (**Figure 97**A). The 2π-MTM results of the time-series of the halite and sylvite percentages shows statistically significant frequency peaks corresponding to cycles of 4.3 years (>99% CL) and 3.0 years (>90% CL) (**Figure 97**B).

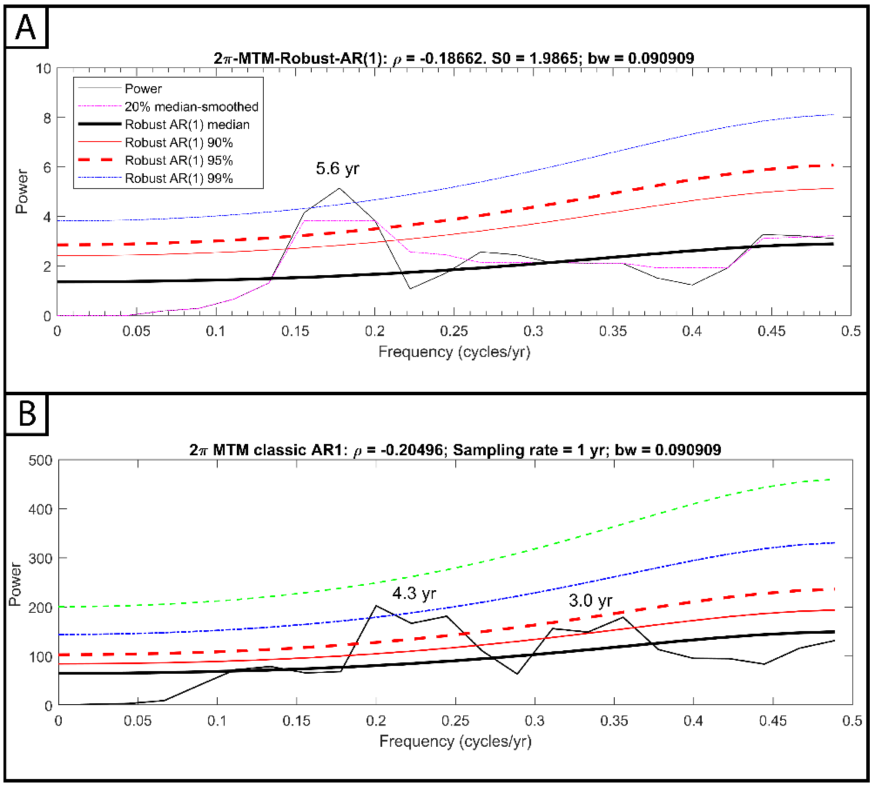

***Figure 97**: 2π-MTM results of the time-series of (A) varve thicknesses and (B) halite and sylvite percentages. As the percentages of halite and sylvite are proportional, their spectral analysis results are the same.*

The 5.6-, 4.3-, and 3.0-years cycles inferred from the spectral analysis of the potash alternations are particularly close to the modern periods of the North Atlantic Oscillation. In the Dead Sea, the investigation of evaporitic varves revealed similar periodicities (~11, 7-8, 4-5 yr) pointing to a North Atlantic Oscillation, and possibly Schwabe cycle control of the hydrology of the Dead Sea watershed (Palchan et al., 2017). Therefore, it seems plausible that the recently formed North Atlantic Oscillation had some control on the Upper Rhine Graben hydrology, influencing the deposition of the potash sediments. However, the investigated time-series are short, and the annual nature of the potash alternations remains to be demonstrated in more detail.

VI.3 : Pechelbronn basin

Thanks to the geothermal exploration and production in the Pechelbronn basin, and thanks to the courtesy of the operators, the Gamma-Ray series of the Cenozoic formations of the Pechelbronn basin of the GRT-1 and GPK-2 boreholes was investigated.

VI.3.a : Preliminary investigations

In contrast with the Mulhouse basin which contains clear mudstone-evaporite alternations, the sedimentary record of the Pechelbronn basin doesn't account for particularly clear sedimentary alternations. However, the "Couches de Pechelbronn Inférieures", "Couches de Pechelbronn Moyennes" (= "Zone Fossilifère"), and "Couches de Pechelbronn Supérieures" have been described as characterized by claystones and marlstones with interbedded sandstones and conglomeratic beds (Duringer et al., 2019; Aichholzer et al., 2016) (see **II.3.c.ii : Pechelbronn basin**). The presence of potentially erosional sandstone and conglomeratic beds suggest that this basin is not particularly fit for cyclostratigraphic investigation. In these boreholes, the depth of the limit between the "Couches de Pechelbronn Inférieures" and "Couches de Pechelbronn Moyennes" is unknown. According to Lavoyer (2013), the thickness of the "Couches de Pechelbron Moyennes" of the nearby GPK-4 borehole is ~90m. These changes in lithology are potentially driven by climate, as they are the contemporary to the astronomically forced alternations of the Mulhouse basin ("Sel III", "Zone Salifère Supérieure"). I therefore performed spectral analysis on the Gamma-Ray series from the GRT-1 and GPK-2 boreholes to investigate such astronomically driven changes in sedimentation. The Gamma-Ray signal is therefore used as a proxy of the proportion of sand and/or thicker grains which could be related to lake-level variations and runoff, similarly to the Mulhouse basin. There is a consequent conglomeratic bed ("Zone Détritique de Glaswinkel") at the base of the "Couches de Pechelbronn Supérieures", which potentially represents a hiatus in the section. Parts of the "Couches de Pechelbronn Moyennes" and "Couches de Pechelbronn Supérieures" are potentially missing due to this conglomeratic bed. The spectral analyses were performed below and above it to avoid its Gamma-Ray signal affecting the results. There is a potentially important unconformity at the top of the "Couches de Pechelbronn Supérieures" in both boreholes, which seems particularly big at the GPK-2 borehole due to the thickness difference of this unit across the boreholes (Duringer et al., 2019; Aichholzer et al., 2016) (**Table 5**).

***Table 5**: Thickness and continuity of the investigated sedimentary intervals of the Pechelbronn basin.*

	GRT-1		GPK-2	
Units	CDP Inf + Moy	CDP Sup	CDP Inf + Moy	CDP Sup
Thickness	193 m	173 m	184.5 m	95 m
Hiatus	Glaswinkel ?	Unconformity (top) Glaswinkel?	Glaswinkel?	Unconformity (top) Glaswinkel?

VI.3.b : Signal analysis, cycle interpretation, minimum durations

VI.3.b.i : GRT-1

Couches de Pechelbronn Inférieures / Couches de Pechelbronn Moyennes

The gamma-ray series of the “Couches de Pechelbronn Inférieures” and “Couches de Pechelbronn Moyennes” of the GRT-1 borhole was interpolated, detrended using the LOWESS method (35%; Cleveland, 1979), and standardized (**Figure 98**A). The 2π-MTM results of the detrended gamma-ray signal (thickness: 193 m) from the GRT-1 borehole reveals statistically significant frequency broadbands related to sedimentary cycles with average thicknesses of 14.1 m, ~2.9 m (> 99% CL) and 44.4 m (> median CL) (**Figure 98**B). The ratios between these cycles in the depth domain (15.3 : 4.9 : 1) are particularly close to those of the orbital cycles (long eccentricity, short eccentricity, precession) in the time domain (18.6 : 4.5 : 1). The ~44.4 m cycle is therefore interpreted as corresponding to the long eccentricity, the ~14.1 m cycle to short eccentricity, and the ~2.9 m cycle to precession. Two other significant frequencies (> 99% CL) related to sedimentary cycles of 2.0 m and 1.4 m are present and could potentially be related to half-precession cycles. Furthermore, the precession broadband contains three main peaks which could be correlated to the three main periodicities of precession.

The EFFT plot and Taner filters suggest that spectrum of the investigated interval is mostly driven by short eccentricity and precession broadbands (**Figure 98**C, D).

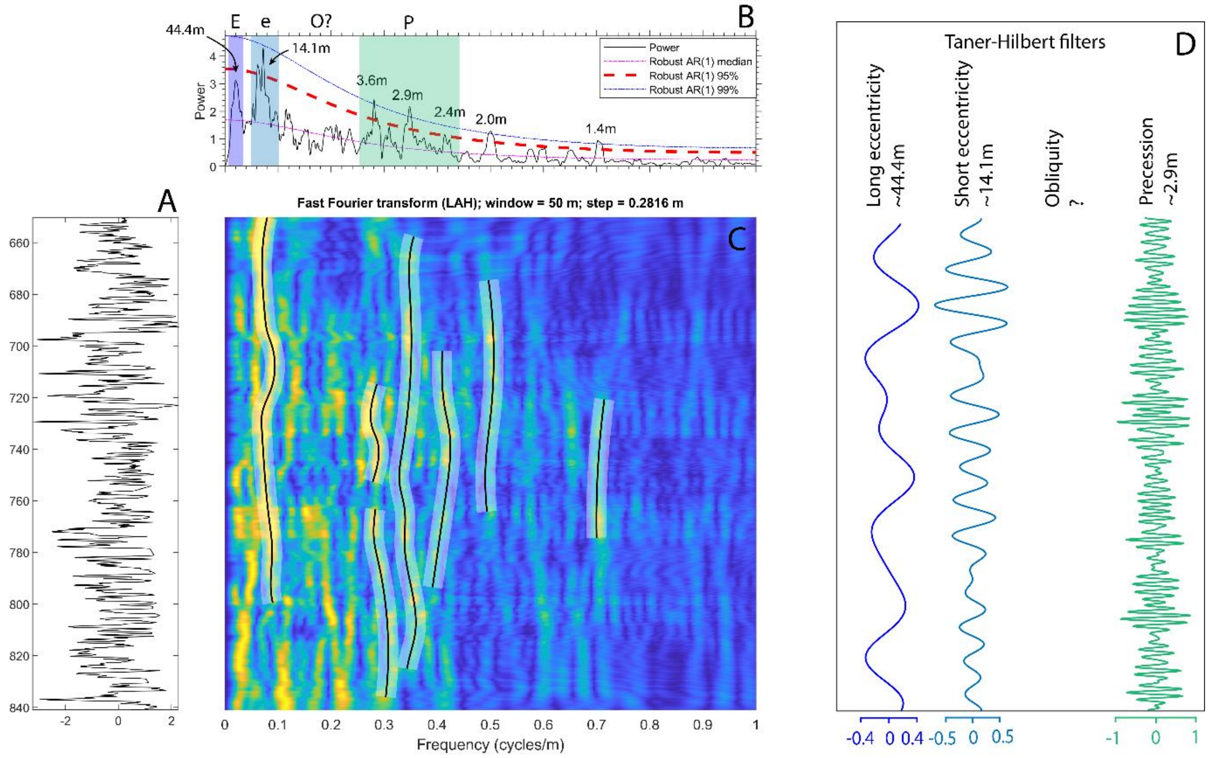

Figure 98: Spectral analysis results of the “Couches de Pechelbronn Inférieures” and “Couches de Pechelbronn Moyennes” of the GRT-1 borehole. (A) Detrended (LOWESS) gamma-ray series. (B) 2π-multitaper spectrum with linearly fitted red-noise modelling. (C) Evolutive Fast Fourier transform (LAH) with a sliding window of 50m and a step of 0.2816m. (D) Taner-Hilbert filters of the interpreted long eccentricity (0.0084 – 0.0366 cycles/m), short eccentricity (0.0492 – 0.0901 cycles/m) and precession (0.2649 – 0.4398 cycles/m) cycles.

Couches de Pechelbronn Supérieures

The gamma-ray series of the "Couches de Pechelbronn Supérieures" of the GRT-1 borehollewas interpolated, detrended using the LOWESS method (35%; Cleveland, 1979), and standardized (**Figure 99**A). The 2π-MTM results of the detrended gamma-ray signal (thickness: 173 m) reveals statistically significant frequency broadbands related to sedimentary cycles with average thicknesses of ~2.6 m (> 99% CL), 57.7 m, 15.6m (> 95% CL), and 4.4 m (> median CL) (**Figure 99**B). The ratios between these cycles in the depth domain (22.2 : 6 : 1.7 : 1) are close to those of the orbital cycles (long eccentricity, short eccentricity, obliquity, precession) in the time domain (18.6 : 4.5 : 1.8 : 1). The ~57.7 m cycle is therefore interpreted as corresponding to the long eccentricity, the ~15.6 m cycle to short eccentricity, the ~4.4 m cycle to obliquity, and the ~2.6 m cycle to precession. Two other significant frequencies (> 99% CL) related to sedimentary cycles of 1.3 m and 1.2 m are present and could potentially be related to half-precession cycles. Furthermore, the precession broadband contains three main peaks which could be correlated to the three main periodicities of precession. The results of this section are particularly similar to those of the "Couches de Pechelbronn Inférieures" and "Couches de Pechelbronn Moyennes".

The EFFT and the Taner filters suggest that the spectrum of the investigated interval is mostly driven by the short eccentricity and precession broadbands, but that the obliquity broadband becomes significant in the top 100 meters (**Figure 99**C, D).

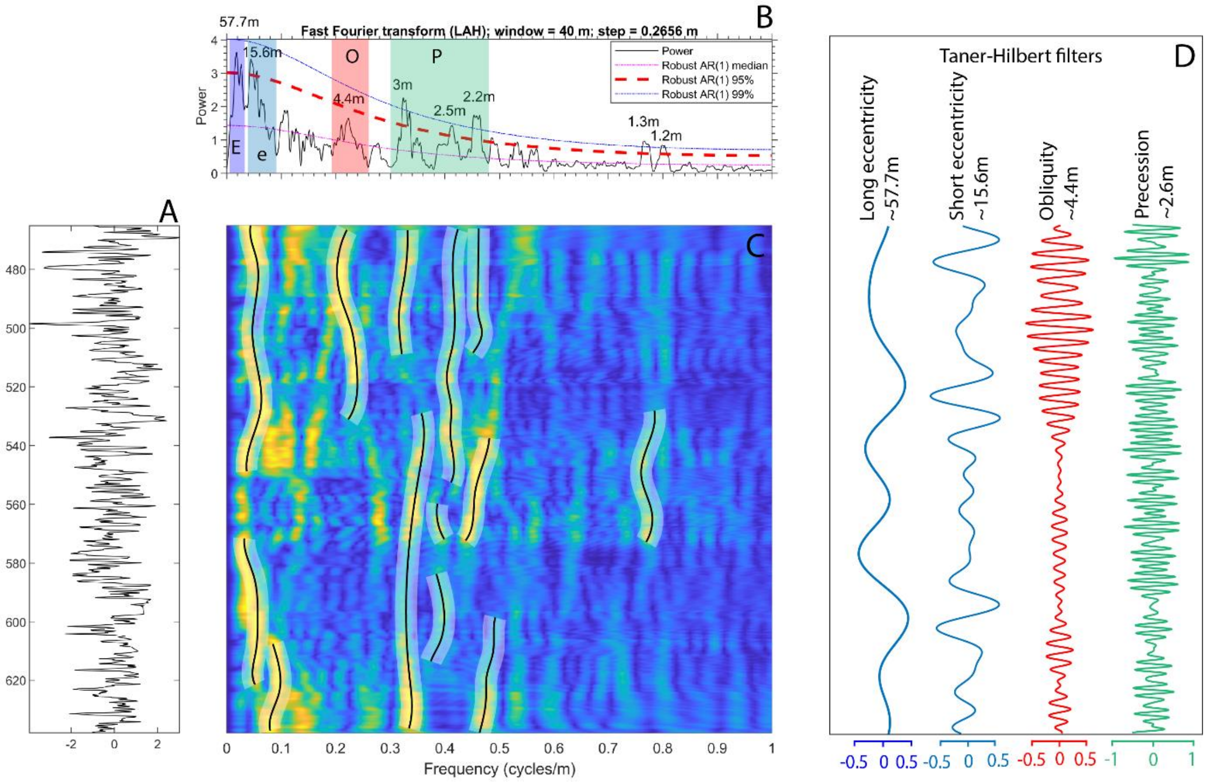

Figure 99: Spectral analysis results of the "Couches de Pechelbronn Supérieures" of the GRT-1 borehole. (A) Detrended (LOWESS) gamma-ray series. (B) 2π-multitaper spectrum with linearly fitted red-noise modelling. (C) Evolutive Fast Fourier transform (LAH) with a sliding window of 40m and a step of 0.2656m. (D) Taner-Hilbert filters of the interpreted long eccentricity (0.0035 – 0.0324 cycles/m), short eccentricity (0.0381 – 0.0902 cycles/m), obliquity (0.1931 – 0.2601 cycles/m) and precession (0.3110 – 0.4798 cycles/m) cycles.

Minimum durations

As there are not clear sedimentary logs on which to correlate Taner filters of the sedimentary cycles, minimum durations are here estimated by counting the number of precession cycles on the Taner filter itself.

As such, the minimum duration of both the “Couches de Pechelbronn Inférieures” and “Couches de Pechelbronn Moyennes” (= “Zone Fossilifère”) in the GRT-1 borehole is estimated to be 1440.5 kyr (67 precession cycles).

The minimum duration of the “Couches de Pechelbronn Supérieures” in the GRT-1 borehole is estimated to be 1483.5 kyr (69 precession cycles).

VI.3.b.ii : GPK-2

Couches de Pechelbronn Inférieures / Couches de Pechelbronn Moyennes

The gamma-ray series of the “Couches de Pechelbronn Inférieures” and “Couches de Pechelbronn Moyennes” of the GPK-2 borehole units was interpolated, detrended using the LOWESS method (35%), and standardized (**Figure 100**A). The 2π-MTM results of the detrended gamma-ray signal (thickness: 184.5 m) reveals statistically significant frequency broadbands related to sedimentary cycles with average thicknesses of 46 m (> 99% CL), 17.5 m (> median CL), 4.9 m, 3.1 m (> 95% CL) (**Figure 100**B). The ratios between these cycles in the depth domain (14.8 : 5.6 : 1.6 : 1) could potentially be related to those of the orbital cycles (long eccentricity, short eccentricity, obliquity, precession) in the time domain (18.6 : 4.5 : 1.8 : 1). The 46 m cycle could be related to the long eccentricity, the 17.5 m cycle to the short eccentricity, the 4.9 m cycle to obliquity, and the 3.1 m cycle to precession. However, the ratios between these cycles compared to the orbital cycles are not as clear as those from the GRT-1 borehole and Mulhouse basin. This could be due to the location of the GPK-2 borehole, which compared to the GRT-1 borehole is further away from the depocenter, and therefore more susceptible to potential erosional processes.

The EFFT and the Taner filters suggest that the spectrum of the investigated interval is influenced all the orbital cycles (**Figure 100**C, D).

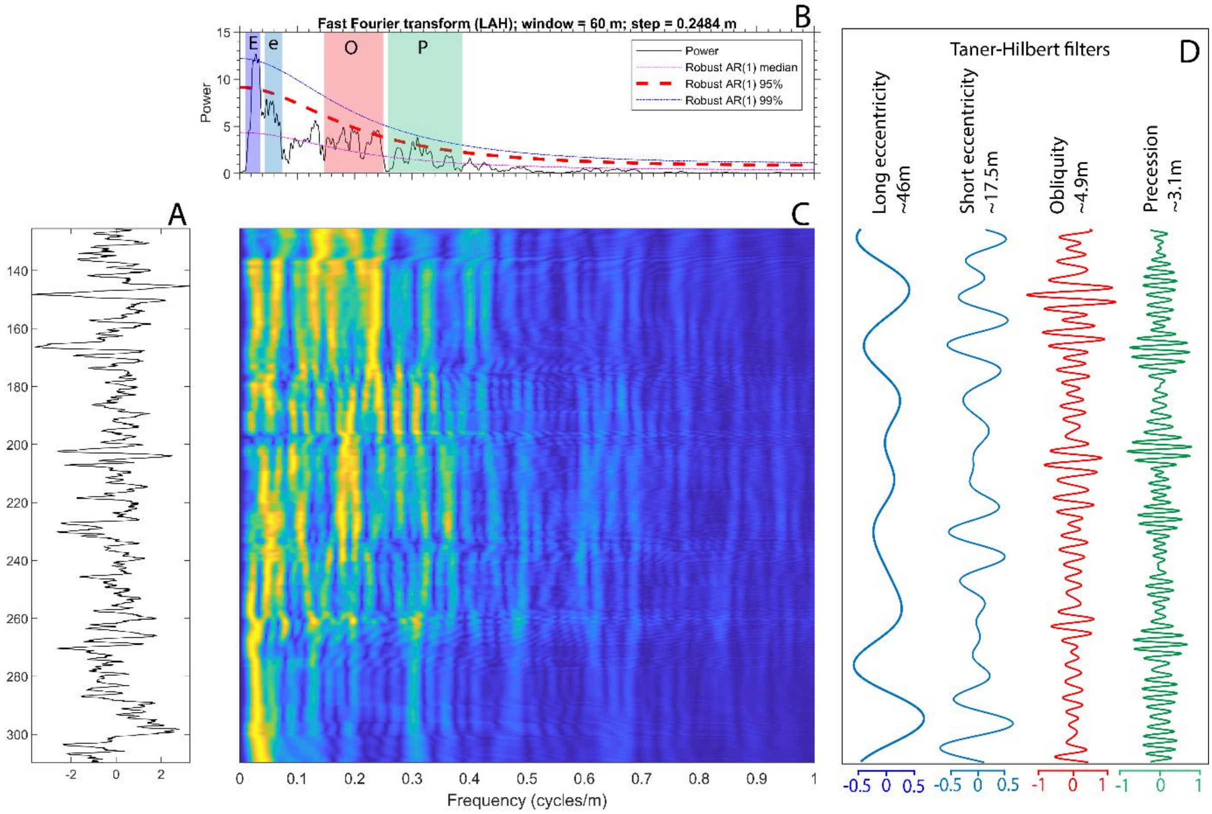

***Figure 100**: Spectral analysis results of the “Couches de Pechelbronn Inférieures” and “Couches de Pechelbronn Moyennes” of the GPK-2 borehole. (A) Detrended (LOWESS) gamma-ray series. (B) 2π-multitaper spectrum with*

linearly fitted red-noise modelling. (C) Evolutive Fast Fourier transform (LAH) with a sliding window of 60m and a step of 0.2484m. (D) Taner-Hilbert filters of the interpreted long eccentricity (0.0054 – 0.0380 cycles/m), short eccentricity (0.0380 – 0.0760 cycles/m), obliquity (0.1465 – 0.2604 cycles/m) and precession (0.2604 – 0.3852 cycles/m) cycles.

Couches de Pechelbronn Supérieures

The gamma-ray series of the “Couches de Pechelbronn Supérieures” unit of the GPK-2 borehole was interpolated, detrended using the LOWESS method (35%), and standardized (**Figure 101**A). The 2π-MTM results of the detrended gamma-ray signal (thickness: 95 m) reveal statistically significant frequency broadbands related to sedimentary cycles with average thicknesses of 46 m (> 99% CL), 17.5 m (> median CL), 4.9 m, 3.1 m (> 95% CL) (**Figure 101**B). The ratios between these cycles in the depth domain (14.8 : 5.6 : 1.6 : 1) could potentially be related to those of the orbital cycles (long eccentricity, short eccentricity, obliquity, precession) in the time domain (18.6 : 4.5 : 1.8 : 1). The 46 m cycle could be related to the long eccentricity, the 17.5 m cycle to the short eccentricity, the 4.9 m cycle to obliquity, and the 3.1 m cycle to precession. However, the ratios between these cycles compared to the orbital cycles are not as clear as those from the GRT-1 borehole and Mulhouse basin. This could be due to the location of the GPK-2 borehole, which compared to the GRT-1 borehole is further away from the depocenter, and therefore more susceptible to potential erosional processes. The precession broadband contains three main peaks which could be correlated with the three main periods of precession.

The EFFT and the Taner filters suggest that the spectrum of the investigated interval is mostly driven by the short eccentricity and obliquity broadbands (**Figure 101**C, D).

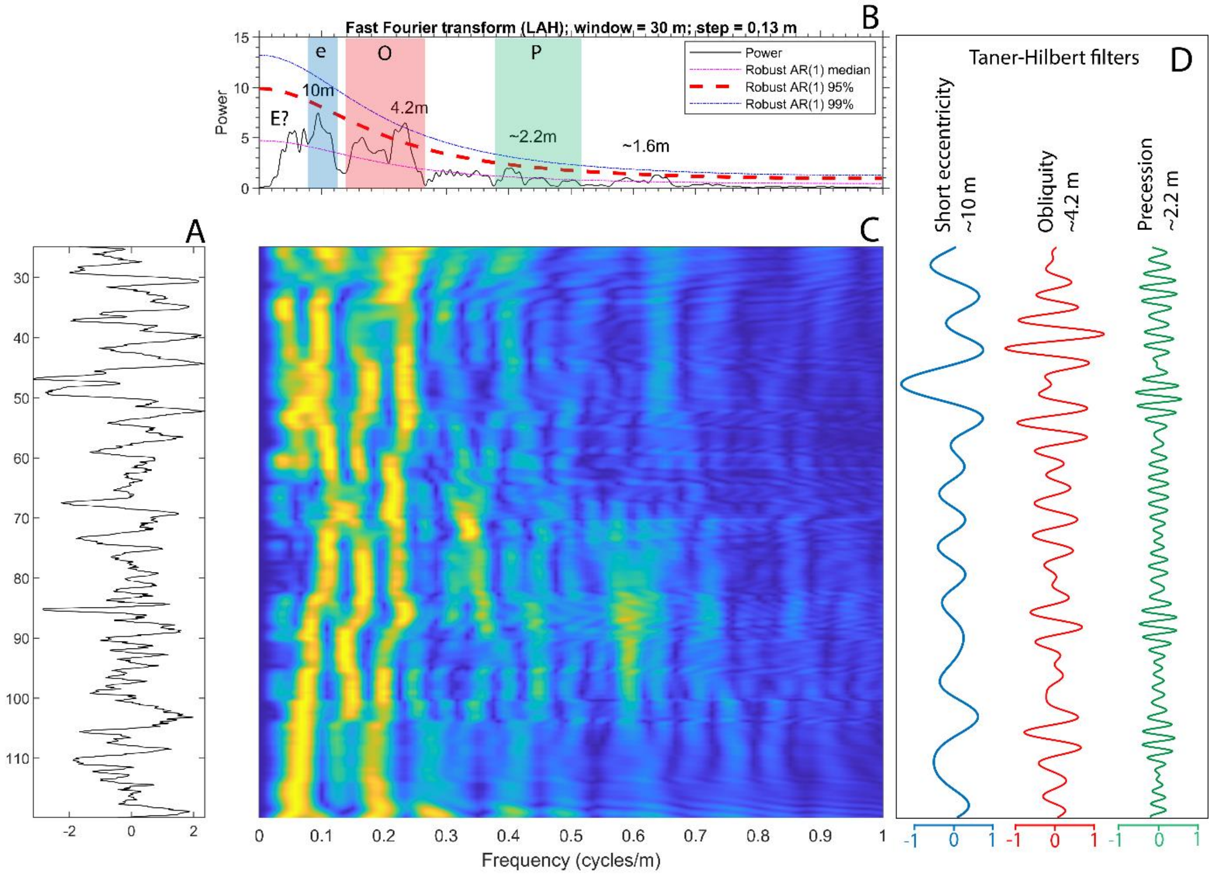

***Figure 101**: Spectral analysis results of the “Couches de Pechelbronn Supérieures” of the GPK-2 borehole. (A) Detrended (LOWESS) gamma-ray series. (B) 2π-multitaper spectrum with linearly fitted red-noise modelling. (C) Evolutive Fast Fourier transform (LAH) with a sliding window of 40m and a step of 0.2656m. (D) Taner-Hilbert filters*

of the interpreted short eccentricity (0.0210 – 0.1262 cycles/m), obliquity (0.1262 – 0.2734 cycles/m) and precession (0.3786 – 0.5363 cycles/m) cycles.

Minimum duration

As there are not clear sedimentary logs on which to correlate Taner filters of the sedimentary cycles, minimum durations are here estimated by counting the number of precession cycles on the Taner filter itself.

As such, the minimum duration of both the "Couches de Pechelbronn Inférieures" and "Couches de Pechelbronn Moyennes" (= "Zone Fossilifère") in the GPK-2 borehole is estimated to be 1311.5 kyr (61 precession cycles). This value is pretty close to the one found for the same interval in the GRT-1 borehole.

The minimum duration of the "Couches de Pechelbronn Supérieures" in the GRT-1 borehole is estimated to be 1483.5 kyr (69 precession cycles).

VI.3.c : Age model

As the "Couches de Pechelbronn Supérieures" unit is comprised between the "Zone Fossilifère" (= "Couches de Pechelbronn Moyennes") and the "Série Grise", it is supposed to be the same duration as the "Zone Salifère Supérieure" of the Mulhouse basin which is comprised between the same units. Due to the hiatuses known in the GRT-1 and GPK-2 boreholes at the top of this unit, it was expected that the minimum durations found for these boreholes would be shorter than those of the Mulhouse basin. These minimum durations are 1440.5 kyr for the "Couches de Pechelbronn Moyennes" and "Couches de Pechelbronn Inférieures", and 1483.5 kyr for the "Couches de Pechelbronn Supérieures". If the cyclostratigraphy results presented earlier are correct, the hiatuses represent at least 788.6 kyr in the "Couches de Pechelbronn Supérieures". It is however not impossible that the hiatus at the top is not that significant and that there are smaller hiatuses across the unit in the GRT-1 borehole.

According to the results found in the Mulhouse basin, the duration of the "Couches de Pechelbronn Moyennes" (= "Zone Fossilifère") is supposed to be ~1200.0 kyr. The minimum duration found for both the "Couches de Pechelbronn Inférieures" and "Couches de Pechelbronn Moyennes" in the GRT-1 borehole being 1440.5 kyr, and the fact that the thickness of the "Couches de Pechelbronn Inférieures" should be relatively close to the one of the "Couches de Pechelbronn Moyennes", suggest that there are significant hiatuses and/or that the cyclostratigraphic results in the Pechelbronn basin are incorrect.

Due to the very likely presence of hiatuses in the GRT-1 and GPK-2 boreholes, I deem their sedimentary records unfit for orbital tuning.

VI.3.d : Astronomical forcing model

Similarly to the Mulhouse basin, I propose that the alternations found in the Pechelbronn basin are driven by astronomically forced changes in runoff regimes. Changes in relative lake-level could influence, close to the rift's shoulders, the distance at which sand-sized and thicker particles are deposited. During humid period, the lake-level would rise and mostly mudstones would be deposited at the location of the GRT-1 and GPK-2 boreholes (**Figure 102**). In deeper parts of the lake, there would be only mudstones, and only sandstone and conglomerate would be deposited near the shore. During dry periods, the lake-level would drop and cause sandstones and conglomerate to reach the location of the boreholes. In deeper parts, there would be mostly mudstone, and the shore of the humid period would get partially eroded. Also, sandstone and conglomerate beds deposited during dry periods were potentially erosive and possibly sometimes erased previous alternations at the location of the boreholes. This would explain the differences in durations compared to the Mulhouse basin, while still allowing the detection of the imprint of climate through the preserved alternations.

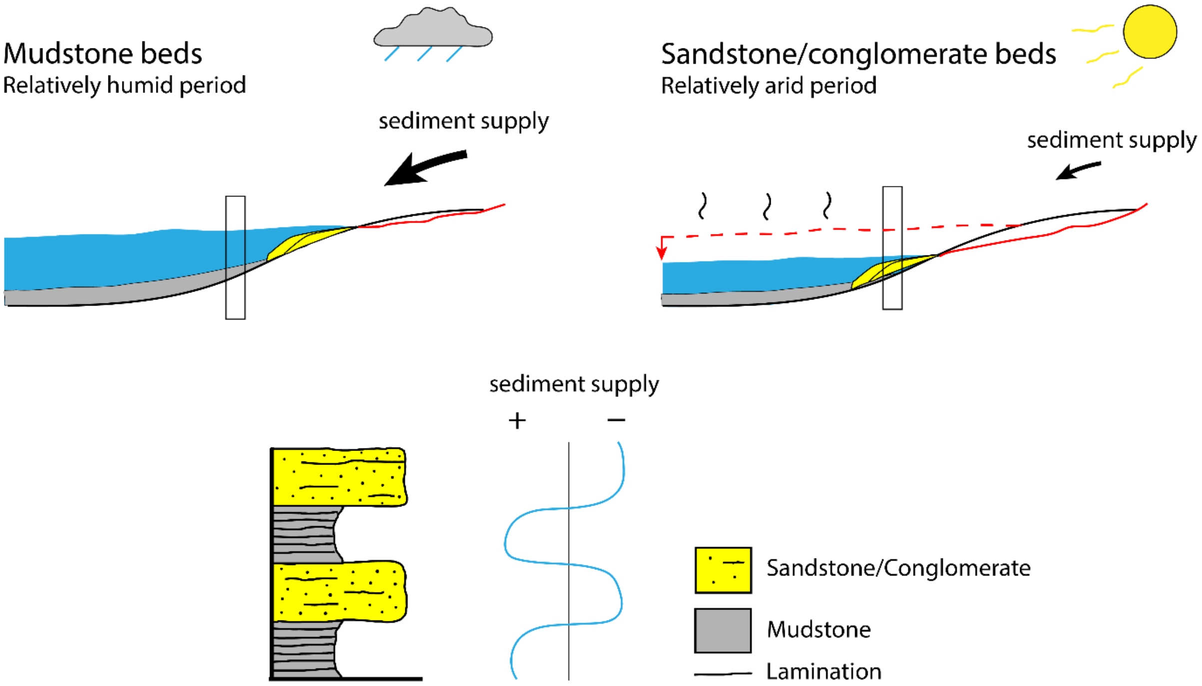

__Figure 102__: Depositional model of the mudstone-sandstone/conglomerate alternations of the Pechelbronn basin in the "Couches de Pechelbronn".

VI.3.e : Summary

- Cyclostratigraphic results account for the imprint of orbital cycles in the deposition of the mudstone-sandstone/conglomerate alternations of the Pechelbronn basin in the "Couches de Pechelbronn".

- The minimum duration of the "Couches de Pechelbronn Inférieures" and "Couches de Pechelbronn Supérieures" units is 1440.5 kyr, and the minimum duration of the "Couches de Pechelbronn Supérieures" unit is 1483.5 kyr. There are substantial differences in minimum durations compared with the Mulhouse basin, implying the presence of non-negligeable hiatuses. An unconformity is known at the top of the "Couches de Pechelbronn Supérieures" (Duringer et al., 2019; Aichholzer et al., 2016), and some sandstone and conglomerate beds could potentially be erosional. In particular, the "Zone Détritique de Glaswinkel" (thick conglomerate bed) could be the cause of a substantial hiatus between the "Couches de Pechelbronn Supérieures" and the underlying units.

- Due to the probable presence of hiatuses across the investigated intervals, orbital tuning was not applicable in the studied boreholes.

- Sandstone/conglomeratic beds were possibly deposited during arid periods and mudstone beds during humid periods, dictated by astronomically forced insolation changes. Further investigations are required to better demonstrate (or refute) this hypothesis and what the underlying climatic mechanisms are.

Chapter VII : Paleoclimatic and paleoenvironmental change in the Pechelbronn basin: insights from the GRT-1 and GPK-2 boreholes based on palynology and geochemistry

Paleoclimatic and paleoenvironmental data in the Pechelbronn basin were produced in the scope of this thesis thanks to the analysis of cuttings and well-logs from the GRT-1 and GPK-2 boreholes provided by ES Géothermie. The GRT-1 and GPK-2 boreholes are located a few kilometers apart from each other on the western side of the graben in the towns of Rittershoffen and Soultz-sous-Forêt (**Figure 44**, **Figure 103**). These boreholes were investigated through the scope of geochemistry and palynology.

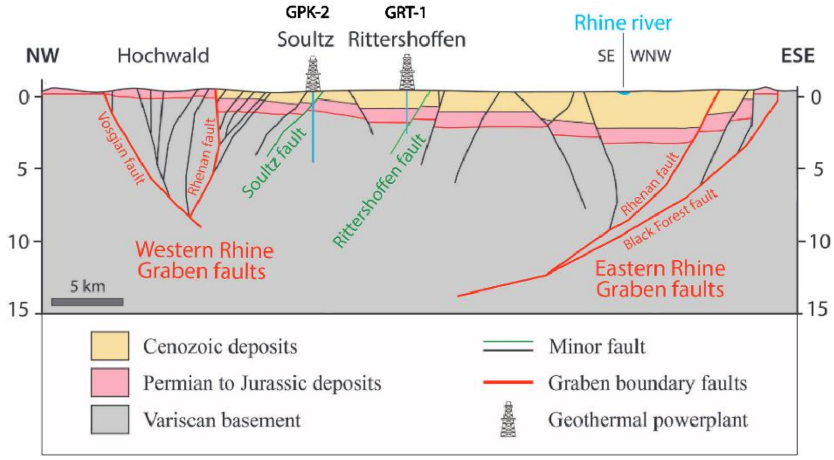

__Figure 103__: Schematic NW-ESE cross-section of the Upper Rhine Graben at the latitude of Rittershoffen. Modified after Duringer et al. (2019).

VII.1.a : Determination of palynomorphs

VII.1.a.i : Pollen grains

Several families of pollen grains have been encountered and determined in the “Couches de Pechelbronn” of the GRT-1 and GPK-2 boreholes (**Figure 104**). They consist of the Pinaceae, Cupressaceae, Ephedraceae, Ulmaceae, Bombacaceae, Nitrariaceae, Polypodiaceae, Rhoipleleaceae, Junglandaceae, Tiliaceae, and Myricaceae families. The Pinaceae and Cupressaceae families represent the large majority of the pollen spectrum in all investigated samples. The Cupressaceae family is mainly represented by Juniperus, which is a major component of arid and semi-arid ecosystems across the Northern Hemisphere (Thorne, 1972; Adams, 2004), and is as such regarded as a marker of aridity in paleoclimate research. Compared to Juniperus, members of the Pinaceae family are typically acclimated to more humid conditions (Schuler, 1988).

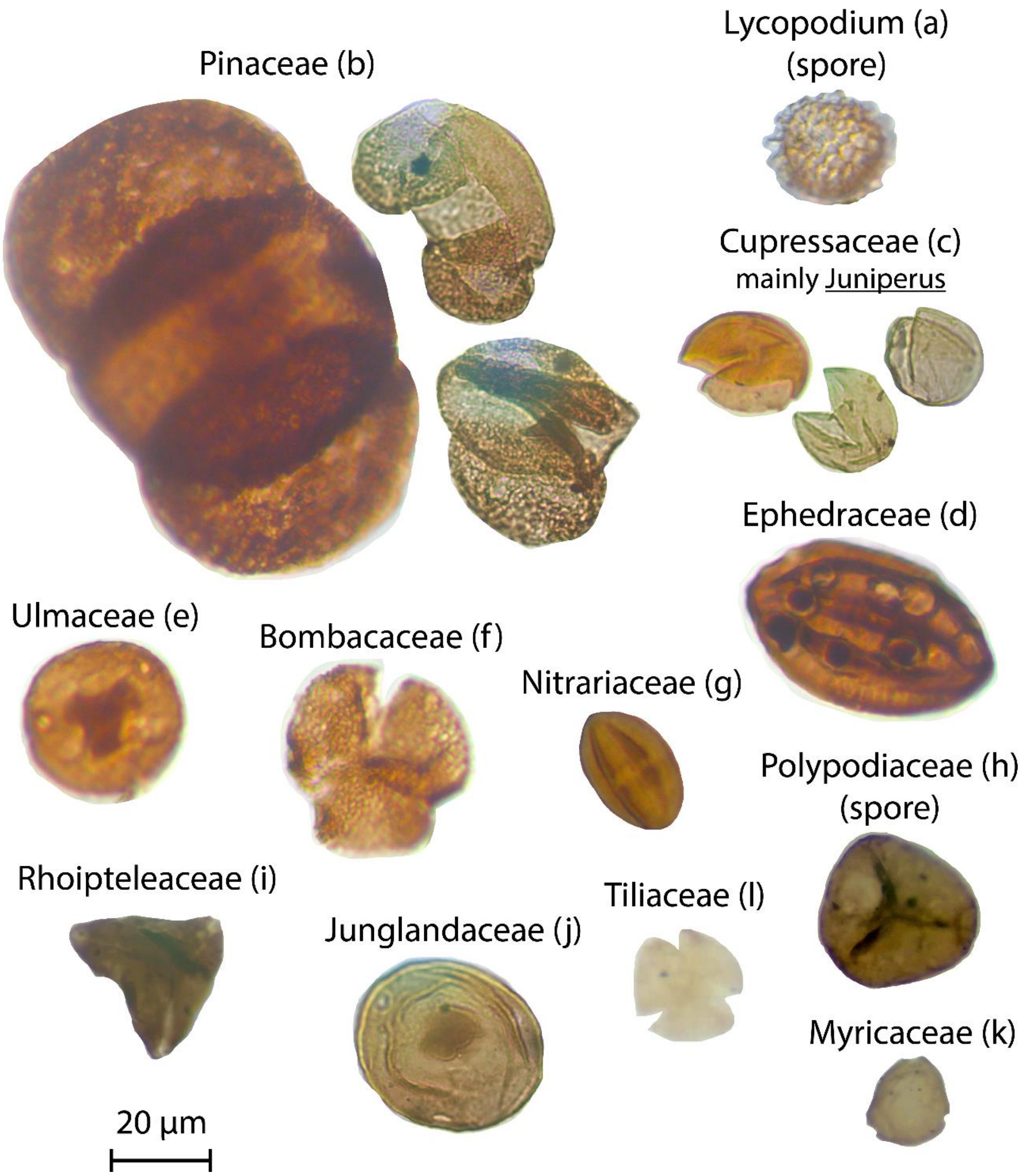

***Figure 104**: List of the families of pollen grains (and spores) encountered in the "Couches de Pechelbronn" in the GRT-1 and GPK-2 boreholes of the Pechelbronn basin.*

VII.1.a.ii : Dinoflagellate cysts

Several species of dinoflagellate cysts have been found in the "Couches de Pechelbronn" of the GRT-1 and GPK-2 boreholes. Those that have been identified with high confidence are *Deflandrea phosphoritica*, *Phtanoperidinium comatum*, *Spiniferites sp.*, *Distanodinium paradoxum*, and *Operculodinium divergens*. The others for which the identification is less certain are *Cordosphaeridinium sp.*?, *Hystrichokolpoma rigaudiae*?, and *Areoligera sp.*?.

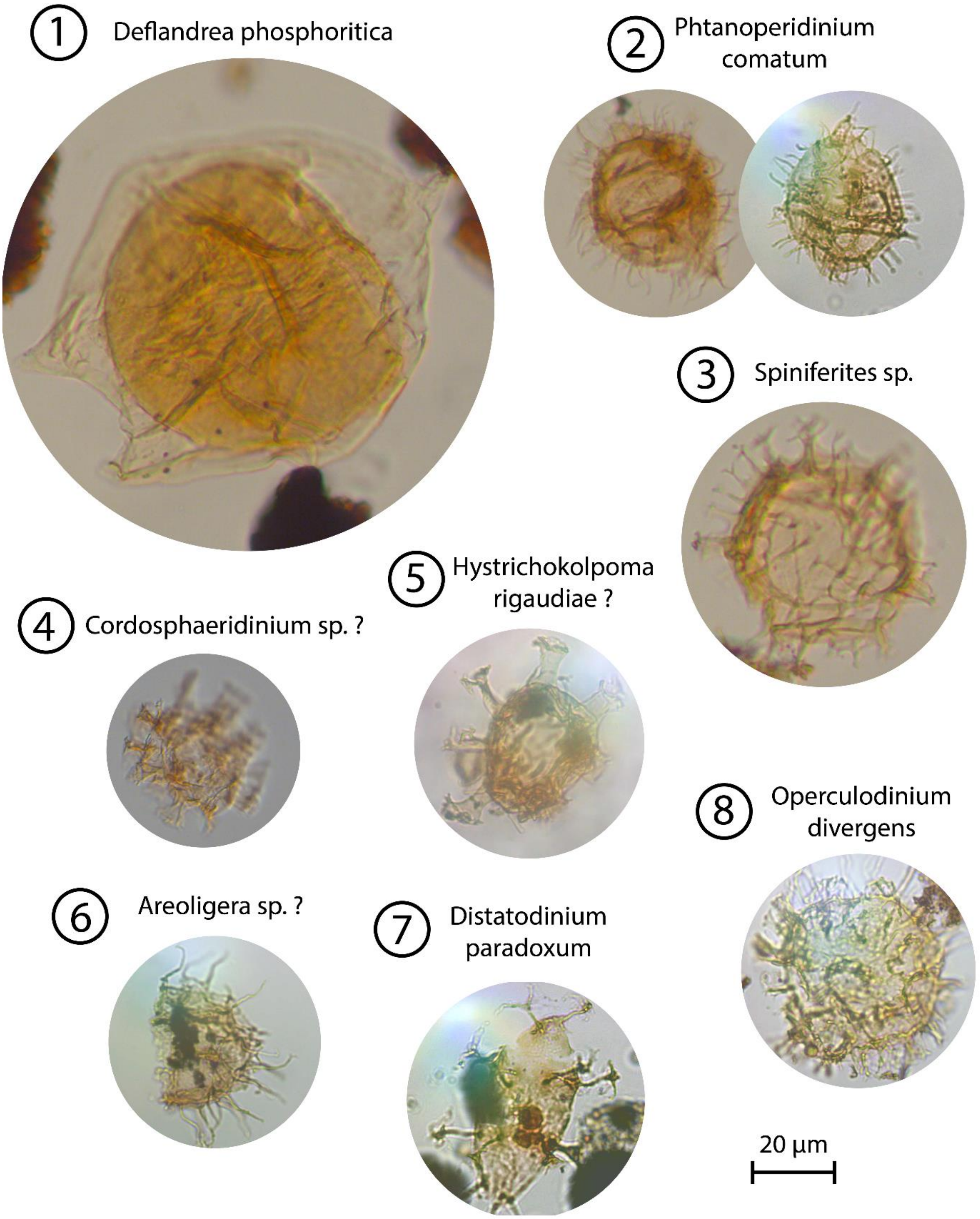

***Figure 105**: List of species of dinoflagellate cysts encountered in the "Couches de Pechelbronn" of the GRT-1 and GPK-2 boreholes of the Pechelbronn basin.*

Dinoflagellate cysts hold precious information about the age of the sediments and the environment inside which they were deposited (Williams et al., 2004; Pross & Brinkhuis, 2005). The information regarding the species of **Figure 105** are detailed in **Table 6**.

***Table 6**: Age range and living environments of the dinoflagellates species encountered in the "Couches de Pechelbronn" of the GRT-1 and GPK-2 boreholes.*

Name	Age range	Environment	References
Deflandrea phosphoritica	54.0 – 21.9 Ma (NML)	**Restricted marine** freshwater input, hypersalinity, terrigenous nutrient input	Pross & Brinkhuis (2005), Williams et al. (2004)
Phtanoperidinium comatum	Eocene – early Oligocene	**Coastal sea-surface** Runoff-related, mixing	Pross & Brinkhuis (2005)
Spiniferites sp.	Mesozoic – Cenozoic	?	Palynodata database
Cordosphaeridinium sp.?	Mesozoic – Cenozoic	**?**	Palynodata database
Hystrichokolpoma rigaudiae?	Eocene - Miocene	**Offshore**	Pross & Brinkhuis (2005)
Areoligera sp.?	Mesozoic – Cenozoic	**Coastal**	Pross & Brinkhuis (2005), Palynodata database
Distatodinium paradoxum	Eocene - Miocene	**Marine**	Piasecki (1980), Costa et al. (1976)
Operculidinium divergens	41.3 – 31.9 Ma (NML)	**Coastal**	Pross & Brinkhuis (2005), Williams et al. (2004)

While no precise age can be inferred from the occurrences of these dinoflagellate species regarding the timing of the Eocene-Oligocene transition, they provide information regarding the influence of marine incursions (detailed in the following sections).

VII.1.b : GRT-1 borehole

VII.1.b.i : Geochemistry

The proxy of the sedimentary carbonate content shows that this sedimentary succession is rich in carbonates, with an average value of 27.3%, ranging from 7.4% to 49.8% (**Figure 106**). This is coherent with the fact that the sedimentary successions of the Pechelbronn basin is known to be mostly made of marls interbedded with sandstones and conglomerates. There could have been two main sources of carbonates in this basin: (1) authigenic precipitation and/or (2) reworking of the Jurassic limestones from the rift's shoulders. The $CaCO_3$ curve appears to be inversely correlated with the gamma-ray signal, suggesting that the latter could be driven by carbonate content. However, conglomeratic, and sandy intervals are clearly marked by lower gamma-ray values, which thus indicate that the gamma-ray signal is driven by multiple factors. A rapid shift in $CaCO_3$ content is observed in the interval containing both the "Couches de Pechelbronn Inférieures" and "Couches de Pechelbronn Moyennes". Multiple interpretations are plausible: (1) it is related to the transgression of the "Zone Fossilifère", marking an increase of marls and a decrease of sandstones through the related lake-level increase, and therefore marks the limit between the two units, or (2) it is part of the "Couches de Pechelbronn Inférieures", in which the EOT is (potentially) positioned (Grimm et al., 2011), suggesting that it could mark a period of increased precipitation of authigenic carbonates linked with aridification. The latter is however pretty unlikely due to the arguments provided by dinoflagellate cysts (see **VII.1.b.ii : Palynology**). The first option is more likely, even more so that the average thickness of the "Zone Fossilifère" fits with this depth.

TOC values are 0.6% on average from the "Zone Dolomitique" to the "Série Grise", reaching up to 3.6% in the lowermost part of the "Couches de Pechelbronn Inférieures", 2% in the uppermost "Couches de Pechelbronn Supérieures", and 3% in the lower part of the "Série Grise" (**Figure 106**). These TOC values can be considered quite high, with the 3.6% value of the “Couches de Pechelbronn Inférieures” likely related to the presence of oil, reason for which the Pechelbronn basin has been exploited in the past.

C/N ratios show that the organic matter is of mixed origin across the entire succession, except in the “Couche Rouge” where it seems to fully consist of algae. Shifts in the C/N ratios in the “Zone Dolomitique” and in the lowermost “Couches de Pechelbronn inférieures”, where several samples show mostly land-based organic matter, could represent periods of accentuated rifting resulting in faster weathering of the rift’s shoulder, and therefore a bigger input of land plants in the lake compared with algal productivity (**Figure 106**). For samples with TOC > 1%, in the in the lower “Couches de Pechelbronn Inférieures”, upper “Couches de Pechelbronn Supérieures”, and lower “Série Grise”, the C/N ratios indicate that the source of the organic matter almost exclusively originated from land plants.

C/S ratios suggest that the depositional environments were exclusively brackish and/or marine through the “Zone Dolomitique” and “Couches de Pechelbronn” (**Figure 106**). Interestingly, several samples of the “Série Grise” contain higher C/S ratios than those of the underlying formation, despite being fully marine according to previous authors (Pirkenseer et al., 2010; 2011; Berger et al., 2005). This suggests that the underlying formation potentially had water with higher salinity than that of seawater.

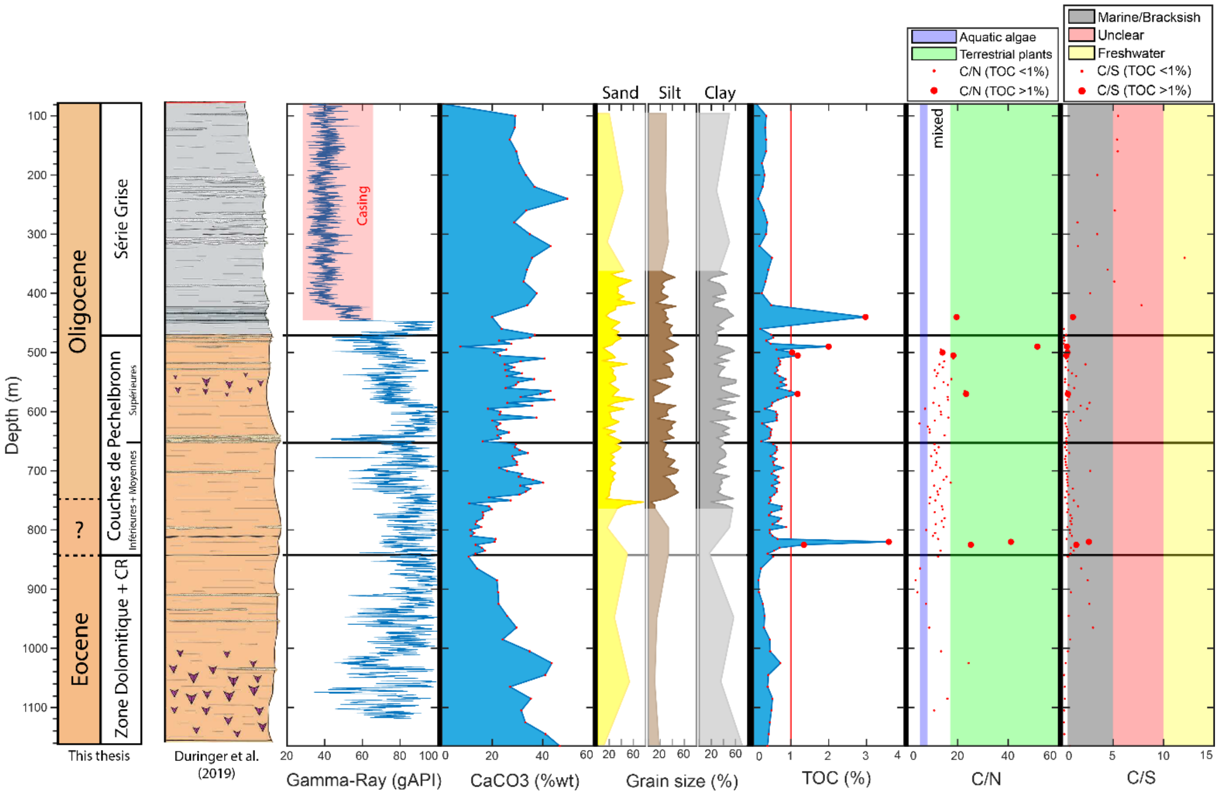

*__Figure 106__: Geochemistry results plotted along with the sedimentary log of Duringer et al. (2019) and gamma-ray data for the GRT-1 borehole. They consist of the carbonate proportion (Total Inorganic Carbon * 8.3), Total Organic Carbon, C/N, and C/S ratios. CR = Couche Rouge. The question mark between the Eocene and Oligocene corresponds to the incertitude on the location of the Eocene-Oligocene boundary.*

VII.1.b.ii : Palynology

The samples of the “Couches de Pechelbronn” from the GRT-1 borehole are relatively poor in pollen grains in the lower half and pretty rich in the upper half. According to the pollen counts, the “Couches de Pechelbronn Inférieures” and “Couches de Pechelbronn Moyennes” are dominated by Pinaceae with few counts of Cupressaceae, along little to no other families.

A clear shift occurs in the “Couches de Pechelbronn Supérieures” where the proportion of Pinaceae reduces while that of Cupressaceae (and other few families) increases (**Figure 107**). Very similar results were found by Schuler (1988) both in the Muhlouse and Pechelbronn basins. The shift from Pinaceae to Cupressaceae can be attributed to a phase of increased aridity, as the Cupressaceae family is mainly represented by Juniperus (Thorne, 1972; Adams, 2004). This shift coincides with the occurrence of the thick conglomeratic bed (“Zone Détritique de Glaswinkel”) at the base of the “Couches de Pechelbronn Supérieures”. This is an additional argument for the interpretation proposed in **VI.3.d : Astronomical forcing model** that coarse-grain beds are related to periods of relative increased aridity while fine-grain beds are related to periods of relative increased humidity (lake-level rise) in the Pechelbronn basin. However, to properly prove it, palynogogical analysis should be performed across the “Couches de Pechebronn” through specific beds to identify Milankovitch-frequency climate cycles, which could only be performed with cores rather than cuttings. Furthermore, based on their position in the stratigraphy (slightly above the “Zone Fossilifère”), it seems very likely that the thick conglomeratic bed at the bottom of the “Couches de Pechelbronn Supérieures” is the equivalent of the lower potash seam of the Mulhouse basin, which if true would further argument the aridity hypothesis.

In the GRT-1 borehole, dinoflagellate cysts were mainly found in the interval that likely corresponds to the lower part of the “Couches de Pechelbronn Moyennes”. This find is in agreement with the proposition that the “Zone Fossilifère” was marked by one or more marine incrusions and/or transgressions (see **II.3.c.iii : About the “Zone Fossilifère”**). The presence *Cordosphaeridinium sp.?* near the bottom of the “Couches de Pechelbronn Inférieures” suggests that one or more marine incursions could have happened even prior to that/those of the “Zone Fossilifère”. Similarily, in the Mulhouse basin, Schuler (1998) found marine dinoflagellate cysts in the upper part of the “Sel III”, suggesting early marine incursions. Furthermore, Schuler (1988) did not find any dinoflagellate cysts in the sediments beneath the “Sel III”, appart from reworked Jurassic species. This is an important information because if the Eocene-Oligocene transition was to be found in the “Couches de Pechelbronn Inférieures”, one would not expect to find marine dinoflagellate cysts inside it as this event marks a sea-level fall of 70m, making connections with the sea quite unlikely. The most likely scenario is that the combination of post-EOT sea-level rise and subsidence led way to marine incursions from the North Sea (Berger et al., 2005a; Berger et al., 2005b). This suggests that in the Pechelbronn basin, the Eocene-Oligocene boundary is therefore located somewhere beneath the first occurrence of tiertiary dinoflagellate cysts, which fits well with the hypothesis that the EOT is located at the bottom of the “Sel III” unit in the Mulhouse basin (see **Chapter V :**). In the “Couches de Pechelbronn Supérieures”, *Deflandrea phosphoritica* is found in some samples while other species are completely absent. This dinoflagellate is known to live restricted marine environments (Pross & Brinkhuis, 2005), it therefore likely survived and proliferated after the connections with the sea were closed through the “Couches de Pechelbronn Superior”, while other marine-acclimated species perished. The dinoflagellate species encountered across the “Couches de Pechelbronn” in the GRT-1 borehole consist of *Deflandrea phosphoritica*, *Phtanoperidinium comatum*, *Spiniferites sp.?, Cordosphaeridinium sp.?*, and *Aeroligera sp.?*.

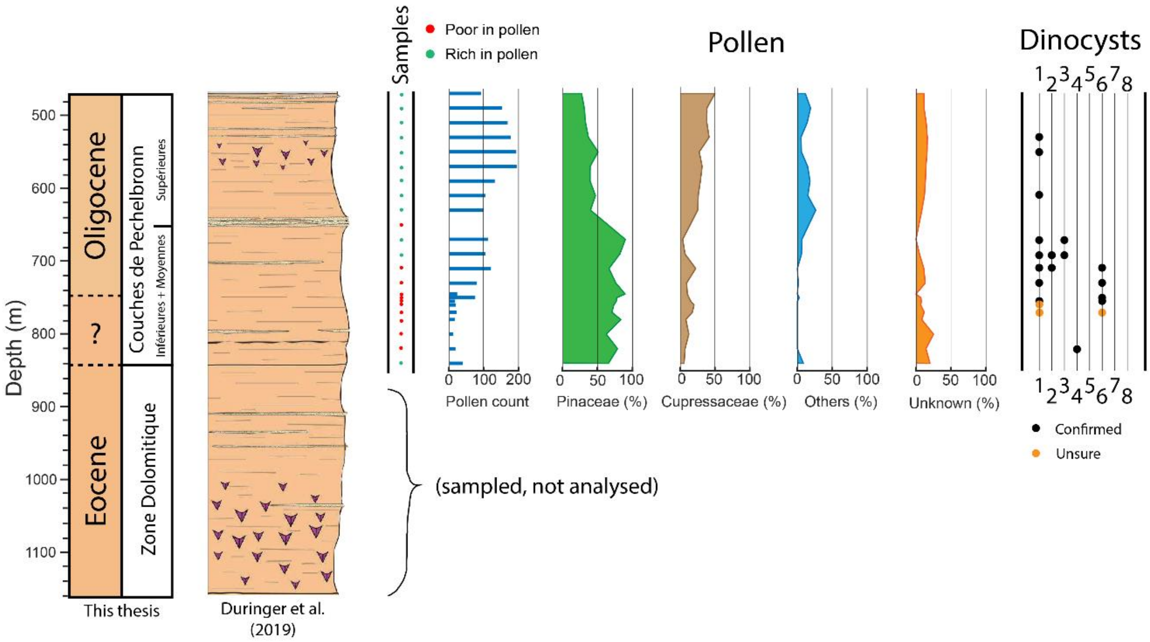

***Figure 107**: Palynology results in the GRT-1 borehole plotted along the sedimentary log of Duringer et al. (2019). They consist of the pollen count, proportions of Pinaceae and Cupressaceae (along other families and undistinguishable grains), and occurrences of specific dinoflagellate cysts. The question mark between the Eocene and Oligocene corresponds to the incertitude on the location of the Eocene-Oligocene boundary.*

VII.1.c : GPK-2 borehole

The investigated section of the GPK-2 borehole goes from the “Zone Dolomitique” up to the “Couches de Pechelbronn Supérieures”. Due to the presence of some fault, it is possible that the lowermost part of the investigated section contains Jurassic sediments (Aichholzer et al., 2016). The uppermost part of the section is marked by an unconformity which cuts a non-negligeable part of the “Couches de Pechelbronn Supérieures” (Aichholzer et al., 2016).

VII.1.c.i : Geochemistry

The proxy of carbonate content in the GPK-2 borehole appears to be similar to that of the GRT-1 borehole, with a maximum value of ~43% and a minimum value of ~6% (**Figure 108**). However, the shift observed in the “Couches de Pechelbronn Inférieures” and “Couches de Pechelbronn Moyennes” of the GRT-1 borehole do not occur as sharply in the GPK-2 borehole, but a similar tendency can be observed. The carbonate content curve of the GPK-2 borehole is in phase with that of the TOC and clay, which is not observed in the GRT-1 borehole. These differences are possibly related to the distance between the two boreholes.

TOC values in the GPK-2 borehole are lower in average than those of the GRT-1 borehole, with only one sample reaching over the 1% benchmark. Several samples are however relatively close to that value. The maximum is reached at the same location in both boreholes, being in the lowermost part of the “Couches de Pechelbronn”.

C/N ratios suggest that the organic matter originates from a mix of land plants and aquatic algae overall. In the case of the sample with a TOC value superior to 1%, the C/N ratio suggests that the organic matter originates primarily from land plants. This is similar to the observations in the GRT-1 borehole samples where almost all values of C/N for TOC values superior to 1% are attributed to land plants.

C/S ratios suggest that the environment was brackish/marine throughout the whole interval, with only a few samples below, inside, and above the conglomeratic interval of the “Couches de Pechelbronn Supérieures” suggesting the occurrence of freshwater environments.

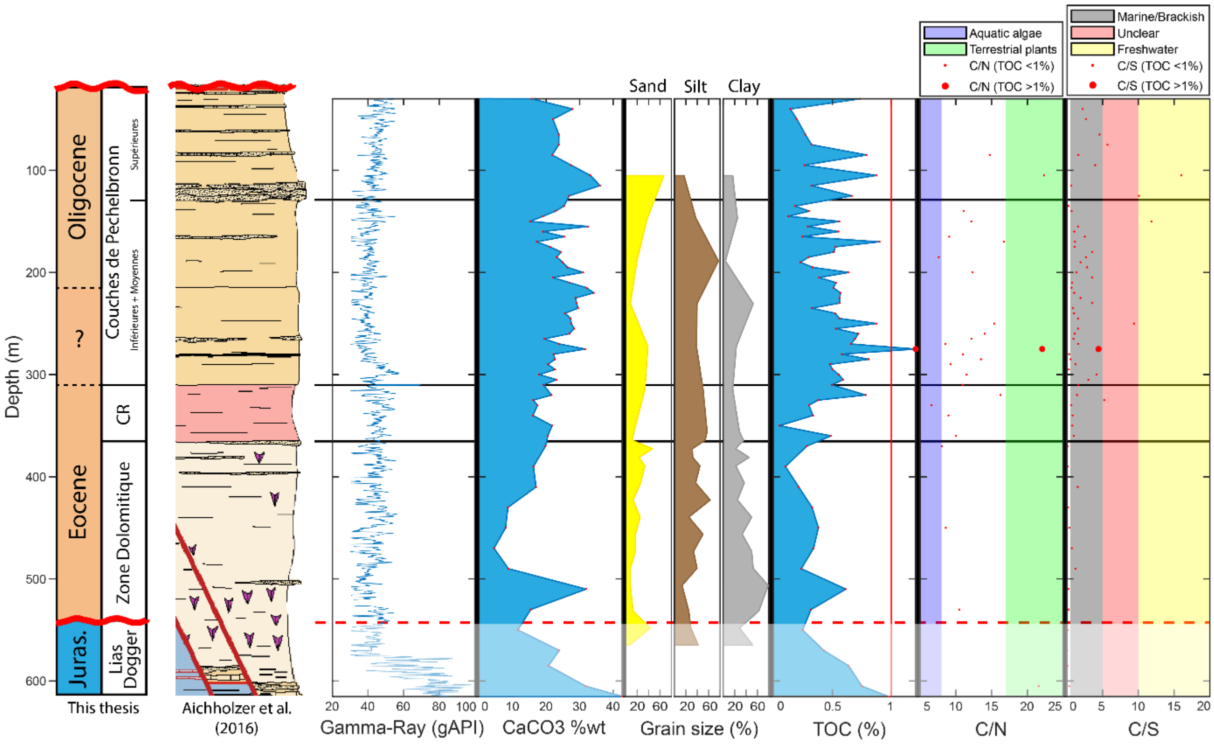

*__Figure 108__: Geochemistry results plotted along with the sedimentary log of Aichholzer et al. (2016) and gamma-ray data for the GPK-2 borehole. They consist of the carbonate proportion (Total Inorganic Carbon * 8.3), Granulometry (sand, silt, clay), Total Organic Carbon, C/N, and C/S ratios. CR = Couche Rouge. The question mark between the Eocene and Oligocene corresponds to the incertitude on the location of the Eocene-Oligocene boundary.*

VII.1.c.ii : Palynology

The samples of the “Couches de Pechelbronn” from the GPK-2 borehole are poor in palynomorphs. Pollen grain count accounts for the dominance of the Pinaceae family in the lower half of the “Couches de Pechelbronn Inférieures” and “Couches de Pechelbronn Moyennes”, after which the Cupressaceae family (Juniperus) starts to largely develop (**Figure 109**). Dinoflagellate cysts were found in the middle of the “Couches de Pechelbronn Inférieures” and “Couches de Pechelbronn Moyennes” across a ~50 m interval. In this interval, the dinoflagellate cysts that were found are *Deflandrea phosphoritica*, *Phtanoperidinium comatum*, *Spiniferites sp.*, *Cordosphaeridinium sp.?*, *Hystrichokolpoma rigaudiae ?*, *Distatodinium paradoxum*, and *Operculodinium divergens*.

In contrast with the samples of the GRT-1 borehole, the samples of the GPK-2 borehole are way poorer in pollen grains, with only three samples exceeding the 100-count mark. The observations are somewhat similar, regarding the fact that the pollen spectrum is dominated by Pineaceae and Cupressaceae grains, however the reduction of Pinaceae and the increase of Cupressaceae happens earlier in the section than in the GRT-1 borehole, where it happened at the transition between the “Couches de Pechelbronn Moyennes” and “Couches de Pechelbronn Supérieures”. As such, and by comparison with the investigations of Schuler (1988), this shift is interpreted as occuring at the transition between the “Couches de Pechelbronn Moyennes” and “Couches de Pechelbronn Supérieures” overall.

Similarly to the GRT-1 borehole, dinoflagellate cysts in the GPK-2 borehole are present across the "Couches de Pechelbronn Inférieures" and the "Couches de Pechelbronn Moyennes", suggesting early marine incursions, and further arguing for the EOT to be located somewhere beneath the first occurrences of tertiary dinoflagellate cysts, in the lower part, or beneath the "Couches de Pechelbronn Inférieures". Interestingly, more dinoflagellate species were encountered in the GPK-2 borehole compared to the GRT-1 borehole. However, apart from *Deflandrea phosphoritica*, each species were present as one or two individuals per sample, meaning that other species were potentially missed.

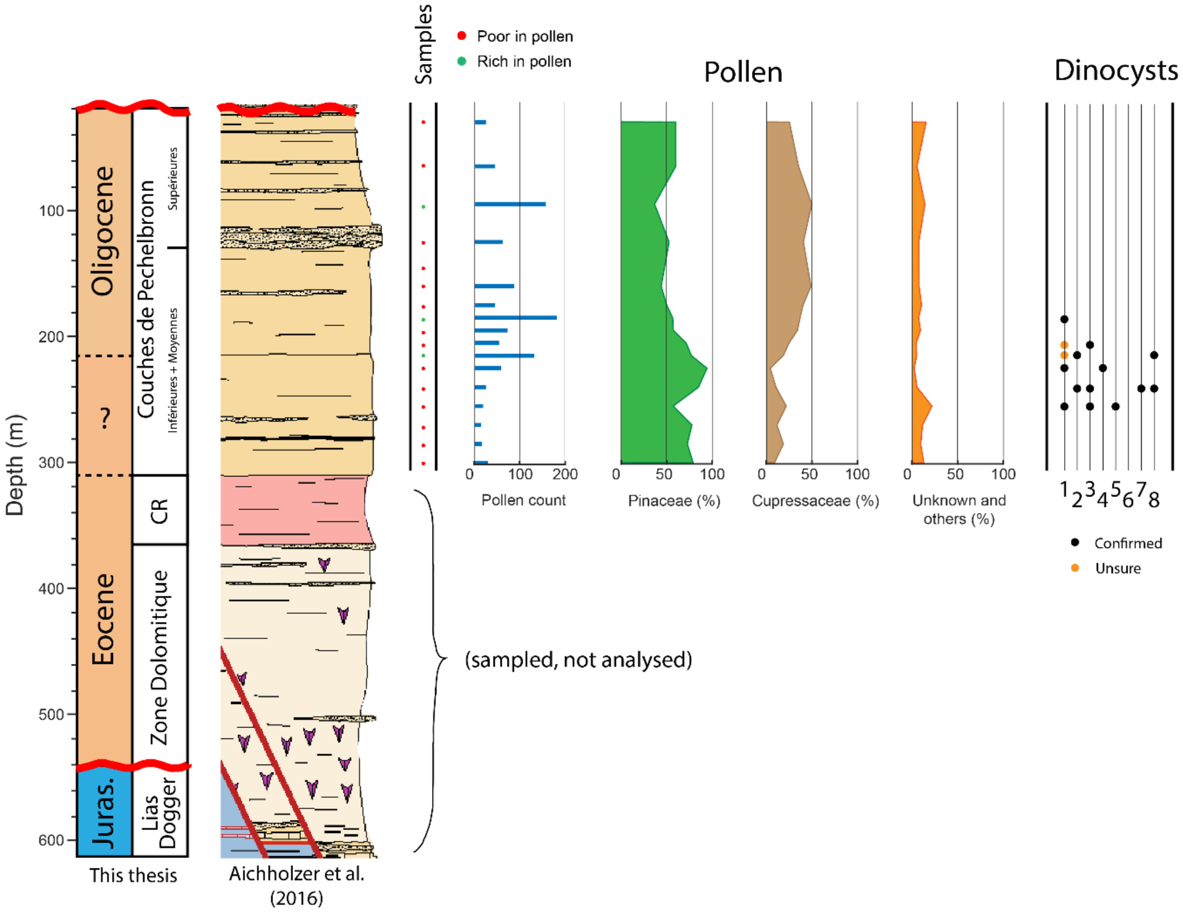

Figure 109: Palynology results in the GPK-2 borehole plotted along the sedimentary log of Aichholzer et al. (2019). They consist of the pollen count, proportions of Pinaceae and Cupressaceae (along other families and undistinguishable grains), and occurrences of specific dinoflagellate cysts. The question mark between the Eocene and Oligocene corresponds to the incertitude on the location of the Eocene-Oligocene boundary.

VII.1.d : Summary

- Geochemistry analyses (carbonate content, C/N ratio, C/S ratio) suggest that the environment was brackish to marine across the whole investigated interval ("Zone Dolomitique" to "Série Grise"), and that the organic matter mostly originated from a mixed sourced of land plants and aquatic algae, except for samples with high TOC values where it mostly originated from land plants. In the "Zone Dolomitique" of the GRT-1 borehole however, C/N ratios show clear variations from algae dominated to land-plant dominated, which could potentially be related to tectonic activity changing the space available for plant communities or inducing higher sediment (and organic debris) fluxes through the uplift of the rift's shoulders.

- Pollen grain counts in the GRT-1 borehole show that the pollen spectrum was dominated by Pinaceae across the “Couches de Pechelbronn Inférieures” and “Couches de Pechelbronn Moyennes”, and that a clear shift occured at the bottom of the “Couches de Pechelbronn Supérieures” where the Pinaceae proportion decreased while the Cupressaceae proportion increased. This shift is interpreted as caused by aridification and occurred along the deposition of a thick conglomeratic interval (”Zone Détritique de Glaswinkel”), suggesting that coarse-grain beds are related to relatively arid intervals in the Pechelbronn basin.

- The occurrence of dinoflagellate cysts across the “Couches de Pechelbronn Inférieures” and “Couches de Pechelbronn Moyennes” is a clear indication of marine incursions, particularly in the lower part of the latter which could be an actual transgression, due to marine-acclimated species being present over multiple tens of meters. The presence of tertiary dinoflagellate cysts in the “Couches de Pechelbronn Inférieures”, even pretty close to bottom of the unit (e.g. *Spiniferites pseudofurcatus* in the GRT-1 borehole) (**Figure 107**), suggests that the Eocene-Oligocene boundary is likely located beneath their first occurrence, as depositing them during a period of sea-level fall of 70m seems very unlikely, even more so that none have been found in underlying sediments (Schuler, 1988).

Chapter VIII : Paleomagnetism measurements

Several cores were extracted from the Westhalten quarry (Strangenberg), Kleinkems quarry, Tagolsheim quarry, Altkirch quarry, and mine gallery using a hand-drill for paleomagnetism measurements as detailed in **III.2.d : Paleomagnetism**. The results are detailed in the following sections for each location.

VIII.1 : Strangenberg quarry

The beds in which the cores were sampled (10 in total) are shown next to the sedimentary log of the Strangenberg quarry (**Figure 69**). They were sampled both in mudstone beds and sandstone beds. Two samples, STR-02A and STR-04A, both sampled in mudstones, gave the best results, with their demagnetization paths clearly indicating that they were deposited during an inverse magnetic chron (**Figure 110**).

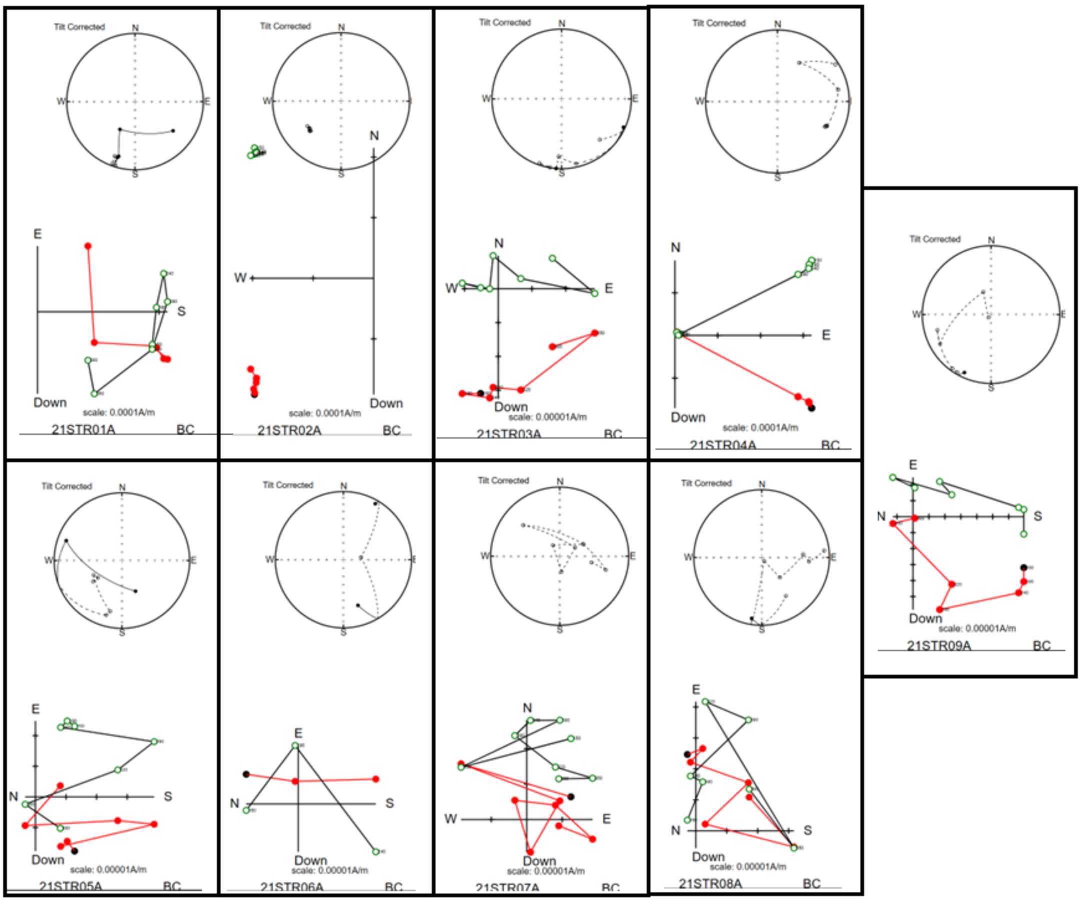

__Figure 110__: Zijderveld diagrams of the paleomagnetism measurements of the samples from the Strangenberg quarry. Most of the samples seem to have been deposited during an inverse magnetic chron. The STR-02A and STR-04A samples gave the most significative results indicating an inverse trend.

Four other samples, STR-01A, STR-03A, STR-05A, and STR-09A, appear to display an inverse trend as well, even though the uncertainties on them are high. The other samples did not have a usable signal. According to the original work of Duringer (1988) in this quarry, back when the lower section was still accessible, the section logged in this thesis (**Figure 69**) is located slightly above the equivalent of the “Zone Fossilifère” which is attributed the NP22 biozone. As such, this information suggests that the investigated section is part of the inverse interval of the C12 magnetic chron, somewhere between ~33.2 Ma and ~31 Ma (**Figure 37**).

VIII.2 : Mine gallery

Three samples were recovered from three laminated marlstone beds in the “Fond du Cuisard” at the Joseph-Else well (**Figure 57**). The demagnetization vectors on the Zijderveld diagrams seem to clearly indicate that these beds were deposited during a normal geomagnetic interval (**Figure 111**). However, it is hard to know if it is the case, as it could potentially have been re-magnetized in the actual magnetic field (common problematic in paleomagnetism studies). When comparing this result with the chronostratigraphy of the URG, having a normal magnetization here is highly unexpected, as these sediments are above the “Zone Fossilifère” (NP22), therefore above the normal interval of the C13 chron (**Figure 37**), and below the “Série Grise” (~29.62 Ma), there under the normal interval of the C12 chron (**Figure 37**). Further demagnetization steps are required to see if an inverse trend appears.

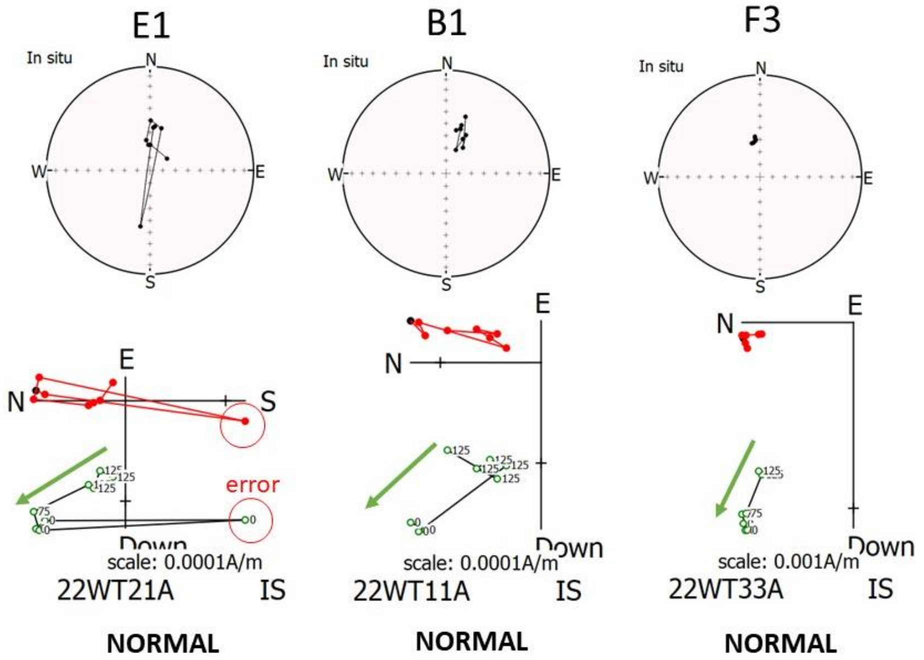

Figure 111: Zijderveld diagrams of the paleomagnetism measurements of the samples from the mine gallery (“Fond du Cuisard”) at the Joseph-Else well. All three samples seem to indicate that they deposited during a normal magnetic chron, but higher demagnetization temperatures would be required to affirm it, as this could be a sign of post-deposition re-magnetization.

VIII.3 : Altkirch quarry, Tagolsheim quarry, Kleinkems quarry

Several samples were collected at the lowermost part of the Altkirch quarry (**Figure 73**), across approximately half of the Tagolsheim quarry (**Figure 71**), and across the whole accessible section of the Kleinkems quarry below the “Zone Fossilifère”, according to the log of Duringer (1988). All the samples from these three locations did not give any usable paleomagnetism signal (**Figure 112**).

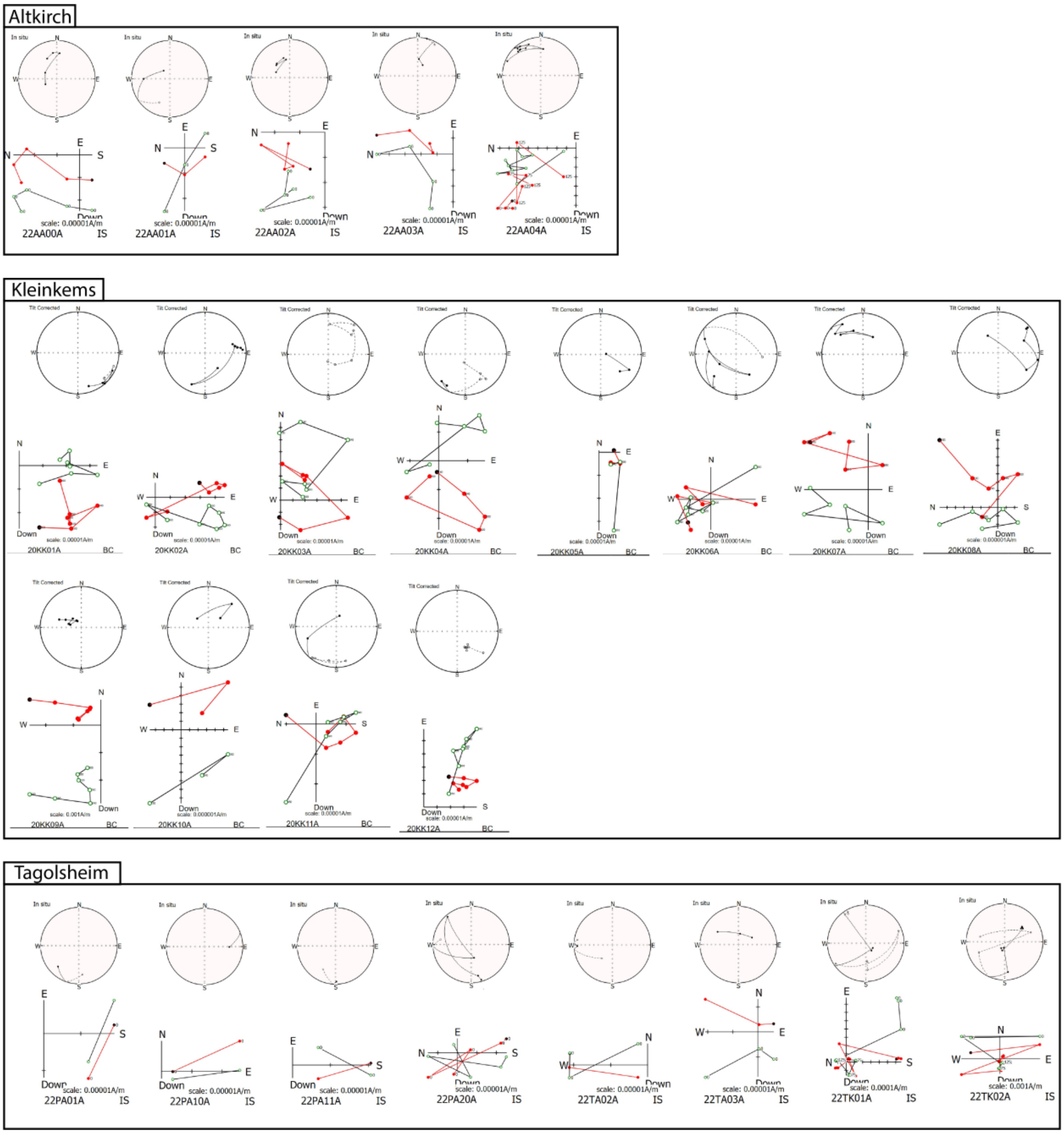

Figure 112: Paleomagnetism results from the samples retrieved from the Altkirch, Kleinkems, and Tagolsheim quarries. All these results show that the investigated samples from these quarries lack a decent magnetic signal, so they are not suitable for the interpretation of the magnetic field's orientation during their deposition.

VIII.4 : Conclusion

Paleomagnetic measurements carried out on certain outcrops have highlighted the fact that certain lithologies, notably marls, give good results. In the case of the Strangenberg quarry, the analyses showed that the outcrop sediments were probably deposited during an inverse magnetic interval, and as the equivalent of the "Fossiliferous Zone" is just below the interval studied, it is likely that the latter belongs to the C12 magnetic chron dated between ~33.2 and ~31 Ma. The majority of samples analyzed from other outcrops were found to be of insufficient magnetic susceptibility to allow any interpretation. Samples taken from a mine drift suggested that the marls of the Mulhouse basin have good magnetic susceptibility. Should a new borehole ever be drilled in this basin, I suggest that a detailed magnetostratigraphic analysis be carried out to enable the formations to be properly anchored in time, with the help of cyclostratigraphic and biostratigraphy results.

General conclusion: major results and perspectives

This research project, funded by two half PhD contracts from both the Region Grand-Est and the Ministère de l'Enseignement supérieur et de la Recherche, as well as by the project EOT-URG (PI M. Schuster) funded by CNRS/INSU/TELLUS/Syster program, represents the first ever initiative to investigate the Tertiary sedimentary archives of the Upper Rhine Graben with regards to the impact of a global climate change (i.e. the Eocene-Oligocene Transition) on continental paleo-environments. This project mainly addresses two main thematics: (1) the significance of the EOT in the URG, and (2) the characterization rift-lakes sedimentary systems.

Findings exposed in this thesis are the result of multi-disciplinary investigations performed on Eocene and Oligocene sedimentary records of the Upper Rhine Graben, notably in the Mulhouse and Pechelbronn basins, and in outcrops. The tools and principles of sedimentology, cyclostratigraphy, palynology, geochemistry, and paleomagnetism were used to unravel the climatic and environmental evolution of the Upper Rhine Graben during and across the climatic shift of the Eocene-Oligocene transition, as well as refining the chronostratigraphic framework of the region.

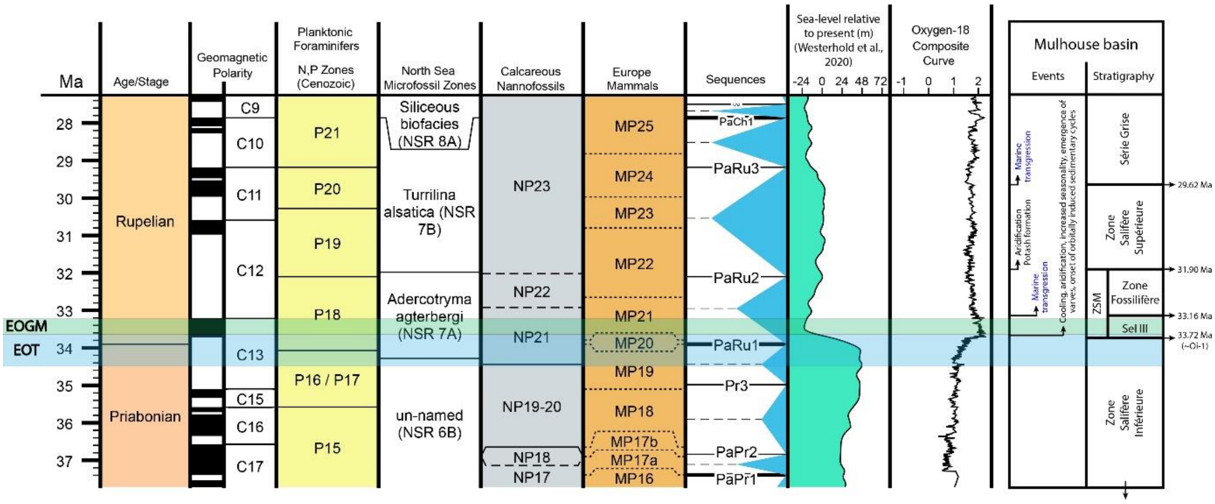

***Figure 113**: New chronostratigraphic framework of the Mulhouse basin based on the results exposed in this thesis, in relation with the biostratigraphy and sea-level sequences and variations. The Earliest Oligocene oxygen Isotope Step (EOIS, Oi-1) is placed at the base of the "Sel III". EOT = Eocene-Oligocene Transition, EOGM = Early Oligocene Glacial Maximum.*

The identified impacts of the Eocene-Oligocene transition on the continental environments of the Upper Rhine Graben include:

- Cooling,
- Aridification,
- Increased seasonal climatic contrast,
- Increased sensitivity of the climate to orbital variations.

Sedimentary and chrono-stratigraphic framework

The sedimentary record of the different sub-basins composing the Upper Rhine Graben has been studied for more than a century, and multiple chrono-stratigraphic frameworks and stratigraphic correlations have been proposed (Simon et al., 2021). Syn-rift sedimentation started during the Lutetian and led to the deposition of red mudstones and conglomerates of the "Basal Eocene" on top of the Jurassic substratum. Throughout the rifting process, several sub-basins differentiated, and the nature of the sedimentary infills varied greatly from North to South, from the silici-clastic dominated Pechelbronn basin to the marlstone and evaporite dominated Mulhouse basin. In the midst of these differences, two formations known as the "Zone Fossilifère" and "Série Grise" form continuous deposits across the Upper Rhine Graben and serve as major correlation surfaces, signing periods of clear water-level rise. The nature of the "Zone Fossilifère" sparked debate amongst the scientific community. Some interpreted the water-level increase as the result of a marine transgression, and others as the result of a purely isolated lacustrine transgression. In this thesis, through the synthesis of previous publications and new palynological investigations in the Pechelbronn basin, I propose that the "Zone Fossilifère" was influenced by a marine transgression notably in its lower part due to the presence of specific marine Tertiary dinoflagellate species and assemblages. These were not found in older deposits, apart from the uppermost "Sel III" and "Couches de Pechelbronn Inférieures" (just below the "Zone Fossilifère") which are probably precursors of the following transgression. Up to now, the Eocene-Oligocene boundary was placed at the base of the "Zone Fossilifère", but this proposition did not make sense as the EOT is marked by a ~70 m sea-level fall, which would have made any marine transgression in the URG very unlikely. Through the synthesis of bio-stratigraphic publications, comparisons with sea-level variations, and the production of age models inferred from cyclostratigraphy, I propose that the base of the "Zone Fossilifère" is most-likely dated at ~33.16 Ma, in the uppermost part NP21 biozone, correlated to the sea-level rise following the PaRu1 sequence, which is related to the partial melting of the Antarctic Icesheet at the end of the EOGM (probably paired with tectonic activity). As a consequence, I propose that the duration of the "Sel III" unit can be estimated through cyclostratigraphy as ~556.8 kyr, suggesting that the Eocene-Oligocene boundary (33.9 Ma) should be located slightly under the base of the "Sel III" (~33.72 Ma). The estimated age for the base of the "Sel III" is almost that of the Oi-1 event (33.65 Ma). This age attribution fits really well with the climatic and sedimentary changes observed at the base of the "Sel III".

Impacts of the EOT on the continental environments of the URG

In the Mulhouse basin, the base of the "Sel III" is marked by a clear increase in seasonality, by aridification, and by cooling, according to past palynological investigations (Schuler, 1988), which I infer as induced by climate change at the Eocene-Oligocene transition based on the newly proposed chrono-stratigraphic framework. Furthermore, the investigation of the DP-XXVIII well and original mining documents show that the base of the "Sel III" marks the transition from structureless mudstones to laminites and varves, as well as the onset of clear orbitally induced sedimentary cycles (Simon et al., 2024, submitted). The appearance of varves is interpreted as the sedimentary record of increased seasonality through the EOT. The onset of orbitally induced sedimentary cycles (precession, obliquity, short eccentricity) at the base of the "Sel III" is consistent with increased sensitivity to orbital forcing across the EOT (Tardif et al., 2021; Westerhold et al., 2020).

Cyclostratigraphy of the Mulhouse and Pechelbronn basins

The cyclostratigraphy investigations performed throughout this thesis indicate the presence of orbitally induced sedimentary cycles recorded in both the Mulhouse and Pechelbronn basins. They are particularly well expressed in the Mulhouse basin ("Sel III", "Zone Salifère Supérieure"). There, the sedimentary cycles consist of clear marlstone-evaporite alternations at various scales. The spectral analysis of these successions through different intervals ("Sel III", "Sel IV", "Sel V", "Marnes sans Sel") shows the imprint of precession, obliquity, and eccentricity in the sedimentary record. The marlstone-evaporite cycles mostly consist of precession cycles, with some cases of obliquity cycles, modulated by short eccentricity. Minimum durations were then proposed for each interval based on the number of cycles within them: 556.8 kyr for the "Sel III", 737.7 kyr for the "Sel IV", 1061.4 kyr for the "Sel V", and 473.0 kyr for the "Marnes sans Sel". An orbital tuning solution has been proposed for the "Zone Salifère Supérieure". It suggests that the very top of the formation (base of the "Série Grise") is dated at 29.62 Ma, which is in accordance with its attribution to the mid P20 biozone (Pirkenseer et al., 2010). Thus, the age of the top of the "Zone Fossilifère" was deduced and estimated at 31.90 Ma, which is coherent with biostratigraphic attributions.

In addition, the high-frequency cyclostratigraphic investigation of the potash seams of the Mulhouse basin reveals, on the assumption that the marlstone-halite-sylvite alternations are of annual origin, the presence of high-frequency cycles (5.6, 4.3, and 3.0 years) that could be related to rapid climatic oscillations such as the North Atlantic Oscillation. This could be a record of the onset of the NAO after the EOT and of its related oceans' structure changes.

Lessons from other investigations

Palynology and geochemistry

A preliminary palynological study was performed on the recently drilled GRT-1 and GPK-2 boreholes of the Pechelbronn basin.

Tertiary dinoflagellate cysts species were found in the "Couches de Pechelbronn Moyennes" (= "Zone Fossilifère") and in the "Couches de Pechelbronn Inférieures" to a lesser extent. These species are marine, and therefore strongly suggest the occurrence of a marine transgression and/or of marine incursions at that time. Counting of pollen grains show that the Pinaceae family is dominant in the "Couches de Pechelbronn Inférieures" and "Couches de Pechelbronn Moyennes", and that the "Couches de Pechelbronn Supérieures" are marked by a clear increase in the Cupressaceae family. This shift could be linked to an increase in aridity, as previously suggested by Schuler (1988). However, the depths at which the Pinaceae family is dominant are relatively the same as those in which marine dinoflagellate species are found, and recent investigations suggest that bissacate pollen types (such as Pinaceae) are over-represented in marine sediments (Mudie, 1982). Therefore, this shift could potentially result in part from a change in depositional environment, but the occurrence of a massive conglomerate deposit at the bottom of the "Couches de Pechelbronn Supérieures" is coherent with an increase in aridity. Similarly, the occurrence of potash seams above the "Zone Fossilifère" in the Mulhouse basin is an additional argument for an increase in aridity at that time. These two specific deposits could be synchronous.

The geochemistry analysis of the whole Eocene and Oligocene sedimentary succession of the GRT-1 and GPK-2 boreholes indicate that these sediments are very rich in carbonates, and that several intervals are rich in Total Organic Carbon (up to ~3.8% in the lowermost “Couches de Pechelbronn Supérieures” of the GRT-1 borehole). The study of C/S ratios suggests that the water was brackish or marine across the whole interval. I suggest that the water is marine where marine dinoflagellate cysts are found, and brackish otherwise (and where *Deflandrea phosphorita* is found alone, as it lived in restricted marine conditions). The study of C/N ratios indicates that the origin of the organic matter was mostly related to a mix of aquatic algae and terrestrial plants, except for sediments with TOC values >1% which mainly relate to terrestrial plants.

Paleomagnetism

The results of the paleomagnetism investigations show that most of the sampled lithologies bear non-interpretable paleomagnetism results, apart from the red mudstones of the Strangenberg quarry (Westhalten) and the laminated marlstones of the mine gallery (Joseph-Else well). All the interpretable results from the Strangenberg quarry show that they were deposited during an reverse geomagnetic period. The investigated sedimentary interval is located slightly above the “Zone Fossilifère” (upper NP21, NP22) by comparison with the sedimentary log of Duringer (1988), which is located in the lower part of the inverse C12 chron, suggesting that it is also part of this inverse period. As such, with the top of the “Zone Fossilifère” being hereby dated at ~31.90 Ma, the investigated sedimentary interval was most certainly deposited somewhere between ~31.90 Ma and ~31.00 Ma. This assumes that there are no major hiatuses and that no normal interval was missed.

Perspectives

This thesis provides the first study of the impacts of the Eocene-Oligocene transition on the continental environments of the Upper Rhine Graben (cooling, aridification, increased seasonality, increased sensitivity to orbital forcing), which will be useful to the scientific community to better understand how this event affected climates and environments worldwide, and how global climate changes in general affect continental environments. This work will also be useful to numerical climate modelers, as the impacts described in this thesis can serve as benchmarks to reach through the testing of various parametrizations (e.g. CO_2 levels, paleogeographic configurations). The observed changes appear to have happened relatively fast (i.e. across a few tens of meters in the Mulhouse basin) which suggests the occurrence of a tipping point that fostered climatic and sedimentary changes. It also reveals the possible links between the formation of the Antarctic Ice-Sheet and the onset of the North Atlantic Oscillation which appears to be recorded in potash alternations, potentially providing arguments for the impact that icesheets in Antarctica have on global climate.

While the Eocene-Oligocene chrono-stratigraphic framework of the URG, and particularly of the Mulhouse basin, has been improved in this thesis, notably through cyclostratigraphic investigations, it could be further improved through the study of continuous coring records using magnetostratigraphy, biostratigraphy, and cyclostratigraphy together. New coring projects will be the key to studying the geological and climatic history of the Upper Rhine Graben in greater detail. Continuous core would also allow the detailed and continuous study of varved intervals, enabling the study of high-frequency cycles over long periods of time and document the evolution of inter-annual climate variability. Such a coring project should be performed in the area where the isopachs of the Eocene-Oligocene sediments reach their maximum, with no faults and limited hiatuses, near the DP-XXVIII well (deepest part of the basin at that time).

The investigation of the Mulhouse basin has shown how hypersaline environments can be rich archives of past climate changes. I suggest that other such environments in other basins should be investigated in detail (cyclostratigraphy in particular), such as the Bourg-en-Bresse basin which holds mudstone-evaporite alternations similar to those of the Mulhouse basin, as well as finely laminated sediments (Moretto, 1987).

The preliminary palynology work performed on the GRT-1 and GPK-2 boreholes of the Pechelbronn basin shows the potential that these boreholes have for palynological studies. While I focused on the “Couches de Pechelbronn”, future research projects could focus on analyzing the whole Tertiary sedimentary record to provide a more complete analysis regarding chronology. Particular interest could be given to the dinoflagellate species found in the “Couches de Pechelbronn Moyennes” (= “Zone Fossilifère”) and “Couche de Pechelbronn Inférieures”, as well as in the “Série Grise”. Regarding pollen, future research should focus on documenting and counting species rather than families to provide temperature and precipitations estimates through the co-existence approach, similarly to what Schuler (1988) did but with more recent methods and tools.

While I mostly focused on the Mulhouse and Pechelbronn basins, the other basins of the Upper Rhine Graben are yet to be investigated in the scope of the EOT, both on the French and German side.

Eurasian sedimentary records show quite homogeneous responses across the EOT, but heterogeneities are clear worldwide. A decent number of records have been studied in the Northern hemisphere, unlike the Southern hemisphere which should be focused on more to get a clearer vision of global heterogeneities. Effort should be made toward extracting numerical values of pCO_2, temperatures, and precipitations from continental records across the EOT.

List of figures

Tables

References

Abello, M. A., Toledo, N., & Ortiz-Jaureguizar, E. (2018). Evolution of South American Paucituberculata (Metatheria: Marsupialia): adaptive radiation and climate changes at the Eocene-Oligocene boundary. *Historical Biology*, 32(4), 476-493.

Abelson, M., & Erez, J. (2017). The onset of modern-like Atlantic meridional overturning circulation at the Eocene-Oligocene transition: Evidence, causes, and possible implications for global cooling. *Geochemistry, Geophysics, Geosystems*, 18(6), 2177-2199.

Adams, R.P. (2004). Junipers of the World: the genus Juniperus. Vancouver, BC, Canada: Trafford Publishing.

Aichholzer, C. (2019). Le log complet de la stratigrahie de la zone rhénane ainsi que les modilités stratigraphiques, sédimentaires et structurales de la transition socle-couverture: application à la géothermie profonde (Doctoral dissertation, Université de Strasbourg).

Aichholzer, C., Duringer, P., Orciani, S., & Genter, A. (2016). New stratigraphic interpretation of the Soultz-sous-Forêts 30-year-old geothermal wells calibrated on the recent one from Rittershoffen (Upper Rhine Graben, France). *Geothermal Energy*, 4(1), 1-26.

Alley, R. B., Clark, P. U., Huybrechts, P., & Joughin, I. (2005). Ice-sheet and sea-level changes. *Science*, 310(5747), 456-460.

Anderle, H. J. (1987). The evolution of the South Hunsrück and Taunus borderzone. *Tectonophysics*, *137*(1-4), 101-114.

Ao, H., Dupont-Nivet, G., Rohling, E. J., Zhang, P., Ladant, J. B., Roberts, A. P., ... & An, Z. (2020). Orbital climate variability on the northeastern Tibetan Plateau across the Eocene–Oligocene transition. *Nature communications*, 11(1), 5249.

Archer, D., Kite, E., & Lusk, G. (2020). The ultimate cost of carbon. *Climatic Change*, 162, 2069-2086.

Barreda, V., & Palazzesi, L. (2010). Vegetation during the Eocene–Miocene interval in central Patagonia: a context of mammal evolution. *The paleontology of Gran Barranca: evolution and environmental change through the Middle Cenozoic of Patagonia*, 375-382.

Bauer, H., Bessin, P., Saint-Marc, P., Châteauneuf, J. J., Bourdillon, C., Wyns, R., & Guillocheau, F. (2016). The Cenozoic history of the Armorican Massif: New insights from the deep CDB1 borehole (Rennes Basin, France). *Comptes Rendus Geoscience*, *348*(5), 387-397.

Ben Dor, Y. B., Neugebauer, I., Enzel, Y., Schwab, M. J., Tjallingii, R., Erel, Y., & Brauer, A. (2019). Varves of the Dead Sea sedimentary record. *Quaternary Science Reviews*, 215, 173-184. https://doi.org/10.1016/j.quascirev.2019.04.011

Berger, A. (1978). Long-term variations of daily insolation and Quaternary climatic changes. *Journal of Atmospheric Sciences*, *35*(12), 2362-2367.

Berger, A. (1988). Milankovitch theory and climate. *Reviews of geophysics*, 26(4), 624-657.

Berger, A. N. D. R. E. (2001). The role of CO2, sea-level and vegetation during the Milankovitch-forced glacial-interglacial cycles. *Geosphere-Biosphere Interactions and Climate*, 119-146.

Berger, A., Loutre, M. F., & Dehant, V. (1989). Astronomical frequencies for pre-Quaternary palaeoclimate studies. *Terra nova*, *1*(5), 474-479.

Berger, J. P. (1996). Cartes paléogéographiques-palinspastiques du bassin molassique suisse (Oligocène inférieur-Miocène moyen). *Neues Jahrbuch für Geologie und Paläontologie-Abhandlungen*, 1-44.

Berger, J. P., Reichenbacher, B., Becker, D., Grimm, M., Grimm, K., Picot, L., ... & Schaefer, A. (2005a). Paleogeography of the upper Rhine Graben (URG) and the Swiss Molasse basin (SMB) from Eocene to Pliocene. *International Journal of Earth Sciences*, *94*, 697-710.

Berger, J. P., Reichenbacher, B., Becker, D., Grimm, M., Grimm, K., Picot, L., ... & Schaefer, A. (2005b). Eocene-Pliocene time scale and stratigraphy of the Upper Rhine Graben (URG) and the Swiss Molasse Basin (SMB). *International Journal of Earth Sciences*, *94*, 711-731.

Bergerat, F. (1985). *Déformations cassantes et champs de contrainte tertiaires dans la plate-forme européenne* (Doctoral dissertation, Université Pierre et Marie Curie-Paris VI).

Bergerat, F. (1987). Stress fields in the European platform at the time of Africa-Eurasia collision. *Tectonics*, *6*(2), 99-132.

Berggren, W. A., Kent, D. V., Swisher, C. C., & Aubry, M. P. (1995). A revised Cenozoic geochronology and chronostratigraphy.

Berner, R. A. (1990). Atmospheric carbon dioxide levels over Phanerozoic time. *Science*, *249*(4975), 1382-1386.

Berner, R. A., & Kothavala, Z. (2001). GEOCARB III: a revised model of atmospheric CO2 over Phanerozoic time. *American Journal of Science*, 301(2), 182-204.

Berner, R. A., & Raiswell, R. (1983). Burial of organic carbon and pyrite sulfur in sediments over Phanerozoic time: a new theory. *Geochimica et Cosmochimica Acta*, *47*(5), 855-862.

Berner, R. A., & Raiswell, R. (1984). C/S method for distinguishing freshwater from marine sedimentary rocks. *Geology*, *12*(6), 365-368.

Blanc-Valleron, M. M. (1990). Les formations paléogènes évaporitiques du bassin potassique de Mulhouse et des bassins plus septentrionaux d'Alsace. Documents BRGM, Vol. 204, 350 p.

Blanc-Valleron, M. M., Foucault, A., & Gannat, E. (1989). Le contrôle climatique, orbital, et solaire de la sédimentation évaporitique: exemple de la base du Salifère supérieur (Oligocène inférieur) du bassin de Mulhouse (Sud du fossé rhénan, France). *Comptes rendus de l'Académie des sciences*, *308*(4), 435-441.

Boës, X., Rydberg, J., Martinez-Cortizas, A., Bindler, R., & Renberg, I. (2011). Evaluation of conservative lithogenic elements (Ti, Zr, Al, and Rb) to study anthropogenic element enrichments in lake sediments. *Journal of Paleolimnology*, 46, 75-87. https://doi.org/10.1007/s10933-011-9515-z

Boggs, S. (2012). Principles of sedimentology and stratigraphy.

Bohacs, K. M., Carroll, A. R., Neal, J. E., & Mankiewicz, P. J. (2000). Lake-basin type, source potential, and hydrocarbon character: An integrated sequence-stratigraphic–geochemical framework. In E. H. Gierlowski-Kordesch and K. R. Kelts, eds., *Lake basins through space and time: AAPG Studies in Geology*, 46, 3–34.

Bohaty, S. M., Zachos, J. C., & Delaney, M. L. (2012). Foraminiferal Mg/Ca evidence for southern ocean cooling across the eocene–oligocene transition. *Earth and Planetary Science Letters*, 317, 251-261.

Bohaty, S. M., Zachos, J. C., & Delaney, M. L. (2012). Foraminiferal Mg/Ca evidence for southern ocean cooling across the eocene–oligocene transition. *Earth and Planetary Science Letters*, *317*, 251-261.

Bordovskiy, O. K. (1965). Accumulation of organic matter in bottom sediments. *Marine Geology*, *3*(1-2), 33-82.

Boulila, S., Dupont-Nivet, G., Galbrun, B., Bauer, H., & Châteauneuf, J. J. (2021). Age and driving mechanisms of the Eocene–Oligocene transition from astronomical tuning of a lacustrine record (Rennes Basin, France). *Climate of the Past*, *17*(6), 2343-2360.

Bourgeois, O., Ford, M., Diraison, M., Veslud, C. L. C. D., Gerbault, M., Pik, R., ... & Bonnet, S. (2007). Separation of rifting and lithospheric folding signatures in the NW-Alpine foreland. *International Journal of Earth Sciences*, *96*, 1003-1031.

Bourquin, S., Durand, M., Diez, J. B., Broutin, J., & Fluteau, F. (2007). The Permian-Triassic boundary and lower Triassic sedimentation in western European basins: an overview. *Journal of Iberian Geology*, *33*(2), 221-236.

Brauer, A., Dulski, P., Mangili, C., Mingram, J., & Liu, J. (2009). The potential of varves in high-resolution paleolimnological studies. *PAGES news*, 17(3), 96-98. https://doi.org/10.22498/pages.17.3.96

Breedlovestrout, R. L., Evraets, B. J., & Parrish, J. T. (2013). New Paleogene paleoclimate analysis of western Washington using physiognomic characteristics from fossil leaves. *Palaeogeography, Palaeoclimatology, Palaeoecology*, *392*, 22-40.

Brenchley, P. J. (1989). Storm sedimentation. *Geology Today*, *5*(4), 133-137.

Bretagnon, P. (1974). Termes à longues périodes dans le système solaire. *Astron. Astrophys*, *30*(1), 141-154.

Brosius, M., & Gramann, F. (1959). Das ältere Tertiär von Großalmerode (Hessische Senke). *Zeitschrift der Deutschen Geologischen Gesellschaft*, 543-558.

Budikova, D. (2009). Role of Arctic sea ice in global atmospheric circulation: A review. *Global and Planetary Change*, 68(3), 149-163.

Budyko, M. I. (1969). The effect of solar radiation variations on the climate of the Earth. *Tellus*, 21(5), 611-619.

Carpenter, A. B. (1978). Origin and chemical evolution of brines in sedimentary basins. *In SPE Annual Fall Technical Conference and Exhibition*. OnePetro.

Carroll, A. R., & Bohacs, K. M. (1999). Stratigraphic classification of ancient lakes: Balancing tectonic and climatic controls. *Geology*, 27(2), 99-102. https://doi.org/10.1130/0091-7613(1999)027<0099:SCOALB>2.3.CO;2

Carroll, A.R., 2017, Xenoconformities and the stratigraphic record of paleoenvironmental change. *Geology*, v. 45, p. 639–642. https://doi.org/10.1130/G38952.1

Catuneanu, O. (2020). Sequence stratigraphy. *Regional Geology and Tectonics*, p. 605-686

Cendón, D. I., Ayora, C., Pueyo, J. J., Taberner, C., & Blanc-Valleron, M. M. (2008). The chemical and hydrological evolution of the Mulhouse potash basin (France): are "marine" ancient evaporites always representative of synchronous seawater chemistry?. *Chemical Geology*, *252*(3-4), 109-124.

Chateauneuf, J. J. (1983). Dinokystes et milieux confines du Paléogene du bassin de Paris. *Sciences Géologiques, bulletins et mémoires*, *36*(4), 223-230.

Châteauneuf, J. J., & Ménillet, F. (2014). Découverte d'une microflore bartonienne dans le Fossé rhénan supérieur: la formation de Mietesheim (Bas-Rhin, Alsace, France). *Géologie de la France*, *1*, 3-20.

Clark, P. U., Pisias, N. G., Stocker, T. F., & Weaver, A. J. (2002). The role of the thermohaline circulation in abrupt climate change. *Nature*, 415(6874), 863-869.

Cleveland, W. S. (1979). Robust locally weighted regression and smoothing scatterplots. *Journal of the American statistical association*, *74*(368), 829-836.

Collinson, J. C., & Mountney, N. P. (2019). Sedimentary Structures. Dunedin Academic Press. *Edinburgh, Scotland, 340 p.*

Colwyn, D. A., & Hren, M. T. (2019). An abrupt decrease in Southern Hemisphere terrestrial temperature during the Eocene–Oligocene transition. *Earth and Planetary Science Letters*, 512, 227-235.

Colwyn, D. A., & Hren, M. T. (2019). An abrupt decrease in Southern Hemisphere terrestrial temperature during the Eocene–Oligocene transition. *Earth and Planetary Science Letters*, *512*, 227-235.

Costa, L. I., Downie, C., & Eaton, G. L. (1976). Palynostratigraphy of some middle Eocene sections from the Hampshire basin (England). *Proceedings of the Geologists' Association*, *87*(3), 273-284.

Courtot, C., Gannat, E., & Wendling, E. (1972). Le bassin potassique de Mulhouse et ses environs. Étude du Tertiaire. *Sciences Géologiques, bulletins et mémoires*, 25(2), 69-91.

Cowling, T. G. (1981). The present status of dynamo theory. *Annual review of astronomy and astrophysics*, *19*(1), 115-135.

Coxall, H. K., Huck, C. E., Huber, M., Lear, C. H., Legarda-Lisarri, A., O'regan, M., ... & Backman, J. (2018). Export of nutrient rich Northern Component Water preceded early Oligocene Antarctic glaciation. *Nature Geoscience*, 11(3), 190-196.

Coxall, H. K., Pearson, P. N. (2007). The Eocene–Oligocene Transition.

Coxall, H. K., Wilson, P. A., Pälike, H., Lear, C. H., & Backman, J. (2005). Rapid stepwise onset of Antarctic glaciation and deeper calcite compensation in the Pacific Ocean. *Nature*, 433(7021), 53-57.

Cramwinckel, M. J., Huber, M., Kocken, I. J., Agnini, C., Bijl, P. K., Bohaty, S. M., ... & Sluijs, A. (2018). Synchronous tropical and polar temperature evolution in the Eocene. *Nature*, *559*(7714), 382-386.

Cramwinckel, M. J., Huber, M., Kocken, I. J., Agnini, C., Bijl, P. K., Bohaty, S. M., ... & Sluijs, A. (2018). Synchronous tropical and polar temperature evolution in the Eocene. *Nature*, *559*(7714), 382-386.

Davies, S. J., Lamb, H. F., & Roberts, S. J. (2015). Micro-XRF Studies of Sediment Cores: Applications of a non-destructive tool for the environmental sciences. *Developments in Paleoenvironmental Research*, 17, 189-226. https://doi.org/10.1007/978-94-017-9849-5_7

DeConto, R. M., & Pollard, D. (2003). Rapid Cenozoic glaciation of Antarctica induced by declining atmospheric CO2. *Nature*, 421(6920), 245-249.

Dèzes, P., Schmid, S. M., & Ziegler, P. A. (2004). Evolution of the European Cenozoic Rift System: interaction of the Alpine and Pyrenean orogens with their foreland lithosphere. *Tectonophysics*, *389*(1-2), 1-33.

Diester-Haass, L., Zachos, J., & Prothero, D. R. (2003). The Eocene-Oligocene transition in the Equatorial Atlantic (ODP Site 925); paleoproductivity increase and positive δ13C excursion. *Greenhouse to Icehouse: The Marine Eocene-Oligocene Transition*, 397-416.

Doebl, F., Müller, C., Schuler, M., Sittler, C., & Weiler, H. (1976). Les Marnes à Foraminifères et les Schistes à Poissons de Bremmelbach (Bas-Rhin). Etudes sédimentologiques et micropaléontologiques. Reconstitution du milieu au début du Rupélien dans le Fossé Rhénan. *Sciences Géologiques, bulletins et mémoires*, *29*(4), 285-320.

Doney, S. C., Fabry, V. J., Feely, R. A., & Kleypas, J. A. (2009). Ocean acidification: the other CO2 problem. *Annual review of marine science*, 1, 169-192.

Dor, Y. B., Neugebauer, I., Enzel, Y., Schwab, M. J., Tjallingii, R., Erel, Y., & Brauer, A. (2019). Varves of the Dead Sea sedimentary record. *Quaternary Science Reviews*, *215*, 173-184.

Dräger, N., Theuerkauf, M., Szeroczyńska, K., Wulf, S., Tjallingii, R., Plessen, B., Kienel, U., & Brauer, A. (2017). Varve microfacies and varve preservation record of climate change and human impact for the last 6000 years at Lake Tiefer See (NE Germany). *The Holocene*, 27(3), 450-464. https://doi.org/10.1177/0959683616660173

Dunham, R. J. (1962). Classification of carbonate rocks according to depositional textures. *AAPG Mem*. 1, 108–121

Dupont-Nivet, G., Krijgsman, W., Langereis, C. G., Abels, H. A., Dai, S., & Fang, X. (2007). Tibetan plateau aridification linked to global cooling at the Eocene–Oligocene transition. *Nature*, 445(7128), 635-638.

Durand, M. (1972). Presence de galets éolisés dans le Buntsandstein moyen lorrain. *CR somm. Soc. géol. France*, *5*, 214-215.

Duringer, P. (1988). Les conglomérats des bordures du rift cénozoïque rhénan : dynamique sédimentaire et contrôle climatique. Thèse d'État, Université de Strasbourg, 287p.

Duringer, P., Aichholzer, C., Orciani, S., & Genter, A. (2019). The complete lithostratigraphic section of the geothermal wells in Rittershoffen (Upper Rhine Graben, eastern France): a key for future geothermal wells. *BSGF-Earth Sciences Bulletin*, *190*(1), 13.

Eagles, G., Livermore, R. A., Fairhead, J. D., & Morris, P. (2005). Tectonic evolution of the west Scotia Sea. *Journal of Geophysical Research: Solid Earth*, 110(B2).

Echols, R. J., Armentrout, J. M., Root, S. A., Fearn, L. B., Cooke, J. C., Rodgers, B. K., & Thompson, P. R. (2003). Sequence stratigraphy of the Eocene/Oligocene boundary interval: Southeastern Mississippi. *From Greenhouse to Ice House: The Marine Eocene–Oligocene Transition*, 189-222.

Edel, J. B., & Fluck, P. (1989). The upper Rhenish Shield basement (Vosges, Upper Rhinegraben and Schwarzwald): main structural features deduced from magnetic, gravimetric and geological data. *Tectonophysics*, *169*(4), 303-316.

Edel, J. B., & Weber, K. (1995). Cadomian terranes, wrench faulting and thrusting in the central Europe Variscides: geophysical and geological evidence. *Geologische Rundschau*, *84*, 412-432.

Edel, J. B., Schulmann, K., & Rotstein, Y. (2007). The Variscan tectonic inheritance of the Upper Rhine Graben: evidence of reactivations in the Lias, Late Eocene–Oligocene up to the recent. *International Journal of Earth Sciences*, *96*(2), 305-325.

Eldrett, J. S., Greenwood, D. R., Harding, I. C., & Huber, M. (2009). Increased seasonality through the Eocene to Oligocene transition in northern high latitudes. *Nature*, *459*(7249), 969-973.

Elsasser, W. M. (1956). Hydromagnetism. II. a review. *American Journal of Physics*, *24*(2), 85-110.

Embry, A. F., & Johannessen, E. P. (1993). T–R sequence stratigraphy, facies analysis and reservoir distribution in the uppermost Triassic–Lower Jurassic succession, western Sverdrup Basin, Arctic Canada. In *Norwegian petroleum society special publications*, 2, 121-146.

Epstein, S., Buchsbaum, R., Lowenstam, H. A., & Urey, H. C. (1953). Revised carbonate-water isotopic temperature scale. *Geological Society of America Bulletin*, 64(11), 1315-1326.

Équipe du projet GeORG. (2013). Potential géologique profonde du Fossé rhénan supérieur. Parties 1 à 4. Internet (Document PDF : http://www.geopotenziale.eu).

Eugster, H.P., Hardie, L.A., Lerman, A., 1978. Saline lakes. Chemistry, Geology and Physics of Lakes. *Springer*, p. 273–293

Fan, M., Ayyash, S. A., Tripati, A., Passey, B. H., & Griffith, E. M. (2018). Terrestrial cooling and changes in hydroclimate in the continental interior of the United States across the Eocene-Oligocene boundary. *GSA Bulletin*, *130*(7-8), 1073-1084.

Fischer, A. G., Silva, I. P., & De Boer, P. L. (1990). Cyclostratigraphy. *Cretaceous Resources, Events and Rhythms: Background and Plans for Research*, 139-172.

Fischer, H. (1965). *Geologie des Gebietes zwischen Blauen und Pfirter Jura (SW Basel): mit einem mikropaläontologischen und einem paläogeographischen Beitrag*. Kuemmerly und Frey.

Förster B. (1911). Ergebnisse der Untersuchung von Bohrproben aus den seit 1904 im Gange befindlichen, zur Aufsuchung von Steinsaltz und Kalisaltzen ausgeführten Tiefbohrungen im Tertiär des Oberelsass. *Mitt. Geol. Landesanst. Els.-Lothr*., 7(4), 349-524.

Foster, G. L., Hull, P., Lunt, D. J., & Zachos, J. C. (2018). Placing our current ‘hyperthermal’ in the context of rapid climate change in our geological past. *Philosophical Transactions of the Royal Society A: Mathematical, Physical and Engineering Sciences*, 376(2130), 20170086.

Francis, J. E., Marenssi, S., Levy, R., Hambrey, M., Thorn, V. C., Mohr, B., ... & DeConto, R. (2008). From greenhouse to icehouse–the Eocene/Oligocene in Antarctica. *Developments in earth and environmental sciences*, *8*, 309-368.

Gale, A. S., Huggett, J. M., Palike, H., Laurie, E., Hailwood, E. A., & Hardenbol, J. (2006). Correlation of Eocene–Oligocene marine and continental records: orbital cyclicity, magnetostratigraphy and sequence stratigraphy of the Solent Group, Isle of Wight, UK. *Journal of the Geological Society*, *163*(2), 401-415.

Gall, J. C. (1971). *Faunes et paysages du Grès à Voltzia du Nord des Vosges. Essai paléoécologique sur le Buntsandstein supérieur*. Mém. Serv. Carte géol. Als. Lorr., 34, 318 p.

Gall, J. C. (1972). Permanence du régime de chenaux et de flaques dans les Vosges du Nord pendant toute la durée du Buntsandstein. *Sciences Géologiques, bulletins et mémoires*, *25*(4), 307-322.

Gall, J. C. (1985). Fluvial depositional environment evolving into deltaic setting with marine influences in the Buntsandstein of Northern Vosges (France). In *Aspects of fluvial sedimentation in the Lower Triassic Buntsandstein of Europe* (pp. 449-477). Springer Berlin Heidelberg.

Gallagher, T. M., & Sheldon, N. D. (2013). A new paleothermometer for forest paleosols and its implications for Cenozoic climate. *Geology*, *41*(6), 647-650.

Gaudant, J. (1979). Sur la présence de Gobiidae (Poissons téléostéens) dans l'Oligocène inférieur de Rouffach (Haut-Rhin). *Sciences Géologiques, bulletins et mémoires*, *32*(3), 131-137.

Gaudant, J. (1981). Un nouveau Cyprinodontidae (poisson téléostéen) de l'Oligocène inférieur de Kleinkems (Pays de Bade, Allemagne): Prolebias rhenanus nov. sp. *Sciences Géologiques, bulletins et mémoires*, *34*(1), 3-12.

Gaudant, J. (2012). Révision de Prolebias stenoura Sauvage, 1874 du Stampien (= Rupélien) de Limagne (centre de la France), espèce type du genre Prolebias (poisson téléostéen, Cyprinodontiformes). *Geodiversitas*, *34*(2), 409-423.

Gaudant, J., & Burkhardt, T. (1984). Sur la découverte de poissons fossiles dans les marnes grises rayées de la zone fossilifère (Oligocène basal) d'Altkirch (Haut-Rhin). *Sciences Géologiques, bulletins et mémoires*, *37*(2), 153-171.

Gélard, J.P. (1978). La fracturation de la Bourgogne méridionale, essai d'interprétation et implications tectoniques régionales. *Revue de Géologie Dynamique et de Géographie Physique*, 2, 5-28.

Gignoux M., Hoffmann C. (1920). Le Bassin Pétrolifère de Péchelbronn (Alsace). Etude géologique (Planches I-III). *Bulletin du Service de la carte géologique d'Alsace et de Lorraine*, 1(1), 1-46.

Gindre-Chanu, L., Pichat, A., Delhaye-Prat, V., Vis, C., Ringenbach, R., & Schlund, J. M. (2022). Depositional and diagenetic model of the Aptian potash-bearing Loémé evaporites in onshore Congo. *Sedimentary Geology*, 427, 106038.

Giot D., Gentilhomme P., Bouiller R., Clozier L., Fleury R., Gagnière G., et al. (1976). Notice de la carte géologique 1/50 000e, Saint Pourçain sur Sioule. *Rapport BRGM*, 16.

Goldner, A., Herold, N., & Huber, M. (2014). Antarctic glaciation caused ocean circulation changes at the Eocene–Oligocene transition. *Nature*, *511*(7511), 574-577.

Gorin, G. (1974). Etude palynostratigraphique des sédiments paléogenes de la Grande Limagne (Massif Central, France), avec applications de la statistique et de l'informatique (Doctoral dissertation, Faculté des Sciences de l'Université de Genève).

Gradstein, F. M., Ogg, J. G., Schmitz, M. D., & Ogg, G. M. (Eds.).(2012). The Geologic Time Scale 2012. Elsevier, p. 435.

Gradstein, F. M., Ogg, J. G., Smith, A. G., Bleeker, W., & Lourens, L. J. (2004). A new geologic time scale, with special reference to Precambrian and Neogene. *Episodes Journal of International Geoscience*, 27(2), 83-100.

Grimm, K. I. (2002). Foraminiferal zonation of early Oligocene deposits (Selztal Group, Latdorfian, Rupelian) in the Mainz Basin, Germany. *Journal of Micropalaeontology*, *21*(1), 67-74.

Grimm, M. C., Wielandt-Schuster, U., Hottenrott, M., Radtke, G., Berger, J. P., Ellwanger, D., Harms, F. J., Hoselmann, C. P., & Weidenfeller, M. (2011). Oberrheingraben (Tertiär des Oberrheingrabens). *Schriftenreihe der Deutschen Gesellschaft für Geowissenschaften*, 57-132. https://doi.org/10.1127/sdgg/75/2011/57

Grygar, T. M., Mach, K., Schnabl, P., Martinez, M., & Zeeden, C. (2019). Orbital forcing and abrupt events in a continental weathering proxy from central Europe (Most Basin, Czech Republic, 17.7–15.9 Ma) recorded beginning of the Miocene Climatic Optimum. *Palaeogeography, Palaeoclimatology, Palaeoecology*, *514*, 423-440.

Grygar, T. M., Mach, K., Schnabl, P., Pruner, P., Laurin, J., & Martinez, M. (2014). A lacustrine record of the early stage of the Miocene climatic optimum in Central Europe from the most basin, Ohře (eger) Graben, Czech Republic. *Geological Magazine*, *151*(6), 1013-1033.

Hager, H. (1986). Peat accumulation and syngenetic clastic sedimentation in the Tertiary of the Lower Rhine Basin (FR Germany). *Mémoires de la Société géologique de France (1924)*, (149), 51-56.

Hamdani, I., Assouline, S., Tanny, J., Lensky, I. M., Gertman, I., Mor, Z., & Lensky, N. G. (2018). Seasonal and diurnal evaporation from a deep hypersaline lake: The Dead Sea as a case study. *Journal of Hydrology*, *562*, 155-167.

Haq, B.U., Hardenbol, J., Vail, P.R., 1988. Mesozoic and Cenozoic chronostratigraphy and cycles of sea-level change. *Soc. Econ. Paleontol. Mineral*, 42, 71–108

Havelcová, M., Sýkorová, I., Mach, K., Trejtnarová, H., & Blažek, J. (2015). Petrology and organic geochemistry of the lower Miocene lacustrine sediments (Most Basin, Eger Graben, Czech Republic). *International Journal of Coal Geology*, *139*, 26-39.

Hay, W. W., Flögel, S., & Söding, E. (2005). Is the initiation of glaciation on Antarctica related to a change in the structure of the ocean?. *Global and planetary change*, *45*(1-3), 23-33.

Hays, J. D., Imbrie, J., & Shackleton, N. J. (1976). Variations in the Earth's Orbit: Pacemaker of the Ice Ages: For 500,000 years, major climatic changes have followed variations in obliquity and precession. *Science*, 194(4270), 1121-1132.

Hilgen, F. J., Hinnov, L. A., Abdul Aziz, H., Abels, H. A., Batenburg, S., Bosmans, J. H. C., ... & Zeeden, C. (2015). Stratigraphic continuity and fragmentary sedimentation: the success of cyclostratigraphy as part of integrated stratigraphy. *Geological Society, London, Special Publications*, 404, 157-197.

Hill, D. J., Haywood, A. M., Valdes, P. J., Francis, J. E., Lunt, D. J., Wade, B. S., & Bowman, V. C. (2013). Paleogeographic controls on the onset of the Antarctic circumpolar current. *Geophysical Research Letters*, *40*(19), 5199-5204.

Hoegh-Guldberg, O., Mumby, P. J., Hooten, A. J., Steneck, R. S., Greenfield, P., Gomez, E., ... & Hatziolos, M. (2007). Coral reefs under rapid climate change and ocean acidification. *Science*, 318(5857), 1737-1742.

Hoehne, F. (1916). Über die geologische Stellung der Blätter Sandsteine von Schwabweiler im Unter-Elsass und ihre Beziehungen zum Septarientone.

Hoffman, P. F., Abbot, D. S., Ashkenazy, Y., Benn, D. I., Brocks, J. J., Cohen, P. A., ... & Warren, S. G. (2017). Snowball Earth climate dynamics and Cryogenian geology-geobiology. *Science Advances*, 3(11), e1600983.

Hooker, J. J., Collinson, M. E., & Sille, N. P. (2004). Eocene–Oligocene mammalian faunal turnover in the Hampshire Basin, UK: calibration to the global time scale and the major cooling event. *Journal of the Geological Society*, *161*(2), 161-172.

Houben, A. J., van Mourik, C. A., Montanari, A., Coccioni, R., & Brinkhuis, H. (2012). The Eocene–Oligocene transition: Changes in sea level, temperature or both?. *Palaeogeography, Palaeoclimatology, Palaeoecology*, *335*, 75-83.

Howell, L. G., & Frosch, A. (1939). Gamma-ray, well-logging. *Geophysics*, 4(2), 106-114.

Hren, M. T., Sheldon, N. D., Grimes, S. T., Collinson, M. E., Hooker, J. J., Bugler, M., & Lohmann, K. C. (2013). Terrestrial cooling in Northern Europe during the Eocene–Oligocene transition. *Proceedings of the National Academy of Sciences*, *110*(19), 7562-7567.

Hsü, K. J., La Brecque, J., Percival, S. F., Wright, R. C., Gombos, A. M., Pisciotto, K., ... & Schreiber, E. (1984). Numerical ages of Cenozoic biostratigraphic datum levels: Results of South Atlantic Leg 73 drilling. *Geological Society of America Bulletin*, *95*(7), 863-876.

Huber, M., & Caballero, R. (2011). The early Eocene equable climate problem revisited. *Climate of the Past*, *7*(2), 603-633.

Hugueney, M. (1984). Évolution du paléoenvironnement dans le tertiaire de Limagne (Massif Central, France) à partir des faunes de mammifères. *Geobios*, *17*, 385-391.

Hutchinson, D. K., Coxall, H. K., Lunt, D. J., Steinthorsdottir, M., De Boer, A. M., Baatsen, M., ... & Zhang, Z. (2020). The Eocene-Oligocene transition: a review of marine and terrestrial proxy data, models and model-data comparisons. *Climate of the Past Discussions*, 2020, 1-71.

Hutchinson, D. K., Coxall, H. K., O'Regan, M., Nilsson, J., Caballero, R., & de Boer, A. M. (2019). Arctic closure as a trigger for Atlantic overturning at the Eocene-Oligocene Transition. *Nature Communications*, 10(1), 3797. https://doi.org/10.1038/s41467-019-11828-z

Illies, H. (1962). Oberrheinisches Grundgebirge und Rheingraben. *Geologische Rundschau*, *52*, 317-332.

Illies, J. H. (1977), Ancient and recent rifting in the Rhinegraben. *Geol. Mijnbouw*, 56, 329–350.

Illies, J. H., Rothé, J. P., & Sauer, K. (1967). Development and tectonic pattern of the Rhinegraben. *The Rhinegraben Progress Report. Abh geol Landesamt Baden-Würtemberg*, *6*, 7-9.

Imbrie, J., Hays, J.D., Martinson, D.G., McIntyre, A., Mix, A.C., Morley, J.J., Pisias, N.G., Prell, W.L., Shackleton, N.J., 1984. The orbital theory of Pleistocene climate: support from a revised chronology of the marine d18O record. In: Berger, A., Imbrie, J., Hays, J., Kukla, G., Saltzman, B. (Eds.), Milankovitch and Climate: Understanding the Response to Astronomical Forcing. D. *Reidel Publishing Co*., Dordrecht, pp. 269-305

Inglis, G. N., Farnsworth, A., Lunt, D., Foster, G. L., Hollis, C. J., Pagani, M., ... & Pancost, R. D. (2015). Descent toward the Icehouse: Eocene sea surface cooling inferred from GDGT distributions. *Paleoceanography*, *30*(7), 1000-1020.

IPCC, 2022: Climate Change 2022: Impacts, Adaptation, and Vulnerability. Contribution of Working Group II to the Sixth Assessment Report of the Intergovernmental Panel on Climate Change [H.-O. Pörtner, D.C. Roberts, M. Tignor, E.S. Poloczanska, K. Mintenbeck, A. Alegría, M. Craig, S. Langsdorf, S. Löschke, V. Möller, A. Okem, B. Rama (eds.)]. Cambridge University Press. Cambridge University Press, Cambridge, UK and New York, NY, USA, 3056 pp., doi:10.1017/9781009325844.

Ivany, L. C., Patterson, W. P., & Lohmann, K. C. (2000). Cooler winters as a possible cause of mass extinctions at the Eocene/Oligocene boundary. *Nature*, *407*(6806), 887-890.

Jaeger J. J. (1971). La faune de mammifères du Lutétien de Bouxwiller (Bas-Rhin) et sa contribution à l'élaboration de l'échelle des zones biochronologiques de l'Eocène Européen. *Bull. Serv. Cart. Géol. Alsace et Lorraine*, 24, 93- 105.

Johnson, J. G., & Murphy, M. A. (1984). Time-rock model for Siluro-Devonian continental shelf, western United States. *Geological Society of America Bulletin*, 95, 1349–1359.

Jones, R. N., McMahon, T. A., & Bowler, J. M. (2001). Modelling historical lake levels and recent climate change at three closed lakes, Western Victoria, Australia (c. 1840–1990). *Journal of Hydrology*, *246*(1-4), 159-180.

Kalanke, J., Mingram, J., Lauterbach, S., Usubaliev, R., Tjallingii, R., & Brauer, A. (2020). Seasonal deposition processes and chronology of a varved Holocene lake sediment record from Chatyr Kol lake (Kyrgyz Republic). *Geochronology*, 2(1), 133-154. https://doi.org/10.5194/gchron-2-133-2020

Katz, M. E., Miller, K. G., Wright, J. D., Wade, B. S., Browning, J. V., Cramer, B. S., & Rosenthal, Y. (2008). Stepwise transition from the Eocene greenhouse to the Oligocene icehouse. *Nature geoscience*, 1(5), 329-334.

Kennedy, A. T., Farnsworth, A., Lunt, D. J., Lear, C. H., & Markwick, P. J. (2015). Atmospheric and oceanic impacts of Antarctic glaciation across the Eocene–Oligocene transition. *Philosophical Transactions of the Royal Society A: Mathematical, Physical and Engineering Sciences*, 373(2054), 20140419.

Kennett, J. P. (1977). Cenozoic evolution of Antarctic glaciation, the circum-Antarctic Ocean, and their impact on global paleoceanography. *Journal of geophysical research*, 82(27), 3843-3860.

Kent, D. V., Olsen, P. E., Rasmussen, C., Lepre, C., Mundil, R., Irmis, R. B., ... & Parker, W. G. (2018). Empirical evidence for stability of the 405-kiloyear Jupiter–Venus eccentricity cycle over hundreds of millions of years. *Proceedings of the National Academy of Sciences*, *115*(24), 6153-6158.

Kiro, Y., Goldstein, S. L., Lazar, B., & Stein, M. (2016). Environmental implications of salt facies in the Dead Sea. *Bulletin*, *128*(5-6), 824-841.

Kobashi, T., Grossman, E. L., Dockery III, D. T., & Ivany, L. C. (2004). Water mass stability reconstructions from greenhouse (Eocene) to icehouse (Oligocene) for the northern Gulf Coast continental shelf (USA). *Paleoceanography*, *19*(1).

Kodama, K. P. (2012). Paleomagnetism of sedimentary rocks: Process and interpretation. John Wiley & Sons.

Kodama, K. P., & Hinnov, L. A. (2014). Rock magnetic cyclostratigraphy (Vol. 5). John Wiley & Sons.

Kohn, M. J., Josef, J. A., Madden, R., Kay, R., Vucetich, G., & Carlini, A. A. (2004). Climate stability across the Eocene-Oligocene transition, southern Argentina. *Geology*, *32*(7), 621-624.

Kohn, M. J., Strömberg, C. A., Madden, R. H., Dunn, R. E., Evans, S., Palacios, A., & Carlini, A. A. (2015). Quasi-static Eocene–Oligocene climate in Patagonia promotes slow faunal evolution and mid-Cenozoic global cooling. *Palaeogeography, Palaeoclimatology, Palaeoecology*, *435*, 24-37.

Korasidis, V. A., Wallace, M. W., Wagstaff, B. E., & Hill, R. S. (2019). Terrestrial cooling record through the Eocene-Oligocene transition of Australia. *Global and Planetary Change*, *173*, 61-72.

Krohe, A., & Eisbacher, G. H. (1988). Oblique crustal detachment in the Variscan Schwarzwald, southwestern Germany. *Geologische Rundschau*, *77*, 25-43.

Kühn, R., & Roth, H. (1979). Beiträge zur Kenntnis der Salzlagerstätte am Oberrhein. *Z. Geol. Wiss.*, 7, 953-966.

Kunzmann, L., Kvaček, Z., Teodoridis, V., Müller, C., & Moraweck, K. (2016). Vegetation dynamics of riparian forest in central Europe during the late Eocene. *Palaeontographica Abteilung B*, 69-89. https://doi.org/10.1127/palb/295/2016/69

Kushner, P. J., Held, I. M., & Delworth, T. L. (2001). Southern Hemisphere atmospheric circulation response to global warming. *Journal of Climate*, 14(10), 2238-2249.

Kvaček, Z., Teodoridis, V., Mach, K., Přikryl, T., & Dvořak, Z. (2014). Tracing the Eocene-Oligocene transition: a case study from North Bohemia. *Bulletin of Geosciences*, 89(1). https://doi.org/10.3140/bull.geosci.1411

Kwiecien, O., Braun, T., Brunello, C. F., Faulkner, P., Hausmann, N., Helle, G., ... & Breitenbach, S. F. (2022). What we talk about when we talk about seasonality–A transdisciplinary review. *Earth-Science Reviews*, *225*, 103843.

Ladant, J. B., Donnadieu, Y., Lefebvre, V., & Dumas, C. (2014). The respective role of atmospheric carbon dioxide and orbital parameters on ice sheet evolution at the Eocene-Oligocene transition. *Paleoceanography*, 29(8), 810-823.

Lamb, A. L., Leng, M. J., Mohammed, M. U., & Lamb, H. F. (2004). Holocene climate and vegetation change in the Main Ethiopian Rift Valley, inferred from the composition (C/N and δ13C) of lacustrine organic matter. *Quaternary Science Reviews*, *23*(7-8), 881-891.

Langereis, C. G., Krijgsman, W., Muttoni, G., & Menning, M. (2010). Magnetostratigraphy-concepts, definitions, and applications. *Newsletters in Stratigraphy*, *43*(3), 207.

Laskar, J. (1989). A numerical experiment on the chaotic behaviour of the solar system. *Nature*, *338*(6212), 237-238.

Laskar, J. (1990). The chaotic motion of the solar system: A numerical estimate of the size of the chaotic zones. *Icarus*, *88*(2), 266-291.

Laskar, J. (1999). The limits of Earth orbital calculations for geological time-scale use. *Philosophical Transactions of the Royal Society of London. Series A: Mathematical, Physical and Engineering Sciences*, *357*(1757), 1735-1759.

Laskar, J., Fienga, A., Gastineau, M., & Manche, H. (2011). La2010: a new orbital solution for the long-term motion of the Earth. *Astronomy & Astrophysics*, *532*, A89.

Lavoyer, T. (2013). Paléontologie et stratigraphie de la partie nord du fossé rhénan supérieur moyen au cours du Paléogène: relations entre le système du rift, les transgressions marines et le paléoclimat. *GeoFocus*, 35, 1–210. Thèse de l’Université de Fribourg.

Le Verrier, U. J. (1856). Ann. Obs. Paris, Vol. 2 (Paris: Mallet-Bachelier)

Lear, C. H., Bailey, T. R., Pearson, P. N., Coxall, H. K., & Rosenthal, Y. (2008). Cooling and ice growth across the Eocene-Oligocene transition. *Geology*, 36(3), 251-254.

Lear, C. H., Mawbey, E. M., & Rosenthal, Y. (2010). Cenozoic benthic foraminiferal Mg/Ca and Li/Ca records: Toward unlocking temperatures and saturation states. *Paleoceanography*, 25(4).

Lear, C. H., Rosenthal, Y., Coxall, H. K., & Wilson, P. A. (2004). Late Eocene to early Miocene ice sheet dynamics and the global carbon cycle. *Paleoceanography*, 19(4).

Lettéron, A., Hamon, Y., Fournier, F., Demory, F., Séranne, M., & Joseph, P. (2022). Stratigraphic architecture of a saline lake system: From lake depocentre (Alès Basin) to margins (Saint-Chaptes and Issirac basins), Eocene–Oligocene transition, south-east France. *Sedimentology*, *69*(2), 651-695.

Lettéron, A., Hamon, Y., Fournier, F., Séranne, M., Pellenard, P., & Joseph, P. (2018). Reconstruction of a saline, lacustrine carbonate system (Priabonian, St-Chaptes Basin, SE France): depositional models, paleogeographic and paleoclimatic implications. *Sedimentary Geology*, *367*, 20-47.

Li, M., Hinnov, L., & Kump, L. (2019). Acycle: Time-series analysis software for paleoclimate research and education. *Computers & Geosciences*, *127*, 12-22.

Li, M., Kump, L. R., Hinnov, L. A., & Mann, M. E. (2018). Tracking variable sedimentation rates and astronomical forcing in Phanerozoic paleoclimate proxy series with evolutionary correlation coefficients and hypothesis testing. *Earth and Planetary Science Letters*, *501*, 165-179.

Lindström, S., & McLoughlin, S. (2007). Synchronous palynofloristic extinction and recovery after the end-Permian event in the Prince Charles Mountains, Antarctica: implications for palynofloristic turnover across Gondwana. *Review of Palaeobotany and Palynology*, *145*(1-2), 89-122.

Lisiecki, L. E., & Raymo, M. E. (2005). A Pliocene-Pleistocene stack of 57 globally distributed benthic δ18O records. *Paleoceanography*, 20(1).

Liu, Z., Pagani, M., Zinniker, D., DeConto, R., Huber, M., Brinkhuis, H., ... & Pearson, A. (2009). Global cooling during the Eocene-Oligocene climate transition. *Science*, *323*(5918), 1187-1190.

Livermore, R., Hillenbrand, C. D., Meredith, M., & Eagles, G. (2007). Drake Passage and Cenozoic climate: an open and shut case?. *Geochemistry, Geophysics, Geosystems*, 8(1).

Lombard, A., Cazenave, A., Le Traon, P. Y., & Ishii, M. (2005). Contribution of thermal expansion to present-day sea-level change revisited. *Global and Planetary Change*, 47(1), 1-16.

Lozier, M. S. (2010). Deconstructing the conveyor belt. *Science*, 328(5985), 1507-1511.

Lüthi, D., Le Floch, M., Bereiter, B., Blunier, T., Barnola, J. M., Siegenthaler, U., ... & Stocker, T. F. (2008). High-resolution carbon dioxide concentration record 650,000–800,000 years before present. *Nature*, 453(7193), 379-382.

Lutz, M., & Cleintuar, M. (1999). Geological results of a hydrocarbon exploration campaign in the southern Upper Rhine Graben (Alsace Centrale, France). *Bulletin für angewandte Geologie*, *4*, 3-80.

Macphail, M. K. (2007). Australian palaeoclimates: Cretaceous to Tertiary A review ofpalaeobotanical and related evidence to the year 2000. *CRC LEME Open File Report*, 151, 1–279. http://hdl.handle.net/1885/35585

Mader, D. (1985). Fluvial conglomerates in continental red beds of the Buntsandstein (Lower Triassic) in the Eifel (FRG) and their palaeoenvironmental, palaeogeographical and palaeotectonic significance. *Sedimentary Geology*, *44*(1-2), 1-64.

Maïkovsky, V. (1941). Contribution à l'étude paléontologique et stratigraphique du bassin potassique d'Alsace. *Mémoires du Service de la Carte géologique d'Alsace et de Lorraine*, Vol. 6, 192 p.

Mancosu, N., Snyder, R. L., Kyriakakis, G., & Spano, D. (2015). Water scarcity and future challenges for food production. *Water*, 7(3), 975-992.

Mann, M. E., & Lees, J. M. (1996). Robust estimation of background noise and signal detection in climatic time series. *Climatic change*, *33*(3), 409-445.

Martin, H. A. (2006). Cenozoic climatic change and the development of the arid vegetation in Australia. *Journal of Arid Environments*, *66*(3), 533-563.

Martini, E. (1990). The Rhinegraben system, a connection between northern and southern seas in the European Tertiary. *Veroffentlichungen aus dem Ubersee-Museum Bremen A*, 10, 83-98.

Martini, E., & Reichenbacher, B. (2007). Nannoplankton und Fisch-Otolithen in den Mittleren Pechelbronn-Schichten (Unter-Oligozän, Oberrheingraben/Mainzer Becken). *Geologische Abhandlungen Hessen*, *116*, 235-273.

Masson-Delmotte, V., Zhai, P., Pörtner, H. O., Roberts, D., Skea, J., & Shukla, P. R. (2022). Global Warming of 1.5 C: IPCC special report on impacts of global warming of 1.5 C above pre-industrial levels in context of strengthening response to climate change, sustainable development, and efforts to eradicate poverty. Cambridge University Press.

Matte, P. (2001). The Variscan collage and orogeny (480–290 Ma) and the tectonic definition of the Armorica microplate: a review. *Terra nova*, *13*(2), 122-128.

Matthews, M. D., & Perlmutter, M. A. (1994). Global cyclostratigraphy: an application to the Eocene Green River Basin. Orbital forcing and cyclic sequences, 459-481.

McCaffrey, M. A., Lazar, B. H. D. H., & Holland, H. D. (1987). The evaporation path of seawater and the coprecipitation of Br (super-) and K (super+) with halite. *Journal of Sedimentary Research*, 57(5), 928-937.

McInerney, F. A., & Wing, S. L. (2011). The Paleocene-Eocene Thermal Maximum: A perturbation of carbon cycle, climate, and biosphere with implications for the future. *Annual Review of Earth and Planetary Sciences*, 39, 489-516.

MDPA (1960). Catalogue des puits et sondages du bassin de Mulhouse, Vol. XIV, 3-119.

Ménillet, F., Durand, M., Genter, A., & Party, J. P. (2015). Notice explicative de la carte géologique de France (1/50 000). *Feuille Haguenau (198)(2e éd.). Orléans: BRGM, 345 p*.

Menning, M. (2018). Die Stratigraphische Tabelle von Deutschland 2016 (STD 2016). The Stratigraphic Table of Germany 2016 (STG 2016). *Zeitschrift der Deutschen Gesellschaft für Geowissenschaften*, *169*(2), 105-128.

Merle, O., Michon, L., Camus, G., & de Goer, A. (1998). L'extension oligocène sur la transversale septentrionale du rift du Massif Central. *Bulletin de la Société Géologique de France*, *169*(5), 615-626.

Michon, L. (2000). Dynamique de l'extension continentale: application au Rift Ouest-Européen par l'étude de la province du Massif Central (Doctoral dissertation, Université Blaise Pascal).

Milankovitch, M. M. (1920). Théorie mathématique des phénomènes thermiques produits par la radiation solaire. Gauthier-Villars et Cie.

Milankovitch, M. M. (1941). Canon of insolation and the iceage problem. *Koniglich Serbische Akademice Beograd Special Publication*, *132*.

Miller, K. G., Cramer, B. S., Wright, J. D., Browning, J. V., Kulpecz, A. A., Barrett, P., & Kominz, M. A. (2008, December). Late Cretaceous to Cenozoic Antarctic Ice-Sheet Evolution From Sea-Level and Deep-Sea Isotope Changes. In *AGU Fall Meeting Abstracts* (Vol. 2008, pp. C34B-07).

Miller, K. G., Wright, J. D., & Fairbanks, R. G. (1991). Unlocking the ice house: Oligocene-Miocene oxygen isotopes, eustasy, and margin erosion. *Journal of Geophysical Research: Solid Earth*, 96(B4), 6829-6848.

Mingram, J. (1998). Laminated Eocene maar-lake sediments from Eckfeld (Eifel region, Germany) and their short-term periodicities. *Palaeogeography, Palaeoclimatology, Palaeoecology*, 140(1-4), 289-305. https://doi.org/10.1016/S0031-0182(98)00021-2

Moretto, R. (1986). Etude sédimentologique et géochimique des dépôts de la série salifère paléogène du bassin de Bourg-en-Bresse (France). (Doctoral dissertation, Université de Lorraine). p. 252.

Mosbrugger, V., & Utescher, T. (1997). The coexistence approach—a method for quantitative reconstructions of Tertiary terrestrial palaeoclimate data using plant fossils. *Palaeogeography, Palaeoclimatology, Palaeoecology*, *134*(1-4), 61-86.

Mosbrugger, V., Utescher, T., & Dilcher, D. L. (2005). Cenozoic continental climatic evolution of Central Europe. *Proceedings of the National Academy of Sciences*, 102(42), 14964-14969. https://doi.org/10.1073/pnas.0505267102

Mudelsee, M., Bickert, T., Lear, C. H., & Lohmann, G. (2014). Cenozoic climate changes: A review based on time series analysis of marine benthic δ18O records. *Reviews of Geophysics*, 52(3), 333-374.

Müller, B., Wehrle, V., Zeyen, H., & Fuchs, K. (1997). Short-scale variations of tectonic regimes in the western European stress province north of the Alps and Pyrenees. *Tectonophysics*, *275*(1-3), 199-219.

Nemec, W., & Steel, R. (1984). Alluvial and coastal conglomerates: their significant features and some comments on gravelly mass-flow deposits. *Tectonics*, 32, 1358-1370.

Neugebauer, I., Brauer, A., Schwab, M. J., Waldmann, N. D., Enzel, Y., Kitagawa, H., ... & Party, D. S. (2014). Lithology of the long sediment record recovered by the ICDP Dead Sea Deep Drilling Project (DSDDP). *Quaternary Science Reviews*, *102*, 149-165.

Nocchi, M., Parisi, G., Monaco, P., Monechi, S., Madile, M., Napoleone, G., ... & Bice, D. M. (1986). The Eocene-Oligocene boundary in the Umbrian pelagic sequences, Italy. *In Developments in Palaeontology and Stratigraphy*, 9, 25-40.

Ojala, A. E., Francus, P., Zolitschka, B., Besonen, M., & Lamoureux, S. F. (2012). Characteristics of sedimentary varve chronologies–a review. *Quaternary Science Reviews*, 43, 45-60. https://doi.org/10.1016/j.quascirev.2012.04.006

Olsen, P. E. (1984). Periodicity of lake-level cycles in the late Triassic Lockatong formation of the Newark basin (Newark Supergroup, New Jersey and Pennsylvania). In *Milankovitch and climate; understanding the response to astronomical forcing: NATO advanced research. Workshop* (pp. 129-146).

Olsen, P. E. (1986). A 40-million-year lake record of early Mesozoic orbital climatic forcing. *Science*, *234*(4778), 842-848.

Oort, A. H. (1983). Global atmospheric circulation statistics, 1958-1973 (No. 14). US Department of Commerce, National Oceanic and Atmospheric Administration.

Page, M., Licht, A., Dupont-Nivet, G., Meijer, N., Barbolini, N., Hoorn, C., ... & Guo, Z. (2019). Synchronous cooling and decline in monsoonal rainfall in northeastern Tibet during the fall into the Oligocene icehouse. *Geology*, *47*(3), 203-206.

Palchan, D., Neugebauer, I., Amitai, Y., Waldmann, N. D., Schwab, M. J., Dulski, P., ... & Enzel, Y. (2017). North Atlantic controlled depositional cycles in MIS 5e layered sediments from the deep Dead Sea basin. *Quaternary Research*, *87*(1), 168-179.

Palter, J. B. (2015). The role of the Gulf Stream in European climate. *Annual Review of Marine Science*, 7, 113-137.

Pan, A. D., Jacobs, B. F., Dransfield, J., & Baker, W. J. (2006). The fossil history of palms (Arecaceae) in Africa and new records from the Late Oligocene (28–27 Mya) of north-western Ethiopia. *Botanical Journal of the Linnean Society*, 151(1), 69-81.

Pearson, P. N., Foster, G. L., & Wade, B. S. (2009). Atmospheric carbon dioxide through the Eocene–Oligocene climate transition. *Nature*, 461(7267), 1110-1113.

Pearson, P. N., McMillan, I. K., Wade, B. S., Jones, T. D., Coxall, H. K., Bown, P. R., & Lear, C. H. (2008). Extinction and environmental change across the Eocene-Oligocene boundary in Tanzania. *Geology*, 36(2), 179-182. https://doi.org/10.1130/G24308A.1

Pearson, P. N., van Dongen, B. E., Nicholas, C. J., Pancost, R. D., Schouten, S., Singano, J. M., & Wade, B. S. (2007). Stable warm tropical climate through the Eocene Epoch. *Geology*, *35*(3), 211-214.

Peck, V. L., Yu, J., Kender, S., & Riesselman, C. R. (2010). Shifting ocean carbonate chemistry during the Eocene-Oligocene climate transition: Implications for deep-ocean Mg/Ca paleothermometry. *Paleoceanography*, 25(4).

Peixoto, J. P., & Oort, A. H. (1992). Physics of climate. American Institute of Physics, p. 520.

Pekar, S. F., Christie-Blick, N., Kominz, M. A., & Miller, K. G. (2002). Calibration between eustatic estimates from backstripping and oxygen isotopic records for the Oligocene. *Geology*, *30*(10), 903-906.

Pelletier, H. (1972). Notes géologiques sur la Limagnes. *Revue des Sciences Naturelles d'Auvergne*, 38, 7-19.

Petersen, S. V., & Schrag, D. P. (2015). Antarctic ice growth before and after the Eocene-Oligocene transition: New estimates from clumped isotope paleothermometry. *Paleoceanography*, *30*(10), 1305-1317.

Piasecki, S. T. E. F. A. N. (1980). Dinoflagellate cyst stratigraphy of the Miocene Hodde and Gram formations, Denmark. *Bulletin of the Geological Society of Denmark*, *29*(1–2), 53-76.

Piga, E. (2020). *How hot is hot? Tropical ocean temperatures and plankton communities in the Eocene Epoch* (Doctoral dissertation, Cardiff University).

Pirkenseer, C., & Berger, J. P. (2011). Paleogene Ostracoda from the southern Upper Rhine Graben: taxonomy, palaeoecology and palaeobiogeography. *Palaeontographica Abteilung A*, 1-152.

Pirkenseer, C., Rauber, G., & Rousse, S. (2018). A revised Palaeogene lithostratigraphic framework for the northern Swiss Jura and the southern Upper Rhine Graben and its relationship to the North Alpine Foreland Basin. *Rivista Italiana di Paleontologia e Stratigrafia*, *124*(1).

Pirkenseer, C., Spezzaferri, S., & Berger, J. P. (2010). Palaeoecology and biostratigraphy of the Paleogene Foraminifera from the southern Upper Rhine Graben and the influence of reworked planktonic Foraminifera. *Palaeontographica, Palaeontographica, Abt. A: Palaeozoology–Stratigraphy*, *293*, 1-93.

Pound, M. J., & Salzmann, U. (2017). Heterogeneity in global vegetation and terrestrial climate change during the late Eocene to early Oligocene transition. *Scientific Reports*, *7*(1), 43386.

Prahl, F. G., Bennett, J. T., & Carpenter, R. (1980). The early diagenesis of aliphatic hydrocarbons and organic matter in sedimentary particulates from Dabob Bay, Washington. *Geochimica et Cosmochimica Acta*, *44*(12), 1967-1976.

Priestley, M. B. (1981). Spectral analysis and time series: probability and mathematical statistics. Academic Press, London, 1-890.

Pross, J., & Brinkhuis, H. (2005). Organic-walled dinoflagellate cysts as paleoenvironmental indicators in the Paleogene; a synopsis of concepts. *Paläontologische Zeitschrift*, *79*, 53-59.

Pross, J., Contreras, L., Bijl, P. K., Greenwood, D. R., Bohaty, S. M., Schouten, S., ... & Brinkhuis, H. (2012). Persistent near-tropical warmth on the Antarctic continent during the early Eocene epoch. *Nature*, *488*(7409), 73-77.

Pusz, A. E., Thunell, R. C., & Miller, K. G. (2011). Deep water temperature, carbonate ion, and ice volume changes across the Eocene-Oligocene climate transition. *Paleoceanography*, 26(2).

Quattrocchio, M. E., Martínez, M. A., Hinojosa, L. F., & Jaramillo, C. (2013). Quantitative analysis of Cenozoic palynofloras from Patagonia, southern South America. *Palynology*, *37*(2), 246-258.

Rahmstorf, S. (2003). Thermohaline circulation: The current climate. *Nature*, 421(6924), 699-699.

Rajchl, M., Uličný, D., Grygar, R., & Mach, K. (2009). Evolution of basin architecture in an incipient continental rift: the Cenozoic Most Basin, Eger Graben (Central Europe). *Basin Research*, *21*(3), 269-294.

Raymo, M. E., & Ruddiman, W. F. (1992). Tectonic forcing of late Cenozoic climate. *Nature*, *359*(6391), 117-122.

Rea, D. K., & Lyle, M. W. (2005). Paleogene calcite compensation depth in the eastern subtropical Pacific: Answers and questions. *Paleoceanography*, *20*(1).

Reading, H. G. (1996). Sedimentary environments: processes, facies and stratigraphy. Blackwell Publishing, p. 688.

Rhines, P., S. Häkkinen, and S. A. Josey (2008), Is Oceanic Heat Transport Significant in the Climate System?, in Arctic-Subarctic Ocean Fluxes, pp. 87–109, Springer, Netherlands.

Ridgway, K. D., & Sweet, A. R. (1995). Climatically induced floristic changes across the Eocene–Oligocene transition in the northern high latitudes, Yukon Territory, Canada. *Geological Society of America Bulletin*, *107*(6), 676-696.

Ritzkowski, S. (1969). Nördliches Hessen. *Führer zur Oligocän-Exkursion*, *1969*, 58-73.

Riveline, J. (1984). Les gisements à charophytes du Cénozoïque (Danien à Burdigalien) d'Europe occidentale.

Riveline, J., Giot, D., Farjanel, G., & Pacquet, A. (1988). Mise en évidence de dépôts Eocène moyen (Lutétien supérieur) à la base des formations Tertiaires du bassin de Moulins (Allier, France): implications tectoniques. *Comptes rendus de l'Académie des sciences. Série 2, Mécanique, Physique, Chimie, Sciences de l'univers, Sciences de la Terre*, *306*(1), 55-62.

Roberts, C. D., LeGrande, A. N., & Tripati, A. K. (2009). Climate sensitivity to Arctic seaway restriction during the early Paleogene. *Earth and Planetary Science Letters*, *286*(3-4), 576-585.

Rodionov, S. N. (2006). Use of prewhitening in climate regime shift detection. *Geophysical Research Letters*, *33*(12).

Rothausen, K., & Sonne, V. (1984). Mainzer Becken. Gebrüder Bornträger, Stuttgart, Germany, 203 p.

Roussé, S. (2006). Architecture et dynamique des séries marines et continentales de l'oligocène moyen et supérieur du sud du fossé rhénan : Evolution des milieux de dépôt en contexte de rift en marge de l'avant-pays alpin (Doctoral dissertation, Université de Strasbourg), p. 474.

Ruddiman, W. F., Raymo, M. E., Prell, W. L., & Kutzbach, J. E. (1997). The uplift-climate connection: a synthesis. *Tectonic uplift and climate change*, 471-515.

Rybka, S. (1981). Répertoire des bancs d’halite et d’insolubles au-dessus et au-dessous des couches potassiques. Mines De Potasse d’Alsace, Département Géologie.

Salam, M. A., & Noguchi, T. (2005). Impact of human activities on carbon dioxide (CO 2) emissions: A statistical analysis. *Environmentalist*, 25, 19-30.

Sanjuan, B., Gourcerol, B., Millot, R., Rettenmaier, D., Jeandel, E., & Rombaut, A. (2022). Lithium-rich geothermal brines in Europe: An up-date about geochemical characteristics and implications for potential Li resources. *Geothermics*, 101, 102385.

Sarkar, S., Basak, C., Frank, M., Berndt, C., Huuse, M., Badhani, S., & Bialas, J. (2019). Late Eocene onset of the proto-Antarctic circumpolar current. *Scientific Reports*, 9(1), 10125. https://doi.org/10.1038/s41598-019-46253-1

Schäfer, A., Utescher, T., Klett, M., & Valdivia-Manchego, M. (2005). The Cenozoic Lower Rhine Basin–rifting, sedimentation, and cyclic stratigraphy. *International Journal of Earth Sciences*, *94*, 621-639.

Schimmelmann, A., Lange, C. B., Schieber, J., Francus, P., Ojala, A. E., & Zolitschka, B. (2016). Varves in marine sediments: A review. *Earth-Science Reviews*, *159*, 215-246.

Schmidt-Kittler, N. (1977). Some aspects of evolution and provincialism of rodent faunas in the European Paleogene. *Geobios*, *10*, 97-106.

Schnaebele, R. (1948). Monographie Géologique du Champ Pétrolifere de Pechelbronn, Strasbourg. *Mémoire de la Carte Géologique d’Alsace et de Lorraine*, *7*, 287 p.

Schneider, S. H., & Dickinson, R. E. (1974). Climate modeling. *Reviews of Geophysics*, 12(3), 447-493.

Schnurrenberger, D., Russell, J., & Kelts, K. (2003). Classification of lacustrine sediments based on sedimentary components. Journal of Paleolimnology, 29, 141-154.

Schuler, M. (1983). Pollens et spores des séries salifères (Eocène/Oligocène) du bassin potassique de Mulhouse (France). Relations entre la microflore et les dépôts évaporitiques. *Sciences Géologiques, bulletins et mémoires*, *36*(4), 255-265.

Schuler, M. (1988). Environnements et paléoclimats paléogènes. Palynologie et biostratigraphie de l'Éocène et de l'Oligocène inferieur dans les fossés rhénan, rhodanien et de Hesse. Documents BRGM, Vol. 190, 503 p.

Schumacher, M. E. (2002). Upper Rhine Graben: role of preexisting structures during rift evolution. *Tectonics*, *21*(1), 6-1.

Schwab, F. L. (1976). Modern and ancient sedimentary basins: comparative accumulation rates. Geology, 4(12), 723-727. https://doi.org/10.1130/0091-7613(1976)4<723:MAASBC>2.0.CO;2

Schwarzacher, W. (1993). Cyclostratigraphy and the Milankovitch theory. *Developments in Sedimentology*, 52, p. 225.

Scotese, C. R., & Wright, N. (2018). PALEOMAP paleodigital elevation models (PaleoDEMS) for the Phanerozoic PALEOMAP Project. *Earthbyte https://www. earthbyte. org/paleodem-resource-scotese-and-wright-2018*.

Seager, R. (2006). The Source of Europe's Mild Climate: The notion that the Gulf Stream is responsible for keeping Europe anomalously warm turns out to be a myth. *American Scientist*, 94(4), 334-341.

Seager, R., Battisti, D. S., Yin, J., Gordon, N., Naik, N., Clement, A. C., & Cane, M. A. (2002). Is the Gulf Stream responsible for Europe's mild winters?. *Quarterly Journal of the Royal Meteorological Society*, 128(586), 2563-2586.

Selkin, P. A., Strömberg, C. A., Dunn, R., Kohn, M. J., Carlini, A. A., Davies-Vollum, K. S., & Madden, R. H. (2015). Climate, dust, and fire across the Eocene-Oligocene transition, Patagonia. *Geology*, *43*(7), 567-570.

Sellers, W. D. (1969). A global climatic model based on the energy balance of the earth-atmosphere system. *Journal of Applied Meteorology and Climatology*, 8(3), 392-400.

Semmani, N., Fournier, F., Suc, J. P., Fauquette, S., Godeau, N., Guihou, A., ... & Borgomano, J. (2023). The Paleogene continental basins from SE France: new geographic and climatic insights from an integrated approach. *Palaeogeography, Palaeoclimatology, Palaeoecology*, *615*, 111452.

Shukla, P. R., Skea, J., Calvo Buendia, E., Masson-Delmotte, V., Pörtner, H. O., Roberts, D. C., ... & Malley, J. (2019). IPCC, 2019: Climate Change and Land: an IPCC special report on climate change, desertification, land degradation, sustainable land management, food security, and greenhouse gas fluxes in terrestrial ecosystems.

Sijp, W. P., von der Heydt, A. S., & Bijl, P. K. (2016). Model simulations of early westward flow across the Tasman Gateway during the early Eocene. *Climate of the Past*, *12*(4), 807-817.

Silva, I. P., & Jenkins, D. G. (1993). Decision on the Eocene-Oligocene boundary stratotype. *Episodes Journal of International Geoscience*, 16(3), 379-382.

Simon, E., Gindre-Chanu, L., Blanchet, C., Dupont-Nivet, G., Martinez, M., Guillocheau, F., Ulrich, M., Nutz, A., Vogel, H., & Schuster, M. (2024, submitted). Lacustrine laminites from the Mulhouse basin (Upper Rhine Graben, France): a sedimentary record of increased seasonality and sensitivity to orbital forcing through the Eocene-Oligocene Transition?. Sedimentologika, 2.

Simon, E., Gindre-Chanu, L., Nutz, A., Boesch, Q., Dupont-Nivet, G., Vogel, H., & Schuster, M. (2021). Regard sur un changement climatique majeur : la transition Éocène-Oligocène dans le Fossé Rhénan. *Géologues*, 210, 26-34.

Sinnesael, M., De Vleeschouwer, D., Zeeden, C., Batenburg, S. J., Da Silva, A. C., de Winter, N. J., ... & Claeys, P. (2019). The Cyclostratigraphy Intercomparison Project (CIP): consistency, merits and pitfalls. *Earth-Science Reviews*, *199*, 102965.

Sirota, I., Enzel, Y., & Lensky, N. G. (2017). Temperature seasonality control on modern halite layers in the Dead Sea: In situ observations. Bulletin, 129(9-10), 1181-1194. https://doi.org/10.1130/B31661.1

Sissingh, W. (1998). Comparative tertiary stratigraphy of the Rhine Graben, Bresse Graben and Molasse Basin: correlation of Alpine foreland events. *Tectonophysics*, *300*(1-4), 249-284.

Sissingh, W. (2006). Kinematic sequence stratigraphy of the European Cenozoic Rift System and Alpine Foreland Basin: correlation with Mediterranean and Atlantic plate-boundary events. *Netherlands Journal of Geosciences/Geologie en Mijnbouw*, *85*(2), 77-129.

Sittler C. (1965). Le Paléogène des fossés rhénan et rhodanien. Études sédimentologiques et paléoclimatiques. *Mém. Serv. Carte géol. Als.-Lorr*., 24, 392 p.

Sittler, C. (1972). Le pétrole dans le département du Haut-Rhin. Bilan d'un siècle et demi de recherches et d'exploitations. *Sciences Géologiques, bulletins et mémoires*, *25*(2), 151-161.

Śliwińska, K. K., Thomsen, E., Schouten, S., Schoon, P. L., & Heilmann-Clausen, C. (2019). Climate-and gateway-driven cooling of Late Eocene to earliest Oligocene sea surface temperatures in the North Sea Basin. *Scientific Reports*, *9*(1), 4458.

Sluijs, A., Pross, J., & Brinkhuis, H. (2005). From greenhouse to icehouse; organic-walled dinoflagellate cysts as paleoenvironmental indicators in the Paleogene. *Earth-Science Reviews*, *68*(3-4), 281-315.

Sluiter, I. R., Holdgate, G. R., Reichgelt, T., Greenwood, D. R., Kershaw, A. P., & Schultz, N. L. (2022). A new perspective on Late Eocene and Oligocene vegetation and paleoclimates of South-eastern Australia. *Palaeogeography, Palaeoclimatology, Palaeoecology*, *596*, 110985.

Stchepinsky, A. (1960). Étude des Ostracodes du Sannoisien de l'Alsace. *Sciences Géologiques, bulletins et mémoires*, *13*(1), 11-34.

Stehlin, H.G. (1910). Remarques sur les faunules de Mammifères des couches éocènes et oligocènes du Bassin de Paris. *Bulletin de la Société Géologique de France*, vol. 4, no 9, 1910, p. 488-520.

STG 2016 (German Stratigraphic Commission, ed.; editing, coordination and layout: Menning, M. & Hendrich, A.) (2016): Stratigraphic Table of Germany 2016. – Potsdam (German Research Centre for Geosciences). in German, (1) Table plain 100 x 141 cm, (2) Table folded A4

Stommel, H. (2022). The Gulf Stream: a physical and dynamical description. Univ of California Press, Berkeley and Los Angeles, USA, p. 248.

Storni, A. (2002). Étude paléontologique et sédimentologique de la carrière d'Altkirch (Alsace, Paléogène) et cartographie des sédiments tertiaires et quaternaires de la région de Porrentruy. *Unpublished Master Thesis, University of Fribourg*, p. 125.

Strasser, A., Hilgen, F. J., & Heckel, P. H. (2006). Cyclostratigraphy-concepts, definitions, and applications. *Newsletters on Stratigraphy*, 42, 75-114.

Straume, E. O., Nummelin, A., Gaina, C., & Nisancioglu, K. H. (2022). Climate transition at the Eocene–Oligocene influenced by bathymetric changes to the Atlantic–Arctic oceanic gateways. *Proceedings of the National Academy of Sciences*, 119(17), e2115346119.

Strömberg, C. A., Dunn, R. E., Madden, R. H., Kohn, M. J., & Carlini, A. A. (2013). Decoupling the spread of grasslands from the evolution of grazer-type herbivores in South America. *Nature communications*, *4*(1), p. 1478.

Strother, S. L., Salzmann, U., Sangiorgi, F., Bijl, P. K., Pross, J., Escutia, C., ... & Woodward, J. (2017). A new quantitative approach to identify reworking in Eocene to Miocene pollen records from offshore Antarctica using red fluorescence and digital imaging. *Biogeosciences*, *14*(8), 2089-2100.

Strum, M. (1979). Origin and composition of clastic varves. In Moraines and varves; origin, genesis, classification. *Proceedings of an INQUA symposium on genesis and lithology of Quaternary deposits*, 281-285.

Stucky A (2005) Der Melanienkalk im südlichen Oberrheingraben: Sedimentationsdynamik pedogenetisch alterierter Karbonate (Tagolsheim, Elsass). MSc Thesis, Geologisch Paläontologisches Institut, Universität Basel, p. 131.

Suc, J. P., & Popescu, S. M. (2005). Pollen records and climatic cycles in the North Mediterranean region since 2.7 Ma. *Geological Society, London, Special Publications*, *247*(1), 147-158.

Sun, J., Ni, X., Bi, S., Wu, W., Ye, J., Meng, J., & Windley, B. F. (2014). Synchronous turnover of flora, fauna and climate at the Eocene–Oligocene Boundary in Asia. *Scientific reports*, *4*(1), 7463.

Taner, M. T. (2000). Attributes Revisited, Technical Publication. *Rock Solid Images, Inc., Houston, Texas. URL: http://www. rocksolidimages. com/pdf/attrib_revisited. htm*.

Tanner, L. H. (2010). Continental carbonates as indicators of paleoclimate. *Developments in Sedimentology*, *62*, 179-214.

Tardif, D., Toumoulin, A., Fluteau, F., Donnadieu, Y., Le Hir, G., Barbolini, N., Licht, A., Ladant, J. B., Sepulchre, P., Viovy, N., Hoorn, C., & Dupont-Nivet, G. (2021). Orbital variations as a major driver of climate and biome distribution during the greenhouse to icehouse transition. *Science Advances*, 7(43). https://doi.org/10.1126/sciadv.abh2819

Taylor, A. H., & Stephens, J. A. (1998). The North Atlantic oscillation and the latitude of the Gulf Stream. *Tellus A: Dynamic Meteorology and Oceanography*, 50(1), 134-142.

Terry, R. D., Chilingar, G. V., & Hancock, A. (1955). Comparison charts for visual estimation of percentage composition. *Journal of Sedimentary Petrology*, *25*, 229-234.

Thomson, D. J. (1982). Spectrum estimation and harmonic analysis. Proceedings of the IEEE, 70(9), 1055-1096. https://doi.org/10.1109/PROC.1982.12433

Thorne, R. F. (1972). Major disjunctions in the geographic ranges of seed plants. *The Quarterly Review of Biology*, 47(4), 365-411.

Thornton, S. F., & McManus, J. (1994). Application of organic carbon and nitrogen stable isotope and C/N ratios as source indicators of organic matter provenance in estuarine systems: evidence from the Tay Estuary, Scotland. *Estuarine, Coastal and Shelf Science*, *38*(3), 219-233.

Thunell, R. C., & Corliss, B. H. (1986). Late Eocene-early Oligocene carbonate sedimentation in the deep sea. In *Developments in Palaeontology and Stratigraphy* (Vol. 9, pp. 363-380). Elsevier.

Tierney, J. E., Poulsen, C. J., Montañez, I. P., Bhattacharya, T., Feng, R., Ford, H. L., ... & Zhang, Y. G. (2020). Past climates inform our future. *Science*, 370(6517), eaay3701.

Toumoulin, A., Tardif, D., Donnadieu, Y., Licht, A., Ladant, J. B., Kunzmann, L., & Dupont-Nivet, G. (2022). Evolution of continental temperature seasonality from the Eocene greenhouse to the Oligocene icehouse–a model–data comparison. *Climate of the Past*, *18*(2), 341-362.

Tramoy, R., Salpin, M., Schnyder, J., Person, A., Sebilo, M., Yans, J., ... & Bauer, H. (2016). Stepwise palaeoclimate change across the Eocene–Oligocene transition recorded in continental NW Europe by mineralogical assemblages and δ15Norg (Rennes Basin, France). *Terra Nova*, *28*(3), 212-220.

Traverse, A. (1988). Paleopalynology. Unwin Hyman, Boston, p. 600.

Tripati, A., Backman, J., Elderfield, H., & Ferretti, P. (2005). Eocene bipolar glaciation associated with global carbon cycle changes. *Nature*, *436*(7049), 341-346.

Usiglio, M. J. (1849). Études sur la composition de l'eau de la Méditerranée et sur l'exploitation des sels qu'elle contient. *Annales Chim. Phys*., ser 3, 27, 172-191.

Utescher, T., Bondarenko, O. V., & Mosbrugger, V. (2015). The Cenozoic Cooling–continental signals from the Atlantic and Pacific side of Eurasia. *Earth and Planetary Science Letters*, 415, 121-133. https://doi.org/10.1016/j.epsl.2015.01.019

Van Aalst, M. K. (2006). The impacts of climate change on the risk of natural disasters. *Disasters*, 30(1), 5-18.

Van Andel, T. H., Heath, G. R., & Moore, T. C. (1975). Cenozoic history and paleoceanography of the central equatorial Pacific Ocean: a regional synthesis of Deep Sea Drilling Project data. https://doi.org/10.1130/MEM143-p1

Van Wervecke, L. (1913) Die Tektonik des Sundgaues, ihre Beziehungen zu den Kalisalzvorkommen im Oberelsass und in Baden und ihre Entstehung. *Mitt. Geol. Landesamt Els.-Lothr*. 6, 323–339.

Villemin, T., Alvarez, F., & Angelier, J. (1986). The Rhinegraben: extension, subsidence and shoulder uplift. *Tectonophysics*, *128*(1-2), 47-59.

Wade, B. S., Houben, A. J., Quaijtaal, W., Schouten, S., Rosenthal, Y., Miller, K. G., ... & Brinkhuis, H. (2012). Multiproxy record of abrupt sea-surface cooling across the Eocene-Oligocene transition in the Gulf of Mexico. *Geology*, *40*(2), 159-162.

Waltham, D. (2015). Milankovitch period uncertainties and their impact on cyclostratigraphy. *Journal of Sedimentary Research*, 85(8), 990-998.

Warren, J. K. (2016). Evaporites: A geological compendium. Springer.

Wattinne, A., Lécuyer, C., Vennin, E., Chateauneuf, J. J., & Martineau, F. (2018). Environmental changes around the Oligocene/Miocene boundary in the Limagne graben, Massif Central, France. *Bulletin de la Société Géologique de France*, *189*(4-6).

Weedon, G. P. (2003). *Time-series analysis and cyclostratigraphy: examining stratigraphic records of environmental cycles*. Cambridge University Press.

Weltje, G. J., Bloemsma, M. R., Tjallingii, R., Heslop, D., Röhl, U., & Croudace, I. W. (2015). Prediction of geochemical composition from XRF core scanner data: a new multivariate approach including automatic selection of calibration samples and quantification of uncertainties. Micro-XRF Studies of Sediment Cores: Applications of a non-destructive tool for the environmental sciences, 507-534. https://doi.org/10.1007/978-94-017-9849-5_21

Westerhold, T., Marwan, N., Drury, A. J., Liebrand, D., Agnini, C., Anagnostou, E., ... & Zachos, J. C. (2020). An astronomically dated record of Earth's climate and its predictability over the last 66 million years. *Science*, *369*(6509), 1383-1387.

White, A. A., & Bromley, R. A. (1995). Dynamically consistent, quasi-hydrostatic equations for global models with a complete representation of the Coriolis force. *Quarterly Journal of the Royal Meteorological Society*, 121(522), 399-418.

Wickert, F., & Eisbacher, G. H. (1988). Two-sided Variscan thrust tectonics in the Vosges Mountains, northeastern France. *Geodinamica Acta*, *2*(3), 101-120.

Williams, G. L., Brinkhuis, H. M. A. P., Pearce, M. A., Fensome, R. A., Weegink, J. W., & Exon, N. F. (2004, April). Southern Ocean and global dinoflagellate cyst events compared: index events for the Late Cretaceous–Neogene. In *Proceedings of the Ocean Drilling Program, scientific results* (Vol. 189, pp. 1-98).

Willis, J. K., Chambers, D. P., & Nerem, R. S. (2008). Assessing the globally averaged sea level budget on seasonal to interannual timescales. *Journal of Geophysical Research: Oceans*, *113*(C6).

Wilson, D. S., Pollard, D., DeConto, R. M., Jamieson, S. S., & Luyendyk, B. P. (2013). Initiation of the West Antarctic Ice Sheet and estimates of total Antarctic ice volume in the earliest Oligocene. *Geophysical Research Letters*, *40*(16), 4305-4309.

Wilson, M. V., & Bogen, A. (1994). Tests of the annual hypothesis and temporal calibration of a 6375-varve fish-bearing interval, Eocene horsefly beds, British Columbia, Canada. *Historical Biology*, 7(4), 325-339. https://doi.org/10.1080/10292389409380463

Wing, S. L. (1987). Eocene and Oligocene floras and vegetation of the Rocky Mountains. *Annals of the Missouri Botanical Garden*, 748-784.

Wunsch, C. (2002). What is the thermohaline circulation?. *Science*, 298(5596), 1179-1181.

Yancey, T. E., Heizler, M. T., Miller, B. V., & Guillemette, R. N. (2018). Eocene–Oligocene chronostratigraphy of ignimbrite flareup volcanic ash beds on the Gulf of Mexico coastal plains. *Geosphere*, *14*(3), 1232-1252.

Zachos, J. C., Quinn, T. M., & Salamy, K. A. (1996). High-resolution (104 years) deep-sea foraminiferal stable isotope records of the Eocene-Oligocene climate transition. *Paleoceanography*, 11(3), 251-266.

Zachos, J., Pagani, M., Sloan, L., Thomas, E., & Billups, K. (2001). Trends, rhythms, and aberrations in global climate 65 Ma to present. *Science*, 292(5517), 686-693.

Zanazzi, A., Judd, E., Fletcher, A., Bryant, H., & Kohn, M. J. (2015). Eocene–Oligocene latitudinal climate gradients in North America inferred from stable isotope ratios in perissodactyl tooth enamel. *Palaeogeography, Palaeoclimatology, Palaeoecology*, 417, 561-568. https://doi.org/10.1016/j.palaeo.2014.10.024

Zanazzi, A., Kohn, M. J., MacFadden, B. J., & Terry, D. O. (2007). Large temperature drop across the Eocene–Oligocene transition in central North America. *Nature*, *445*(7128), 639-642.

Zhang, Y. G., Pagani, M., Liu, Z., Bohaty, S. M., & DeConto, R. (2013). A 40-million-year history of atmospheric CO2. *Philosophical Transactions of the Royal Society A: Mathematical, Physical and Engineering Sciences*, *371*(2001), 20130096.

Ziegler, P. A. (1992). European Cenozoic rift system. *Tectonophysics*, *208*(1-3), 91-111.

Ziegler, P. A. (1992). North Sea rift system. *Tectonophysics*, *208*(1-3), 55-75.

Zijderveld, J. D. A. (1967). AC demagnetization of rocks: Analysis of results, Methods in Paleomagnetism DW Collinson, KM Creer, SK Runcorn, 254–286.

Zijderveld, J. D. A. (2013). AC demagnetization of rocks: analysis of results. In *Developments in solid earth geophysics* (Vol. 3, pp. 254-286). Elsevier.

Zolitschka, B., Francus, P., Ojala, A. E., & Schimmelmann, A. (2015). Varves in lake sediments–a review. *Quaternary Science Reviews*, 117, 1-41. https://doi.org/10.1016/j.quascirev.2015.03.019

Emile SIMON

Impacts des changements climatiques globaux sur les environnements continentaux : étude de cas de la transition Éocène-Oligocène dans le Fossé Rhénan

Résumé

Comprendre l'impact des perturbations climatiques passées sur les environnements continentaux est crucial pour mieux anticiper le futur de notre Terre. Cette thèse contribue à l'effort collectif des études concernant la Transition Éocène-Oligocène (TEO) au prisme des environnements continentaux du Fossé Rhénan (FR). C'est une période de ~790 ka qui correspond à la transition de conditions « greenhouse » à « icehouse ». La chronostratigraphie du FR a été améliorée et les changements à travers la TEO documentés. Ces changements sont un refroidissement, une aridification, un contraste climatique saisonnier accru, et une plus grande sensibilité du climat aux variations orbitales. Dans le bassin de Mulhouse, la transition de pélites sans structures à des sédiments laminés et varves, ainsi que l'apparition de cycles sédimentaires forcés par les variations orbitales, sont les marqueurs de ces deux derniers changements. Des investigations géochimiques et palynologiques menées dans le bassin de Pechelbronn suggèrent l'occurrence d'une transgression marine proche de la base de la « Zone Fossilifère ».

Mots-clés : Transition Éocène-Oligocène, Dérèglement climatique, Fossé Rhénan, Paléoclimats, Paléoenvironnements, Sédimentologie, Cyclostratigraphie, Bassin de Mulhouse

Impacts of global climate changes on continental environments: case study of the Eocene-Oligocene transition in the Upper Rhine Graben

Résumé en anglais

Understanding the impact of past climatic perturbations on continental environments is crucial to better assess and anticipate the future of our Earth. This thesis contributes to the collective effort of paleoclimate studies regarding the Eocene-Oligocene Transition (EOT) through the prism of the continental environments of the Upper Rhine Graben (URG). The EOT is a ~790 kyr period that corresponds to the transition from "greenhouse" to "incehouse" conditions. The chronostratigraphic framework of the URG has been improved and the changes across the EOT documented. These changes consist of cooling, aridification, increased seasonal climatic contrast, and a greater sensibility of the climate to orbital variations. In the Mulhouse basin, the transition from structureless mudstones to laminated sediments and varves at the base of the "Sel III", along the onset of orbitally induced sedimentary cycles, are the markers of these last two changes. Geochemical and palynological investigations performed in the Pechelbronn basin suggest the occurrence of a marine transgression near the base of the "Zone Fossilifère".

Keywords: Eocene-Oligocene transition, Climate change, Upper Rhine Graben, Paleoclimates, Paleoenvironments, Sedimentology, Cyclostratigraphy, Mulhouse basin